Impact of metabolic disorders on the structure, function, and immunological integrity of the blood-brain barrier

Thesis presented by

Madeeha Hamid Sheikh

For the degree of

Doctor of Philosophy

Centre for Translational Medicine and Therapeutics

William Harvey Research Institute

Queen Mary, University of London

Statement of Originality

I, Madeeha Hamid Sheikh, confirm that the research included within this thesis is my own work or that where it has been carried out in collaboration with, or supported by others, that this is duly acknowledged below and my contribution indicated. Previously published material is also acknowledged below.

I attest that I have exercised reasonable care to ensure that the work is original, and does not to the best of my knowledge break any UK law, infringe any third party's copyright or other Intellectual Property Right, or contain any confidential material.

I accept that the College has the right to use plagiarism detection software to check the electronic version of the thesis.

I confirm that this thesis has not been previously submitted for the award of a degree by this or any other university.

The copyright of this thesis rests with the author and no quotation from it or information derived from it may be published without the prior written consent of the author.

Signature:
Date: 15th July 2020

This work was supported by the British Heart Foundation - Award number: FS/16/60/32739.

Details of collaboration: Thank you to Professor Daniella Virgintino, Dr Marielle Errede and Dr Antonio d'Amati from Bari University, Italy for carrying out the confocal imaging, immuno-histochemical analysis, and quantification on mouse brains.

Abstract

Metabolic disorders induce a low-grade chronic inflammatory state that is damaging to the peripheral vasculature, leading to cardiovascular diseases. In recent years, there has been mounting evidence linking metabolic disease to neurovascular disorders and cognitive decline. However, the pathophysiological response occurring at the brain microvasculature, the blood-brain barrier (BBB), remains largely unexplored.

Using a mouse model of Type II diabetes mellitus, the results of this project demonstrate pro-inflammatory mediators and altered immune responses to impair the protective BBB functionality. Disruption to tight junctions and basal lamina, due to loss of control in activation/production of MMPs and their inhibitors, causes complete BBB breakdown. Metabolic stress triggers endothelial dysfunction resulting in altered metabolism and receptor expression, enhanced ROS production and up-regulated adhesion molecules. Immunologically, there is an increase in the percentage of activated effector and central memory T-cells along with an imbalance in the T_H17/Treg subsets. Together these factors augment transmigration of leukocytes across the BBB to trigger activation and shift of microglia to a pro-inflammatory phenotype, initiating neuroinflammation. Loss of the physical, transport and metabolic properties of the BBB will consequently have detrimental effects on neuronal function.

Additionally, this thesis explores the use of a pharmacological and dietary intervention to reduce and restore the damage incurred to the BBB. Treatment with human recombinant annexin A1 (a well know anti-inflammatory molecule) and reversion from a high-fat high-sugar diet to a chow diet both attenuate T2DM development, reduce peripheral inflammation and dampen the immune response, resulting in restored BBB integrity. Both interventions confer neuroprotection through stabilisation of cell-cell contacts, consequently limiting leukocyte extravasation and downstream pathological events.

This thesis emphasises the growing understanding of long-term impact of metabolic disease and their contribution to the development of neuroinflammatory/ neurodegenerative disorders. Preventive and therapeutic strategies that mediate anti-inflammatory effects are key in limiting the disease progression.

Acknowledgements

Alhamdulillah, all praise is due to Allah SWT who has given me the strength, health, ability, knowledge, and patience through these PhD years.

Nothing can ever be accomplished without enthusiasm; so, thank you to my supervisor Dr Egle Solito whose passion for science is unwavering. I am sincerely grateful for your knowledge and guidance throughout this project. Thank you for the opportunities to participate in international conferences, those memories are ones I will treasure for life.

A huge thank you to my 'PhD family' – Caroline, Jack, Noorafza, Sabrina, Liz, Sura, Zahid, Lauren, Johannes, Alice and Anitha for being my life support every day and for never letting me give up. I know in you all, I have found forever friends. Dearest Caroline: you are my best friend, comrade, ally, sidekick, partner in crime, alter ego, yin to my yang. Basically, there is no other person I would pick to have completed this rollercoaster of a journey with me - thank you for making so many ordinary moments extraordinary. Dearest Jack, you could put a smile on my face just by walking into the room. Thank you for all our life chats and for keeping me sane (or basically me doing that to you!). To both of you, through all the good and bad times, one thing has been clear: Our laughs? Limitless. Our memories? Countless. Our Friendship? Endless. To my TMT crew, we have been quite the group of friends over the years and I am certain everyone is going to miss our chatter!

The best kind of friendships are the fierce lady friendships where you believe in each other, defend each other and think the other deserves the world. To my closest ladies – Naomi, Tapiwa, Sara, Laura and Lisha, thank you for being the circle of friends who always want to see me win, the ones who always clap and cheer the loudest and for always having my back. Dearest Naomi: you have been the one who has seen me through all my life phases. From the first day of freshers back in undergrad to me finishing my PhD, you have been my personal cheerleader. I will forever cherish those

evenings and weekends treats; London is always better when you are around. Dearest Tapiwa: you are my soul sister, the one who probably knows me better than I know myself and never judges. I cannot thank you enough for all your words of kindness and encouragement, you make me feel like I can achieve anything and friends like that are golden. Those countless hours on the phone are not about to end here though!

To my beloved Family: It is your prayers and your belief in me that carries me through everything I do in my life. Family is really everything. To Bahn Phoppo, Pollay Phoppo and Sobia Aunty: Your support and well wishes are never forgotten. My loveliest Jaji Uncle & Baba: I know you are with me every step of the way. To my two guardian angels, Dadi Ami and Aunty Bhathool, thank you for watching over me.

My most beautiful sisters, Zainab, Hiba & Anam: Thank you for the much-needed distractions and the girly chats. Distance does not mean anything when you have a bond like ours.

To my one and only brother, Ahmad: you perhaps will never truly know how much I looked forward to those morning coffees or those evenings desserts with you. Thank you for always looking out for me and bringing me endless joy and happiness; you really are irreplaceable. Sometimes being a big brother is better than being a superhero, and sometimes being a little sister is better than being a princess.

Dearest Dad, Mum and Billay Phoppo: You hear my pain when everyone else ignores it. You always make me smile when I think I cannot. You listen to my worries and make them yours. You give me a hug when I cannot find my voice. You wipe away the tears that the world makes me weep. You straighten my crown and give me hope and strength. I am the person I am today, because of you. Thank you will never be enough for all the love and support you constantly give me to accomplish my dreams. My success, in everything I do, equally belongs to the three of you.

Finally, to Me: If there ever comes a day in life when you feel like you cannot achieve your goals, look back and remember this period - the darkness and the light. I want you to remember that through hard work and perseverance even the impossible becomes possible. Keep your vision in sight, stand up for yourself, and keep going. You can do it.

Publications

M. H. Sheikh, M. Errede, A. d'Amati, S, McArthur, N.Q. Khan, R. A. Loiola, C. E. O'Riordan, G. S. Purvis, J. Keswich, M. Collino, D. Lucchesi, C. Reutelingsperger, M. Yaqoob, C. Thiemermann, F. Marelli-Berg, D. Virgintino and E. Solito, Impact of metabolic disorders on the structural, functional and immunological integrity of the blood-brain barrier (*In Submission – Nature Communications*).

C. E. O'Riordan, G. S.D. Purvis, D. Collotta, N. Krieg B. Wissu**a, M. H. Sheikh**, G. F. Alves, S. Mohammad, L. Callender, S. M. Coldewey, M. Collino, D. R. Greaves and C. Thiemermann, X-linked immunodeficient mice with no functional Bruton's Tyrosine Kinase are protected from sepsis-induced multiple organ failure, Front. Immunol. (2020), doi:10.3389/fimmu.2020.581758

M. H. Sheikh, S. M. Henson, R. A. Loiola, S. Mercurio, A. Colamatteo, G. T. Maniscalco, V. De Rosa, S. McArthur and E. Solito, Immuno-metabolic impact of the multiple sclerosis patients' sera on endothelial cells of the blood-brain barrier, J. Neuroinflammation (2020), doi:10.1186/s12974-020-01810-8.

A. Colamatteo, E. Maggioli, R. Azevedo Loiola, **M. Hamid Sheikh**, G. Calì, D. Bruzzese, G. T. Maniscalco, D. Centonze, F. Buttari, R. Lanzillo, F. Perna, B. Zuccarelli, M. Mottola, S. Cassano, M. Galgani, E. Solito and V. De Rosa, Reduced Annexin A1 Expression Associates with Disease Severity and Inflammation in Multiple Sclerosis Patients, J. Immunol. (2019), doi:10.4049/jimmunol.1801683.

G. S. D. Purvis, M. Collino, R. A. Loiola, A. Baragetti, F. Chiazza, M. Brovelli, **M. H. Sheikh**, D. Collotta, A. Cento, R. Mastrocola, M. Aragno, J. C. Cutrin, C. Reutelingsperger, L. Grigore, A. L. Catapano, M. M. Yaqoob, G. D. Norata, E. Solito and C. Thiemermann, Identification of Annexina1 as an endogenous regulator of RhoA, and its role in the pathophysiology and experimental therapy of type-2 diabetes, Front. Immunol. (2019), doi:10.3389/fimmu.2019.00571.

E. Zub, G. Canet, R. Garbelli, M. Blaquiere, L. Rossini, C. Pastori, **M. Sheikh**, C. Reutelingsperger, W. Klement, F. de Bock, E. Audinat, L. Givalois, E. Solito and N. Marchi, The GR-ANXA1 pathway is a pathological player and a candidate target in epilepsy, FASEB J. (2019), doi:10.1096/fj.201901596R.

M. H. Sheikh and E. Solito, Annexin A1: Uncovering the many talents of an old proteinInt. J. Mol. Sci. (2018), doi:10.3390/ijms19041045.

Table of Contents

List of Figures

List of Tables

List of Abbreviations

AD	Alzheimer's disease
2-DG	2-deoxyglucose
ABC	ATP-binding cassette
AJs	Adherens junctions
ALS	Amyotrophic lateral sclerosis
AMPs	Anti-microbial peptides
ANXA1	Annexin A1
ApoB	Apolipoprotein B
APOE	Apolipoprotein E
APP	Amyloid precursor protein
AUC	Area under the curve
Aβ	Amyloid beta
Bad	Bcl-2-associated death promoter
BBB	Blood-brain barrier
BCA	Bicinchoninic acid method
BCRP	Breast cancer resistance proteins
BCSFB	Blood-cerebrospinal fluid barrier
bFGF	Basic fibroblast growth factor
BM	Basement membrane
BMECs	Brain microvascular endothelial cells
COX-2	Cyclooxygenase-2
CRP	C-reactive protein
CSF	Cerebrospinal fluid
CVOs	Circumventricular organs
CVD	Cardiovascular disease
DCFDA	Dichlorofluorescin diacetate
DMSO	Dimethyl sulfoxide
EAE	Experimental Autoimmune Encephalomyelitis
ECAR	Extracellular acidification rate
ECM	Extracellular matrix
ETC	Electron transport chain
FAO	Fatty acid oxidation

FBS	Fetal bovine serum
FCCP	Carbonyl cyanide-4 (trifluoromethoxy) phenylhydrazone
FFAs	Free fatty acids
FITC	Fluorescein isothiocyanate
FOXO1	Forkhead box transcription factor 1
Foxp3	Fork head/winged-helix transcription factor 3
FPR2	Formyl peptide receptor 2
GFAP	Glial fibrillary acidic protein
GLUT1	Glucose transporter 1
GPCR	G-protein coupled receptor
HAD	Human immunodeficiency virus-1-associated dementia
HDL	High density lipoprotein
Hepes	hydroxyethyl piperazineethanesulfonic acid
HFHS	High-fat high-sugar
hrANXA1	Human recombinant Annexin A1
i.p.	Intraperitoneal
i.v.	Intravenously
ICAM-1	Intercellular Adhesion Molecule 1
IFN-γ	Interferon-gamma
IKK-β	IκB kinase-β
IL	Interleukin
iNOS	Inducible nitric oxide synthase
IPAD	Intramural Peri-Arterial Drainage
IRS-1	Insulin receptor substrate 1
ISF	Interstitial fluids
ITT	Insulin tolerance test
JAMs	Junctional adhesion molecules
LAT1	L-type neutral amino acid transporter 1
LDL	Low density lipoprotein
MAPK	Mitogen-activated protein kinase
MDR	Multi-drug resistance
MetS	Metabolic Syndrome
MFI	Median intensity of fluorescence

MMPs	Matrix metalloproteinases
MS	Multiple Sclerosis
NF-κB	Nuclear factor kappa-light-chain-enhancer of activated B cells
NK	Natural Killer cells
NO	Nitric oxide
NVU	Neurovascular unit
OCR	Oxygen consumption rate
OGTT	Oral glucose tolerance test
OPCs	Oligodendrocyte precursor cells
OxPhos	Oxidative phosphorylation
PBMCs	Peripheral blood mononuclear cells
PCR	polymerase chain reaction
PD	Parkinson's disease
PDAC	Pancreatic ductal adenocarcinoma
Pe	Permeability coefficient
PFA	Paraformaldehyde
Pgp	P-glycoprotein
PLA_2	phospholipase A_2
pMBMECs	Primary mouse brain microvascular endothelial cells
RAGE	Receptor for advanced glycation end products
RNS	Reactive nitrogen species
RoRγt	Retinoic acid-related orphan receptor gamma t
ROS	Reactive oxygen species
SDS–PAGE	Sodium dodecyl sulphate polyacrylamide gel electrophoresis
SIP	Stock isotonic percoll
SLE	Systemic lupus erythematosus
STZ	Streptozotocin
T1DM	Type I Diabetes Mellitus
T2DM	Type II Diabetes Mellitus
T3DM	Type III Diabetes Mellitus
TACE	TNF-α-converting enzyme
TBI	Traumatic brain injury
TCA	Citric acid cycle

T_{CM}	Central memory T-cells
TEER	Transendothelial electrical resistance
T_{eff}	Effector T-cells
TEM	Transendothelial migration
T_{EM}	Effector memory T-cells
TGF-β	Transforming growth factor-beta
T_H	T-helper cells
TIMPs	Tissue inhibitor of matrix metalloproteinases
TJs	Tight junctions
TLR4	Toll-like receptor 4
TNF-α	Tumour necrosis factor-alpha
Treg	Regulatory T-cells
VaD	Vascular dementia
VBL	Vessel basal lamina
VCAM-1	Vascular cell adhesion protein 1
VEGF	Vascular endothelial growth factor
VLDL	Very low-density lipoprotein
ZO	Zona occludens

Chapter 1 – Introduction

Metabolic syndrome (MetS) is a complex condition characterised by a series of traits including elevated glucose levels, insulin resistance, dyslipidaemia, hypertension and central obesity (1,2), which subsequently results in the development of Type II Diabetes Mellitus (T2DM). Each trait is associated with inducing a low-grade chronic inflammatory state and immune imbalance responsible for exacerbating stress and damage upon cells and tissues. Consequently, the traits of MetS and T2DM are risk factors for heart and circulatory diseases (cardiovascular disease, CVD) encompassing coronary heart disease, atrial fibrillation, heart failure, stroke, and vascular dementia (VaD). CVDs are the leading cause of death worldwide, responsible for 17.9 million deaths in 2016 (3).

Whilst the effect of metabolic disorders on the peripheral system has been greatly investigated, little attention has been provided to investigating the effect of MetS and T2DM on the brain, particularly at the blood-brain barrier (BBB) level. The BBB, formed of specialised endothelial cells, forms a protective barrier to limit the entry of unwanted toxic components into the brain. Studies have found that damage at the BBB level can be responsible for the development of neurological disorders such as Multiple Sclerosis (MS) and cerebrovascular dementia. This is due to alterations of BBB characteristics leading to recruitment of inflammatory cells into the brain, resulting in neurological damage (4). In recent years, research has implicated metabolic disorders to be a risk factor for cognitive decline (5,6) and the development of dementias (7,8). Individuals with T2DM have twice the risk of developing dementia, particularly Alzheimer's disease (AD), compared to those without T2DM (9). The underlying feature of metabolic disorders is insulin resistance. Recent research has discovered abnormalities in the brain which can be linked to insulin resistance ensuing in a course of pathological events similar to AD (10,11). This has therefore let to the concept of insulin resistance of the brain, and has been termed Type III DM (T3DM) (12).

Both T2DM and dementias are progressive long-term conditions largely affecting individuals >65 years old (13). Given that people are living longer and obesity is on the rise due to westernisation (increased intake of energy dense foods high in saturated fats and sugar and decreased physical activity levels) (14) we are facing an epidemic crisis; placing an increasing burden on healthcare systems. The need for preventative

and therapeutic strategies to reduce the development of metabolic disorders and subsequent cardiovascular and neurological diseases has never been greater.

However, investigations are still required to understand the mechanisms by which metabolic disorders lead to T3DM development. In order to achieve this, it is first paramount to understand the effect of metabolic disorders on the BBB at the cellular and molecular level. This will allow for development and investigation of compounds that can help to reduce the progression, restore the damage incurred and combat the development of neurovascular/neurodegenerative disorders. This is the broad aim of this thesis.

1.1 Central Nervous System: the brain & its barriers

The Central Nervous system (CNS) consists of the brain and spinal cord; it is the control centre of the body involved in processing information into motor function (voluntary and involuntary movements), thoughts, perceptions and emotions (15). To allow for optimal neuronal communication and signalling, the surrounding microenvironment (ionic balance, pH & nutrient supply) must be precisely regulated. Homeostatic maintenance of the neural microenvironment is provided by three principal barriers, which are present at the interface between the CNS and the peripheral system (16,17). The three principal barriers are the BBB, the blood-cerebrospinal fluid barrier (BCSFB) and the meninges-arachnoid barrier (Figure 1.1). There is also a fourth barrier, the tanycytic barrier that is present at the circumventricular organs (CVOs) (18,19).

1.1.1 The blood-brain barrier (BBB)

The BBB is present at the interface between blood and the cerebral tissue and is constructed of endothelial cells that form the capillary walls (Figure 1.1a) (20). The BBB has a unique phenotype attributed to the high expression of tight junctions (TJs) and specialised transport mechanisms that provide exceptional protection to the brain from invading pathogens, toxins and immune cells (21). Basement membranes (BMs), pericytes and astrocytes form close associations with the endothelial cells to provide a complex and highly restrictive 3D structure (22). Together with basement membranes (BMs), pericytes, astrocytes, microglia and neurons, these cells form the neurovascular unit (NVU). The highly restricted and regulated structure of the BBB gives rises to its ability to function as a physical, transport and metabolic barrier (22). Further detail of the BBB structure and the cells of the NVU is provided in Section 1.3.

1.1.2 The Blood-Cerebrospinal fluid barrier (BCSFB)

The BCSFB is present within the choroid plexus of the lateral, third and fourth ventricles of the brain (23). The choroid plexus is an epithelial-endothelial convolute that is comprised of a vascularised stroma containing connective tissue and a continuous single layer of cuboidal epithelial cells that are linked together by TJs (24–

26). It should be noted that the epithelium of the choroid plexus is continuous with the ependymal cell layer that lines the ventricular system (24). One of the primary functions of the choroid plexus is to produce the cerebrospinal fluid (CSF) that is secreted into the brain ventricular system (27,28). Microvilli project from these epithelial cells on the CSF-facing surface to increase the surface area to aid in fluid secretion (26). Secondly, the choroid plexus serves as a barrier in the brain separating the blood from the CSF forming the BCSFB. In comparison to the BBB, the capillaries of the BCSFB are fenestrated to allow for the movement of molecules across the endothelial cells through intercellular gaps (29). Instead the barrier function is performed by the choroid plexus epithelial cells that are linked together by TJs (Figure 1.1b) (29). Notably, similar to the BBB, the BCSFB is also lined with polarised transporters for selective transport of ions and solutes into the brain ventricles (16,23). In addition to these vital functions, the choroid plexus also secretes various growth factors that maintain the stem cell pool in the subventricular zone of the lateral ventricle (30).

1.1.2.1 The Cerebrospinal fluid (CSF) and the interstitial fluid (ISF)

The CSF is a clear, colourless fluid which is found in the CNS, intracerebrally within the brain ventricles (20% of CSF volume) or extracerebrally in the subarachnoid space (80% of CSF volume). Within a human, the total volume of CSF is 150mL and within 24 hours approximately 500-600mL is produced therefore the CSF is replaced 3-4 times per day (28,31). The CSF functions to provide mechanical support against the real weight of the brain, to provide protection as a shock absorber or to sudden changes in pressure or temperature and to allow for maintenance of a metabolic equilibrium and homeostatic environment by supply of nutrients and disposal of waste products (32).

The CSF is synthesised via two processes. The large majority ~50-70% of secretion occurs through the epithelial cells of the choroid plexus and the ventricular ependyma, whilst the remainder is produced by ultrafiltration of blood plasma through choroidal capillaries (33). The CSF is secreted across the choroid plexus into the brain ventricles. The ventricles of the brain are interconnected cisterns and thus the CSF circulates from the lateral ventricles through the foramina of Monro into the third ventricle and further through the aqueduct of Sylvius to the fourth ventricle. From the fourth ventricle, part

of the CSF flow into the central canal of the spinal cord whilst the rest flows into the subarachnoid space by the foramina of Luschka and Magendie (32,33). In the subarachnoid space, the CSF is separated from the outer surface of the brain by the pia matter. Resorption of the CSF takes place by the arachnoid granulations and the arachnoid villi, these are protrusions of the arachnoid through the dura mater that project further into the intracranial venous sinuses to allow flow of CSF back into the blood circulation (34). In some pathological conditions, the increase in intracranial pressure can force the CSF into the extracellular space of the periventricular white matter (35).

Whilst the CSF fills the ventricles and the subarachnoid space, the remainder of the brain extracellular fluid is the brain interstitial fluid (ISF) (36,37). The brain ISF, similar to the CSF, also functions to cushion and support the cells of the NVU. Within the brain, the ISF occupies the brain interstitial system (ISS); an irregular and tortuous space among neural cells and capillaries (38,39). Of the total brain volume, the brain ISS occupies 15-20% and it contains both ISF and the extracellular matrix (ECM) (39,40). The brain ISF is a water solvent that contains ions, gaseous and organic molecules including proteins, peptides, enzymes and extracellular vesicles. The ISF surrounds neural cells to provide a supply of nutrients. There is extensive communication between the CSF and ISF and hence the CSF is considered a reservoir for the ISF and the site of removal of waste products from the brain ISF (39,41), discussed later in Section 1.3.5.

1.1.3 The meninges-arachnoid barrier

The meninges consist of three layers: the dura mater (pachymeninx) which is an outer fibrous sheet adjacent to the skull, the arachnoid mater and the pia mater (together referred to as the leptomeninges) which lay under the dura mater and just above the brain and spinal cord parenchyma (42,43). The dura mater is a tough, collagenous membrane, it is highly vascularised and contains the lymphatics (44,45). In comparison to the dura mater, the leptomeninges are relatively thin (42,43). The arachnoid mater is formed of several layers of epithelial cells that have tight junctions to strictly regulate movement of molecules, similar to the BBB. The regulation by this meningeal membrane confers the meninges-arachnoid barrier (Figure 1.1c) (16,21). Underneath the arachnoid mater lies the subarachnoid space through which the CSF,

produced by the choroid plexus epithelium, flows. The last meningeal membrane, the pia mater covers the brain and spinal cord parenchyma and is semi-permeable to the CSF (42,43,46).

The meninges serve to protect the brain and spinal cord from trauma, support blood vessels and form a continuous cavity to allow for the flow of the CSF through the arachnoid and pia mater (42,43). The purpose of the meninges-arachnoid barrier is to completely enclose the brain and the CNS from the rest of the body (21), to prevent the mixing of peripheral ISF with brain ISF and CSF (47).

1.1.4 The Tanycytic barrier

The brain regions located around the brain ventricles are named the CVOs; three sensory and four secretory CVOs have been identified. The sensory CVOs include the subfornical organ, organum vasculosum of the lamina terminalis, and area postrema; the cells located here monitor blood and CSF-derived information (48). The secretory CVOs consist of the neurohypophysis, median eminence, and pineal gland that release brain-derived hormones into the blood circulation (48). Together the CVOs help to maintain homeostasis; allowing for a two-way exchange of metabolic information (49) thus the CVOs also form an interface between the blood - brain (50), giving rise to another barrier between the blood - CSF called the tanycytic barrier (18,19).

The CVOs have distinct features such as fenestrated capillaries, lack of tight junctional complexes, enlarged perivascular spaces and highly specialised ependymal cells called tanycytes (18,51). However, observations of the tanycytes have revealed these cells to express TJ proteins in comparison to the fenestrated endothelial cells present at the CVOs (19,52,53); suggesting a shift of the barrier from the vascular to the ventricular side (18). This shift of the barrier allows for diffusion of blood-borne materials through the permeable vasculature into the parenchyma of the CVO and from here the tanycyte TJs control their diffusion into the CSF (19,49). Thus, the tanycytic barrier forms a barrier between the blood-CSF at the CVOs. Tanycytes were initially identified at the median eminence (19) but have since found to be a characteristic feature of all of the CVOs (18).

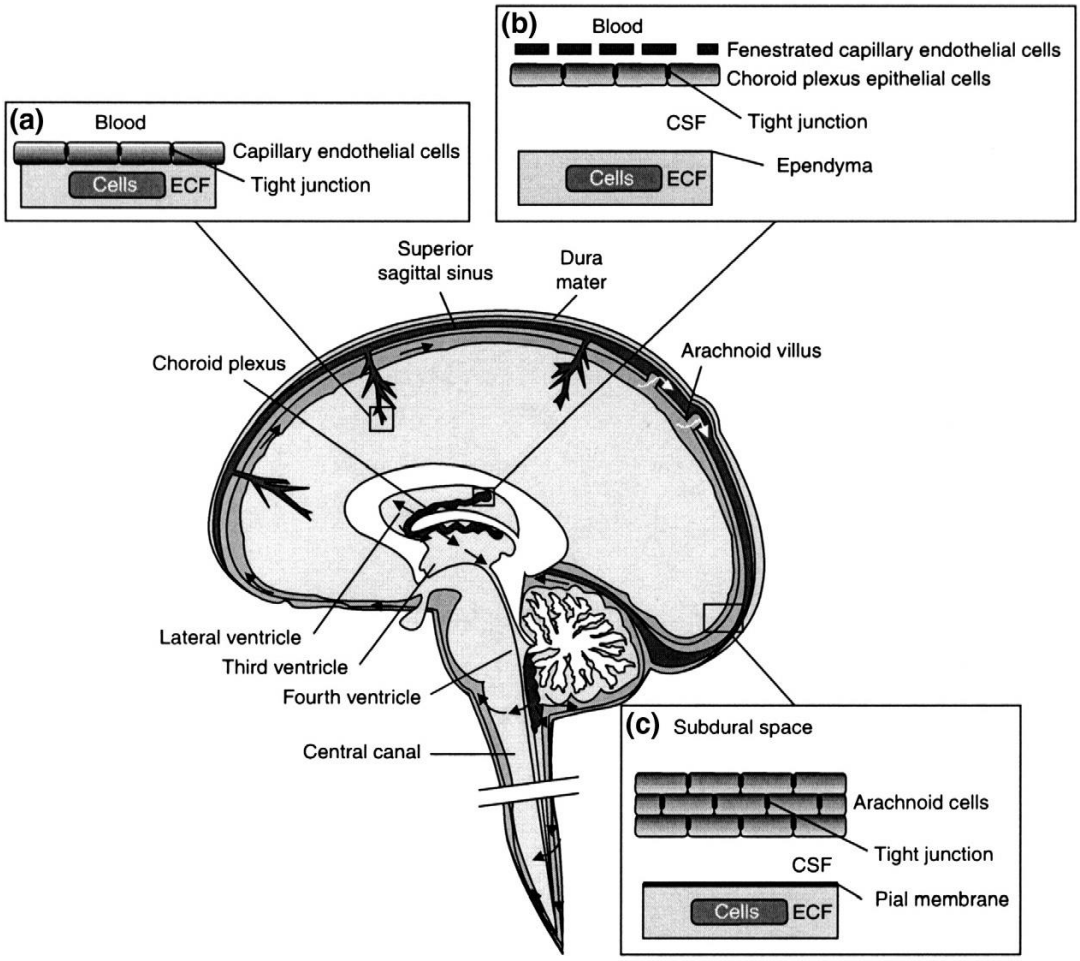

Figure 1.1 | The three barriers of the brain

a) A BBB is present in all organisms with a well-developed CNS. It is formed of capillary endothelial cells held together by tight junctions, creating the largest surface area for exchange between the blood and brain. In the average human adult the surface area of the BBB is approximately 12-18m^2 (54) b) The endothelial cells of the choroid plexus are fenetestrated instead the BCSFB is formed by the epithelial cells of the choroid plexus present at the lateral, third and fourth ventricles of the brain that are held together by tight junctions; the CSF is secreted across this barrier into the brain ventricular system. The remainder of the brain is surrounded in ISF. c) The epithelial cells of the arachnoid membrane, which lies under the *dura mater*, encloses the brain and the CNS from the peripheral system. The meninges-arachnoid barrier is formed of several layers of epithelial cells creating an effective barrier that is avascular in nature and has a small surface area to prevent exchange between the blood and the CNS. CSF drains out of the brain via arachnoid villi that project into the sagittal sinus. Figure taken from Abbott et al., 2009 (16)**.**

1.2 The brain vasculature system

The brain is one the most perfused organs in the body. The arterial supply to the brain consists of two pairs of large arteries - the right and left internal carotid arteries and the right and left vertebral arteries. The carotid arteries run along the front of the neck to supply the cerebrum whereas the vertebral arteries run along the back, coming together to form the basilar artery to supply the cerebellum and the brain stem. At the base of the brain, the carotid and basilar arteries join to form an anastomotic ring known as the circle of Willis. The circle of Willis gives rise to three further main arteries - the anterior, middle, and posterior cerebral arteries. Each of these divides progressively into smaller arteries and arterioles that run along the surface of the brain, providing blood supply to all regions of the brain (55,56). Figure 1.2 shows the major arteries of the brain.

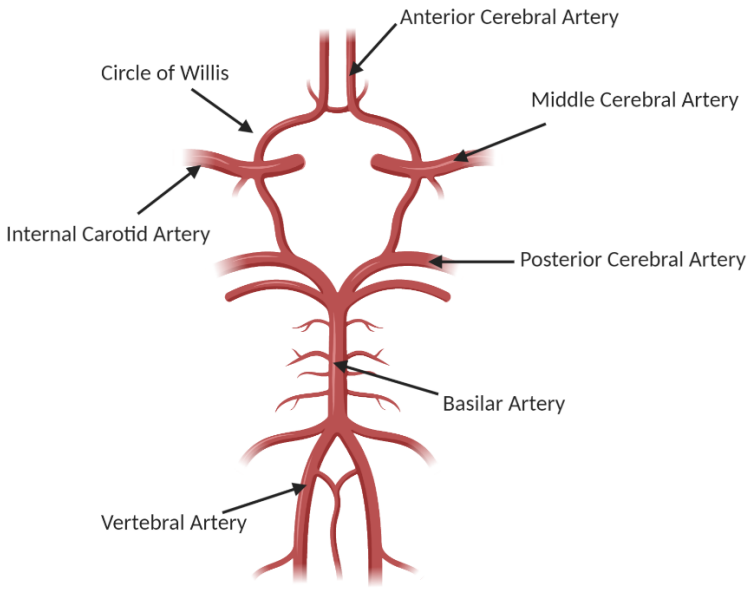

Figure 1.2 | The main arterial supply to the brain

The main arterial supply to the brain is provided by two pairs of arteries – the right and left carotid and the right and left vertebral artery. The right and left vertebral artery come together to from the basilar artery. Where the basilar and carotid arteries join, at the base of the brain, an anastomotic ring is formed known as the circle of Willis. The circle of Willis gives rise to three cerebral arteries - anterior, middle, and posterior, to supply the brain (55,56).

Arteries enter the brain into two ways; either by running parallel to the surface of the cerebral cortex as pial arteries or perpendicularly to the surface of the brain resulting in a V-shaped depression in the pia mater (43,57). Parallel pial arteries are surrounded by a single layer of pia; pial cells can be identified by the presence of intercellular gap junctions and diffuse BMs (43,57). The arteries which enter the brain parenchyma perpendicular to the surface also carry a single-layered sheath of pial cells. Unlike arteries in the periphery, there are no true perivascular (Virchow-Robin) spaces around the arteries in human cerebral cortex (43,58,59). Instead the perivascular compartment of the arteries in the cerebral cortex consists of compacted layers of smooth muscle cells, endothelial cell BM and pia that associate closely with the BM of astrocyte end-feet (43,58). Mouse brains show a similar arrangement of arteries (60). Importantly, whilst there are no perivascular spaces in the arteries of the cerebral cortex, perivascular spaces do exist in the arteries of the cerebral white matter, basal ganglia and midbrain (61,62); with the capacity to dilate due to the presence of two leptomeningeal layers in these regions versus the one layer of leptomeninges that surrounds the arteries in the cerebral cortex (43,58,63). The layers of leptomeningeal cells facilitate the entry of CSF into the CNS tissue (60). Additionally, the BMs of the arteries and capillaries are also routes for the flow of fluid and solutes into and out of the brain (60,64) and is termed the Intramural Peri-Arterial Drainage (IPAD) pathway; IPAD has been discussed in Section 1.3.5.

As the arteries narrow deeper into the brain parenchyma they transition into parenchymal arterioles which branch off into capillaries to supply the cells of the NVU (56,65). The pial and penetrating arteries are covered by vascular smooth muscles cells which remain separated from brain tissue by the parenchymal BM. The descending parenchymal arterioles and capillaries on the other hand, become associated with astrocytes and inter-neurons (66). The parenchymal arterioles are covered with a single layer of smooth muscle cells whereas the capillaries are formed of endothelial cells supported by BMs, pericytes and astrocytes (56,66) (described in section 1.2.4). The structure of the capillaries gives rise to the BBB (67–71). Figure 1.3 shows the transition from pial arteries through to capillaries.

From the cerebral capillaries, the blood continues into the post-capillary venules where perivenous spaces exist and fill with CSF. There are two groups of valve-less veins which allow for the drainage of venous blood from the cerebral hemispheres. One group is the superficial cortical veins, which are located in the pia mater and drain the cerebral cortex and white matter. The second group is the deep or central veins that drain the brain's interior including the deep white and grey matter that surrounds the lateral and third ventricles. These veins drain into the superior sagittal sinus, and venous outflow is directed via a confluence of sinuses towards the sigmoid sinuses and jugular veins (68).

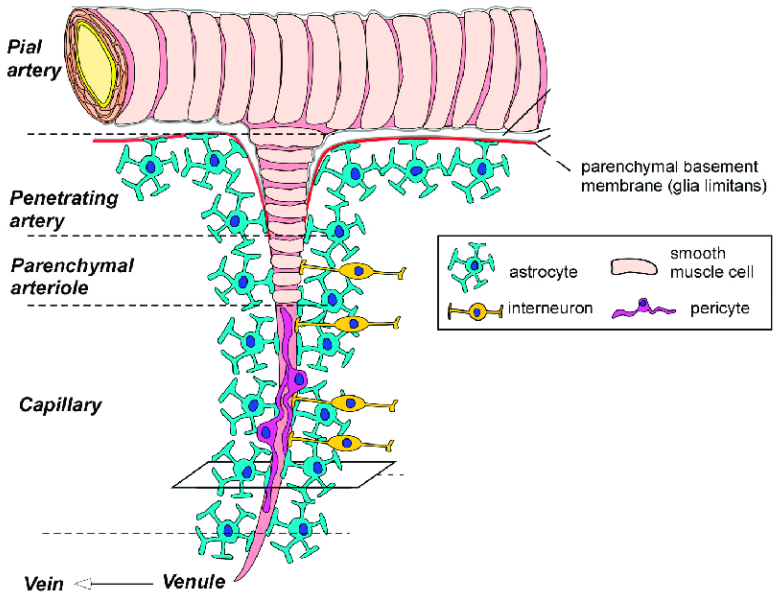

Figure 1.3 | Arteries to capillaries in the brain

The pial arteries are present on the surface of the brain in contact with the pia. Branching arteries penetrating into the brain tissue are termed penetrating arteries. As these penetrating arterioles narrow deeper into the brain parenchyma they transition into parenchymal arterioles which branch off into capillaries to supply the cells of the NVU. The descending parenchymal arterioles and capillaries are associated with astrocytes and neurons. The transition between the two can be seen through smooth muscle cell cover, provided at the parenchymal arteries. Whereas the capillaries are formed of endothelial cells supported by basement membranes, pericytes, astrocytes and neurons, to give rise to the BBB. From the cerebral capillaries, the blood continues into the post-capillary venules, which drain into the major veins to be carried away from the brain. Figure taken from Yamazaki et al., 2017 (69).

1.2.1 Cerebral blood flow

As an organ, the brain has the highest energy-density demands of all of the organs, utilising 20% of the body's resting metabolic rate (72). Interestingly, the high metabolic demand of the brain is not matched by the presence of larger intrinsic energy stores within the cells of the NVU. Instead the brain relies on a continuous supply of substrates from the peripheral vasculature (73). Consequently, the cerebral blood flow (CBF) is critical to ensure proper delivery of oxygen and nutrients and subsequent removal of waste products of metabolism (74). The CBF is maintained by the coordinated action of the arteries, capillaries and veins, which form a 400-mile long vascular network within the brain (75). Changes in blood flow i.e. hypoperfusion (insufficient CBF) and hyperperfusion (excessive CBF) can cause ischemic injury or BBB breakdown resulting in seizures, encephalopathy and ischemic or haemorrhagic strokes.

In order to maintain regional CBF, the brain has unique mechanisms known as functional hyperaemia (increase in CBF occurring in response to brain activity) or neurovascular coupling (dynamic functional change in CBF in response to local neuronal activity) (76,77). These mechanisms allows for rapid upregulation in CBF in activated brain regions. All of the cells within the NVU contribute to neurovascular coupling, however the vascular smooth muscle cells are responsible for the contractile properties of the vessel to control diameter and blood flow (75–78). Therefore, the flow through the capillaries is regulated by the contraction or dilation of vascular smooth muscle cells at either the arterial or venous ends resulting in changes in blood flow ranging from 0.3mm/s to 3.2mm/s (79,80). There are number of modulators which can contribute to the alterations in the vascular tone and thus alter CBF. For example, nitric oxide (NO) produced by neurons acts on vascular smooth muscle cells leading to hyperpolarisation and relaxation (76,81). The release of ATP or adenosine by neurons can cause vascular smooth muscle constriction when bound to purinergic receptors P2X and P27 (82,83) or relaxation when bound adenosine A_{2A} receptors (78,84). Other modulators include arachidonic acid metabolic products including epoxyeicosatetraenoic acids, prostaglandin E2via and cyclooxygenase 1 (81,85,86).

Impaired myogenic autoregulation, endothelial dysfunction and neurovascular uncoupling, can result in a mismatch between CBF, oxygen/nutrient delivery and neuronal activity. This disruption in functional connectivity, as a consequence of

vascular conditions and aging, is often seen in early stages of a number of neurological disorders including AD, stroke and Amyotrophic lateral sclerosis (ALS) and initiates the neurodegenerative process (75–77,87).

1.3 The BBB: structure & function

The BBB is the defining feature of the brain vasculature, limiting the contact of peripheral blood and peripheral blood-borne materials with the brain. In order for the BBB to provide a specialised protective function, the endothelial cells of the BBB are distinctly different in structure from all other endothelial cells in the body (88). Firstly, the brain microvascular endothelial cells (BMECs) have an absence of fenestrations, which correlates with a high expression of TJs. Secondly there is little pinocytosis and paracellular diffusion of hydrophilic compounds; as a result a number of membrane receptors and transporters are present on both the luminal and abluminal sides of the BMECs (20,89). Due to the high metabolic demands of the BMECs to conduct their cellular activities, they are lined with a high number of mitochondria (22,90).

1.3.1 Physical barrier

The extreme tightness of the BBB, which limits the diffusion of the majority of macromolecules, can be attributed to the presence of TJs and adherens junction (AJs) that provide cell-cell adhesion contacts. The TJs help to form a continuous blood vessel with high electrical resistance in the range of 1500-2000 $\Omega.cm^2$ giving rise to low paracellular permeability and high transendothelial electrical resistance (TEER) (91,92). The role of the AJs on the other hand is to initiate, mature and maintain cell-cell contacts (93). Within epithelial cells, including the choroid plexus epithelium, TJs are the most apical component of the junctional complexes and can clearly be distinguished from the AJs however, in the endothelial cells, particularly those of the BBB, the complexes appear intermingled (94–97).

1.3.1.1 Tight junctions

TJs are composed of three major transmembrane proteins – occludins, claudins and junctional adhesion molecules (JAMs) connected to a series of cytoplasmic proteins such as zona-occludens (ZO)-1, ZO-2, ZO-3 and regulatory proteins such as cingulin (Figure 1.4). In the brain, claudins-3, -5 and -12 have been identified; these bind homotypically to claudins present on adjacent cells thereby forming the TJ seal (98). The 65-kDa occludin protein has a much higher expression in brain endothelium compared to endothelial barriers in non-neuronal tissues, hence it is key in regulating the paracellular permeability through association with ZO proteins (99). All of the junctional proteins form a multi-complex junction that links to cytoskeleton component actin. Together this maintains the structural and functional integrity of the brain endothelium (100–102).

1.3.1.2 Adherens junctions

The AJs are intermingled with the TJs in the basolateral membrane of BMECs (Figure 1.4); these AJs help to form a continuous adhesion belt (103). The major transmembrane protein of AJs is Ca^{2+}-regulated VE-cadherin, which is linked to scaffolding proteins α-, β-, γ- and p120 catenin that couple the entirety of the complex to the actin cytoskeleton (104,105). Proteins of the AJs and TJs are known to interact (97), for example VE-cadherin engagement through Akt activation and inhibition of β-catenin nuclear translocation, causes phosphorylation of the transcription factor forkhead box factor 1 (FOX1). FOXO1 induces the transcription of TJ protein claudin-5 (106). Hence AJs are essential in establishment and maintenance of the endothelial cell-cell contact.

1.3.1.3 The cytoskeleton

The inter-endothelial junctional integrity is provided by the cytoskeleton, consisting of actin microfilaments, intermediate filaments and microtubules (107). There are two different conformations of actin filaments; globular monomers of G-actin that upon polymerisation form helical structures, or asymmetrical filaments of F-actin which come together to form contractile bundles. The actin cytoskeleton is essential in providing a tension force to BMECs that allows them to retain their shape, driven by the interaction of actin with myosin to form stress-fibres. The polymerisation of actin

fibres is widely recognised to alter the structure of cells; this is important for normal cellular physiological tasks such as cell cytokinesis or endo- and exocytosis (108–111). Intermediate filaments are 10nm in diameter and are responsible for providing tensile strength, the major intermediate filament is vimentin which links to VE-cadherin (112). Microtubules consist of polymers of α- & β- tubulin involved in the rapid assembly of actin filaments and focal adhesions, cellular contraction and increased transendothelial migration (113,114).

1.3.1.4 Cell polarity

TJs and AJs play an important role in providing cell polarity in order to separate the apical and the basolateral sides of endothelial cells, this polarity is more pronounced in the BBB compared to all other endothelial barriers (115). The lipid and glycoprotein composition at plasma membranes is an important mediator of cellular polarity (116,117). They aide in the distribution and localisation of transporters which are essential for movement of nutrients and ions to meet the metabolic demand of the brain. Polarisation is also crucial for the response to stimuli such as cytokines and growth factors e.g. VEGF or histamine, as these factors increase BBB permeability when administered at the basolateral membrane but not at the apical membrane (49). Overall, this cellular polarity ensures active regulation of the internal milieu of the brain.

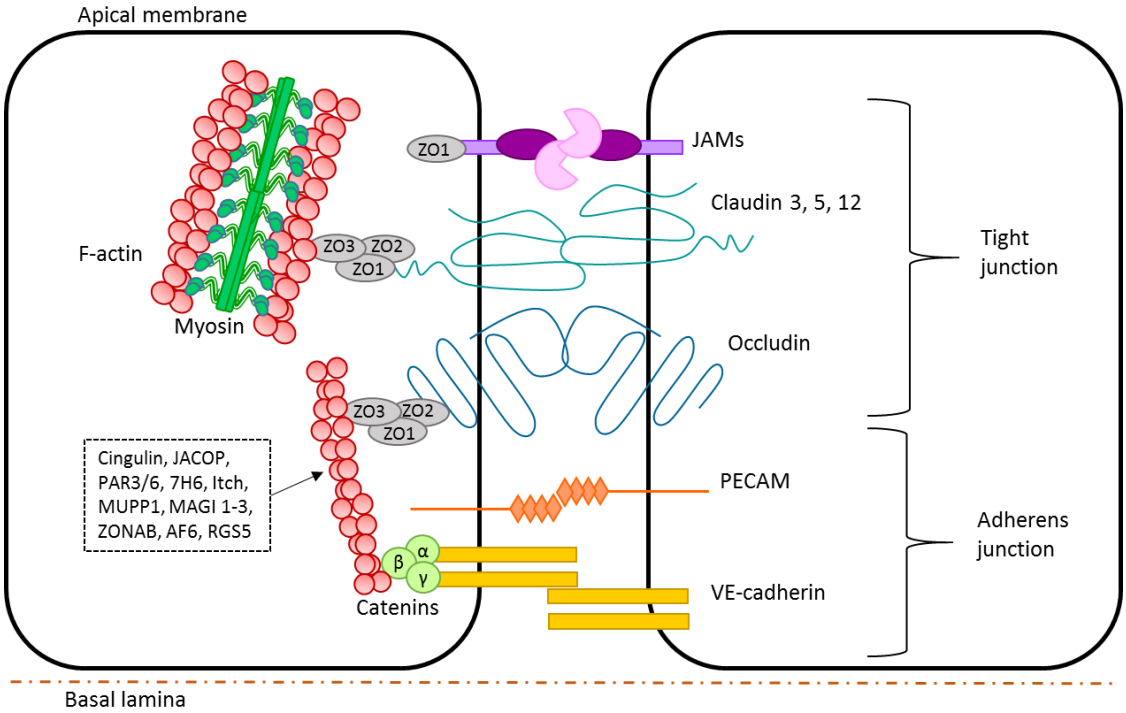

Figure 1.4 | Molecular composition of BBB endothelial tight junctions

Cell-cell adhesion in the BBB is provided by the presence of tight junctions (TJs) and adherens junctions (AJs), allowing the formation of a continuous vessel. The TJs are composed of occludins, claudins and junctional adhesion molecules (JAMs) A, B & C connected to a series of scaffolding proteins zona-occludens (ZO)-1, ZO-2 & ZO-3, TJ-associated protein 7H6 and Itch (E3 ubiquitin protein ligase). The AJs sit below the TJs; the major component is VE-cadherin linked to scaffolding proteins α-, β-, γ- and p120 catenin. The platelet–endothelial cell adhesion molecule (PECAM) is also part of the AJs and is involved in mediating homophilic adhesion. The scaffolding proteins connect with the actin-myosin cytoskeleton to retain the cellular shape through interaction with cingulin and junction-associated coiled-coil protein (JACOP). A series of secondary adaptor proteins including membrane-associated guanylate kinase with inverted orientation of protein–protein interaction domains (MAGI 1-3), partitioning defective proteins (PAR3/6) and multi-PDZ-protein 1 (MUPP1) help to organise regulatory and signalling molecules such as the regulator of G-protein signalling 5 (RGS5), afadin (AF6), and the transcription regulator ZO-1-associated nucleic acid-binding protein (ZONAB) (16,21).

1.3.2 Transport barrier

Molecules can pass across endothelial cells using a paracellular (between adjacent cells) or transcellular (through the cell) route (89). Due to the restrictive nature of the BBB provided by the junctional complexes, the paracellular pathway is largely occluded. Whilst small non-polar molecules such as oxygen and carbon dioxide and lipophilic molecules such as ethanol can freely diffuse across the BBB, larger hydrophilic molecules require facilitated diffusion in the form of transporters, channels or carriers outlined in Figure 1.5 (114). The brain has a high energy consumption therefore the transport of nutrients such as glucose and amino acids are necessary for metabolism. Consequently the brain is enriched with glucose transporter-1 (GLUT1) (20) and the L-type neutral amino acid transporter-1 (LAT1) (119,120). The BBB also contains several ATP-binding cassette (ABC) transporters required for the efflux of molecules from the brain into the bloodstream to clear waste products and prevent the entry of neurotoxic or xenobiotic compounds. The major ABC transporters present in the brain are p-glycoprotein (Pgp), multi-drug resistance (MDR) proteins 1-6 and breast cancer resistance protein (BCRP) (121–125). Cellular polarity is a major determinant on the localisation of all transporters to the luminal or abluminal plasma membranes. The BBB endothelium also possesses a number of ion channels, required for ionic balance, transport and secretion of signalling molecules including Ca^{2+}, nitric oxide (NO) and von Willebrand factor (103). On the other hand, the transcellular pathway involves receptor-mediated shuttling largely used by hormones and adipokines or by leukocytes. Notably leukocytes are also capable of diapedesis through TJs via the paracellular pathway (126).

1.3.2.1 Transport of glucose and insulin across the BBB

The focus of this thesis is to examine the impact of T2DM on the BBB. In T2DM, the role of glucose and insulin in the peripheral system is of paramount of importance, with hyperglycaemia and hyperinsulinaemia resulting in T2DM progression as discussed later, in Section 1.5. The brain is very metabolically active and utilises glucose as its primarily fuel to generate energy (127,128). As a result, the transport of glucose and insulin across the BBB are of paramount importance.

To date, 14 different GLUTs have been identified with GLUT-1, -2, -4 and -4 being the most well characterised. Brain endothelial cells express GLUT-1 on both the apical and basolateral membranes, astrocytes express GLUT-1 and GLUT-3, microglia express GLUT-5 and neurons express isoforms GLUT-3 and GLUT-4 (129–132).

Within the peripheral system, insulin is a major regulator of blood glucose levels through stimulating uptake of glucose by liver, muscle and adipose tissue (133). Insulin is produced within the beta-cells in the islets of Langerhans of the pancreas and is immediately released from granular stores upon raises in blood glucose. Released insulin acts on insulin specific receptors which signal via intercellular insulin receptor substrate-1 (IRS-1). Under basal conditions, the IRS-1 complex is rendered inactive through phosphorylation on serine-307. However, upon hyperglycaemic conditions, insulin binding to the insulin receptor allows for phosphorylation of typrosine-608/638 instead, thereby allowing signal transduction through phosphoinositide 3-kinase (PI3K)/protein kinase B (Akt) (134). This signalling cascade initiated by insulin binding to its receptor facilitates the translocation of glucose transporters to cell membranes (135). Insulin crosses the BBB by a saturable transport mechanism (133).

Interestingly, glucose transport in the brain is largely insulin-independent with GLUT-1 and GLUT-3 not requiring insulin to regulate glucose uptake (136). However, GLUT-4 present on neurons does require insulin-mediated glucose uptake (136) for neuronal growth, plasticity or neurotransmitters release (137) and thus insulin plays a key role in learning, memory and cognition. It has been reported that the highest concentration of insulin receptors are found in olfactory bulb, cerebral cortex, hypothalamus, hippocampus, and cerebellum; regions associated with learning and memory (138–140).

Aside from cognition, insulin affects feeding behaviour (141). In contrast to the effects of peripheral insulin, CNS insulin increases blood glucose levels and decreases feeding and body weight (142–144). Other effects of insulin at the BBB include enhanced transport of amino acids tyrosine and tryptophan, increased transport of adipokine leptin (141) and enhanced expression and function of Pgp (145).

1.3.3 Metabolic barrier

Isolated human brain microvessels reveal the BBB to contain a number of drug transporters and drug metabolising enzymes (146) responsible for restricting entry of neurotoxic drugs and eliminating foreign compounds from the CNS (Figure 1.5). In the human BBB, phase I enzymes such as cytochrome P450 and phase II enzymes such as UDP-glucuronosyltransferase and glutathione S-transferase have been identified; this strongly impacts the ability of pharmacological agents to target CNS diseases (147). The function of these transporters is effected during disease such as AD resulting in enhanced exposure of the brain to neurotoxic molecules such as β-amyloid thereby augmenting neurodegeneration (8,148).

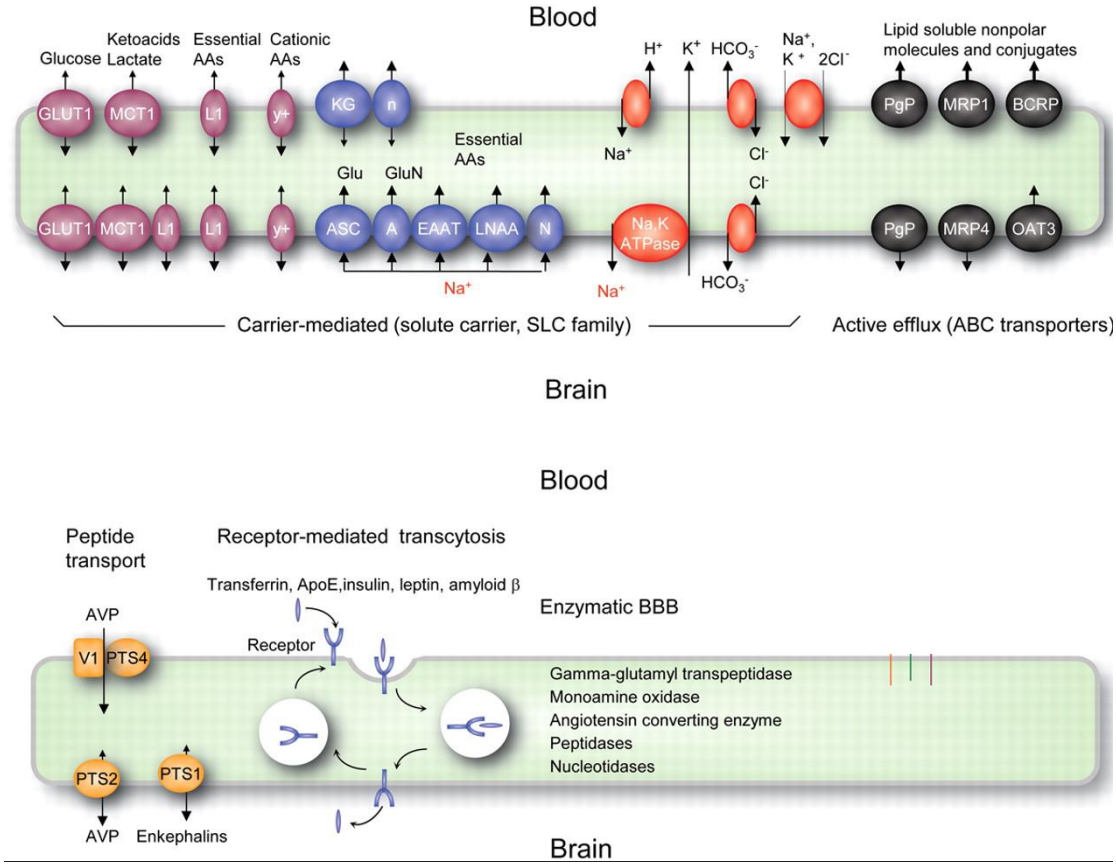

Figure 1.5 | The transport mechanisms present at the BBB

As the BBB provides a restricted environment for the free movement of molecules a number of transport mechanisms must be present to facilitate entry of enzymes, metabolites and leukocytes. These transporters have polarised distribution on either the luminal or abluminal surfaces of the BBB endothelium. The BBB is lined with a number of solute carrier (SLC) transporters e.g. GLUT1, ion channel pumps to allow entry of metabolites required for ATP generation, along with Na^+-dependent amino acid and organic acid transporters. In addition, there are specific transporters for neuroactive peptides such as arginine-vasopressin (AVP). The movement of larger molecules e.g. insulin, transferrin, leptin, β-amyloid is facilitated by receptor-mediated transcytosis. Additional protection of the brain is provided by the presence of active efflux ABC transporters (Pgp, MDR1, BCRP) which are involved in pumping toxic compounds out of the brain. Enzymes are also present at the BBB to metabolise any foreign material. Figure adapted from Bennaroch, 2012 (149).

1.3.4 The NVU

Beyond the BMECs, other components and cells of the NVU also contribute to the maintenance and functionality of the BBB. The structure of the NVU is shown in Figure 1.6.

1.3.4.1 Basement membranes and the glycocalyx

The basal lamina is an ECM that is produced by both endothelial cells and the surrounding astrocytes to form BMs (150). The different cells are responsible for producing different laminin isoforms, with laminin α4 and α5 being derived from BMECs and laminin α1 and α2 being derived from astrocytes (151,152). The BMs are also composed of various types of collagen, glycoproteins and proteoglycans that are termed the glycocalyx (153). The attachment of the endothelial BM to endothelial cells is mediated via α-dystroglycan whereas the parenchymal BM attachment to astrocytic end-feet is mediated by β-dystroglycan (154). The combination of the parenchymal BM and astrocyte foot processes is termed the glia limitans (4). The glia limitans covers the entire surface of the brain and spinal cord on the external face towards the subarachnoid space and is termed the glia limitans *superficialis* whereas the glia limits that surrounds the vessels is called the glia limitans *perivascularis* (155). Between the endothelial BM and the glia limitans, there is a collagen IV-containing middle layer, called the perivascular space (155). In the capillaries, the BMs fuse together to form a gliovascular membrane that closes the perivascular space (156).

The endothelial glycocalyx, present on the luminal side (157), is involved in regulating vascular permeability through transmission of physical forces, induced by fluid shear stress, to the cytoskeleton of endothelial cells (158,159). The extracellular matrix (ECM) of the BBB also contains a number of matrix metalloproteinases (MMPs) and their inhibitors, tissue inhibitor of metalloproteinases (TIMPs) which are involved in the dynamic regulation of the BBB (160).

1.3.4.2 Pericytes

Pericytes are in close contact with endothelial cells to provide a variety of supportive roles. This includes development and maturation of endothelial cells and assistance in the metabolic performance of myocytes. The latter helps in the pericyte-aided control of capillary diameter and modulation of blood flow in response to neuronal activity (161–163). In addition, pericytes secrete growth factors and adhesion molecules as well as assisting with angiogenesis and phagocytosis at the BBB (162,163).

1.3.4.3 Glial cells – astrocytes, microglia and oligodendrocytes

The maintenance of a number of BBB properties, including the formation of TJs and polarised expression of transporters relies on the close association of astrocytes with the BMECs (164). From an anatomical point of view, neurovascular communication takes place through the astrocyte end-foot, which is an extension of the astrocytes that encase the endothelial cells and pericytes (165). The astrocyte foot processes provide an additional layer of structural support and defence at the BBB. The astrocytes can also produce and release substances such as prostaglandins, neurotrophic factor, angiopoietin-1 or NO, that contribute to BBB integrity and vascular tone (166).
Astrocytes also provide simultaneous support to neurons; making them one of the most diverse cells in the brain (167). Astrocytes are involved in the regulation and maintenance of neuronal synapses through provision of metabolic support, neurotransmitter precursors and ion buffering via specialised gap junctions or direct contact (168,169). The close association of astrocytes to neurons allows for neuronal mediators to affect vessel dynamics and BBB integrity (170).

Astrocytes are a type of glial cell, the other glial cells in the brain parenchyma include the microglia and oligodendrocytes. Microglia are the resident macrophage of the brain and form the first line of immune defence in the brain (171). In a healthy state, microglia are involved in surveillance of the CNS, with motile processes that constantly monitor the extracellular space (172). Upon activation, microglia become activate, proliferate and migrate to the site of injury or inflammation to phagocytose bacteria, degenerating cells and neurons to help clear the damage (173). However, activated microglia can also release cytokines, chemokines, interleukins and other

inflammatory molecules which can contribute to the initiation of a neuroinflammatory response (171,173). The activation and role of astrocytes and microglia in neuroinflammation has been discussed in Section 1.7.

With regard to the maintenance of the BBB, early migration of macrophages to capillary walls in response to CCL5 release by brain endothelial cells has been observed and this results in TJ formation by microglia cells with endothelial cells through expression of claudin-5 (174). This additional support helps to maintain BBB integrity; indeed, ablation of microglia or blockage of CCL5 signalling early on in inflammation increases BBB permeability (174). Sustained inflammation causes microglia transformation to a phagocytic phenotype with the ability to release pro-inflammatory mediators and thus contribute adversely to BBB damage (174,175).

Oligodendrocytes are smaller and have fewer branches than astrocytes (176). The most well documented function of oligodendrocytes is myelin formation to produce the myelin sheath that insulates neuronal axons for the transmission and propagation of action potentials for signal conduction (177). In addition, oligodendrocytes surround cerebral blood vessels and help to maintain BBB permeability (178–181). This is via trophic communication between oligodendrocyte precursor cells (OPCs) and brain endothelial cells (182). Endothelial cells provide fibroblast growth factor-2, brain-derived neurotrophic factor and vascular endothelial growth factor (VEGF) for proliferation, survival and migration of OPCs (182,183). In turn, OPCs secrete transforming growth factor β (TGF-β) for maintenance of BBB integrity via the MEK/ERK signalling pathway which increases the expression of TJ proteins (184). Interestingly, oligodendrocytes can also contribute negatively to BBB permeability through the production of ECM degradation proteins, the matrix metalloproteinases (MMPs) (185,186). MMPs are expressed by OPCs and are required for the maturation into oligodendrocytes and sensitivity to growth factors (185,186). However, MMPs increase BBB permeability through degradation of junctional proteins and the BMs and can also contribute to neuroinflammation-induced neurotoxicity (187).

1.3.4.4 Neurons

Neurons are the pacemakers of the NVU (188). With the ability to detect small variation in nutrient or oxygen supply, they can influence the vessel dynamics and BBB integrity through the release of electrical or chemical messengers via astrocytes (170). Neuronal functioning is necessary for the co-ordination of sensory and motor function. Therefore the precise regulation of the microenvironment is essential for signalling (168). The cells and components of the NVU come together to ensure that the properties of the BBB are maintained for optimal brain functioning (189).

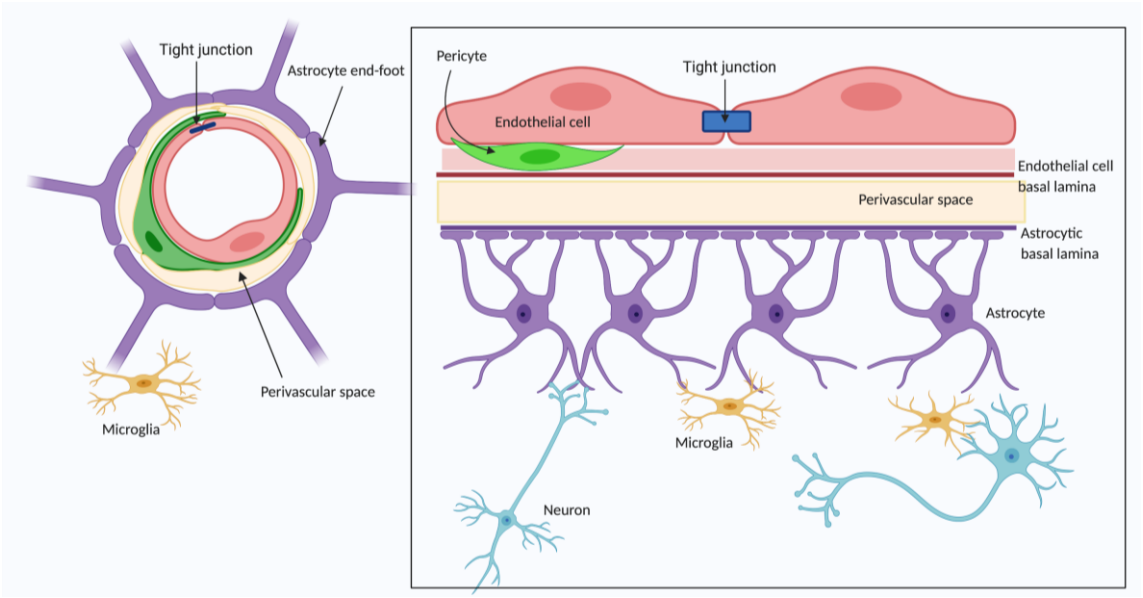

Figure 1.6 | Structural diagram of the neurovascular unit (NVU)

The NVU is made up of endothelial cells, basement membranes, pericytes (smooth muscle cells), astrocytes, neurons, and microglia. Collectively, the NVU is responsible for maintaining the homeostasis of the brain microenvironment to allow for optimal CNS functioning. The cells of the NVU come together to form the blood-brain barrier (BBB), which acts as a protective barrier against potentially cytotoxic agents. As a result, brain capillaries have a very distinct structure from general capillaries in the peripheral system. Tight junctions between cerebral endothelial cells form a very restrictive seal to block free movement of solutes. Instead, a number of transporters localise to the luminal and abluminal sides of the cerebral endothelial cells to ensure the delivery of nutrients to meet brain metabolic demand. Further support in regulating permeability and cerebral blood flow is provided by the close association of pericytes. Astrocytes encase the endothelial cells of the BBB via end-foot processes, to provide an additional layer of protection, assist in biochemical maintenance and allow for transduction of signals to neurons. Astrocytes and neurons form close associations through transmission of metabolites and neurotransmitters, which can control vessel dynamics and BBB integrity. Endothelial cells and astrocytes both also secrete laminins to form two distinct basement membranes, which are composed of collagen IV, laminins, fibronectins, proteoglycans, and glycoproteins to add additional layers of support, protection and BBB maintenance. All together these layers ensure a tightly enclosed and regulated system of the brain from peripheral blood.

1.3.5 The Glymphatic system

An important aspect of tissue homeostasis is the efficient removal of excess fluid and waste products, and the return of soluble materials and proteins back into the circulation. In the peripheral tissues, the lymphatic system serves to provide this function (190). The lymphatic vascular network is a unidirectional flow system that is present in every organ of the body to remove ISF; the major lymphatic systems are the cardiopulmonary, hepatic, meningeal, and dermal lymphatic vessels (191). Lymph drains into the lymphatic capillary vessels that are present within the interstitial spaces of tissues and organs. Lymph is moved into the lymphatic system present within lymph nodes and are returned to the blood circulation through the left and right subclavian veins and into the vena cava (192). The lymph nodes filter the lymph fluid to remove pathogens and other waste products. Importantly, the lymphatic is not only responsible for the removal and filtration of ISF from tissues, but it also involved in the transport of antigens and immune cells to the lymph nodes, where adaptive immune responses are often triggered (190). Thus, the lymphatic system is also implicated in the pathogenesis of several diseases such as lymphomas, lymphedema, lymphangitis, lymphocytosis and lymphadenitis (193).

Usually the density of lymph vessels correlates with the rate of tissue metabolism; it would therefore be expected that the brain and spinal cord, with the highest metabolic rate of the body, would be served by the greatest number of lymphatic vessels (194,195). However, the CNS lacks a conventional lymphatic system. Instead the brain has a unique clearance system that utilises perivascular tunnels formed by astroglial cells, and this is termed the glymphatic system (196). Similar to the peripheral lymphatic system, the glymphatic system also serves to facilitate the distribution of soluble compounds throughout the brain and spinal cord such as glucose, lipids, amino acids, growth factors and neuromodulators through the mixing of CSF and ISF (71).

Given the anatomy of the brain and restrictive environment provided by the 3 brain barriers, the glymphatic system can be defined into 3 distinct steps. Firstly, the CSF produced by the choroid plexus cells is moved by bulk-flow from the basal cisterns into the subarachnoid space that cover the cerebral hemispheres. The CSF enters into periarterial spaces (area surrounding pericytes and smooth muscle cells) in a bulk-flow-driven manner. Next, the CSF moves into the perivascular space surrounding

arteries (58) through a combination of arterial pulses, respiration, slow vasomotion and CSF pressure gradients. The CSF continues its flow into the perivascular spaces around arterioles, capillaries, and venules where the extracellular matrix of the BMs provides a continuity of the fluid space and low resistance. The surrounding astrocytic end-feet which ensheath these perivascular spaces express aquaporin 4 (AQP4) through which CSF can move into the brain parenchyma to enable the mixing of CSF and ISF as well as waste product removal (70,197,198). The CSF movement drives ISF waste towards perivenous spaces of larger central veins surrounding the meninges and cranial nerves, and exiting the skull from where it can drain into the peripheral lymphatic system via the cervical lymph nodes (199,200).

The glymphatic system and clearance mechanism is of significant interest in neurodegenerative disorders. In conditions such as AD, the accumulation of β-amyloid (A) proteins and tau tangles are central to disease progression. In fact, the first pioneering study that lead to the discovery of the glymphatic system was through the injection of fluorescent or radiolabelled amyloid-β1-40 into mouse striatum; in which it was seen that the protein was transported from the ISF and out of the brain via a novel clearance mechanism (197,201). This implicates the glymphatic system as a novel therapeutic target for preventing cognitive decline (198,202). The glymphatic system is so named, due to its reliance of AQP4 channels located on the astroglial cells; with $AQP4^{-/-}$ mice showing 55% reduction in amyloid-β1-40 clearance compared to wild-type controls (197,201). The dependence of the AQP4 channels located on astrocytic end-feet implicates how damage and BBB breakdown could result in the accumulation of waste products and excess fluids that contribute to adverse CNS pathology.

Aside from the glymphatic system formed by perivascular tunnels created by astrocytes, fluid and solutes drain from the brain to the cervical lymph nodes along the BMs in the walls of cerebral capillaries and arteries (60,64,203). This drainage mechanism has been named the IPAD pathway (204). It has been suggested that this perivascular lymphatic drainage is dependent on vascular smooth muscle cell contractions and biochemical interactions with BMs and therefore reduced contractility of the vascular smooth muscle cells with age or vascular dysfunction such as atherosclerosis results in reduced efficiency of this lymphatic drainage (205–209). Over time this results in the accumulation of Aβ in the IPAD pathways of cerebral

arteries and capillaries, known as cerebral amyloid angiopathy (210). The accumulation of Aβ and indeed of other waste products or metabolites will affect the CNS environment and lead to altered homeostasis. Similar to the glymphatic system, targeting the IPAD could provide a novel therapeutic strategy to improve outcomes in cerebral amyloid angiopathy and AD (204).

1.3.6 Disruption to BBB integrity

A variety of different factors can disrupt the permeability of the BBB. One of the biggest group of agents to induce BBB alterations are vasogenic agents such as histamine, VEGF, basic fibroblast growth factor and TGF-β (211–214). Inflammatory mediators of cytokines (IL-1β, TNF-α & IFN-γ), chemokines (CCL2, CXCL8), matrix metalloproteinases (MMP-2 & MMP-9), free radicals (H_2O_2, OH^- & NOO^-) and prostaglandins (E2 & F2a) have also largely been implicated in causing BBB breakdown (215–219).

The contractile forces generated by the endothelial cytoskeleton, in combination with the adhesive forces of the TJ and AJ proteins, are responsible for maintaining the integrity and restrictive nature of the BBB. Increased paracellular permeability and low TEER can be associated with alterations in the junctional complex, resulting in the formation of intercellular gaps to large plasma proteins, leukocytes and foreign molecules (44,63). Changes to the adhesive properties can be correlated to the phosphorylation state of the junctional proteins. The TJ and AJ proteins undergo phosphorylation and dephosphorylation by protein kinases and phosphatases at serine, threonine, or tyrosine residues affecting protein-protein interaction, protein localisation and distribution (222–225). In unison, the actin cytoskeleton undergoes reorganisation whereby the actin filaments polymerise to form stress fibres. Association of the actin with myosin results in the generation of contractile forces that ‘pull’ apart the endothelial cells to disrupt the junctional complexes hence forming small gaps in the barrier (226,227). Downstream effects of changes in the TJs and AJs integrity include disruption of cell polarity, subsequently affecting the distribution and localisation of transporters and enzymes. Overall a tightly regulated BBB ensures limited permeability, aiding in preserving the homeostatic environment of the brain.

In order to maintain the correct brain microenvironment, the BBB must function as a dynamic system which can sense and response to local changes and requirements, such as adjustment of nutrient supply, protection from circulating infections or facilitation in local repair (21). However BBB dysfunction has been associated with a large number of CNS pathologies including MS, AD, Parkinson's disease (PD), epilepsy, hypoxia and ischemia, tumours, glaucoma and lysosomal storage disease (16). The variation in barrier dysfunction can range from mild transient TJ opening to complete perturbation and breakdown of the BBB. The loss of BBB integrity can result in altered transport, accumulation of toxins such as β-amyloid, activation of microglia cells and neuronal damage/loss (228).

1.4 The concept of inflammation: involvement of the immune system

Inflammation is an evolutionary-conserved response initiated by the innate arm of the immune system upon destruction of tissue or against foreign materials (229). The aim is to destroy the harmful agent and limit the tissue injury. Inflammation can be recognised by its classic signs of heat (*calor*), redness (*rubor*), swelling (*tumor*), pain (*dolor*) and loss of function (*function laesa*) (230); which correspond to physiological changes occurring during the inflammatory process as seen by blood vessel dilation, increased blood vessel permeability and leukocyte extravasation (231).

Inflammation can be categorised as either acute or chronic. Acute inflammation refers to the initial response generated by the host organism in order to eliminate the source of damage and restore homeostasis (232). The acute phase response causes the release of a number of pro-inflammatory cytokines such as IL-1, IL-6 and TNF-α (233). If the original source of inflammation is unable to be resolved, long-term chronic inflammation can result. This occurs due to persistence of inflammatory mediators and activated immune cells that cause on-going tissue damage (229,234).

Innate immune responses form part of the acute response, whereas chronic inflammation also involves the adaptive arm. The innate immune system is composed of granulocytes (neutrophils, basophils, eosinophils), mast cells, macrophages, and dendritic cells. In contrast, the adaptive immune system is comprised of $CD4^+$ T-helper (T_H) cells, $CD8^+$ cytotoxic T-cells and B-cells. Natural killer (NK) cells are at the interface of the two immune systems, with cytotoxic and antigen-presenting ability (235). $CD4^+$ T-helper cells can be divided into different subsets; the pro-inflammatory T_H1 and T_H17 and the anti-inflammatory T_H2 and T-regulatory (Treg). T_H1 cells are responsible for the production of IFN-γ, TNF-α and IL-12 to trigger cell-mediated immunity and phagocytic-dependent inflammation as well as inducing macrophage switching to a pro-inflammatory M1 phenotype (235). T_H2 cells produce IL-4, IL-6, IL-10 and IL-13 to regulate antibody responses and T_H17 cells predominately secrete IL-17 and IL-22 (235,236). Treg cells secrete IL-10 and TGF-β to prevent excessive inflammatory responses, including autoimmunity, by regulating the other T-cell subsets and innate immune cells (237,238).

1.4.2 The immunologically unique CNS: interaction with the peripheral immune system

During the mid-20th century, studies of successful tissue transplantation into the brain parenchyma without rejection gave rise to the concept of the CNS as an immune privileged site (239,240). However, research in the past 20 years has altered this view with an understanding that peripherally-generated inflammatory mediators and xenotoxic agents can enter the brain and contribute to neurodegeneration suggesting that the CNS cannot be entirely immune-privileged (241,242). The protective barriers of the brain establish an interface between the peripheral and central immune systems to prevent damage to neurons, through restriction of immune cell entry. Therefore immune cell trafficking into the brain, like the movement of all molecules, is strictly regulated (4).

1.4.3 Breaching the BBB: leukocyte transmigration

Transendothelial migration (TEM) is a highly established process, allowing immune cells to cross endothelial cell barriers to the site of interest. The classic steps of TEM include capture-rolling, activation-adhesion, crawling-arrest and extravasation-diapedesis (Figure 1.7). Each step requires the involvement of different adhesion or signalling molecules on endothelial cells and circulating leukocytes (4,243). There are two distinct migration routes, either paracellularly through endothelial junctions or transcellularly through the formation of pores. *In vitro* and *in vivo* studies implicate the paracellular route to be favoured peripherally whereas healthy brain vascular endothelium support higher transcellular leukocyte migration, due to the BBB requiring a more complex and coordinated opening and resealing of the tight junctions (59,96,100,102).

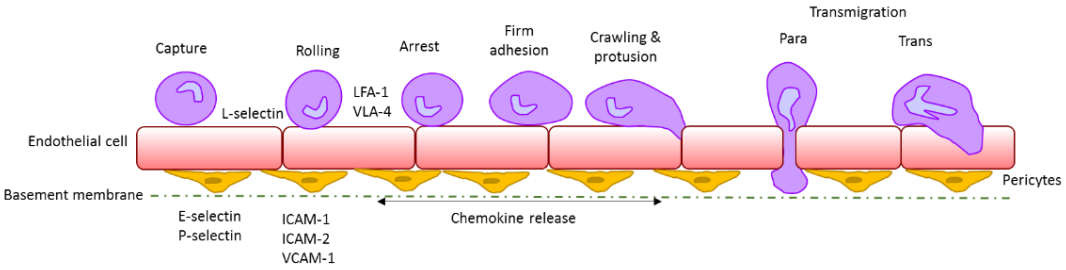

Figure 1.7 | Transendothelial migration of leukocytes

The initial step of TEM is the capture and rolling of leukocytes along the endothelium mediated by the selectin family of adhesion molecules (E-, L- and P-selectin), which bind to their respective ligands e.g. P-selectin glycoprotein ligand (PSGL-1) (88,89). Tethering and firm adhesion is provided by β2-integrins (LFA-1 and VLA-4) present on leukocytes that bind the immunoglobulin (Ig) superfamily of adhesion molecules (ICAM-1, ICAM-2, and VCAM-1). The adhered immune cell can bind a number of chemotactic factors such as CXCL8 via G-protein coupled receptors to induce conformational changes through inside-out signalling allowing for the arrest of immune cells along the vascular endothelium (90). After arrest, leukocytes rapidly protrude and translocate through the endothelial barrier at TJs or alternatively they use their integrins to crawl along the endothelium in search of exit cues. There are two distinct migration routes, either paracellularly through endothelial junctions or transcellularly through the formation of pores (93).

Crucially, passage of leukocytes across or through brain endothelial cells is not sufficient to reach the brain parenchyma. Instead the migration of leukocytes across the BBB is a multi-step process requiring penetration across cells and BMs, a mechanism unique to the CNS. Notably, some leukocytes may also enter into the CSF via the BCSFB, bypassing this mechanism (247).

As described in section 1.3.4, the BMECs are surrounded by two distinct BMs (150). The first is the endothelial BM composed of laminin α4 and α5 and the second is the parenchymal BM composed of lamina α1 and α2 which attaches to the astrocytic end-feet that ensheath the blood vessel (151,152). The combination of the parenchymal BM and astrocyte foot processes is termed the glia limitans, which acts as the second supportive barrier in TEM (4). Immune cells must penetrate this second barrier to enter into the CNS parenchyma (Figure 1.8) (4,248,249).

Once leukocytes have crossed the BMECs, they transverse the endothelial BM to enter into the perivascular space. T-cells preferentially migrate at sites containing laminin α4 and lacking α5 (250). The final challenge for T-cells to invade the CNS parenchyma is the glia limitans (4,248,249). T-cells are unable to interact with laminin α1 and α2 expressed on the parenchymal BM (156), therefore immune cell migration out of the perivascular space requires cleavage of the anchoring cell surface receptor β-dystroglycan present on astrocyte end-feet by MMP-2 and MMP-9 (251).

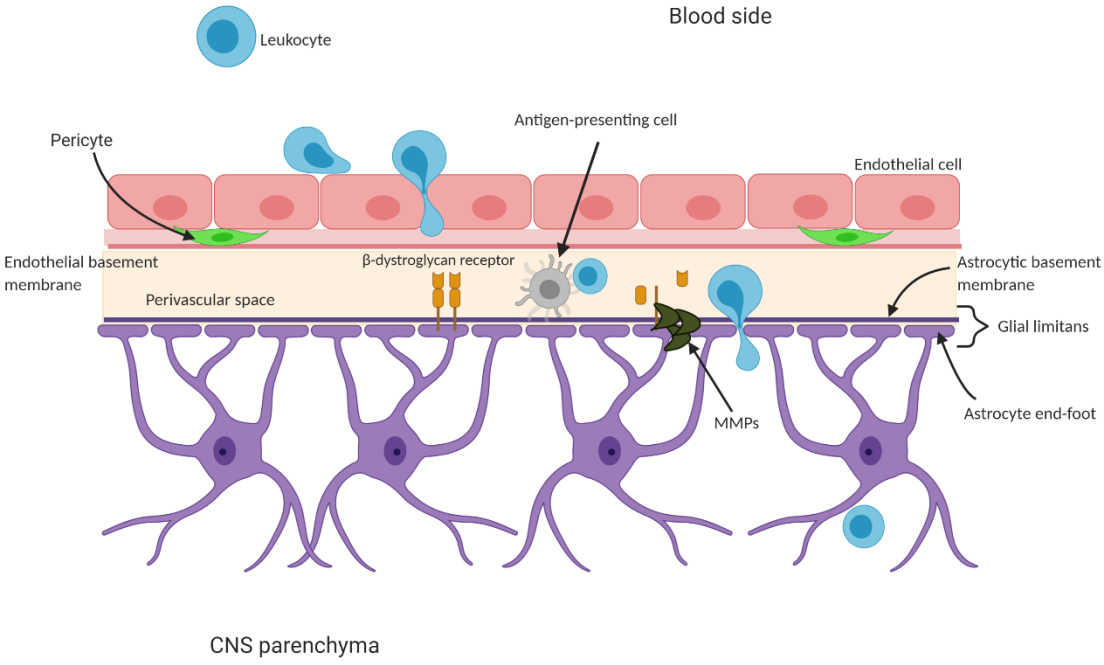

Figure 1.8 | Crossing the BBB

Immune cells invading the BBB must penetrate through a series of membranes to reach the CNS parenchyma. The endothelial cells of the BBB initially deposit an endothelial BM in which pericytes are embedded; in order to cross into the perivascular space T-cells preferentially migrate at sites containing laminin α4 and lacking laminin α5 (156). Next the T-cells must cross the glia limitans, formed by the astrocytic end-feet, by MMP-mediated cleavage of cell surface receptor β-dystroglycan (251). It is believed that invading cells must already be activated and primed from the periphery to cross the glia limitans, or T-cells must interact with the correct antigen presenting cells within the perivascular space to become activated. This complex vascular structure prevents damage with the brain parenchyma, particularly to neurons.

In healthy individuals and rodents, T-cells have been detected to cross the BBB, but are retained within the CSF-drained perivascular, leptomeningeal or ventricular spaces and do not enter the CNS parenchyma (252,253). It is thought that these immune cells are present for immunosurveillance, with flow cytometric analysis revealing these cells to largely be inactivated $CD4^+$ memory T-cells (254). The glymphatic system drains ISF containing CNS antigens into the perivascular spaces or into the CSF of the ventricles allowing for immunosurveillance within the CNS (247). Alternatively, the glymphatic system drains into the large veins existing the brain and as a result CNS antigens can also be detected in cervical lymph nodes (255). The importance of drainage of extracellular fluid from the CNS into the cervical lymph nodes for antigen detection was shown by Cserr and colleagues. Cserr et al., showed that micro-injections of antigens into the brain and CSF could elicit both cell and antibody-mediated immune response in the cervical lymph nodes and spleen (256). Moreover, antigens confer greater immune responses when administered into the CNS than into conventional extracerebral sites (256). These results implicate that the CNS is far from immune-privileged, instead there is highly regulated communication between the brain and the immune system response.

Importantly, opening the BBB alone e.g. during grafting of foreign tissue into the CNS is not sufficient to result in leukocyte TEM into the CNS parenchyma (257). Instead the loss of BBB integrity must be accompanied by a pro-inflammatory response (258). For example, in stroke, following cerebral ischemia and reperfusion (259) there is rapid alteration in the BMECs, with the release of oxidants, proteolytic enzymes and inflammatory cytokines (260). These mediators contribute to increased BBB permeability and result in migration of circulating activated leukocytes towards the ischemic lesion (261). The activated leukocytes release MMPs, specifically MMP-9, which degrade the laminin of BMs and TJ-associated protein complexes to further contribute to brain damage (262,263).

A number of CNS disorders such as MS, AD, brain tumours and bacterial meningitis, have been associated with the disruption of the BBB correlated with enhanced immune cell infiltration across the BBB, secondary to changes in systemic levels of molecules that are able to disrupt the TJ structure (22). The role of MMPs in BBB breakdown is paramount. MMPs levels are controlled by their inhibitors, TIMPs (264,265). In MS patients, disruption of the BBB coupled with macrophage infiltration is amongst the

earliest indicator of disease (266). Studies have shown MS patients to have higher serum levels of MMP-9 than healthy controls, along with higher MMP-9/TIMP-1 ratios (267). This contributes to decreased expression of TJ proteins occludin and VE-cadherin in cultured human brain endothelial cells, when stimulated with MS patient serum (268,269). Involvement of MMPs/TIMPs in the breakdown of the BBB in other CNS disorders implicates its potential to cause disruption in the current study of T2DM effects on the brain, particularly as T2DM patients have higher MMP-9 levels in their serum (270).

1.4.4 Resolution of inflammation

The purpose of inflammation is to restore tissue homeostasis after tissue damage. Uncontrolled and unresolved inflammation can be destructive, with ongoing chronic inflammation resulting in loss of tissue or organ function. The host's natural control of inflammation is conducted by switching from pro-inflammatory programmes to pro-resolving programmes, involving a shift to anti-inflammatory cytokines (IL4, IL-10, IL-13 & TGF-β) and cell types (Treg and M2 macrophages). The pro-resolution programme involves:

1. Reversal of vasodilation and vascular permeability.
2. Switching off signalling pathways associated with pro-inflammatory cytokine production responsible for leukocyte infiltration, proliferation, and survival.
3. Induction of apoptosis and clearance of recruited inflammatory and apoptotic cells.

1.4.4.1 Annexin A1: in the peripheral system

Anti-inflammatory therapies can either focus on neutralising the level of pro-inflammatory mediators or enhancing pro-resolution programmes (229,271). A well-established class of anti-inflammatory and immuno-suppressive drugs is the glucocorticoids. Annexin A1 (ANXA1), previously known as lipocortin-1, belongs to the annexin superfamily of proteins and is one of the molecules upregulated by glucocorticoids. ANXA1 is a 37kDa calcium-dependent phospholipid-binding protein that binds to the negatively charged phospholipids of cell membrane and the G-protein coupled receptor (GPCR) – formyl peptide receptor 2 (FPR2) (272). Binding of

ANXA1 to its receptor causes the activation of a number of signalling pathways through p38 mitogen-activated protein (MAP) kinase – ERK1/2 stimulation (273). During inflammatory reactions, ANXA1 is up-regulated and translocated from the cytosol to cell membrane, whereby it prevents the activation of phospholipase A_2 (PLA_2) and inhibits subsequent synthesis of eicosanoids (274,275); $ANXA1^{-/-}$ mice show exacerbated inflammation with increased PLA_2 activity (276). ANXA1 has also been shown to inhibit cyclooxygenase (COX)-2 enzyme production in microglia and pro-inflammatory mediators such as histamine whilst inducing anti-inflammatory cytokines e.g. IL-10 through the ERK signalling pathway (277) and activating caspase-3 signalling to promote apoptosis and chemotaxis of macrophages for clearance of immune cells (278).

One of the most well-documented properties of ANXA1 is its ability to inhibit leukocyte TEM. ANXA1 mediates its effect through modulating adhesion molecule-based leukocyte to endothelium interactions via two mechanisms. Firstly, ANXA1 co-localises with α4β1 integrin on leukocytes to prevent binding to vascular cell adhesion molecule (VCAM-1) on endothelium (279). Secondly, ANXA1 induces L-selectin shedding from leukocytes to prevent tethering, rolling and firm adhesion (280). Leukocytes mobilise their endogenous ANXA1 to the plasma membrane, upon cellular activation by chemokines, to promote leukocyte detachment. In this manner, ANXA1 serves as a negative regulator of TEM (166,167).

ANXA1 also mediates inflammation resolution through accelerating apoptosis through activation of caspase-3 (283) and Bcl-2-associated death promoter (Bad) activity (284,285). ANXA1 further aids in the removal of apoptotic cells through co-localising with ‘eat-me’ signal phosphatidylserine, serving as a signalling molecule for efferocytosis/phagocytosis (286).

In contrast to the well described effects of ANXA1 in innate immune responses, the role of ANXA1 in adaptive immunity, particularly in T_H cells, is less clear. ANXA1 is expressed in T-cells however the expression levels are almost 100-fold lower than in neutrophils and monocytes (287). The effect of ANXA1 on T-cell responses have been contrasting. One particular group reported ANXA1 could induce proliferation, activation and differentiation of T_H cells responses, through promoting T_H1

development and supressing T_H2 development (288,289). In contrast, it has been seen across separate studies that T-cell-expressed ANXA1 functions to attenuate pro-inflammatory T_H1 and T_H17 responses through limiting T-cell proliferation and reducing expression of pro-inflammatory cytokines IL-17, IFN-γ, TNF-α and IL-6 (290,291). In a mouse model of uveitis, the effect of ANXA1 on T_H17 cell development was regulated through the SOCS2/STAT3 pathways (291). Early studies in peripheral blood mononuclear cells (PBMCs) from atopic patients reported that exogenous peptides of ANXA1 could inhibit T-cell proliferation and differentiation (292). Indeed, in our lab we have reported that ANXA1 reduces T-cell activation and proliferation secondary to STAT3 hyperactivation. Moreover, it has been observed that T_H17 cells have reduced ANXA1 production and this can be correlated with an increased migratory capacity across an *in vitro* model of the BBB (293).

Due to ANXA1's diverse capacity to resolve inflammation, its role in various different diseases and conditions including immune repair (inflammatory bowel disease, rheumatoid arthritis), cardiovascular disease, cancers and in the endocrine system (HPA axis modulation) has been extensively researched. These have been discussed in detail in my published review – "Annexin A1: Uncovering the Many Talents of an Old Protein" (294).

1.4.4.2 Annexin A1: implications at the BBB

The presence of ANXA1 can be detected as early as in pre-natal brain development (295). During foetal development, the expression of ANXA1 was detected in BMECs and microglia-like cells (296). ANXA1 mediates its affect through the FPR2 receptor, which is present on BMECs implicating the ability of ANXA1 to bind to the BBB and mediate its anti-inflammatory effects through the mechanisms described above. Aside from limiting the impact of peripheral challenge on the CNS through blockage of TEM, ANXA1 has also shown to be important in maintaining BBB integrity at the TJs, through co-localisation with actin microfilaments (297). Evaluation of the BBB in $ANXA1^{-/-}$ mice showed disruption in occludin, VE-cadherin and the actin cytoskeleton along with loss of cell polarity indicating its importance in regulating BBB permeability and receptor distribution, with implications on meeting nutrient demand for the brain (296,297).

Studies have found a significant role of ANXA1 in the pathological development of aging and neurological disorders such as AD, MS, and stroke. In MS patients, there is a loss of ANXA1 expression in the brain parenchymal capillaries distant from lesion sites suggesting that there is a loss of BBB integrity (297,298). The opening of the BBB would allow for enhanced extravasation of activated leukocytes that attack and damage the myelin sheaths on neurons. Natalizumab, the current treatment for MS, is a humanised monoclonal antibody against α4β1 integrin with the aim to prevent leukocyte infiltration (299). Interestingly, this is the mode of action of ANXA1 thereby suggesting the potential of ANXA1 to be exploited for therapeutic potential, particularly as it is an endogenous protein and therefore is likely to induce a lower risk of side-effects. The benefit of ANXA1 treatment has also been tested in murine model of stroke. ANXA1 Ac2-26 peptide application reduced infarct volume, leukocyte adherence and markers of inflammation; neurological scores of treated mice also showed improvement versus non-ANXA1-treated mice (300). An alternative analogue of ANXA1, peptide 1-188 conferred similar beneficial effects in stroke (301).

Within the brain, microglia are the tissue-resident macrophages which are activated upon brain injury or neurological disorders (302,303). Similar to the peripheral system where macrophages phagocytose apoptotic cells, microglia remove unwanted cells within the brain and this is encouraged by ANXA1 which co-localises with 'eat-me' signal phosphatidylserine on the cell surface of apoptotic neurons surface thus serving as a efferocytosis/phagocytosis signal to microglia (279). In response to Aβ, in AD, microglia become constitutively activated. ANXA1 treatments *in vivo* and *in vitro* reduces Aβ levels by inducing efferocytosis/phagocytosis and enzymatic degradation (304). In ischemia-induced injury of neurons, treatment with ANXA1-derived peptide Ac2-26 promoted the transition of activated microglia from a pro-inflammatory M1 phenotype to an anti-inflammatory, pro-resolving M2 phenotype (305), suggesting ANXA1 confers neuroprotection.

1.5 An overview of T2DM

T2DM is a chronic metabolic disorder characterised by the loss of insulin sensitivity due to insulin resistance in target organs coupled with reduced production of insulin due to pancreatic β-cell dysfunction. Insulin resistance results in reduced uptake of glucose into liver, muscle and fat cells thereby raising blood sugar levels, resulting in glycated haemoglobin (306) measured as HbA1c levels.

The development of T2DM is affected by genetic and lifestyle factors. There is a strong heritable genetic connection, with approximately 25% of the disease having a family history and almost 100% concordance amongst monozygotic twins (307). Nevertheless, modifiable lifestyle factors such as reduced physical activity, increased consumption of energy-dense diets, alcohol intake and smoking levels play a fundamental role in the onset of the disease (308).

1.5.1 Epidemiology of CVDs & T2DM

In 2017, 425 million people were living with DM and this number is projected to increase to 552 million by 2030 (309); of which 439 million will have T2DM (310). People suffering from T2DM are 2.5 times more likely to suffer from a heart attack and 2 times more like to have a stroke, compared to those without diabetes (311). CVDs represent the greatest cause of mortality and morbidity associated with T2DM (312).

Globally CVDs are the leading cause of death, claiming more than 17 million deaths per year which accounts for 31% of all deaths (313). In the UK alone, 7.4 million people are living with a CVD and the annual healthcare cost spent on CVDs accounts for £9 billion (314). An ageing and growing population are likely to increase these numbers further, particularly as obesity and its associated complications of hypertension and hypercholesterolaemia are on the rise. In fact, between 1980 and 2004 the worldwide incidence in obesity, sedentary lifestyle and ageing population has quadrupled the prevalence of T2DM (315). Overall, this is placing an increasing burden on the economic system therefore highlighting the importance of understanding and managing T2DM and its related complications.

1.5.2 T2DM – micro and macrovascular complications

Diabetes and its related complications are associated with vascular disease which can lead to long-term damage and failure of organs including the heart, brain, kidney, eyes, muscle, and skin. These vascular complications, both at the macrovasculature and microvasculature level, are induced via a variety of mechanisms largely attributable to endothelial dysfunction and low-grade chronic inflammation. Some specific etiological mechanisms involved in causing vascular disease include oxidative stress, advanced glycation end products (AGEs) accumulation, haemodynamic dysregulation, enhanced platelet aggregation, impaired fibrinolytic ability, ECM protein synthesis, capillary BM thickening, smooth muscle dysfunction, overproduction of endothelial growth factors and NO response inhibition (316,317).

Diabetic macrovascular disease involves the aorta and large to medium-sized arteries. Atherosclerosis accelerates the progression of macrovascular complications, which include cardiovascular, cerebrovascular, and peripheral arterial disease. The atherosclerotic plaque build-up is the main factor in contributing to the development of these diseases, whereby reduced blood flow along with ruptured plaques and subsequent clots can lead to occlusion of arteries in the heart, brain and lower limbs resulting in myocardial infarctions, stroke and amputations respectively (318).

The microvascular complications of diabetes include nephropathy, neuropathy, and retinopathy. It is these complications which place an extreme burden on health care systems; in the UK the NHS spends approximately 80% of its diabetes-allocated budget on managing and treating microvascular complications (311). Worldwide, diabetes is response for being the leading cause of end-stage renal disease (>55%), neuropathy (60-70%) and non-trauma induced amputations (>60%), as well as being the main reason for partial or complete vision loss in individuals over 20 (309,319).

Given that the BBB serves as the interface between the peripheral and CNS systems, for inflammation and immunological integrity, it can be hypothesised that damage at the brain microvasculature arising from metabolic disorders, that results in adverse brain pathology, is also a secondary complication of T2DM.

1.5.3 Endothelial dysfunction in Diabetes

Endothelial cells serve as a determinant of vascular health. Endothelial cells were once thought of a quiescent barrier serving as an interface between vascular smooth muscle cells and circulating blood, however decades of research has broken this paradigm. Endothelial cells are important in upholding vascular homeostasis which involves maintenance of arterial tone (vasodilation and vasoconstriction), maintenance of blood fluidity through regulating platelet activity, the clotting cascade and the fibrinolytic system, and regulating production of pro-inflammatory and anti-inflammatory mediators that regulate inflammatory and regenerative processes. The term endothelial cell dysfunction refers to the loss or the impairment of the vascular endothelium to uphold these properties (320,321).

1.5.3.1 Vascular tone – maintenance by nitric oxide (NO)

Endothelial cells regulate vascular tone by balancing the production of vasodilators e.g. NO, prostacyclin, and endothelium-derived hyperpolarizing factor and vasoconstrictors e.g. endothelin-1 and angiotensin II (322). The balance between the production and response to these mediators is essential in maintaining a constant and adequate blood supply around the body. Endothelium-derived NO is important in maintaining an anti-proliferative and anti-apoptotic environment (323). NO also prevents the adhesion of leukocytes (322). In T2DM, the activation of endothelial NO synthase (eNOS) and subsequent production of NO is altered.

Within the peripheral system, insulin is a major regulator of blood glucose levels through stimulating uptake of glucose by liver, muscle and adipose tissue (133). Under physiological conditions, insulin binding to the insulin transmembrane receptor leads to IRS-1 phosphorylation which activates phosphoinositide-3 kinase (PI3K) and Akt. Akt phosphorylates eNOS to stimulate NO production (324,325). However, in the context of T2DM the increased presence of glucose, lipids (in the form of free fatty acids) and diacylglycerol leads to the activation of protein kinase C-β and subsequently NF-κB. This blocks insulin signalling via IRS-1 and thus reduces NO production via PI3K/Akt (326,327). Interestingly, insulin also activates MAPK via small GTPase Ras leading to cellular growth and proliferation. In endothelial cells, this leads to the increased expression of endothelin-1 and pro-inflammatory adhesion

molecules e.g. ICAM-1. In T2DM, the insulin-mediated Ras/MAPK activation remains active (320,328,329).

1.5.3.2 Oxidative Stress

Increased glucose and free fatty acids (FFAs) result in increased superoxide production. The production of reactive oxygen species (ROS) at low concentrations is useful to act as regulators of signalling involved in functions such as cell growth, however at higher concentration ROS induces cellular injury and death. This oxidative stress increases vascular permeability thereby allowing for greater leukocyte transmigration. Additionally, superoxides reduce NO bioavailability. Human-based studies have found increased markers of oxidative stress e.g. F2 isoprostanes in individuals with obesity, insulin resistance and T2DM (330,331). Clinical studies have shown improved endothelial function of patients infused with antioxidant ascorbic acid (332).

Importantly, mitochondrial-derived ROS in T2DM activates AMP kinase – a regulator of cellular energy status. As with non-mitochondrial ROS, low levels are required physiologically however under pathological conditions the mitochondrial-generated ROS can have detrimental effects on the lifecycle and function of mitochondria leading to impaired ATP production (333,334). Impaired mitochondrial ability reduces its ability to metabolise fatty acids thereby resulting in activation of PKC, which blocks insulin signalling (335). Antioxidants directed at mitochondria e.g. lipoic acid can help to reduce free radical production, improve sensitivity of insulin and downstream NO-mediated vasodilation (336).

1.5.4 Inflammation in metabolic disorders

The first molecular link between inflammation and obesity came from the identification of raised levels of TNF-α in adipose tissue of obese mice (337); in parallel human adipose tissue was also shown to overexpress TNF-α (338). Over the decades this association has been strengthened with identification of large numbers of inflammatory markers e.g. IL-1, IL-6, c-reactive protein (CRP), serum amyloid and soluble adhesion molecules showing upregulation in metabolic disorders with a graded increase with increasing features of MetS/T2DM (339,340). These molecules can activate the endothelial cells to become activated, promoting a pro-atherogenic phenotype via reduced NO bioavailability and expression of adhesion molecules leading to the recruitment of immune cells and their extravasation into tissues (231,341–343).

Under normal conditions, once the trigger of inflammation has been removed, the inflammatory mediators are terminated. However in metabolic disorders the trigger events such as hyperglycaemia and dyslipidaemia are persistent and therefore the aberrant activation of the innate immune system and its signalling cascades in multiple tissues such as adipose tissue, liver, heart etc. lead to the failure of inflammatory regulation (344). The consumption of carbohydrate-rich and lipid-dense foods also disrupts metabolism (345,346). Impaired insulin action results in IRS-1 serine phosphorylation consequently switching on p38 MAPK, PKC, JNK, AP-1 and NF-κB pathways (347,348). Increased free fatty acid presence places an increased demand on mitochondria for the use of the electron transport chain (ETC) for fatty acid oxidation (FAO), resulting in overproduction of mitochondrial superoxide. Similarly, hyperglycaemia evokes the production of AGEs. The presence of ROS and AGE causes oxidative stress and further amplifies the induction of pro-inflammatory pathways (340,349–351) such as NF-κB signalling. TNF-α and overexpression of IκB kinase-β (IKK-β) can lead to insulin resistance; pharmacological inhibition of IKK-β by salicylates prevents this from occurring. In fact, treatment of obese patients with salicylates reduces NF-κB activation in isolated endothelial cells, allowing for improved insulin sensitivity and endothelial cell-associated vasodilation (352). This suggests that control of endothelial cell function via anti-inflammatory drugs may improve the outcome of vascular disease.

The role of inflammatory events in metabolic disease, can be confirmed using anti-inflammatory drug aspirin in T2DM patients. After 2 weeks of treatment, aspirin lowers fasting blood glucose concentration by 25%, triglycerides by 50%, CRP by 17% and increases insulin sensitivity by 30% (353). This therefore highlights that metabolic disorders are not just characterised by biochemical abnormalities alone, such as altered insulin production or secretion; instead they also involve a strong inflammatory and immune signalling component (354). It is this long-lasting, low-grade chronic inflammation that is the distinguishing feature in metabolic disorders and CVDs (355), and is often referred to as metaflammation (356,357).

1.5.5 The innate immune system in metabolic disorders

Of the innate immune system, the role of macrophages is the most well-defined in T2DM and CVDs. Macrophages can largely be divided into two subtypes, the pro-inflammatory M1 phenotype and the anti-inflammatory, pro-resolving M2 phenotype (358). In lean adipose tissue, the M2 phenotype are dominant, maintaining the insulin sensitivity by the secretion of TGF-β and IL-10 (359). However, upon sustained weight gain, adipose tissue becomes hypertrophic, insulin resistant, hypoxic, and apoptotic. This causes the macrophages to become metabolically activated due to the high glucose, insulin and FFA concentration, causing a switch to the M1 phenotype and subsequent release of pro-inflammatory cytokines such as IFN-γ, TNF-α and IL-1β (360,361). Overall the number of macrophages in obese adipose tissue is substantially increased (362). The involvement of the innate immune system and its inflammatory effects are clearly identifiably in atherosclerotic plaques. The build-up of cholesterol-rich lipid drives macrophage accumulation, foam cell formation and monocyte migration resulting in atherosclerosis progression and CVD development.

1.5.6 The adaptive immune system in metabolic disorders

In the adaptive arm of the immune system, the $CD4^+$ T-cells play a large role in obesity and insulin resistance (363), with numbers of naïve $CD4^+$ T-cells declining in T2DM patients (364). In T2DM patients, the levels of T_H1-associted cytokines is increased and in contrast, the T_H2 cell-mediated immunity is impaired and delayed (365). Specifically T_H1 along with cytotoxic $CD8^+$ T-cells are increased in obese adipose tissues whereas the numbers of T_H2 and Treg cells are decreased (366). The balance between the different subsets is important for modulating immune responses. It has been reported that both Treg/T_H17 and Treg/T_H1 ratios are decreased in T2DM patients (367,368).

The innate immune response is fast-acting however does not confer any memory. In contrast the adaptive immune response, specifically of $CD4^+$ T-cells are activated to induce effector and central memory phenotypes. Upon antigen-presentation, naïve T-cells become activated, proliferate, and differentiate into effector T-cells (T_{eff}) for migration to site of infection/inflammation. These effector subsets are short-lived and therefore memory subsets for long-term survival are generated. Memory cells located in secondary lymphoid organs are known as central memory T-cells (T_{CM}) and those located in tissues are known as effector memory T-cells (T_{EM}). Memory subsets allow for quicker and more effective responses upon re-exposure of an antigen (369). A study by Mauro et al., found high-fat feeding in rodents primed $CD4^+$ T-cells towards an effector memory-like phenotype with no major changes in the size of the central memory pool (370). Similarly, there was an increased T_{EM} phenotype in obese patients. In another study of T2DM patients with and without CVD, the number of T_{CM} and T_{EM} cells were increased in individuals with T2DM regardless of CVD status compared to controls; however no changes were seen in the Treg population (371).

$CD8^+$ T-cells also play a crucial role in adaptive immune response through the secretion of IFN-γ, TNF-α and IL-17 and by the release of cytotoxic granules (372). Reports in patients with T2DM and high-fat feeding in mice show higher percentages of $CD8^+$ T-cells (373,374). B-cell antibody responses are important in the development of insulin resistance; with increased numbers of the cells present in visceral adipose tissues (375). B-cells can affect T_H17 and macrophage activation (376).

1.6 Dysfunction of the BBB: the role of endothelial cells

The cells of the NVU together form a dynamic functional unit for signal transduction. Thereby any damage occurring to the BMECS can be transduced across the brain and affect cellular functions e.g. reduced NO alters synaptic plasticity (377). In addition, the changes in the microenvironment have wider implications on the activity of the brain and thus its control via the sympathetic and parasympathetic nervous system on the entire body.

Cerebrovascular endothelium-derived NO is responsible for the maintenance of cerebral blood flow. Aside from this, cerebrovascular endothelial cell-derived NO regulates neurogenesis, axonal outgrowth and synaptic plasticity in the hippocampus and cortex which is essential for memory formation and learning (378). Within the CNS, eNOS and neuronal NOS (nNOS) are responsible for producing a constitutive level of NO to maintain vascular homeostasis. In conditions of inflammation, inducible NOS (iNOS) is activated to produce excessive NO, causing neurotoxicity, impairment of mitochondrial function and induction of apoptosis through uncoupling and free radical generation (378). The lack of available NO in inflammatory conditions activates the endothelium and generates oxidative stress. As described previously this leads to leukocyte adhesion and has important implications for the transmigration of inflammatory cells and toxins to pass through the BBB.

1.6.1 Pathophysiology – MetS to T2DM

MetS is the cluster of risk factors (obesity, hyperglycaemia, hyperinsulinemia, dyslipidaemia, and hypertension) which leads to the development of T2DM and subsequent CVD. It is the combined multifactorial nature of the disease which makes it hard to medically manage. The stage at which MetS becomes T2DM is not easily defined, as the nature of the disease is progressive over a long-term period. However usually, the main defining factor between MetS and T2DM is the level of hyperglycaemia and hyperinsulinemia correlated with β-cell dysfunction.

1.6.1.1 Hyperglycaemia

Hyperglycaemia arises in MetS and T2DM due to the loss of insulin sensitivity. Glucose levels are maintained through cross-talk between insulin-producing β-cells in the pancreas and insulin-sensitive tissues. Usually β-cell stimulation releases insulin, which stimulates an uptake of glucose, amino acids and fatty acids by muscle and adipose tissue and supresses the production of glucose by the liver. The tissues feedback to the islets regarding their requirement for insulin, likely mediated by neuronal and humoral mechanisms. In conditions such as obesity, in which there is accumulation of fat deposition, insulin resistance begins to develop. Initially, β-cells try to combat increased glucose levels by producing more insulin however when the β-cells cannot maintain this production, impaired glucose tolerance develops. As the β-cell dysfunction progresses there is a complete loss of euglycemia eventually resulting in T2DM (379). The compensatory hyperinsulinemia is often considered a trait of MetS, whereby the fasting glucose levels are maintained to combat insulin resistance. It is when the insulin secretion diminishes, that MetS can be differentiated from T2DM (380).

1.6.1.2 Hyperinsulinemia

Hyperinsulinemia not only exists from trying to combat hyperglycaemia, but also in response to increased fatty acids. Usually, insulin inhibits the lipolysis of fatty acids from triglyceride-rich lipoproteins stores in adipose tissue however when insulin resistance develops, there is no brake and uncontrolled lipolysis results in abundant levels of circulating FFAs (1). Excessive FFAs alter downstream signalling of the PKC pathway and IRS-1 phosphorylation as well as increasing hepatic glucose production and lipogenesis (381,382). Taking this into consideration, central obesity is a key diagnostic measure of MetS, as excessive subcutaneous and visceral abdominal tissue can contribute to raised levels of circulating FFAs.

1.6.1.3 Dyslipidaemia

Dyslipidaemia is a combination of several factors including increased flux of FFAs, raised triglyceride levels, reduced high-density lipoprotein (HDL), increased small, dense low-density lipoprotein (LDL) and raised apolipoprotein B (apoB). Increased FFA presence stimulates hepatic triglyceride synthesis, which in turn results in the production of apoB-containing triglyceride-rich very low-density lipoprotein (VLDL). When the VLDL is lipolysed, it produces a population of small dense LDL particles which fail to efficiently bind to LDL receptors and hence have prolonged circulatory time due to reduced clearance. The small dense LDL particles are thus considered pro-atherogenic. In combination with this, there is reduced production of good HDL cholesterol because of reduced triglyceride-cholesterol ester exchange between VLDL and HDLs. This results in production of HDL lacking their major apoA component; the apoA component is thought to be protective against atherosclerosis (383,384).

1.6.1.4 Hypertension

The development of high blood pressure is thought to be due to a series of factors including central obesity, insulin resistance, sympathetic nervous system overactivity, increased inflammatory mediators, oxidative stress, endothelial dysfunction, and activated/altered renin-angiotensin system. The combination of these effects can result in decreased vasodilation, increased vasoconstriction, and the loss of elasticity in the peripheral blood vessels. Lipid accumulation (atherosclerosis), glycated haemoglobin (raised HbA1) and hypertension together restrict the delivery of oxygen and nutrients to tissues resulting in organ damage and/or failure (385).

All of these risk factors have been discussed in the peripheral system, however the potential for damage to the microvasculature of the brain implicates how these risk factors could contribute significantly to altered brain signalling and subsequent brain damage.

1.7. From the BBB to neuronal damage: Dementia

Various models demonstrate that the dysfunction and perturbation of the BMECs results in subsequent damage to the brain. This is characterized by astrogliosis, microglial activation, white matter damage, impaired synaptic plasticity, neural inflammation, and apoptosis leading to cognitive impairment and eventually dementias. In fact, BBB damage can be used as a predictor of cognitive impairment in elderly patients (386,387).

Currently there are 50 million individuals worldwide living with dementia and this number is projected to triple by 2050 (388). Dementia is the fifth leading cause of death worldwide, of which AD constitutes 60-70% of cases (389). Although the understanding between the involvement of T2DM and the brain is still being understood, hypotheses are starting to arise to describe AD as T3DM (12) due to the role played by insulin resistance. In fact, high-fat feeding in an AD transgenic mouse model results in T2DM-like peripheral insulin resistance concomitant with decreased insulin receptor signalling in the brain, increased β-amyloid and cognitive defects (390,391).

For now, the majority of links of DM are made to the development of VaD, however VaD may just be a predecessor to the development of AD (133,392,393). Intriguingly, T2DM and transgenic AD mice present with similar vascular dysfunction resulting in cognitive decline that can be attributed to increase β-amyloid accumulation in both conditions (394,395). It is these similarities which have given rise to the T3DM concept (133,396) and implicate the need to understand the role of metabolic disorders in causing neurodegenerative disorders.

1.7.1 Astrogliosis

Astrocytes account for the majority of the cells in the brain with an abundance of approximately 50% (397). As astrocytes provide the link between the BMECs and neurons, they play a crucial role in providing metabolic support and control of the ion and neurotransmitter environment and thus are involved in providing the balance between neuroprotection, destruction and regeneration (398). In a rodent brain, a single astrocyte covers approximately 140,000 synapses (399); in humans, astrocytes are larger and more complex and therefore can link to approximately 2 million

synapses highlighting the complexity of glia to neuronal signalling (400). The astrocytic end-feet which bind the BMECs are key in mediating the transmission of nutrients, neurotransmitters and second messengers from the peripheral side into the CNS.

The close link between astrocytes and neurons therefore underlies that astrocytic activation and performance is a key contributor to neuropathological diseases. Acute or chronic insults to the brain can trigger glial-specific morpho-functional changes resulting in reactive astrocytes known as astrogliosis. Astrogliosis initially serves to be protective mechanism, isolating the damaged area and facilitating remodelling of brain circuits (401). However, as in all chronic inflammatory conditions, the over-activation of these cells can release neurotoxic substances, damaging BBB permeability and neurons. In animal models of VaD, there is marked astrogliosis and astrocytic end-feet swelling (402). Activation of HIF-1α in astrocytes can lead to the subsequent elevated expression of MCP-1, MMP-12 and VEGF which are responsible for attacking the BBB integrity (403). MCP-1 acts via the Rho signalling pathway to induce TJ redistribution altering paracellular permeability (227). MMP-13 can lead to the degradation of junctional proteins for example VE-cadherin and ZO-1 (404). VEGF secretion from astrocytes can bind to receptors on BMECs and lead to increased BBB permeability via activating phospholipase C, thereby down-regulating claudin-5 expression (405).

Astrocytes can become activated through several pathways. For example, secretion of VEGF by BMECs in inflammation can promote proliferation of astrocytes and result in the expression of glial fibrillary acidic protein (GFAP) via the MAPK/ERK and PI3K pathways (406). GFAP marks astrocytes for activation, resulting in the deposition of chondroitin sulphate proteoglycans and subsequently glial scar formation (407). Fibrinogen deposition has been found in patients with brain small vessel disease and correlated with the increased risk of dementia development (408,409). Moreover, the over-expression of endothelin-1 by BMECs can lead to their binding on the endothelin receptor type B on astrocytes, leading to the activation of JNK and p38 MAPK signalling pathways causing astrogliosis (410). Notably in humans with dementia, there is a marked increase in the number of astrocytes in the frontal-temporal lobes in the early stages of the disease (411).

1.7.2 Microglia activation

Microglia are the resident immune cells of the CNS, accounting for approximately 16% of the total number of cells within the brain. Activation of microglia reduces synaptic plasticity and affects the long-term potentiation of the brain thereby leading to memory loss and cognitive impairment (412).

Microglial cells are rapidly activated upon CNS tissues damage. Microglia, as with all macrophages, can present with a pro-inflammatory M1 phenotype or an anti-inflammatory M2 phenotype. M2 microglia secrete protective cytokines in an attempt to alleviate the immune response and phagocytose necrotic tissue to promote survival and repair of neurons (413). Conversely, excessive M1 microglia activation contributes to inflammation within the brain, damaging the BBB, neurons, and oligodendrocytes. In VaD, microglia activation has shown to contribute to white matter damage and cognitive dysfunction (414).

Components such as fibrinogen, present during vascular injury, can enter the brain parenchyma via a leaky BBB and promote microglia activation and assembly at sites of injury (415). Moreover, conditions of hypoxia and sugar deprivation are known to activate microglia cells resulting in the expression of TNF-α, IL-1β, IL-16 and MCP-1. Activated microglia are also the main source of MMP-2, MMP-3, MMP-9 and ROS within the brain (416). All these mediators can further degrade the BBB, thereby resulting in the loss of protection of the CNS.

1.7.3 White matter lesions, demyelination, and neuronal injury

White matter constitutes half of the brain volume and is sensitive to changes in blood flow and the delivery of nutrients (417). Endothelial cell dysfunction at the BBB, due to the risk factors of T2DM is likely to induce the sensitivity of white matter to the development of lesions. White matter hyperintensities have been linked to the occurrence of cognitive impairment (418) and are characterised by the loss of oligodendrocytes and the demyelination of neurons (378).

Oligodendrocytes wrap around axons to form myelin sheaths that are well known to be involved in the rapid conduction of nerve impulses. Oligodendrocytes also support axonal growth and survival through providing nutrients. Damage to oligodendrocytes causes demyelination resulting in axonal degeneration (177,419). In patients with VaD, the density of the myelin sheath and number of myelin precursor cells is decreased within the white matter (420). The expression of myelin basic protein and myelin-associated protein is also significantly reduced in the brain of VaD patients (419,421). Disruption to TJs, TNF-α and fibrinogen, amongst others, entering the brain can cause demyelination. In these areas, there is notable astrogliosis and activated microglia presence, suggesting that these cells contribute to the dysfunction of oligodendrocytes (422). Demyelination prevents nerve impulse conduction thereby impairing memory and cognition. Although oligodendrocyte progenitor cells proliferate upon tissue injury to induce spontaneous remyelination (423), chemokines, cytokines and other factors released during inflammation decrease the remyelination ability of these precursor cells (424). Oxidative stress from BBB dysfunction is a major factor in causing oligodendrocyte precursor cell dysfunction through free radical presence (425) and by reducing expression of genes such as sonic hedgehog required for differentiation (426). Activated astrocytes release hyaluronan, which further inhibits oligodendrocyte precursor cell maturation (427). Moreover, in an inflammatory condition the ability of microglia and macrophages to phagocytose myelin fragments is reduced; the presence of these fragments inhibits precursor cells from becoming mature (428).

Astrocyte and microglia activation as a result of BBB dysfunction can directly affect synaptic plasticity. Activated microglial cells overexpress iNOS inhibiting long-term potentiation formation and impairing cognition (429). In addition, the leakage of the BBB results in transmigration of leukocytes into the brain parenchyma. These infiltrated leukocytes release a variety of toxic proteins e.g. granzyme-B resulting in neuronal injury and death (430). Release of MMPs by the BBB cells can directly induce neuronal apoptosis; moreover these MMPs, specifically MMP-9, can enter the nucleus of neuronal cells to cause DNA damage resulting in neuronal cell death (431). The raise of inflammatory mediators within the brain from astrocytes and microglia can result in the accumulation of glutamate that causes cell-death (432). Elevation of

TNF-α in elderly patients has shown to initiate the phagocytosis of stressed neurons (433).

The method by which inflammation is induced in the brain can be accounted for by BBB disruption, suggesting the dysfunction of BMECs as a major contributing factor. Therefore, controlling risk factors which can affect vascular health and cause endothelial cell damage, such as those involved in T2DM, is incredibly important in preventing dementia development. Studies have found that control of blood pressure and a low-fat diet can reduce white matter hyperintensities and dementia risk (87). To date there are no drugs that can improve endothelial cell function however traditional remedies such as ginseng have well documented anti-inflammatory and anti-oxidant effects and have been used pre-clinically and clinically to treat dementia (434).

1.8 Metabolic disorders, BBB dysfunction & cognitive decline

There is a huge array of data focussing on the effect of metabolic disorders in context of CVDs however research on the effect of neurodegenerative diseases is still limited. So far, research investigating the link between metabolic disorders and brain dysfunction has shown significant alterations in the NVU and regions in the brain associated with memory and learning, supporting the notion that metabolic overload can be causative in development of neurological disorders through loss of BBB integrity.

Obesity and diabetes in rodent models induced by high-fat feeding (approximately 45% fat) show reduction in pericyte number, activation of astrocytes and microglial alongside neuronal loss (435). Together these effects suggest a neuroinflammatory response induction, secondary to BBB disruption. BBB permeability studies in these rats revealed increased permeability to sodium fluorescein dye particularly in the hippocampus region. Several BBB permeability studies have identified decreased expression of the TJ proteins claudin-5, claudin-12 and occludin alongside increased MMP-2 expression and raised oxidative stress levels (436–439). Furthermore, analysis by flow cytometry reveals macrophage infiltration into the perivascular space and activation of microglial cells in diabetic mice (440).

Clinically, neuro-imaging of human brains using a tensor-based morphometry technique has revealed obese patients to have atrophy of frontal lobes, hippocampus, thalamus, white and grey matter (441–443). In diabetic patients, brain post-mortem studies also find reduced grey and white matter in the hippocampus region (444–446) suggesting a connection between metabolic disorders and brain deficit.

Normal brain functioning requires the maintenance of nutrient transport across the BBB. Normally when a substrate is in excess the body will down-regulate the receptor expression to modulate its supply. The role of hyperglycaemia, hyperlipidaemia and hyperinsulinemia could therefore have major effects on transport receptors on the BMECs and subsequent neuronal function. Current research shows limited understanding of the effect of T2DM on GLUT-1 and lipid uptake. However, there is significant interest in understanding the transport of insulin. Insulin transport across the BBB is important for regulating tau phosphorylation via inactivation of glycogen

synthase kinase-3 and β-amyloid, preventing tauopathies and development of AD (447,448).

Western diets have been show to increase peripheral circulating levels of β-amyloid that disrupt the BBB and accumulate within the hippocampus (449). The hippocampus has a major role in learning and memory. Dementias are characterised by progressive memory loss and cognitive decline. Patients with MetS show loss of neurons and brain matter in the hippocampus (392,450). In rodents, the association of cognitive decline has been tested using spatial memory tests (Morris water maze and arm maze). Rodents fed western diets show impaired memory retention in as little as 72 hours of feeding in comparison to chow-fed counterparts (451,452), implicating the role of metabolic-induced disruption on affecting brain cognition.

The association of western diets to cognitive decline has raised interest in the role of nutritional intake on dementia development. A number of epidemiological and animal studies have found particular food groups or individuals nutrients to be important in conferring neuroprotective effects; leafy green vegetables provide a good source of folate, vitamin E and carotenoids, seafoods provide a source of n-3 fatty acids and berries provide a source of polyphenols which reduce oxidative stress (453,454).

Currently, there is no cure for dementia and therefore preventive strategies are key. It is well recognised that nutritional therapy positively influences glycaemic control, contributes to weight loss and reduces hypertension and LDL-cholesterol (455,456) in the peripheral system, contributing to improved T2DM and CVD outcomes. This implicates that dietary changes could also improve cognition and brain disorders; however current data is limited. A large systematic review found that adherence to Mediterranean, Dietary Approaches to Stop Hypertension (DASH), and Mediterranean-DASH Intervention for Neurodegenerative Delay (MIND) diets is associated with a reduced cognitive decline and lower risk of AD (457). The majority of these studies are observational and there is insufficient evidence to support the development of dietary guidelines for dementia. In the first study of its kind, a randomised clinical trial is underway to evaluate the MIND diet intervention in AD prevention, in 600 participants aged between 65-84 years old. These individuals are being tracked over a period of 3 years to assess changes in cognitive score and total brain and hippocampal volume (458). The study is due to end in April 2021. Such

studies will be influential in healthcare strategies. Nevertheless, comprehensive approaches using laboratory and animal models are required to understand how diet can affect the brain through structural, function and immunological alterations at the BBB.

Chapter 2 – Rationale, Aims & Outline of Thesis

2.1 Rationale & Hypotheses

Over the past twenty years, evidence has been accumulating to indicate that metabolic disorders such as MetS and T2DM can strongly affect brain health, leading to cognitive decline and AD-like pathology. Given that T2DM can result in microvasculature complications of the peripheral system, it is highly plausible that brain dysfunction in metabolic disorders arises due to damage at the brain microvasculature - the BBB.

The focus of this project was to investigate how metabolic disorder-induced inflammation, termed metaflammation, can disrupt the BBB, with focus on alterations to the structural and immunological integrity of the barrier.

⇒ **Hypothesis 1:**

It is hypothesised that metaflammation arising in T2DM will result in a leaky BBB phenotype resulting in the infiltration of immune cells from the peripheral side into the brain parenchyma to cause neuroinflammation.

Anti-inflammatory drugs have shown to improve T2DM and CVD outcomes. In this manner, the effect of using ANXA1 as an anti-inflammatory therapeutic has been explored at the BBB. ANXA1 is well-established as a positive regulator of BBB structure and it has also been shown to provide neuroprotection, indicating its potential to reduce and repair damage at the BBB and beyond.

⇒ **Hypothesis 2:**

It is hypothesised that treatment with human recombinant ANXA1 (hrANXA1) will restore the leaky BBB phenotype through restoring TJs. Improved BBB integrity along with hrANXA1's effect on leukocytes will prevent leukocyte TEM and reduce neuroinflammation.

Aside from therapeutic strategies, the simplest method to resolve inflammation is to remove the source. In patients, lifestyle modifications are key to reduce the progression of T2DM and CVD, with the aim to reduce the inflammation arising from hyperglycaemia, hyperinsulinemia, and hyperlipidaemia. Moreover, the understanding on dietary intake and brain health is growing. As a result, the effect of a dietary intervention has been explored to understand whether preventive measures can reinstate the integrity of the BBB and subsequent development of neurodegenerative disorders.

⇒ **Hypothesis 3:**

It is hypothesised that reverting to a healthy diet will remove the source of metaflammation and therefore improve the integrity of the BBB by reducing endothelial dysfunction and subsequently reduce neuroinflammation.

Disruption to the BBB because of metaflammation will also impair its ability as a functional, transport and metabolic barrier.

⇒ **Hypothesis 4:**

It is hypothesised that the metabolism of the BBB endothelial cells will be disrupted and this together with impaired BBB structure will alter the transport of essential nutrients e.g. glucose across the BBB into the brain to contribute to neurodegeneration. Treatment with hrANXA1, which is shown to repair the BBB TJs, could therefore also repair the metabolic integrity of the BBB endothelial cells.

2.2 Project design

This study used a diet-induced mouse model of T2DM, fed a combination of high-fat and high-sugar (HFHS) for 10 weeks, to investigate the effect of metabolic overload on the BBB. Diet-induced diabetic models work through causing obesity from imbalanced food intake and low energy expenditure (459). Obesity is the single biggest risk factor for developing T2DM, with research suggesting that obese individuals are 80 times more likely to develop T2DM than non-obese individuals (311). Obesity raises the levels of fatty acids, glucose, pro-inflammatory markers and alters hormones and metabolism due to the accumulation of fat deposition, leading to the development of insulin resistance (460). The diet-induced models of diabetes are used to replicate the westernised lifestyle in humans, with increased intake of foods dense in fats and sugars along with a sedentary lifestyle. This was the rationale for using a diet that was high in both fats and sugars.

The comparison of the effects of HFHS-induced T2DM on the BBB was made against mice which were fed a standardised chow-based diet. The composition of the two diets and further information on the protocol e.g. length of time used to induce and confirm T2DM can be found in the Methods Section 3.1.1.1. The effect of HFHS-induced T2DM on the BBB has been presented in Chapter 4 and in Chapter 6.

Pharmacological intervention in this study was delivered by treating mice fed a HFHS-diet with hrANXA1. Details on the protocol of the treatment provided, e.g. which group, length of time, dosage can be found in Methods Section 3.1.1.2. The effect of hrANXA1 treatment at the BBB in HFHS-induced T2DM mice has been presented in Chapter 5 and Chapter 6.

Dietary intervention was provided by firstly inducing T2DM by feeding mice a HFHS-diet for 10 weeks, after which the diet was reversed back to a standard chow diet for a further 5 weeks. Details on the dietary intervention protocol can be found in Methods Section 3.1.1.3. The effect of dietary intervention on T2DM-induced BBB damage has been presented in Chapter 5.

2.3 Aims

The following are the general aims of this entire study, the specific aims/objectives have been provided at the beginning of each results chapters.

1. To characterize the early vascular defects occurring in the BBB during HFHS-feeding *in vivo*, *ex vivo* and *in vitro*.
    - Identify the functional changes occurring to the BBB through measuring vascular leakage.
    - Identify structural alterations through immuno-histochemical analysis of brain endothelium junctional proteins, BM components and the cytoskeleton.

2. To define the pathogenic events leading to cerebrovascular damage at the BBB induced by HFHS-feeding.
    - Examine the role of inflammatory mediators and soluble factors present in the sera such as cytokines, chemokines, interleukins, metabolic factors, extracellular matrix components, on inducing BBB permeability and endothelial dysfunction.
    - Define the effect of metabolic disorders on the innate and adaptive arms of the peripheral immune system. Determine whether the priming of immune cells within the peripheral system can correlate with the transmigration across the BBB and subsequently activate the microglia, the resident immune cell of the CNS to initiate neuroinflammation in a diabetic state.

3. To assess the potential therapeutic effect of hrANXA1 on HFHS-induced BBB alterations.
    - hrANXA1 treatment will be given *in vivo* to animals to examine whether the protein has the ability to restore, resolve and revert the damage induced to the BBB, to the pre-diabetic state. This will serve as a pharmacological intervention. Structural and immunological integrity will be assessed as aforementioned in Aims 1 & 2.

4. To investigate whether the metabolic stress induced BBB defects are reversible upon dietary intervention.
    - In order to assess reversibility of diabetes-induced BBB damage, mice fed a HFHS diet for 10 weeks will be re-introduced to a normal chow diet for a further 5 weeks Structural and immunological integrity will be assessed as aforementioned in Aims 1 & 2.

5. To investigate how nutrient imbalance in T2DM induced by HFHS-feeding can affect the BBB endothelium metabolic programming by examining cellular metabolism pathways of glycolysis and oxidative phosphorylation. The potential of hrANXA1 treatment to restore the metabolic integrity will also be assessed.

2.4 Outline of Results of Thesis

The following provides an outline of the arrangement of the results chapters 4-6 of this thesis, to clarify where the general aims have been investigated and discussed. It should be noted that all methods of used in thesis have been provided in Chapter 3 and a general discussion of the implications of all of the results have been provided in Chapter 7.

Chapter 4 - The impact of MetS/T2DM at the BBB: structural and immunological alterations

This chapter investigates the effect of a HFHS-induced T2DM at the BBB, by examining the functional, structural and immunological alterations. This chapter will cover Aims 1 & 2. The results in this chapter will specifically compare the effect of a HFHS-fed diet that induces T2DM with a standard chow-based diet.

Chapter 5 – Examining the effect of a pharmacological (hrANXA1 treatment) and dietary (HFHS – Chow reversion) intervention to restore the BBB to the pre-diabetic state

This chapter investigates the effect a pharmacological intervention provided by hrANXA1 treatment and a dietary intervention provided by altering diet on restoring the BBB to the pre-diabetic state. This chapter will cover Aims 3 and 4. The results in this chapter will compare the effects of a pharmacological and dietary intervention against the HFHS-diet and chow-diet fed mice, as well as a comparison against each other. As a result, there will be 4 experimental groups:

1. Chow diet-fed mice
2. HFHS diet-fed mice
3. HFHS diet-fed mice given hrANXA1 treatment
4. HFHS – Chow reversion diet-fed mice

Chapter 6 – Metabolism at the blood-brain barrier

This chapter investigates how metabolism of the BBB endothelial cells is altered with HFHS-induced T2DM. The effect of hrANXA1 treatment in restoring BBB endothelial cell metabolism is also investigated. This chapter covers Aim 5. Therefore, the results in this chapter are compared between 3 experimental groups:

1. Chow diet-fed mice
2. HFHS diet-fed mice
3. HFHS diet-fed mice given hrANXA1 treatment

Chapter 3 – Materials & Methods

This chapter includes all of the materials and methods used in this thesis. Unless otherwise stated, all materials, reagents and solutions were purchased from Sigma-Aldrich Ltd (Poole, Dorset, UK).

This Chapter has been organised into the following:

- **3.1 *In vivo* methods**

  This section covers the experimental models and *in vivo* animal-based experiments. These models are relevant to chapters 4, 5 & 6 and the methodology covered here is referred to in Chapters 4 & 5.

- **3.2 *In vitro* methods**

  This section covers all methods that have been conducted *in vitro* using primary cultured cells, cell lines, primary brain microvessels and mouse serum. The methodology used here is covered across Chapters 4, 5 and 6.

- **3.3 Immunofluorescence & Immunophenotyping**

  This section details the information on immunohistochemistry conducted on mouse brain tissue which is relevant to chapters 4 & 5. The methodology in this section also includes the flow cytometry and antibody details relevant to Chapters 4, 5 & 6.

- **3.4 Measuring cellular metabolism**

  This section provides the methodology used in Chapter 6.

- **3.5 Statistical Analysis**

  This section provides the statistical analysis used throughout the thesis.

3.1 *In vivo* methods

3.1.1 Animals

All animal experiments in this study were performed in accordance with the UK Animals Scientific Procedures Act 1986 and with approval of the Animal Welfare Ethics Review Board (AWERB) of Queen Mary, University of London. The study purchased 9-week-old male wild-type C57BL/6 mice from Charles River Laboratories UK Ltd., Kent, U.K. Animals were allowed to acclimatise to laboratory settings for a period of one week prior to initiation of experimental procedures. All mice were 10-weeks old at the initiation of study. The mice were housed 6 per cage, in individually ventilated cages, in a temperature-controlled room with 12-hour light/dark cycle. All mice had free access to food and water, body weight was recorded weekly. The body weight of all animals was measured at the same time at the beginning of each week using the same balance for the whole experiment for determination of body weight gain for measuring obesity. New fresh food (stored at -20°C) was supplied, once defrosted, to mice at the beginning of each week and observed every few days during the week for colour or consistency changes. High-quality feed is necessary to ensure an animal's nutritional needs are met. Feed and bedding can influence experimental outcomes as they can impact an animal's physiology. Provision of high-quality feed is therefore essential to maintain the health and welfare of the animals. Any suspected changes in consistency or colour, deviated from the frozen food was removed, if necessary. Daily assessments on mouse welfare were conducted by the biological services unit technicians on a daily basis. Mice were separated if there was an issue with fighting. Mice were identified by ear marking and were house together based on diet and treatment received. Mice were assigned to diet and treatment on random, no blinding was performed.

3.1.1.1 Induction of T2DM by the use of a HFHS diet

10-week old male C57BL/6 mice were fed either a standard chow-based diet (5053, LabDiet Ltd) or a HFHS diet (58R3, TestDiet Ltd) for 10 weeks. Both chow and HFHS-fed mice were 20-weeks old at cull. The compositions and nutritional profile of the two diets are shown in Table 3.1. The HFHS diet has been termed 'high-fat' and 'high-sugar' due to its high concentration of saturated fats (hydrogenated coconut oil) and sucrose.

Table 3.1 | Diet composition and nutritional intake of chow and high-fat high-sugar (HFHS) diets

		Chow	High-Fat High-Sugar (HFHS)
Energy from (kcal %)	Protein	24.5	14.9
	Fat	13.1	59.4
	Carbohydrate	62.4	25.7
Fat composition (%)	Cholesterol, ppm	142	0
	Linoleic Acid	2.12	1.28
	Linolenic Acid	0.27	0.19
	Arachidonic Acid	0.01	0
	Omega-3 Fatty Acids	0.45	0.19
	Total Saturated Fatty Acids	0.78	31.55
	Total Monounsaturated Fatty Acids	0.96	0.62
	Polyunsaturated Fatty Acids	0	1.47
Additional ingredients (%)	Sucrose	3.25	17.5
	Hydrogenated coconut oil	N/A	33.3

In this study, a diet-induced diabetic model was favoured due to its ability to mimic the human condition more accurately that genetic models of obesity-induced diabetes (461). Diet-induced diabetic models work through causing obesity from imbalanced food intake and low energy expenditure (459), therefore the diet-induced models replicate the westernised lifestyles in humans, of increased intake of foods dense in fats and sugars along with a sedentary lifestyle.

The use high-fat feeding has been examined in a number of rodent models (459,462,463), however the C57BL/6 mouse strain has shown to most closely parallel the pathophysiology of T2DM as seen in humans (464). A high-fat (58%) diet in these mice has clearly shown to cause weight gain, insulin resistance and hyperglycaemia in comparison to mice fed a chow-diet (11% fat) (465). Furthermore studies have found male mice to be more prone to the development of diabetes in comparison to females (466). Obesity inevitably leads to metabolic syndrome that can progress to T2DM and hence the C57BL/6 male diet-induced obese mouse model is highly suitable for this study (467,468).

It should be noted that there are no 'gold-standard' reference values, which are used to confirm development of T2DM in an animal model (467). All studies will compare the development or induction of T2DM against a control, in this case this will be the chow diet mice, and comparison to other studies. The lack of 'gold-standard' reference values may be due the number of different models that can be used to induce T2DM. With regard to diet-induced diabetes, there is no single standard protocol with variations in the use of mouse strains, formulations of high fats (fat fractions ranging from 20-60%), duration of feeding periods (ranging from a few weeks to more than one year) and age of mice at induction of diet (469,470).

Nevertheless, there are certain clinical measures that are used to confirm T2DM in animal models and these are based on the criteria of traits seen in MetS/T2DM in humans. Notably, the assessment and definition of these metabolic disorders is still of considerable debate in humans, with a number of guidelines available which have variations in their diagnostic criteria (471). To confirm the development of T2DM in this study, I have used clinical measures that have been previously used by Surwit et al., in development of the original high-fat diet-induced model (464) and reversal of diet-induced obesity (472) in C57BL/6 mice as well as by others in our group (473–475). The list of these clinical measures or traits along with the methodology used to determine these have been presented in Table 3.2. Further information on each of these traits can be found in section 1.6.1. and in the relevant sections of the methods that follows. Summary of the chow and HFHS-fed mouse model is provided in Figure 3.1.

Table 3.2 | The traits of MetS/T2DM

The table defines the traits of MetS/T2DM that are often used to confirm development of T2DM in mice. The methodology to determine the development of these traits or clinical measures has also be listed. OGTT – oral glucose tolerance test, ITT – insulin tolerance test.

Clinical Measure	Definition (taken from WHO)	Which methodology is used to determine the measure?
Obesity	Overweight and obesity are defined as abnormal or excessive fat accumulation that presents a risk to health. Based on Body Mass Index in humans.	Body weight (taken weekly to determine weight gain) & adiposity (epididymal and inguinal fat pad measurements)
Hyperglycaemia & Insulin resistance	Impaired fasting glucose levels and impaired glucose tolerance. Often results from insulin resistance thereby raising blood glucose levels	Fasted and non-fasted blood glucose, OGTT, ITT
Hyperinsulinemia	Occurs in response to high glucose and fatty acid levels	OGTT, ITT and serum insulin
Dyslipdaemia	Elevation of blood cholesterol, triglycerides, or both, or a low HDL cholesterol level.	Serum triglycerides and serum total cholesterol

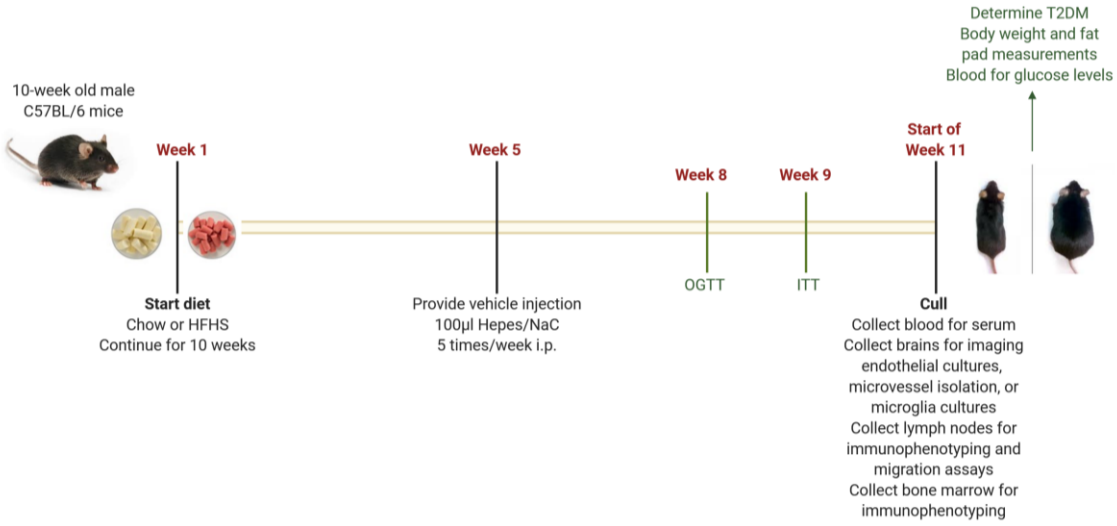

Figure 3.1 | Summary of the experimental model used to establish diet induced T2DM

10-week old male C57BL/6 mice were fed either a chow or HFHS for 10 weeks. From week 5, mice were injected with a sham injection of 100µL Hepes/NaCl, 5 times/week via intraperitoneal (i.p.) injection for 6 weeks. Assessment for glucose tolerance and insulin resistance were conducted via oral glucose tolerance tests (OGTT) and insulin tolerance tests (ITT) respectively. Mice were culled at the beginning of week 11. Confirmation of T2DM was made by weight and various blood/serum analyses. At cull, blood, brain, lymph nodes and bone marrow were collected.

3.1.1.2 Pharmacological intervention: Treatment with human recombinant ANXA1 (hrANXA1)

Pharmacological intervention was provided by treating mice fed a HFHS-fed diet with hrANXA1. 10-week-old male C57BL/6 mice were fed a HFHS diet for 10 weeks. Pharmacological intervention was provided from weeks 5-10, whilst mice remained on the HFHS diet. Mice were treated with 1µg hrANXA1 in 100µl of 50mM Hepes (hydroxyethyl piperazineethanesulfonic acid) and 140mM NaCl, pH 7.4, daily (5 times/week) intraperitoneal (i.p.). The daily dose of 1µg was selected based on previous report that show the half-life of ANXA1 to be approximately 6 hours through i.p. or intravenous (i.v.) injection (476,477). I.p. injection is preferred because 0.5% of the injected dose remains in the circulation 24 hours post injection versus almost 0% through i.v. administration (478). The dose of hrANXA1 remained the same throughout the duration of the study and was not changed with increasing weight gain in the mice.

To allow for accurate comparison against the chow-fed and HFHS-fed mice; mice not assigned to receive hrANXA1 where treated with vehicle 100µl of 50mM Hepes, 140mM NaCl, pH 7.4, daily (5 times/week) i.p.

Assignment to diet and treatment was random and no blinding was performed. All groups of mice were 20-weeks old at cull. Summary of the HFHS-fed + hrANXA1 treated mice model is provided in Figure 3.2.

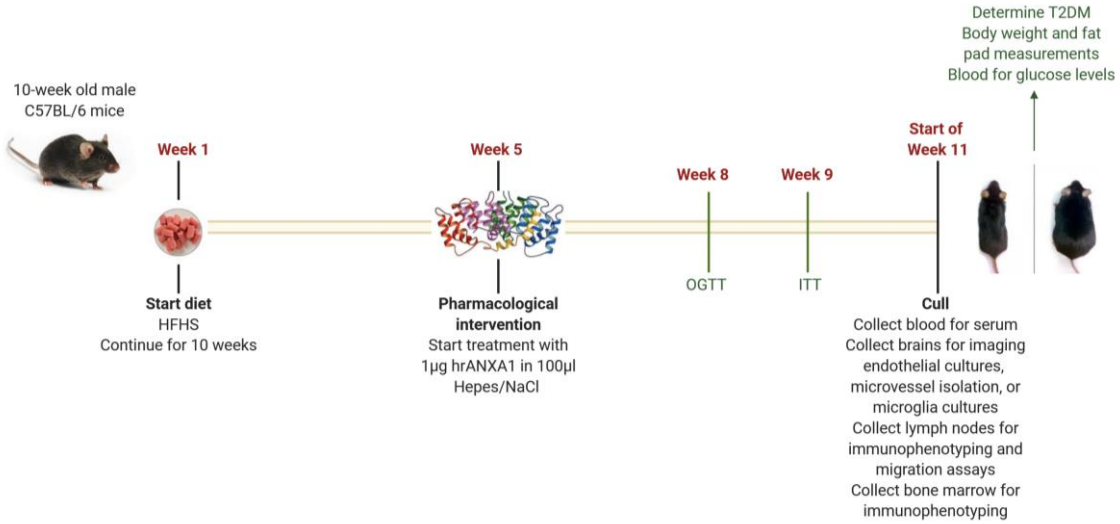

Figure 3.2 | Summary of the experimental model used to provide pharmacological intervention with hrANXA1 treatment

10-week old male C57BL/6 mice were fed a HFHS for 10 weeks. From week 5, mice were injected with a 1µg hrANXA1 in 100µL Hepes/NaCl, 5 times/week via intraperitoneal (i.p.) injection for 6 weeks. Assessment for glucose tolerance and insulin resistance were conducted via oral glucose tolerance tests (OGTT) and insulin tolerance tests (ITT) respectively. Mice were culled at the beginning of week 11. Confirmation of T2DM was made by weight and various blood/serum analyses. At cull, blood, brain, lymph nodes and bone marrow were collected.

The hrANXA1 was kindly provided by our collaborator Chris P. M. Reutelingsperger (University of Maastricht, The Netherlands) who produced and purified the hrANXA1 as per procedures described below. The hrANXA1 was provided at a stock concentration of 2.1mg/mL in 50mM Hepes, 140mM NaCl pH 7.4. When stored at 4°C in the Hepes/NaCl buffer, hrANXA1 is stable for at least 1 year. For longer periods of time, hrANXA1 can be stored at -80°C. Throughout the study a single synthesis/purification of hrANXA1 was used. The hrANXA1 was aliquoted and stored in the freezer upon arrival. The required amounts were defrosted and prepared to the required concentration prior to use in the mice.

hrANXA1 was produced according to previously described procedures (478). Briefly, cDNA coding for hrANXA1 was amplified by polymerase chain reaction (PCR) using the primers: 5'-GGTATCGAGGGAAGGGCAATGGTATCAGAATTC-3' and 5'-GCTCAGCTAATTAAGCTTTAGTTTCCTCCACAAAGAGC-3'. The PCR was run for 35 cycles consisting of incubation for 1 minute at 94°C, 1 minute at 55°C, and 1 minute 20 seconds at 72°C. The primers allowed for the introduction of Stu-I and Hind-III restriction sites, which were required for the ligation into the expression vector pQE30Xa (Qiagen). This expression vector introduced a His-tag upstream of the N-terminal tail. The N-terminal tail of ANXA1 mediates the anti-inflammatory activities of the protein and contain protease-sensitive sites. *Escherichia coli cells* (SG13009 pREP4) (Novagen) were transformed with the vector. Cells were fermented in Luria-Bertani broth medium supplemented with Ampicillin (50ug/ml, Roche), Kanamycin (30ug/ml, Gibco) and 0.5% glycerol. ANXA1 expression was induced by incubating sub-confluent culture (optical density of >6) with of 5mM isopropyl β-D-1-thiogalactopyranoside (IPTG, Eurogentec). hrANXA1 proteins were purified using immobilized metal affinity chromatography. In order to verify that procedure yielded full-length recombinant protein, purified hr-anxA1 was subjected to structural analyses including Matrix Assisted Laser Desorption/ Ionization (MALDI TOF/TOF), silver stained SDS-PAGE and Western blotting and tryptic digestion. The analysis confirmed the production and purification of full-length hrANXA1 with a purity of >95%. Biological functionality of the N-terminal tail and Ca^{2+}-dependent phospho-lipid-binding C-terminal core were assessed by the calcium flux induced in FPR-2 transfected HEK-293 cells and ellipsometry, respectively (478).

Importantly it is not only the full-length ANXA1 molecule which has the ability to mediate its widespread effects; ANXA1's N-terminal derived peptides Ac2-26, Ac2-12 and Ac2-6 have also been reported to induce activation of FPR1 and FPR2 (479–481). However treatment is provided by using full length hrANXA1, as the dose required to induce biological function is up to 20 times less than that required by the peptide Ac2-26 (482) and 14 times less than that needed to induce gene expression changes (483). Furthermore, Ac2-26 peptide has a weak ability in reducing leukocyte adhesion unlike full-length hrANXA1 (484). Notably, the sequence homology of conserved and variable residues between mouse to human ANXA1 is 87%, making it viable for treatment use in mice (485).

3.1.1.3 Dietary intervention: Reversion to Chow Diet

Dietary intervention was provided by reverting mice fed a HFHS diet onto a chow diet. 10-week old male C57BL/6 mice were fed a HFHS diet for 10 weeks, after which mice were placed back on a chow diet for a further 5 weeks, the total dietary period for these mice was 15 weeks. Importantly, comparisons of this group have been made to mice given chow or HFHS-diet for 10 weeks and hence there is an element of age, which will be a confounder in these results. Chow, HFHS and HFHS + hrANXA1 mice were 20-weeks old at cull whereas HFHS – Chow reversion mice were 25-weeks old at cull.

Importantly, these mice were also treated with vehicle 100µl of 50mM Hepes, 140mM NaCl, pH 7.4, daily (5 times/week) i.p., similar to chow-fed and HFHS-fed mice for the first 10 weeks on the intervention. Summary of the HFHS – Chow reversion diet mice model is provided in Figure 3.3.

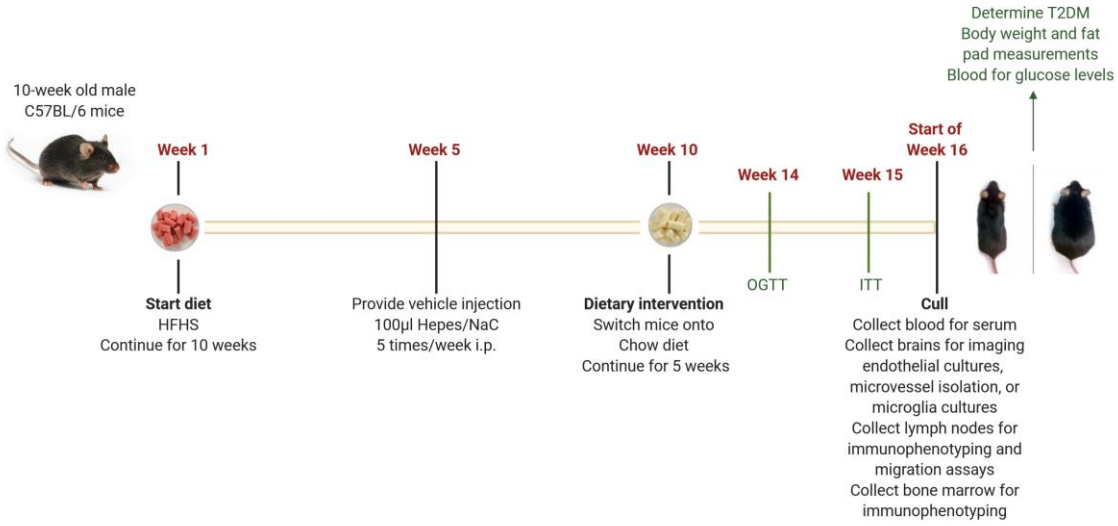

Figure 3.3 | Summary of the experimental model used to provide dietary intervention

10-week old male C57BL/6 mice were fed a HFHS for 10 weeks. From week 5, mice were injected with a sham injection of 100µL Hepes/NaCl, 5 times/week via intraperitoneal (i.p.) injection for 6 weeks. From week 10, mice were switched onto a chow diet for 5 weeks. Assessment for glucose tolerance and insulin resistance were conducted via oral glucose tolerance tests (OGTT) and insulin tolerance tests (ITT) respectively. Mice were culled at the beginning of week 16. Effect on T2DM was made by weight and various blood/serum analyses. At cull, blood, brain, lymph nodes and bone marrow were collected.

A summary of the 4 experimental groups has been provided in Table 3.3.

Table 3.3 | Experimental groups used to establish a mouse model of diet induced T2DM and the models used to provide a pharmacological and dietary intervention.

Group name and age	Diet and period of time	Treatment and period of time	Age at cull	Total number
Chow 10-week old male C57BL/6 mice	Chow from weeks 1 - 10	Vehicle of 100µl of 50mM Hepes, 140mM NaCl, pH 7.4, 5 times/week i.p. Given weeks 5-10	20 weeks	55
HFHS 10-week old male C57BL/6 mice	HFHS from weeks 1 - 10	Vehicle of 100µl of 50mM Hepes, 140mM NaCl, pH 7.4, 5 times/week i.p. Given weeks 5-10	20 weeks	55
HFHS + hrANXA1 10-week old male C57BL/6 mice	HFHS from weeks 1 - 10	**Pharmacological intervention of** 1µg hrANXA1 in 100µl of 50mM Hepes, 140mM NaCl, pH 7.4, 5 times/week i.p. Given weeks 5-10	20 weeks	55
HFHS - Chow reversion 10-week old male C57BL/6 mice	HFHS from weeks 1 - 10 Chow from weeks 11-15 **(dietary intervention)**	Vehicle of 100µl of 50mM Hepes, 140mM NaCl, pH 7.4, 5 times/week i.p. Given weeks 5-10	25 weeks	15

3.1.2 Measuring body weight and feeding behaviour

The body weight and food and calorie take of mice were measured at the beginning of each week to ensure good health and monitor feeding habits. Body weight was measured at the beginning of each week at the same time, using the same balance throughout the entire study. The body weight gain was calculated at the end of the study.

Fresh food (150 grams/cage) was also supplied at the beginning of each week and was regularly monitored through the week for colour or consistency change. The diet from each cage was weighed before being changed to measure food (g/mouse/day) and calorie intake (kcal/mouse/day) using the following equations (473):

$$\text{Food intake} = \frac{\text{weight of diet at beginning of week} - \text{weight of diet at end of week}}{(\text{number of mice in cage x number of days})}$$

$$\text{Calorie intake} = \text{food intake x } [\text{protein\%}, \text{x4} + \text{ fat \%}, \text{x9}, + \text{carb\%}, \text{x4})]$$

Note that energy (kcal/gm) – is the sum of decimal fractions of protein, fat and carbohydrate x4, x9, x4 kcal/gm respectively, where a gram of protein and carbohydrate give 4 calories and fat gives 9 calories.

3.1.3 Collection of blood, brain tissue, lymph nodes and bone marrow

For chow, HFHS and HFHS + hrANXA1 mice, culls were conducted at the beginning of week 11, when a full 10 weeks of diet manipulation had been completed. For HFHS – Chow reversion mice, culls were conducted at the beginning of week 16, when 15 weeks of dietary manipulation had been completed.

Mice were anaesthetised using a cocktail of xylazine (20mg/mL) and ketamine (100mg/mL) in a 1:2 ratio, given i.p. as a dose of 1.5mL/kg. The heart was revealed by cutting through both sides of the rib cage and the diaphragm, blood samples were collected by cardiac puncture of the left ventricle and the right atrium was cut to allow release of blood. Cardiac puncture was performed using a G25 BD hypodermic needle (BD Biosciences). Blood was washed out by perfusion of the left ventricle with 12ml 0.9% saline at 4°C given over 3 minutes. To perform the perfusion, the needle was left

in place after the cardiac puncture, and the syringe used to collect blood was removed and replaced with a syringe containing saline. An incision was made at both sides of the skull to reveal the brain. Brains were removed and placed in ice-cold $PBS^{-/-}$ containing 100 units/mL Gentamycin (Gibco) and 2.5µg/mL Amphotericin B (Gibco) on ice for endothelial primary culture isolation. For microglial isolation, brains were placed in ice-cold $PBS^{-/-}$ containing 1M Hepes, 45% D-Glucose and 10mL/L penicillin/streptomycin solution (All reagents from Sigma-Aldrich). Alternatively for tissue imaging each hemisphere of the brain was cut into 3 transversal slices, placed in 3mL of 2% paraformaldehyde (PFA, pH 7.4) and 0.2% glutaraldehyde (Sigma-Aldrich) in $PBS^{+/+}$ for 4 hours at 4°C. Brain slices were then washed several time in $PBS^{+/+}$ at 4°C and stored in 0.002% PFA in $PBS^{+/+}$. Blood was centrifuged at 9000g for 3mins at room temperature (RT) and the serum fraction (supernatant) was obtained. Lymph nodes were isolated from the superficial and deep cervical regions (Figure 3.3) and stored in ice-cold 0.01M PBS for lymphocyte isolation. Mouse femurs were harvested for bone marrow collection and stored in 0.01M PBS. The adiposity of the mice was measured, by collecting epididymal and inguinal fats pads. These were weighed using the same balance throughout the entire study and presented as a percentage of the total body weight of the mouse. The fat pad measurements along with the overall body weight helped to determine obesity.

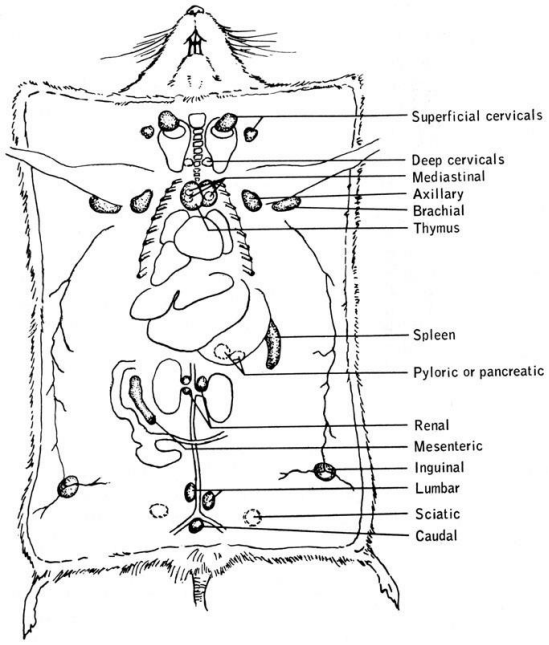

Figure 3.4 | Figure to show location of lymph nodes in rodent

Deep cervical lymph nodes were collected. Figure taken from (486).

3.1.4 Measurement of glucose, insulin and lipid levels

T2DM is characterised by hyperglycaemia arising due to the loss of insulin sensitivity. Initially, β-cells try to combat increased glucose levels by producing more insulin however when the β-cells cannot maintain this production, impaired glucose tolerance and insulin resistance develops (379).

The Oral Glucose tolerance tests (OGTT) is the only means of identifying impaired glucose tolerance and is widely used in literature as means of testing for T2DM. It should be noted that even a relatively simple procedure such as the OGTT also has little consensus on a specific protocol, with variables such as length of fasting period, glucose dose and route of administration affecting outcome; making direct comparisons between studies complicated (487). Therefore, the protocol per study should be carried out in the same procedure. A period of fasting is required before glucose administration which can be given either via an oral bolus or i.p.; fasting is required to provide a stable baseline blood glucose level. Fasting periods are either over night for approximately 16 hours or starting in the morning for approximately 6 hours (487). Overnight fasting has the advantage of producing a low and stable baseline blood glucose however overnight fasting is not often ideal as mice, due to their nocturnal nature (488,489). Nocturnal animals consume most of their calories overnight, this coupled with a high metabolic rate as seen in mice means an overnight fast can often induce a state of starvation rather than fast because of the relatively long period in which mice are food deprived (490). Overnight fasting in mice can also increase insulin sensitivity (491). Administration of glucose can be via oral gavage or a single i.p. injection; both routes are considered appropriate methods for administration. Dynamically, peak plasma is reached more quickly in response to oral glucose at 15 minutes compared to 30 mins with i.p. injection (490). The dose administered for OGTT is typically either 1 or 2g/kg, it should be noted that insulin resistance may only be revealed in response to higher glucose loading (490).

Although OGTT tests are often considered to be adequate to monitor glucose tolerance and insulin resistance (490), often some form of insulin measurement is also provided to complement the measurements of glucose tolerance (487). Similar to the OGTT, an insulin tolerance test (ITT) is often used in literature. The ITT involves monitoring

blood glucose in response to insulin administration that can only be administered as an i.v. or i.p. injection. Typically, a 6 hour fasting is preferential to an overnight fast to prevent hypoglycaemia (487).

Taking the above into account, OGTTs and ITTs were conducted prior to termination of animals using the following protocol to determine glucose tolerance and insulin resistance. The mice were fasted for 6 hours (8am – 2pm) by being moved to clean cages with no food but with free access to water. At the end of 6 hour feeding period, the body weight of each mouse was measured. A small incision was made to side of the tail to obtain blood. Fasting blood glucose was measured, followed by administration of an oral bolus of glucose (2g/kg in PBS) or insulin (1unit/kg in PBS). Blood glucose was measured via the tail vein puncture at 15-minute intervals for a total duration of 120 minutes using a glucometer (Accu-Chek Compact System; Roche Diagnostics, Basel, Switzerland), and expressed as a time course of absolute blood glucose measurements and area under the curve (AUC). Non-fasting blood glucose values were obtained using a glucometer immediately after cardiac exsanguination. Non-fasted and fasted blood glucose levels allow for the determination of hyperglycaemia. Compensatory hyperinsulinemia often occurs in response to hyperglycaemia in an attempt to maintain fasting glucose combat insulin resistance (380). ELISA kits were used to measure serum levels of insulin (ThermoFisher Scientific), cholesterol (Abcam Plc.) and triglycerides (Abcam Plc.) for the determination of hyperinsulinemia and dyslipidaemia.

3.1.5 $CD4^+$ T-cell isolation and expansion

Isolated lymph nodes were placed on a 70µm cell strainer (Fisher Scientific) placed over a 50mL falcon tube. Lymph nodes were kept wet with $PBS^{-/-}$. The lymph nodes were homogenized using a total of 5mL $PBS^{-/-}$. Isolated lymphocytes were centrifuged at 1800rpm for 5 minutes at 4°C, the supernatant was discarded, and the cell pellet was re-suspended in 3mL 0.01M PBS. The number of cells were counted and seeded on a 24-well plate (Corning) at a density of $1x10^6$ cells/well. For stimulation of $CD4^+$ T-cells, plates were previously coated with 1µg/mL of anti-CD3 (E-bioscience) and 5µg/mL of anti-CD28 (E-bioscience) diluted in 50mM Tris (pH 8.5) in a volume of 200µl/well for 1 hour at 37°C. The coating solution was removed and the isolated cells

were suspended in 1mL of RPMI medium supplemented with 10% fetal bovine serum (FBS), 2mM Glutamine, 10mM HEPES, 1mM Sodium Pyruvate, 50µM β-mercaptoethanol and 100 units/ml Gentamycin containing 10ng/mL IL-2 (Roche, all other reagents Gibco). Cells were expanded for 5 days for transmigration assays or for flow cytometric analysis.

3.1.6 Bone marrow isolation

Mouse femurs were flushed several times with 1mL 0.001M $PBS^{-/-}$. To lyse out red blood cells, 4mL of 1X cold lysis solution (155mM NH_4Cl, 12mM NaHCO3, 0.1mM EDTA) was added to 1mL of PBS-cell fraction. The PBS-cell fraction was placed on a rocking platform for 10 minutes at RT, followed by centrifugation for 10 minutes at 250g at 4°C. The supernatant was discarded, and the cells were washed in FACS buffer (2% FBS in $PBS^{+/+}$) for a further 10 minutes at 250g at 4°C. The supernatant was discarded, and the cells were re-suspended in 1mL of FACS buffer. The cell solution was divided equally into FACS tube ready for staining. Antibodies are listed in Table 3.7

3.1.7 *In vivo* administration of Evans Blue dye

Evans blue dye extravasation is an effective technique to analyse permeability changes occurring *in vivo*. This method relies upon small molecules of Evans blue binding to serum albumin present in blood; a small proportion remains uncoupled (0.11%-0.31%) (492). Evans blue dye has a molecular weight of 961Da and is highly soluble (280g/L), it specifically binds to serum albumin both *in vivo* and *in* vitro and therefore becomes a high molecular weight protein tracer of 69kDa (492–494). When injected, either i.v. or i.p., albumin-bound Evans blue dye remains stable in the blood, the dye distributes throughout the body and stains the animal with an intense blue colour (495). Under normal conditions, the endothelium of the BBB restricts the entry of the dye, however under certain stimuli or damage which disrupts the tightness of the BBB, the leakage of the dye into the brain parenchyma increases via a paracellular route (496,497). It is the increased presence of Evans blue dye into the brain that is a measure of disrupted BBB integrity.

To measure Evans blue dye leakage in the study, mice were placed in a warming chamber for 5 minutes to dilate the tail vein to facilitate i.v. injection of 100µl of 2% Evans blue dye in 0.9% saline. The dye was allowed to circulate for 1 hour for diffusion from the circulation to tissues, after which mice were anaesthetised. Cardiac exsanguination and perfusion were performed, as described in section 3.1.3. Brains were isolated, sliced into two hemispheres and stored in 0.01M PBS on ice for permeability assessment.

3.1.8 Evans blue detection in brain homogenates and serum samples

The following protocol was adapted from previously published methods (495,498). Brain hemispheres collected after *in vivo* Evans blue dye administration were weighed and homogenized through maceration. 2.5mL of 60% tricholoracetic acid (TCA) in dH_2O was added to each homogenized tissue preparation, samples were mixed and incubated on ice for 30 minutes. Samples were centrifuged at 1000g for 30 minutes at 4°C, 200µL of the supernatant was assessed using a spectrophotometer at 620nm (Infinite M200 PRO plate reader, TECAN). The serum was obtained from blood samples taken from the mice as described in section 3.1.2. Serum samples were also analysed spectrophotometrically in a 1:40 dilution with 0.9% saline in a final volume of 200µl. Final values were normalized to tissue weight and expressed as percentage of serum dye content. BBB integrity loss is signified by a greater percentage of Evans blue dye leakage into the brain.

$$\frac{(\mu g \text{ of dye in brain}) \,/\, (\text{mg of tissue})}{(\mu g \text{ of dye in serum})} \text{ x } 100$$

3.1.9 Culturing of primary mouse brain microvascular endothelial cells (pMBMECs)

pMBMECs were cultured from all mice groups – Chow, HFHS, HFHS + hrANXA1 and HFHS – Chow reversion mice. In addition, pMBMECs were also cultured from a group of 6-week old chow-fed mice. This group was compared against the 20-week old chow mice group, to assess the effect of age. The results from this experiment can be found in Chapter 4.

The following volumes are calculated for isolation of endothelial cells from a total of 10 mice brains. Isolated whole brains were placed on sterile chromatography paper. The brain stems, cerebellum and thalamus were removed with forceps and the meninges were detached by gentle rolling. The remaining brain tissue was cut into 1mm pieces with a scalpel and transferred to a 50mL falcon containing 12.5ml DMEM/F12 (ThermoFisher), 1.5mL 10mg/mL collagenase II (Sigma) and 200µl 1mg/mL DNase I (Sigma). The brain tissue was mixed thoroughly using a 5mL pipette and incubated at 37°C in a shaker (200rpm) for 55mins to generate a milky-looking homogenate. Following incubation, 10mL DMEM/F12 was added and the mixture was centrifuged at 1000g for 8mins. The supernatant was removed and 10mL 20% BSA-DMEM/F12 was added to the cell pellet, mixing thoroughly with a 5mL pipette; the mixture was centrifuged at 1000g for 20mins at 4°C. After centrifugation, the myelin layer at the top containing neurons, glia and the BSA-DMEM/F12 solution was transferred into a 15mL falcon and shaken vigorously before centrifuging again at 1000g for 20mins at 4°C. This process was repeated 3-4 times. The cell pellets (whitish-red in colour) containing the microvessels were stored on ice.

For obtaining brain microvessels for proteome analysis (section 3.2.8), the brain microvessels pellets were pooled into a single eppendendorf and stored in 1mL of radioimmunoprecipitation assay (RIPA) buffer containing inhibitors (1µg/mL aprotinin, 1µg/mL leupeptin, 1mM PMSF, 1mM NaF, 1mM Na_3VO_4). Pellets were stored at -80°C until required. Protein quantification was determined before use for experiments (described in section 3.2.9).

For obtaining pMBMECS for culture, the brain microvessel pellets were pooled into a single falcon tube and further digested in 7.5mL DMEM/F12, 833µl 10mg/mL collagenase-dispase (Roche) and 83µl 1mg/mL DNase I. The brain vessels were mixed with a 1mL pipette and incubated at 37°C in a shaker (200rpm) for 35mins to generate a reddish-pink fluid. Following incubation, 10mL DMEM/F12 was added to the mixture and centrifuged at 700g for 6mins, the washing step was repeated, and the cells were ready to plate. pMBMECs were plated in 35mm culture dishes (Falcon); 1 dish was used for every 2-3 mice. The surface of the culture dishes were coated with 500µl of 0.2% Rat Tail Collagen I (Corning) in $PBS^{-/-}$, the coating was pipetted up & down 10 times to ensure whole surface coverage and the solution was transferred to the next dish. The plates were allowed to dry in a 5% CO_2 incubator for approximately 3 hours prior to plating cells.

pMBMECs were initially cultured in DMEM/F12 supplemented with 15% FBS, 1ng/mL basic fibroblast growth factor (bFGF, Roche), 100µg/mL heparin (Sigma), 1 x Insulin-Transferrin-Selenium (ITS, Gibco), 4µg/mL puromycin (Sigma) and 100 units/ml Gentamycin. Cells are grown at 37°C in a 5% CO_2 incubator. Fresh medium was added on day 3 containing only 10% FBS and from day 4, medium was prepared without puromycin. Puromycin is initially supplemented into the medium in order to obtain a pure monoculture. Cells reach confluency between days 5-7, however cells are used for experiments or passaged at 75% confluency (around day 4). For passaging, cells were washed twice with $PBS^{-/-}$ followed by incubation with 200µl/dish 0.25% Trypsin at 37°C for 2-3 minutes. Growth medium was added in a 1:4 ratio to trypsin to inhibit the action of trypsin, cells were counted using a disposable haemocytometer (Kova International). Further passages were plated at a density of $7\text{-}8x10^4$ cells/cm^2. pMBMECs were used at p1.

3.1.10 Culturing of primary mouse microglia cells

The following volumes are calculated for isolation of microglia cells from a total of 10 mice brains. Isolated brains were placed into a sterile petri dish; brain tissue was cut into 1mm pieces with a scalpel and transferred to a 50mL falcon containing ice-cold $PBS^{-/-}$. Tissue fragments were centrifuged at 300g for 2 minutes at 4°C and the supernatant discarded. The fragments were mixed thoroughly using a 5mL glass pipette in 20mL of enzyme buffer ($PBS^{-/-}$, 10ml/L penicillin/streptomycin solution, 1M Hepes, 30% BSA, 0.5mg/ml DNAse1, 5mM L-Cysteine (Sigma-Aldrich) and 1.5 units/mL papain and incubated at 37°C in a shaker (200rpm) for 30 minutes. After incubation, the cell suspension was passed through a 40µm strainer (Fisherbrand Scientific) rinsing with warm $PBS^{-/-}$. The cell suspension was centrifuged at 300g for 10 minutes at 20°C, the supernatant was discarded and the pellet re-suspended in 20mL of myelin removal buffer (0.9M sucrose in $PBS^{+/+}$), followed by further centrifugation at 300g for 10 minutes at RT. Stock isotonic percoll (SIP) was used to separate microglial cells using density dependent centrifugation; SIP was prepared at 30% and 70% gradients in Hanks balanced salt solution (HBSS,). The cells were washed in $PBS^{-/-}$ and re-suspended in ice-cold 70% SIP (3.5mL/brain) and distributed across 15mL falcons (one/brain). An overlay was created, first using 5mL ice-cold 30% SIP and then 3mL ice-cold PBS. The cells were centrifuged at 800g for 30 minutes at 4°C, removing the brake to avoid disruption of the interphase containing microglia. The microglia cells were collected using pasteur pipettes at the 25/75 interphase and diluted with 3X ice-cold PBS, followed by centrifugation at 1000g for 10 minutes at RT. The pellet was suspended in warm medium (1mL/brain) and plated at a density of 3×10^5 cells/well in 24 well plates. Microglia cells were cultured in DMEM with L-glutamine, 20% FBS, 100units/mL gentamycin and 50ng/mL M-CSF (Gibco) and maintained at 37˚C in 5% CO_2. Microglia were allowed to adhere for 3 hours, after which fresh medium was given. Medium was changed every 2-3 days thereafter. Microglia cells were used for experiments between days 7-10.

3.2 *In vitro* methods

3.2.1 Origin of bEnd3 cell line

All *in vitro* studies examining the effect of mice sera on the BBB have used the mouse brain-derived endothelial cell line – bEnd3. The cell line was established by W. Risau (Max-Planck Institute) through transformation of primary brain endothelial cultures obtained from BALB/c mice with the NTKmT retrovirus vector expressing polyomavirus middle T antigen coding for the Polyoma virus middle T oncogene (499). bEnd3 cells are commercially available and were purchased from The European Collection of Authenticated Cell Cultures (ECACC), Public Health, England.

3.2.2 Routine cell culture of bEnd3 cell line

bEnd3 cells were cultured in DMEM 1g/L D-glucose culture medium (Gibco) supplemented with 10% FBS, 4mM Glutamax, 100 units/mL Gentamycin, 50µM β-Mercaptoethanol, 1mM Na-Pyruvate and 1x non-essential amino acids. Expansion of cells was carried out in T75 flasks at a plating density of 4 x 10^6 cells, in a 5% CO_2 incubator at 37°C; previously coated with gelatin solution (Gibco), diluted 1:20 in $PBS^{-/}$. Cells were checked daily for confluency and passaged approximately every 4-5 days when they had reached the log phase of their division. bEnd3 passages 24-34 were used throughout the study.

3.2.3 Thawing, Passaging & Cryopreservation of cell lines

Frozen stock vials were stored in liquid nitrogen. Cells were thawed using warmed culture medium and centrifuged at 1800rpm for 5 minutes to remove the dimethyl sulfoxide (DMSO). The supernatant was aspirated, and fresh medium was added to resuspend the pellet, which was transferred to a T75 flask. Fresh medium was replaced 24 hours after thawing and every 2-3 days after.

For passaging, cells were first washed in $PBS^{-/-}$ followed by incubation with 1.5ml 0.25% Trypsin at 37°C for 2-3 minutes. Growth medium was added in a 1:4 ratio to trypsin to inhibit the action of trypsin, cells were counted using a disposable haemocytometer and harvested at 1800rpm at RT for 5 minutes. The pellet was resuspended in fresh medium and transferred into a T75 flask. Any cells not required

for experiments or for culturing, were cryopreserved using 10% DMSO in FBS. Cells were stored in cryovials (Nalgene) in a freezing container at -80°C for 24 hours after which vials were transferred to -196°C liquid nitrogen tank.

3.2.4 Stimulation of cell lines with serum or inflammatory mediators

Any experimental studies using bEnd3 cells were stimulated overnight with decomplemented 10% mouse serum in place of FBS in the culture medium. Serum stimulation was used to model the effect of peripheral mediators on the BBB. All serum was decomplemented for 20 minutes in a 56°C water bath prior to use.

3.2.5 Paracellular permeability assay

The paracellular permeability of pMBMECs and bEnd3 serum-stimulated cells was assessed using the fluorescent marker protein fluorescein isothiocyanate (FITC)-dextran, MW 55-77kDA (Sigma-Aldrich).

The assay was conducted using transwell polyester membrane inserts (Corning, pore size 0.4 μm, membrane diameter 12 mm) coated with 200μL of laminin (50ug/mL, Sigma) diluted in $PBS^{-/-}$ for 30 minutes in a 5% CO_2 humidifier at 37°C. Cells were harvested and seeded on the top compartment of the transwells in 500μL culture medium; 700μL culture medium was added to the bottom compartment of each transwell. Cells were allowed to reach confluency (3-4 days) after which the medium was changed. The cells were left for another 3-4 days to allow full tight junction formation. Fresh medium was only replaced every few days to prevent shear stress.

Prior to assessment using FITC-dextran, cell lines were stimulated overnight with 500μL medium containing 10% mouse serum. Cell-free transwells were served to measure the resistance of the plastic filter alone to paracellular movement of molecules.

After 24 hour stimulation, the medium from the top compartment was aspirated and replaced with 500μL FITC-dextran (3mg/mL) dissolved in transport buffer (2% FBS in DMEM 4.5g/L glucose without phenol red). Each set of transwells were transferred to a new 12-well plate (Corning) containing 1.5mL of transport buffer and incubated in a 5% CO_2 incubator at 37°C. Every 10 minutes, the insert was moved to the next

row of wells, containing 1.5mL transport buffer for a total duration of 60 minutes. At the end of the 60 minutes the filters were removed and the fluorescence of each well measured to determine the amount of diffused FITC-dextran. Refer to Figure 3.4 for a schematic representation of the assay. Fluorescence was measured using a spectrophotometer (Tecan Infinite M200 Pro, Tecan, Austria) at excitation wavelength 485nm and emission wavelength 535nm. The endothelial permeability coefficient (Pe) was calculated in cm/min as previously described (297,500,501). Briefly, the clearance principle was used to define the concentration-dependent transport parameter. The cleared volume ([V]cl) for each time interval was calculated using the following equation:

$$[V]cl = \frac{[C]l \times [V]l}{[C]u}$$

Where [C]u represents the fluorophore concentration on the upper chamber, while [V]l and [C]l represents the volume and the fluorophore concentration in the lower chamber, respectively. The concentration values of the lower chamber were calculated by plotting a standard curve of known amounts of FITC-dextran. An increment of cleared volumes was plotted against time of measurement (60 minutes). The slope of the linear curve the proportionally represents the permeability properties of the monolayer and defines PS, the permeability surface area. The PS indicates the resistance opposed to the clearance:

$$\text{PS (permeability surface area)} = \text{slope}$$

The total resistance opposed to the passage of the dye is the sum of the resistance offered by the monolayer and the resistance offered by the filter:

$$\text{Total resistance of PS (PS TOT)} = \text{PS monolayer} + \text{PS filter}$$

Therefore, PS monolayer can be calculated by subtracting PS filter from PS TOT.

The permeability coefficient (also called conductance) is defined as the inverse of the resistance, the permeability coefficient of the endothelium (Pe) can be calculated as follows:

$$\mathrm{Pe} = \mathrm{PS\ TOT} - \mathrm{PS\ filter} = \frac{1}{\mathrm{PS\ TOT}} - \frac{1}{\mathrm{PS\ filter}}$$

Pe was calculated in unitary value cm/min (500,501).

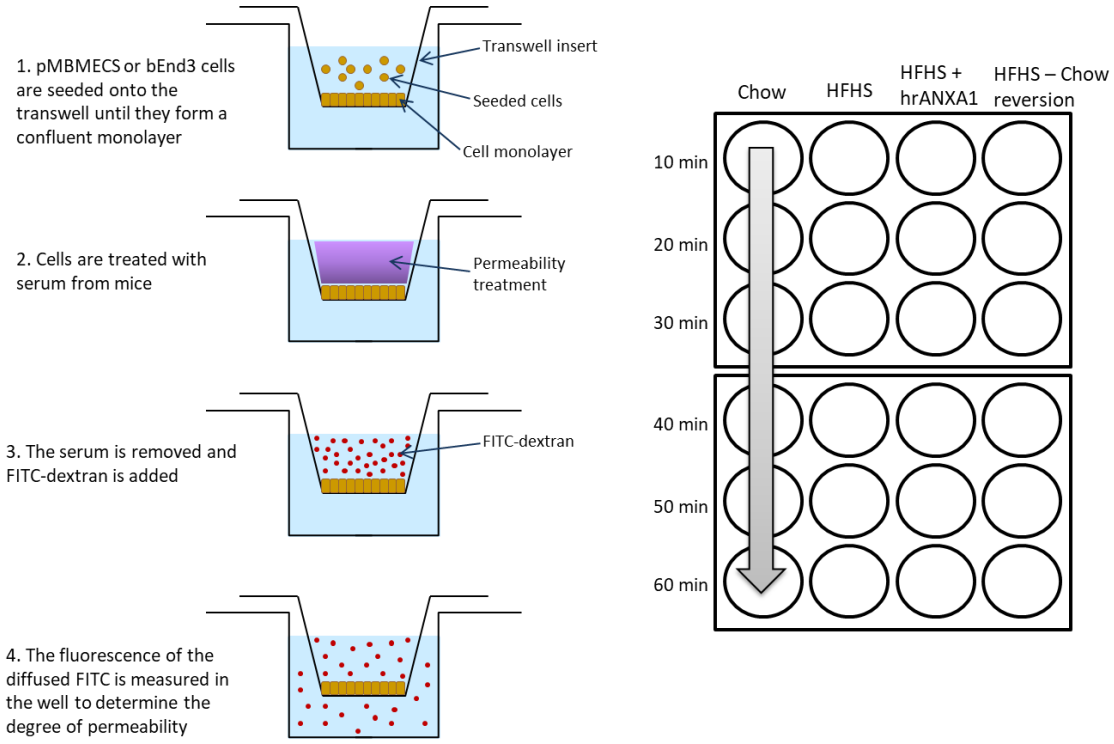

Figure 3.5 | Representation of the permeability assay performed using 55-77kDA FITC-dextran

3.2.6 Transendothelial electrical resistance (TEER)

The TEER is another measure of permeability, it provides an indication on the tightness of the endothelium barrier. TEER measurements were performed on the same transwells as described in the paracellular permeability experiments. The TEER was measured 3 hours prior to the paracellular permeability assays to allow the monolayers to resettle. TEER was measured using the Epithelial Volt/Ohm (EVOM2) Meter (World Precision Instruments, USA) consisting of two electrodes. One electrode is place in the upper chamber of the transwell and the other electrode is place in the lower chamber allowing the two electrodes to be separated by the endothelial layer. Electrical resistance was expressed as Ohms/cm^2 (Ω/cm^2). Collagen-coated cell-free resistance values were subtracted from the values of obtained in the presence of endothelial cells.

3.2.7 Transmigration assays

Polycarbonate transwell inserts (24-well, 0.33cm^2 surface area, pore size 5µm; Sigma-Aldrich, UK) were coated with 50µg/mL laminin. Cells were seeded on the top compartment of the transwells and cultured in 200µL medium for 72 hours to allow confluent monolayers to form; no medium was added to the bottom compartment. On the day of the assay, 600µl of complete medium was added to the bottom compartment of the transwells. 1 x 10^6 mouse leukocytes were added per tranwells were added to the top compartment and incubated for 4 hours at 37°C in 5% CO_2. After 4 hours, inserts were removed, and the entire volume of the bottom compartment was collected to assess the transmigrated lymphocyte population. Lymphocytes adhered to monolayers were collected by washing inserts with 100µl $PBS^{-/-}$ to remove non-bound cells, followed by 50µL 5mM EDTA for 5 minutes. Cells recovered in the EDTA washing step were considered the adherent cell population. Adherent and migrated cells were stained with mouse antibodies as shown in Table 3.7 and analysed via flow cytometry. To standardise the result collection, all samples were run at the flow cytometer for a period of 2 minutes as oppose to setting an x number of events to be collected.

3.2.8 Proteome analysis – cytokine analysis

The Mouse Cytokine Array XL Kit (R&D Systems) was used to analyse 111 different cytokines, chemokines and acute phase proteins using mouse serum or mouse brain microvessels. The kit is a membrane-based sandwich immunoassay. The kit contains nitrocellulose membranes onto which capture, and control antibodies have been spotted in duplicate. Each membrane was blocked for 1 hour on a rocking platform at RT with blocking buffer. After 1 hour, the block buffer was removed and replaced with the different samples. For serum 200µL/sample was used and for tissue lysates 200µg/sample was used; the final volumes of the samples/membrane were made up to 1.5mL in blocking buffer. Samples were incubated overnight at 4°C on a rocking platform. Following overnight incubation, the membranes were washed 3 times in wash buffer for 10 minutes each. For each membrane, 30µL of detection antibody cocktail was added to 1.5mL of 1X Array buffer 4/6 (provided in kit). The detection antibody was incubated for 1 hour on a rocking platform at RT followed by a series of 3 washes. Next 2mL of 1X Streptavidin-HRP was added to each membrane followed by a series of 3 washes. For detection, the Chemi Reagent mix was prepared and 1mL of the mix was added to each membrane for 1 minute. Membranes were exposed to x-ray film for multiple exposure times between 1-15 minutes. Signal was produced at the different capture sports which corresponded to the amount of protein bound. Negative control spots were used for background subtraction. Image Studio™ Lite (LI-COR Biosciences, USA) software was used to analyse the data.

Mouse serum analysis of TIMP-1 was additionally measured using a quantikine ELISA kit (R&D systems).

3.2.9 Protein extraction and quantification

Protein concentration was determined by homogenising cells or brain microvessels with RIPA buffer containing inhibitors. Plated cells were homogenised using a multichannel pipette, vortexed for 1 minute on a plate shaker at 200rpm followed by centrifugation at 2500rpm for 15 minutes at 4°C and the supernatant collected. Brain microvessels stored at -80°C in RIPA buffer were thawed, and homogenised using a homogeniser (Omni Int, USA), centrifuged and the supernatant was collected.

To determine the protein concentration the bicinchoninic acid method (BCA) was applied, using the Pierce BCA Protein Assay Kit (ThermoFisher Scientific). The assay is based on the principle that under alkaline conditions copper Cu^{2+} ions form a complex with peptide bonds of proteins and are reduced to Cu^{+}. The BCA reagent is highly stable and specific for this purpose and forms a purple compound when reduced whose intensity is proportional to the amount of protein present in the sample.

A calibration curve was constructed using albumin standard samples containing 2mg/ml of bovine serum albumin (BSA). Concentrations of 1mg/mL, 0.8mg/mL, 0.6mg/mL, 0.4mg/mL and 0.2mg/mL were made up with RIPA buffer. In a 96-well ELISA plate (Nunc MaxiSorp, ThermoScientific, UK), 20µL of the standard curve or 20µL or each sample were plated. BCA Reagent A and BCA Reagent B were mixed in a 1:50 ratio and 200µL of the reagent solution was added to each well containing the standard curve or samples. The plate was placed in 37°C incubator for 10 minutes after which the values were read using a spectrophotometer at 562nm. The concentration value was extrapolated using the standard curve.

3.2.10 Zymography

Zymography is an electrophoretic technique used for measuring proteolytic activity. Gelatin zymography was used for the detection of gelatinases MMP-2 and MMP-9 in brain microvessels. For each sample, 1µg/lane was loaded for separation by non-reducing gel electrophoresis on a 7.5% acrylamide gel containing 1mg/mL porcine skin gelatin (Sigma). After electrophoresis, the gel was washed extensively with 50mM Tris-HCL containing 2.5% Triton X-100, 5mM $CaCl_2$ and 1µM $ZnCl_2$ to remove SDS. During this step, the enzymes partially renature and recover their activity. Subsequently the gel was incubated overnight in activation buffer (50mM Tris-HCl containing 1% Triton X-100, 5mM $CaCl_2$ and 1µM $ZnCl_2$) at 37°C. During this incubation, the concentrated renatured MMPs will digest the substrate. After incubation, the gel is stained in Coomassie brilliant blue, the MMPs are detected as clear bands against a blue background of undegraded substrate. Images were acquired with a ChemidocMP imaging system (Bio-Rad) and analysed using ImageJ (NIH).

3.3 Immunofluorescence & Immunophenotyping

3.3.1 Immunofluorescence on tissues

Brains were collected from mice, fixed and stored (described in section 3.1.2) until ready for staining. Fixed brain tissue was cut using a vibratome (Leica Microsystems) into 30-35µm thick sagittal sections at 200µM internals. Brain slices were stored in 0.002% PFA in PBS at 4°C. Approximately 60-120 sections/hemisphere were cut using the vibratome. Staining was carried out in an IF chamber that was kept moist at all times. First, tissue slices were permeabilised using 0.5% Triton X-100 in $PBS^{+/+}$ for 40 minutes at RT followed by 3 washes using $PBS^{+/+}$. Next tissue slices were blocked with immunofluorescence buffer (1% BSA & 2% FBS in $PBS^{+/+}$ for 40 minutes at RT. Primary antibody staining was carried out using 200µL immunofluorescence buffer overnight at 4°C, tissues sections were washed 3 times using $PBS^{+/+}$ and the secondary antibody was added in 200µL immunofluorescence buffer for 40 minutes at RT. Following a further 3 washes using $PBS^{+/+}$, sections were counterstained for nuclei using TO-PRO3. Finally, the sections were mounted on SuperFrost slides (Menzel). Vectashield coverslips were applied using mounting medium (Vector Laboratories). Slides were allowed to cure overnight at RT, for long-term storage, slides were stored at 4°C. Antibodies used are shown in Table 3.4 and Table 3.5.

Sections were examined using a confocal laser scanning microscope Leica TCS SP5 (Leica Microsystems) using a sequential scan procedure. Confocal images were taken at 0.35µm intervals through the x-, y-, and z- axes of the section with 40x and 63x oil lenses. Fluorescence intensity analysis was performed by two independent observers on ten randomly selected fields at the 63x magnification using Cell F image analysis software (Olympus Italia).

Table 3.4 | Primary antibodies used to stain mouse cerebral cortical brain sections

Primary Abs	Host species	Dilution Factor	Supplier	Catalogue Number
Claudin-5	Mouse	1:100	Invitrogen	35-2500
Occludin	Mouse	1:100	Invitrogen	33-1500
Pan-laminin	Rabbit	1:100	Sigma-Aldrich	L9393
Laminin α4	Mouse	1:1000	Novus Biologicals	NBP-42393
Laminin α1	Rabbit	1:1000	LifeSpan BioSciences	LS-C119557
GFAP	Rat	1:100	Invitrogen	I3-0300
ICAM-1	Rat	1:100	Novus Biologicals	NBP2-12360
P-selectin	Rabbit	1:100	LifeSpan BioSciences	LS-B3578
CD45	Rat	1:100	Bio-Rad	MCA
Iba1	Goat	1:100	Abcam	ab5076
iNOS	Mouse	1:1000	BD Biosciences	610329

Table 3.5 | Secondary antibodies used to stain mouse cerebral cortical brain sections

Secondary Abs	Fluoro-chrome	Dilution Factor	Supplier	Catalogue Number	Primary antibody combination
Goat anti-mouse IgG	AF488	1:500	Invitrogen	A11001	Claudin-5, Occludin, Laminin α4 & iNOS
Goat anti-rabbit IgG	AF488	1:500	Invitrogen	A11070	P-selectin
Goat anti-rat IgG	AF488	1:500	Invitrogen	A11006	ICAM-1
Goat anti-rabbit IgG	AF568	1:500	Invitrogen	A11011	Pan-laminin & Laminin α1
Donkey anti-goat IgG	AF568	1:500	Invitrogen	A11057	Iba1
Goat anti-rat IgG	AF555	1:500	Invitrogen	A21434	GFAP & CD45

3.3.2 Flow Cytometry - Fluorescence-activated cell sorting (FACS)

Collected cells were placed in FACS tubes and washed using FACS buffer (2% BSA in $PBS^{+/+}$); samples were vortexed and centrifuged at 1800rpm for 5 minutes at 4°C. The supernatant was discarded, and the cells were fixed using 100µL of 2% PFA for 10 minutes at RT. Cells which required live-imaging e.g. for metabolism monitoring were not fixed, but instead staining was carried out on ice. Fractions were topped up 200µL of FACS buffer vortexed and centrifuged at 1800rpm for 5 minutes at 4°C. The supernatant was discarded, and antibody staining was conducted.

3.3.2.1 Cell surface staining

Samples which were being stained for cell surface markers were stained using a primary antibody in 100µL of FACS buffer/tube; cells were incubated in the dark at RT for 20-30 minutes. After 20-30 minutes, each of the tubes was topped up with 300µL FACS buffer and centrifuged as before. Any primary antibodies that were not conjugated, required secondary antibody staining. This was carried out in 100µL of FACS buffer/tube; cells were incubated in the dark at RT for 20-30 minutes. After 20-30 minutes, each of the tubes was topped up with 200µL FACS buffer and centrifuged as before. Antibodies used are shown in Table 3.6 and Table 3.7.

3.3.2.2 Intracellular staining

Cells that were stained for intracellular markers required permeabilisation to open up the cellular membrane. Any cell surface marker staining was conducted prior to permeabilisation.

The BD Bioscience Mouse FoxP3 buffer kit was used for permeabilisation. The permeabilisation buffer was diluted 1:5 in $PBS^{-/-}$ and 200µL of permeabilisation buffer was added to each tube, vortexed and incubated for 30 minutes in the dark at RT. After 30 minutes, 2mL of FACS buffer was added to each tube, vortexed and centrifuged at 1800rpm for 5 minutes at 4°C. The supernatant was discarded, and antibodies were added in 100µl of FACS buffer/tube; cells were incubated in the dark at RT for 20-30 minutes. After 20-30 minutes, each of the tubes was topped up with 200µL FACS buffer and centrifuged as before.

Once all staining was conducted, cell pellets was re-suspended in 200µL of $PBS^{+/+}$ ready for FACS analysis; tubes were stored at 4°C. Analysis of flow cytometry was performed using a BD LSR Fortessa (BD, Biosciences). Compensation was conducted and applied to panels to ensure there was minimal spectral overlap. In general, approximately 100,000 viable cells were collected from all samples, after which a gating strategy was applied. FlowJo (BD Biosciences, UK) was used to analyse data. Data was presented as median intensity of fluorescence (MFI), as cell percentages or whole cell numbers. Antibodies used are shown in Table 3.8.

Table 3.6 | Antibodies used to stain for cell surface markers

Primary Antibody	Fluorochrome	Dilution factor	Supplier	Catalogue Number
Ly6G	FITC	1:200	Abcam	ab25024
F4/80	PE-Cy7	1:200	Biolegend	123114
CD11c	APC-Cy7	1:200	Biolegend	117311
CD11b	PE-Cy7	1:200	Biolegend	101208
NK1.1	BV421	1:200	Biolegend	108731
CD45	APC-Cy7	1:200	Biolegend	103116
CD3	-	1:200	eBioscience	10-0032-85
CD4	PE-Cy7	1:200	Biolegend	552775
CD8	BV450	1:200	Biolegend	100741
CD19	APC	1:200	eBioscience	17-0193-82
CD25	BB515	1:200	BD Horizon	564424
CD44	BV421	1:200	BD Horizon	563970
LFA1	PE	1:200	eBioscience	12-0111-82
CXCR31	PE	1:200	Biolegend	126505
CD62L	BB515	1:200	BD Horizon	565261
CCR7	AF647	1:200	BD Pharmingen	560766
CX3CR1	BV711	1:200	Biolegend	149031
MHC II	BV421	1:200	Biolegend	107631
CD86	PE-Cy7	1:200	Biolegend	105116
CD206	BV785	1:200	Biolegend	141729
ICAM-1	APC	1:100	Biolegend	116119
VCAM-1	Pacific blue	1:100	Biolegend	105722
Occludin	AF488	1:100	ThemoFisher Scientific	33-1500
PECAM-1	AF488	1:100	eBioscience	11-0311-81
VE-Cadherin	-	1:100	Abcam	ab33168
CD220	APC	1:100	R&D Systems	FAB1544A
GLUT-1	-	1:100	Abcam	ab653
Pgp transporter	AF488	1:100	Invitrogen	MA1-26528

Table 3.7 | Secondary antibodies used for FACS

Secondary Antibody	Fluoro-chrome	Dilution factor	Supplier	Catalogue Number	Primary Antibody combination
Goat anti-mouse IgG	AF488	1:100	Life Technologies	A11001	VE-Cadherin
Goat anti-mouse IgG	Pacific Orange	1:100	Invitrogen	p31585	CD3
Goat anti-rabbit IgG	Cy3	1:100	Abcam	ab6939	GLUT-1

Table 3.8 | Antibodies used for intracellular staining

Primary Antibody	Fluorochrome	Dilution factor	Supplier	Catalogue Number
FoxP3	AF647	1:100	BD Pharmingen	560401
RoRγt	BV421	1:100	BD Horizon	562894
Phalloidin (F-actin)	AF568	1:40	ThermoFisher	A12380
DNase1 (G-actin)	AF488	1:1800	ThermoFisher	A11096

3.4 Measuring cellular metabolism

Metabolism is a critical component of all cells playing a role in activation, proliferation, differentiation, apoptosis, and disease. Using Agilent Seahorse XF technology, the glycolytic and mitochondrial function (oxidative phosphorylation, OxPhos) of bEnd3 cells stimulated with mouse serum was investigated.

Briefly, a 96-well Seahorse culture plate was coated with 50µL 0.1% gelatin/well (1:20 dilution in $PBS^{-/-}$) and incubated for 30 minutes in 10% CO_2, the plate was washed with $PBS^{-/-}$ prior to the addition of cells. bEnd3 cells were harvested and plated in a density of 15,000 cells/well in 200µL of bEnd3 medium. Wells A1, A8, L1 and L8 did not have cells seeded as these wells are used by the Seahorse XFe96 Analyzer (Agilent Technologies) to calculate the background.

bEnd3 cells were left to grow for 3 days to ensure an even and confluent monolayer was formed, after which cells were serum stimulated. pMBMECs were left to grow for 4 days. The day before the assay, a Seahorse utility plate was filled with 180µL/well of calibrant solution (Seahorse, Agilent Technologies). A sensor cartridge was lowered onto the utility plate to submerge the sensors in calibrant. The cartridge plate was placed at 37°C in a non-CO_2 incubator overnight. The following day, the medium was aspirated from the cell culture plate and replaced with 180µL/well of assay medium, the plate was transferred to the non-CO_2 incubator to stabilize the conditions of the cells with the medium and absence of CO_2 for 1-2 hours.

The assay medium was prepared by supplementing the Seahorse XF Base Medium with the requirements for each kit:

- For glycolytic function - 1mM of glutamine was added
- For mitochondrial function -1 mM sodium pyruvate, 2 mM glutamine and 10 mM glucose were added

The assay medium for each kit was adjusted to pH 7.4 and filter sterilized before use. In the meantime, the drugs for each kit were prepared and loaded into the cartridge. Each vial of drug was diluted with 3mL of the respective assay medium for the assay. All drugs were protected from light and stored at 4°C once prepared. The drugs were loaded into the cartridge using the ports provided in the kit, and the cartridge was

returned to the CO_2-free incubator for a further 30 minutes. Table 3.9 shows the port and volume of drugs loaded per assay.

After 30 minutes, the calibration of the Seahorse XFe Analyzer was initiated, the cells were placed into the machine when prompted and the experiment was allowed to run. After running the assay, the data was normalized to protein concentration. Analysis was conducted using Wave Software 2.3 (Agilent Technologies) and Microsoft Excel.

Table 3.9 | Name, concentration and volume of the drugs used in the glycolysis and oxidative phosphorylation metabolism assay

Glycolysis - ECAR			
Port	**Drug**	**Final Concentration**	**Volume added to port**
A	Glucose	10mM	20
B	Oligomycin	1µM	20
C	2DG	50mM	25

Mitochondrial respiration (OxPhos) - OCR			
Port	**Drug**	**Final Concentration**	**Volume added to port**
A	Oligomycin	1µM	20
B	FCCP	0.5µM	22
C	Rotenone/Antimycin A	0.5µM	25

3.4.1 Glycolytic Function

The glycolytic function of cells was determined by measuring the extracellular acidification rate (ECAR), which is the extrusion of protons, produced by glucose conversion to pyruvate and lactate, into the extracellular medium. A Seahorse XF Glycolysis Stress Test Kit (Agilent Technologies) was used to assess the parameters of glycolytic flux including basal glycolysis, glycolytic capacity, glycolytic reserve, and the non-glycolytic acidification (Figure 3.5).

The assay works by initially incubating the cells in glycolysis stress test assay medium that lacks glucose or pyruvate to determine the non-glycolytic acidification, which is caused by processes other than glycolysis. The first injection given is a saturating concentration of glucose to determine glycolysis of the cells under basal conditions. The second injection given is oligomycin, an ATP synthase inhibitor that blocks

mitochondrial ATP production thereby shifting all energy production to glycolysis. This determines the maximum glycolytic capacity of the cells. The glycolytic reserve is the difference between the cells maximum capacity and the basal rate of glycolysis; it serves to indicate if the cells are capable to respond to an energetic demand and also how close the basal rate of glycolysis is to the theoretical maximum. The third injection given is 2-deoxyglucose (2-DG), a glucose analogue that inhibits glycolysis by binding to the first enzyme in the glycolytic pathway – hexokinase. The subsequent decrease after 2-DG serves to confirm that ECAR production in the experiment was due to glycolysis.

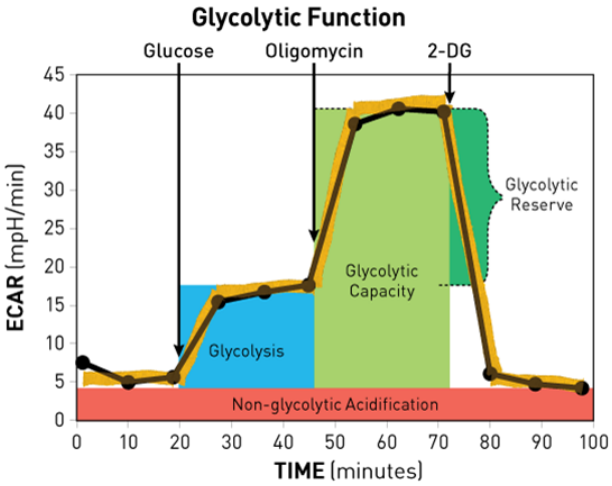

Figure 3.6 | Glycolytic Function Stress Test

The graph shows the expected profile to be obtained when conducting the Glycolysis Stress Test. Injections are added sequentially to determine basal glycolysis, glycolytic capacity, glycolytic reserve, and non-glycolytic acidification. Figure taken from Agilent Technologies (502).

After running the assay, the ECAR data was normalized to protein concentration which could be used to calculate each parameter by using the equation in Table 3.10.

Table 3.10 | Equations used to calculate the different parameters for assessing glycolytic function

Parameter value	Equation
Glycolysis	ECAR value after glucose injection – ECAR value after 2DG injection
Glycolytic capacity	ECAR value after oligomycin injection – ECAR value after 2DG injection
Glycolytic reserve	ECAR value after oligomycin injection – ECAR value after glucose injection
Non-glycolytic acidification	ECAR value after 2DG injection

3.4.2 Mitochondrial function

The mitochondrial function of cells was determined by measuring the oxygen consumption rate (OCR). A Seahorse XF Cell Mito Stress Test (Agilent Technologies) was used to assess the parameters of metabolic function including basal respiration, ATP production, proton leak, maximal respiration, spare respiratory capacity, and non-mitochondrial respiration (Figure 11). The assay works by initially incubating the cells in mito stress test assay medium supplemented with sodium pyruvate, glutamine, and glucose to determine basal respiration. The kit uses different compounds, which target various points of the ETC to modulate respiration. The first injection given is oligomycin that inhibits ATP synthase (complex V of the ETC), the resultant decrease in the OCR relates to the mitochondrial respiration that is used to drive cellular ATP production. The second injection is carbonyl cyanide-4 (trifluoromethoxy) phenylhydrazone (FCCP), an uncoupling agent that collapses the proton gradient to disrupt the mitochondrial membrane production. The resultant increase in OCR is due to uncontrolled electron flow through the ETC, this serves to provide the maximal respiration or O_2 consumption by complex IV. Maximal respiration is achieved by causing rapid oxidation of substrates such as sugars, fats & amino acids to meet an increased metabolic demand. The third injection is a combination of rotenone and antimycin A that inhibit complexes I and III respectively, effectively shutting down mitochondrial respiration to determine non-mitochondrial associated respiration rate.

The proton leak is measure of any mitochondrial damage and the spare respiratory capacity is an indicator of a cell's flexibility to respond to an increased energetic demand as well as showcasing how close the basal rate of respiration is to the theoretical maximum.

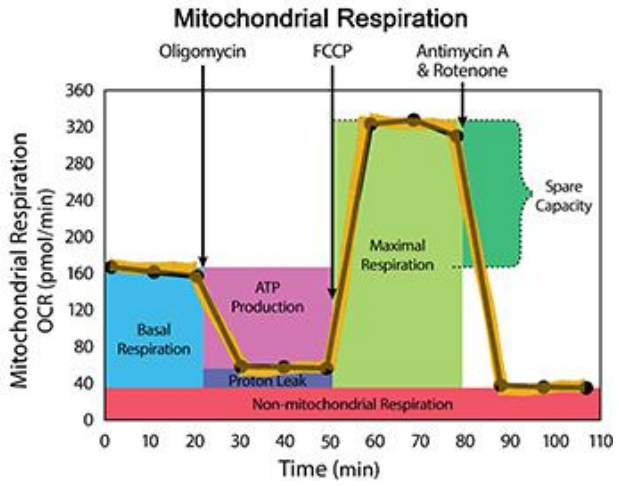

Figure 3.7 | Mitochondrial (Oxidative Phosphorylation) Stress Test

The graph shows the expected profile to be obtained when conducting the Mito Stress Test. Injections are added sequentially to determine basal respiration, ATP production, proton leak, maximal respiration, spare respiratory capacity, and non-mitochondrial respiration. Figure taken from Agilent Technologies (503).

After running the assay, the OCR data was normalized to protein concentration, which could be used to calculate each parameter by using the equations in Table 3.11.

Table 3.11 | Equations used to calculate the different parameters for assessing mitochondrial function in the Mito Stress Test

Parameter value	Equation
Basal respiration	OCR value prior to oligomycin injection – OCR value after Rotenone/Antimycin A injection
ATP production	OCR value prior to oligomycin injection – OCR value after oligomycin injection
Proton leak	OCR value after oligomycin injection – OCR value after Rotenone/Antimycin A injection
Maximal respiration	OCR value after FCCP injection – OCR value after Rotenone/Antimycin injection
Spare capacity	OCR value after FCCP – OCR value prior to oligomycin
Non-mitochondrial respiration	OCR value after Rotenone/antimycin A injection

3.4.3 Glucose uptake

bEnd3 cells were cultured in 24 well plates for 72 hours to form confluent monolayers. Once confluency had been reached, cells were stimulated overnight with 200µL of mouse serum. The following day, cells were washed with 200µL $PBS^{-/-}$ and collected in FACS tubes using 5mM EDTA. Cells were washed with FACS buffer and resuspended in 200µL/tube of glucose-free culture medium for 1 hour at 37°C in a 5% CO_2 incubator. Glucose uptake was measured using 6-NBDG (a fluorescent nonhydrolyzable glucose analogue) at a final concentration of 20µM made in FACS buffer. Cells were incubated with 6-NBDG for 20 minutes at 37°C. After staining, cells were washed with FACS buffer, centrifuged for 5 minutes at 1800rpm and resuspended in $PBS^{+/+}$ for flow cytometric analysis at Ex/Em = 465/540 (B530/30 laser).

3.4.4 ATP production

ATP is a marker of cell viability; it is present in all metabolically active cells. The ATPLite Detection Assay kit (Perkin Elmer) was used to measure ATP production.

Briefly, a 96-well black-bottom plate was coated with 50µL 0.1% gelatin/well (1:20 dilution in $PBS^{-/-}$) and incubated for 30 minutes in 10% CO_2, the plate was washed with $PBS^{-/-}$ prior to the addition of cells. bEnd3 cells were harvested and plated in a density of 15,000 cells/well in 200µL of bEnd3 medium and grown for 72 hours. The cells were stimulated overnight with 100µL medium containing 10% mouse serum. On the day of the assay, reagents were equilibrated to RT. Lyophilised substrate solution was reconstituted, as per manufacturers instruction, by adding 5mL of substrate buffer to one vial. A standard was constructed using the ATP stock solution (10mM); concentration of 0.1µM to 5µM were made up in dH_2O. To all wells, 50µL/well of mammalian cells lysis solution was added, the plate was placed on an orbital shaker for 5 minutes at 700rpm. In the standard wells, 10µL of the ATP standard dilution series was added, the plate was placed on an orbital shaker for 5 minutes at 700rpm. To all wells, 50µL/well of substrate cells lysis solution was added, the plate was placed on an orbital shaker for 5 minutes at 700rpm. The plate was dark-adapted for 10 minutes, the luminescence was read (1 sec/well) on a plate reader (Infinite M200 PRO plate reader, TECAN). The concentration value was extrapolated using the standard curve.

3.4.5 DCFDA – cellular ROS

Cellular ROS was measured using the DCFDA kit (Abcam). The kit uses the cell permeant reagent 2', 7' – dichlorofluorescin diacetate (DCFDA), a fluorogenic dye that measure the hydroxyl, peroxyl and other ROS species activity within the cell.

Briefly, a 96-well black-bottom plate was coated with 50µL 0.1% gelatin/well (1:20 dilution in $PBS^{-/-}$) and incubated for 30 minutes in 10% CO_2, the plate was washed with $PBS^{-/-}$ prior to the addition of cells. bEnd3 cells were harvested and plated in a density of 15,000 cells/well in 200µL of bEnd3 medium and grown for 72 hours. On the 3rd day, cells were serum starved overnight in medium without phenol-red. The following day, cells were washed in 100µL 1X buffer. The cells were stained with

25µM DCFDA (100µL/well), prepared in 1X buffer for 45 minutes at 37°C. Following incubation with DCFDA, the cells were washed and replaced with fresh medium containing 10% mouse serum; cells were stimulated for 6 hours. The production of ROS was measured using a plate reader at 37°C, Ex/Em = 485nm/535nm.

3.4.6 MitoSOX Red – mitochondrial superoxide indicator

MitoSOX Red permeates live cells and selectively targets mitochondria. It is rapidly oxidised by superoxide but not by other ROS or reactive nitrogen species (RNS). The oxidised product is highly fluorescent upon binding to nucleic acid; therefore, the accumulation of dye positively correlates with increased mitochondrial superoxide production and is a marker of oxidative stress.

Briefly, a 96-well black-bottom plate was coated with 50µL 0.1% gelatin/well (1:20 dilution in $PBS^{-/-}$) and incubated for 30 minutes in 10% CO_2, the plate was washed with $PBS^{-/-}$ prior to the addition of cells. bEnd3 cells were harvested and plated in a density of 15,000 cells/well in 200µL of bEnd3 medium and grown for 72 hours. On the 3rd day, cells were serum starved overnight in medium without phenol-red. The following day, cells were incubated with 2µM of MitoSOX in phenol red-free medium at 37°C. The mitochondrial respiratory chain complex I inhibitor rotenone was used as a positive control, used at a concentration of 2.5µM. The medium was aspirated and replaced with fresh medium containing 10% serum; cells were stimulated for 6 hours. The production of mitochondrial superoxide was measured using a plate reader at 37°C, Ex/Em = 510nm/580nm.

3.5 Statistical Analysis

All data are presented as mean ± standard error of mean (SEM) of n observations, where n denotes the number of animals studied. The numbers of animals used, repeats per carried out per experimental procedure and/or technical replicates have been reported in each figure legend. Outliers were identified on Microsoft Excel using the Interquartile Range (IQR). Briefly, data is divided into quartiles:

- 1st quartile, Q1 – 25% of the data are less than or equal to this value
- 3rd quartile, Q3 – 25% of the data are greater than or equal to this value
- IQR – 50% of the data, calculated as the difference between Q3 – Q1

Outliers are defined as any values that fall outside of the range of the following equations:

- Q1 – (1.5 x IQR) or Q3 + (1.5 x IQR)

All statistical analysis was conducted using GraphPad Prism 8 (GraphPad Software, San Diego, California, USA). All data was tested for normality and analysed by a student's t-test, Mann-Whitney U test or one-way ANOVA for multiple comparisons with post-hoc analysis using Bonferonni's. Significance is indicated as *p<0.05, **p<0.01, ***p<0.001, ****p<0.0001 vs chow or $p<0.05, $$p<0.01, $$$p<0.001, $$$$p<0.0001 vs HFHS or #p<0.05, ##p<0.01, ###p<0.001, ####p<0.0001 vs HFHS + hrANXA1.

Chapter 4 – The impact of MetS/T2DM at the BBB: structural and immunological alterations

4.1 Introduction

Animal models are regularly used to investigate T2DM pathophysiology and its secondary complications, as a well as evaluate potential therapeutic treatments and preventive strategies (504). In order for an animal model to be relevant in the study of T2DM in humans, the animal model should mirror the aetiology and pathophysiology of T2DM seen in the human condition. T2DM is closely linked to obesity and therefore the majority of animal models of T2DM are obese. Obesity is the single biggest risk factor for developing T2DM, with research suggesting that obese individuals are 80 times more likely to develop T2DM than non-obese individuals (311). Obesity raises the levels of fatty acids, glucose, pro-inflammatory markers and alters hormones and metabolism due to the accumulation of fat deposition, leading to the development of insulin resistance (460). Insulin resistance presents with an impairment in β-cell function; the continued decline of β-cell function with inadequate insulin production causes a loss of glucose control resulting in T2DM (379). Due to this continuum between obesity, insulin resistance and T2DM, research into metabolic disorders is based across the spectrum of these stages. Of course, in humans it is far easier to assess the stage of the disease, as this is progressive and long-term. Weight loss and reducing BMI are therefore key in preventing T2DM development (347). In comparison, in rodents the definition of each stage is not as easily determined.

The major ways to induce development of T2DM in rodents is via genetic manipulation (monogenic or polygenic) or through diet by feeding on primarily high fat (505) which causes obesity and insulin resistance (468).

The most common monogenic models of T2DM are defective in leptin signalling. Leptin is a satiety hormone and therefore lack of functional leptin removes the 'hunger' control mechanism to induce excessive food consumption that ultimately results in obesity (506). These models include the Leptin ob/ob mouse which are deficient in leptin or the Leptin db/db mice and Zucker Diabetic Fatty rats which are deficient in the leptin receptor (506).

Notably, obesity in human is rarely caused by a monogenic mutation and therefore polygenic models of obesity, glucose intolerance and T2DM may provide a more accurate model of the human condition in which a more varied approach is used. These

polygenic models include KK mice, OLETF rat, NZO mice, TallyHo/Ing mice and NoncNZO10/LtJ mice (504). Nonetheless polygenic models are still unable to mimic the multifaceted nature of the disease in humans, in which over 50 genes have been identified to play a role in inducing T2DM (507). Moreover, the polygenic models do not have a true wild-type control and the male sex bias is more extreme (508).

In this study, we used a diet-induced mouse model of T2DM, fed a combination of high-fat and high-sugar. Diet-induced diabetic models work through causing obesity from imbalanced food intake and low energy expenditure (459). The diet-induced models of diabetes are used to replicate the westernised lifestyle in humans, with increased intake of foods dense in fats and sugars along with a sedentary lifestyle. Since the obesity is induced by environmental manipulation rather than genes, diet-induced models are thought to mimic the human condition more accurately that genetic models of obesity-induced diabetes (461).

Numerous studies have examined the effect of high-fat feeding in rodent models (459,462,463); of the strains tested the C57BL/6 mouse progression of metabolic abnormalities parallels the dysfunction seen in humans. The model of high-fat feeding in C56BL/6J mice was first described in 1988 (464). A high-fat (58%) diet in these mice has clearly shown to cause weight gain, insulin resistance and hyperglycaemia in comparison to mice fed a chow-diet (11% fat) (465). Furthermore studies have found male mice to be more prone to the development of diabetes in comparison to females (466). Obesity inevitably leads to metabolic syndrome that can progress to T2DM and hence the C57BL/6 male diet-induced obese mouse model is highly suitable for our investigations (467,468)

Importantly, to date, no single standard protocol of high fat induced T2DM has been established. Within the literature, there are a vast variety of protocols with variations in mouse strains, formulation of high fats (fat fractions ranging from 20-60%), duration of feeding periods (ranging from a few weeks to more than one year) and age of mice at induction of diet (469,470). Importantly, it is not just the percentage of fat but the origin and exact composition of fat which can induce different biological responses, for example animal-derived fat or saturated fatty acids are more obesogenic compared to plant-derived (e.g. coconut oil) or unsaturated fatty acids (509,510).

In this particular study, a combination of high-fat and high-sugar (fat 59.4%, carbohydrate 25.7 %, protein 14.9%) was used (see Table 3.1 for full composition) compared to a standard chow diet (fat 13.2%, carbohydrate 62.3 %, protein 24.5%). This HFHS diet was used to closely mimic consumption of a high-fat, high-sugar and energy dense diet seen in modern day society. The C57BL/6 strain was used as the B6 mouse has been shown to be a good model for mimicking the multi-factorial nature and progression of MetS/T2DM as seen in humans, through the development of obesity, hyperglycaemia, hyperinsulinemia and hypertension when fed a HF diet *ad libitum*. In comparison, when fed a chow diet *ad libitum*, the B6 mouse model remains lean (467,511).

Moreover, we have previously established this particular mouse model of HFHS in our lab for inducing T2DM related secondary complications and cardiomyopathy with a feeding period between 10-16 weeks (473–475). In particular, using the same 10-week feeding model used in the current study, previously results have shown HFHS-feeding caused hepatosteatosis resulting in liver injury, seen through lipid deposition and accumulation in the liver (512). Additionally, HFHS-feeding induced renal dysfunction as seen through decreased creatinine clearance resulting in proteinuria and vacuolar degeneration in the kidney (512). The ability of HFHS-feeding to induce microvascular complications in the peripheral systems suggests that this model is efficient in producing a low-grade chronic inflammatory state, as seen in conditions of MetS/T2DM, thereby making it viable to use for the aims of this thesis.

4.1.1 Aims and objectives

The focus of this chapter was to investigate how metabolic disorder-induced inflammation, termed metaflammation, can disrupt the BBB, with focus on alterations to the structural and immunological integrity of the barrier.

The chapter addresses the first hypothesis mentioned in Chapter 2, this is as follows:

⇒ **Hypothesis 1:**

It is hypothesised that metaflammation arising in T2DM will result in a leaky BBB phenotype resulting in the infiltration of immune cells from the peripheral side into the brain parenchyma to cause neuroinflammation.

This chapter addresses Aims 1 & 2 mentioned in Chapter 2, these are as follows:

1. To characterize the early vascular defects occurring in the BBB during HFHS-feeding *in vivo*, *ex vivo* and *in vitro*.
    - Identify the functional changes occurring to the BBB through measuring vascular leakage.
    - Identify structural alterations through immuno-histochemical analysis of brain endothelium junctional proteins, BM components and the cytoskeleton.

2. To define the pathogenic events leading to cerebrovascular damage at the BBB induced by HFHS-feeding.
    - Examine the role of inflammatory mediators and soluble factors present in the sera such as cytokines, chemokines, interleukins, metabolic factors, extracellular matrix components, on inducing BBB permeability and endothelial dysfunction.
    - Define the effect of metabolic disorders on the innate and adaptive arms of the peripheral immune system. Determine whether the priming of immune cells within the peripheral system can correlate with the transmigration across the BBB and subsequently activate the microglia, the resident immune cell of the CNS to initiate neuroinflammation in a diabetic state.

The following objectives were covered in this chapter to address these aims:

- To induce T2DM in mice via diet by feeding mice on a HFHS-diet for 10-weeks
- To measure disruption of BBB integrity (vascular leakage) using *in vivo* Evans blue dye and *ex vivo/in vitro* via measuring the paracellular permeability coefficient and TEER.
- To imaging structural alterations occurring at the BBB via confocal microscopy of cerebral cortical mouse brain sections for expression of junctional proteins occludin and claudin-5 and endothelial and astrocytic BM laminins, α4 and α5.

- To determine the role played by MMPs and their inhibitor, TIMP-1 in BBB degradation through measurement of expression and activity.
- To compare the inflammatory profile in chow and HFHS-fed mice via examination of cytokines, interleukins and chemokines.
- To determine whether the endothelial cells become activated by metaflammation and expression adhesion molecules.
- To phenotype the activation of the innate and adaptive immune cells in bone marrow and cervical lymph nodes.
- To characterise, using FACS, the effect of HFHS-induced T2DM on $CD4^+$ T_{eff}, T_{CM}, $T_{EM,}$ T_H17 and Treg cells present in cervical lymph nodes.
- To image the infiltration of $CD45^+$ leukocytes cells into the brain parenchyma, and classify the different $CD4^+$ T-cell phenotypes migrating across the BBB using an *in vitro* model.
- To characterise the effect of HFHS-induced T2DM on microglia cell activation and microglia M1 or M2 phenotype via FACS analysis of primary microglia cultures and imaging cerebral cortical brain sections.
- To characterise the initiation of neuroinflammation through measuring expression of iNOS in the brain parenchyma using confocal microscopy.

In order to study these aims, 10-week old male C57BL/6 mice were fed either a standard chow-based diet (5053, LabDiet Ltd) or a HFHS diet (58R3, TestDiet Ltd) for 10 weeks. The latter was used to induce diet induced T2DM. Both chow and HFHS-fed mice were 20-weeks old at cull. A summary of the experimental groups, experimental plan and the methods used to quantify each measure have been provided in Table 4.1, Figure 4.1 and Table 4.2, respectively.

Table 4.1 | Experimental groups used to establish a mouse model of diet induced T2DM

Group name and age	Diet and period of time	Treatment and period of time	Age at cull	Total number
Chow 10-week old male C57BL/6 mice	Chow from weeks 1 - 10	Vehicle of 100µl of 50mM Hepes, 140mM NaCl, pH 7.4, 5 times/week i.p. Given weeks 5-10	20 weeks	55
HFHS 10-week old male C57BL/6 mice	HFHS from weeks 1 - 10	Vehicle of 100µl of 50mM Hepes, 140mM NaCl, pH 7.4, 5 times/week i.p. Given weeks 5-10	20 weeks	55

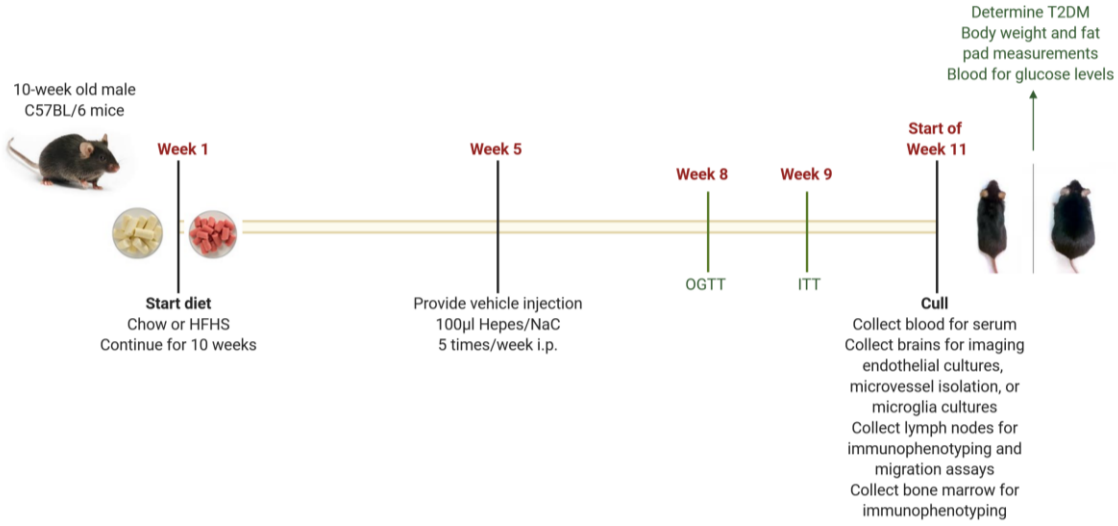

Figure 4.1 | Summary of the experimental plan used to establish diet induced T2DM

10-week old male C57BL/6 mice were fed either a chow or HFHS for 10 weeks. From week 5, mice were injected with a sham injection of 100µL Hepes/NaCl, 5 times/week via intraperitoneal (i.p.) injection for 6 weeks. Assessment for glucose tolerance and insulin resistance were conducted via oral glucose tolerance tests (OGTT) and insulin tolerance tests (ITT) respectively. Mice were culled at the beginning of week 11. Confirmation of T2DM was made by weight and various blood/serum analyses. At cull, blood, brain, lymph nodes and bone marrow were collected.

Table 4.2 | Summary of the central and individual measures used to evaluate the aims and objectives of Chapter 4, with reference to the respective methodology used to conduct these experiments.

Central measure	Individual measures	Method section
T2DM development	Obesity - weight gain and fat pads	3.1.1.1, 3.1.2 & 3.1.3
	Hyperglycaemia- fasted glucose, non-fasted glucose OGTT	3.1.1.1 & 3.1.4
	Hyperinsulinaemia - ITT, serum insulin	3.1.1.1, 3.1.2 & 3.1.4
	Dyslipidaemia - serum & cholesterol triglycerides	3.1.1.1, 3.1.2 & 3.1.4
Vascular integrity	Evans blue dye leakage *in vivo*	3.1.7 & 3.1.8
	Paracellular permeability *in vitro*	3.1.9 & 3.2.5
	TEER	3.1.9 & 3.2.6
BBB structure	Imaging junctional proteins occludin and claudin-5	3.1.3 & 3.3.1
	Imaging BM laminins α4 and α2	3.1.3 & 3.3.1
MMP involvement	MMP-2, -3, -9 expression at brain microvessels via cytokine array	3.1.9 & 3.2.8
	MMP-2 and -9 activity at brain microvessels via zymography	3.2.9 & 3.2.10
	TIMP-1 ELISA	3.2.8
Inflammatory profile	Cytokine array for interleukins, chemokines, cytokines in serum and brain microvessels	3.2.8
	Imaging and characterising adhesion molecule expression at BBB	3.2.8 & 3.4.3
Immuno-phenotyping	Cell frequency of innate and adaptive immune cells in bone marrow and deep cervical lymph nodes	3.1.3, 3.1.5, 3.1.6, 3.4.3
	$CD4^+$ T-cell activation for Teff	3.1.3 & 3.4.3
	T_{CM} vs T_{EM}	3.1.3 & 3.4.3
	T_H17 vs Treg	3.1.3 & 3.4.3
Leukocyte TEM across BBB	Imaging CD45 infiltration into brain parenchyma	3.1.3 & 3.3.1
	In vitro adhesion/migration assays	3.1.3, 3.2.1, 3.2.2, 3.2.3, 3.2.7
Microglia phenotyping	Activation and M1 vs M2 phenotyping	3.1.10 & 3.4.3
Neuro-inflammation	Imaging IBA1 activated microglia cells	3.1.3 & 3.3.1
	Imaging for iNOS expression	3.1.3 & 3.3.1

4.2 Results: *In vivo & ex vivo*

4.2.1 Induction of MetS/T2DM in a mouse model

Confirmation of metabolic disruption (obesity, hyperglycaemia, dyslipidaemia and insulin resistance) in this mouse model was conducted by measurements of weight gain, fat mass (epididymal & inguinal), fasting and non-fasting blood glucose, OGTT and ITT as well as serum insulin, cholesterol and triglyceride levels (Figure 4.2). At the end of the 10-week feeding period, mice fed a HFHS diet presented with significantly increased body weight (Figure 4.2A,D) and fat mass (Figure 4.2E,F) in comparison to mice fed a chow diet. All mice fed a HFHS diet had lower food intake than chow-fed mice, however the calorific intake of the HFHS diet was substantially higher than the chow diet (Fig 4.2B,C)

Tests for hyperglycaemia found raised non-fasted and fasted blood glucose levels in HFHS-fed mice when compared to chow-fed mice (Figure 4.2G,J). Insulin resistance was confirmed using OGTT and ITT; measurement of the area under the curve (AUC) in both tests found HFHS-fed mice to have an impaired insulin response compared to chow-fed mice (Figure 4.2H-L). Although notably, the ITT in HFHS-fed mice was not significant, which may have been due to small n numbers of 6 vs 48 in OGTT. Similarly, serum insulin levels were also elevated in HFHS-fed mice compared to chow-fed mice (Figure 4.2M). HFHS-fed mice were also found to have hyperlipidaemia, as seen by elevated serum cholesterol and triglyceride levels compared to chow-fed mice (Figure 4.2N,O).

Conclusively the HFHS diet induced obesity and contributed to the development of MetS/T2DM as noted by hyperglycaemia, hyperinsulinemia, hypercholesterolemia, and hypertriglyceridemia.

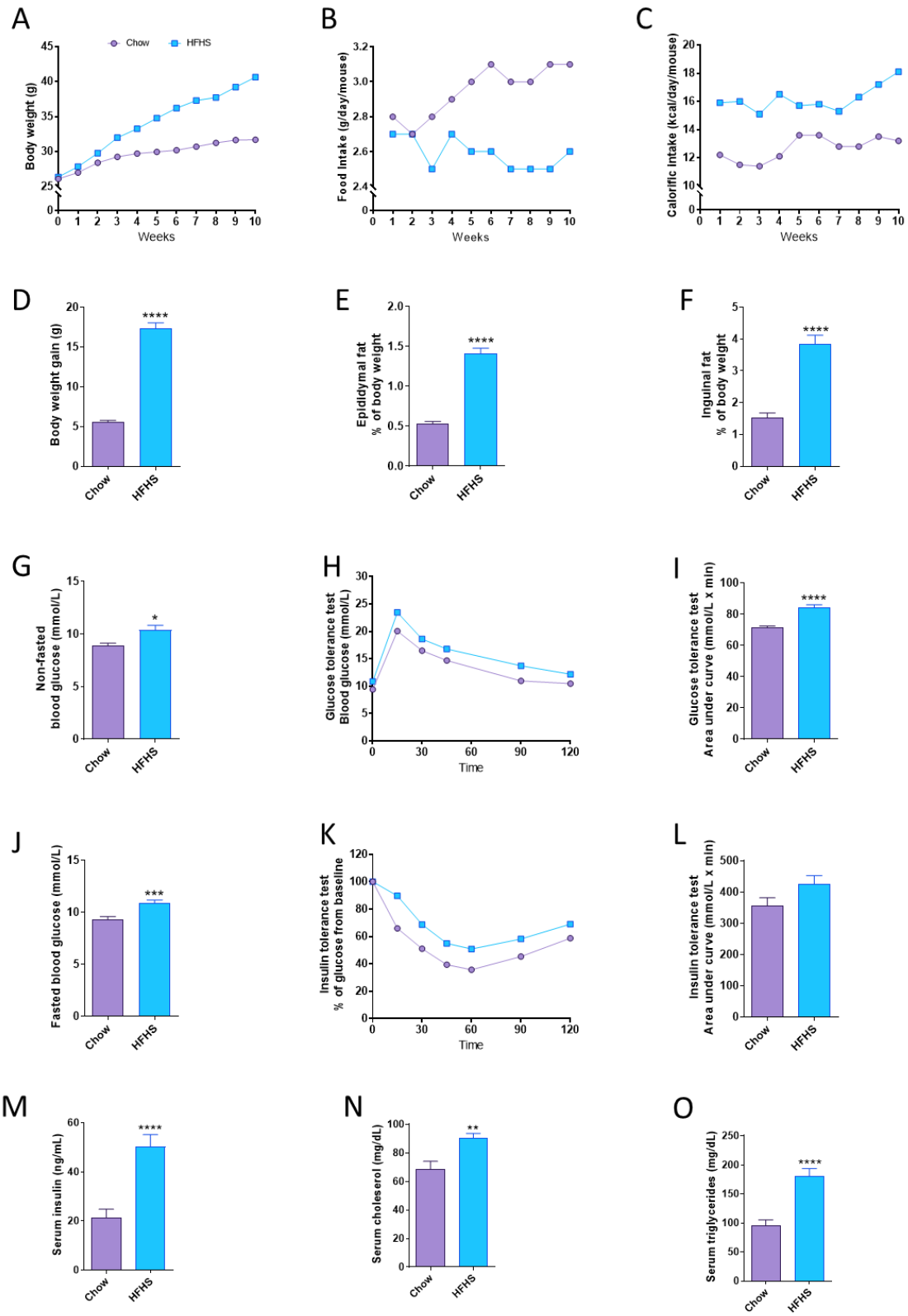
A
Chow
HFHS
Body weight (g)
Weeks
B
Food Intake (g/day/mouse)
Weeks
C
Calorific Intake (kcal/day/mouse)
Weeks
D
Body weight gain (g)
****
Chow
HFHS
E
Epididymal fat
% of body weight
****
Chow
HFHS
F
Inguinal fat
% of body weight
****
Chow
HFHS
G
Non-fasted
blood glucose (mmol/L)
*
Chow
HFHS
H
Glucose tolerance test
Blood glucose (mmol/L)
Time
I
Glucose tolerance test
Area under curve (mmol/L x min)
****
Chow
HFHS
J
Fasted blood glucose (mmol/L)
***
Chow
HFHS
K
Insulin tolerance test
% of glucose from baseline
Time
L
Insulin tolerance test
Area under curve (mmol/L x min)
Chow
HFHS
M
Serum insulin (ng/mL)
****
Chow
HFHS
N
Serum cholesterol (mg/dL)
**
Chow
HFHS
O
Serum triglycerides (mg/dL)
****
Chow
HFHS

Figure 4.2 | Characteristics of mice fed a chow or HFHS diet for 10 weeks

C57BL/6 male mice were fed either a chow or HFHS diet for 10 weeks; n=55/group. Food (B) and calorific intake (C) was recorded (n=10/group). Weekly body weight measurements (A), final body weight gain (D) and epididymal (E) & inguinal fat mass (F) was recorded to confirm obesity onset; n=54-55/group. Non-fasting (G; n=38/group) and fasting (J; n=39-40/group) blood glucose was measured to confirm hyperglycaemia. Serum insulin levels (M; n=22-23/group), glucose (H, I; n=38/group) and insulin tolerance testing (K, L; n=6) was conducted to confirm insulin resistance. Serum cholesterol (N) and serum triglycerides (O) levels were measured to confirm hypercholesterolemia and hypertriglyceridemia (n=11-16/group). Statistical analysis was performed by either an Independent Student's T-test or Mann-Whitney U test. Data is expressed as mean ± SEM., *p< 0.05, **p<0.01, ***p<0.001, ****p< 0.0001.

4.2.2 Effect of metabolic overload on the integrity of the BBB

A central function of the BBB is to restrict and control the entry and exit of molecules such as nutrients, enzymes, hormones, and waste products. The endothelial TJs maintain strict control of paracellular permeability movement; instead the plasma membranes of brain endothelial cells are lined with transporters, carriers and ion channels (513). The contractile and adhesive forces produced by the endothelial cytoskeleton and cell-cell junctions respectively maintain the paracellular permeability of the BBB (220,514). The first assessment in this study therefore required investigating whether metabolic overload could perturb the adhesive properties of the junctions to create intracellular gaps, thereby increasing the permeability of the BBB and altering its integrity as a barrier.

4.2.2.1 Measuring permeability in vivo using Evans blue dye

Evans blue dye was used to assess the permeability of the BBB *in vivo*. The dye was injected into the tail vein of all mice and allowed to circulate for 1 hour. Spectrophotometer analysis of the brain dye content revealed a significantly greater leakage of the BBB by almost 3-fold in HFHS-fed mice in comparison to chow-fed mice (Figure 4.3A).

4.2.2.2 Ex vivo analysis of paracellular permeability & TEER

To further investigate the abnormal permeability observed in vivo and depict any molecular change at the endothelium level, pMBMECs were isolated and cultured from the two different experimental mice groups, as well as from an additional group of 6-week old male mice fed a chow diet. These 6-week old mice vs 20-week old mice represented a young vs aged phenotype to determine the change in BBB integrity as a factor of time (age). When comparing the effects of age, young chow-fed mice had the lowest permeability coefficient, and this was statistically significant when compared to older chow-fed mice (Figure 4.3B). The young chow fed-mice had the highest TEER, which was significant when compared to older chow-fed mice (Figure 4.3C).

When comparing the HFHS-fed mice to their age-matched chow-fed counterparts, it was seen that a diabetic phenotype further increased paracellular permeability (Figure 4.3B) and further reduced the TEER (Figure 4.3C).

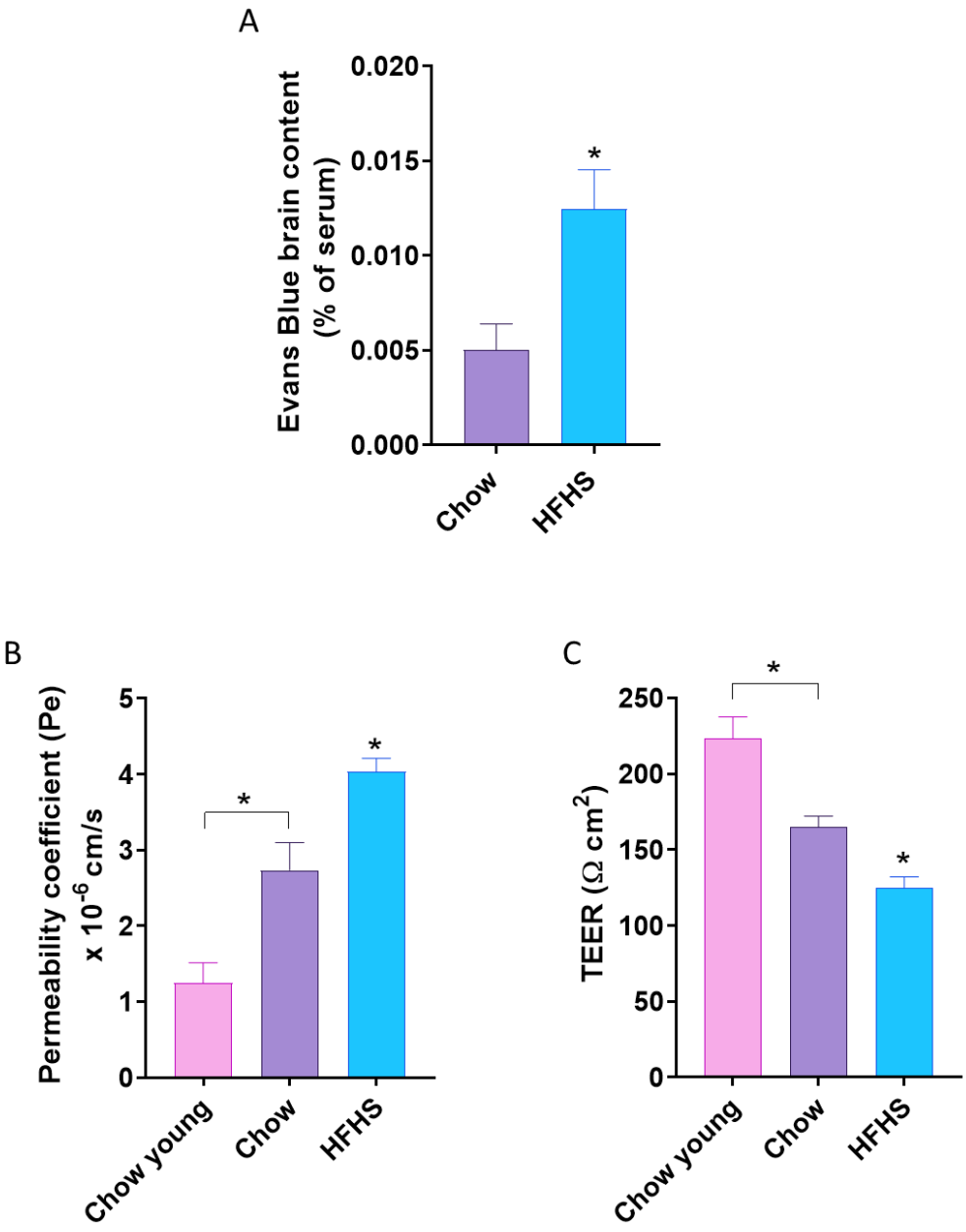
A
Evans Blue brain content
(% of serum)
0.020
0.015
0.010
0.005
0.000
*
Chow
HFHS
B
Permeability coefficient (Pe)
x 10-6 cm/s
5
4
3
2
1
0
*
*
Chow young
Chow
HFHS
C
TEER (Ω cm2)
250
200
150
100
50
0
*
*
Chow young
Chow
HFHS

Figure 4.3 | Measuring permeability *in vivo* & *ex vivo*

Assessment of BBB permeability *in vivo* was conducted using Evans blue dye extravasation into the brain (A). 100µl of 2% Evans blue dye was given i.v. to mice (n=6/group) and allowed to circulate for 1 hour. The dye content was analysed spectrophotometrically at an absorbance of 620nm, values were normalized to brain tissue weight and are expressed as percentage of serum dye content. Isolated and cultured pMBMECs from 20-week old chow-fed and 20-week old HFHS-fed mice were grown on transwell inserts for 7 days to measure e*x vivo* paracellular permeability (B) and transendothelial electrical resistance (TEER) (C) using 70kDA FITC-dextran and the Epithelial Volt/Ohm (EVOM2) Meter (World Precision Instruments, USA), respectively (n=10 pooled/group per experiment, two technical replicates, performed as three independent experiments with a total of n=30 per/group). pMBMECs were also isolated and cultured from young 6-week old male chow-fed mice against 20-week old chow-fed and HFHS-fed mice for a comparison of age-effect. Statistical analysis was performed by either an Independent Student's T-test or One-Way ANOVA followed by a Bonferonni post-hoc test. Data is expressed as mean ± SEM., *$p < 0.05$.

4.2.3 Imaging the structural changes occurring to the brain endothelial cells

Increased BBB permeability results due to changes in the structural arrangement and interaction of the TJ and AJ proteins. It has been observed that these proteins undergo phosphorylation or modifications, resulting in their redistribution and reorganisation (225,515–517). As the results of this study highlighted that there was increase in the BBB permeability upon metabolic overload, the next part of the study aimed to examine whether this could be correlated to changes in the junctional proteins within the endothelial cells. Additionally, for immune cells and other cells or molecules to enter the brain parenchyma, there must be degradation of key components of BBB structure including the BM components and surrounding cells of the NVU. As described in section 1.3.4, the BMECs are surrounded by two distinct BMs (150). The first is the endothelial BM composed of laminin α4 and α5 and the second is the parenchymal BM composed of lamina α1 and α2 which attaches to the astrocytic end-feet that ensheath the blood vessel (151,152). Therefore, in order to assess the impact of HFHS-induced T2DM on the BMs, staining was conducted for laminin forms present on both endothelial cells (laminin α4) and astrocytes (laminin α2). In order for immune cells, toxins or other molecules to enter into the CNS parenchyma, they must be able to transverse both BMs (4,248,249).

4.2.3.1 Changes occurring to the junctional proteins of brain endothelium

Immuno-histochemical analysis of TJ proteins claudin-5, occludin and vessel basal lamina (VBL) component pan-laminin was conducted on cerebral cortex microvessels of mice. Confocal microscopy analysis showed claudin-5 and occludin in chow-fed mice had a regular, linear and continuous pattern of staining along the microvessel along with intense VBL reactivity for pan-laminin (Figure 4.4A,B). In comparison, in HFHS-fed mice claudin-5 and occludin showed thinner linear TJ strands and reduced VBL pan-laminin reactivity (Figure 4.4A,B). The differences in junctional proteins and laminin staining was confirmed by quantification of fluorescence intensity, in which HFHS-fed mice has significantly lower amounts of claudin-5, occludin and laminin when compared to chow-fed mice.

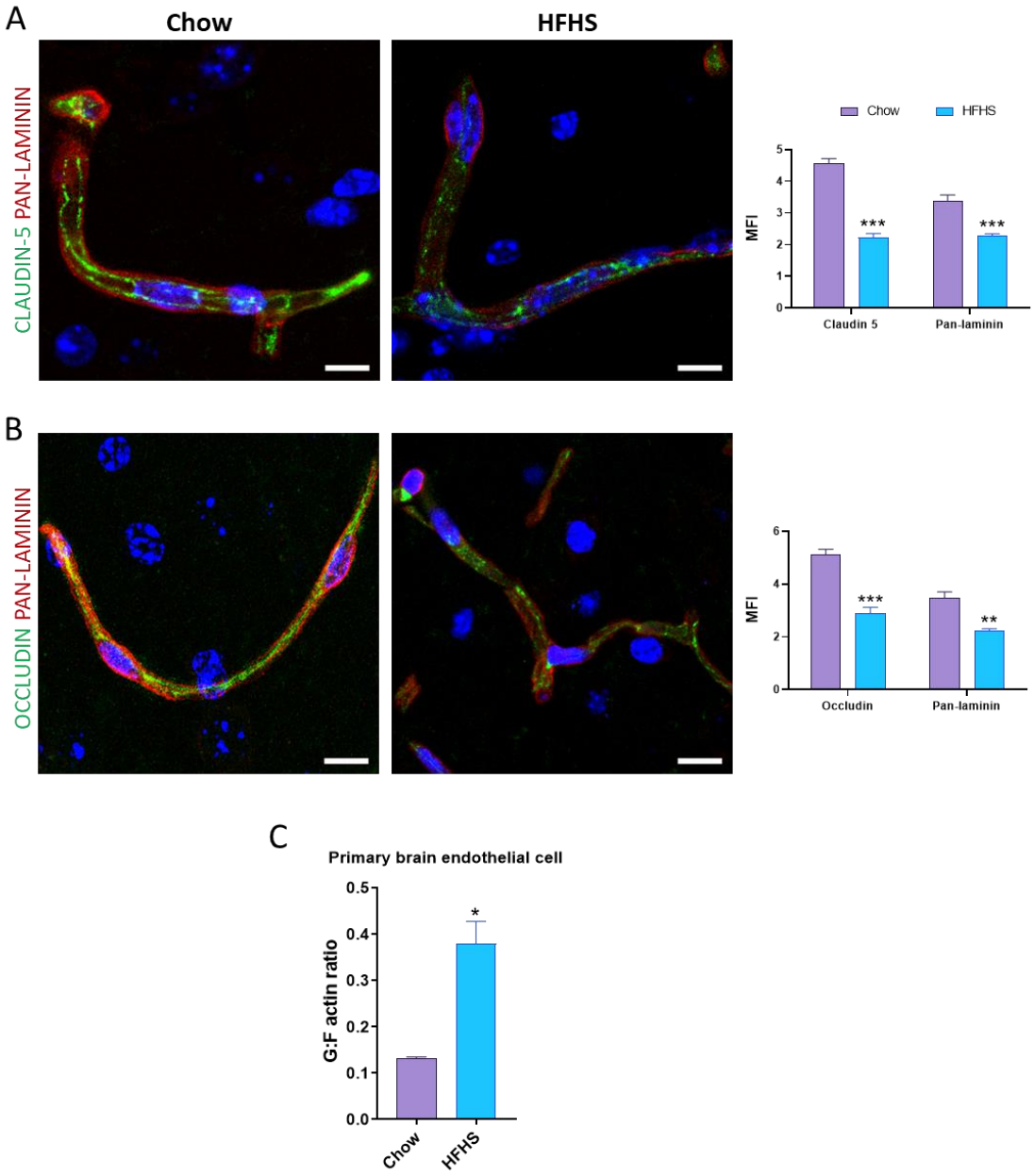

Figure 4.4 | Immuno-histochemical analysis of brain endothelium junctional proteins and flow cytometrical analysis of actin cytoskeleton

Confocal microscopy of cerebral cortical sections of mouse brains double immune-labelled with claudin-5/pan-laminin (A) and occludin/pan-laminin (B). Nuclear counterstain with TO-PRO3. Confocal images are representative images from n=4 mice/group, 35 section/animal (scale bar: 25µm). Quantification of staining shown as mean fluorescence intensity (arbitrary units) of markers on ten randomly selected fields. Flow cytometric analysis of G/F actin ratio in pMBMECs (C). Statistical analysis was performed by an Independent Student's T-test. Data is expressed as mean ± SEM., **p<0.01, ***p<0.001.

4.2.3.2 Changes occurring to the basement membranes of endothelial cells & astrocytes

The BM forms an integral part of BBB, therefore immuno-histochemical analysis of the BMs on endothelial cells of capillaries and astrocytes were conducted in cerebral cortical brain sections. Firstly, VBL component pan-laminin and endothelial laminin α4 was examined (Figure 4.5A). Chow-fed mice showed an intense expression of both laminin forms; however, it was noticeable that pan-laminin immunoreactivity prevailed on the outer VBL layer and showed limited co-localization with laminin α4. Laminin α4 staining was localised at the basal and the inter-endothelial sides suggestive of junctional-like immunostaining and diffused in the endothelial cytoplasm. In comparison, staining in HFHS-fed mice revealed substantive loss of immune-reactivity of both pan-laminin and laminin α4, which was confirmed by quantification. Importantly there was no change in the general distribution of the laminins.

Astrocytes form close associations with endothelial cells of the BBB, ensheathing the cerebrovasculature to provide an added layer of protection. Hence double immune-staining was conducted for the distribution and localisation of laminin α2 present on astrocyte end-feet and for laminin α4 on the endothelial cells (Figure 4.5B). In chow-fed mice it can be seen that the astrocytic laminin α2 was localised on the outer vessel surface whereas the endothelial laminin α4 was present within the vessel, surrounding and between the cells. In chow-fed mice, the two laminins never co-localised however there was clear noticeable linear tract of both laminins suggesting an intact vessel morphology. In comparison, in HFHS-fed mice, both laminin α2 and α4 immuno-reactivity was significantly reduced when compared to chow-fed counterparts, as quantified using mean fluorescence intensity.

To further elucidate whether a HFHS diet induced structural changes to the BBB, staining for the presence and distribution of astrocytes was conducted using astrocytic marker GFAP in conjunction with the astrocytic laminin α2 (Figure 4.5C). In chow-fed mice laminin α2 and GFAP showed clear co-localization, suggestive of astrocytic end-feet embracing the microvessel structure, forming an intact vessel. Astrocytes protruded from the vessel structure outward into the brain parenchyma. In contrast, in HFHS-fed mice where there was a loss of laminin α2, the astrocyte end-feet lost contact with the endothelial cells of the microvessel, indicative of loss of the BBB

structure and hence barrier properties. It is important to note, that whilst the mean fluorescence intensity of laminin α2 was significantly lower in HFHS-fed mice, the overall intensity of the astrocytic marker GFAP did not differ between the two groups.

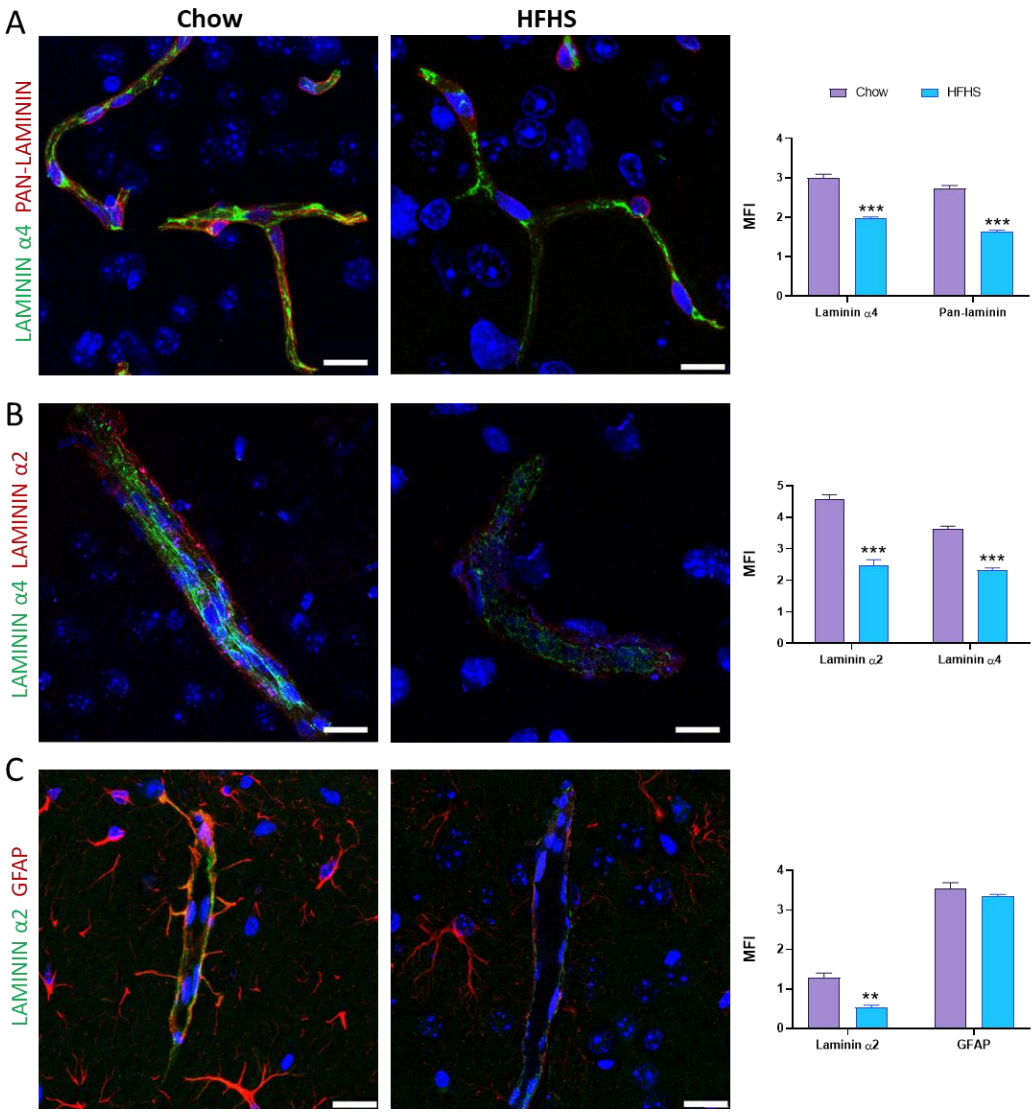

Figure 4.5 | Immuno-histochemical analysis of basement membranes & astrocytes

Confocal microscopy of cerebral cortical sections of mouse brains double immune-labelled with endothelial laminin α4/vascular basement membrane pan-laminin (A), endothelial laminin α4/astrocytic laminin α2 (B) and endothelial laminin α4/astrocytic marker glial fibrillary acidic protein (GFAP) (C). Nuclear counterstain with TO-PRO3. Confocal images are representative images from n=4 mice/group, 35 section/animal (scale bar: 25µm). Quantification of staining shown as mean fluorescence intensity (arbitrary units) of markers on ten randomly selected fields. Statistical analysis was performed by an Independent Student's T-test. Data is expressed as mean ± SEM., **p<0.01, ***p<0.001.

4.2.3.3 The role of MMPs in BBB disruption

The breakdown of the BBB structure in HFHS diet-fed mice led to the investigation of MMPs in the brain microvessels, which could be responsible for the degradation of junctional proteins and BMs. Proteomic analysis of brain microvessels using a membrane-based sandwich immuno-assay showed significantly increased levels of MMP-2, MMP-3 and MMP-9 in brain microvessels extracts of mice fed a HFHS diet in comparison to mice fed a chow diet (Figure 4.6A). In conjunction, the endogenous regulator of MMP activity - tissue inhibitor of metalloproteinases (TIMPs) concentration was reduced in the serum of HFHS-fed mice compared to chow-fed mice by 1.5-fold (Figure 4.6B).

The proteomic analysis of brain microvessels only revealed the presence of the MMPs through expression, therefore, to evaluate the proteolytic activity of these enzymes, a zymography of MMP-2 and MMP-9 was conducted (Figure 4.6C). Zymography resolves the gelatinases by molecular mass, thereby allowing detection of the active and latent forms of the enzymes. The inactive pro-peptide domain must be cleaved to allow enzymatic activity of the MMPs. Quantification of the zymogram showed increased pro-MMP-2 and active MMP-2 forms (Figure 4.6D) along with increased pro-MMP-9 and active MMP-9 forms (Figure 4.6E) in the brain microvessels of HFHS-fed mice when compared to chow-fed mice.

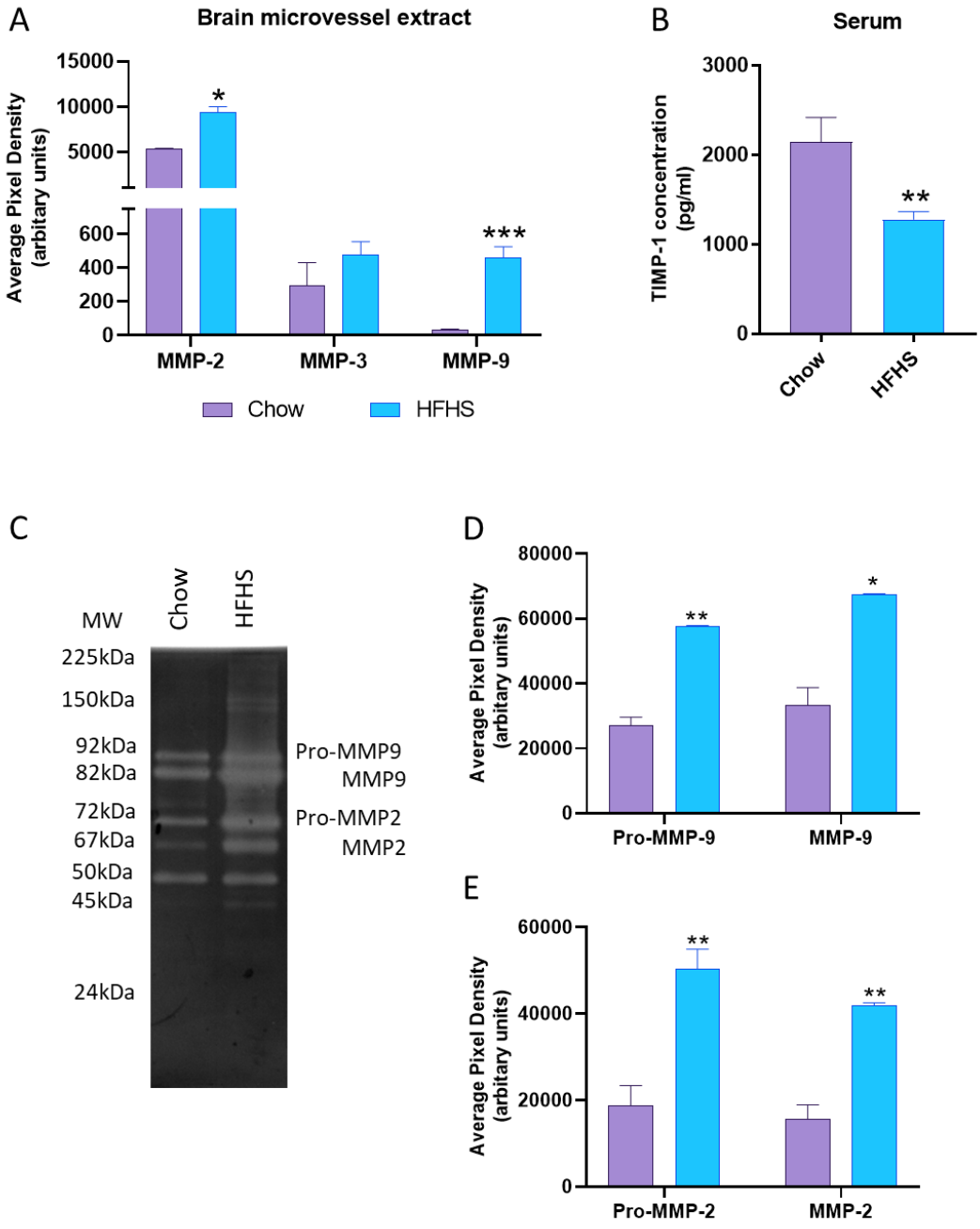
A
Brain microvessel extract
Average Pixel Density (arbitary units)
15000
10000
5000
600
400
200
0
*
***
MMP-2
MMP-3
MMP-9
Chow
HFHS
B
Serum
TIMP-1 concentration (pg/ml)
3000
2000
1000
0
**
Chow
HFHS
C
MW
Chow
HFHS
225kDa
150kDa
92kDa
82kDa
72kDa
67kDa
50kDa
45kDa
24kDa
Pro-MMP9
MMP9
Pro-MMP2
MMP2
D
Average Pixel Density (arbitary units)
80000
60000
40000
20000
0
**
*
Pro-MMP-9
MMP-9
E
Average Pixel Density (arbitary units)
60000
40000
20000
0
**
**
Pro-MMP-2
MMP-2

Figure 4.6 | The role of MMPs in BBB disruption

Expression of MMP-2, MMP-3, MMP-9 was analysed in brain microvessel extracts of chow and HFHS-fed mice using a Mouse Proteome Profiler (R&D Systems). The membrane-antibody array was loaded with 500ng of protein/group overnight (n=10 pooled/group, two technical replicates per experiment, performed as two independent experiments total n=20/group). Membranes were exposed to x-ray film and the signal produced at the different capture spots was used to quantify the amount of protein bound using ImageStudio Lite (LI-COR Biosciences) and expressed as arbitrary units (A). Serum levels of tissue inhibitor of metalloproteinases (TIMP-1) were measured using a quantikine ELISA kit (R&D Systems) (B; n=11/group). Proteolytic activity of MMP-2 and MMP-9 in brain microvessel extracts was determined via zymography, based on separation of proteins by non-reducing sodium dodecyl sulphate-polyacrylamide gel electrophoresis (SDS–PAGE). Molecular weight markers were used to estimate the molecular masses of inactive 'pro' and active/cleaved forms of MMP-2 and MMP-9 (C). Blots were scanned (BioRad Imager) and densitometry analysis was performed using ImageJ software (C,D). Each lane was loaded with 100ng of protein (n=10 pooled/group, representative of two independent experiments total n=20). Statistical analysis was performed by an Independent Student's T-test. Data is expressed as mean ± SEM., *p< 0.05, **p<0.01, ***p<0.001, ****p< 0.0001.

4.2.4 The inflammatory state: measuring inflammatory molecules in circulating serum and in the brain microvessels

It is well documented that T2DM induces a low-grade chronic inflammatory state within the peripheral vasculature and is damaging to peripheral blood vessels over time. To measure if there is a raised state of inflammation within the HFHS-fed mice compared to chow-fed mice, cytokines, chemokines and other inflammatory proteins in the serum (Figure 4.7A) were simultaneously measured using the R&D Mouse Cytokine Array Panel A Kit (R&D Systems). Within the serum of HFHS-fed, there were raised levels of chemokines CXCL1 and CXCL12, sICAM-1 and pro-inflammatory interleukins IL-1a, IL-16 and TNF-α. There was also a noticeable reduction in the anti-inflammatory IL-13 levels, chemokine CXCL13 and TIMP-1 in HFHS-fed mice compared to chow-fed mice. There appeared to be no major differences in the C5a and CXCL13 levels between the two groups, within the serum (Figure 4.7A).

Further analysis of the presence and potential impact of inflammatory mediators at the brain microvasculature was detected by conducting a similar proteome profile of the cytokines, chemokines, and other acute phase proteins in isolated brain microvessels protein extract of chow and HFHS-fed mice. Review of general inflammatory markers revealed HFHS-fed mice to have raised C5a, Chitinase 3-like 1, IFN-γ, TNF-α, receptor for advanced glycation end products (RAGE) and VEGF compared to chow-fed mice. HFHS-fed mice had reduced levels of periostin when compared to chow-fed mice and no difference was seen in CRP levels. Review of pro- vs anti-inflammatory interleukins found all listed pro-inflammatory interleukins to be raised in HFHS-fed mice compared to chow-fed mice with the exception of IL-1β and IL-7, whose levels remained similar between the two groups (Figure 4.7D). Similarly, the levels of all listed anti-inflammatory interleukins were also increased in HFHS-fed mice compared to chow-fed mice with the exception of IL-1ra and IL-5, whose levels were decreased with HFHS-feeding (Figure 4.7E). The interleukins that showed the greatest abundance were IL-1a, IL-7, IL-15, IL-27 p28 and IL-11. Likewise, chemokines that induced both neutrophil/monocyte and T/B-cells were markedly raised on the whole in mice fed a HFHS-compared to mice fed a chow diet (Figure 4.7C). Overall, the results indicate a raised inflammatory profile in the HFHS-fed mice.

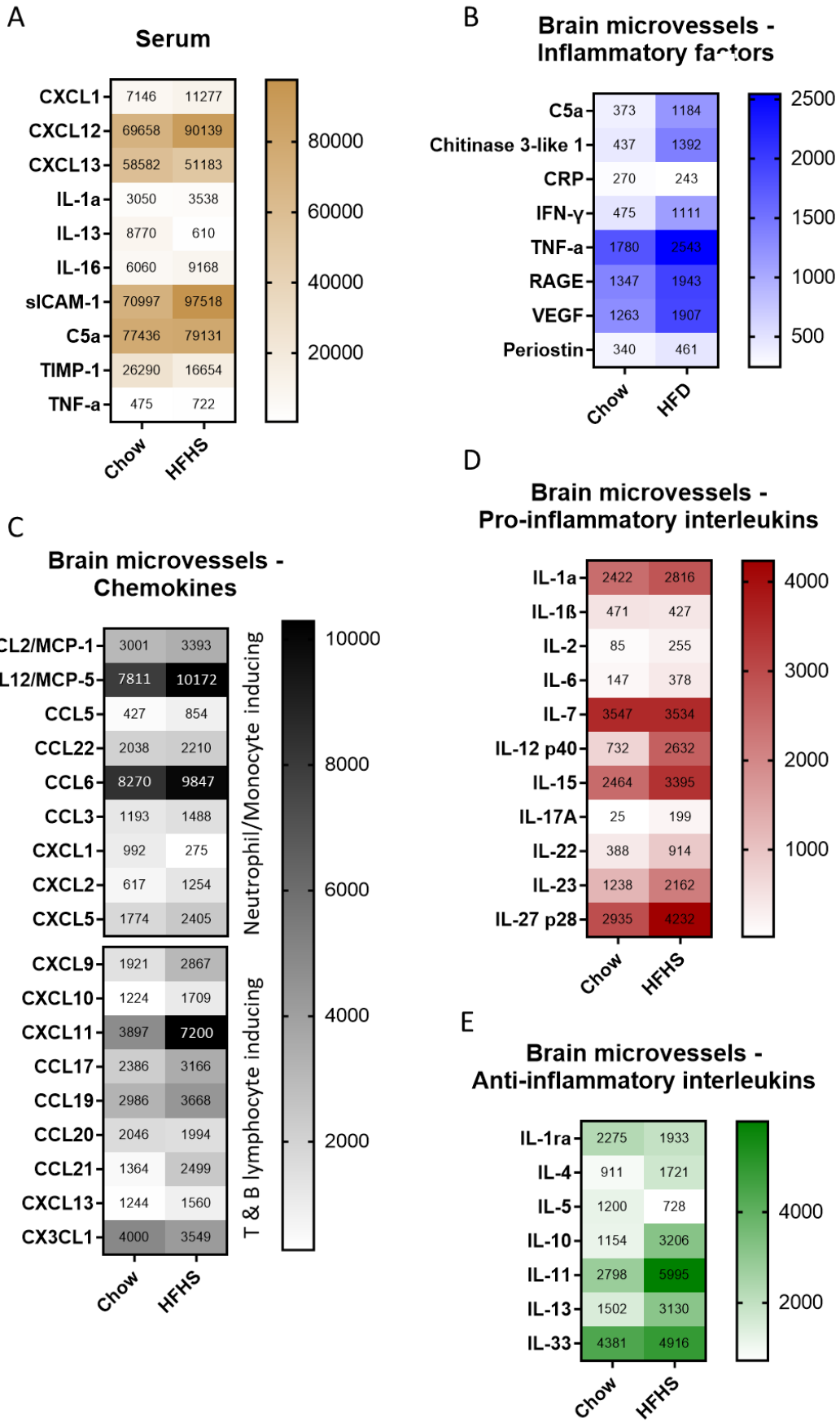
A
Serum
CXCL1 7146 11277
CXCL12 69658 90139
CXCL13 58582 51183
IL-1a 3050 3538
IL-13 8770 610
IL-16 6060 9168
sICAM-1 70997 97518
C5a 77436 79131
TIMP-1 26290 16654
TNF-a 475 722
Chow
HFHS
80000
60000
40000
20000
B
Brain microvessels - Inflammatory factors
C5a 373 1184
Chitinase 3-like 1 437 1392
CRP 270 243
IFN-γ 475 1111
TNF-a 1780 2543
RAGE 1347 1943
VEGF 1263 1907
Periostin 340 461
Chow
HFD
2500
2000
1500
1000
500
C
Brain microvessels - Chemokines
CCL2/MCP-1 3001 3393
CCL12/MCP-5 7811 10172
CCL5 427 854
CCL22 2038 2210
CCL6 8270 9847
CCL3 1193 1488
CXCL1 992 275
CXCL2 617 1254
CXCL5 1774 2405
Neutrophil/Monocyte inducing
CXCL9 1921 2867
CXCL10 1224 1709
CXCL11 3897 7200
CCL17 2386 3166
CCL19 2986 3668
CCL20 2046 1994
CCL21 1364 2499
CXCL13 1244 1560
CX3CL1 4000 3549
T & B lymphocyte inducing
Chow
HFHS
10000
8000
6000
4000
2000
D
Brain microvessels - Pro-inflammatory interleukins
IL-1a 2422 2816
IL-1ß 471 427
IL-2 85 255
IL-6 147 378
IL-7 3547 3534
IL-12 p40 732 2632
IL-15 2464 3395
IL-17A 25 199
IL-22 388 914
IL-23 1238 2162
IL-27 p28 2935 4232
Chow
HFHS
4000
3000
2000
1000
E
Brain microvessels - Anti-inflammatory interleukins
IL-1ra 2275 1933
IL-4 911 1721
IL-5 1200 728
IL-10 1154 3206
IL-11 2798 5995
IL-13 1502 3130
IL-33 4381 4916
Chow
HFHS
4000
2000

Figure 4.7 | Evaluation of inflammation in mouse serum and at the brain microvasculature through measuring inflammatory markers, interleukins & chemokines

Simultaneous measurement of multiple cytokines, chemokines, interleukins and other inflammatory markers in both serum and protein extract from brain microvessels of chow and HFHS-fed mice using Mouse Cytokine Array Kits (R&D Systems). Membrane-based immunoassays detected the relative expression levels of analytes detected as arbitrary units. Analytes were measured in serum (A; n=10 pooled/group, two technical replicates per experiment, performed as two independent experiments total n=20/group) or in brain microvessels (C-E, n=10 pooled/group, performed in duplicate) and categorised as inflammatory factors (B), chemokines (C), pro-inflammatory interleukins (D) or anti-inflammatory interleukins (E).

4.2.5 Activation of endothelial cells of the BBB

It is widely acknowledged that an inflammatory state causes the activation and extravasation of leukocytes particularly in atherosclerosis and coronary heart disease, for which obesity and MetS are risk factors (518). In order for leukocytes to transmigrate, the endothelium must be primed and activated to allow immune cells to roll, tether and adhere. Both *in vitro* and *in vivo* studies have linked hyperglycaemia and hyperlipidaemia in T2DM to cause endothelium activation with enhanced expression of activation markers such as ICAM-1 (519). In parallel, research has indicated glucose and lipid presence to also activate lymphocytes (520–522).

To observe if an enhanced metabolic state induces the BBB endothelial in the same manner, the expression of ICAM-1 and P-selectin on microvessels in the cerebral cortex of the brain was examined using immunofluorescence. Confocal microscopy illustrates major differences in ICAM-1 (Figure 4.8A) and P-selectin (Figure 4.8B) expression on the microvessels between chow-fed and HFHS-fed mice, whereby both cell adhesion molecules have a higher constitutive expression in HFHS-fed mice; statistically confirmed via mean fluorescence intensity (Figure 4.8A,B). Moreover, transversely cut sections of the microvessels of HFHS-fed mice showed the localisation of ICAM-1 and P-selectin prevalently at the luminal side of the vessel, to allow TEM into the brain parenchyma.

Proteomic analysis of isolated brain microvessel tissue (Figure 4.8C) confirmed the confocal imaging results. HFHS-fed mice had raised ICAM-1, P-selectin and VCAM-1 compared to chow-fed mice. HFHS-fed mice also showed a trend of increased co-stimulatory molecule CD40 compared to chow-fed mice however, however no changes were seen in E-selectin expression.

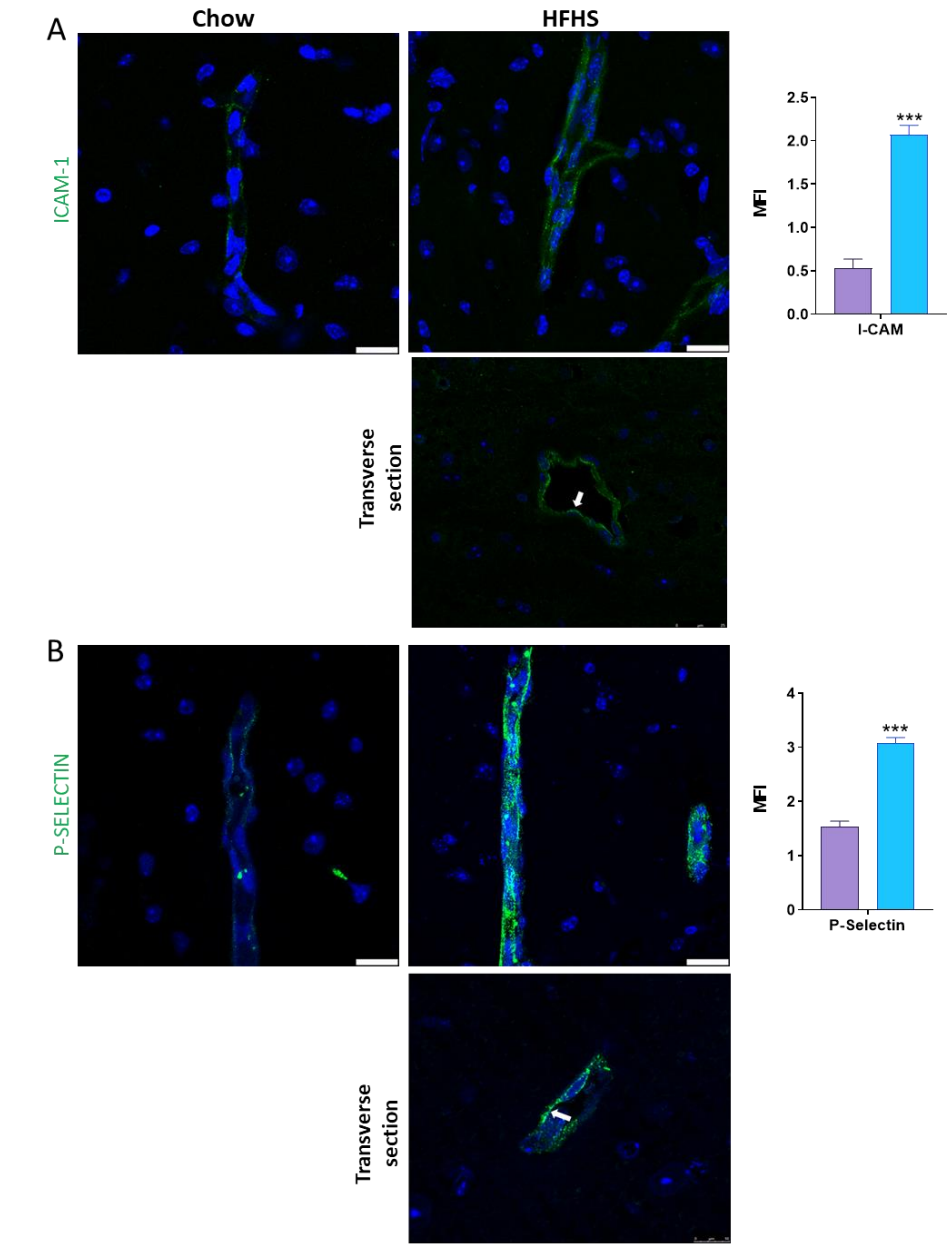
A
Chow
HFHS
ICAM-1
Transverse section
MFI
I-CAM
***
B
P-SELECTIN
Transverse section
MFI
P-Selectin
***
C
Average Pixel Density (arbitary units)
Chow
HFD
CD40
E-selectin
ICAM-1
P-selectin
VCAM-1
*

Figure 4.8 | Activation of the BBB endothelium to a pro-inflammatory state - cell adhesion molecule expression on brain microvessels

Cerebral cortical sections of the brain were immunofluorescently stained for endothelial cell adhesion molecules ICAM-1 (A) and P-selectin (B); nuclei were labelled with TO-PRO3. Typical images from n=4 animals, 35 section/animals (scale bar: 25µm). Quantification of staining shown as mean fluorescence intensity (arbitrary units) of markers on ten randomly selected fields. Proteomic analysis of adhesion molecules on brain microvessel extracts from chow and HFHS-fed mice using a membrane-based immunoassay (Mouse Cytokine Array XL Kit, R&D Systems) to detect the relative presence of E-selectin, ICAM-1, P-selection and VCAM-1 and co-stimulatory molecule CD40 by x-ray film exposure (C, n=10 pooled/group, two technical replicates per experiment, performed as two independent experiments total n=20/group); quantified using ImageStudio Lite (LI-COR Biosciences). Statistical analysis was performed by an Independent Student's T-test. Data is expressed as mean ± SEM., *p< 0.05, **p<0.01, ***p<0.001, ****p< 0.0001.

4.2.6 Induction of the immune system in metabolic overload

The pathogenesis of T2DM is considered to involve both the innate and adaptive immune systems. The progressive tissue damage occurring to the heart, liver, kidney, and adipose tissue are characterised by abnormal immune cell function. It is therefore likely that the damage occurring at the BBB and subsequently within the brain parenchyma would involve peripherally activated and primed immune cells.

4.2.6.1 Examining the innate and adaptive arms of the immune system in the peripheral system

In order to evaluate whether the immune system is primed and activated in this mouse model, the frequency of different immune cells types from the innate and adaptive arms was assessed.

Bone marrow was isolated and stained for cells of the innate (neutrophils, macrophages & dendritic cells) and adaptive (NK cells, T-cells, and B-cells) immune system (Figure 4.9A). Percentage cell frequency of all innate immune cell types were higher in the HFHS-fed mice when compared to chow-fed mice. In the adaptive immune cells, only $CD8^+$ T-cells had a higher frequency in HFHS-fed mice when compared to chow-fed mice. In comparison, NK cells and B-cells had a reduced frequency in HFHS-fed mice when compared to chow-fed mice and no differences were seen with $CD4^+$ T-cells.

The T- and B-cell frequency was also analysed from the cervical lymph nodes of mice, the main lymph drainage points from the brain (Figure 4.9B). Again no differences were seen in $CD4^+$ T-cells however opposite to the bone marrow, in the cervical lymph nodes HFHS-fed mice showed a reduced frequency of $CD8^+$ T-cells and higher frequency of $CD19^+$ B-cells compared to chow-fed mice.

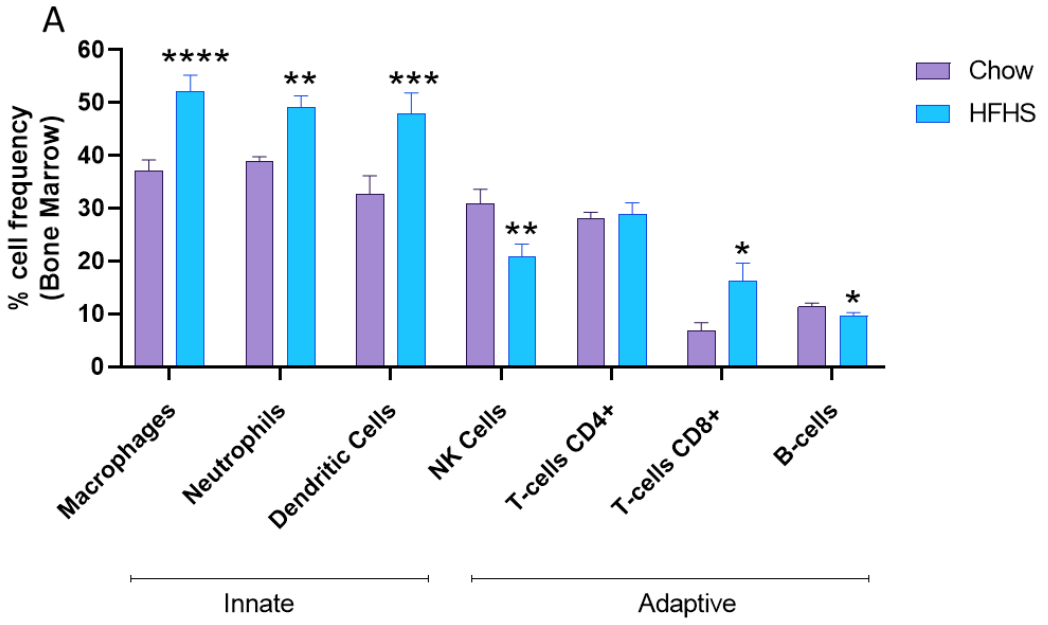
A
% cell frequency (Bone Marrow)
60
50
40
30
20
10
0
****
**
***
**
*
*
Chow
HFHS
Macrophages
Neutrophils
Dendritic Cells
NK Cells
T-cells CD4+
T-cells CD8+
B-cells
Innate
Adaptive

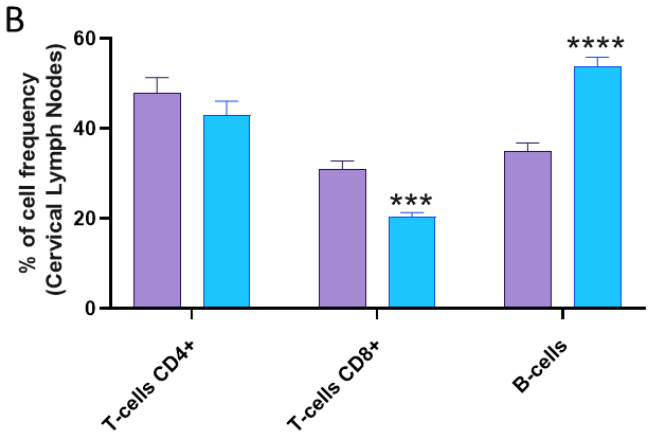
B
% of cell frequency (Cervical Lymph Nodes)
60
40
20
0
***
****
T-cells CD4+
T-cells CD8+
B-cells

Figure 4.9 | Activation of the innate and adaptive arms of the immune system

Bone marrow and deep cervical lymph nodes were collected from chow and HFHS-fed mice. Bone marrow was flushed with PBS-/- to obtain white blood cells, red blood cells were lysed using lysis buffer. Cells were stained using fluorescently conjugated antibodies for cell-surface markers on cells of the innate – neutrophils (Ly6G), macrophages (CD11b), dendritic cells (F4/80, CD11c), and adaptive – NK cells (NK 1.1), T-cells (CD4, CD8), B-cells (CD19) immune system and underwent flow cytometric analysis (n=19-23/group). Deep cervical lymph nodes were homogenised to obtain lymphocytes and underwent flow cytometric analysis after staining to obtain percentage frequency of T-cell subsets CD4+ and CD8+ and B-cells (CD19+) (n=12-16/group). Statistical analysis was performed by either an Independent Student's T-test or Mann-Whitney U Test. Data is expressed as mean ± SEM., *p< 0.05, **p<0.01, ***p<0.001, ****p< 0.0001.

4.2.6.2 Examining the activation of $CD4^+$ T-cells in T2DM

$CD4^+$ T-cells are also known as T-helper (T_H) cells and play an important role in shaping the response of the adaptive immune system by releasing cytokines to enhance or supress immune responses. Mature T_H cells express the cell surface protein CD4. The $CD4^+$ cells are vital in B-cell antibody class switching, activation of cytotoxic T-cells and in maximising the phagocytic activity of macrophages. In this part of project, we investigated the role of this specific subset of T-cells in more detail. Lymphocytes were always isolated from deep cervical lymph nodes.

HFHS-feeding enhanced activation of $CD4^+$ T-cells, as represented by immune-staining with activation marker CD44, which is typically upregulated after activation of naïve T lymphocytes during immune response. Results showed that when compared to chow-fed mice, HFHS-fed mice had a greater percentage of $CD4^+$ $CD44^+$-expressing T-cells, however this was not statistically significant (Figure 4.10A).

In order for immune cells to illicit immune response and combat microbes or infection, they must be able to reach the site of target by passing across endothelial cell barriers from bloodstream to tissue. Transmigration not only requires the expression of adhesion molecules on endothelial cells but also co-receptors on the leukocytes to allow for firm arrest. CD44 itself can regulate the tethering and rolling interaction. Nonetheless within the $CD4^+$ $CD44^+$-expressing T-cells the expression of adhesion molecule lymphocyte function-associated antigen 1 (LFA-1) that binds to ICAM-1 on endothelial cells was assessed (Figure 4.10B). Results showed a significant increase in percentage of $CD4^+$, $CD44^+$, LFA-1^+-expressing T-cells by 1.5-fold in HFHS-fed mice when compared to chow-fed mice.

T-cells which respond to immune cues in the short-term can be named as effector T-cells (T_{eff}). Chemokine receptor, CXCR3 is highly expressed on these T_{eff} cells and is key in the trafficking and function of these cell types in response to chemokines. Within the $CD4^+$ $CD44^+$-expressing T-cells, the expression of CXCR3 was also measured (Figure 4.10C). Results showed a significant increase in the percentage of $CD4^+$, $CD44^+$, $CXCR3^+$-expressing T_{eff} cells by 2-fold in HFHS-fed mice when compared to chow-fed mice.

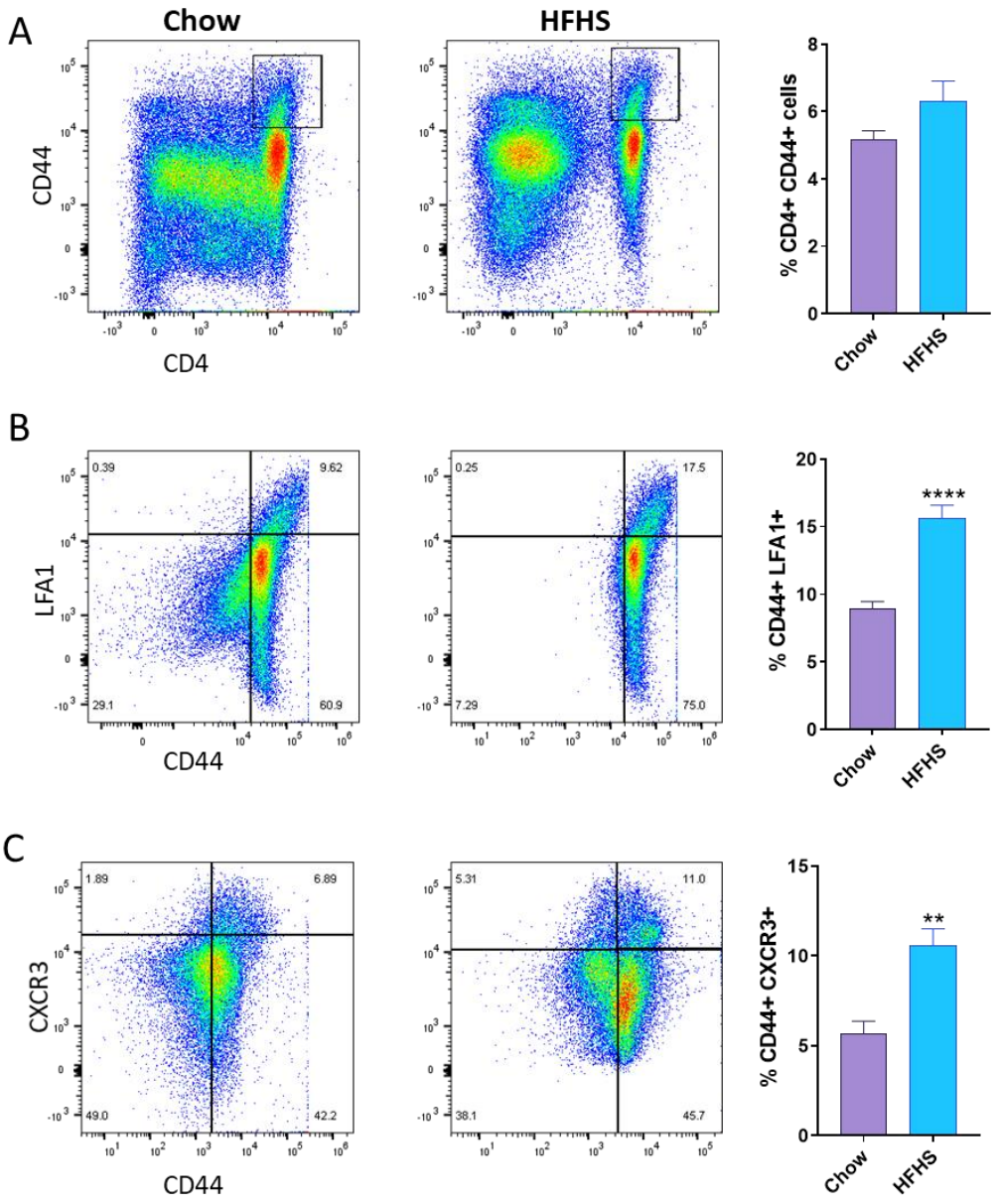

Figure 4.10 | T-effector cell activation in T2DM

Deep cervical lymph nodes were collected from chow and HFHS-fed mice. Lymph nodes were homogenised to obtain lymphocytes. All T-cells were stained for CD4, within this subset of T-cells staining was conducted for activation marker CD44 (A). On $CD4^+$ $CD44^+$-expressing T-cells, the expression of lymphocytic adhesion molecule LFA-1 (B) and chemokine receptor CXCR3 (C) was evaluated (n=5-11/group). Statistical analysis was performed by either an Independent Student's T-test or Mann-Whitney U Test. Data is expressed as mean ± SEM., **p<0.01, ****p< 0.0001.

4.2.6.3 Involvement of central memory vs effector memory T-cells

Memory T-cells are often termed antigen-experienced T-cells due to their characteristic to have encountered and responded to their antigen previously. Such memory T-cells can reproduce faster and stronger responses upon re-encounters to their cognate antigens. Memory T-cells can be divided into several subsets, of which central memory (T_{CM}) and effector memory (T_{EM}) are the two major groups. T_{CM} have a self-renewal ability and confer powerful responses against viruses, bacteria, and cancer cells. In comparison T_{EM} cells are responsible for cytotoxic action.

As MetS and T2DM confers a low-grade chronic inflammatory state whereby the same antigens will be encountered by the immune cells, the relative numbers of T_{CM} and T_{EM} in the HFHS model was investigated. The expression of CD44 is retained on memory T-cells, therefore cells were initially defined as $CD4^+$ $CD44^+$-expressing T-cells. Within this population, the expression of chemokine receptor CCR7 (Figure 4.11A) and L-selectin CD62L was analysed (Figure 4.11B). It is the differential expression of these ligands as high (hi) or low (lo) which defines whether, these cells are central or effector memory. T_{CM} cells are defined as CD44hi CD62Lhi CCR7hi whereas T_{EM} cells are defined as CD4hi CD62Llo CCR7lo.

In HFHS-fed mice there is a significantly greater percentage of CD44hi CCR7hi cells when compared with chow-fed mice. The HFHS-fed mice have a slightly increased percentage of CD44hi CD62Lhi-expressing cells when compared to chow-fed mice, however this is not statistically significant. Overall, the results implicate HFHS-fed mice to have a greater proportion of T_{CM} cells when compared with chow-fed mice.

Similarly, in HFHS-fed mice there is a significantly greater percentage of CD44hi CCR7lo and CD44hi CD62Llo-expressing cells when compared with chow-fed. Overall the results implicate HFHS-fed mice to have greater numbers of T_{EM} cells when compared with chow-fed.

Given the differences in percentages and statistically significance, it appears as though HFHS-fed mice have a greater proportion of T_{EM} to T_{CM} cells ratio.

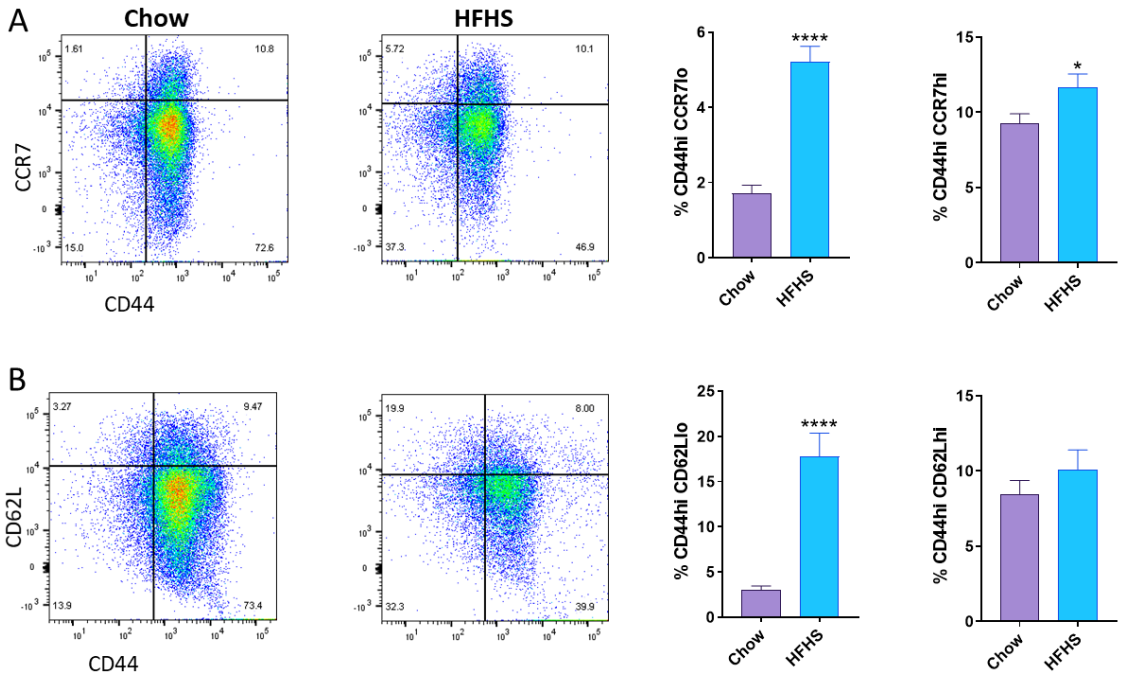

Figure 4.11 | Effector Memory vs Central Memory T-cells

Deep cervical lymph nodes were collected from chow and HFHS-fed mice. Lymph nodes were homogenised to obtain lymphocytes. All T-cells were stained for CD4 antigen, within this subset of T-cells staining was conducted for high (hi) or low (lo) expression of activation antigen marker CD44 (A). On $CD4^+$ $CD44^+$-expressing T-cells, the high and low expression of L-selectin CD62L (A) and chemokine receptor CCR7 (B) was evaluated (n=5-11/group) to characterise the presence of central memory (CD44hi, CD62Lhi, CCR7lo) or effector memory (CD44hi, CD62Llo, CCR7lo) T-cells. Statistical analysis was performed by either an Independent Student's T-test or Mann-Whitney U Test. Data is expressed as mean ± SEM., **p<0.01, ****p< 0.0001.

4.2.6.4 Pro vs Anti-inflammatory T-cells: Treg vs Th17 cells

$CD4^+$ T-helper subsets can be categorised into different effector subsets including the pro-inflammatory T_H1, T_H2 and T_H17 and the anti-inflammatory Treg. A combination of different cytokine signals determines the fate and production of the T_H cells. The different subsets orchestrate varied responses and conduct specific functions dependent on their cytokine production.

T_H17 cells are RAR-related orphan receptor gamma (RoRγt)-expressing cells involved in inflammation and autoimmune responses. In contrast, the Treg cells are vital in supressing excessive inflammatory responses and to limit tissue damage. Treg cells are characterised by the expression of fork head/winged-helix transcription factor, Foxp3.

The involvement of T-cells in T2DM has been widely reported in mice and humans; with a skew towards the pro-inflammatory T_H1 and T_H17 subsets and a decrease in Treg; culminating in inflammation, insulin tolerance and T2DM progression (523–526). Importantly, the T_H17 cells were negatively correlated to plasma levels of HDL and Treg were positively correlated to IL-6 levels; suggesting the relationship between $CD4^+$ T-cells subsets and dyslipidaemia and hyperglycaemia (368). Therefore, the presence and ratio of T_H17 to Treg was investigated in the experimental mice to see if there was an imbalance in their proportion (Figure 4.12).

Flow cytometric analysis of lymphocytes isolated from deep cervical lymph nodes found that in HFHS-fed mice the percentage of RoRγt-expressing T_H17 cells was significantly upregulated (Figure 4.12A) compared to chow-fed mice. The percentage of Foxp3-expressing Treg cells (Figure 4.12B) showed a trend towards downregulation in HFHS-fed mice compared to chow-fed mice, but this was not significant. However, in the HFHS-fed mice there was a higher T_H17/Treg ratio compared to chow-fed mice (Figure 4.12C), thereby highlighting a skew towards a pro-inflammatory T-cell phenotype.

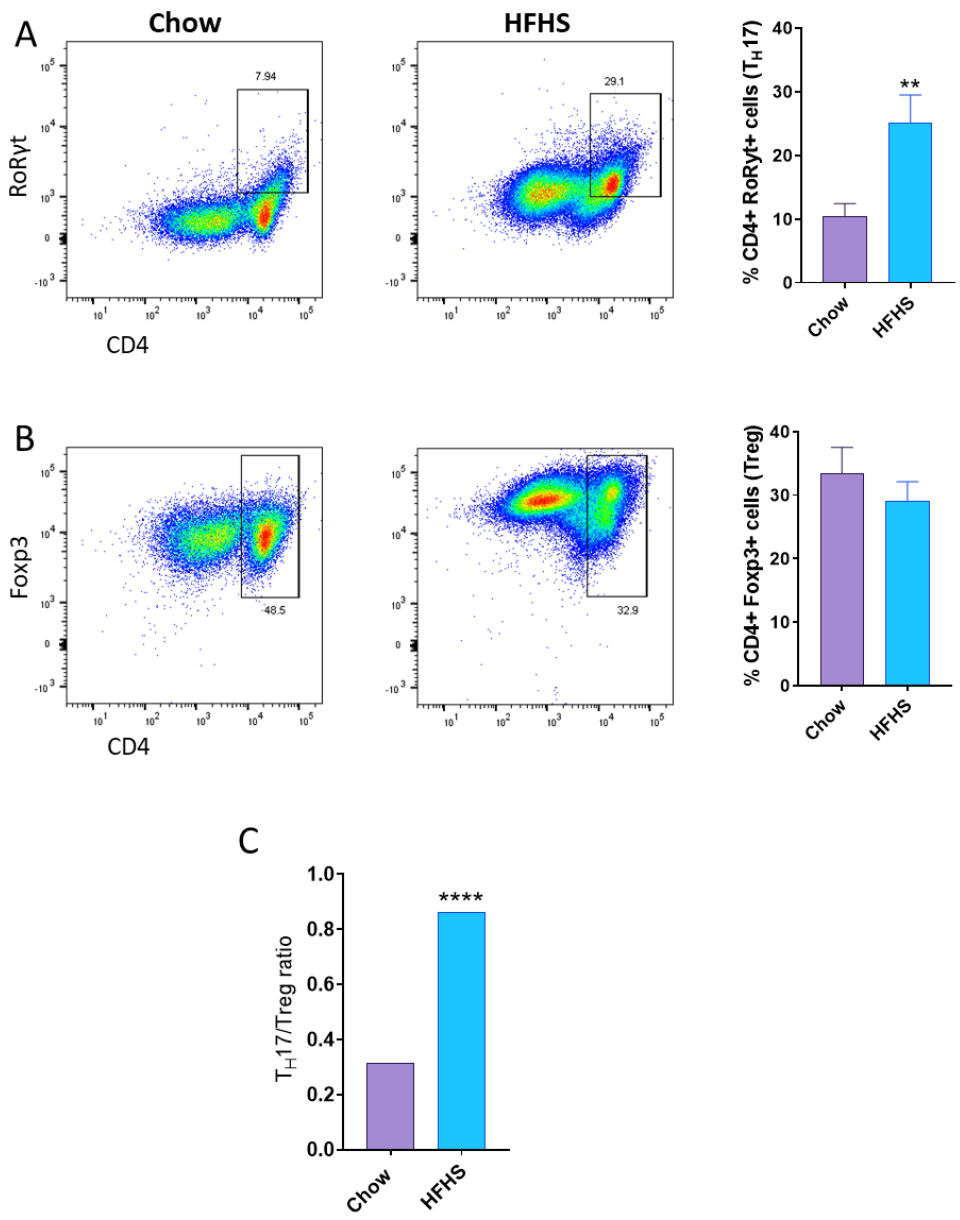

Figure 4.12 | Pro vs Anti-inflammatory T-cells: T_H17 vs Treg cells

Deep cervical lymph nodes were collected from chow and HFHS-fed mice. Lymph nodes were homogenised to obtain lymphocytes. All T-cells were stained for CD4, within this subset T-cells were categorised as pro-inflammatory T-helper (T_H17) cells based on their expression of RoRγt (A) or as anti-inflammatory regulatory T-cells (Treg) based on their expression of Foxp3 (B) The skew towards a pro- or anti-inflammatory phenotype was determined by the ratio of T_H17/Treg cells (C) (n=9=11/group). Statistical analysis was performed by either **a**n Independent Student's T-test or Mann-Whitney U Test. Data is expressed as mean ± SEM., **p<0.01

4.2.6.5 Transmigration of peripherally activated leukocytes across the BBB

Having previously shown that the HFHS diet damages the BBB and its barrier properties, and activates T-cells, we measured the migratory activity of T-cells through the endothelium into the brain parenchyma.

Confocal microscopy of cortical brain sections double-stained with CD45 and pan-laminin (Figure 4.13A) revealed numerous $CD45^+$ cells in the vessel lumen of HFHS-fed mouse brains, which appeared trapped between the VBL layers. In comparison, in chow-fed mice brains, $CD45^+$ cells were rarely detected and there was absence of perivascular leukocytes infiltrates.

To further dissect the mechanism of action of T-cell migration, *in vitro* adhesion/migration experiments were performed using lymphocytes isolated from deep cervical lymph nodes. Isolated lymphocytes from chow-fed and HFHS-fed mice were activated and expanded for 4 days using CD3 and CD28, after which they were placed in contact for 4 hours with an *in vitro* model of the BBB; using bEnd3 cells plated on transwells to conduct a transmigration assay (see Figure 4.13B). The migrated cells represented those which had crossed the BBB, whereas the adhered cells were equivalent to the immune cells which had arrested on the endothelium but had not crossed the BBB (Figure 4.13B).

FACS analysis of double immune-stained $CD4^+$ $CD45^+$ T-cells from lymph nodes (Figure 4.13D) showed that the numbers of adhered and migrated cells were higher in the HFHS-fed mice when compared to chow-fed mice, however this was only significant in the migrated population.

T-cells expanded from lymph nodes were also stained for pro-inflammatory T_H17 and anti-inflammatory Treg cells (Figure 4.13E,F). Results showed a greater number of adhered and migrated T_H17 and Treg cells in the HFHS-fed mice when compared to chow-fed mice, all results were significant.

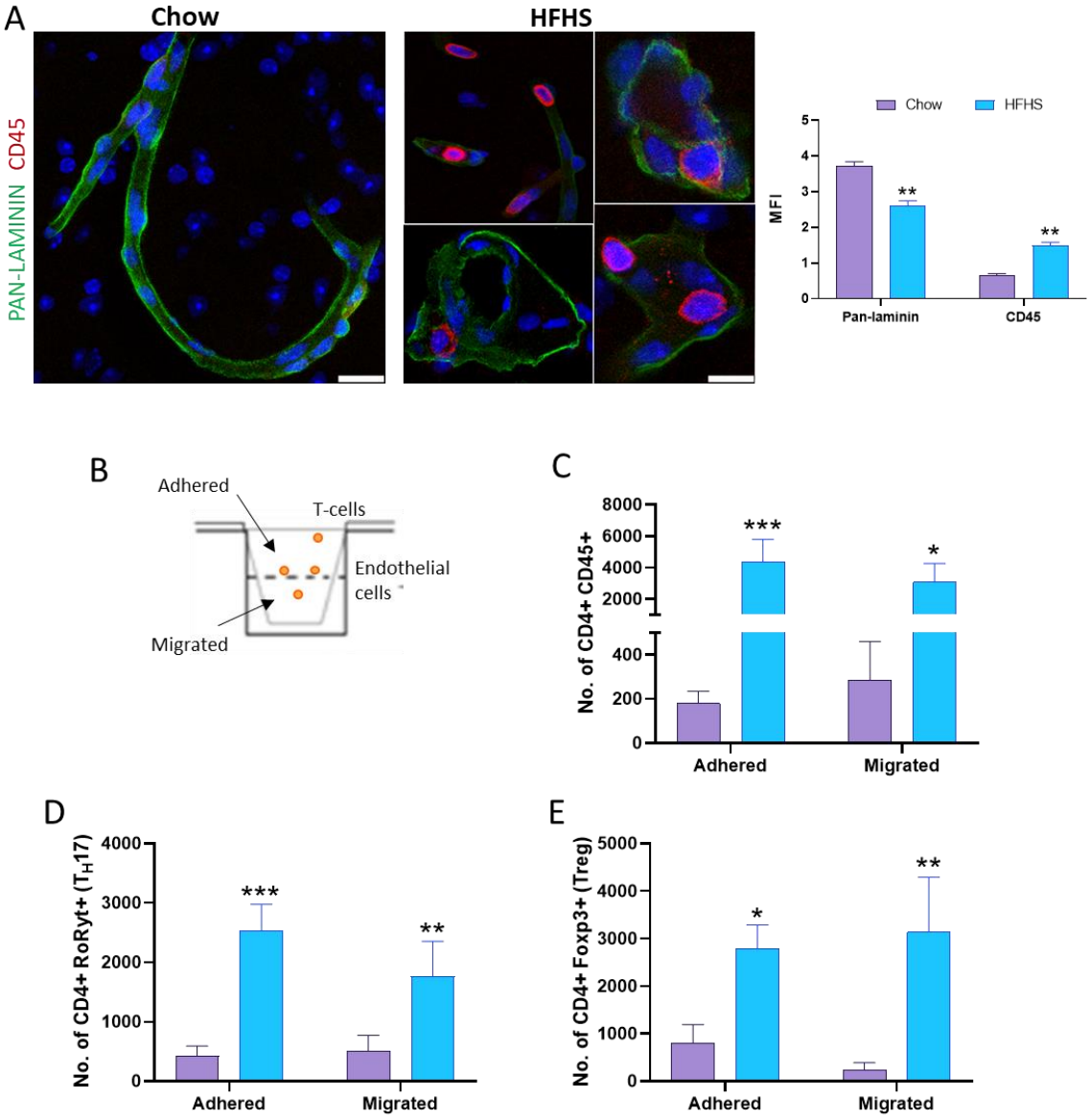
A
Chow
HFHS
PAN-LAMININ CD45
Chow
HFHS
MFI
Pan-laminin
CD45
B
Adhered
T-cells
Endothelial cells
Migrated
C
No. of CD4+ CD45+
Adhered
Migrated
D
No. of CD4+ RoRyt+ (TH17)
Adhered
Migrated
E
No. of CD4+ Foxp3+ (Treg)
Adhered
Migrated

Figure 4.13 | Transmigration of peripherally activated leukocytes across the BBB

Cerebral cortical sections of the brain were immunofluorescently stained for antigen CD45, present on all activated leukocytes, to examine the transmigration of immune cells across the BBB (A); nuclei were labelled with TO-PRO3. Typical images from n=4 animals, 35 section/animals (scale bar: 25μm). Quantification of staining shown as mean fluorescence intensity (arbitrary units) of markers on ten randomly selected fields. Further assessment of T-cell migration was conducted using deep cervical lymph nodes, collected from chow and HFHS-fed mice (B-E). Lymph nodes were homogenised to obtain lymphocytes and expanded for 4 days in the presence of CD3 and CD28. On day 4, a transmigration assay was conducted, with 1 x 10^6 cells placed in contact with bEnd3 cells grown on transwell inserts. T-cells were placed in contact with the *in vitro* BBB model for a period of 4 hours, after which the cells collected from the top compartment of the transwell served as the adhered component and the cells collected from the bottom compartment served as the migrated component (B). All collected cells were stained for CD4; within this subset cells were stained for activation marker CD45 (C), RoRγt-expressing T_H17 cells (D) or Foxp3-expressing Treg (E) (n=5-9/group). Statistical analysis was performed by either an Independent Student's T-test or Mann-Whitney U Test. Data is expressed as mean ± SEM., *p< 0.05, **p<0.01, ***p<0.001.

4.2.7 Activating the brain-tissue resident immune cells: The microglia

The data provided until now have proved that a HFHS diet causes inflammation and activates the peripheral immune system; together these factors disrupt the structural and immunological integrity of the BBB. The next step was to investigate how the brain innate response and functionality was affected. A protagonist at the centre of brain immunity is the microglia cells; and hence their activation and behaviour were investigated.

4.2.7.1 M1 vs M2 Microglia

Microglial cells were identified from macrophages by gating on the CD45lo $CD11b^+$ population (Figure 4.14A). Results showed a higher percentage of microglial cells in the HFHS-fed mice when compared to chow-fed mice. Microglial cells also highly express the fracktaline receptor $CX3CR1^+$ which responds to the fracktaline (chemokine) CX3CL1 produced by neurons. Interestingly the expression of $CX3CR1^+$, as measured by MFI, was reduced in HFHS-fed mice when compared to chow-fed mice (Figure 4.14B). Activated microglial cells were identified by the markers $CD11c^+$ and $MHCII^+$ on CD45lo $CD11b^+$-expressing cells (Figure 4.14C); the results showed HFHS-fed mice to have a higher percentage of activated microglial cells compared to chow-fed mice. These activated cells were further differentiated as a pro-inflammatory M1 phenotype ($CD86^+$-expressing cells) or as an anti-inflammatory/resolving M2 phenotype ($CD206^+$-expressing cells, Figure 4.14D). Notably HFHS-fed mice had more than double the percentage of M1 $CD86^+$ cells compared to chow-fed mice; this correlated with a decrease of M2 $CD206^+$ cells by more than 50%. In summary, the HFHS-fed mice had a greater ratio of M1:M2 microglia cells (Figure 4.14E).

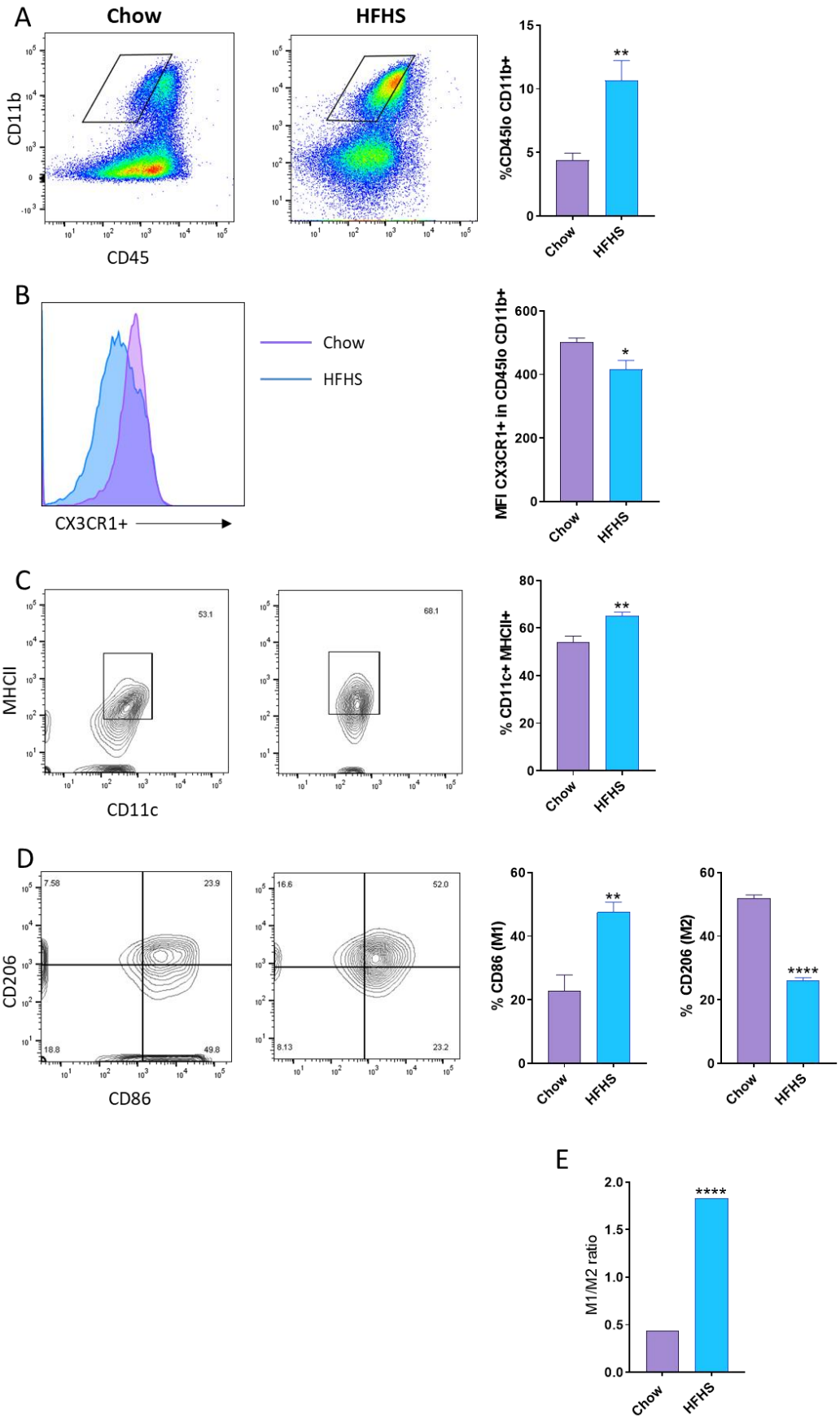
A
Chow
HFHS
CD11b
CD45
%CD45lo CD11b+
Chow
HFHS
B
Chow
HFHS
CX3CR1+
MFI CX3CR1+ in CD45lo CD11b+
C
MHCII
CD11c
% CD11c+ MHCII+
D
CD206
CD86
% CD86 (M1)
% CD206 (M2)
E
M1/M2 ratio

Figure 4.14 | Activation of brain tissue resident macrophages – the microglia cells

Microglia cells were isolated and cultured from chow and HFHS-fed mice (n=6-12/group, pooled in pairs). Microglia cells were identified by gating on CD45lo $CD11b^+$ cells to differentiate from macrophages (A). Expression of fracktaline receptor $CX3CR1^+$ in CD45lo $CD11b^+$-expressing cells (B), as median intensity of fluorescence (MFI). Percentage of activated microglial cells identified as $CD11c^+$ $MHCII^+$-expressing cells (C) differentiated into pro-inflammatory M1 (CD86+-expressing) and anti-inflammatory M2 (CD206+-expressing cells) phenotypes (D) and presented as a ratio of M1/M2 (E). Statistical analysis was performed by an Independent Student's T-test. Data is expressed as mean ± SEM., *p< 0.05, **p<0.01, ****p<0.0001.

4.2.7.2 Oxidative damage in the diabetic brain

NO is key in modulating physiological responses such as vasomotor tone and neuronal function. The production of ROS and RNS forms a part of innate defence mechanism; however, their overproduction can cause apoptosis and promote tissue damage. Endothelial cells, macrophages/microglia and neurons are the main producers of NO (527).

Immune staining of IBA1, a microglia activation marker, showed activated microglia of a pro-inflammatory phenotype in the HFHS-fed mice, which are known to be source of iNOS production (Figure 4.15A). In comparison, in the chow-fed mice there is low expression of microglia activation marker IBA1. Confocal imaging of cortical brain sections reveals HFHS-fed mice to have a higher constitutive expression of iNOS when compared to chow-fed mice (Figure 4.15B). The localisation of iNOS is consistent with the formation of a vessel, suggesting that the endothelial cells are producing iNOS. This is confirmed in through the co-localisation of iNOS with endothelial cells via nuclei staining of TO-PRO3 (Figure 4.15B). iNOS presence outside of the vessel formation in the brain tissue suggests production by brain parenchymal cells such as the microglia.

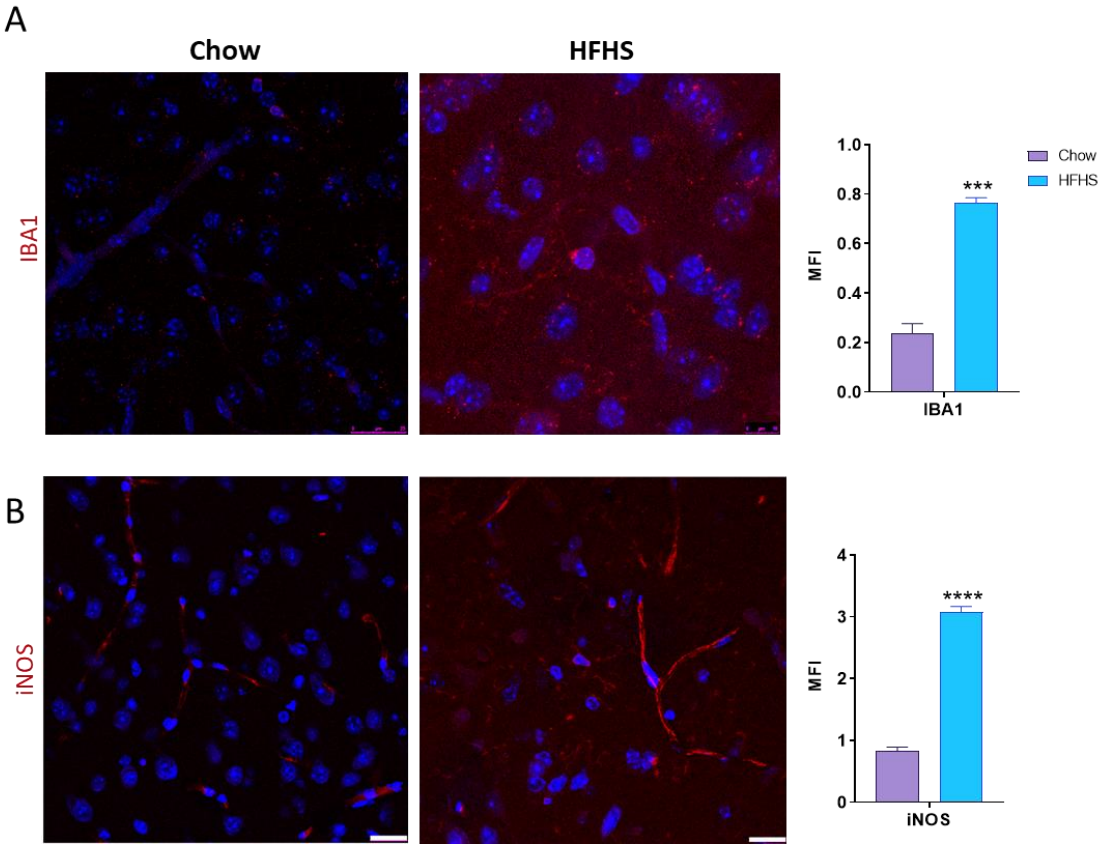

Figure 4.15 | Oxidative stress in the brain

Cerebral cortical sections of the brain were immunofluorescently stained for IBA1 (A) and iNOS (B) expression; nuclei were labelled with TO-PRO3. Typical images from n=4 animals, 35 section/animals (scale bar: 25µm). Quantification of staining shown as mean fluorescence intensity (arbitrary units) of markers on ten randomly selected fields. Statistical analysis was performed by an Independent Student's T-test. Data is expressed as mean ± SEM., *p< 0.05, **p<0.01, ****p<0.0001.

4.3 Discussion

This chapter investigates the use of a combination of high-fat and high-sugar feeding to serve as a diet-induced model of MetS/T2DM. As mentioned previously, there are no gold-standard reference values for confirmation of T2DM in mice (467), therefore results have been compared to previous literature and studies.

Feeding on a HFHS diet for 10 weeks resulted in progressive increase in body weight compared to chow-fed mice. Previous studies using C57BL/6 mice indicate that an increase in body weight is noticeable as early as 2 weeks and becomes clearly apparent after 4 weeks (505), which parallels the results in this HFHS model. Literature reports that after 16-12 weeks of high-fat feeding, mice will exhibit a 20-30% increase in body weight compared to chow-fed mice (505); in the results of our study it can be seen that HFHS feeding results in approximately a 40% weight gain in comparison to chow-fed counterparts. These results are similar to those reported previously in our group using the same HFHS diet for a period of 10-12 weeks (473,474,512). According to Surwit et al., this increase in body weight gain in chow-fed versus high fat-fed mice can be termed as obesity (464,472). We also similarly report an increase in the percentage of epididymal and inguinal fat in HFHS-fed mice compared to chow-fed mice, as measures of adiposity and thus obesity (472).

The HFHS-fed mice in this study also show a significant impairment in oral glucose tolerance at week 8. Similar results have also been shown by Andrikopoulos et al., at 8 weeks of high-fat feeding in C57BL/6 mice (490) and have also been shown by our group using the same HFHS diet for a period of 10, 12, 14 or 16 weeks (473–475). In fact, it has been reported that an impairment in glucose tolerance can be seen as early as 1 week after dietary manipulation (528).

According to the initial establishment of the T2DM using a high-fat diet model in C57BL/6 mice, fasting blood glucose and serum insulin levels are sufficient to confirm glucose in tolerance and insulin resistance, respectively (464,472). Based on these criteria alone, it would be sufficient to suggest that the HFHS-fed mice in this study have impaired glucose tolerance and insulin resistance due to high fasted and non-fasted blood glucose and high serum insulin levels compared to controls; this criteria has been used by other studies too (490). Nevertheless, the advancement in obesity and diabetes research has led to more in-depth measures of insulin resistance of which

insulin tolerance testing in the most popular. The results in the HFHS-fed mice indicate that there is an impaired insulin response, but this is not significant. This may simply be due to a small n number of 6 animals, however other studies that have reported impaired insulin response, as measured by ITT in mice place on a high-fat diet for 12-16 weeks or more (473,528–530). Therefore, it is plausible to say that the HFHS-fed mice in this study have moderate insulin resistance as opposed to overt insulin resistance. In fact, it is well known that compensatory hyperinsulinemia is often considered a trait of MetS or mild diabetes, whereby the fasting glucose levels are maintained to combat insulin resistance (380). In this manner, the high serum insulin levels are an attempt to combat the hyperglycaemia and therefore the insulin resistance is not fully established. Indeed, in mice it is more difficult to assess the stage of disease and there is significant continuum between obesity, MetS, insulin resistance and T2DM (379).

Dyslipidaemia with high cholesterol and high triglyceride levels is significantly apparent in the HFHS-fed mice compared to chow-fed mice. This parallels previous reports by our group and others (474,512,529–532).

Therefore initially the results of this chapter showcase that the use of a combination of high-fat and high-sugar feeding appropriately serves as a diet-induced model of MetS/T2DM through the development of obesity, hyperglycaemia, hyperinsulinemia, mild insulin resistance and dyslipidaemia compared to a normal chow diet. Furthermore, the HFHS diet impairs the structural, functional, and immunological integrity of the brain through a rise in pro-inflammatory mediators including IL-1, IL-6, TNF-α and IFN-γ, in the serum and at the BBB.

4.3.1 Disruption of BBB integrity & permeability: the role of MMPs and TIMPs

Endothelial cells serve as a key interface between the blood and organs; therefore, vascular health is a key determinant in disease progression. Here, we show that metabolic disorders also disrupt the endothelial cells of the BBB. The important barrier function of these endothelial cells is perturbed with consumption of a HFHS diet, as seen by increased paracellular permeability and decreased TEER; which can be attributed to the loss of TJ proteins occludin and claudin-5 and loss of fibrillar actin. Loss of cell-cell contact through reduced TJ and AJ proteins hinders the correct association with the cell cytoskeleton resulting in loss of cell shape and reduced tension (100–102), which is further reduced upon actin depolymerisation (108–111). Loss of tensile strength hinders the ability of the brain endothelial cells to maintain their properties as a strict barrier.

BMs add an additional supportive layer to the BBB structure. Research by Sorokin and team has shown that different laminins transverse the BM dependent on layers in the brain and regions within the vascular beds, as well as stage of development (151,152). Within the capillaries of the CNS parenchyma, endothelial BMs ubiquitously express laminin α4 and laminin α5 and astroglial BMs express laminin α1 and α2 (152,533).

In this study, confocal imaging was conducted on brain capillaries and the relevant BM markers were utilised. Staining revealed loss of lamina components in both endothelial cells and astrocytes in HFHS-fed mice thereby preventing the association of astrocytic end-feet, suggesting a complete breakdown of the BBB. Under normal conditions, model systems have shown BMs to exclude macromolecules the size of albumin (hydrodynamic diameter 7nm) and limit transport of molecules in size from 40kDa (534,535,535–537). With a complete breakdown of the brain microvessel structure, molecules can readily pass through into the brain parenchyma and this correlated with enhanced albumin-bound Evans blue dye leakage in the brains of HFHS-fed mice compared to chow-fed mice. Other rodent studies using high-fat feeding also report increased BBB permeability using Evans blue dye (538), sodium fluorescein dye (539) or antibodies against endothelial barrier antigen (540), specifically in the hippocampal region of the brain. Notably, cerebral cortical brain

imaging in our study has not differentiated between brain regions. Future studies would benefit from determining whether the loss of TJs and BMs of the BBB occur within specific regions of the brain and the correlation of these brain regions with motor and neuronal function.

Breakdown of junctional proteins and BMs involves digestion by MMPs. Physiologically MMPs are required for normal tissue homeostasis. Specifically within the brain, the degradation of the ECM allows for tissue remodelling, cell migration, axonal elongation, angiogenesis and breakdown of Aβ peptides (Aβ40 and Aβ42) (187,541). However, MMPs are also involved in adverse pathophysiological processes. A number of CNS diseases including MS, AD, gliomas and stroke have implicated MMPs to be involved with undesirable effects including BBB breakdown, demyelination, tumour invasion, metastasis and promotion of leukocyte migration (187,542). A number of studies have also reported increased MMP-2 and MMP-9 concentrations in the serum (543), plasma (544), kidney arteries (545) and eyes (546) of diabetic patients. To our knowledge, our study is the first to correlate MMPs with BBB breakdown in a T2DM model, shown through increased expression of MMP-2, MMP-3 and MMP-9 within the brain microvessels of HFHS-fed mice, and enhanced activity of MMP-2 and MMP-9 via gel zymography.

MMP activity is regulated transcriptionally by cytokines, growth factors, ROS and hormones (187,547,548); this correlates with the inflammatory profile witnessed in the HFHS-fed mice with increased cytokines, interleukins, chemokines and iNOS. Inhibition of MMPs on the other hand, is mediated by TIMPs; through their binding to MMP domains (264,265). Therefore, to maintain a favourable balance of tissue homeostasis and neuroprotective events vs pathological events, a balance is required between the MMP and TIMP ratio. In the HFHS-fed mice, TIMP-1 activity was significantly reduced when compared to chow-fed mice in combination with raised MMP-2, MMP-3, and MMP-9 activity, indicating a disruption in the balance and control of MMP activity. Notably, it would be beneficial to also examine the serum levels of TIMP-2, TIMP-3 and TIMP-4, as the TIMPs interact with the MMPs with varying degrees of affinity (264). TIMP-2 has a higher affinity for MMP-2 whereas TIMP-1 forms strong interactions with MMP-9; TIMP-3 possess the broadest range of inhibition through targeting all family members of the MMPs (264).

Numerous studies have reported pro-inflammatory IL-1 and TNF-α to upregulate TIMP-1 levels in both endothelial cells and astrocytes (549,550). In mouse models of Experimental Autoimmune Encephalomyelitis (EAE), a widely-accepted model of demyelinating diseases such as MS, GFAP-expressing astrocytes increase TIMP-1 expression to aid remodelling of the brain ECM (551). Similarly, in human T-lymphotropic virus, T_H1 cells interact with astrocytes causing them to become reactive; reactive astrocytes secrete pro-inflammatory cytokines and express TIMP-1 and TIMP-3 (552). Additionally, in CNS morbillivirus infection of mouse, TIMP-1 mRNA is up-regulated in affected brain areas which can be correlated with increased T_H1 cytokines, IFN-γ, TNF-α and IL-6 (553). Although in our diabetic model, there is a substantial increase in the presence of T-cell inducing chemokines, the serum and brain microvessel protein levels of TIMP-1 are decreased. This contrast, between our results and other studies showing upregulated TIMP-1 may in fact represent the switch between a protective vs detrimental effect of MMPs/TIMPs.

For example, reports have shown differential expression of TIMP-1 in human immunodeficiency virus (HIV)-1-associated dementia (HAD). In HAD, IL-1 produced by mononuclear phagocytes induces acute activation of astrocytes resulting in significantly increased TIMP-1 mRNA and protein, despite astrocytes being rarely infected (550). In contrast, CSF and brain tissue examination from HAD patients at the end-stage of the neurological disease shows significant downregulation of TIMP-1 (554). Studies by Ghorpade and team propose differential regulation of TIMP-1, specifically in astrocytes of HAD or AD patients, to correlate with acute vs chronic inflammatory state of the disease (542,550,554). In inflammation, astrocytes initially become activated to serve as a protective mechanism, isolating the damaged area and facilitating brain circuit remodelling (401). As such, acute activation of astrocytes along with microglial activation may enhance the levels of TIMP-1 in the brain microenvironment to allow positive remodelling. However, under sustained inflammation, the levels of TIMP-1 cannot be maintained and therefore decline significantly. In a similar manner, in the diabetic mouse model where there is underlying chronic inflammation, the results show an imbalance of TIMP-1 and MMPs. In fact, a study of T2DM patients found serum concentrations of MMP-2 and MMP-9 to be lower in diabetic patients vs non-diabetic controls during short-lasting

hyperglycaemia induced by OGTT whereas chronic hyperglycaemia, reflected by HbA1c levels, correlated with higher MMP-9 levels in T2DM patients (270).

To fully consolidate the theory of acute vs chronic inflammatory MMP/TIMP balance, evaluation of brain tissue before 10 weeks of HFHS-feeding would be necessary or equivalently an acute dose of inflammation e.g. via LPS could be administered in the HFHS-fed mice before sacrificing and collecting brain tissue. Nevertheless, in this study the MMP/TIMP levels have been observed in the brain microvessels, which represents a better overall understanding of the impact at the BBB. Even so, culturing brain endothelial cells and astrocytes individually will provide a clear picture of the activity levels in each cell type. Particularly as results in models of stroke and middle cerebral artery occlusion have shown release of MMP-2, MMP-3 and MMP-9 in the acute phase (2-24 hours), by endothelial cells and infiltrating leukocytes to correlate with BBB dysfunction through degradation of the BMs; this predisposed the brain capillaries to rupture and impacted the extent of the infarct (555–560). In contrast, 7 days post-stroke when the BBB is presumably restored, the astrocytes and microglia produce MMPs which may contribute positively to the ECM remodelling (561,562). With this in mind, it is plausible that long-term presence of circulating inflammatory factors cause endothelial dysfunction inducing BBB degradation via loss of the feedback mechanism that maintains proportional levels of MMPs to TIMPs. Whilst the roles of astrocytes have not been investigated in this study, it was noted that intensity of GFAP-expressing astrocytes was not altered between chow and HFHS-fed groups despite the loss of astrocytic end-feet attachment to the endothelial cells in the HFHS-fed mice. Instead the astrocytes may respond to these inflammatory cues by becoming reactive in HFHS-fed mice. Future studies would benefit from exploring astrogliosis in a diabetic condition to understand the protective vs detrimental effect of this response, as no studies have done this to date.

It should also be noted, that TIMPs may have several diverse roles that can be either positive or negative in the brain. For instance, TIMP-3 can inhibit ADAM17 to reduce TNF-α production; ADAM17, also known as TNF-α-converting enzyme (TACE), regulates the cleavage of pro-TNF-α to its active form (563,564) to limit inflammation. On the other hand, TIMP-3 inhibition of ADAM10 and ADAM17 results in Aβ-peptide accumulation and thus plaque formation involved in AD pathogenesis (565). Indeed, increased TIMP-3 levels have been reported in AD brains of humans and

mouse models, where it associates with neurofibrillary tangles and neuritic senile plaques (566). However, this upregulation of TIMP-3 in these plaques has also been proposed as a potential compensatory mechanism to reduce inflammation through controlling TNF-α levels (567). The differential positive and negative effects of TIMP-3 in AD suggest a more complex nature of MMP/TIMP regulation.

Interestingly, increased TIMP-3 in the brain has not been reported in any other neuropathologies, suggesting a specific role in AD and β-amyloid build up (567). Studies have shown that T2DM results in cognitive decline that can be attributed to increase Aβ accumulation, similar to the pathology seen in transgenic AD mice (394,395); thus the role of TIMP-3 requires particular attention in the future, in the HFHS-fed mice.

4.3.2 The inflammatory state at the BBB: impact of metaflammation

A critical component of T2DM is the low-grade chronic inflammation that is characterised by cytokine expression and immune cell infiltration that remains unresolved over time (344). In metabolic disorders, the excessive nutrient consumption leading to hyperglycaemia and dyslipidaemia is accompanied by a plethora of inflammatory and metabolic responses in multiple cell types, and is termed metaflammation i.e. metabolism-induced inflammation (356,357).

Chronic hyperglycaemia and hyperlipidaemia induce the production of pro-inflammatory cytokines from various cells and tissues including the liver, pancreas, kidney, heart, adipose tissue and immune cells; a distinct signature of cytokines includes raised TNF-α, IL-1, IL-6, IL-8, CRP and MCP-1 (337,339,340,568). The excessive production of these peripheral pro-inflammatory mediators contributes to molecular alterations that lead to the development of T2DM-related secondary conditions such as nephropathy, neuropathy, retinopathy, ischemic heart disease and peripheral vasculopathy (316,317).

In the HFHS-fed mice, there is a rise in TNF-α, IL-1α, IL-6 and MCP-1 in the serum and brain microvessels; along with a rise in a range of other inflammatory mediators e.g. C5a and IFN-γ, receptors e.g. RAGE, interleukins e.g. IL-12p40 and IL-23 and chemokines e.g. CCL5 and CXCL12 (Figure 4.7). A number of these mediators have

been implicated to induce BBB damage. For example, complement activation and generation of C5a in systemic lupus erythematosus (SLE) damages brain endothelial cells and astrocytes. The loss of BBB integrity in SLE has been attributed to the activation of NF-κB signalling by C5a, resulting in loss of claudin-5 and ZO-1 at the TJs and rearrangement of actin fibres at the cytoskeleton (569). Similarly, RAGE alters the cell cytoskeleton through increasing β-catenin levels resulting in decreased F-actin stress fibres, with implications for loss of BBB structure (570). In the HFHS-fed model, there is disruption to the brain endothelial junctional proteins and cytoskeleton, which can be attributed to the up-regulation of these inflammatory mediators.

Moreover, a number of studies have reported correlations between high peripheral inflammation and risk of neurodegenerative diseases such as AD, PD, HD, ALS and MS (392,571). For example, a meta-analysis of forty studies showed AD development to be linked to higher peripheral blood cytokine concentrations of TNF-α, IL-1β, IL-6, IL-8, IL-12 and TGF-β (572), as well as the activation of circulating peripheral immune cells (573).

What then, is the mechanism by which peripheral immune system activation results in brain pathology? One particular study has shown that stimulation of the mouse immune system results in AD pathology, with increased deposition of amyloid precursor protein (APP) and it's proteolytic fragments, build-up of Aβ, tau aggregation, microglia activation and reactive gliosis (574). The activation of astrocytes and microglia contributes to disease progression and neurodegeneration through subsequent release of acute-phase proteins, complement components, prostaglandins, cytokines and ROS/RNS that promote neuronal cell death (575,576). Moreover the release of MMPs by the BBB cells can directly induce neuronal apoptosis; MMP-9 can enter the nucleus of neuronal cells to cause DNA damage resulting in neuronal cell death (431). These studies demonstrate a clear link between peripheral inflammation and neuroinflammatory response that leads to neurodegeneration (577). In conditions such as MetS/T2DM where peripheral inflammation is chronic and sustained, the pro-inflammatory microenvironment is likely to propagate a vicious cycle of self-propelling inflammation from endothelial cells, astrocytes, microglia and neurons that ultimately leads to chronic neuroinflammation and neurodegeneration (578).

In the HFHS-fed mice there is an initiation of a neuroinflammatory response as seen by the activation of $CD11c^+$ $MHCII^+$ $CD86^+$ IBA1-expressing microglia cells. Importantly, the intact BBB in the chow-fed mice vs the damaged BBB in the HFHS-fed mice along with greater M1 phenotype microglia cells consolidates the theory that peripheral inflammation arising as a result of metabolic disorders plays a significant role in causing disruption to the brain microvasculature resulting in neuroinflammation. In our diabetic model, investigation into neuronal loss is beyond the scope of this study; however future studies would benefit to review the effect on neurons to confirm that metaflammation-triggered neuroinflammation leads to neurodegeneration.

Furthermore, the evidence for the role of peripheral inflammation in contributing to neurodegeneration has been evidenced via blocking this inflammation (575). For example, IL-12 and IL-23 influence the development of T_H1 and T_H17 cells and have been shown to be upregulated in the microglia of AD mice (579). Targeting IL-12p40, the common subunit of IL-12 and IL-23, reduced Aβ burden and improved cognition (580). Both IL-12p40 and IL-23 levels are increased in the HFHS-fed mice, indicating the potential for these cytokines to induce adverse microglial responses. Indeed, within mouse models of MS it has been demonstrated that IL-12p40 produced by microglia plays a critical role in the encephalitogenicity during the effector phase of the disease (581).

Aside from the rise in pro-inflammatory mediators in the HFHS-fed mice, there is also an increase in the anti-inflammatory cytokines e.g. IL-4, IL-10 and IL-13. These classical anti-inflammatory cytokines have been previously associated with obesity and insulin resistance (582–586) and have been suggested to offer a degree of protection through recruiting eosinophils and T_H2 cells (587). In MS, IL-4 and IL-10 help modulate the balance between $T_H1/T_H2/T_H17$/Treg cells which is crucial for determining disease progression (588). Anti-inflammatory cytokines have also shown to reduce neuronal damage, for example IL-10 represses sepsis-associated hippocampal neuronal damage (589) and IL-1ra significant reduces the extent of neuronal cell death through binding to IL-1 receptors in ischemia, trauma and excitotoxicity (590).

The rise in these anti-inflammatory interleukins in the HFHS-fed mice could perhaps represent an attempt to balance and resolve the ongoing inflammation. In fact, in T2DM, adipose tissue is also a key producer of anti-inflammatory interleukins such as IL-4 and IL-10 (582,583). Nevertheless, other reports suggest hypo-responsiveness or a 'resistance' to IL-10 in T2DM (591) and the increased production may be a mechanistic response to overcome this issue. Importantly, within the brain, different mediators have differential effects dependent on disease. In EAE or PD mice, IL-10 ameliorates the disease phenotype (592,593). However in AD mice, IL-10 administration leads to Aβ accumulation through impaired microglia phagocytosis (594). Further contrasting studies find hippocampal targeted expression of IL-10 and IL-4 to decrease gliosis and improve spatial memory in AD mice (595,596). Importantly, the administration of IL-10 in EAE mice is largely only beneficial when provided at disease onset (597) and through intracranial administration (598).

These studies highlight the complex nature of chronic inflammation as well as the brain microenvironment. The simultaneous rise of pro- and anti-inflammatory mediators activate and alter multiple signalling cascades (340,349–351) and perhaps it is this disarray that results in the self-perpetuating inflammatory environment that contributes to overall disease progression. Rebalancing the immune response, is therefore not as simple as blocking inflammation but rewiring the immune response in a spatial and temporal manner (599). In depth studies are required to understand the role played by pro- and anti-inflammatory mediators arising from metaflammation, and the signalling pathways involved in inducing BBB damage, reactive gliosis, and microglial activation. In doing so, useful targets to help alleviate or decelerate the damage to the brain can be discovered.

4.3.3 Immune imbalance

$CD4^+$ T_H subsets play a crucial role in modulating immune response. Of the subsets, the T_H1 and T_H2 subsets have been well studied in relation to T2DM and contribute to chronic inflammation and insulin resistance. T_H1 cells are responsible for the production of IFN-γ, TNF-α and IL-12 to trigger cell-mediated immunity and phagocytic-dependent inflammation (236). T_H2 produces a variety of cytokines including IL-4, IL-6, IL-10 and IL-13 to regulate antibody responses (600). In our diabetic model of HFHS-feeding, although the percentage of the T_H1 and T_H2 subsets were not evaluated, all of the above mentioned cytokines were increased at the brain microvasculature in the HFHS-fed mice compared to chow-fed mice thereby suggesting that these cytokine-producing cells are likely to have been present to try and combat the disease and reduce inflammation.

Another T-cell subset of importance are the Treg cells which maintain immune homeostasis by preventing excessive inflammatory response; this is achieved through regulating the response of other T-cell subtypes and by influencing the activities of innate immune cells (601,602). T_H1 and Treg cells in visceral adipose tissue play a key role in regulating body weight, insulin resistance, glucose tolerance and thus T2DM progression, in both mice and humans (525,526). Generally, the skew of $CD4^+$ T-cell subsets in T2DM patients are towards the pro-inflammatory subsets (368). However a study by Zeng et al., have demonstrated that it is not only the balance between T_H1/T_H2 but also the balance of T_H17/Treg that influences pathogenesis of T2DM (368). T_H17 are reported to be increased in obese and T2DM patients and have been linked to altered lipid metabolism (603–605). T_H17 cells produce IL-17, which stimulates the production of TNF-α and correlates to obesity (606), with IL-$17^{-/-}$ mice on a high-fat diet showing improved insulin sensitivity despite being overweight (607). In the HFHS-fed mice there is an increase in IL-17 and TNF-α levels compared to chow-fed mice, that are likely to contribute to the increase weight gain.

Additionally within the gut, T_H17 cells induce anti-microbial peptides (AMPs) which increase intestinal permeability within mice fed a high-fat diet (603,608). AMPs are part of the innate immune response, and within the brain, Aβ itself is recognised as an AMP when it forms aggregates under inflammatory response (609). These aggregates cause CNS inflammation, inducing microglial cells and promote further Aβ production resulting, over time, in AD. The enhanced presence of T_H17 cells in a

diabetic inflammatory state may therefore induce AMPs at the BBB and further contribute to the development of negative immune responses within the brain, enhancing the rate of neurodegenerative disease development.

The involvement of T_H17 cells in the brain has been most well studied in MS. T_H17 cells and IL-17 is increased in peripheral blood, the brain parenchyma, CSF and lesions of MS patients or EAE rodents; with the numbers of T_H17 cells linked to disease severity (610–612). The contribution of T_H17 to MS progression is confirmed by IL-$17^{-/-}$ mice which are protected against EAE development (613). The role of T_H17 cells have also been of interest in AD, with studies reporting elevated T_H17 cells in AD brains (614), that can be correlated to the degree of amyloidopathy (615). The infiltration of T_H17 cells into the brain parenchyma of AD mice contribute to neuroinflammation and neurodegeneration either indirectly through increasing the release of pro-inflammatory cytokines IL-17 and IL-22 or directly by the Fas/FasL apoptotic pathway (616). These studies implicate the potential of T_H17 cells to contribute to neuroinflammation/neurodegeneration in the HFHS-fed model, in which numbers of migrated RoRγt^+ cells are elevated.

Furthermore, T_H17 cells have largely been implicated in the microvascular diabetic complication of diabetic nephropathy. In patients with diabetic nephropathy the T_H17 counts increased along with the ratio of T_H17/Treg cells (367). Similarly, in our diabetic model of HFHS-feeding within the cervical lymph nodes, the percentage of T_H17 cells are increased along with the ratio of T_H17/Treg cells in the HFHS-fed mice compared to chow-fed mice. Moreover, in the same study of diabetic nephropathy patients, it was seen that the ratio of T_H17/Treg increased over disease duration, whereas there was no change in the ratio of T_H1/T_H2 cells over disease duration (367) suggesting therefore that T_H17 and Treg cells may have stronger roles to play in the pathology of metabolic disorders and its associated complications. Indeed, in the brain, Treg confer neuroprotection and have shown to attenuate T_H17-mediated neurodegeneration in PD brains (617). In contrast, the levels of Treg and their role is in AD is still under debate. Some studies have shown Treg to be reduced and thus linked to cognitive impairment; the administration of Treg into mouse models have thus shown to have suppressive activity, slow down disease progression and restore cognition (618,619). On the other hand, other studies report increased Treg numbers in AD which positively correlate to the level of tau protein in AD brains (614,615).

Interestingly, there was also increased migration of Treg cells along with T_H17 cells in a BBB model, this could be an attempt to provide neuroprotection.

Overall lack of Treg in the peripheral systems results in reduced immunosuppression of monocytes/macrophages, which are strong contributors to the inflammatory process and development of secondary complications (238). Within the HFHS-fed mice, it was seen that percentages of neutrophils, macrophages and dendritic cells are all increased in the bone marrow compared to chow-fed mice, further implicating the loss of Treg to dampen immune response and thus loss of immune balance control within metabolic disorders.

$CD8^+$ T-cells are also key in inducing the recruitment and differentiation of macrophages in obese adipose tissues, with studies showing early infiltration of $CD8^+$ T-cells into adipose tissue with high-fat feeding (372). In the present study, the percentage of $CD8^+$ T-cells is increased in the bone marrow of HFHS-fed mice compared to chow-fed mice however, surprisingly the percentage of $CD8^+$ T-cells in draining cervical lymph nodes of HFHS-fed mice is decreased. In traumatic brain injury mouse models, it has been seen that $CD8^+$ T-cells are increased in the brain preceding increased $CD4^+$ $RoR\gamma t^+$ T-cells; and a pharmacological or genetic depletion of $CD8^+$ T-cells improved neurological outcomes through providing a T_H17/T_H2 immunological shift (620). In addition, B-cells can also impact the proliferation of T_H17 cells with depletion of B-cells in T2DM patient resulting in reduced T_H17 cell proliferation (621). Within the HFHS-fed mice, in the bone marrow there was a reduction of B-cells compared to chow-fed mice. The reduction of B-cells may be an attempt to improve glucose tolerance, through inactivating T_{eff} cell response. Mice which are unable to produce mature B-cells and are fed a high-fat diet have improved glucose levels compared to wild-type controls on high-fat diet (375). Therefore overall, it can be assumed that increases in levels of particular anti-inflammatory cytokines or alteration in cell types in the diabetic state are likely to be a compensatory mechanism induced by the immune system in an attempt to attain back control. To gain clarity, further work would be required to look at the infiltration and differential subset ratios within the brain parenchyma of these mice to determine exact neurological impact with metabolic disorders.

On the other hand, the reduction of NK cells in HFHS-fed mice compared to chow-fed mice is not unexpected, with a large majority of studies reporting decreased NK cells and function in obese individuals compared to healthy controls (363,622). In fact, NK cell-deficient mice have worse metabolic disorders and enhanced weight gain (622–625). Injections of Galactosylceramide (αGalCer), a potent lipid ligand that induces NK cells, in obese mice increased NK cell activity resulting in weight loss, reversal of glucose and insulin insensitivity along with differentiation of macrophages to an anti-inflammatory phenotype (626–628).

Crucially, the assessment of the innate and adaptive immune cells has been conducted in the bone marrow and cervical lymph nodes of these mice, and adhesion/migratory capacity of these cells across the BBB into the brain parenchyma has only been assessed in CD4+ T-cells. Without doubt, future work is required to understand the migration of other immune cells into the brain parenchyma, and the regional distribution between parenchymal and leptomeningeal compartments.

4.3.4 Immune cell recruitment to the BBB

BBB breakdown is considered a significant event in the start of neuroinflammatory and neurodegenerative disorders. Notably, models of EAE clearly showcase that symptoms of disease do not occur until leukocytes have migrated across the BBB; thus suggesting that leukocyte migration is a rate-limiting step in disease onset (156,251). Damage to the structural and functional integrity of the BBB therefore allows for an easier passage of immune cells, amongst other molecules, from the peripheral system into the brain either transcellularly or paracellularly.

Importantly, opening the BBB alone is not sufficient to result in leukocyte TEM into the CNS parenchyma (257). Instead the loss of BBB integrity must be accompanied by a pro-inflammatory response (258). There are several conditions which are required to allow for the optimal migration of leukocytes across an endothelium barrier. First and foremost, chemokine signals must induce the chemotaxis of immune cells. Review of the chemokines at the brain microvasculature in HFHS-fed mice revealed a raised presence of chemokines that induce monocytes, neutrophils, and T-cells. Examination of $CD45^+$ leukocytes staining is indicative of chemotaxis in the HFHS-fed mice. In

viral models of lymphocytic choriomeningitis virus and mouse hepatitis virus, the generation of CXCL10 in the CNS precedes leukocyte infiltration and development of disease (629–631). This suggests that brain cells in the parenchyma are also responsible for production of chemokines; and in fact astrocytes, microglia and neurons were confirmed to produce CXCL10 in these particular viral models (253). Moreover, a transgenic mouse with astrocyte-targeted CXCL10 gene found that despite the ability of CXCL10 to recruit leukocytes into the CNS, the leukocytes were not fully activated until additional pro-inflammatory cytokines provided by a peripheral immune challenge was given (253). In the HFHS-fed mouse model, this latter condition has been met by the sustained metaflammation and indeed we see increased CXCL10 and increased migration of leukocytes across the BBB *in vivo* and *in vitro.* Without doubt, there are several chemokines which work by similar mechanisms to induce chemotaxis that will be relevant in the HFHS-fed model. It would be interesting to evaluate the chemokines produced by the different cell types in future studies, particularly as the ability of brain parenchymal cells to produce chemokines and thus induce leukocyte infiltration suggests that these cells can detect perturbations in the brain or blood milieu very early on and thus contribute to the disease pathology.

Whilst there is a higher level of the majority of chemokines noted in the brain microvessels and serum of the HFHS-fed mice compared to chow-fed mice, it should be noted that a number of chemokines are also categorised as homeostatic. The constitutive expression of chemokines CCL19, CCL20, CCL21, CXCL12 and CX3CL1 are also detected in uninflamed brain tissue (632,633); as seen in the chow-fed mice. For example, the presence of CXCL12 protein at the BBB under normal conditions is found to be located on the abluminal surface of the endothelium. During EAE or MS in mouse and humans respectively, CXCL12 relocates to the luminal surface thereby increasing the entry of immune cells, which express the co-receptor CXCR4, into the brain (633,634). Localisation of CXCL12 therefore represents a method of homeostatic protection in the brain to limit immune cell extravasation. Whilst the levels of CXCL12 have not been measured at the brain microvessels in our model using the cytokine kit, there are increased levels of this chemokine in the serum of HFHS-fed mice suggesting increased production and therefore chemotactic

properties. Again, there are likely to be several chemokines which function within the same manner and examining the differential location of chemokines under inflammation could be an interesting line of work to pursue to determine the particular subsets of immune cells that migrate across the BBB.

Moreover activated or memory T-cells are known to be favoured for migration from blood to tissues (635,636). Interestingly, Kivisäkk et al., characterised the phenotype of T-cells in the CSF of normal humans and found activated T_{CM} cells with high expression levels of CCR7, CXCR3 and L-selectin (637,638). It is therefore not surprising that in the draining cervical lymph nodes of HFHS-fed mice there is a higher percentage of $CD4^+$ T-cells expressing CD44, LFA1 and CXCR3 compared to chow-fed mice. In addition, the HFHS-fed mice also had a higher percentage of both T_{CM} CD44hi CD62Lhi CCR7hi-expressing cells and T_{EM} CD44hi CD62Llo CCR7lo-expressing cells in cervical lymph nodes, compared to chow-fed mice. The activation and memory status of $CD4^+$ T-cells, along with cytokine presence and antigen-presentation therefore may account for the significantly larger number of both adhered and migrated $CD4^+$ $CD45^+$, $RoR\gamma t^+$ and $Foxp3^+$ cells in the HFHS-fed mice compared to the chow-fed mice. Indeed work by Marelli-Berg and colleagues in a high-fat model of western diet, have shown T_{EM} cells (CD44hi-CCR7lo-CD62Llo-$CXCR3^+$-$LFA1^+$) to preferentially migrate to non-lymphoid inflammatory sites (370) and Shirakawa et al., showed an increase of these T_{EM} cells in the visceral adipose tissue of obese mice (639). Furthermore in a human cohort study of 1172 subjects, defined as lean (BMI <25), overweight (BMI <25-<30) and obese (BMI >30), flow cytometric analysis of $CD4^+$ T-cell subsets found obesity to be strongly associated with reduced naïve T-cells and increased T_{EM} cells ($CD4^+RA^+$ $RO^-CCR7^+HLA\text{-}DR^+CXCR3^+$) (370). More research is required into looking at human patient samples in BBB models to determine the migratory profiles.

Although an inflammatory cytokine environment is required as a contributing factor to activation and thus migration of leukocytes across the BBB, the underlying presence of chemokines in normal chow-fed mice suggests that immune cells must be present in normal conditions too. In fact, studies have shown presence of peripherally-derived

T-cells, macrophages and dendritic cells localised in the perivascular compartments outside the parenchyma acting as immune-surveillance; importantly the number of these cells is relatively small compared to peripheral organs (171,640). One key role during immune surveillance is to act as an antigen-presenting cell; some reports suggest the ability of dendritic cells to present antigens detected in the CNS to T-cells in the periphery. Nonetheless, dendritic cells injected into the CSF of patients have been detected in B-cell follicles of cervical lymph nodes (641). Although the cell frequency of dendritic cells in cervical lymph nodes was not evaluated in chow or HFHS-fed mice, it was noted that there was a significantly greater B-cell frequency in the HFHS-fed mice suggesting that B-cells had been stimulated to proliferate, perhaps by antigen-presentation from the CNS. Without antigen presentation, the T-cells will simply not become activated despite the inflammatory environment.

One other factor preceding TEM, is the requirement of the endothelium to become activated to express adhesion molecules thus allowing for the initiation of the transmigration cascade (capture, rolling, tethering, firm adhesion & diapedesis) (642). In the HFHS-fed mice, the serum contains higher levels of sICAM-1 and the endothelium clearly expresses higher levels of ICAM-1, VCAM-1 and P-selectin with confocal imaging confirming presence on the luminal side. Increased adhesion molecule presence on endothelial cells along with increased expression of co-receptors on T-cells allows for enhanced adhesion, as confirmed by greater numbers of adhered $CD4^+$ leukocytes in the HFHS-fed mice compared to chow-fed mice.

4.3.5 Leukocyte TEM across the BBB

In peripheral tissues, transmigration allows cells to directly enter the tissue parenchyma. However due to the tightly controlled nature of the brain, the transmigration of leukocytes across the BBB into the brain parenchyma is in fact a two-step process (643–645). Invading leukocytes must initially pass across the endothelial cells whereby they become trapped in specialised compartments termed the perivascular space; defined by the inner endothelial BM and the outer astrocytic BM. To cross into the brain parenchyma, the invading cells must be able to transverse both BMs. In models of EAE, it has been seen that leukocytes can accumulate within this region and this accumulation of leukocytes is dubbed as the perivascular cuff (156,251). In the HFHS-fed mice, double immunostaining with pan-laminin (a marker for both endothelial and astrocytic BM) and general leukocyte marker CD45 shows clear entrapment of $CD45^+$ leukocytes between the two BM layers or perivascular space and some infiltration into the brain parenchyma. Staining in the chow-fed mice does not show this type of perivascular cuffing. Although migration studies with isolated and activated leukocytes in transwells confirmed far greater numbers of migrated $CD4^+$ $CD45^+$ leukocytes in the diabetic model of HFHS-feeding compared to control chow-fed mice, it must be noted that *in vitro* modelling did not use co-culture methods with endothelial cells and astrocytes. This would be a true indicator of the passage of activated leukocytes across both BMs.

Initial passage across the endothelial cells requires a β1-integrin-mediated process. Research by Sixt et al., demonstrated that upon approaching the endothelial BM, T-cells preferentially infiltrate across regions containing only laminin α4 due to the high expression of α6β1-integrin located here (156). As noted, the number of migrated leukocytes was far greater in the HFHS-fed model indicating that these cells were interacting via integrins to allow the TEM cascade. Electron microscopy studies could help to reveal the pores through which leukocyte migration occurs and identify if these are at laminin α4 regions. Importantly the ability of some cells to adhere and migrate in the chow-fed model is indicative of immune surveillance. Studies in healthy patients and rodents have shown the presence of inactivated $CD4^+$ T-cells to reside in the perivascular region for this purpose (254). The astrocytic BM lacks α6 and therefore in order for leukocytes to pass from the perivascular space into the brain parenchyma β-dystroglycan, a transmembrane receptor, that anchors astrocyte end-feet to the

parenchyma must be cleaved (156,646). *In vivo* studies in EAE models have shown that MMP-2 and MMP-9 selecting cleave β-dystroglycan, with double $MMP^{-/-}$ mice conferring resistance to leukocyte infiltration through inhibiting this cleavage (251). Within the HFHS-fed mice, the increased activity of the gelatinases implicates the ability of β-dystroglycan to be cleaved; corresponding with loss of the astrocytic end-feet association to the microvessels in the HFHS-fed mice compared to chow-fed mice. Additionally, activated leukocytes also release MMPs to aid in passage across the BBB (262,263).

The production of MMPs by tissue and immune-cell sources have been implicated to be strongly affected by cytokine levels. Work by Agrawal and colleagues show that the balance of TNF-α vs IFN-γ regulates activation of astrocytes and secretion of MMP-9 (647). TNF-$\alpha^{-/-}$ mice show enlarged perivascular cuffs due to the accumulation of leukocytes that are unable to breach the astrocytic BM barrier due to lack of MMP production thereby delaying disease onset in EAE models (647,648). On the contrary, IFN-γ acts a negative regulator of secretion, activation and subsequent transmigration (649,650). Interestingly, in the HFHS-model there is an increase of both TNF-α and IFN-γ at the brain microvessels; notably the relative expression of TNF-α to IFN-γ is much higher. Moreover, the balance of TNF-α/IFN-γ production is controlled by the T_H17/T_H1 cell populations. T_H1 cells are characterized by secretion of TNF-α and IFN-γ whereas T_H17 cells produce TNF-α and IL-17 (651) suggesting that the ratio of the cells at the BBB and the perivascular space have important roles to play in MMP secretion and subsequent astrocyte induction (647). In this regard, the increased percentage of $CD4^+$ $RoR\gamma t^+$ cells in the cervical lymph nodes and in the adhesion/migration model in the HFHS-fed mice versus the chow-fed mice implicate that cells of the T_H17 lineage are a likely contributor to the source of increased TNF-α, IL-17a and MMPs detected in the brain microvessels. Nevertheless, as eluded to previously the exact ratio of different T-cell subsets within the cervical lymph nodes, at the perivascular space, and in the CNS parenchyma requires further investigation. It should be noted that in the HFHS-fed model, there is also an equally large proportion of adhered and migrated cells of the Treg subpopulation, again perhaps representing a compensatory mechanism by the brain to combat the enhanced inflammation at the BBB.

The work of this project has focused on leukocyte TEM across the BBB, however it is should be acknowledged that some leukocytes may also enter the brain parenchyma in the CSF via the BCSFB (247). In MS patients, the number of T-cells, B-cells and macrophages in the CSF correlates with the number of CNS lesions (652). Although the BCSFB does not have the two-step process of leukocyte TEM, with leukocytes held in the perivascular space due to the glia limitans, the BCSFB epithelial cells are also interconnected with TJs (653). Disruption of the TJ molecule claudin-3 in choroid plexus cells in EAE models coincides with enhanced levels of infiltrating leukocytes in the CSF of these mice (653). It has been proposed that leukocytes passing across the BCSFB produce large amounts of inflammatory mediators and cytokines that activate the endothelial cells of the brain vasculature to induce adhesion molecule expression. Thus, this facilitates an influx of immune cells across the BBB (654). Increased permeability of the BCSFB has also been noted in mild cognitive impairment and AD accompanied by the passage of interleukins such as IL-17 and IL-4 (655). Future studies would benefit in examining the extent to which the disruption of the BCSFB contributes to the immune cell passage in HFHS-fed mice.

Moreover, this study has largely focused on the correlation of BM degradation with leukocyte TEM. However, it is important to note that degradation of the BM also has wider implications in disrupting the CNS environment; through impacting the drainage of ISF. Fluid and solutes from the brain drain to the cervical lymph along the BMs in the walls of capillaries and arteries (60,64,203). This drainage mechanism has been named the IPAD pathway (204). Reduced lymphatic drainage via IPAD can result in the accumulation of Aβ and results in cerebral amyloid angiopathy, which appears as white matter hyperintensities during scans of the brain (210). The accumulation of Aβ and indeed of other waste products or metabolites will affect the CNS environment and lead to altered homeostasis. Indeed, this could be one potential mechanism by which T2DM results in T3DM. It would be interesting to explore the IPAD in these HFHS-fed mice, to determine whether degradation of the BMs in endothelial cells and astrocytes also correlates with the loss of ISF drainage, and Aβ accumulation.

4.3.6 Metaflammation induced microglial activation

To understand if the metabolic disruption at the BBB has implications within the brain parenchyma, the status of the microglia cells was investigated. Microglia cells are the primary resident immune cells of the brain. Typically, microglia are described to be in either their resting or activated state. However, microglia are not truly 'resting' even in a healthy CNS. Instead microglia form close associations with neurons, contacting synapses with their processes in order to monitor synapse function, state and stability by providing trophic support (171) and engaging in environmental surveillance to maintain homeostasis. Once microglia sense harm or encounter an antigen that is foreign, they enter into an 'activated' state; inducing changes in morphology, proliferation, phagocytic activity and immunoreactivity with increased expression of pro- and anti-inflammatory mediators (656). Within the activated state, microglia can be categorised into two broad states, which are the pro-inflammatory M1 phenotype or the anti-inflammatory, pro-resolving M2 phenotype. Activation of microglia, aims to resolve, retain and limit the infection and/or tissue damage (657). Dysfunction and uncontrolled activation or skew towards the M1 phenotype therefore has huge implications for vascular breakdown, neuronal death and synaptic plasticity, and forms the neuroinflammatory response (412). Reactive gliosis has been implicated in a number of brain disorders including AD, PD, ALS, traumatic brain injury (TBI), Stroke and Epilepsy amongst others. In AD, there is an increase in proliferation of activated microglia of the M1 phenotype, with impaired ability of microglia to take up Aβ for phagocytosis, resulting in its accumulation (658,659). Confocal images in the HFHS-fed mice showed activated microglia through the expression of $IBA1^{+}$ staining and in primary culture cells there was an upregulation of activation markers MHCII and CD11c compared to the chow-fed mice, indicating that an immune response was being elicited within the brain. In line with this, in HFHS-fed mice there is a significant rise in the M1 phenotype accompanied with a decrease in the resolving M2 phenotype. The initiation of neuroinflammation with a skew towards the M1 phenotype in HFHS-mice implicates how the altered brain responses may lead to the development of AD pathology (660–663). In diabetic retinopathy patients, activation of microglia cells leads to nerve fibre thinning, apoptosis of neurons and visual loss (656); it is possible that similar effects may be occur in diabetic brains.

Of particular interest in the HFHS-fed mice was the loss of the CX3CR1 receptor expression compared to chow-fed mice. Under both normal and pathological conditions, the CX3CR1 receptor present on microglia interacts with neuronally-derived CX3CL1 to mediate cross-talk for controlling functions such an intracellular calcium mobilisation, chemotaxis and Fas-mediated apoptosis (664,665). In mouse models of T1DM, loss of CX3CR1 signalling increased systemic inflammation through increased IL-1β production by proliferating microglia. Further studies found the deletion of CX3CR1 in T1DM sped up diabetic retinopathy onset through increased apoptosis in the retina (666). This implicates, that the loss of CX3CR1 expression in the microglia of HFHS-fed mice could potentially have detrimental effects on neurons within the brain parenchyma; particularly as $CX3CR1^{-/-}$ mice have aberrant IL-1β expression, loss of long-term potentiation and loss of synapse plasticity/activity resulting in impaired cognition (667,668). Nevertheless, knockout of CX3CR1 in mouse models of AD (APP/PS1 transgenics) found CX3CR1 deficiency to reduce amyloid plaque aggregation and microglia-mediated neuronal death despite microglia hyperactivation (669–671). However *in vitro*, microglia treated with β-amyloid show downregulation of CX3CR1 with increased expression of IL-6 and TNF-α (672). Patients with AD also exhibit lower levels of CX3CR1 and CX3CL1 (672). In summary, this suggests that reduced CX3CR1-CX3CL1 can induce both negative and beneficial effects. Further work is required to substantiate the true role of CX3CR1-CX3CL1 in T2DM, as studies in other models of disease including ALS, PD and stroke show differential signs of benefit vs harm (673).

Overall, a low grade chronic inflammatory state within the peripheral system because of MetS/T2DM has major implications in inducing and causing sustained neuroinflammatory responses. As a consequence of sustained BBB breakdown through inflammatory mediators there will be constant activated leukocyte transmigration and therefore subsequent astrocyte and microglial activation. The sustained neuroinflammatory response, like the immune response within the peripheral system, will have negative and destructive effects on the neurons within the brain. In the HFHS-fed mice, the loss of astrocyte association to the brain endothelial cells will impact the transmission of nutrients, neurotransmitters and second messengers to neurons (400). Moreover, iNOS production by microglial cells, as seen in the HFHS-fed mice, is known to inhibit long-term potentiation formation thereby

impairing cognition (429). The blindness induced by microglial activation in diabetic retinopathy, highlights the potential impact of widespread degeneration within the brain. Although further research is required on the impact on the neurons in the HFHS-fed mice, research has shown that diabetes induces a loss of memory or impaired cognition in both patients (392,450) and rodents (451,452) with T2DM. In C56BL/6J mice fed a high-fat high-fructose diet for 24 weeks there is a significant deterioration in cognitive function as assessed by the Morris Water Maze test compared to control on a normal diet (451,452). In line with cognitive decline, staining for astrocytes and degenerating neurons using GFAP and Fluro-Jade C respectively in diabetic rats, showed significantly enhanced expression, astrogliosis and neurodegeneration (674).

4.3.3 Conclusion

In summary, this chapter shows that the development of MetS/T2DM induces an inflammatory state both at the serum level and at the brain microvasculature. The increased presence of interleukins and chemokines has an impact at both an immune system level but also at the BBB by inducing breakdown and thus enhancing permeability. The complete breakdown of the BBB, resulting from loss of TJs, cytoskeleton and BMs as a result of dysregulated MMPs/TIMPs ratio allows for the passage of $CD45^+$ leukocytes to transverse the BBB and enter into the brain parenchyma. The peripherally activated T_{eff}, $T_{CM,}$ T_{EM} and T_H17/Treg imbalance along with chemokine/cytokine disruption induce activation of the brain resident immune cell - the microglia. The disbalance of M1/M2 microglia phenotype could have a huge impact on causing further inflammation within the CNS parenchyma and affecting the astrocytes and neuronal cells. In conclusion, a diabetic phenotype has a negative impact on the brain and begins to initiate an inflammatory response which could have detrimental effects for neuroinflammatory and neurodegenerative disorder development.

It should be noted that this study is examining the effect of peripherally derived inflammation arising from a HFHS-diet on the BBB and the NVU. There is a vast amount of research detailing the pathophysiology and development of T2DM in the peripheral system. Although, the brain is no longer considered immune-privileged, the BBB and the other central barriers described in Section 1.1 indicates the unique and

enclosed structure of the brain. Therefore, manifestation and development of disease at the BBB and within the brain arising from T2DM may differ from the atypical pathology seen in the peripheral system. Equally, as the T2DM is a disease of the peripheral system, it is also likely to differ from the pathology of atypical CNS disorders. Therefore, when examining the development of neuroinflammation or neurodegeneration arising from T2DM, the interplay of the two system must be considered in greater depth. This has huge implications for not only understanding the development and progression of the disease but also when considering treatments to combat the disease.

Of final note, this chapter studies the differences in chow vs HFHS fed mice and does not look at the effects of aging, which formulates a study within itself. However, a simple evaluation of permeability and TEER of young vs aged pMBMECs showcases that there is a significant degree of damage to the BBB overtime with age; this is perhaps not unexpected as it is well documented that health and immune response declines with age (675,676). The natural inflammatory state is raised with age, and is referred to as inflammaging (677). However, the ability of a HFHS-fed diet to further enhance permeability and reduce TEER significantly against age matched chow-fed counterparts is indicative of how metaflammation can accelerate brain microvasculature damage and thus initiate detrimental pathology within the brain. This is a cause for concern, given that the worldwide incidence for obesity, sedentary lifestyle and ageing population is on the rise (315); suggesting that not only will CVDs rise but also neuroinflammatory and neurodegenerative disorders too.

Chapter 5 – Examining the effect of a pharmacological (hrANXA1 treatment) and dietary (HFHS – Chow reversion) intervention to restore the BBB to the pre-diabetic state

5.1 Introduction

The findings from Chapter 4 showed how metabolic disorders disrupt the BBB and can lead to adverse immune events both peripherally and within the brain parenchyma. These results implicate that controlling metabolic disease is not just essential for prevention of typical diabetes-related peripheral secondary complications and cardiovascular disease but also for secondary complications of the brain (initiation of neuroinflammation and development of potential neurovascular/neurodegenerative disorders).

Management of T2DM in patients is achieved through medications and lifestyle changes such as dietary intake, physical activity levels and behavioural therapy. Medical management of T2DM requires the control of hyperglycaemia, dyslipidaemia, and high blood pressure to reduce chronic inflammation and its associated tissue damage. Therefore, the identification of drugs or molecules that combat the underlying low-grade chronic inflammatory state, alongside medications specifically for glucose, lipid or blood-pressure lowering could have huge implications in preventing or slowing the progression of macrovascular and/or microvascular complications.

Annexin A1 (ANXA1) is an endogenous anti-inflammatory molecule that is upregulated by glucocorticoids. ANXA1 reduces inflammation by preventing the activation of PLA_2 (274,275)., inhibiting COX-2 and inducing anti-inflammatory cytokines such as IL-10 (277). At the immune system, ANXA1 prevents leukocyte TEM through inducing L-selectin shedding and co-localising with α4β1 integrin to prevent leukocyte-endothelial interactions (279). In addition, ANXA1 promotes clearance of apoptotic cells through inducing efferocytosis by macrophages (278). ANXA1 levels are modulated in a number of different diseases and hrANXA1 or it's n-terminal peptide Ac2-26 have been shown to produce therapeutic benefits in many diseases, including rheumatoid arthritis, MS and atherosclerosis, amongst others (294).

Previous studies undertaken in our lab, have investigated the potential of hrANXA1 to act as a therapeutic agent in modulating T1DM and T2DM-related microvascular disease. The results from these studies found that prophylactic hrANXA1 treatment had the ability to prevent development of microvascular complications (nephropathy

and cardiomyopathy) in STZ-induced T1DM mice (678). Similarly, therapeutic hrANXA1 treated in STZ-induced T1DM mice, in which microvascular complications had already developed, prevented further decline in cardiac and renal function (678). Likewise, in a T2DM model of high-fat high-sugar feeding treatment with hrANXA1 prevented further deterioration of T2DM through restoring insulin sensitivity (512). Moreover, hrANXA1 treatment reduced the development of microvascular complications specifically renal nephropathy and lipid accumulation within the liver of T2DM mice.

ANXA1 signals through the GPCR - FPR2, which is present on brain endothelial cells thus implicating its potential for limiting microvascular complications of the brain. In fact, studies from our lab have shown that ANXA1 is pivotal in maintaining cellular polarity, cytoskeleton integrity and consequently tightness of the BBB through the inhibition of the small G protein RhoA (297). Other cells of the NVU including astrocytes, microglia and neurons also express ANXA1 (679), further implicating its potential as neuromodulating agent.

In this study, mice fed a HFHS-diet are treated with hrANXA1 as a pharmacological intervention. Treatment is provided by using full length hrANXA1, as the dose required to induce biological function is up to 20 times less than that required by the peptide Ac2-26 (482) and 14 times less than that needed to induce gene expression changes (483). Furthermore, Ac2-26 peptide has a weak ability in reducing leukocyte adhesion unlike full-length hrANXA1 (484). The daily dose of 1µg was selected based on previous report that show the half-life of ANXA1 to be approximately 6 hours through i.p. or i.v. injection. I.p. injection is preferred because 0.5% of the injected dose remains in the circulation 24 hours post injection versus almost 0% through i.v. administration (478).

Lifestyle modifications are essential in managing T2DM development and progression. A meta-analysis of 89 studies indicates that nutritional therapy alone has the largest impact on producing weight loss and improving metabolic control (680). A number of nutritional guidelines are available from NICE (681), International Diabetes Federation (682), American Diabetes Association (683) and Joint British Societies (684). These guidelines provide recommendations for reference intake of food groups and nutrients (e.g. protein 0.75g/kg of ideal body weight, saturated fat <10% of daily intake, salt<6g/day) as well as proposed targets to reduce risk factors of MetS/T2DM (e.g. blood pressure <130/80mmHg, LDL cholesterol <2mmol/L, HbA1c levels <6.5%). These guidelines are for proposed for both patients that are at high risk of developing T2DM and CVDs or patients already diagnosed with T2DM with or without CVD complications.

The majority of dietary recommendations are based on the consumption of a Mediterranean-style diet which is high in monounsaturated fats and fish oils with abundance of fruits, vegetables, legumes, and grains. Together these food groups help combat inflammation due to the high presence of omega-3 fatty acids, antioxidants and polyphenols that reduce free radical and cytokine production. This limits the activation of pro-inflammatory signalling pathways and helps to alleviate a chronic inflammatory state (685).

Dietary recommendations form a crucial part of chronic disease management for a number of other diseases too, such as cancer, osteoporosis and dental disease. Consequently, the role of a paleo diet has also been investigated for the prevention of brain disorders, specifically dementias. Reports from large systematic reviews, made up of largely observational-based longitudinal studies, propose Mediterranean diets to improve cognitive function, decrease risk of cognitive impairment and lower risk of dementia development (686,687).

As previously shown in Chapter 4, a diet high in fat and sugar causes inflammation which is damaging to the brain microvasculature and can start to initiate a neuroinflammatory response. In this study, mice fed a HFHS-fed diet for 10 weeks have been reverted to a normal chow diet for a following 5 weeks to review whether dietary intervention can also help to alleviate metabolic disorder-induced damage at the BBB.

5.1.1 Aims and objectives

The chapter addresses Hypotheses 2 and 3 mentioned in Chapter 2, this is as follows:

Anti-inflammatory drugs have shown to improve T2DM and CVD outcomes. In this manner, the effect of using ANXA1 as an anti-inflammatory therapeutic has been explored at the BBB. ANXA1 is well-established as a positive regulator of BBB structure and it has also been shown to provide neuroprotection, indicating its potential to reduce and repair damage at the BBB and beyond.

⇒ **Hypothesis 2:**

It is hypothesised that treatment with human recombinant ANXA1 (hrANXA1) will restore the leaky BBB phenotype through restoring tight junctions. Improved BBB integrity along with hrANXA1's effect on leukocytes will prevent leukocyte TEM and reduce neuroinflammation.

Aside from therapeutic strategies, the simplest method to resolve inflammation is to remove the source. In patients, lifestyle modifications are key to reduce the progression of T2DM and CVD, with the aim to reduce the inflammation arising from hyperglycaemia, hyperinsulinemia, and hyperlipidaemia. Moreover, the understanding on dietary intake and brain health is growing. As a result, the effect of a dietary intervention has been explored to understand whether preventive measures can reinstate the integrity of the BBB and subsequent development of neurodegenerative disorders.

⇒ **Hypothesis 3:**

It is hypothesised that changing to a chow diet will remove the source of metaflammation and therefore improve the integrity of the BBB by reducing endothelial dysfunction and subsequently reduce neuroinflammation.

This chapter addresses Aims 3 & 4 mentioned in Chapter 2, these are as follows:

3. To assess the potential therapeutic effect of hrANXA1 on HFHS-induced BBB alterations.
    - hrANXA1 treatment will be given *in vivo* to animals to examine whether the protein has the ability to restore, resolve and revert the damage induced to the BBB, to the pre-diabetic state. This will serve as a pharmacological intervention.

4. To investigate whether the metabolic stress induced BBB defects are reversible upon dietary intervention.
    - In order to assess reversibility of diabetes-induced BBB damage, mice fed a HFHS diet for 10 weeks will be re-introduced to a normal chow diet for a further 5 weeks.

The following objectives were covered in this chapter to address these aims, the relevant methodology section has been referenced in brackets:

- To determine whether pharmacological intervention provided by hrANXA1 for 6 weeks and dietary intervention provided for 5 weeks can revert HFHS-induced T2DM in mice.
- To determine whether both interventions can restore BBB integrity (vascular leakage). Measurement will be conducted using *in vivo* Evans blue dye and *ex vivo/in vitro* via measuring the paracellular permeability coefficient and TEER.
- To determine whether both interventions can restore the junctional proteins and BMs laminins. Expression of junctional proteins occludin and claudin-5 and endothelial and astrocytic BM laminins, α4 and α5 to be imaged using confocal microscopy.
- To determine whether both interventions can restore the expression and activity of MMPs and its inhibitor TIMP-1 to baseline, as seen in chow-fed mice.
- To determine whether both interventions can resolve the inflammatory profile seen in HFHS-fed mice via examination of cytokines, interleukins and chemokines.

- To determine whether both interventions can reduce metaflammation-induced activation and expression adhesion molecules on endothelial cells.
- To determine the effect of both interventions on the phenotype the of the innate and adaptive immune cells in bone marrow and cervical lymph nodes.
- To determine the effect of both interventions, restore the activation status and ratio of $CD4^+$ T_{eff}, T_{CM}, $T_{EM,}$ T_H17 and Treg cells present in cervical lymph nodes.
- To determine whether both interventions can reduce the infiltration/migration of leukocytes into the brain parenchyma.
- To determine whether both interventions can reduce microglia cell activation and restore microglia M1 or M2 phenotype via FACS analysis of primary microglia cultures and imaging cerebral cortical brain sections.
- To determine whether hrANXA1 can reduce neuroinflammation through measuring expression of iNOS in the brain parenchyma using confocal microscopy.

In order to study these aims and objectives, interventions were provided in the following manner:

- ❖ Pharmacological intervention was provided by treating mice fed a HFHS-fed diet with hrANXA1. 10-week old male C57BL/6 mice were fed a HFHS diet for 10 weeks. Pharmacological intervention was provided from weeks 5-10, whilst mice remained on the HFHS diet. Mice were treated with 1µg hrANXA1 in 100µl of 50mM Hepes and 140mM NaCl, pH 7.4, daily (5 times/week) intraperitoneal (i.p.). The dose of hrANXA1 remained the same throughout the duration of the study and was not changed with increasing weight gain in the mice. To allow for accurate comparison against the chow-fed and HFHS-fed mice; mice not assigned to receive hrANXA1 where treated with vehicle 100µl of 50mM Hepes, 140mM NaCl, pH 7.4, daily (5 times/week) i.p.

- Dietary intervention was provided by reverting mice fed a HFHS diet onto a chow diet. 10-week old male C57BL/6 mice were fed a HFHS diet for 10 weeks, after which mice were placed back on a chow diet for a further 5 weeks, the total dietary period for these mice was 15 weeks. Importantly, comparisons of this group have been made to mice given chow or HFHS-diet for 10 weeks and hence there is an element of age, which will be a confounder in these results. Chow, HFHS and HFHS + hrANXA1 mice were 20-weeks old at cull whereas HFHS – Chow reversion mice were 25-weeks old at cull.

  Importantly, this group of mice were also treated with vehicle 100µl of 50mM Hepes, 140mM NaCl, pH 7.4, daily (5 times/week) i.p. similar to chow-fed and HFHS-fed mice for the first 10 weeks on the intervention.

Comparisons of both interventions have been made to mice fed a HFHS-diet or chow-diet for 10 weeks. A summary of the experimental groups, experimental plan and the methods used to quantify each measure have been provided in Table 5.1, Figure 5.1 and Table 5.2, respectively.

Table 5.1 | Experimental groups used to establish a mouse model of diet induced T2DM and the models used to provide a pharmacological and dietary intervention.

Group name and age	Diet and period of time	Treatment and period of time	Age at cull	Total number
Chow 10-week old male C57BL/6 mice	Chow from weeks 1 - 10	Vehicle of 100µl of 50mM Hepes, 140mM NaCl, pH 7.4, 5 times/week i.p. Given weeks 5-10	20 weeks	55
HFHS 10-week old male C57BL/6 mice	HFHS from weeks 1 - 10	Vehicle of 100µl of 50mM Hepes, 140mM NaCl, pH 7.4, 5 times/week i.p. Given weeks 5-10	20 weeks	55
HFHS + hrANXA1 10-week old male C57BL/6 mice	HFHS from weeks 1 - 10	**Pharmacological intervention of** 1µg hrANXA1 in 100µl of 50mM Hepes, 140mM NaCl, pH 7.4, 5 times/week i.p. Given weeks 5-10	20 weeks	55
HFHS - Chow reversion 10-week old male C57BL/6 mice	HFHS from weeks 1 - 10 Chow from weeks 11-15 **(dietary intervention)**	Vehicle of 100µl of 50mM Hepes, 140mM NaCl, pH 7.4, 5 times/week i.p. Given weeks 5-10	25 weeks	15

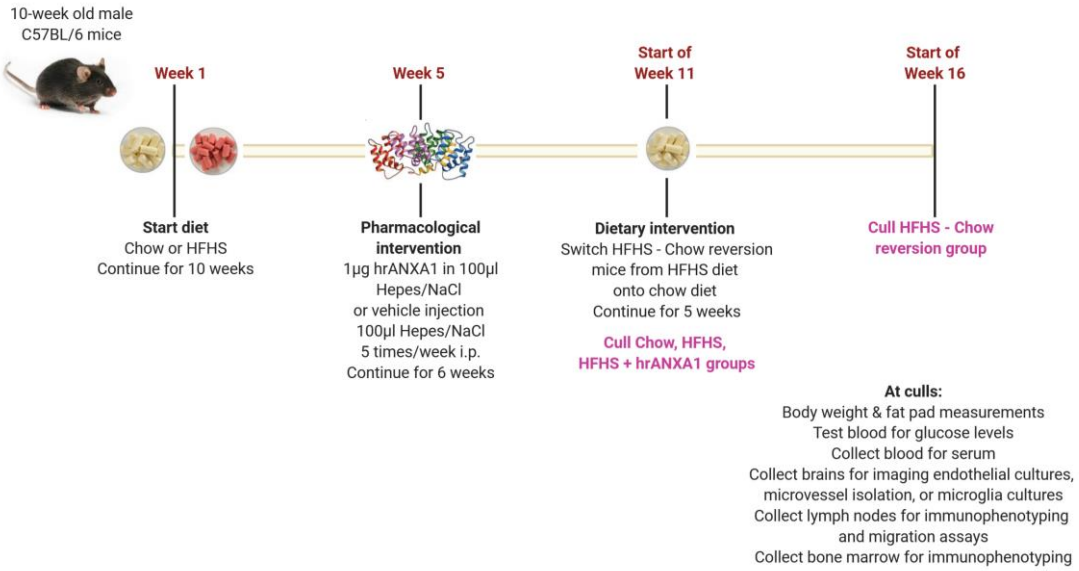

Figure 5.1 | Summary of the experimental plan used to induce T2DM and provide pharmacological and dietary intervention.

Table 5.2 | Summary of the central and individual measures used to evaluate the aims and objectives of Chapter 5, with reference to the respective methodology used to conduct these experiments.

Central measure	Individual measures	Method section
T2DM development	Obesity - weight gain and fat pads	3.1.1.1, 3.1.2 & 3.1.3
	Hyperglycaemia- fasted glucose, non-fasted glucose OGTT	3.1.1.1 & 3.1.4
	Hyperinsulinaemia - ITT, serum insulin	3.1.1.1, 3.1.2 & 3.1.4
	Dyslipidaemia - serum & cholesterol triglycerides	3.1.1.1, 3.1.2 & 3.1.4
Vascular integrity	Evans blue dye leakage *in vivo*	3.1.7 & 3.1.8
	Paracellular permeability *in vitro*	3.1.9 & 3.2.5
	TEER	3.1.9 & 3.2.6
BBB structure	Imaging junctional proteins occludin and claudin-5	3.1.3 & 3.3.1
	Imaging BM laminins α4 and α2	3.1.3 & 3.3.1
MMP involvement	MMP-2, -3, -9 expression at brain microvessels via cytokine array	3.1.9 & 3.2.8
	MMP-2 and -9 activity at brain microvessels via zymography	3.2.9 & 3.2.10
	TIMP-1 ELISA	3.2.8
Inflammatory profile	Cytokine array for interleukins, chemokines, cytokines in serum and brain microvessels	3.2.8
	Imaging and characterising adhesion molecule expression at BBB	3.2.8 & 3.4.3
Immuno-phenotyping	Cell frequency of innate and adaptive immune cells in bone marrow and deep cervical lymph nodes	3.1.3, 3.1.5, 3.1.6, 3.4.3
	$CD4^+$ T-cell activation for Teff	3.1.3 & 3.4.3
	T_{CM} vs T_{EM}	3.1.3 & 3.4.3
	T_H17 vs Treg	3.1.3 & 3.4.3
Leukocyte TEM across BBB	Imaging CD45 infiltration into brain parenchyma	3.1.3 & 3.3.1
	In vitro adhesion/migration assays	3.1.3, 3.2.1, 3.2.2, 3.2.3, 3.2.7
Microglia phenotyping	Activation and M1 vs M2 phenotyping	3.1.10 & 3.4.3
Neuro-inflammation	Imaging IBA1 activated microglia cells	3.1.3 & 3.3.1
	Imaging for iNOS expression	3.1.3 & 3.3.1

5.2 Results

5.2.1 Effect of pharmacological and dietary intervention on the development of MetS

Confirmation of metabolic disruption (obesity, hyperglycaemia, dyslipidaemia and insulin resistance) in this mouse model was conducted by measurements of weight gain, fat mass (epididymal & inguinal), fasting and non-fasting blood glucose, OGTT and ITT as well as serum insulin, cholesterol and triglyceride levels (Figure 5.2). Mice fed a chow diet, HFHS diet or HFHS diet + hrANXA1 treatment were culled at 10 weeks, a total of 55 mice/group were used. Mice placed on a reversion diet were fed a HFHS diet for 10 weeks followed by reversion to a chow diet for 5 weeks; these mice were culled at 15 weeks; a total of 15 mice were used.

At the end of the 10-week feeding period, HFHS-fed + hrANXA1 treated mice had significantly increased body weight and fat mass compared to chow-fed mice (Figure 5.2A,D-F). Interestingly, treatment with hrANXA1 significantly reduced the overall weight gain and epididymal fat mass compared to HFHS-fed mice (Figure 5.2D,E). In the HFHS – Chow diet reversion group, the switch to a chow diet led to a decrease of body weight, with final body weight at 15 weeks significantly lower than the HFHS-fed and HFHS-fed + hrANXA1 treated mice (Figure 5.2A,D) . In the HFHS – Chow reversion diet mice, there was a trend towards decreased percentage of fat mass however this was only statistically significant for percentage of epididymal fat compared HFHS-fed mice (Figure 5.2E,F).

Food and calorific intake were only measured for chow-fed, HFHS-fed and HFHS + ANXA1 treated mice. The food intake of mice on HFHS diet was substantially lower than the chow diet however calorific intake was substantially higher (Figure 5.2B,C). Treatment with hrANXA1 in HFHS-fed had no effect on feeding patterns when compared to HFHS-fed, suggestive that hrANXA1 does not affect eating habits e.g. hunger or satiety directly.

Treatment with hrANXA1 and reversion diet significantly reduced the non-fasted blood glucose levels when compared to HFHS-fed diet mice, however no changes were seen in the fasted blood glucose levels, with concentrations significantly higher across all HFHS-fed groups when compared to chow-fed mice (Figure 5.2G,J).

Insulin resistance was confirmed using OGTT and ITT. HFHS-fed + hrANXA1 treated mice had improved glucose tolerance when compared to HFHS-fed mice although the tolerance remained worse than chow-fed mice (Figure 5.2H,I). HFHS – Chow reversion diet mice had impaired glucose tolerance when compared to chow-fed and HFHS-fed + hrANXA1 treated mice; and were similar to HFHS-fed mice. In the ITT, treatment with hrANXA1 did not alter the insulin tolerance when compared to HFHS-fed mice (Figure 5.2K,L). Nevertheless, treatment with hrANXA1 did significantly lower serum insulin levels compared to HFHS-fed mice, comparable to concentrations seen in chow-fed mice (Figure 5.1M). Dietary reversion showed a trend towards improved insulin tolerance, similar to the tolerance seen in chow-fed mice. Dietary reversion lowered serum insulin levels when compared to HFHS-fed mice however the concentration of serum insulin remained higher than in concentrations in chow-fed and HFHS-fed + hrANXA1 mice (Figure 5.1M).

Correspondingly, serum cholesterol and triglyceride levels were significantly reduced with hrANXA1 treatment; the serum cholesterol levels were comparable to chow-fed mice whereas the serum triglyceride levels were non-significantly higher (Figure 5.2N,O). Similarly, HFHS – Chow reversion diet mice also had reduced serum cholesterol and triglyceride levels compared to HFHS-fed mice. The concentrations were comparable to those in chow-fed and HFHS-fed + hrANXA1 treated mice; however, these results were not statistically significant.

In summary, it was seen that the HFHS-diet induced obesity and contributed to the development of MetS as noted by hyperglycaemia, hyperinsulinemia, hypercholesterolemia, and hypertriglyceridemia. Treatment with hrANXA1 in HFHS-fed mice attenuated the development of MetS as seen through reduced weight gain (independent of affecting satiety), lower non-fasted blood glucose levels, improved OGTT and lower serum insulin, serum cholesterol and serum triglyceride levels. Likewise, reversion from a HFHS diet to a chow diet also resulted in a reduction in

weight gain, lower non-fasted blood-glucose levels, improved ITT and lower serum insulin, serum cholesterol and serum triglyceride levels.

Generally, whilst both pharmacological and dietary interventions attenuate MetS development, treatment with hrANXA1 showed greater improvement across the majority of measures when compared to HFHS-fed mice, with particular effect on improving serum levels and glucose tolerance. Furthermore, results showed the levels/concentrations in HFHS-fed + hrANXA1 treated mice were largely similar to those in chow-fed mice, with the exception of weight gain. The reduction of weight gain, in comparison, was the strongest indicator of improvement in HFHS – Chow reversion diet group suggestive that diet has a huge impact on obesity.

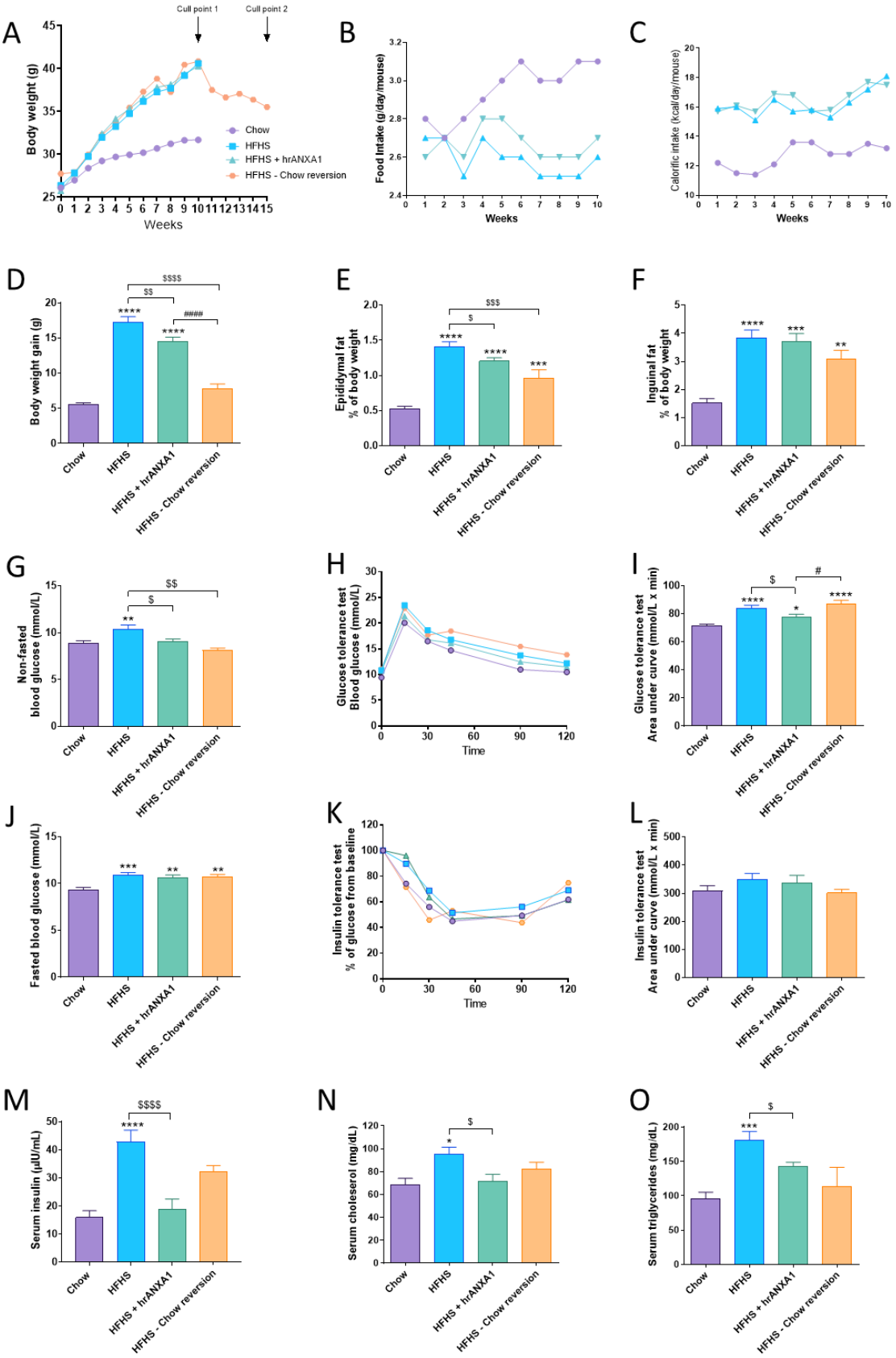
A
Cull point 1
Cull point 2
Body weight (g)
Weeks
Chow
HFHS
HFHS + hrANXA1
HFHS - Chow reversion
B
Food Intake (g/day/mouse)
Weeks
C
Calorific intake (kcal/day/mouse)
Weeks
D
Body weight gain (g)
E
Epididymal fat % of body weight
F
Inguinal fat % of body weight
G
Non-fasted blood glucose (mmol/L)
H
Glucose tolerance test Blood glucose (mmol/L)
Time
I
Glucose tolerance test Area under curve (mmol/L x min)
J
Fasted blood glucose (mmol/L)
K
Insulin tolerance test % of glucose from baseline
Time
L
Insulin tolerance test Area under curve (mmol/L x min)
M
Serum insulin (µIU/mL)
N
Serum choleserol (mg/dL)
O
Serum triglycerides (mg/dL)

Figure 5.2 | Characteristics of mice fed a chow diet, HFHS diet, HFHS diet + hrANXA1 treatment or HFHS-diet for 10 weeks + 5 weeks of chow diet (HFHS – Chow reversion)

C57BL/6 mice were fed either a standard diet (Chow) or a high-fat high-sugar diet (HFHS) for 10 weeks. Pharmacological intervention was given with either vehicle or human recombinant (hr) ANXA1 (1µg/100µl, i.p.) five times/week from weeks 5 to 10 (n=55). Dietary intervention was provided by placing mice on a HFHS for 10 weeks, followed by a chow diet for 5 weeks (HFHS – Chow reversion; n=15). Food (B) and calorific intake (C) was recorded for chow, HFHS and HFHS + hrANXA1 mice (n=10/group). Weekly body weight measurements (A), final body weight gain (D) and epididymal (E) & inguinal fat mass (F) was recorded to confirm obesity onset (n=15-55/group). Non-fasting (G; n=15-44/group) and fasting (J; n=15-39/group) blood glucose levels were measured to confirm hyperglycaemia. Serum insulin levels (M; n=8-27/group), glucose (H, I; n=15-38/group) and insulin tolerance testing (K,L; n=6-15) was conducted to confirm insulin resistance. Serum cholesterol (N) and serum triglycerides (O) levels were measured to confirm hypercholesterolemia and hypertriglyceridemia (n=9-23/group). Statistical analysis was performed by one-way ANOVA followed by a Bonferroni post-hoc test. Data is expressed as mean ± SEM., *p< 0.05, **p<0.01, ***p<0.001, ****p< 0.0001 vs. Chow; $p<0.05, $$p<0.01, $$$p<0.001, $$$$p<0.0001 vs. HFHS. #p< 0.05, ####p< 0.0001 vs. HFHS + hrANXA1.

5.2.2 Treatment with hrANXA1 and healthy dietary changes reduces the vascular leakage of the BBB

The first measure to determine whether the interventions could improve BBB integrity was to measure the *in vivo* permeability (Figure 5.3A). Both treatment with hrANXA1 and dietary changes reduced the BBB leaky phenotype, as seen by a reduction in the Evans blue dye leakage. However, the reduction in leakage when compared to HFHS-fed mice was slightly better in the HFHS-fed + hrANXA1 treated mice with approximately a 65% reduction compared to 50% reduction in HFHS – Chow reversion diet mice. Levels of Evans blue brain content in HFHS-fed + hrANXA1 mice were comparable to levels of Evans blue in chow-fed mice.

Further measurements for BBB integrity assessment were conducted *ex vivo* using cultured pMBMECs. Both intervention arms significantly decreased the paracellular permeability when compared to HFHS-fed mice (Figure 5.3B). Interestingly, the reduction in the *in vitro* paracellular permeability was significantly greater in the HFHS – Chow reversion diet mice with a 4-fold decrease compared to a 3-fold decrease in HFHS-fed + hrANXA1 mice and was in fact even better than the chow-fed mice by 1.5-fold, suggesting a tighter restriction of paracellular flow. In combination with reduced permeability, both intervention arms showed a significant increase in the TEER which was better in the HFHS-fed + hrANXA1 treated mice, suggesting a tighter restriction in the ionic conductance (Figure 5.2C).

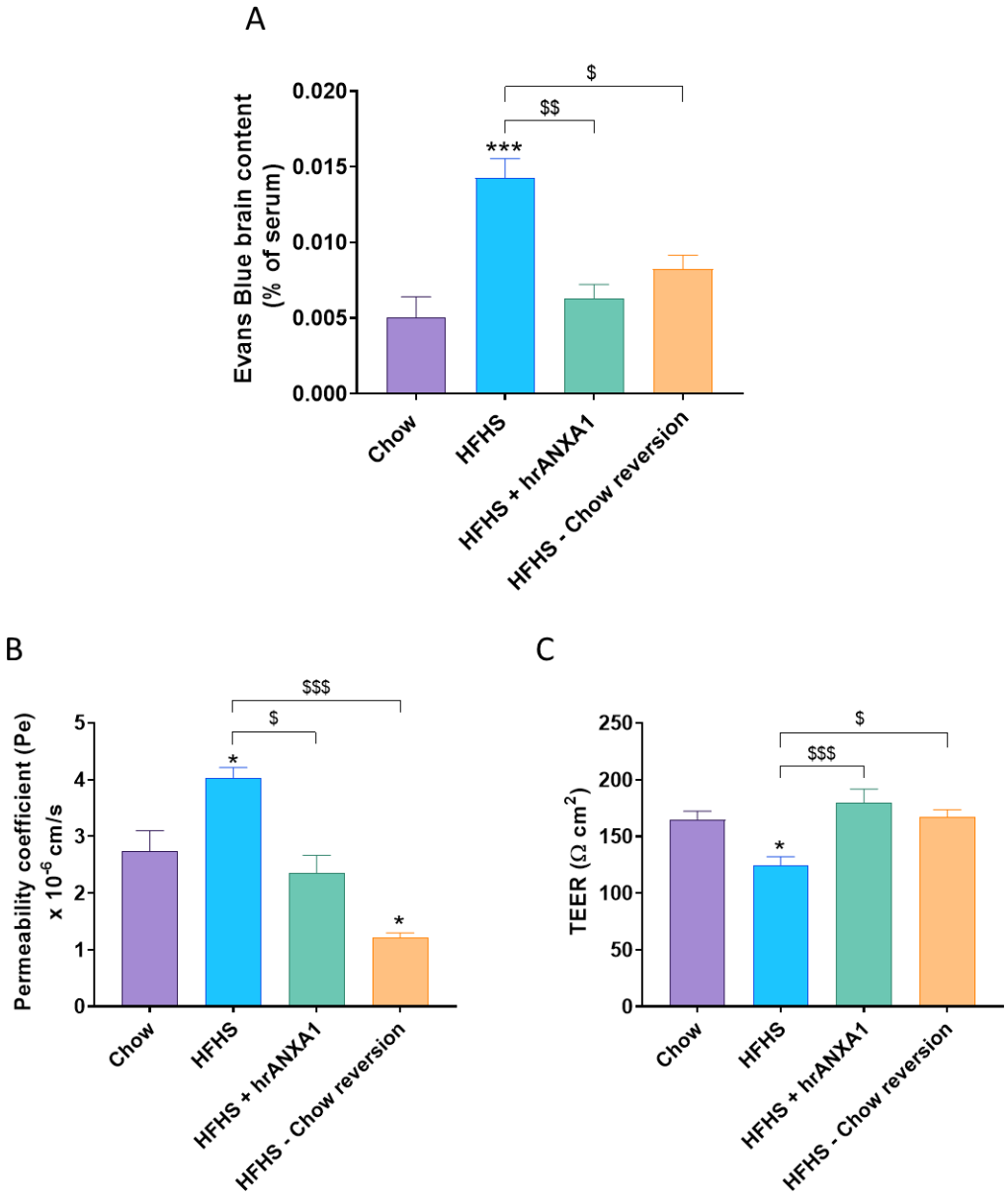
A
Evans Blue brain content (% of serum)
0.020
0.015
0.010
0.005
0.000
***
$
$$
Chow
HFHS
HFHS + hrANXA1
HFHS - Chow reversion
B
Permeability coefficient (Pe) x 10-6 cm/s
5
4
3
2
1
0
*
*
$
$$$
Chow
HFHS
HFHS + hrANXA1
HFHS - Chow reversion
C
TEER (Ω cm2)
250
200
150
100
50
0
*
$
$$$
Chow
HFHS
HFHS + hrANXA1
HFHS - Chow reversion

Figure 5.3 | *In vivo* and *in vitro v*ascular permeability measurements

Assessment of BBB permeability *in vivo* was conducted using Evans blue dye extravasation into the brain (A). 100µl of 2% Evans blue dye was given i.v. to mice (n=6/group) and allowed to circulate for 1 hour. The dye content was analysed spectrophotometrically at an absorbance of 620nm, values were normalized to brain tissue weight and are expressed as percentage of serum dye content. Isolated and cultured pMBMECs from mice were grown on transwell inserts for 7 days to measure e*x vivo* paracellular permeability (B) and transendothelial electrical resistance (TEER) (C) using 70kDA FITC-dextran and the Epithelial Volt/Ohm (EVOM2) Meter (World Precision Instruments, USA), respectively (For chow, HFHS, HFHS + hrANXA1 n=10 pooled/group per experiment, two technical replicates, performed as three independent experiments with a total of n=30 per/group. For HFHS – Chow reversion n=6pooled/group, with two technical replicates, performed as two independent experiments with a total of n=12). Statistical analysis was performed by one-way ANOVA followed by a Bonferroni post-hoc test. Data is expressed as mean ± SEM., *p< 0.05, ***p<0.001 vs. Chow; $p<0.05, $$p<0.01, $$$p<0.001, vs. HFHS.

5.2.3 Treatment with hrANXA1 restores the BBB integrity through restoring tight junctions and the basement membranes. Dietary intervention begins to improve BBB morphology.

5.2.3.1 Changes occurring to the junctional proteins of brain endothelial cells

The impaired BBB integrity in the HFHS-fed mice could be correlated to the disruption of TJs and BMs of endothelial cells and astrocytes. The significantly reduced leakage of the BBB in the HFHS-fed + hrANXA1 and HFHS – Chow reversion diet mice, therefore proposed an improvement in the cell-cell contacts and vascular structure of the brain microvessel.

Confocal imaging of cerebral cortical brain sections revealed treatment with hrANXA1 restored TJ protein, claudin-5 and occludin and BM, pan-laminin (Figure 5.4A,B) distribution, with staining showing a regular and continuous pattern. Further re-instatement of the cell-cell contacts was correlated to the actin cytoskeleton, with results showing HFHS-fed + hrANXA1 mice to have restored F-actin fibre formation, as seen with a reduction in the G/F actin ratio compared to HFHS-fed mice (Figure 5.4B).

Intriguingly, in the HFHS – Chow reversion diet mice there was a trend towards improved occludin deposition when compared to HFHS-fed mice, though this was not statistically significant. The reverse diet mice also retained weak laminin reactivity similar to the HFHS-fed mice (Figure 5.4C). Both occludin and pan-laminin reactivity was significantly lower than the chow-fed and HFHS-fed + hrANXA1 treated mice.

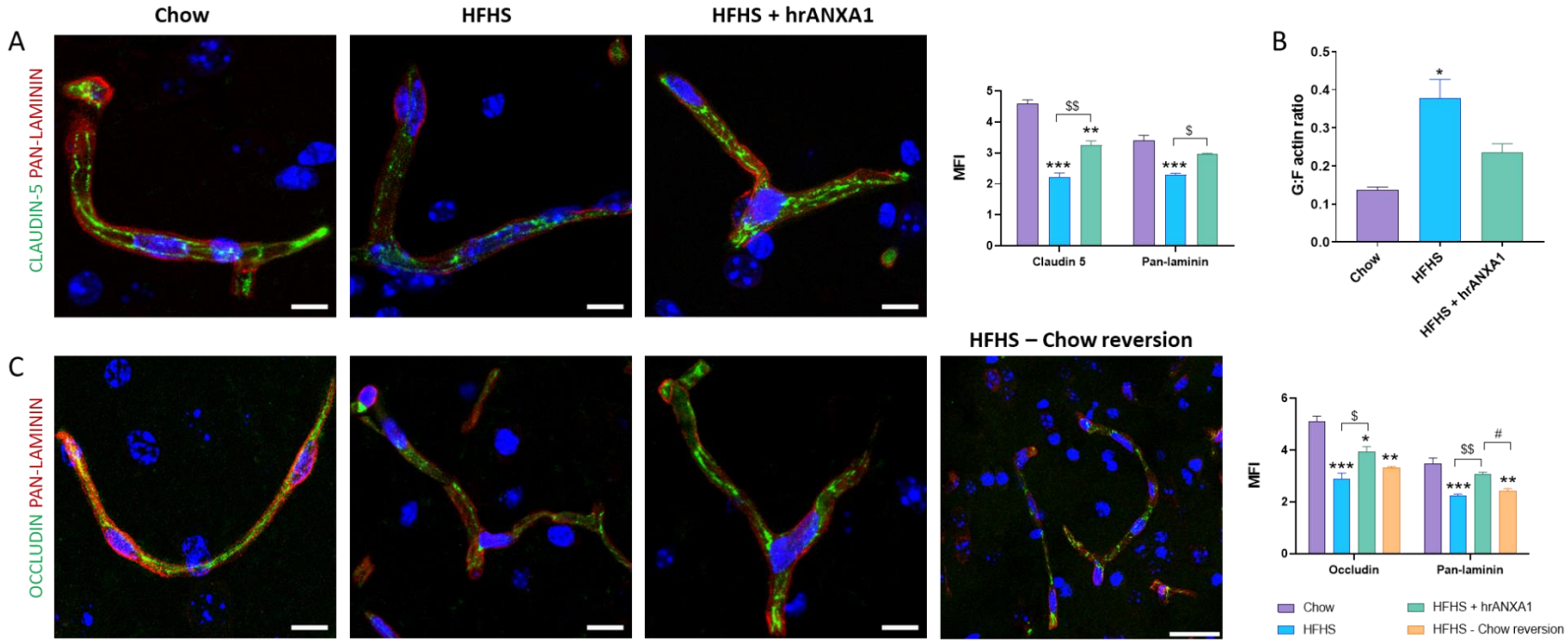

Figure 5.4 | Immuno-histochemical analysis of brain endothelium junctional proteins and flow cytometrical analysis of cytoskeleton

Confocal microscopy of cerebral cortical sections of mouse brains double immune-labelled with claudin-5/pan-laminin (A) and occludin/pan-laminin (C). Nuclear counterstain with TO-PRO3. Confocal images are representative images from n=4 mice/group, 35 section/animal (scale bar: 25µm). Quantification of staining shown as mean fluorescence intensity (arbitrary units) of markers on ten randomly selected fields. Flow cytometric analysis of G/F actin ratio in primary brain endothelial cells (B). Statistical analysis was performed by one-way ANOVA followed by a Bonferroni post-hoc test. Data is expressed as mean ± SEM., *p< 0.05, **p<0.01, ***p<0.001, vs. Chow; $p<0.05, $$p<0.01, vs. HFHS. #p< 0.05, vs. HFHS + hrANXA1

5.2.3.2 Changes occurring to the BMs of brain endothelial cells & astrocytes

Treatment with hrANXA1 also recovered the presence of BMs that were disrupted with HFHS-feeding, with both laminin α2 and α4 showing a regular and continuous staining pattern, as was observed in chow-fed mice brains (Figure 5.5A,B). The pan-laminin immunoreactivity was also restored, prevailing on the outer VBL layer (Figure 5.5A). Importantly, the recovery of laminin α2 allowed for re-association of co-localised astrocytic end-feet (labelled with GFAP) back to the vessel, reforming an intact-looking BBB (Figure 5.5C).

In contrast, in the HFHS – Chow reversion diet mice the laminin α2 presence on astrocytic end-feet was not fully restored like the HFHS-fed + hrANXA1 treated mice, and thus prevented the reattachment of the astrocytes to the vessel (Figure 5.5C). Interestingly there was no difference in the overall intensity of GFAP between with groups, with the exception of HFHS – Chow reversion diet mice, in which there appeared to be significantly fewer astrocytes compared to chow-fed mice.

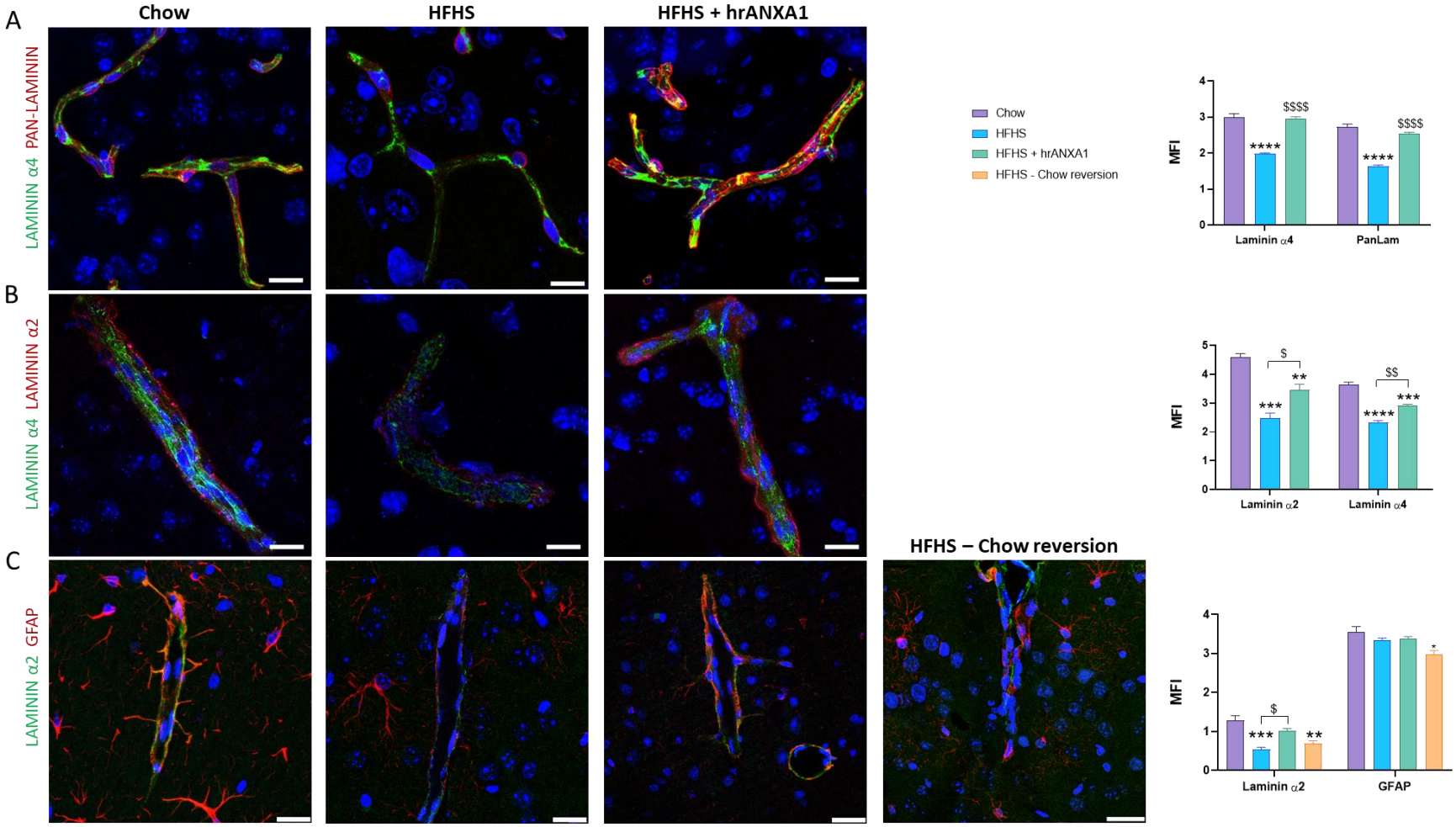
A
Chow
HFHS
HFHS + hrANXA1
LAMININ α4 PAN-LAMININ
B
LAMININ α4 LAMININ α2
C
LAMININ α2 GFAP
HFHS – Chow reversion
Chow
HFHS
HFHS + hrANXA1
HFHS - Chow reversion
MFI
Laminin α4
PanLam
Laminin α2
Laminin α4
Laminin α2
GFAP

Figure 5.5 | Imaging the basement membrane in hrANXA1 treated and dietary reversion mice

Confocal microscopy of cerebral cortical sections of mouse brains double immune-labelled with endothelial laminin α4/vascular basement membrane pan-laminin (A), endothelial laminin α4/astrocytic laminin α1 (B) and endothelial laminin α4/astrocytic marker glial fibrillary acidic protein (GFAP) (C). Nuclear counterstain with TO-PRO3. Confocal images are representative images from n=4 mice/group, 35 section/animal (scale bar: 25µm). Quantification of staining shown as mean fluorescence intensity (arbitrary units) of markers on ten randomly selected fields. Statistical analysis was performed by one-way ANOVA followed by a Bonferroni post-hoc test. Data is expressed as mean ± SEM., *p< 0.05, **p<0.01, ***p<0.001, ****p<0.0001 vs. Chow; $p<0.05, $$p<0.01, vs. HFHS. #p< 0.05, vs. HFHS + hrANXA1.

5.2.3.3 Effect of hrANXA1 treatment and dietary intervention on MMPs at the BBB

In chapter 4, the loss of the TJs and BMs in the HFHS-fed mice was associated to the rise in MMPs that degrade the junctional and ECM proteins. Similarly the restoration of the TJs and BMs in the HFHS-fed + hrANXA1 mice could be correlated to a reduction in MMP-2-, MMP-3 and MMP-9 expression at the brain microvessels compared to HFHS-fed mice; however this was only statistically significant when examining MMP-9 (Figure 5.6A). In HFHS – Chow reversion diet mice, the levels of MMP-3 and MMP-9 decreased when compared to HFHS-fed mice comparable with levels in HFHS-fed + hrANXA1 treated mice. Interestingly, the levels of MMP-2 in the reversion diet mice remained the same as the levels observed in the HFHS-fed mice.

Confirmation of reduced MMP proteolytic activity was conducted via a zymography of MMP-2 and MMP-9 (Figure 5.6C). Results showed treatment with hrANXA1 in HFHS-fed mice reduced pro-MMP-9, MMP-9, pro-MMP-2 and MMP-2 when compared to HFHS-fed mice however these results were not statistically significant (Figure 5.6D,E). In the HFHS – Chow reversion diet mice, the levels of all MMPs were dramatically reduced, which were statistically significant when compared to HFHS-fed mice; levels of proteolytic activity in the reversion mice were similar to those seen in chow-fed mice (Figure 5.6D,E).

MMPs levels are kept in check by their inhibitors - TIMPs. In the HFHS-fed mice, the increased MMP expression at the brain microvessels was marked by a significant reduction in the TIMP-1 serum concentration. In the HFHS-fed + hrANXA1 mice, where the MMP levels were shown to decrease, the concentration of TIMP-1 in the serum increased but the levels were still lower than in chow-fed mice, albeit not significantly (Figure 5.6B). Similarly, the HFHS – Chow reversion diet mice also showed restored TIMP-1 levels in the serum when compared to HFHS-fed mice, however this was not significant; and concentrations remained lower than those seen in HFHS-fed + hrANXA1 treated and chow-fed mice (Figure 5.6B).

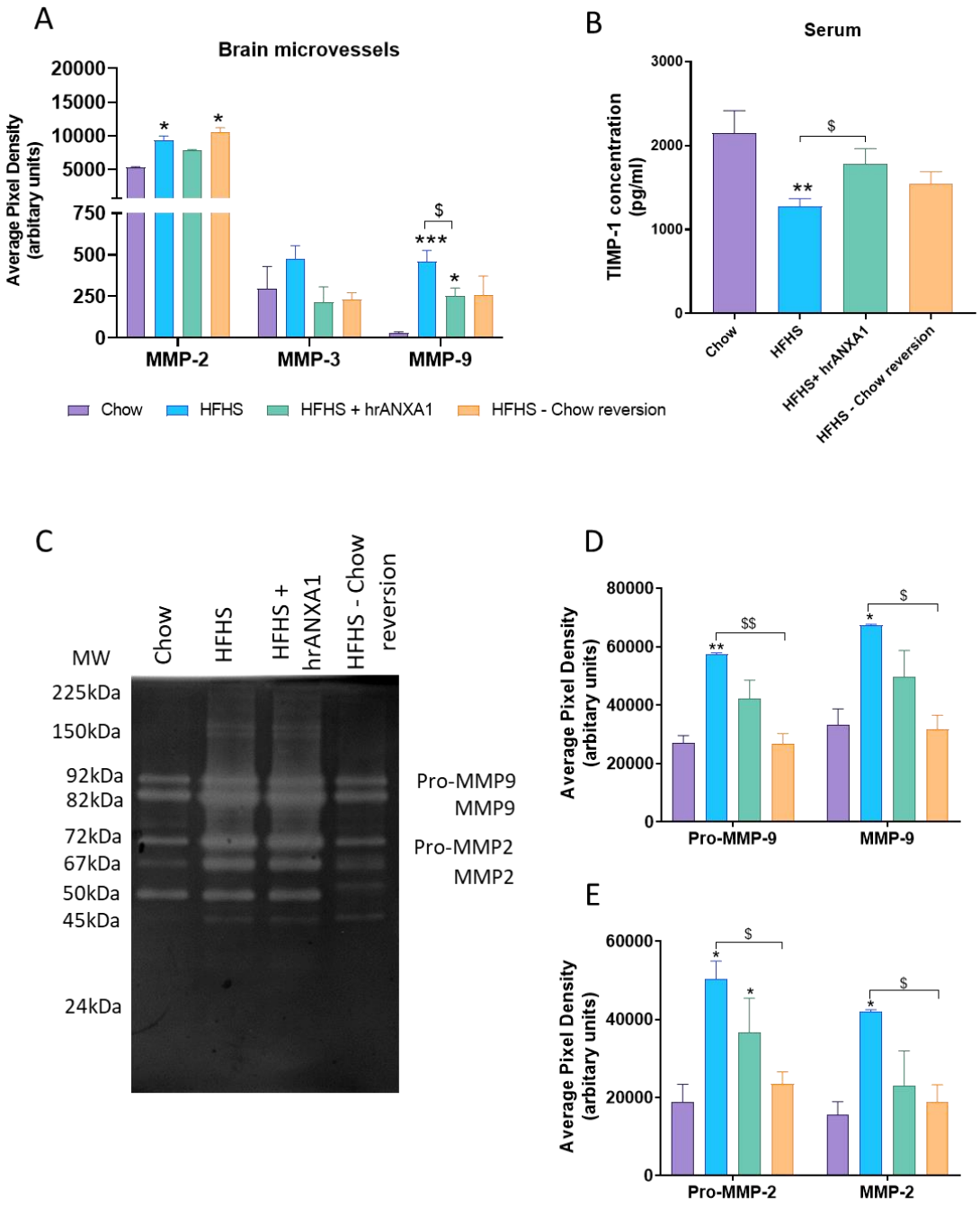
A
Brain microvessels
Average Pixel Density (arbitary units)
20000
15000
10000
5000
750
500
250
0
MMP-2
MMP-3
MMP-9
Chow
HFHS
HFHS + hrANXA1
HFHS - Chow reversion
B
Serum
TIMP-1 concentration (pg/ml)
3000
2000
1000
0
Chow
HFHS
HFHS+ hrANXA1
HFHS - Chow reversion
C
MW
Chow
HFHS
HFHS + hrANXA1
HFHS - Chow reversion
225kDa
150kDa
92kDa
82kDa
72kDa
67kDa
50kDa
45kDa
24kDa
Pro-MMP9
MMP9
Pro-MMP2
MMP2
D
Average Pixel Density (arbitary units)
80000
60000
40000
20000
0
Pro-MMP-9
MMP-9
E
Average Pixel Density (arbitary units)
60000
40000
20000
0
Pro-MMP-2
MMP-2

Figure 5.6 | Effect of hrANXA1 treatment and dietary intervention on MMPs at the BBB

Expression of MMP-2, MMP-3, MMP-9 was analysed in brain microvessel extracts of mice using a Mouse Proteome Profiler (R&D Systems). The membrane-antibody array was loaded with 500ng of protein/group overnight (n=10 pooled/group, two technical replicates per experiment, for chow, HFHS and HFHS + hrANXA1 performed as two independent experiments total n=20/group). Membranes were exposed to x-ray film and the signal produced at the different capture spots were used to quantify the amount of protein bound using ImageStudio Lite (LI-COR Biosciences), expressed as arbitrary units (A). Serum levels of tissue inhibitor of metalloproteinases (TIMP-1) were measured using a quantikine ELISA kit (R&D Systems) (B; n=11/group). Proteolytic activity of MMP-2 and MMP-9 in brain microvessel extracts was determined via zymography, based on separation of proteins by non-reducing sodium dodecyl sulphate polyacrylamide gel electrophoresis (SDS–PAGE). Molecular weight markers were used to estimate the molecular masses of active "pro" and inactive forms of MMP-2 and MMP-9 (C). Blots were scanned (BioRad Imager) and densitometry analysis was performed using ImageJ software (C,D). Each lane was loaded with 100ng of protein (n=10 pooled/group for chow HFHS, HFHS + hrANXA1, total n=20 and n=6 pooled for HFHS – Chow-reversion, total n=12, this gel is representative of two independent experiment). Statistical analysis was performed by one-way ANOVA followed by a Bonferroni post-hoc test. Data is expressed as mean ± SEM., *p< 0.05, **p<0.01, ***p<0.001 vs. Chow; $p<0.05, vs. HFHS.

5.2.4 Treatment with hrANXA1 and dietary changes reduce the inflammatory profile seen in diabetic mice

Results from Chapter 4 clearly demonstrated an enhanced pro-inflammatory profile in the HFHS-fed mice, both in the serum and at the brain microvasculature.

Within the serum, treatment with hrANXA1 in HFHS-fed mice resulted in a reduction in inflammation, with restoration in the levels of CXCL1, CXCL12, IL-1a, IL-16, s-ICAM-1 and TNF-α (Figure 5.7) when compared to HFHS-fed mice. However, the levels of anti-inflammatory IL-13 were further decreased when compared to HFHS-fed mice and there was no change in the C5a expression. Notably, hrANXA1 appeared to have a potent effect on reducing the interleukins; with levels reduced beyond those seen in control chow-fed mice.

Further in-depth analysis of mediators, interleukins, cytokines, chemokines, and acute phase proteins at the brain microvessels was conducted across all animal groups.

Figure 5.8A reviews general inflammatory markers. Results show that hrANXA1 treatment restored levels of IFN-γ, chitinase 3-like 1 and C5a (in contrast to serum values) when compared to HFHS-fed mice. On the other hand, hrANXA1 treatment exacerbated the levels of TNF-α and VEGF, beyond those seen in HFHS-fed mice and in comparison, the levels of CRP and periostin were improved beyond those seen in chow-fed mice; there was no change in expression of RAGE. Comparatively, HFHS – Chow reversion diet mice improved a larger proportion of these mediators, with reduction in C5a, IFN-γ, TNF-α, RAGE and VEGF levels when compared to HFHS-fed mice; notably the levels of IFN-γ were considerably higher than in HFHS-fed + hrANXA1 treated mice. The HFHS – Chow reversion diet mice also worsened the periostin and CRP levels beyond those seen in chow-fed mice (Figure 5.8A).

Review of pro- vs anti-inflammatory interleukins found all listed pro-inflammatory interleukins to be raised in HFHS-fed mice compared to chow-fed (Figure 5.8B). Treatment with hrANXA1 in HFHS-fed mice further increased the levels of IL-1α, IL-1β, IL-7, IL-22 and IL-23 when compared to HFHS-fed mice; levels of IL-2, IL-6, IL-12 p40 and IL-27 p28 where improved whilst there was no large differences in IL-15 and IL-17A. In the HFHS – Chow reversion diet group there was reduction in the

levels of IL-15, IL-17A, IL-23 and IL-27 p28 when compared to HFHS-fed mice. Notably in the reversion group, there was also a reduction in the levels of IL-1α, IL-6, IL-7 and IL-22 when compared to HFHS-fed mice and chow-fed mice. However, the reversion diet increased levels of IL-1β and IL-2 when compared to HFHS-fed mice (Figure 5.8B).

When examining the anti-inflammatory interleukins (Figure 5.8D), treatment with hrANXA1 in HFHS-fed mice reduced the levels of IL-1ra, IL-4, IL-5 and IL-13, whilst levels of IL-10 and IL-11 did not change compared to HFHS-fed mice. The levels of IL-33 did not differ across the groups. Dietary intervention managed to lower the levels of all anti-inflammatory cytokines when compared to HFHS-fed mice, except for IL-5.

Review of chemokines (Figure 5.8C) found the large majority of chemokines to be increased in the HFHS-fed mice. Treatment with hrANXA1 in HFHS-fed mice further increased the levels of all chemokines when compared to a HFHS-fed diet with the exception of CX3CL1 which was further decreased. On the whole, HFHS – Chow reversion diet mice had reduced levels of all chemokines when compared to HFHS-fed mice with the exception of CCL5, CXCL1 and CX3CL1.

In summary, the results showed both pharmacological and dietary intervention to have anti-inflammatory effects. Nevertheless, the reversion of diet was more potent at reducing the overall inflammatory phenotype.

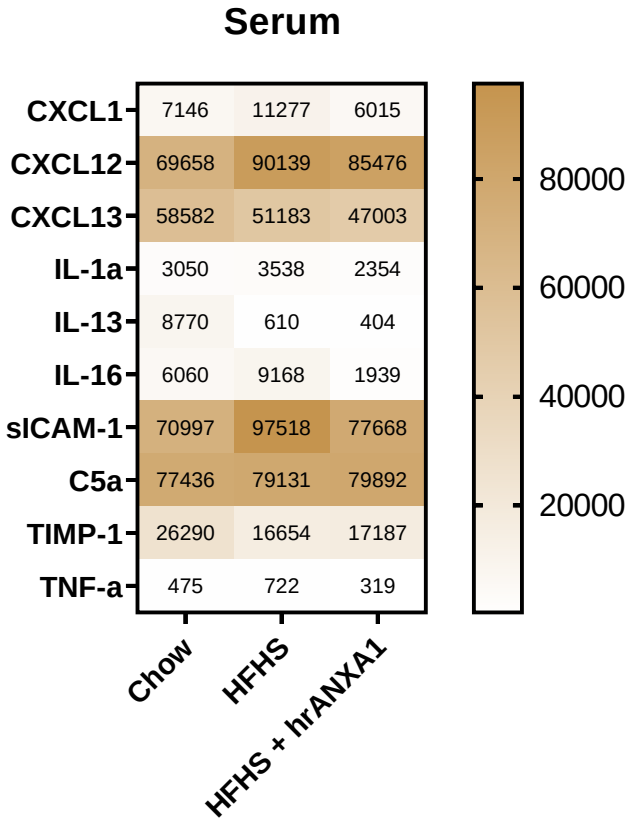

Figure 5.7 | Cytokine measurements in the serum

Inflammatory mediator analysis was conducted to reveal the relative level of inflammation occurring within the serum of chow, HFHS or HFHS + hrANXA1 mice. The Mouse Cytokine Array Panel A kit (R&D Systems) was used to analyse the presence of acute phase proteins, interleukins and chemokines using a membrane-based sandwich immunoassay; results are presented as arbitrary units, n=10 pooled/group, two technical replicates.

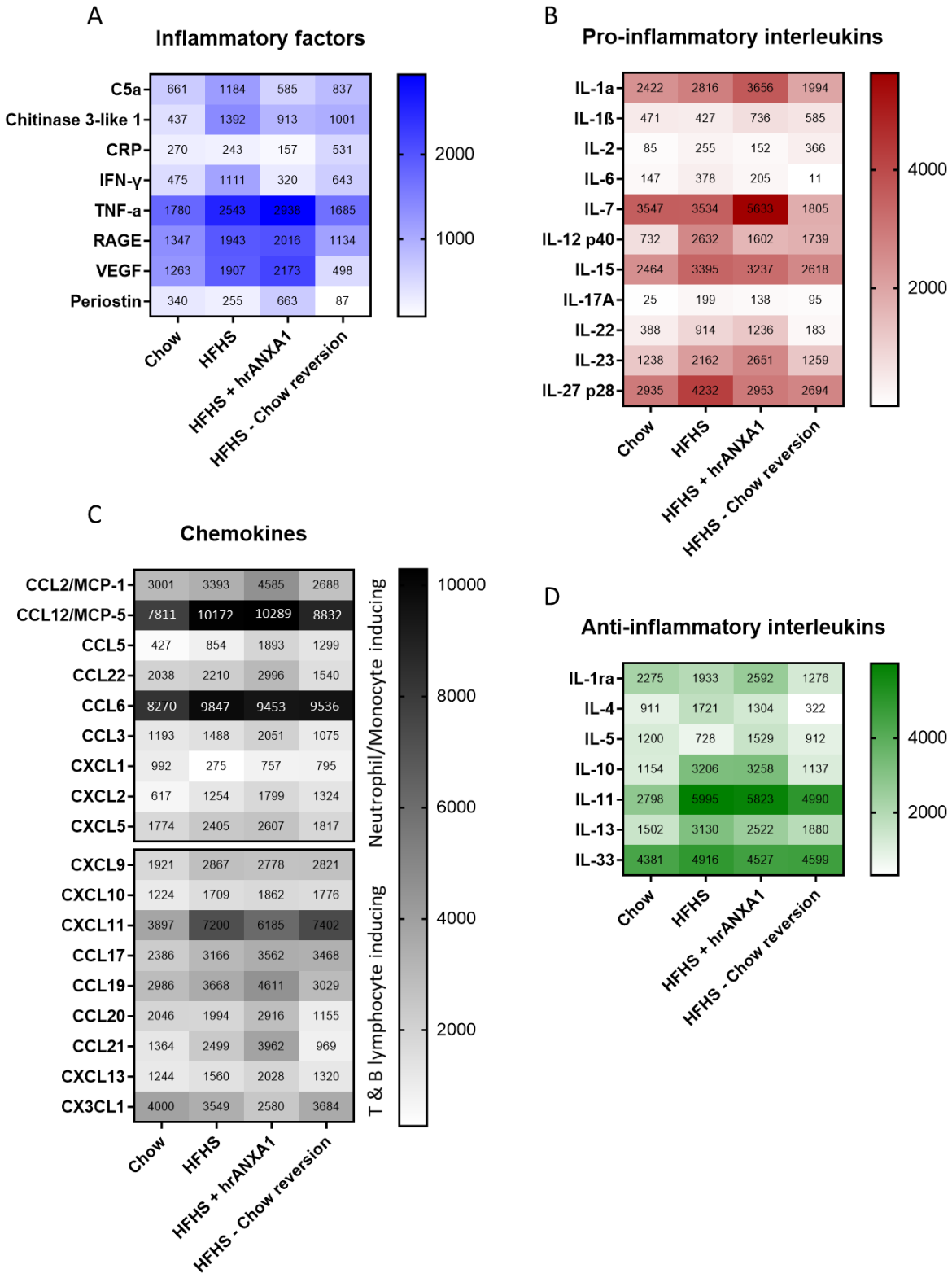
A
Inflammatory factors
C5a 661 1184 585 837
Chitinase 3-like 1 437 1392 913 1001
CRP 270 243 157 531
IFN-γ 475 1111 320 643
TNF-a 1780 2543 2938 1685
RAGE 1347 1943 2016 1134
VEGF 1263 1907 2173 498
Periostin 340 255 663 87
2000
1000
Chow
HFHS
HFHS + hrANXA1
HFHS - Chow reversion
B
Pro-inflammatory interleukins
IL-1a 2422 2816 3656 1994
IL-1ß 471 427 736 585
IL-2 85 255 152 366
IL-6 147 378 205 11
IL-7 3547 3534 5633 1805
IL-12 p40 732 2632 1602 1739
IL-15 2464 3395 3237 2618
IL-17A 25 199 138 95
IL-22 388 914 1236 183
IL-23 1238 2162 2651 1259
IL-27 p28 2935 4232 2953 2694
4000
2000
Chow
HFHS
HFHS + hrANXA1
HFHS - Chow reversion
C
Chemokines
CCL2/MCP-1 3001 3393 4585 2688
CCL12/MCP-5 7811 10172 10289 8832
CCL5 427 854 1893 1299
CCL22 2038 2210 2996 1540
CCL6 8270 9847 9453 9536
CCL3 1193 1488 2051 1075
CXCL1 992 275 757 795
CXCL2 617 1254 1799 1324
CXCL5 1774 2405 2607 1817
CXCL9 1921 2867 2778 2821
CXCL10 1224 1709 1862 1776
CXCL11 3897 7200 6185 7402
CCL17 2386 3166 3562 3468
CCL19 2986 3668 4611 3029
CCL20 2046 1994 2916 1155
CCL21 1364 2499 3962 969
CXCL13 1244 1560 2028 1320
CX3CL1 4000 3549 2580 3684
Neutrophil/Monocyte inducing
T & B lymphocyte inducing
10000
8000
6000
4000
2000
Chow
HFHS
HFHS + hrANXA1
HFHS - Chow reversion
D
Anti-inflammatory interleukins
IL-1ra 2275 1933 2592 1276
IL-4 911 1721 1304 322
IL-5 1200 728 1529 912
IL-10 1154 3206 3258 1137
IL-11 2798 5995 5823 4990
IL-13 1502 3130 2522 1880
IL-33 4381 4916 4527 4599
4000
2000
Chow
HFHS
HFHS + hrANXA1
HFHS - Chow reversion

Figure 5.8 | Profiling the inflammation at the brain microvasculature

Simultaneous measurement of multiple cytokines, chemokines, interleukins and other inflammatory markers in protein extracts from brain microvessels using Mouse Cytokine Array Kits (R&D Systems). Membrane-based immunoassays detected the relative expression levels of analytes detected as arbitrary units (n=10 pooled/group, two technical replicates per experiment, for chow, HFHS and HFHS + hrANXA1 performed as two independent experiments total n=20/group) and categorised as inflammatory factors (A), chemokines (C), pro-inflammatory interleukins (B) or anti-inflammatory interleukins (D).

5.2.5 Both pharmacological and dietary intervention reduce the activation and expression of adhesion molecules at the BBB

In line with a reduced inflammatory phenotype, histological analysis of *ex vivo* cortical brain sections showed treatment with hrANXA1 in HFHS-fed mice to downregulate the expression of ICAM-1 and P-selectin when compared to HFHS-fed mice (Figure 5.9A,B). Nevertheless, the expression levels were still significantly higher when compared to chow-fed mice.

Proteomic analysis of isolated brain microvessel tissue (Figure 5.9C) confirmed the confocal imaging results, with hrANXA1 treatment significantly decreasing expression of ICAM-1 and VCAM-1. Interestingly, treatment with hrANXA1 showed no change in P-selectin expression and trend towards increased CD40 and E-selectin expression when compared to HFHS-fed. Dietary reversion, on the other hand, decreased expression of all adhesion molecules when compared to HFHS-fed and chow-fed mice, however this was only statistically significant for ICAM-1 and VCAM-1 levels.

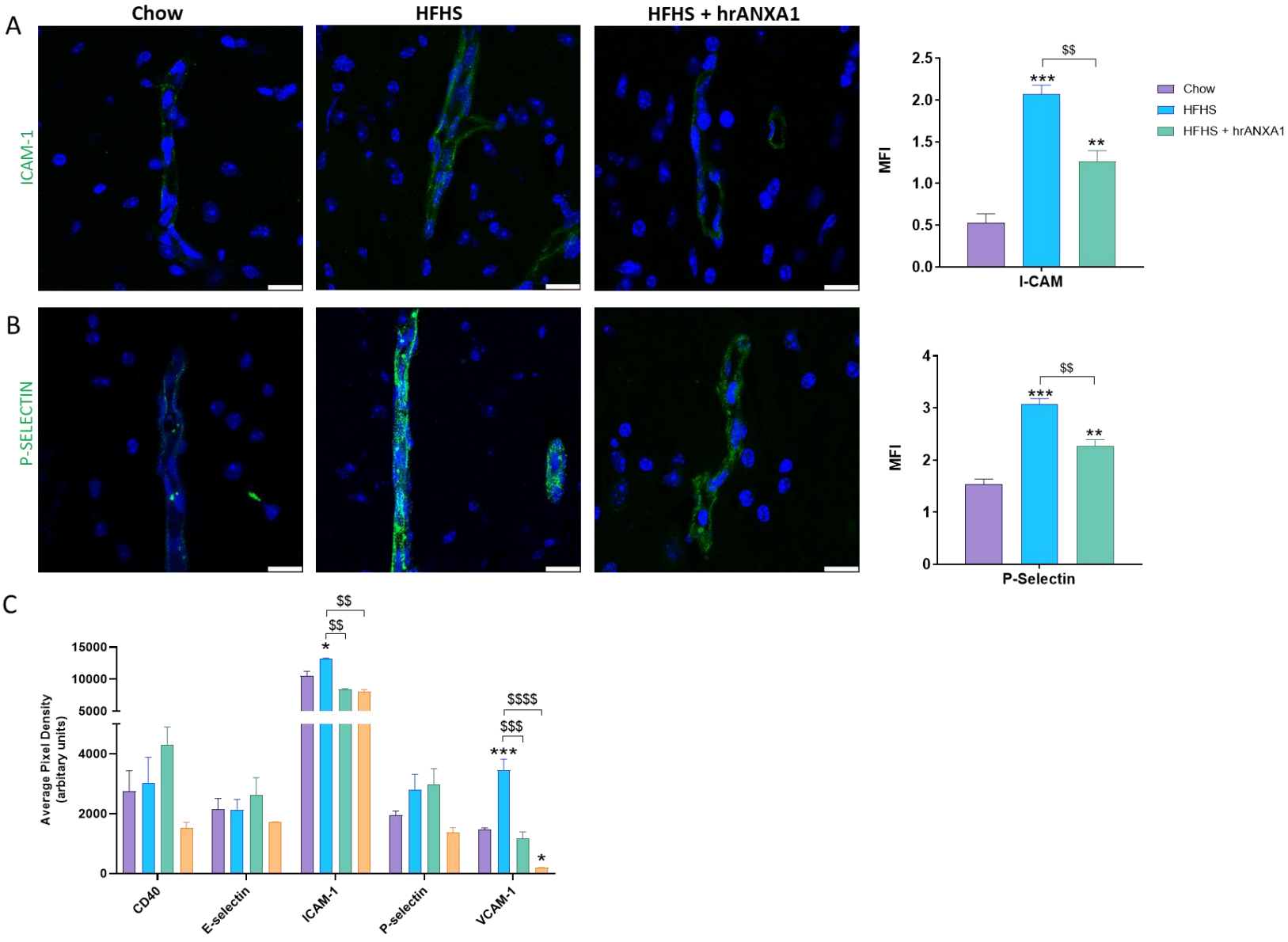
A
Chow
HFHS
HFHS + hrANXA1
ICAM-1
B
P-SELECTIN
MFI
I-CAM
Chow
HFHS
HFHS + hrANXA1
P-Selectin
C
Average Pixel Density (arbitary units)
CD40
E-selectin
ICAM-1
P-selectin
VCAM-1

Figure 5.9 | Changes in the expression of adhesion molecules on the BBB with hrANXA1 treatment and dietary intervention

Cerebral cortical sections of the brain were immunofluorescently stained for endothelial cell adhesion molecules ICAM-1 (A) and P-selectin (B); nuclei were labelled with TO-PRO3. Typical images from n=4 animals 35 section/animals (scale bar: 25μm). Quantification of staining shown as mean fluorescence intensity (arbitrary units) of markers on ten randomly selected fields. Proteomic analysis of brain microvessel extracts using a membrane-based immunoassay (Mouse Cytokine Array XL Kit, R&D Systems, Minneapolis, USA) to detect the relative presence of adhesion molecules E-selectin, ICAM-1, P-selection and VCAM-1 and co-stimulatory molecule CD40 by x-ray film exposure (n=10 pooled/group, two technical replicates per experiment, for chow, HFHS and HFHS + hrANXA1 performed as two independent experiments total n=20/group); quantified using ImageStudio Lite (LI-COR Biosciences). Statistical analysis was performed by one-way ANOVA followed by a Bonferroni post-hoc test. Data is expressed as mean ± SEM., *p< 0.05, **p<0.01, ***p<0.001 vs. Chow; $$p<0.01, $$$p<0.001, $$$$p<0.0001 vs. HFHS.

5.2.6 The effect of pharmacological and dietary intervention on the immune system

5.2.6.1 The innate and adaptive arms of the immune system

As previously described in Chapter 4, the HFHS-fed mice increased both innate and adaptive immune cells. Assessments have been carried out using bone marrow and cervical lymph nodes.

The percentage of macrophages and neutrophils remained significantly high in the HFHS-fed + hrANXA1 treated and HFHS – Chow reversion diet mice (Figure 5.10A). Interestingly, the percentage of macrophages was significantly higher in the reversion group compared to hrANXA1 treated group and this was also the same for dendritic cells. The percentage of dendritic cells however was decreased in the HFHS-fed + hrANXA1 treated mice when compared to HFHS-fed mice. Remarkably the percentage of NK cells in the HFHS-fed mice where further depleted with hrANXA1 treatment, and no change was seen with dietary modification (Figure 5.10A).

In the other adaptive immune cells (Figure 5.10B), both HFHS-fed + hrANXA1 treated and HFHS – Chow reversion diet mice had significantly depleted $CD4^+$ and $CD8^+$ T-cells in the bone marrow when compared to HFHS-fed mice. The percentage of T-cells in HFHS – Chow reversion diet mice was in fact lower than both the HFHS-fed + hrANXA1 treated mice and the chow-fed mice, however only significantly in $CD4^+$ cells. Furthermore, hrANXA1 treatment reverted the inhibitor effect of the HFHS-diet on the percentage of $CD19^+$ B-cells. In contrast, no changes were seen with HFHS – Chow reversion diet mice (Figure 5.10B).

Interestingly, hrANXA1 treatment did not have any effect on the percentage of $CD4^+$ T-cells or $CD8^+$ T-cells in the cervical lymph nodes when compared to HFHS-fed mice (Figure 5.10C). However, hrANXA1 slightly reduced the percentage of $CD19^+$ B-cells compared to HFHS-fed mice, but this was not significant. Similarly, the reversion diet had no effect on the $CD8^+$ T-cells or the $CD19^+$ B-cells in cervical lymph nodes when compared to HFHS-fed mice. However, the reverse diet depleted the percentage of $CD4^+$ T-cells, to percentages lower than in the chow-fed mice.

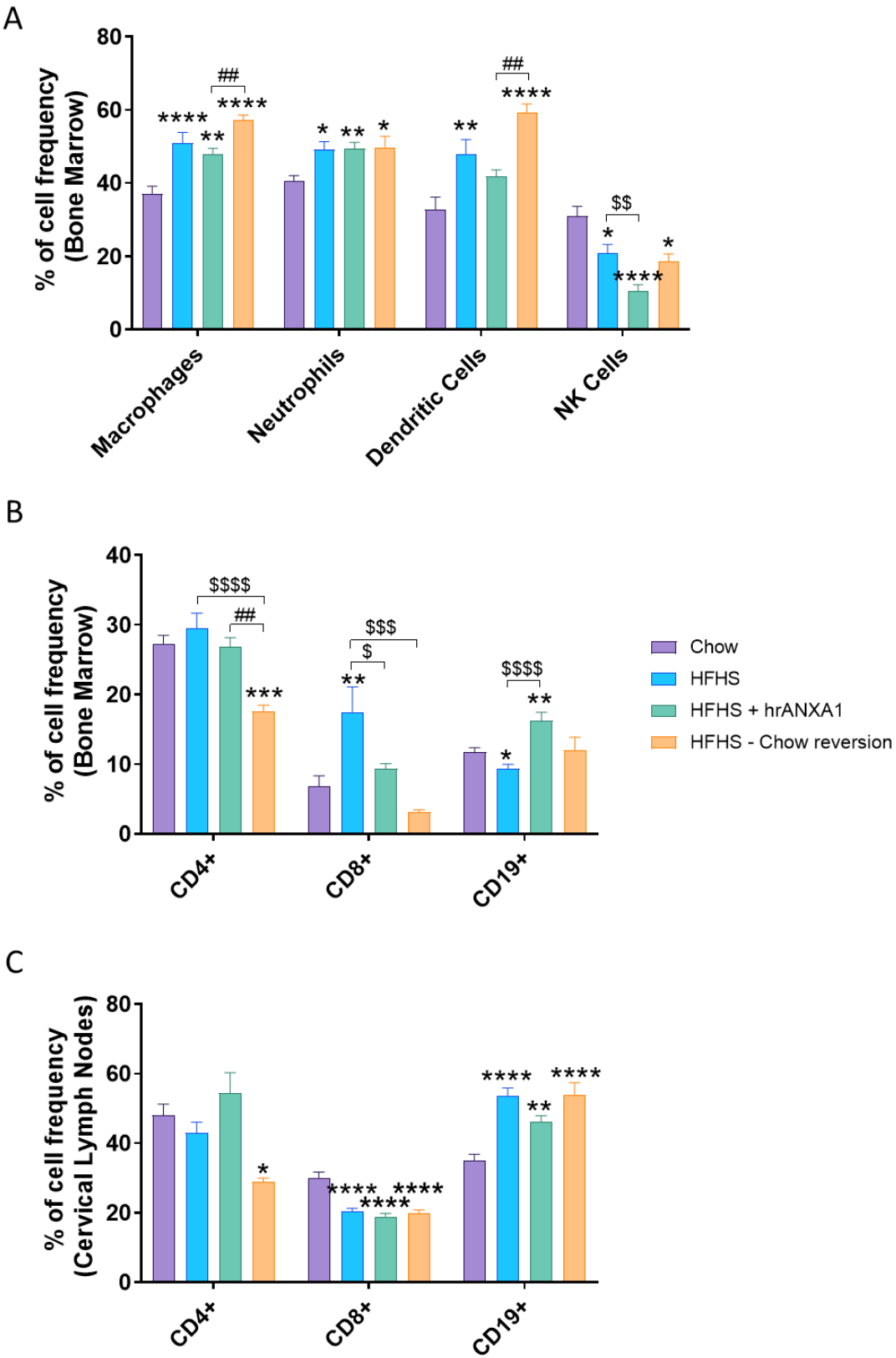
A
% of cell frequency (Bone Marrow)
Macrophages
Neutrophils
Dendritic Cells
NK Cells
B
% of cell frequency (Bone Marrow)
CD4+
CD8+
CD19+
Chow
HFHS
HFHS + hrANXA1
HFHS - Chow reversion
C
% of cell frequency (Cervical Lymph Nodes)
CD4+
CD8+
CD19+

Figure 5.10 | Effect of hrANXA1 and diet on the activation of the innate and adaptive arms of the immune system

Bone marrow and deep cervical lymph nodes were collected from mice. Bone marrow was flushed with $PBS^{-/-}$ to obtain white blood cells, red blood cells were lysed using lysis buffer. Cells were stained using fluorescently conjugated antibodies for cell-surface markers on cells of the innate – neutrophils (Ly6G), macrophages (CD11b), dendritic cells (F4/80, CD11c), and adaptive – NK cells (NK 1.1), T-cells (CD4, CD8), B-cells (CD19) immune system and underwent flow cytometric analysis (n=13-23/group). Deep cervical lymph nodes were homogenised to obtain lymphocytes and underwent flow cytometric analysis after staining to obtain percentage frequency of T-cell subsets CD4+ and CD8+ and B-cells (CD19+) (n=11-16/group). Statistical analysis was performed by one-way ANOVA followed by a Bonferroni post-hoc test. Data is expressed as mean ± SEM., *p< 0.05, **p<0.01, ***p<0.001, ****p<0.0001 vs. Chow; $p<0.05, $$p<0.01, $$$p<0.001, $$$$p<0.0001 vs. HFHS; ##p<0.01, vs HFHS + hrANXA1.

5.2.6.2 Treatment with hrANXA1 reduces the activation of $CD4^+$ T-cells

Pharmacological and dietary intervention had no effect on the activated $CD4^+$ $CD44^+$-expressing T-cells with percentages similar to those seen in the HFHS-fed mice (Figure 5.11A). Despite this, treatment with hrANXA1 did reduce the percentages of $CD4^+$ $CD44^+$ LFA-1^+ and $CD4^+$ $CD44^+$ $CXCR3^+$-expressing T-cells compared to HFHS-fed mice (Figure 5.11B,C). In contrast, the reversion diet significantly increased the percentages of $CD4^+$ $CD44^+$ LFA-1^+ and $CD4^+$ $CD44^+$ $CXCR3^+$-expressing T-cells; and these percentages were even higher than those seen in the chow-fed mice (Figure 5.11B,C).

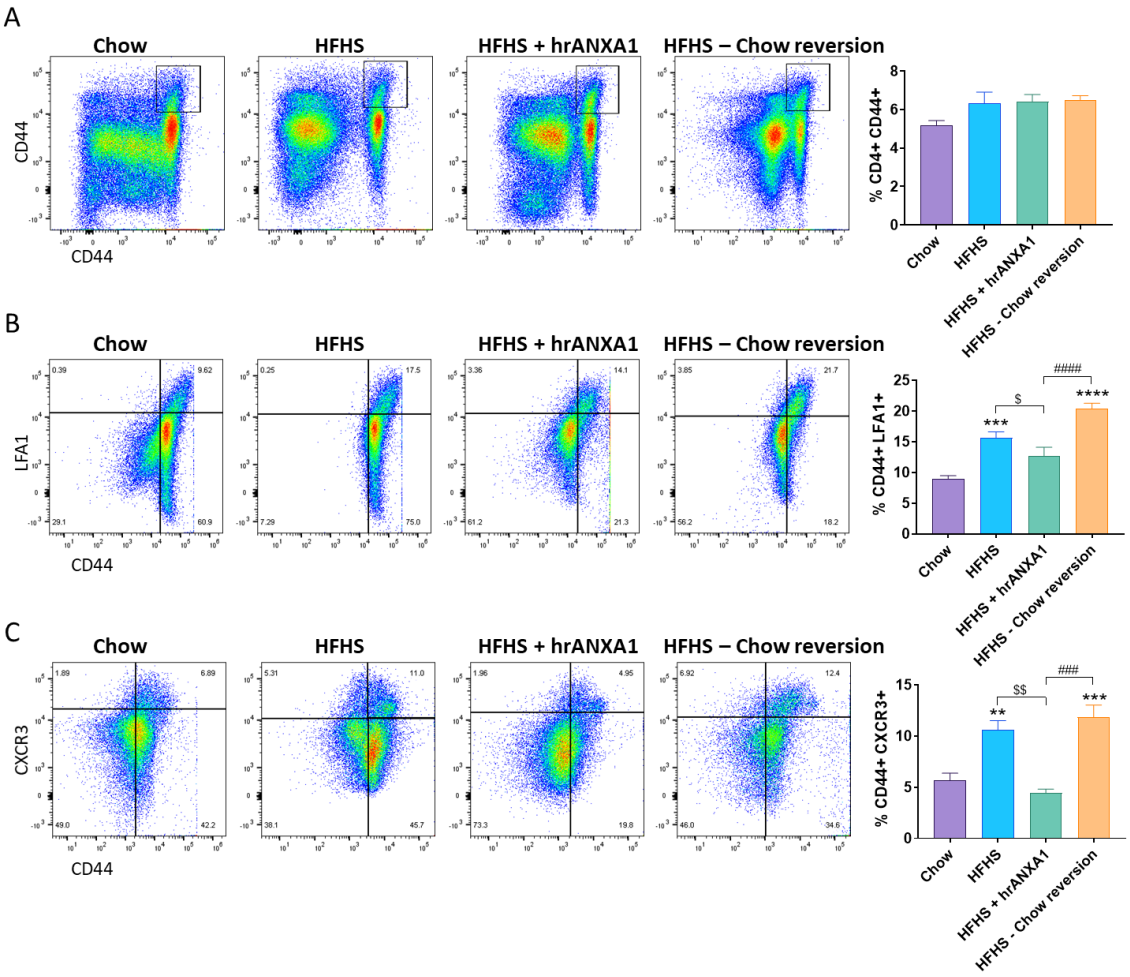

Figure 5.11 | Effect of hrANXA1 and diet on CD4$^+$ T-cell activation

Deep cervical lymph nodes were collected and homogenised to obtain lymphocytes. All T-cells were stained for CD4, within this subset of T-cells staining was conducted for activation marker CD44 (A). On CD4$^+$ CD44$^+$-expressing T-cells, the expression of lymphocytic adhesion molecule LFA-1 (B) and chemokine receptor CXCR3 (C) was evaluated (n=5-11/group). Statistical analysis was performed by one-way ANOVA followed by a Bonferroni post-hoc test. Data is expressed as mean ± SEM., *p< 0.05, **p<0.01, ***p<0.001, ****p<0.0001 vs. Chow; $p<0.05, $$p<0.01, $$$p<0.001, $$$$p<0.0001 vs. HFHS; ##p<0.01, vs HFHS + hrANXA1.

5.2.6.2 Both pharmacological and dietary intervention show greater presence of T_{CM} vs T_{EM} cells

The memory status of the $CD4^+$ T-cells found HFHS-fed mice to have increased percentages of T_{CM} and T_{EM} cells compared to chow-fed mice, and with slightly higher T_{EM} percentages. T_{CM} cells are defined as CD44hi CD62Lhi CCR7hi whereas T_{EM} cells are defined as CD44hi CD62Llo CCR7lo.

Treatment with hrANXA1 did not change the percentage of CD44hi CCR7hi cells when compared to HFHS-fed mice (Figure 5.12A). However, the percentage of CD44hi CD62Lhi cells was lower compared to HFHS-fed mice, and similar to chow-fed mice percentages (Figure 5.12B), although this was not significant. In contrast, in the HFHS – Chow reversion diet mice, the percentage of CD44hi CCR7hi cells was further elevated when compared to all other groups, whereas the percentage of CD44hi CD62Lhi cells was depleted when compared to all other groups. In summary, both hrANXA1 and diet reversion induced loss in the high expression of CD62L (Figure 5.12B).

Both pharmacological and dietary intervention caused a significant loss of CD44hi CCR7lo expressing cells when compared to HFHS-fed mice (Figure 5.12A). The percentage of CD44hi CC62Llo cells in both intervention arms remained elevated, with percentages equal to HFHS-fed mice (Figure 5.12B). This suggests that hrANXA1 treatment and dietary intervention cause the loss of CCR7lo expression.

Given the differences in percentages and statistically significance, it appears as though HFHS-fed + hrANXA1 mice have a greater ratio of T_{CM} vs T_{EM} cells. In the HFHS – Chow reversion mice, there appears to be more disarray in the expression levels of receptors, with perhaps an equal balance of T_{CM} and T_{EM} cells.

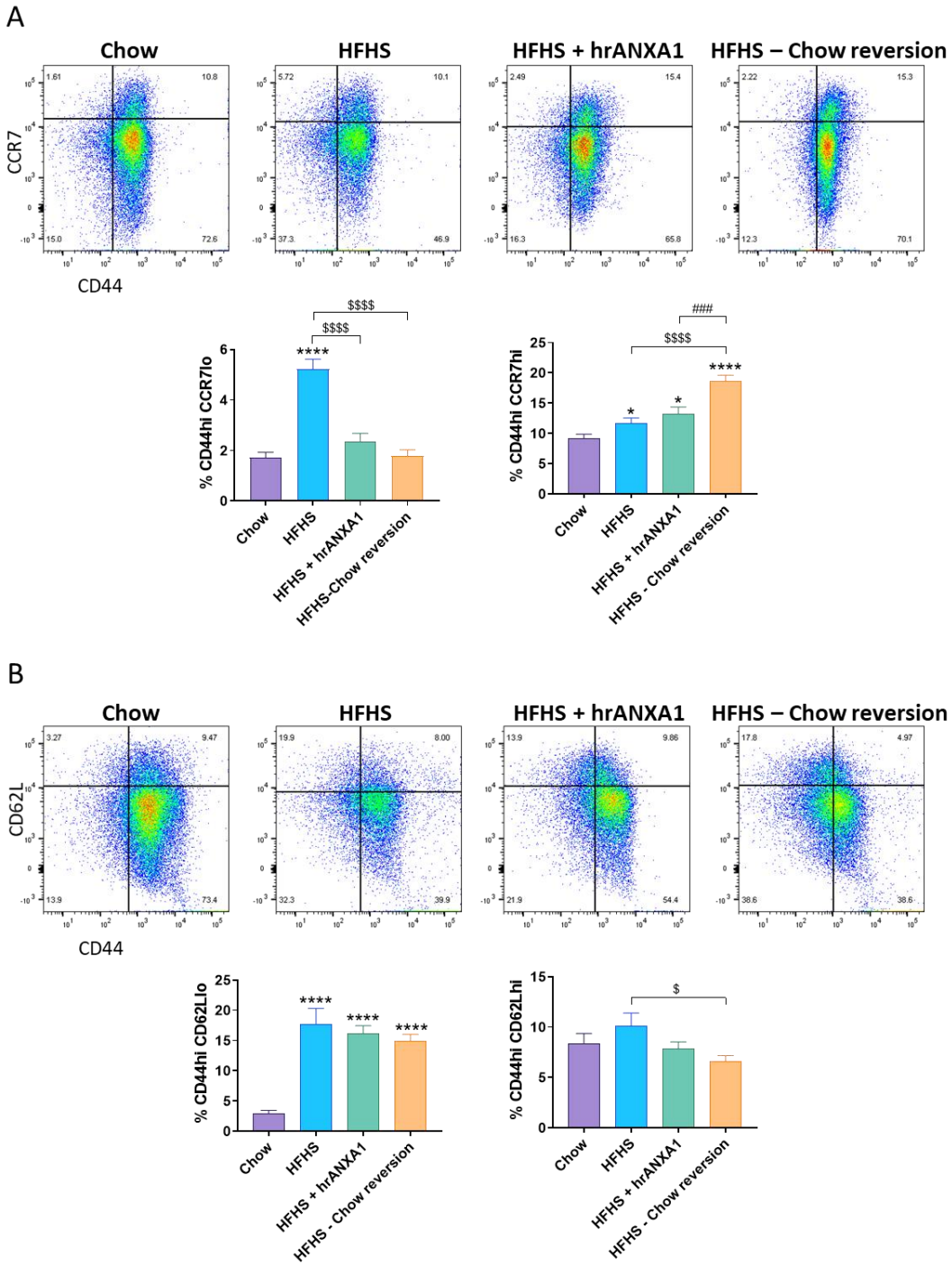
A
Chow
HFHS
HFHS + hrANXA1
HFHS – Chow reversion
CCR7
CD44
1.61
10.8
15.0
72.6
5.72
10.1
37.3
46.9
2.49
15.4
16.3
65.8
2.22
15.3
12.3
70.1
% CD44hi CCR7lo
$$$$
$$$$
****
Chow
HFHS
HFHS + hrANXA1
HFHS-Chow reversion
% CD44hi CCR7hi
###
$$$$
****
*
*
Chow
HFHS
HFHS + hrANXA1
HFHS - Chow reversion
B
Chow
HFHS
HFHS + hrANXA1
HFHS – Chow reversion
CD62L
CD44
3.27
9.47
13.9
73.4
19.9
8.00
32.3
39.9
13.9
9.86
21.9
54.4
17.8
4.97
38.6
38.6
% CD44hi CD62Llo
****
****
****
Chow
HFHS
HFHS + hrANXA1
HFHS - Chow reversion
% CD44hi CD62Lhi
$
Chow
HFHS
HFHS + hrANXA1
HFHS - Chow reversion

Figure 5.12 | Effect of hrANXA1 and diet on Effector vs Central Memory T-cells

Deep cervical lymph nodes were collected and homogenised to obtain lymphocytes. All T-cells were stained for CD4, within this subset of T-cells staining was conducted for high (hi) or low (lo) expression of activation marker CD44 (A). On $CD4^+$ $CD44^+$-expressing T-cells, the high and low expression of L-selectin CD62L (A) and chemokine receptor CCR7 (B) was evaluated (n=5-11/group) to characterise the presence of central memory (CD44hi, CD62Lhi, CCR7lo) or effector memory (CD44hi, CD62Llo, CCR7lo) T-cells. Statistical analysis was performed by one-way ANOVA followed by a Bonferroni post-hoc test. Data is expressed as mean ± SEM., *p< 0.05, ****p<0.0001 vs. Chow; $p<0.05, $$$$p<0.0001 vs. HFHS; ####p<0.0001, vs HFHS + hrANXA1.

5.2.6.3 Both pharmacological and dietary intervention reduce the T_H17/Treg ratio

Treatment with hrANXA1 and dietary reversion significantly reduced the percentage RoRγt-expressing T_H17 cells when compared with the HFHS-fed mice (Figure 5.13A). Although there were no changes in the Foxp3-expressing Treg cells in the intervention arms when compared to HFHS-fed mice (Figure 5.13B), the drop in T_H17 cells resulted in a large reduction in the T_H17/Treg ratio in these intervention strategies (Figure 5.13C).

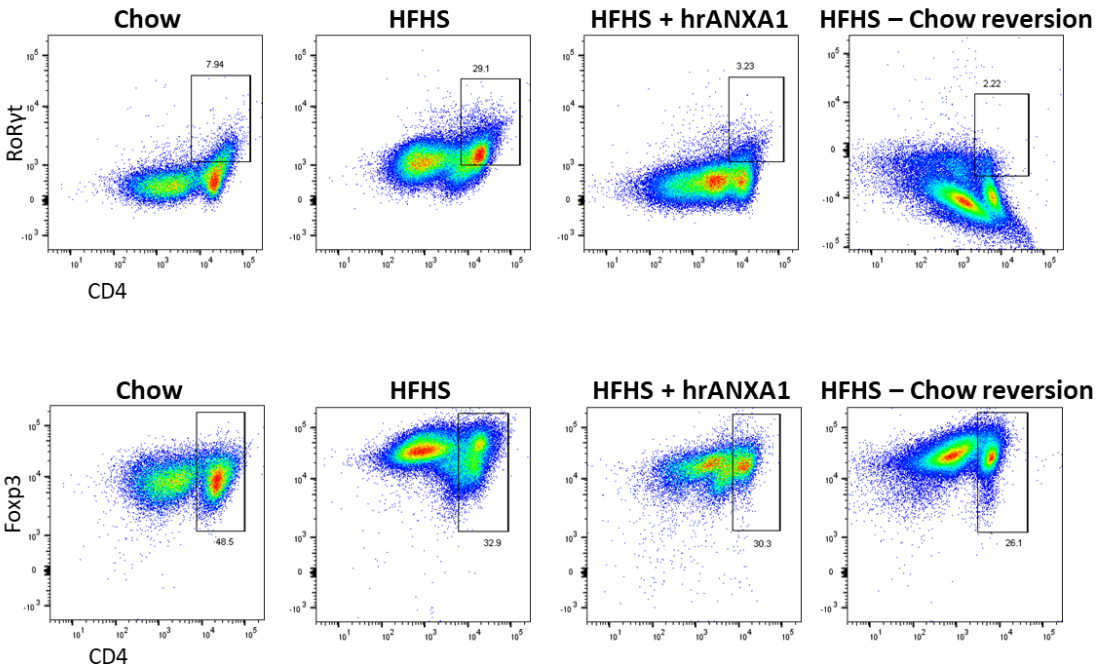
Chow
HFHS
HFHS + hrANXA1
HFHS – Chow reversion
RoRyt
CD4
7.94
29.1
3.23
2.22
Foxp3
48.5
32.9
30.3
26.1

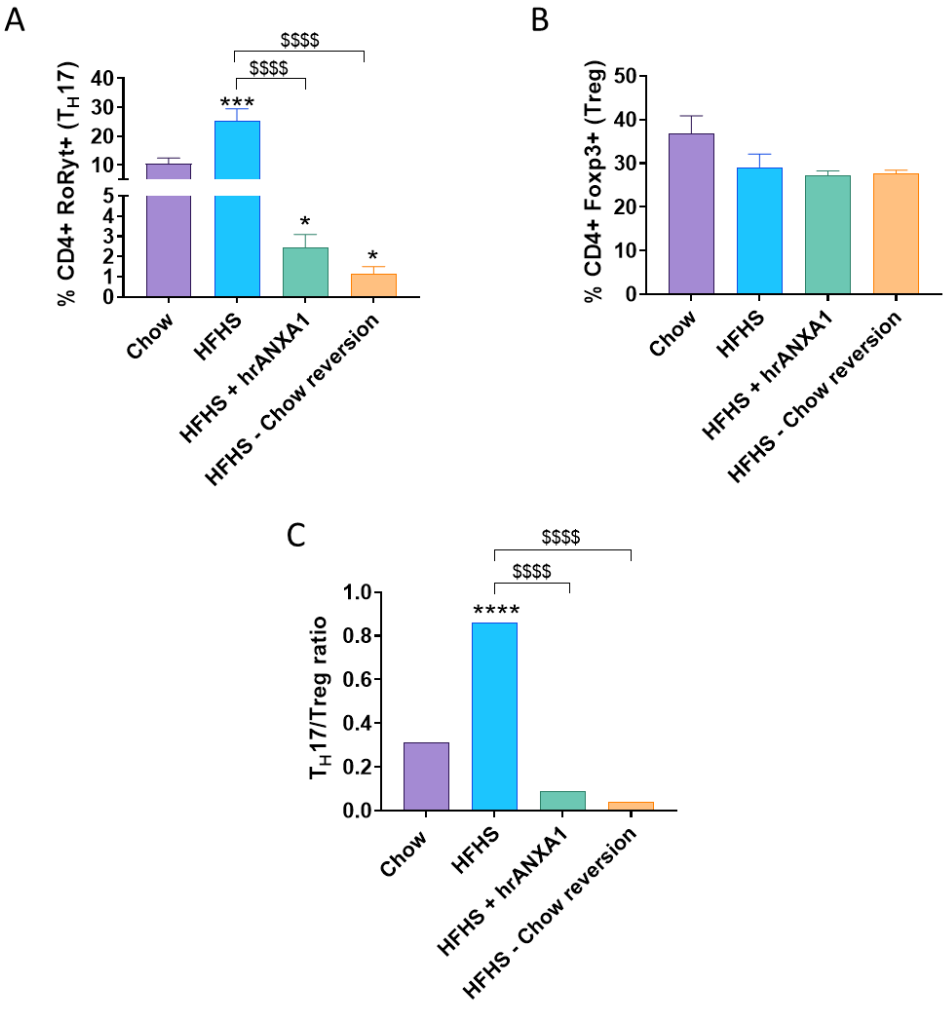
A
% CD4+ RoRyt+ (TH17)
$$$$
$$$$
***
*
*
Chow
HFHS
HFHS + hrANXA1
HFHS - Chow reversion
B
% CD4+ Foxp3+ (Treg)
C
TH17/Treg ratio
****

Figure 5.13 | Effect of hrANXA1 and diet on Th17 vs Treg cells

Deep cervical lymph nodes were collected from chow and mice. Lymph nodes were homogenised to obtain lymphocytes. All T-cells were stained for CD4, within this subset T-cells were categorised as pro-inflammatory T-helper (T_H17) cells based on their expression of RoRγt (A) or as anti-inflammatory regulatory T-cells (Treg) based on their expression of Foxp3 (B). Ratio between T_H17/Treg cells (C) (n=9=11/group). Statistical analysis was performed by one-way ANOVA followed by a Bonferroni post-hoc test. Data is expressed as mean ± SEM., *p< 0.05, ***p<0.001 vs. Chow; $$$$p<0.0001 vs. HFHS.

5.2.6.4 Treatment with hrANXA1 reduces the transmigration of peripherally activated leukocytes across the BBB. Dietary modifications reduce T_H17 TEM across the BBB.

In the HFHS-fed mice, the loss of BBB integrity coupled with a pro-inflammatory status and increased immune cell numbers resulted in increased TEM of leukocytes across the BBB. In contrast, treatment with hrANXA1 showed no or rare $CD45^+$ cells infiltration into the brain parenchyma (Figure 5.14A). However, diet reversion did not have any apparent differences in the $CD45^+$ infiltration when compared to HFHS-fed mice, with confocal imaging showing entrapped $CD45^+$ cells within the VBL layers.

In vitro transmigration assays found similar results, with hrANXA1 treatment significantly reducing the number of $CD4^+$ $CD45^+$ of adhered and migrated T-cells when compared to the HFHS-fed mice (Figure 5.14B). Intriguingly, the reversion diet did not abolish the higher adhered or migratory numbers of $CD4^+$ $CD45^+$ T-cells. Although, a more detailed analysis on the T_H17 and Treg cells showed that dietary reversion significantly reduced the adhered and migrated $RoR\gamma t^+$-expressing T_H17 cells compared to HFHS-fed mice (Figure 5.14C) but did not affect the $Foxp3^+$-expressing Treg cells adherence or migration (Figure 5.14C,D). In contrast, treatment with hrANXA1 affected both the T_H17 and Treg numbers, causing significant reduction in the adherence and migratory capacity of these T-cells when compared to HFHS-fed mice (Figure 5.14C,D).

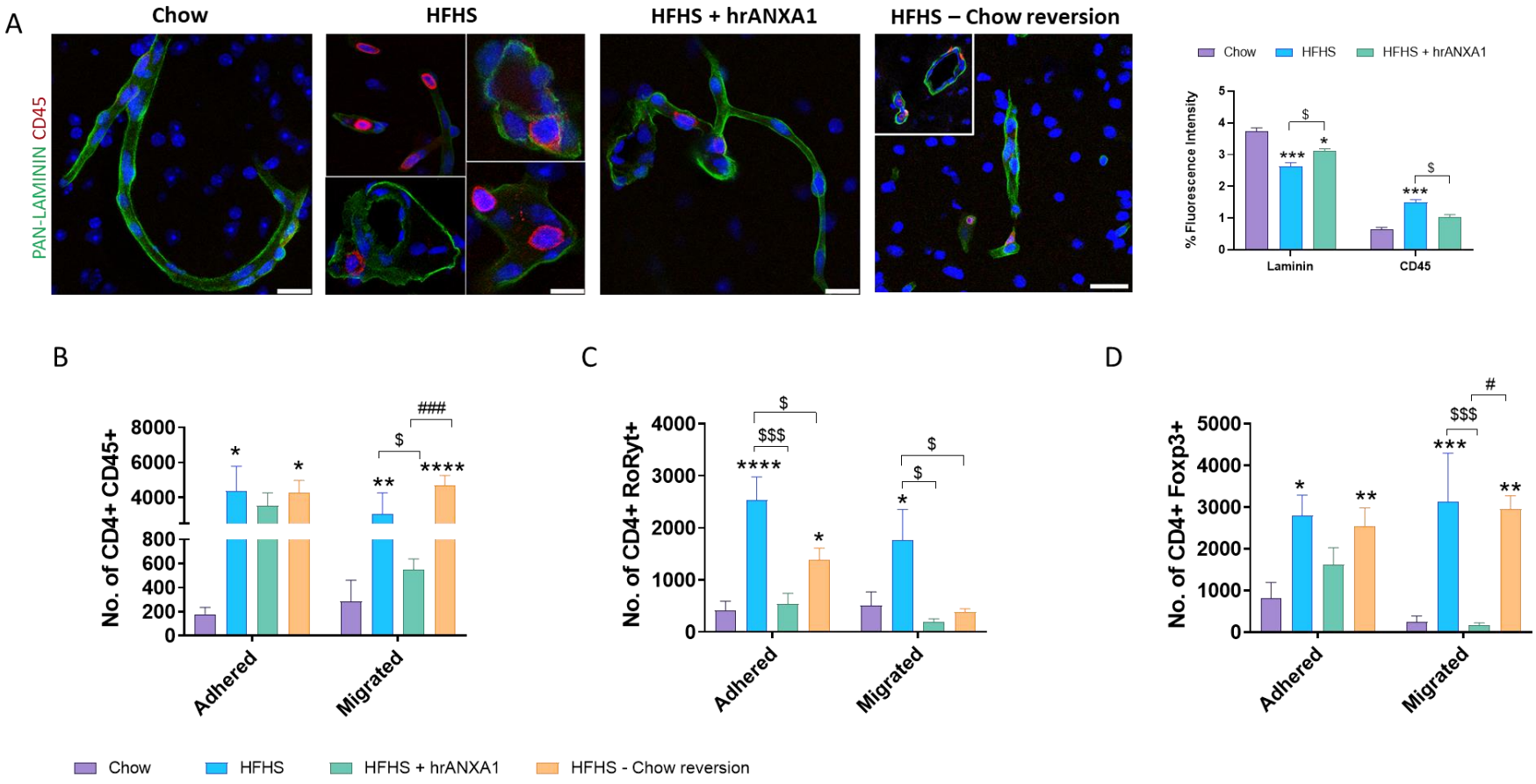
A
Chow
HFHS
HFHS + hrANXA1
HFHS – Chow reversion
PAN-LAMININ CD45
Chow
HFHS
HFHS + hrANXA1
% Fluorescence Intensity
Laminin
CD45
B
No. of CD4+ CD45+
Adhered
Migrated
C
No. of CD4+ RoRyt+
Adhered
Migrated
D
No. of CD4+ Foxp3+
Adhered
Migrated
Chow
HFHS
HFHS + hrANXA1
HFHS - Chow reversion

Figure 5.14 | Transmigration of peripherally activated leukocytes across the BBB

Cerebral cortical sections of the brain were immunofluorescently stained for activation marker CD45, present on all leukocytes, to examine the transmigration of immune cells across the BBB (A); nuclei were labelled with TO-PRO3. Typical images from n=4 animals, 35 section/animals (scale bar: 25μm). Quantification of staining shown as mean fluorescence intensity (arbitrary units) of markers on ten randomly selected fields. Deep cervical lymph nodes were collected from chow and HFHS-fed mice. Lymph nodes were homogenised to obtain lymphocytes and expanded for 4 days in the presence of CD3 and CD28. On day 4, a transmigration assay was conducted, with 1 x 10^6 cells placed in contact with bEnd3 cells grown on transwell inserts. T-cells were placed in contact with the *in vitro* BBB model for a period of 4 hours, after which the cells collected from the top compartment of the transwell served as the adhered component and the cells collected from the bottom compartment served as the migrated component. All collected cells were stained for CD4; within this subset cells were stained for activation marker CD45 (B), RoRγt-expressing Th17 cells (C) or Foxp3-expressing Treg (D) (n=5-9/group). Statistical analysis was performed by one-way ANOVA followed by a Bonferroni post-hoc test. Data is expressed as mean ± SEM., *p< 0.05, **p<0.01, ***p<0.001, ****p<0.0001 vs. Chow; $p<0.05, $$$p<0.001 vs. HFHS; #p<0.05, ###p<0.001 vs HFHS + hrANXA1.

5.2.7 Pharmacological and dietary interventions restore the M1/M2 microglia phenotypic balance.

5.2.7.1 M1 vs M2 Microglia

Results show treatment with hrANXA1 reduces the percentage of microglia cells (CD45lo CD11b^{+}) when compared to HFHS-fed mice (Figure 5.15A). On the contrary, dietary reversion further increases the percentage of microglial cells when compared to all groups. In microglia cells, the expression of fracktaline receptor CX3CR1^{+} expression was restored with pharmacological and dietary intervention when compared to HFHS-fed mice; however, results were only significant for the HFHS-fed + hrANXA1 treated mice (Figure 5.15B).

Interestingly, although HFHS-fed + hrANXA1 treated mice had a reduced percentage of microglia cells, an equivalent percentage of these cells were activated (CD11c^{+} MHCII^{+}-expressing) as in HFHS-fed mice (Figure 5.15C). In contrast, the percentage of activated microglia cells was significantly lower with dietary reversion, with percentages even lower than those seen in chow-fed mice. These activated cells were further differentiated as a pro-inflammatory M1 phenotype (CD86^{+}-expressing cells, Figure 5.15D) or as an anti-inflammatory/resolving M2 phenotype (CD206^{+}-expressing cells, Figure 5.15D). In the HFHS-fed + hrANXA1 treated mice, the percentage of M1 cells remained equivalently elevated as the HFHS-fed mice however there was an increase in the M2 phenotype of cells resulting in a restoration of the M1/M2 phenotypic balance (Figure 5.15E). In the HFHS – Chow reversion diet mice, there was a trend towards reducing M1 phenotypic cells and a trend towards an increased M2 phenotype balance when compared to HFHS-fed mice. Like hrANXA1 treatment, dietary changed restored the balance of M1/M2 cells (Figure 5.15E).

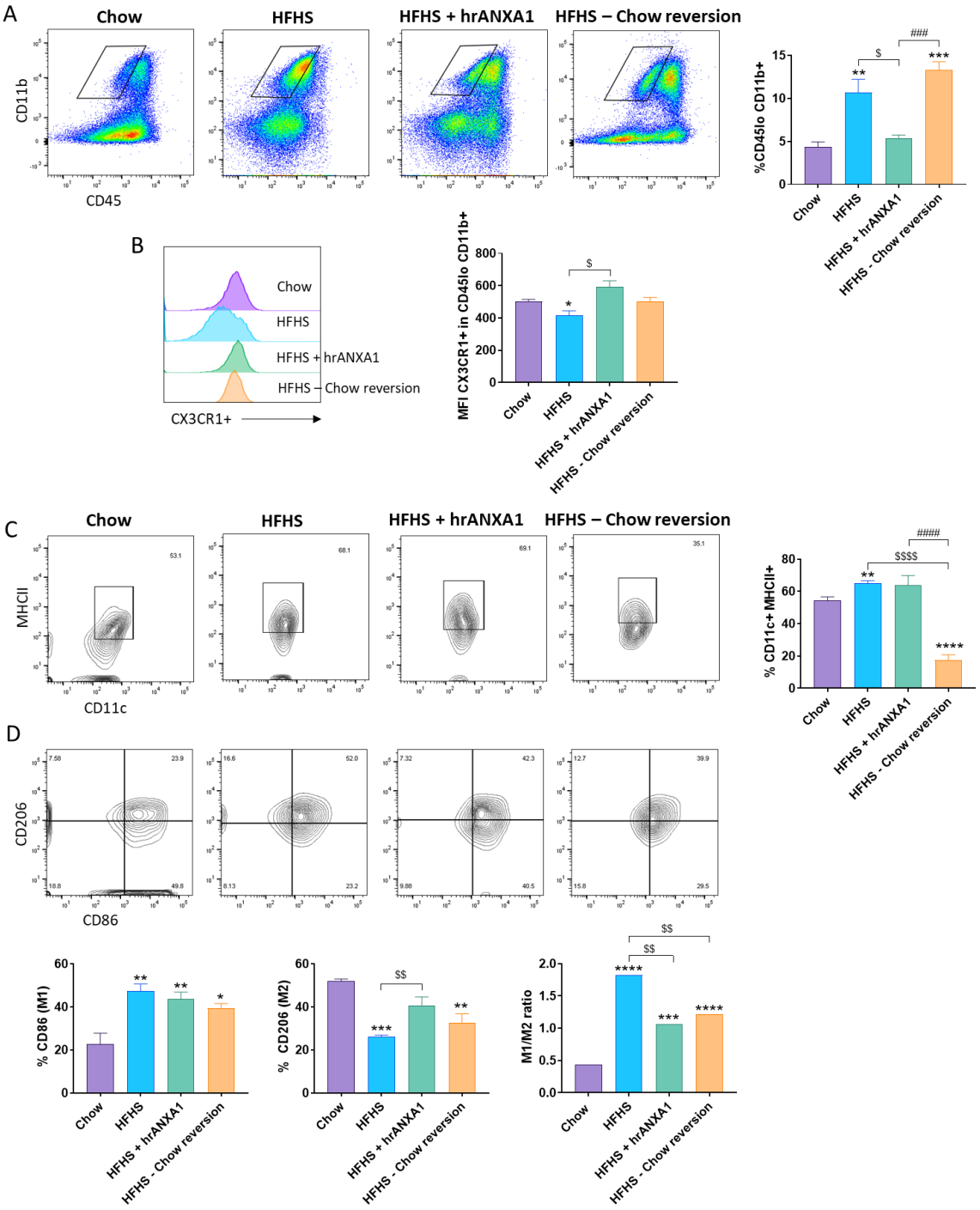
A
Chow
HFHS
HFHS + hrANXA1
HFHS – Chow reversion
CD11b
CD45
%CD45lo CD11b+
B
Chow
HFHS
HFHS + hrANXA1
HFHS – Chow reversion
CX3CR1+
MFI CX3CR1+ in CD45lo CD11b+
C
MHCII
CD11c
% CD11c+ MHCII+
D
CD206
CD86
% CD86 (M1)
% CD206 (M2)
M1/M2 ratio

Figure 5.15 | Changes in the phenotype of microglia cells with hrANXA1 treatment and dietary modifications

Microglia cells were isolated and cultured from chow, HFHS, HFHS + hrANXA1 and HFHS – Chow reversion mice (n=6-12/group, pooled in pairs). Microglia cells were identified by gating on CD45lo $CD11b^+$ cells to differentiate from macrophages (A). Expression of fracktaline receptor $CX3CR1^+$ in CD45lo $CD11b^+$-expressing cells (B), as median intensity of fluorescence (MFI). Percentage of activated microglial cells identified as $CD11c^+$ $MHCII^+$-expressing cells (C) differentiated into pro-inflammatory M1 (CD86+-expressing) and anti-inflammatory M2 (CD206+-expressing cells) phenotypes and ratio of M1/M2 cells (D). Statistical analysis was performed by one-way ANOVA followed by a Bonferroni post-hoc test. Data is expressed as mean ± SEM., *p<0.05, **p<0.01, ***p<0.001, ****p<0.0001 vs. Chow; $p<0.05, $$p<0.01, $$$p<0.001 vs. HFHS; ###p<0.001, ####p<0.0001 vs HFHS + hrANXA1.

5.2.7.2 Oxidative damage in the diabetic brain

In addition, confocal imaging confirmed reduced microglia cell activation in the HFHS-fed + hrANXA1 treated mice, as seen by reduced $IBA1^{+}$-expressing cells compared to HFHS-fed mice (Figure 5.16A). Treatment with hrANXA1 lowered the production of iNOS by both endothelial cells and by microglial cells (Figure 5.16B) when compared to HFHS-fed mice. Notably, the levels of IBA1 and iNOS were equivalent to the levels in chow-fed mice.

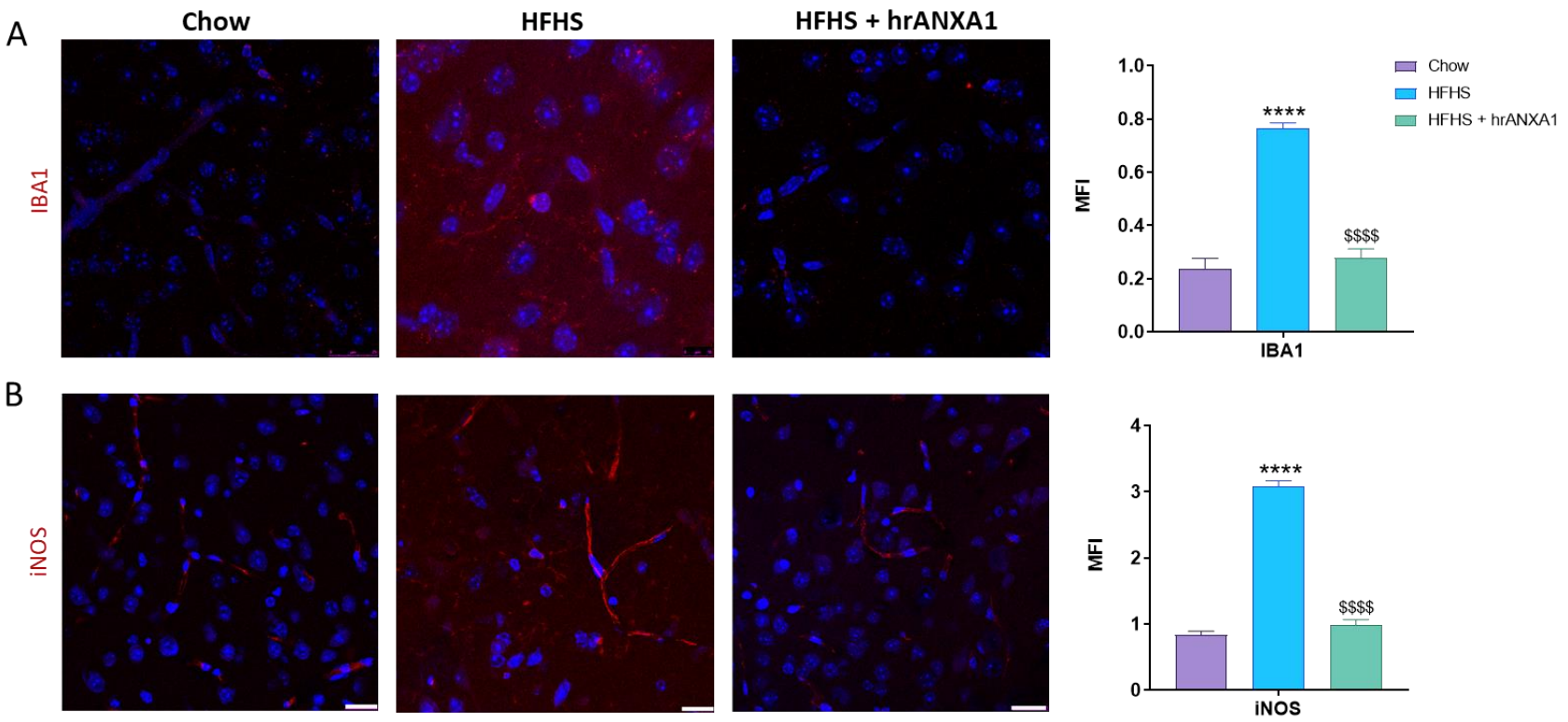
A
Chow
HFHS
HFHS + hrANXA1
IBA1
B
iNOS
MFI
1.0
0.8
0.6
0.4
0.2
0.0
****
$$$$
IBA1
Chow
HFHS
HFHS + hrANXA1
4
3
2
1
0
iNOS

Figure 5.16 | Effect of hrANXA1 on IBA1 and iNOS expression in endothelial cells and microglia

Cerebral cortical sections of the brain were immunofluorescently stained for IBA1 (A) and iNOS (B) expression; nuclei were labelled with TO-PRO3. Typical images from n=4 animals 35 section/animals (scale bar: 25μm). Quantification of staining shown as mean fluorescence intensity (arbitrary units) of markers on ten randomly selected fields. Statistical analysis was performed by one-way ANOVA followed by a Bonferroni post-hoc test. Data is expressed as mean ± SEM., *p< 0.05, **p<0.01, ****p<0.0001 vs Chow.

5.2.8 Summary and comparison of results

Overall, this chapter has evaluated the effect of two interventions – pharmacological and dietary on improving HFHS-feeding induced T2DM. As there are multiple different effects measured, a summary table has been provided (Table 5.3). HFHS-fed mice data is compared to chow-fed mice data, which serves as the 'control'. The effects of pharmacological treatment and dietary intervention have been compared to HFHS-fed mice. The table also compares which intervention fared better against each effect measured.

Table 5.3 | Summary and comparison of results from HFHS-induced T2DM mice and pharmacological and dietary intervention

A summary of the main effects measured in this study has been provided. HFHS-fed mice data is compared to chow-fed mice, which serves as a 'control'. The effects of pharmacological treatment and dietary intervention have been compared to HFHS-fed mice. The table also provides information on which intervention served better against each effect measured.

Effect measured	HFHS vs Chow	HFHS + hrANXA1 vs HFHS	HFHS - Chow reversion vs HFHS	Which intervention scored better?
T2DM development	Induces T2DM	Improves T2DM – reduces glucose, insulin, cholesterol & triglycerides levels	Improves T2DM – reduces obesity and insulin and triglyceride levels	hrANXA1 treatment
Evans blue dye	Increased leakage	Decreased leakage, similar to chow diet	Decreased leakage	hrANXA1 treatment
Paracellular permeability co-efficient	Increased paracellular permeability	Decreased paracellular permeability, similar to chow diet	Decreased paracellular permeability, better than to chow diet	Reversion diet
TEER	Decreased TEER	Increased TEER, similar to chow diet	Increased TEER, similar to chow diet	Similar
G:F actin ratio	Decreased F-actin	Restored F-actin	Not measured	N/A
Claudin-5 expression	Decreased	Restored	Not measured	N/A
Occludin expression	Decreased	Restored	Restored	hrANXA1 treatment
Endothelial laminin α4 expression	Decreased	Restored, similar to chow diet	Not measured	N/A
Astrocytic laminin α2 expression	Decreased	Restored, similar to chow diet	Decreased	hrANXA1 treatment
Pan-laminin	Decreased	Restored, similar to chow diet	Restored	hrANXA1 treatment

Effect measured	HFHS vs Chow	HFHS + hrANXA1 vs HFHS	HFHS - Chow reversion vs HFHS	Which intervention scored better?
MMP expression	Increased	Decreased	Decreased	Similar
MMP-2 and MMP-9 activity (zymography)	Increased	Remained high	Decreased, similar to chow	Reversion diet
TIMP-1 expression	Decreased	Restored	Restored	hrANXA1 treament
Overall inflammatory profile	Increased	Inflammatory mediators largely remain high	Majority of inflammatory mediators decreased	Reversion diet
Innate arm of immune system	Activated	Remains activated	Remains activated	Similar
Adaptive arm of immune system	Activated	Remains activated	Remains activated	Similar
T-effector cells	Increased %	Decreased %	Remains similar to HFHS diet	hrANXA1 treatment
T_{CM} and T_{EM} cells	Increased T_{CM} and T_{EM}	Greater ratio of T_{CM} vs T_{EM}	Equal balance of T_{CM} and T_{EM}	
T_H17 vs Treg celss	Increased T_H17 vs Treg	Decreased T_H17 vs Treg	Decreased T_H17 vs Treg	Similar
CD45 infilitration into brain parenchyma (imaging)	Decreased	Increased	Not measured	N/A
Adhered/Migrated cells in vitro	Increased CD45, T_H17 and Treg cells	Decreased CD45, T_H17 and Treg cells	Increased CD45 and Treg, decreased T_H17 cells	hrANXA1
Microglia	Increased % activated, increased M1 vs M2	Decreased % activation, equal M1 vs M2	Decreased % activation, equal M1 vs M2	similar
iNOS production	Increased	Decreased	Not measured	N/A

5.3 Discussion

The focus of this chapter was to evaluate how the damage induced by metabolic disorders, both immunologically and at the BBB, can potentially be reversed using either pharmacological or dietary intervention. Data in this chapter provides evidence that treatment with hrANXA1 and switch to a diet low in fat and sugars reduces metaflammation and attenuates T2DM development to restore the damage to the BBB. These interventions could have huge implications on future treatments and healthcare guidance for managing metabolic disorders.

5.3.1 The use of ANXA1 as a pharmacological agent to reduce, revert and restore the damage to the BBB in metabolic disorders

5.3.1.1 The role of ANXA1 in attenuating T2DM development

First and foremost, the findings of this chapter reveal the administration of hrANXA1 in HFHS-fed mice to attenuate MetS/T2DM development; as seen by lower serum insulin, cholesterol and triglycerides along with lower blood glucose levels and improved OGTT. Previous work in our lab found the therapeutic administration of hrANXA1 in a HFHS-fed mouse model to improve insulin resistance by attenuating hepatosteatosis (lipid accumulation in the liver) and renal dysfunction (proteinuria) (512). Purvis et al., showed that the impaired glucose tolerance in HFHS-fed mice was mediated by the IRS-1/Akt/GSK-3β signalling cascade which is involved in energy metabolism (glycolysis) (688). Treatment with hrANXA1 restored this signalling cascade to allow for GSK-3β-dependent enzymatic conversion of glucose to glycogen thus lowering blood glucose levels (689,690).

The beneficial role of ANXA1 as a therapeutic agent in diabetes has been further confirmed by our team's previous studies using ANXA$^{-/-}$ mice fed a HFHS diet. These ANXA1$^{-/-}$ mice have a more severe diabetic phenotype compared to wild-type HFHS-fed mice, with severe dyslipidaemia, hepatic steatosis and renal dysfunction (512). Treatment with hrANXA1 also halts microvascular disease development in a mouse model of T1DM through restoring Akt signalling (678); notably these STZ-induced mice also have improved cardiac function. Studies using LDLR$^{-/-}$ mice have shown

hrANXA1 treatment to reduce atherosclerotic plaque burden and improve plaque stability through reduced lipid accumulation (691), demonstrating the therapeutic benefit of ANXA1 in treating metabolic disease and its associated peripheral co-morbidities. These studies already implicate the potential for ANXA1 in improving diabetes-induced brain microvascular disease.

5.3.1.2 ANXA1 and BBB integrity

In the BBB community, the role of endogenous ANXA1 in maintaining BBB integrity has long been recognised. Work by Cristante and colleagues showed ANXA$^{-/-}$ mice to have constitutively elevated BBB permeability compared to wild-type controls (297). The leaky BBB phenotype in ANXA1$^{-/-}$ mice can be attributed to loss of occludin and VE-cadherin at sites of cell-cell contact; in contrast wild-type mice show high abundance of ANXA1 at junctional sites. The role of ANXA1 in tight junction stability has been clearly demonstrated through use of hCMEC/D3 ANXA1 knock-down cells, in which rescue experiments using hrANXA1 restored F-actin organisation via co-localisation with β-actin (297). Similarly, the disrupted tightness of the brain microvasculature as a loss of claudin-5, occludin and F-actin in the HFHS-fed mice was restored with hrANXA1 treatment. This reinstatement of the TJs and cytoskeleton can be correlated with reduced paracellular permeability measures and increased TEER compared to HFHS-fed mice. The ability of hrANXA1 to re-establish cell-cell contacts suggests a depletion of endogenous ANXA1 at the brain microvasculature that impacts the BBB tightness. In fact, ANXA1$^{-/-}$ mice have a similar leaky BBB phenotype to HFHS-fed mice, and rescue experiment with hrANXA1 in these ANXA1$^{-/-}$ mice also improves BBB tightness (297). Together, these data strongly support the therapeutic effect of hrANXA1, which remains to date, the best endogenous molecule exploitable as a therapeutic target in the neuroinflammatory pathology of a leaky BBB.

Moreover, in this chapter we extend our findings of the therapeutic effect of hrANXA1 treatment also on the essential components of the BM; with clear restoration of endothelial and astrocytic laminin α4 and laminin α2, respectively. This allowed for the re-attachment of astrocytic end-feet to the brain endothelial cells to restore the full structure of the BBB in HFHS-fed + hrANXA1 treated mice. In the HFHS-fed mice, the breakdown of the BBB was linked to digestion by MMPs namely MMP-2 and

MMP-9, as discussed in depth in Chapter 4.3.1. Treatment with hrANXA1 in HFHS-fed mice down-regulated the presence/activity of MMP-2, MMP-3, and MMP-9. The reduced permeability measures and clear confocal imaging of brain microvessels in the HFHS-fed + hrANXA1 treated mice overrides the lack of statistical significance seen in the MMP studies which is likely a factor of small n numbers and repeats.

Previous studies investigating the link of ANXA1 and MMPs have largely been carried out in the cancer field however results find differential expression and effect depending on cancer type. For example in breast cancer cells, the ablation or silencing of ANXA1 leads to decreased MMP-9 expression that is associated with reduced migration and invasion (692). In comparison, the decrease of ANXA1 in pancreatic ductal adenocarcinoma (PDAC) was associated with worse disease progression, as seen by lymph node metastasis and advanced TNM stage (693). Indeed extensive research of the literature implicates that ANXA1 can act as both a tumour suppressor and oncogene (694,695), suggesting that the role of ANXA1 may be dependent on tissue type and disease phenotype.

Furthermore, in conjunction with reduced MMPs, there is a significant increase in TIMP-1 concentrations in the serum with hrANXA1 treatment. The restoration of TIMPs/MMPs is a key contributor in the remodelling and restoration of the BBB (187,542). In Chapter 4, the expression and ratio MMPs/TIMPs have been discussed regarding changes in acute to chronic inflammation. In HFHS-fed + hrANXA1 treated mice, there is a reduction in the pro-inflammatory profile and therefore hrANXA1 may aid the restoration of MMPs/TIMPs balance through reduction of chronic metaflammation. The role of ANXA1 to restore the TIMP ratios is confirmed in ANXA1 knockout cells. Knockout of ANXA1 in PDAC results in the disbalance of MMP/TIMP, with increased MMP-9 activity to be correlated with a decreased TIMP-1 expression (693).

In diabetes, MMPs have been associated with microvascular complications. Altered MMP expression in diabetic nephropathy contributes to glomerular hypertrophy (696). Likewise, increased plasma MMP-2 and MMP-9 in peripheral arterial disease has been associated with disease progression and severity (697). In diabetes, it appears that increased MMP expression is associated with a negative outcome and this appears to be the case at the brain microvasculature in our HFHS-fed model, with ANXA1

treatment positively restoring MMPs/TIMPs levels and thus preventing BBB degradation.

5.3.1.3 ANXA1 and its role in preventing TEM

The most well-documented property of ANXA1 is its ability to inhibit leukocyte TEM. ANXA1 mediates its effect through modulating adhesion molecule-based leukocyte to endothelium interactions. Firstly, ANXA1 co-localises with α4β1 integrin on leukocytes to prevent binding to VCAM-1 on endothelium (482). Usually leukocytes, upon cellular activation by particular chemokines, mobilise and release their endogenous ANXA1 to promote leukocyte detachment (281). Treatment with exogenous hrANXA1 will further promote this detachment by increasing ANXA1 levels; indeed HFHS-fed + hrANXA1 treated mice have a significant reduction in both adhesion and TEM of $CD4^+$ leukocytes across the BBB compared to HFHS-fed mice and akin to numbers seen in chow-fed mice. Moreover, we have previously shown that ANXA1 expression (total and surface) is reduced in T_H17 and Treg cells of MS patients and this was connected to an increase migratory potential of T_H17 cells across an *in vitro* model of the BBB (293). Given the inflammatory nature of T2DM, we can hypothesise that ANXA1 is likely to be reduced within these T-cell subsets in the HFHS-fed model, thus accounting for the increased T_H17 cell migration in HFHS-fed mice which is reduced upon hrANXA1 treatment. Future studies should examine the expression of ANXA1 in these T-cells subsets to elucidate whether treatment with exogenous ANXA1 restores the intracellular stores of ANXA1 in the leukocytes to contribute to reduce TEM.

Notably, previous work in our lab has shown that exogenous ANXA1 increases endogenous ANXA1 in the human brain endothelial cell line hCMEC/D3 to restore the actin cytoskeleton (297). Moreover, in the HFHS-fed model we have shown that endogenous ANXA1 is depleted in the kidney, liver and skeletal muscle (512). Treatment with hrANXA1 restored the intracellular stores of ANXA1 contributing to attenuation of T2DM development in the HFHS-fed + hrANXA1 treated mice (512). In this manner, we can hypothesise that treatment with hrANXA1 will restore endogenous ANXA1 at the brain endothelial cells of the BBB in the HFHS-fed + hrANXA1 treated mice, which will further contribute to the reduced leukocyte TEM through mobilisation of ANXA1 and restored tightness of the BBB. *In vivo*

inflammatory models show increased endothelial ANXA1 mobilisation post neutrophil diapedesis (measured over 4hours) (698) to support this theory. Here, we have also shown ANXA1's ability to reinstate the TJ and BMs, therefore future studies would also benefit from examining the ANXA1 localisation in accordance with actin and laminin isoforms.

ANXA1 also inhibits leukocyte TEM through inducing L-selectin shedding from leukocytes to prevent tethering, rolling and firm adhesion (280). In the HFHS-fed + hrANXA1 treated mice, there is a reduction in the percentage of $CD4^+$ $CD44^+$ CD62Lhi-expressing cells compared to HFHS-fed mice, and hence reduced adhesion of $CD4^+$ cells. Notably there was also a marked reduction in the number of $CD4^+$ $CD44^+$ LFA-1^+-expressing cells. Importantly, whilst glucocorticoid treatment has shown to reduce LFA-1 expression (699), this effect is not attributed to ANXA1 (700). Results also showed a significant reduction in several adhesion molecules including ICAM-1, P-selectin, and VCAM-1. Although ANXA1 does not modulate the expression of CAM molecules it has been proposed that ANXA1 induces functional/conformation changes on the surface of CAM molecules contributing to diminished adhesion and TEM (700).

During inflammation resolution, β2 integrins can themselves act as efferocytic receptors; for example ICAM-3 is known to serve as an "eat-me" signal through binding to CD14 on apoptotic cells (701). In fact, ANXA1 can be recruited to the cell surface of apoptotic cells to co-localise with the "eat-me" signal phosphatidylserine thus regulating cell removal. Although further studies are required to determine whether integrin/ANXA1 co-localise, the combination of these efferocytic integrins and ANXA1 serving as apoptotic markers suggests a potential mechanism by which leukocyte-endothelial cell interaction is reduced during the resolution phase of inflammation (286). Undeniably, in the HFHS-fed + hrANXA1 treated mice the overall inflammatory profile is improved when compared to HFHS-fed mice. In the literature, ANXA1 is documented to reduce IL-6, TNF-α, IL-1β, IL-12p40 levels whilst increasing IL-10 (702). In the HFHS-fed + hrANXA1 treated mice, there is reduced expression of IL-6 and IL-12p40 at the brain microvessels with increased IL-10 levels; TNF-α levels increased at the brain microvessels however were decreased

within the serum. Without doubt there is a large degree in variation in the levels of inflammatory mediators expressed in the serum and brain microvessels of ANXA1 treated mice, nevertheless the alteration and differentiation in the markers compared to HFHS-fed mice suggest that inflammation resolution is being undertaken. Taking all the above into consideration, the reduction of adhesion and TEM at the BBB in the hrANXA1 treated mice can be attributed to both direct and indirect effects of ANXA1.

Nonetheless, it is noteworthy that all the chemokines measured at the brain microvasculature, except CX3CL1, increased in the HFHS-fed + hrANXA1 treated mice when compared to HFHS-fed mice suggestive that chemotaxis of leukocytes is still occurring in these mice and the adhesion is the rate limiting factor. Besides it is documented that upregulated ANXA1 in circulating leukocytes, after glucocorticoid treatment, are responsible for the prolonged diapedesis time (703). This serves to explain why in the HFHS-fed + hrANXA1 treated mice the number of adhered $CD4^+$ cells are far greater than the number migrated, whereas the proportion of adhered/migrated cells in each of the other experimental groups are roughly equivalent.

5.3.1.4 ANXA1 and its effect on adaptive immunity

Whilst the role of ANXA1 on innate immunity has thoroughly been investigated, the function of ANXA1 in adaptive immunity remains largely undiscovered. Nevertheless, T-cells express ANXA1 and its deficiency has been associated with autoimmune diseases. For example, PBMCs isolated from MS patients show reduced ANXA1 expression in T-cell subsets $CD4^+$ $CD25^+$, $CD4^+$ $CD25^-$, $CD4^+$ $RoR\gamma t^+$ and $CD4^+$ $Foxp3^+$ compared to healthy patients and this was associated with an increased migratory capacity of $CD4^+$ $CD25^-$ and T_H17 cells across an *in vitro* model of the BBB (293). In a mouse model of uveitis, in which there is reduced ANXA1 expression, hrANXA1 administration rescues the severity of the disease through restricting T_H17 development (291). Although we have not measured the expression of ANXA1 in T-cells in the HFHS-fed mice, it is evident that metabolic disorders cause a shift in the T_H17/Treg ratio with increase in the percentage of T_H17 cells in HFHS-fed mice compared to chow-fed mice, in line with other studies (367,368). hrANXA1 treatment corrected this shift and reduced the T_H17/Treg ratio, with T_H17 percentages lower than

those in chow-fed counterparts; suggestive that hrANXA1 treatment is affecting T_H17 development concomitant with reduced IL-17 production. In addition, the number of T_H17 cells migrating in the HFHS-fed + hrANXA1 treated mice was reduced.

Some studies have eluded to the role of ANXA1 in modulating the differentiation of naïve T-cells into T_H cells, with ANXA1 promoting development of the T_H1 subset and supressing T_H2 subsets (288). Another study found ANXA1-derived peptide Ac2-26 to inhibit the proliferation and cytokine production of both T_H1 and T_H2 cells via interfering with T-cell activation through antigen presentation (292). To date, the role of ANXA1 in modulating T_H differentiation largely remains disputed. Nevertheless, studies in human PBMCs show ANXA1 reduces T-cell proliferation and activation due to altered T-cell priming by the reduction of co-stimulatory molecules CD80, CD86 and CD83 on monocytes (293). Interestingly in the HFHS-fed + hrANXA1 treated mice, the cell frequency of macrophages and neutrophils remained similar to HFHS-fed mice; both were significantly higher than chow-fed mice. However, the cell frequency of dendritic cells was reduced in HFHS-fed + hrANXA1 treated mice compared to HFHS-fed mice. Although this was not statistically significant, it perhaps represents a reduction in antigen presentation by dendritic cells involved in the reduced T-cell activation seen in HFHS-fed + hrANXA1 treated mice as seen by reduced $CD4^+$ $CD44^+$ $CXCR3^+$-expressing T_{eff} cells. Studies in a rodent models of high feeding have shown increased T_{EM} cells (CD44hi-CCR7lo-CD62Llo-$CXCR3^+$-$LFA1^+$) compared to control mice (370). Interestingly in the HFHS-fed + hrANXA1 treated model there appears to be a greater ratio of T_{CM}/T_{EM} cells indicative of a resolving inflammation phenotype with reduced circulating T_{EM} cells.

5.3.1.5 ANXA1 and its involvement in conferring neuroprotective

Overall, treatment with hrANXA1 has a profound effect on restoring the BBB integrity; ANXA1 also reduces inflammatory mediators resulting in fewer T_{eff} cells and is key in preventing leukocyte attachment to the brain endothelial cells. Together these properties help to reduce the migration of peripherally-activated immune cells into the brain parenchyma thereby limiting the potential for inflammation within the brain. This is clearly apparent by the lower percentage of microglia cells (CD45lo $CD11b^+$) within the HFHS-fed + hrANXA1 treated mice compared to the HFHS-fed

mice whereby microglia cells had proliferated in response to inflammation. Interestingly, flow cytometrical analysis revealed that despite the fewer microglia cells, a similar percentage of these CD45lo CD11b^{+} microglia cells were activated in the HFHS-fed + hrANXA1 treated mice as in the HFHS-fed mice. Of these activated microglia cells, HFHS-fed mice had a higher M1/M2 phenotype ratio whereas treatment with hrANXA1 balanced the ratio of M1/M2 phenotype with a prominent increase in the percentage of M2 cells. Intriguingly, confocal imaging reveals lower IBA1 expression in HFHS-fed + hrANXA1 treated mice compared to HFHS-fed mice and reduced iNOS expression by endothelial cells and microglia. iNOS is largely produced by activated M1 phenotypic microglia cells and is responsible for causing neurotoxicity and neuronal apoptosis (378), decreased M1 cells will contribute to the reduction in iNOS production.

In macrophages, presence of ANXA1 drives a phenotypic switch from pro-inflammatory M1 to pro-resolving M2 (704–706). Furthermore in ischemic-injured neurons, treatment with ANXA1 peptide Ac2-26 promoted the transition of activated microglia from an M1 to M2 phenotype through peptide-FPR engagement (305). The importance of this phenotypic switch is highlighted in studies conducted by McArthur and colleagues; in which they illustrate the role of ANXA1 in contributing to microglia surveillance and maintenance of brain homeostasis. Under inflammatory conditions, induced by LPS or Aβ *in vitro,* BV2 microglia cells had aberrant upregulation of efferocytosis/phagocytosis of both apoptotic and non-apoptotic neurons, accompanied by surges in pro-inflammatory cytokines TNF-α and IL-6 (279). Treatment with ANXA1 reduced the phagocytosis of non-apoptotic neurons by LPS-stimulated BV2 cells, highlighting that ANXA1 is key in regulating microglia activity to limit uncontrolled neuronal damage. In fact, it was noted that ANXA1 reduced the production of NO in these LPS-stimulated BV2 cells. Microglia-derived NO and its associated RNS are neurotoxic thereby highlighting the role of ANXA1 in conferring neuroprotection (279). In the diabetic model of HFHS-feeding, it was noted that iNOS production was reduced upon treatment with hrANXA1.

It is noteworthy that endogenous production and release of ANXA1 by microglia occurs under basal conditions, this is to enable the removal of damaged neurons through binding with phosphatidylserine that signals to microglia via the FPR2

receptor for engulfment (279); serving to explain the high percentage of M2 cells seen in chow-fed mice. McArthur et al., demonstrated that in early phases of AD, ANXA1 expression is upregulated in human microglia and this may serve to control microglia response to amyloid plaques and subsequent neurodegeneration (279). Further studies by Ries et al, however found microglia become constitutively activated under inflammatory conditions (304). The secretion of endogenous ANXA1 is not enough to maintain control and therefore treatment with ANXA1, *in vitro* and *in vivo,* stimulated Aβ phagocytosis by microglia through inducing endocytosis of the Aβ/FPRL1 complex, thus reducing plaque burden (304). It is well documented that $A\beta_{1\text{-}42}$ peptide binds to FPRL1/FPR2 and is rapidly internalised by phagocytic cells (707). ANXA1 which co-localises with F-actin in the cell cytoskeleton facilitates the interaction of F-actin and phagosomes in macrophages and therefore facilitates endocytosis (708).

Microglial upregulation of ANXA1 has also been detected in mouse models of excitotoxic neuronal injury and transmissible spongiform encephalopathies particularly around lesional sites indicative of mechanisms to restore brain homeostasis (709–711). Without doubt, these studies implicate the neuroprotective effects of ANXA1; and the loss of ANXA1-dependent microglia regulation appears to occur under conditions where inflammation changes from acute to chronic. Future research would benefit from examining the ability of metabolic disorders to damage neurons and the role played by ANXA1 in conferring protection against neurodegeneration with particular focus on the point at which endogenous ANXA1 loses control. However, for now, it is clear treatment with ANXA1 in metabolic disease is aiding inflammation resolution beyond the peripheral system.

5.3.2 Can the switch to a healthy diet reduce, revert and restore the damage to the BBB caused by metabolic overload?

5.3.2.1 Effect of dietary modifications on T2DM development & BBB integrity

Initial observation of results from this chapter clearly highlight the switch of diet from HFHS-feeding to chow-feeding reduces obesity; a key risk factor in the development of MetS/T2DM (148) . Whilst HFHS – Chow reversion diet mice had lower non-fasted blood glucose levels, the glucose tolerance as measured by OGTT did not improve compared to HFHS-fed mice, however the HFHS – Chow reversion mice did show an improvement in the ITT. Nonetheless, reversion mice showed a decrease in concentrations of serum insulin, serum cholesterol and serum triglyceride compared to HFHS-fed mice. Excessive subcutaneous and visceral abdominal tissue can contribute to raised levels of circulating FFAs (1), therefore the weight loss in these mice is central to the reduction in lipid levels. Lack of statistical significance here may in part be reflective of smaller n numbers in the HFHS – Chow reversion diet mice group

It is well recognised that an improved diet can help control and manage T2DM and the development of CVDs (712–716) and there is growing evidence of the role of Mediterranean and Dietary Approaches to Stop Hypertension (DASH) diets in reducing cognitive decline and lowering AD risk (457). However, the majority of these studies are large longitudinal observation studies or meta-analyses. To our knowledge, our study is the first to examine the effect of diet on the structural and functional changes of the brain microvasculature in a diabetic model induced by HFHS-feeding.

From the results, it is clearly noticeable that dietary changes have a huge impact on BBB integrity with significantly reduced Evans blue dye extravasation, reduced paracellular permeability of FITC-dextran and increased TEER compared to HFHS-fed mice. Reduced leakage can be accounted for by restoration of junctional proteins; although whilst occludin presence at junctional sites is beginning to be re-established, the laminin reactivity remains low preventing the ensheathment of astrocytes. When examining the MMP levels, there is a significant reduction in the expression and activity of MMP-2 and MMP-9 in HFHS – Chow reversion diet mice compared to HFHS-fed mice, comparable to levels in chow-fed mice which can be accounted for

by decreased inflammatory mediators such as TNF-α and IFN-γ; therefore the lack of BBB vessel restoration is of surprise. Notably, the TIMP-1 levels are not increased in the HFHS – Chow reversion diet mice and perhaps it is this balance which is required to prevent MMP-induced degradation.

As a result of the lack of complete BBB restoration, in the HFHS – Chow reversion diet mice $CD45^+$ leukocytes are still present within the VBL layers and appear to show migration outwards into the brain parenchyma. These results together illustrate that brain endothelial cells contacts are repaired with dietary changes however the BBB vasculature in its entirety, is not restored. The endothelial cells are the first cells of the BBB structure and therefore it is logical that the most immediate improvement is apparent at this cellular level. It would be interesting to assess the role of ANXA1 in improving BBB integrity in the HFHS – Chow reversion diet mice, thus future studies should examine the endogenous levels of ANXA1 in the BBB and T-cells in these mice.

Importantly, this study has only placed mice back onto a chow diet for a period of 5 weeks, which may not be sufficient to re-instate the conformational changes of the TJs and BM required for a tight BBB. Studies which have investigated dietary changes in diabetic rodents by food or calorie restriction (717–719), ketogenic diets (720), herbal formulas (721), reduced glycoxidation products (722) or addition of extra virgin olive oil (723) report improved insulin sensitivity with feeding over a duration of 8 – 24 weeks on intervention. In our study, a 5-week intervention begins to improve insulin and lipid levels however optimal glycaemic control has not been achieved. It would without doubt be beneficial to examine a longer intervention period, as well as comparing to chow-fed or HFHS-fed mice that have been on their respective diets for an equivalent duration of time to remove age as a confounding factor.

5.3.2.2 Diet and the immune system: metaflammation

In the HFHS – Chow reversion diet mice, remarkably there is a significant reduction in the percentage of activated microglia cells compared to chow-fed and HFHS-fed mice, despite the larger population of microglia cells (CD45lo $CD11b^+$). Of these activated microglia cells, there is a restoration in the M1 to M2 phenotype balance, compared to HFHS-fed mice which are skewed towards M1. The reduced activation status and movement towards a resolving phenotype is indicative of less triggering of microglial response (724). A closer look at the effect of diet intervention on immune cells however reveals that there are still highly activated percentages of $CD4^+$ $CD44^+$ $LFA1^+$ $CXCR3^+$ cells within the cervical lymph nodes of the HFHS – Chow reversion diet mice, even higher than those seen in HFHS-fed mice. These two sets of results appear to be contradictory. Conversely, upon further examination of the activation status of the brain microvessels of HFHS – Chow reversion diet mice, there is reduced expression of adhesion molecules (CD40, E-selectin, P-selectin, ICAM-1 and VCAM-1) to levels lower than those even in chow-fed mice. Reduced adhesion molecule expression would prevent the TEM cascade (642). Therefore, despite the higher percentage of activated T-cells, fewer passage would reduce the activation of microglia from this source. Interestingly, the cell frequency of dendritic cells in the HFHS – Chow reversion diet mice was particularly high, which may account for the large number of activated $CD4^+$ T-cells; however overall the frequency of $CD4^+$ cells in the bone marrow and cervical lymph nodes was considerably reduced, even when compared to chow-fed mice.

Nevertheless, review of $CD4^+$ T-cell subsets finds a significantly lower percentage of T_H17 cells in the HFHS – Chow reversion diet mice compared to both HFHS-fed and chow-fed mice thereby reducing the ratio of T_H17/Treg cells. The ratio of T_H17/Treg cells have been suggested to play a key role in the pathology of metabolic disorders and its secondary complications (367). In line with this, *in vitro* experiments show a significant reduction of the adhered and migrated T_H17 cell subset across the BBB compared to HFHS-fed mice whereas the numbers of adhered and migrated Treg and $CD4^+$ $CD45^+$ leukocytes remain the same as HFHS-fed mice. Here, we have not evaluated the proportion of the T_H1 subset; T_H1 cells are known to play a substantial role in regulating body weight, insulin resistance, glucose tolerance in visceral adipose tissue (368) and may account for high presence of $CD4^+$ cells at the BBB.

Furthermore, T_H1 cells presence may aid in explaining the lack of insulin sensitivity restoration within the HFHS – Chow reversion diet mice. Future studies would benefit from examining the role played by other subsets under dietary changes.

Generally, it is documented that individuals with T2DM are more prone to infectious disease and cancer as a result of the hyperglycaemic environment that favours immune dysfunction (725–728). An important concept of inflammation is to remember than intact inflammatory pathways are required for maintenance of tissue health and response to acute triggers. Therefore disruption of immune state results in tissue damage (357). As described in Chapter 4, in the HFHS-fed mice there is a large disruption in the inflammatory mediator profile (pro- and anti-inflammatory interleukins, cytokines and chemokines). In the HFHS-fed – Chow reversion mice, the inflammatory profile is greatly improved with reduction in cytokines TNF-α and IFN-γ, interleukins e.g. IL-1α, IL-6, IL-1ra, IL-4, IL-10 and IL-1 and chemokine e.g. CCL2, amongst many others (Figure 4.7). Studies report improved diabetic outcomes in rodents which have been treated with IL-1 inhibitors (729). Therefore, the improved inflammatory mediator profile in HFHS – Chow reversion diet mice plays a strong role in the overall improvement seen in these mice both immunologically and at the BBB. Indeed, the benefit of Mediterranean diets, rich in polyunsaturated fats, flavonoids, vitamins and minerals (calcium, iron, zinc etc), are associated to the high presence of omega-3 fatty acids, antioxidants and polyphenols that reduce free radical generation and cytokine production, thereby inhibiting pro-inflammatory signalling pathways (685,730). Similarly, the use of these diets in humans have been associated with improved cognition and learning by facilitating synaptic plasticity and/or enhancing synaptic membrane fluidity through reduction of inflammation and oxidative stress (730–732). Support of the role of diet in cognition, has been seen through rodent studies. Rodents fed on diets high in saturated fats and sucrose show declining cognitive performance and reduced synaptic plasticity (451,452,733).

Metaflammation involves a number of signalling pathways that affect both metabolism and the immune system (357). Ingestion of foods rich in lipids, can activate toll-like receptor 4 (TLR4) subsequently initiating the inflammasome to trigger immune response (734,735). TLR4 activation by fatty acids is thought to be due the LPS component. Certainly, diabetes and obesity have been associated with high LPS levels which are negatively correlated to insulin sensitivity (736,737). LPS in the intestine increases the gut-barrier leakiness (738). Mice with loss of TLR4 function, under high fat diets are protected from insulin resistance (739). Additionally, deletion of TLR adaptor molecule MyD88 in the CNS also protects mice from diet-induced insulin-resistance (740). Alternatively, nutrients such as long-chain omega-3 polyunsaturated fatty acids can also interfere with the TLR4 activation to prevent its signalling pathway (741). A healthy diet is associated with lower levels of endotoxemia in the gut (742) and this has been linked to not only improving the gut health but also to improving neuroinflammation in conditions such as PD (743). This has led to a vast amount of research in the area of the gut-brain axis. These concepts highlight a possible mechanism through which BBB leakage has been reduced in HFHS – Chow reversion diet mice. Although insulin sensitivity is not entirely re-established, the serum cholesterol and triglycerides are considerably lower than in HFHS-fed mice and overall, this leads to a reduction in metaflammation with beneficial effects on improving brain microvasculature health. It is likely that a longer duration of a chow-diet would provide considerable improvements across all measurement of diabetic health.

5.3.3 Pharmacological intervention vs dietary intervention

All current existing anti-diabetic medications such as metformin, incretin agonists, thiazolidinediones and DPP4 inhibitors have an anti-inflammatory component (744). Essentially the use of ANXA1 as a pharmacological intervention or dietary changes to a healthier intake aim to reduce metaflammation and thereby limit the primary macrovascular and secondary microvascular complications. In this chapter, it is seen that both a therapeutic treatment delivered by ANXA1 and dietary intervention from a HFHS diet to a chow diet have the ability to slow the progression of T2DM.

In summary, treatment with hrANXA1 clearly attenuates the development of T2DM, by restoring insulin sensitivity and preventing hepatosteatosis and proteinuria (512). At the level of the BBB, treatment with hrANXA1 in the HFHS model has profound effects on restoring the BBB integrity through restoration of TJs (actin-mediated) and BM laminins to allow a resealing of the BBB vasculature through astrocytic end-feet association, resulting in reduced permeability and TEM. At the immunological level, hrANXA1 treatment limits T-cell activation, reducing T_{eff} cells and reduces the T_H17/Treg ratio, which can be accounted for by alterations in the interleukins and cytokines. Reduced T-cell activation accompanied by prevention of leukocyte adhesion via L-selectin shedding, amongst possible other mechanisms such as endothelial cell ANXA1 shedding, significantly reduces the migration of peripherally activated immune cells into the brain parenchyma. Within the brain, hrANXA1 reduces the number of microglia cells, restores the expression of CX3CR1 and induces a shift from the pro-inflammatory M1 to the pro-resolving M2 phenotype, this can have a huge impact on improving cross-talk and preventing damage to neurons through reduced iNOS production and controlled apoptosis.

To sum up, dietary intervention of HFHS – Chow reversion diet causes significant weight loss and reduces obesity. Changes in nutritional intake affects a number of metabolic and immune signalling pathways to reduce inflammation. Most notably, HFHS – Chow reversion diet mice have significant improvement in their inflammatory profile. After 5 weeks of diet intervention, brain endothelial cells show improvement in TJs, and reduced activation via adhesion molecules accounting for improved permeability. Overall dietary changes do not reduce the activation of all T-cells; nevertheless, there is a reduction in the T_H17/Treg ratio which are implicated in diabetes. Along with this, TEM studies show presence of $CD45^+$ leukocytes at the

BBB. Whilst there is a reduction in adhesion/migration of T_H17 cells, the Treg cells still transmigrate implicating that T-cells have not lost their ability to migrate however there are changes being made immunological to restore the disease status. In particular, Treg cells are known to be present to allow for brain surveillance; migration of $CD4^+$ $CD45^+$ T-cells and $CD4^+$ $Foxp3^+$ cells perhaps represents T-cells required for immune surveillance, inflammation resolution and immune suppression to slow down disease progression and restore cognition (617–619). In fact, within the brain parenchyma there is considerably reduced microglia activation suggesting that less damaging cells or molecules are passing through. Microglia also show a restoration of balance between M1/M2 phenotype and the CX3CR1 receptor. In can be concluded that dietary changes begin to show changes in diabetes and its associated brain microvascular complications however a longer duration of diet may be required to allow for the complete reversal of diabetes-induced damage.

Taking the results of this chapter into consideration, what then is a better treatment for diabetes-induced BBB damage and neuroinflammation inflammation – pharmacological intervention by hrANXA1 or dietary changes? Without doubt, hrANXA1 therapeutic treatment appears to have a much more significant effect on reducing the overall diabetic phenotype compared to dietary change. Nonetheless, when examining permeability and TEER, both hrANXA1 and dietary change show equivalent improvement highlighting that both are beneficial in restoring BBB integrity. It appears that ANXA1 has more direct effects on the BBB restoration through its links with the actin cytoskeleton, BMs and TEM prevention. On the other hand, the attributes of a healthy diet are through reduced inflammatory mediators, downstream this would result in the altering of signalling pathways associated with T2DM. Both interventions also show significantly better microglia outcomes indicative of reduced neuroinflammation.

Importantly, the HFHS – Chow reversion mice are 5 weeks older compared to the chow-fed, HFHS-fed and HFHS-fed + hrANXA1 mice, and as shown in Figure 4.2, there is an effect of age that can contribute to BBB leakage. Therefore, it is likely that beneficial effects of a dietary change are likely to be even greater than those shown here by our HFHS – Chow reversion mice in this preliminary study. Confirmation is required by comparing mice all at the same age at cull. Nevertheless, our results

provide a baseline for the potential of diet in improving BBB integrity and neurovascular health.

It is well-documented that a multi-factorial approach of lifestyle, drug and behavioural therapy produces greater improvements in HbA1c, blood pressure, total cholesterol and triglycerides than conventional drug therapy alone (716). Therefore, in the future, it would be beneficial to combine HFHS – Chow reversion diet mice with treatment of hrANXA1, both prophylactically from week 5 in HFHS-feeding through to the end of chow-feeding and therapeutically from week 11 when dietary intervention is implemented.

In conclusion, this chapter highlights that both a pharmacological and dietary intervention can have huge potential for improving brain health that has been impaired as a result of metabolic disorders. Research is being undertaken for using hrANXA1 as a therapeutic treatment in human disease as its benefits have been documented in a variety of conditions including heart disease, MS and rheumatoid arthritis (294). In fact, the ability of hrANXA1 to prevent α4β1 integrin-VCAM1 interaction is the main mechanism of action of the MS drug, Natalizumab. As ANXA1 is an endogenous protein it has the potential of reducing side effects and could be highly beneficial in conditions of T2DM whereby patients are already prescribed a number of other medications.

The ability of dietary changes to reduce BBB leakage suggests that MetS/T2DM effects are not only limited to the peripheral system but also the brain. In fact, large clinical trials are underway to assess the role of diet in conditions of dementia and MS, with a focus on foods high in poly-unsaturated fatty acids, antioxidants and polyphenols and a reduction of saturated fats, refined sugars and salt content. Taking these results into consideration, whereby it is clear that reduced peripheral inflammation benefits the brain, it would be valuable to educate individuals on the effect of diet not just on causing T2DM and heart disease but also on causing brain disorders. The role of diet in improving brain health, has huge implications in national and international strategies of preventing and lowering the burden of neuroinflammatory and neurodegenerative disorders.

Chapter 6 – Metabolism at the blood-brain barrier

6.1 Introduction

Maintenance of healthy cellular and systemic function requires the constant supply of metabolites for cellular energy metabolism in order to generate ATP. It is widely recognised that the brain has the highest energy consumption of all organs in the body, utilising 20% of the body's resting metabolic rate (72). Of this, neurons consume 70-80% of the total energy for neuronal functions such as restoration of membrane potential, vesicle recycling and neurotransmitter transport (745–748). However the high metabolic demand of the brain is not matched by the presence of large intrinsic energy stores within cells of the NVU, instead the brain depends on a continuous influx of substrates from the peripheral vasculature (73). Therefore the BBB, along with the BCSFB, is integral in providing transport of essential nutrients, ions and signalling molecules from the peripheral blood into the brain parenchyma (21,749).

The BBB controls the influx of metabolites such as glucose, amino acids and ketones whilst limiting the entry of unwanted toxic molecules or immune cells (16,749). Results from the previous chapters have clearly demonstrated the loss of BBB integrity in T2DM. As previously shown in Chapters 4 & 5, the BBB endothelial cells of HFHS-fed mice become activated through increased expression of inflammatory mediators such as cytokines, chemokines, interleukins, adhesion molecules and MMPs. This results in enhanced leukocyte TEM and subsequently leads to microglia activation. All these processes confer increased energetic demands. Moreover, loss of the BBB will impact the transport functionality, altering the energy availability and supply to the brain (750) impacting neuronal function and thus leaving the brain susceptible to neurodegeneration and cognitive impairment.

Indeed, disruption in glucose and oxygen metabolism and mitochondrial function have been attributed to the pathology of a number of neurodegenerative diseases including AD, MS, PD and Huntington's Disease (73,751). However to date, research has primarily focused on understanding the metabolism of neurons and astrocytes in health and disease (73,751). To our knowledge the only other study reporting metabolic status of the BBB endothelial cells was conducted by our own lab which was investigating the effect of MS patient's serum on brain endothelial cells. We reported that factors in the serum of MS patients reduced the glycolytic and mitochondrial activity of BBB endothelial cells (269).

6.1.1 Aims and objectives

Since BBB endothelial cells are sensing for metabolic-related factors, disruption to the BBB because of metaflammation will also impair its ability as a functional, transport and metabolic barrier. This is likely to be crucial to the downstream effects occurring in microglia, astrocytes, and neurons.

The chapter addresses Hypothesis 4 mentioned in Chapter 2, this is as follows:

⇒ **Hypothesis 4:**

It is hypothesised that the metabolism of the BBB endothelial cells will be disrupted and this together with impaired BBB structure will alter the transport of essential nutrients e.g. glucose across the BBB into the brain to contribute to neurodegeneration. Treatment with hrANXA1, which is shown to repair the BBB TJs, could therefore also repair the metabolic integrity of the BBB endothelial cells.

This chapter addresses Aim 5 mentioned in Chapter 2, this are as follows:

5. To investigate how nutrient imbalance in T2DM induced by HFHS-feeding can affect the BBB endothelium metabolic programming by examining cellular metabolism pathways of glycolysis and oxidative phosphorylation. The potential of hrANXA1 treatment to restore the metabolic integrity will also be assessed.

In order to study this aim, the mouse brain endothelial cell line, bEnd3 was used and stimulated with serum collect from the three experimental mice groups: chow-fed diet, HFHS-fed diet and HFHS-fed diet + hrANXA1 treatment.

The following objectives were covered in this chapter to address this aim:

- To determine whether serum stimulation with mouse serum on the mouse brain endothelial cell line, bEnd3 serves as a relevant *in vitro* model. Serum from chow-fed diet, HFHS-fed diet, HFHS-fed diet + hrANXA1 treatment and HFHS – Chow reversion diet mice was used to stimulate bEnd3 cells. Confirmation of the model was determined by measuring BBB integrity via *in vitro* paracellular permeability, TEER, junctional proteins and adhesion molecules expression.
- To investigate the effect of HFHS-induced T2DM and hrANXA1 treatment in HFHS-feeding on the glycolytic activity of BBB endothelial cells.
- To investigate the effect of HFHS-induced T2DM and hrANXA1 treatment in HFHS-feeding on glucose uptake and transport.
- To investigate the effect of HFHS-induced T2DM and hrANXA1 treatment in HFHS-feeding on the mitochondrial respiration of BBB endothelial cells.
- To investigate the effect of HFHS-induced T2DM and hrANXA1 treatment in HFHS-feeding on ATP production of BBB endothelial cells.
- To investigate the effect of HFHS-induced T2DM and hrANXA1 treatment in HFHS-feeding on ROS production by BBB endothelial cells.
- To investigate the effect of HFHS-induced T2DM and hrANXA1 treatment in HFHS-feeding and dietary intervention on lipid and adipokine expression at the BBB.

A summary of the experimental plan and the methods used to quantify each measure have been provided in Figure 5.1 and Table 5.1, respectively.

Table 6.1 | Summary of the central and individual measures used to evaluate the aims and objectives of Chapter 6, with reference to the respective methodology used to conduct these experiments.

Central measure	Individual measures	Method section
Confirmation of in vitro model - mouse serum stimulation of bEnd3 cells	Cell culture & serum stimulation	3.2.1-3.2.4
	Paracellular permeability & TEER	3.2.5 & 3.2.6
	FACS analysis of junctional proteins and cytoskeleton	3.4.3
	FACS analysis of adhesion molecules	3.4.3
Glycolytic activity	Seahorse assay for glycolysis of bEnd3 cells	3.4.1 & 3.2.9
	Glucose uptake (6NBDG) and glucose transport (GLUT1 expression)	3.4.3 & 3.4.3
	Insulin receptor expression	3.4.3
Mitochondrial respiration	Seahorse assay for oxidative phosphorylation of bEnd3 cells	3.4.2 & 3.2.9
	ROS production (DCFDA and mitosox)	3.4.5 & 3.4.6
Lipids and adipokines	Cytokine array on brain microvessels	3.1.8 & 3.2.8

6.2 Results

The results from the previous chapters clearly demonstrate that metabolic disorders impact the brain microvasculature, causing the BBB to lose its inherent properties as a barrier interface between the central and peripheral systems. The leaky phenotype of the BBB predisposes the brain to a neuroinflammatory response. Therapeutic treatment with hrANXA1 or dietary intervention from a HFHS diet to a chow diet dampened the pro-immuno-inflammatory status thus improving the structural, functional, and immunological integrity of the BBB, which will thereby reduce the neuroinflammatory status.

The anti-inflammatory effect of ANXA1 or a healthy diet versus HFHS-feeding mice implicates that damage to the BBB occurs due to peripheral pro-inflammatory mediators attacking and damaging the brain microvasculature. To replicate such effects *in vitro*, serum collected from chow-fed, HFHS-fed, HFHS-fed + hrANXA1 treated and HFHS – Chow reversion-fed mice was used to stimulate an immortalised cell line of mouse brain endothelial cells - bEnd3. The benefit of using an *in vitro* model is to replace, reduce and refine the number of rodents used; particularly as primary brain endothelial or microglial cultures require several mice per each culture which only remain viable for a few passages.

6.2.1 Effect of serum stimulation on BBB integrity

Firstly, the integrity of the BBB was measured through assessing the permeability and electrical resistance of bEnd3 cells stimulated with mouse serum from chow-fed, HFHS-fed, HFHS-fed + hrANXA1 treated and HFHS – Chow reversion-fed mice. Serum stimulation was provided by switching the FBS in complete bEnd3 medium with mouse serum. The serum was decomplemented before use, to ensure the effects seen were not due to the interference of the complement system. The cells were also left unstimulated e.g. in normal complete medium with FBS to ensure that the effect seen was due to factors present in the mouse serum. Additionally, cells were also stimulated with 100ng/mL TNF-α overnight to mimic an inflammatory state, as means of confirmation that this is the trigger for BBB damage.

The permeability of the BBB was tested using an *in vitro* system whereby bEnd3 cells were cultured on transwell inserts until confluent. Cells were either left unstimulated, stimulated with 100ng/mL TNF-α or stimulated with 10% mouse serum in culture medium for 16 hours. The permeability of the tight junctions to 55-77kDa FITC-dextran was assessed (Figure 6.1A). The results showed a 2.5-fold increase in paracellular permeability of cells stimulated with HFHS-fed mice serum when compared to chow-fed mice serum-stimulated cells. Stimulation of bEnd3 cells with serum from HFHS-fed + hrANXA1 treated and HFHS – Chow reversion diet mice reduced the permeability compared to HFHS-fed mice serum-stimulated cells; comparable to the permeability seen with chow-fed mice serum stimulation. Results from the permeability assay reveal unstimulated cells to have a similar coefficient to chow-fed mice serum-stimulated cells. TNFα-stimulated cells had increased permeability compared to unstimulated cells, which was similar to the HFHS-fed mice serum-stimulated cells, confirming that pro-inflammatory interleukins and other mediators are indeed present in the serum to induce increased permeability and these are reduced in the pharmacological and dietary intervention arms (also confirmed by the serum analytes analysis on chow-fed, HFHS-fed and HFHS-fed + hrANXA1 treated mice in Figure 5.7).

The TEER was also tested in the transwells as another measure of BBB tightness (Figure 6.1B). Cells stimulated with HFHS-fed mice serum had reduced electrical resistance compared to cells stimulated with chow-fed mice serum. Serum from HFHS-fed + hrANXA1 treated and HFHS – Chow reversion diet mice significantly increased the TEER when compared to HFHS-fed mice serum-stimulated cells and the TEER was in fact higher that in chow-fed mice serum-stimulated cells, albeit not significantly. Unstimulated cells had a similar TEER to cells stimulated with chow-fed mice serum, and TNF-α, like the HFHS-fed mice serum, reduced the TEER.

A

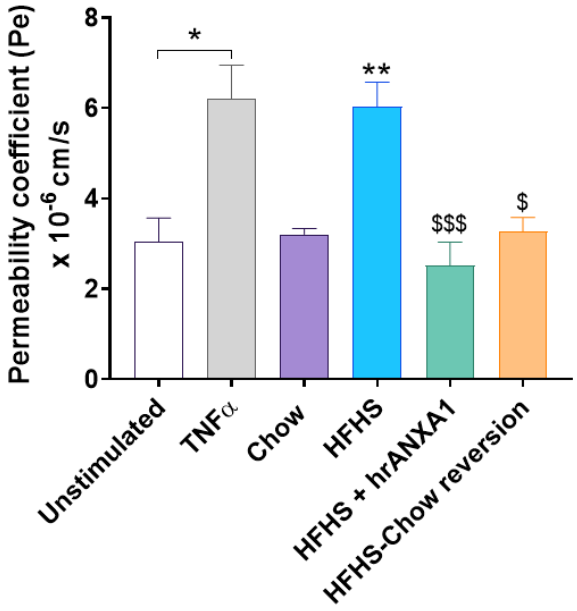
Permeability coefficient (Pe)
x 10-6 cm/s
8
6
4
2
0
*
**
$$$
$
Unstimulated
TNFα
Chow
HFHS
HFHS + hrANXA1
HFHS-Chow reversion

B

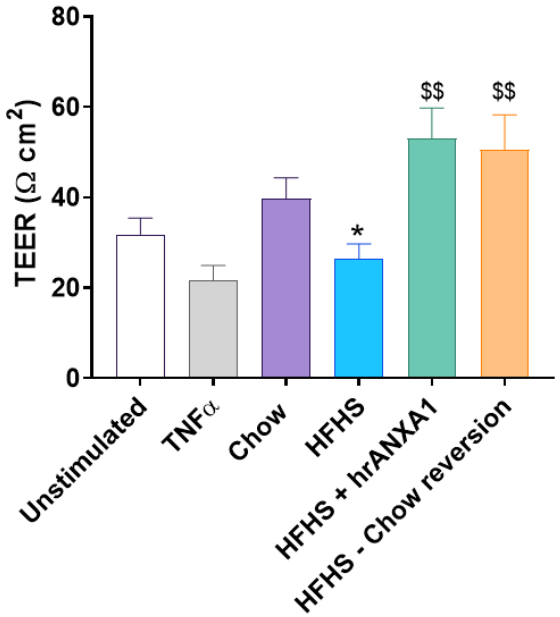
TEER (Ω cm2)
80
60
40
20
0
*
$$
$$
Unstimulated
TNFα
Chow
HFHS
HFHS + hrANXA1
HFHS - Chow reversion

Figure 6.1 | Measuring the permeability and TEER of bEnd3 cells stimulated with mouse serum

FITC-dextran (55-77kDa) was used to assess the *in vitro* paracellular permeability of bEnd3 cells grown on transwell inserts. Cells were stimulated overnight (16 hours) with 10% serum collected from chow, HFHS, HFHS + hrANXA1 or HFHS – Chow reversion mice (A). The TEER of bEnd3 cells with serum stimulation was also measured using the Epithelial Volt/Ohm (EVOM2) Meter (World Precision Instruments, USA) (B); cells were also left unstimulated in complete culture medium with FBS or stimulated with 100ng/mL of TNF-α (n=30/group, 10 mice pooled/group, per 3 independent experiments, two technical replicates per experiment). Statistical analysis was performed by one-way ANOVA followed by a Bonferroni post-hoc test. Data is expressed as mean ± SEM., *p< 0.05, **p<0.01 vs. Chow; $p<0.05, $$p<0.01, $$$p<0.001, vs. HFHS.

Previously, the changes in permeability and TEER could be correlated to the alterations in the structure and alignment of TJs, AJs and cytoskeleton. To confirm that the *in vitro* results were replicable to the *in vivo* and *ex vivo* results, the effect of serum stimulation of on junctional proteins, the actin cytoskeleton and adhesion molecules was also assessed using flow cytometry (Figure 6.2).

Stimulation with HFHS-fed mice serum reduced the expression of occludin and VE-cadherin compared to chow-fed mice serum-stimulated cells (Figure 6.2A). Serum from HFHS-fed + hrANXA1 treated and HFHS – Chow reversion diet mice restored the expression of occludin and VE-cadherin when compared to HFHS-fed mice serum, comparable to chow-fed mice serum-stimulated cells. Interestingly, there was no change in the expression of PECAM-1 across all groups.

Figure 6.2B showed HFHS-fed mice serum stimulation to disrupt the actin cytoskeleton arrangement, with a 2-fold increase in the G/F actin ratio compared to chow-fed mice serum-stimulated cells. Both HFHS-fed + hrANXA1 treated and HFHS – Chow reversion diet mice serum-stimulated cells restored the G/F actin ratio when compared to HFHS-fed mice serum-stimulated cells.

The expression of ABC transporter, Pgp was also measured via flow cytometry. Pgp is an efflux pump and is important in protecting the brain from the accumulation of toxic substances (752). Figure 6.2C shows a decrease in the expression of the Pgp transporter in HFHS-fed mice serum-stimulated cells compared to chow-fed mice serum-stimulated cells. HFHS-fed + hrANXA1 treated and HFHS – Chow reversion diet mice serum-stimulated cells show increased Pgp expression compared to HFHS-fed mice serum-stimulated cells. Although there was a trend, there was no statistical significance in these results.

Review of the activation status of the endothelium upon serum stimulation (Figure 6.2D), revealed that HFHS-fed mice serum significantly increased expression of ICAM-1 compared to chow-fed mice serum, this was reduced upon serum stimulation from HFHS-fed + hrANXA1 treated and HFHS – Chow reversion diet mice. Interestingly there was no change in expression of VCAM-1 across all groups.

Another marker used to measure the activation of the BBB endothelium, was the co-stimulatory molecule CD86. CD86, is normally presented by antigen presenting cells an accessory signal for optimal T-cell activation and proliferation. Previous studies using human brain microvascular endothelial cells have found CD86 to be upregulated after TNF-α or IFN-γ stimulation, suggesting that endothelial cells may act as an antigen presenting cell themselves to trigger T-cell activation (753,754). Using the bEnd3 model, it was seen that stimulation with HFHS-fed mice serum resulted in upregulation of CD86 compared to chow-fed mice serum. HFHS-fed + hrANXA1 treated mice serum reduced the expression of CD86 on bEnd3 cells, whereas the expression of CD86 remained high in cells stimulated with HFHS – Chow reversion diet mice serum.

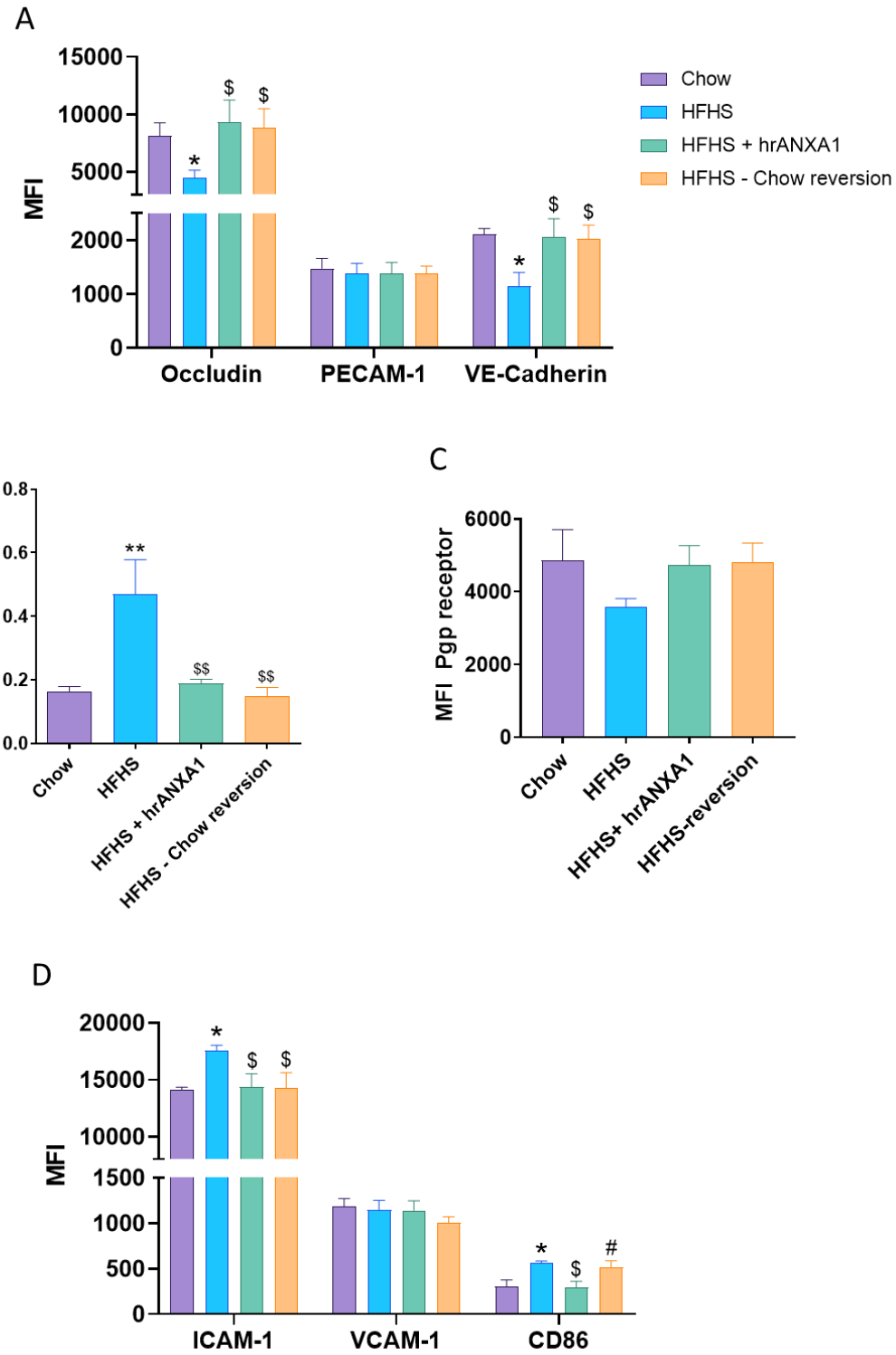
A
15000
10000
5000
2000
1000
0
MFI
Occludin
PECAM-1
VE-Cadherin
Chow
HFHS
HFHS + hrANXA1
HFHS - Chow reversion
B
G:F actin ratio
0.8
0.6
0.4
0.2
0.0
Chow
HFHS
HFHS + hrANXA1
HFHS - Chow reversion
C
MFI Pgp receptor
6000
4000
2000
0
Chow
HFHS
HFHS+ hrANXA1
HFHS-reversion
D
MFI
20000
15000
10000
1500
1000
500
0
ICAM-1
VCAM-1
CD86

Figure 6.2 | Effect of mouse serum on junction proteins and the adhesion molecules

bEnd3 cells were stimulated overnight (16 hours) with 10% mouse from chow, HFHS, HFHS + hrANXA1 and HFHS – Chow reversion mice. Cells were collected and stained for junctional proteins, G/F-actin and adhesion molecules. The expression (median fluorescence intensity, MFI) of junctional proteins occludin, PECAM-1 and VE-cadherin (A), G/F actin ratio pool (B), P-glycoprotein (Pgp) transporter (C) and adhesion molecules ICAM-1, VCAM-1 and co-stimulatory molecule CD86 (D) was analysed flow cytometrically (n=6-26/group, mouse serum pooled in pairs, conducted as at least 3 independent experiments). Statistical analysis was performed by one-way ANOVA followed by a Bonferroni post-hoc test. Data is expressed as mean ± SEM., *p< 0.05, **p<0.01 vs. Chow; $p<0.05, $$p<0.01, vs. HFHS, #p<0.05 vs HFHS + hrANXA1.

6.2.2 HFHS-feeding alters the metabolism of BBB endothelium cells

Brain endothelial cells primarily use glucose and lipid-derived fatty acids as energy sources (346), which are metabolised to produce ATP via a series of metabolic pathways.

Briefly, glucose is metabolised via glycolysis to produce pyruvate, which is further oxidised to Acetyl-CoA. Fatty acids are metabolised via β-oxidation to also produce Acetyl-CoA. Acetyl-CoA from glycolysis and β-oxidation enters the citric acid cycle (TCA). The conversion of glucose to pyruvate, pyruvate to Acetyl-CoA, fatty acid to Acetyl-CoA and oxidation of Acetyl-CoA results in the production of electrons and H^+ ions which are transferred via NADH or $FADH_2$ to the ETC for oxidative phosphorylation. Oxidative phosphorylation involves the reduction of O_2 to H_2O with electrons donated by NADH and $FADH_2$, through a series of electron carries (Figure 6.3). All of these metabolic pathways are ATP yielding (755,756).

Using the Seahorse metabolic assays (Agilent, UK), the glycolytic pathway and downstream metabolic respiration at the ETC was assessed in brain endothelial cells stimulated with serum from chow-fed, HFHS-fed and HFHS-fed + hrANXA1 treated mice.

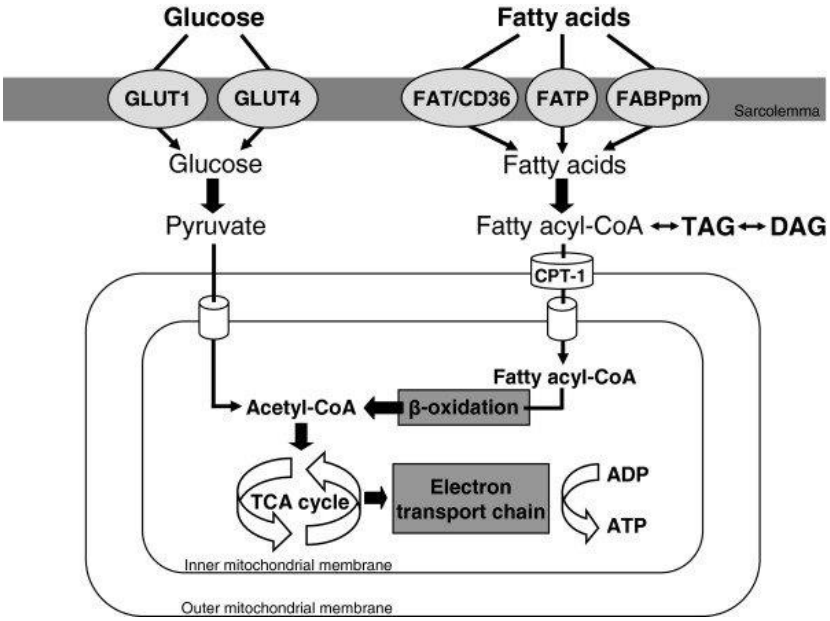

Figure 6.3 | Linking glycolysis & β-oxidation to mitochondrial respiration of the TCA cycle and ETC

Different metabolic pathways are used to metabolise different nutrients for production of ATP. Glucose is metabolised via glycolysis to produce pyruvate in the cytosol. Pyruvate is taken up by the mitochondria and further metabolised to Acetyl-CoA. Fatty acids are metabolised by co-enzymes to fatty acyl-CoA, which undergo β-oxidation to produce Acetyl-CoA. Acetyl-CoA from glucose and fatty acids enters into the TCA cycle for oxidation. In each of these conversion steps - glucose to pyruvate, pyruvate to Acetyl-CoA, fatty acid to Acetyl-CoA and oxidation of Acetyl-CoA, electrons and H^+ ions are produced. These are transferred via NADH or FADH2 to the electron transport chain for oxidative phosphorylation. Oxidative phosphorylation involves the reduction of O_2 to H_2O with the donated electrons. The TCA and oxidative phosphorylation pathways collectively are termed as mitochondrial respiration. Figure taken from van den Brom et al., (757).

The Glycolytic Stress Kit was used to measure glycolytic function and thus assess the use of glycolysis in brain endothelial cells. In glycolysis, the conversion of glucose to pyruvate and subsequently lactate results in the production and extrusion of protons into the extracellular medium. The extrusion of protons causes acidification of the medium and hence the extracellular acidification rate (ECAR) is used to determine the glycolytic function of the cells.

The ECAR profile (Figure 6.4A) shows HFHS-fed mice serum-stimulated cells have a higher ECAR than the chow-fed mice serum-stimulated cells, indicative of greater glycolysis taking place in these cells. This can be seen through all parameters of glycolytic rate, glycolytic capacity and glycolytic reserve (Figure 6.4 B-D) whereby HFHS-fed mice serum-stimulated cells have a higher ECAR compared to chow-fed mice serum-stimulated cells. Cells stimulated with serum from HFHS-fed + hrANXA1 treated mice have a lower ECAR profile when compared to HFHS-fed mice serum-stimulated cells, with a statistically significant reduction only seen in the glycolytic capacity. The non-glycolytic acidification rate does not differ between the groups suggesting that only glycolysis is the source of extracellular acidification in these cells.

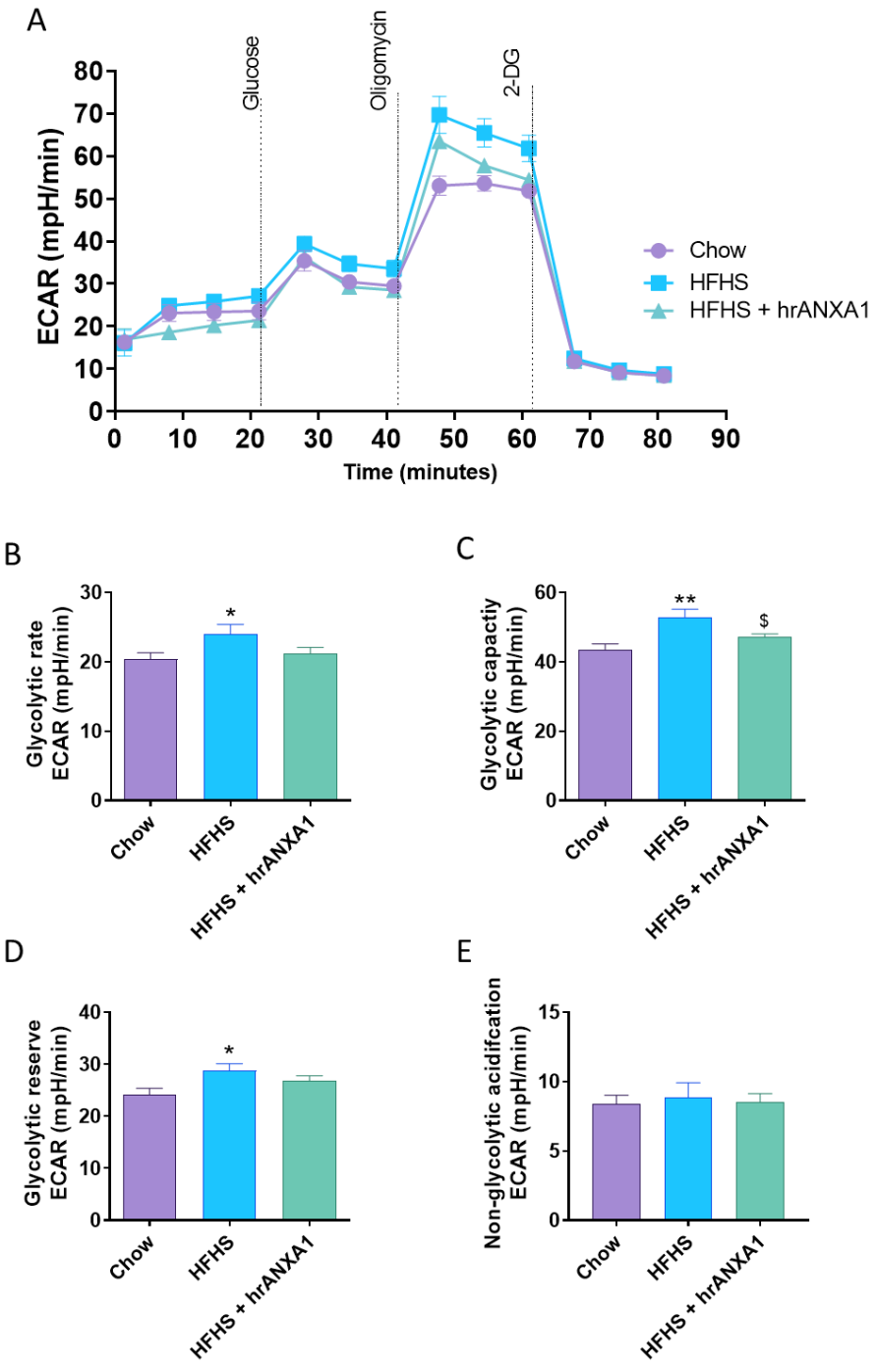
A
Glucose
Oligomycin
2-DG
ECAR (mpH/min)
Time (minutes)
Chow
HFHS
HFHS + hrANXA1
B
Glycolytic rate ECAR (mpH/min)
C
Glycolytic capactiy ECAR (mpH/min)
D
Glycolytic reserve ECAR (mpH/min)
E
Non-glycolytic acidifcation ECAR (mpH/min)

Figure 6.4 | Effect of chow, HFHS, HFHS + hrANXA1 mouse serum on the glycolytic activity of brain endothelial cells

bEnd3 cells were stimulated for 16 hours with 10% mouse serum from chow, HFHS, HFHS + hrANXA1 mice. Using the Glycolysis Stress Test (Seahorse, Agilent, UK) sequential injections of glucose, oligomycin and 2-deoxy-glucose (DG) were added to measure glycolytic function (extracellular acidification rate, ECAR, mpH/min). The kinetic profile of glycolytic function (A) was used to quantify the glycolytic rate (B), maximum glycolytic capacity (C), glycolytic reserve (D) and non-glycolytic acidification (E) (n=12/group, three replicates per mouse). Statistical analysis was performed by one-way ANOVA followed by a Bonferroni post-hoc test. Data is expressed as mean ± SEM., *p< 0.05, **p<0.01 vs. Chow; $p<0.05 vs. HFHS.

To gain a better understanding of glucose as a fuel for these cells as well as the transport of glucose across the BBB, the expression of glucose receptor - glucose transporter-1 (GLUT-1), and the uptake of glucose was measured using flow cytometry (Figure 6.5). When measuring glucose uptake by the cells using 6NBDG, a fluorescent nonhydrolyzable glucose analogue, there was a trend towards increased uptake by HFHS-fed mice serum-stimulated cells compared to chow-fed mice serum-stimulated cells, and a trend towards reduced uptake by HFHS-fed + hrANXA1 treated mice serum-stimulated cells. There was no change in the expression of GLUT-1 between HFHS-fed and chow-fed mice serum-stimulated cells however there was a decrease in the expression of GLUT-1 expression in HFHS-fed + hrANXA1 treated mice serum-stimulated cells, to levels lower than in chow-fed mice serum-stimulated cells; however no results were significant.

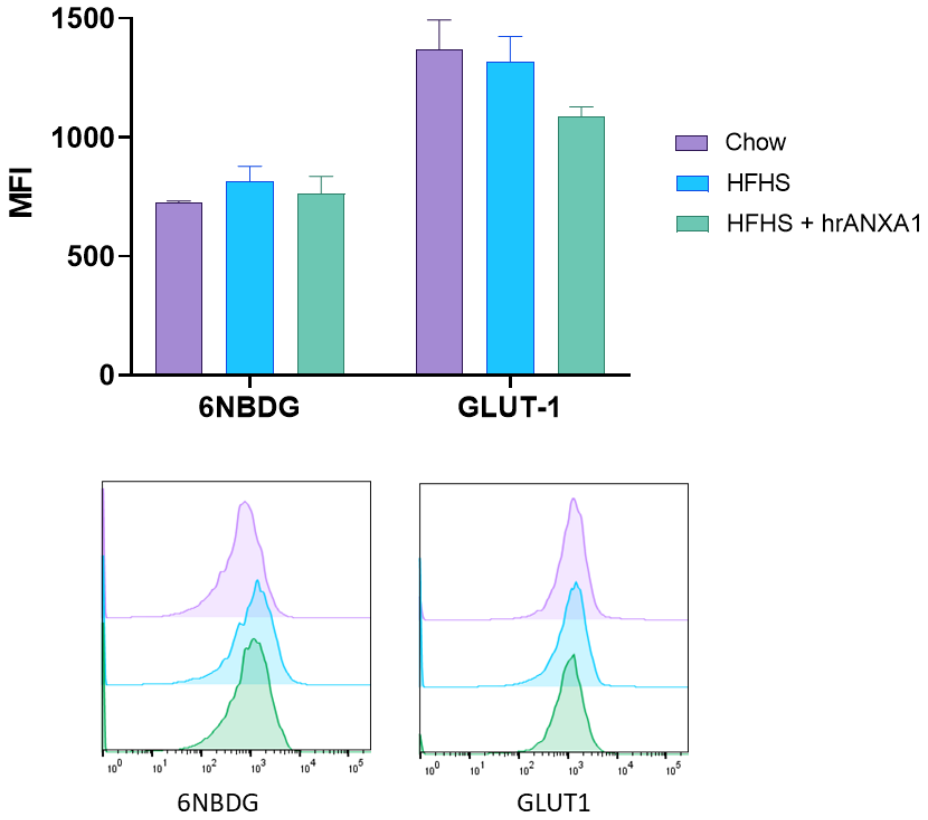

Figure 6.5 | Glucose uptake and transport

The expression (median fluorescence intensity, MFI) of receptors involved in glucose transport in brain endothelial cells were assessed using flow cytometry (n=4-8/group, duplicates per mouse). bEnd3 cells were stimulated for 16 hours with 10% mouse serum from chow, HFHS, HFHS + hrANXA1 mice after which cells were stained for glucose transporter-1 (GLUT-1). To measure glucose uptake, cells were first incubated in glucose free medium for 1 hour followed by the addition of 200µM 6NBDG, a glucose analogue; cells were analysed live at the flow cytometer. Statistical analysis was performed by one-way ANOVA followed by a Bonferroni post-hoc test. Data is expressed as mean ± SEM.

In addition, as metabolic disorders cause hyperinsulinemia and subsequent insulin resistance, the expression of the insulin receptor by bEnd3 cells was also measured (Figure 6.6). There was no stark change in the expression of insulin receptor across all 3 groups, however there appeared to be a trend towards decreased expression in the HFHS-fed and HFHS-fed + hrANXA1 treated mice groups.

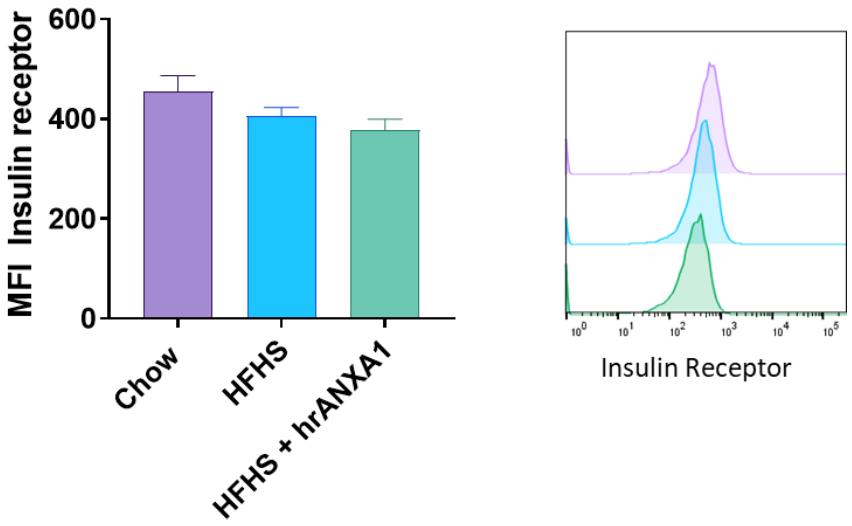

Figure 6.6 | Expression of insulin receptor on brain endothelial cells

The expression (median fluorescence intensity, MFI) of the insulin receptor in brain endothelial cells were assessed using flow cytometry (n=4-8/group, duplicates per mouse). bEnd3 cells were stimulated for 16 hours with 10% mouse serum from chow, HFHS, HFHS + hrANXA1 mice after which cells were stained and were passed by the flow cytometer. Statistical analysis was performed by one-way ANOVA followed by a Bonferroni post-hoc test. Data is expressed as mean ± SEM.

The Mito Stress test was used to measure mitochondrial respiration at the ETC (oxidative phosphorylation) and thus assess the mitochondrial function (Figure 6.7). Mitochondrial respiration was measured by oxygen consumption rate (OCR). Cells stimulated with serum from HFHS-fed mice had a significantly higher OCR profile compared to chow-fed mice serum-stimulated cells (Figure 6.7A), indicative of higher mitochondrial respiration. The OCR of all parameters - basal respiration, ATP production, proton-leak, maximal respiration and spare capacity (Figure 6.6 B-G) is higher in HFHS-fed mice serum-stimulated cells compared to chow-fed mice serum-stimulated cells; indicative of increased oxidative phosphorylation taking place within these cells. Overall, cells stimulated with serum from HFHS-fed + hrANXA1 treated mice have a lower OCR profile when compared to HFHS-fed mice serum-stimulated cells. Although the basal respiration and proton leak remain high in the HFHS-fed + hrANXA1 treated mice, there is a significant reduction in the maximal respiration and spare capacity of these cells when compared to HFHS-fed mice serum-stimulated cells; the latter two measurements are similar to chow-fed mice serum-stimulated cells. The high basal respiration rate in HFHS + hrANXA1 accounts for the high ATP production via the ETC. Importantly the non-mitochondrial oxygen consumption does not differ between the groups suggesting that this test is an accurate measure for mitochondrial respiration occurring via oxidative phosphorylation.

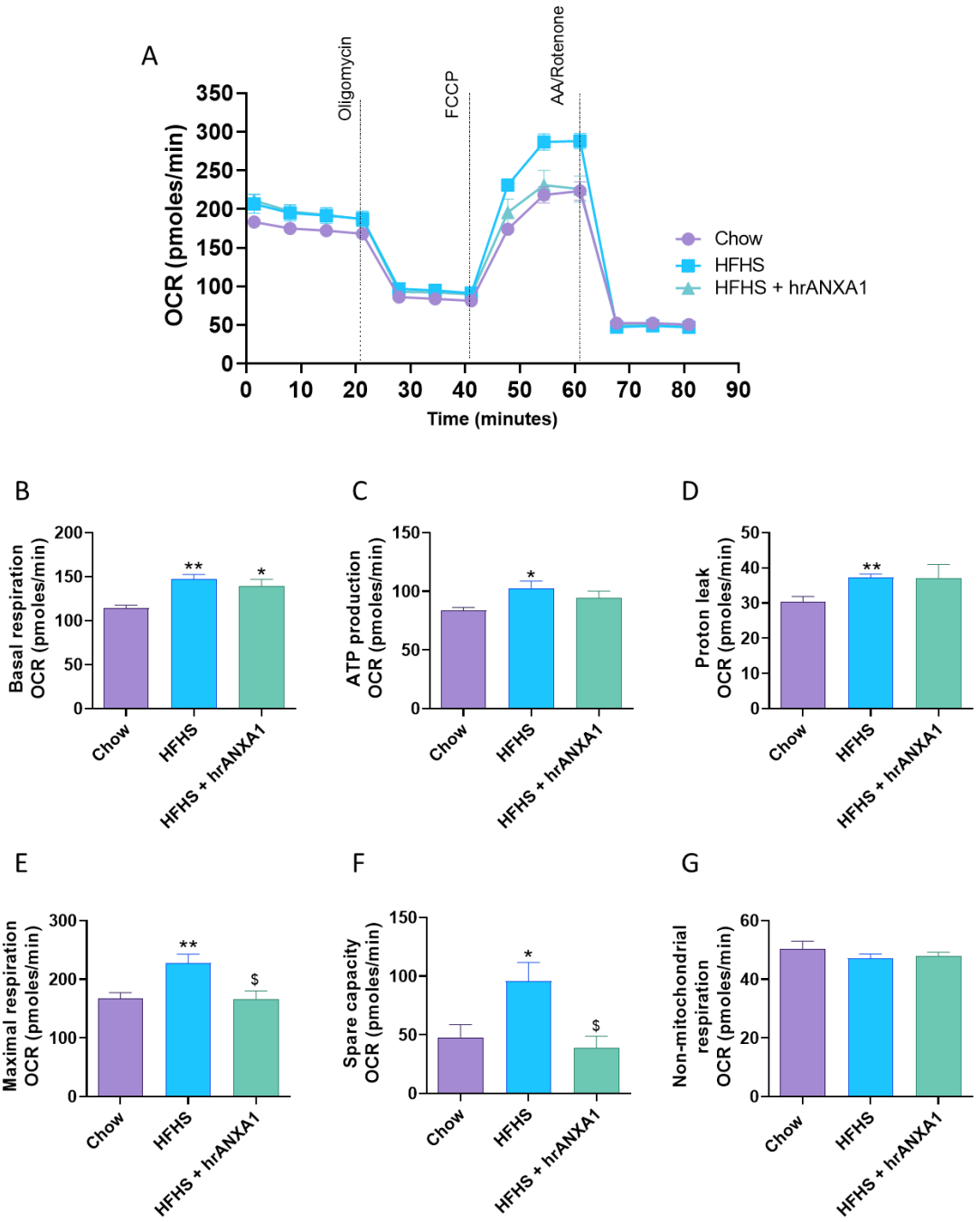
A
Oligomycin
FCCP
AA/Rotenone
OCR (pmoles/min)
Time (minutes)
Chow
HFHS
HFHS + hrANXA1
B
Basal respiration OCR (pmoles/min)
C
ATP production OCR (pmoles/min)
D
Proton leak OCR (pmoles/min)
E
Maximal respiration OCR (pmoles/min)
F
Spare capacity OCR (pmoles/min)
G
Non-mitochondrial respiration OCR (pmoles/min)

Figure 6.7 | Effect of chow, HFHS, HFHS + hrANXA1 mouse serum on the mitochondrial respiration of brain endothelial cells

bEnd3 cells were stimulated for 16 hours with 10% mouse serum from chow, HFHS, HFHS + hrANXA1 mice. Using the Mito stress kit (Seahorse, Agilent, UK) sequential injections of oligomycin, FCCP, Antimycin A & Rotenone were added to measure mitochondrial respiration (oxygen consumption rate, OCR, pmoles/min) by inhibiting different complexes of the electron transport chain. The kinetic profile to quantify mitochondrial respiration (A) was used to quantify the other indices of mitochondrial function – basal respiration (B), ATP production (C), proton leak (D), maximal respiration (E), spare capacity (F), non-mitochondrial respiration (G) (n=6/group, three replicates per mouse). Statistical analysis was performed by one-way ANOVA followed by a Bonferroni post-hoc test. Data is expressed as mean ± SEM., *p< 0.05, **p<0.01 vs. Chow; $p<0.05 vs. HFHS.

To measure the production of all ATP generated by the cell, an ATP luminescence detection kit (Perkin-Elmer, USA) was used (Figure 6.8). Results reveal there to be an increase in the production of ATP by HFHS-fed mice serum-stimulated cells compared to chow-fed mice serum-stimulated cells, however the production of ATP is further increased in HFHS-fed + hrANXA1 treated mice serum-stimulated cell. None of these results were statistically significant.

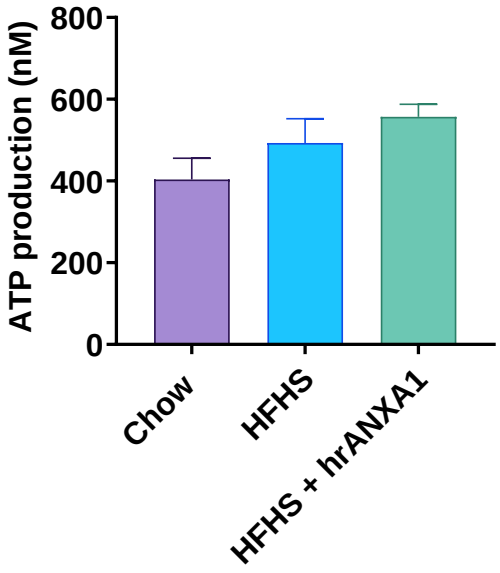

Figure 6.8 | ATP production by bEnd3 cells stimulated with mouse serum

ATP production by bEnd3 cells stimulated with mouse serum (n=5/group, five replicates per mouse) was measured using the ATP luminescence detection kit (Perkin Elmer, USA). Luminescence was read (1 sec/well) on a plate reader (Infinite M200 PRO plate reader, TECAN). Statistical analysis was performed by one-way ANOVA followed by a Bonferroni post-hoc test. Data is expressed as mean ± SEM.

The combination of hyperglycaemia and insulin resistance causes oxidative stress through disruption of NO release; coupled with increased AGE and ROS production thereby enhancing activation of inflammatory pathways (758).

Firstly cellular and mitochondrial ROS production was measured using DCFDA and MitoSOX respectively (Figure 6.9A,B). Fluorescence assays showed stimulation with HFHS-fed mice serum induced a greater production of both cellular and mitochondrial ROS when compared to chow-fed mice serum stimulation, as seen by higher fluorescence emission (relative fluorescence unit, RFU). Cells stimulated with serum from HFHS-fed + hrANXA1 treated mice had significantly reduced cellular and mitochondrial ROS production when compared to HFHS mice.

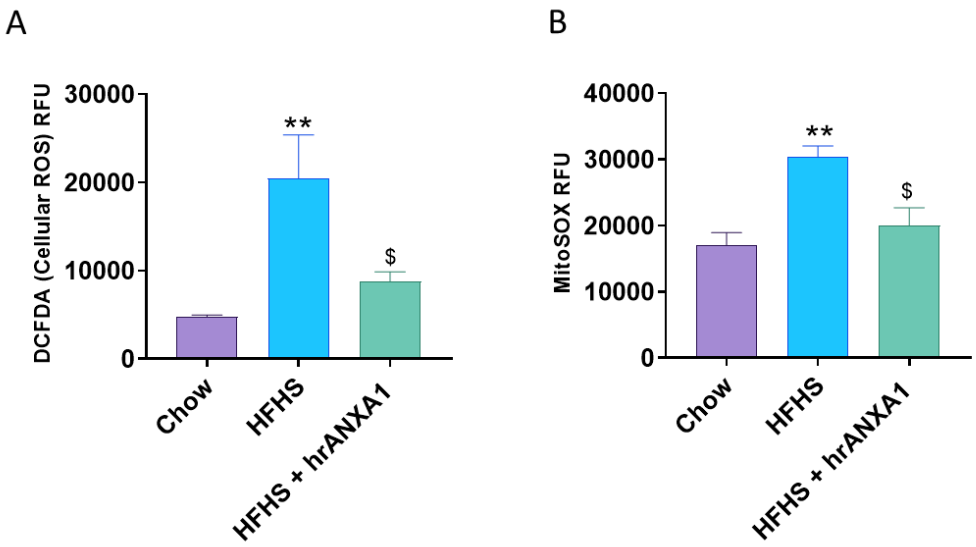

Figure 6.9 | Measurement of cellular and mitochondrial ROS production in bEnd3 cells stimulated with mouse serum

ROS production, cellular and mitochondrial was measured using fluorescence assays. bEnd3 cells were grown in 96-well plates until confluent; cells were stained using 25µM DCFDA (cellular ROS, Ex/Em 485/535nm; A) or 2.5µM of MitoSOX (mitochondrial ROS, Ex/Em 510/580nm; B) followed by stimulation with 10% serum from chow, HFHS or HFHS + hrANXA1 mice. Using a plate reader, the accumulation of ROS was measured by fluorescence emission and the relative fluorescence unit (RFU) taken as a readout for ROS production. (n=12/group, pooled in pairs, three replicates per pair).

6.2.3 The role of lipids and adipokines in metabolism at the BBB

Aside from glycolysis and oxidative phosphorylation there are several other cellular metabolism pathways that could be impacted by T2DM. Aside from hyperglycaemia, T2DM also causes hyperlipidaemia, as seen by raised levels of cholesterol and triglycerides in the HFHS-fed mice (Figure 4.2). Here, we briefly investigated how lipid metabolism may be altered by briefly investigating the expression of LDL receptor (LDL-R) and PCSK9, a protein that can bind to LDL-R, in primary brain microvessels of chow-fed, HFHS-fed, HFHS-fed + hrANXA1 treated and HFHS – Chow reversion mice (Figure 6.10A).

The results showed that the expression of LDL-R is significantly decreased in HFHS-fed mice compared to chow-fed mice. The expression of LDL-R is restored in HFHS-fed + hrANXA1 treated and HFHS – Chow reversion diet mice. PCSK9 is a protein that competes with lipids to bind to the LDL receptor and prevent lipid uptake; results show significantly increased PCSK9 protein expression in HFSH-fed mice compared to chow-fed mice, the expression is reduced in HFHS-fed + hrANXA1 treated and HFHS – Chow reversion diet mice.

In addition, research in recent years has suggested that expression of adipose-derived factors called adipokines, that act has hormones, may disrupt CNS homeostasis and thereby play a role in the development of neuroinflammatory disorders. Four adipokines have been measured at the brain microvessels of the mice, these include adiponectin, chemerin, leptin and resistin (Figure 6.10B).

Adiponectin is involved in regulating glucose levels; results show that its expression is decreased in HFHS-fed mice compared to chow-fed mice and levels are improved in HFHS-fed + hrANXA1 treated and HFHS – Chow reversion diet mice.

Chemerin regulates adipocyte development and glucose metabolism; results show that its expression is significantly increased in HFHS-fed mice compared to chow-fed mice and levels are restored in HFHS-fed + hrANXA1 treated and HFHS – Chow reversion diet mice.

Leptin is a satiety hormone, there are no significant differences across the groups however there appears to be a slight trend towards increased leptin expression in HFHS-fed + hrANXA1 treated and HFHS – Chow reversion diet mice compared to chow-fed and HFHS-fed mice.

Resistin has been shown to induce inflammation; results at the brain microvessels indicate an increased expression of resistin in HFHS-fed mice compared to chow-fed mice and this is decreased in HFHS-fed + hrANXA1 and HFHS – Chow reversion mice.

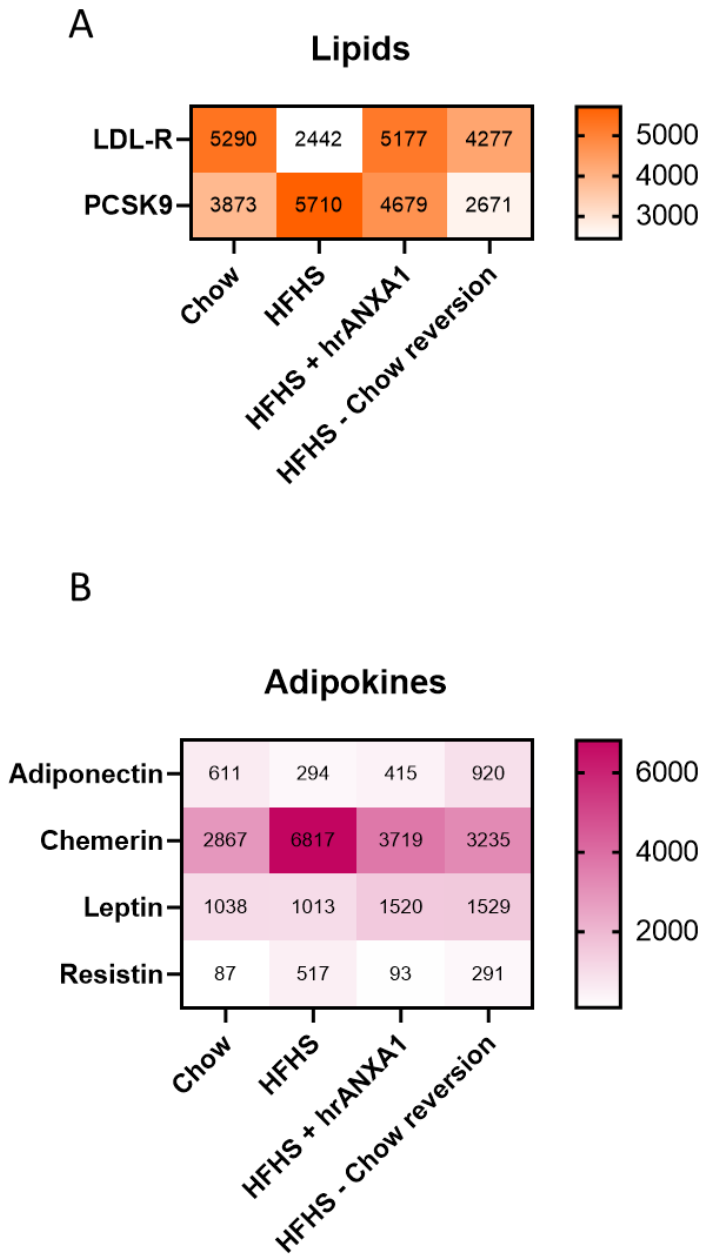

Figure 6.10 | Expression of metabolic factors in primary brain microvessels

Simultaneous measurement of adipokines and lipid mediators in protein extracts from primary brain microvessels of chow, HFHS, HFHS + hrANXA1 and HFHS – Chow reversion mice, using Mouse Cytokine Array Kits (R&D Systems, Minneapolis, USA). Membrane-based immunoassays detected the relative expression levels of analytes detected as arbitrary units by x-ray film exposure (n=10 pooled/group, two technical replicates per experiment, for chow, HFHS and HFHS + hrANXA1 performed as two independent experiments total n=20/group); quantified using ImageStudio Lite (LI-COR Biosciences).

6.3 Discussion

The results from the first part of this chapter using serum stimulation, show stimulation with HFHS-fed mice serum increases the leakage of the brain endothelial cells with heightened permeability and reduced TEER compared with chow-fed mice serum-stimulated cells, which can be accounted for by the reduction of junctional proteins such as occludin and VE-cadherin as well as loss of the actin filamentous fibres. Moreover, the HFHS-fed mice serum activates the bEnd3 cells to upregulate adhesion molecule expression. In addition, cells stimulated with HFHS-fed mice serum show an upregulation of co-stimulatory molecule CD86, indicating that the brain endothelial cells themselves act as antigen presenting cells under inflammatory stimuli, as previously reported (753,754). This coincides with the increased adhesion and migratory profile of T_H17 and Treg cells seen in the HFHS-fed mice (Figure 5.14) Stimulation with HFHS-fed + hrANXA1 treated and HFHS – Chow reversion diet mice serum retains the cellular integrity as seen in chow serum-stimulated cells.

All of these results are comparable to the *in vivo* and *ex vivo* data shown in Chapters 4 & 5, measuring the same parameters. It can therefore be concluded, that pro-inflammatory mediators (interleukins, chemokines, cytokines, acute phase proteins etc.) are present in the serum collected from the mice and these induce the same phenotypic changes seen in the primary brain endothelial cells or microvessels. The restoration of the parameters with both an anti-inflammatory agent (ANXA1) and dietary switch implicates the role played by chronic inflammation in causing endothelial dysfunction and vascular damage induced by the traits of MetS (obesity, hyperglycaemia and dyslipidaemia).

Primarily, these results demonstrate that an *in* vitro BBB model stimulated with mouse serum serves as a comparable model to *ex vivo* primary cultures. This has major implications for the 3Rs (reduction, replacement, and refinement) of research. It would therefore seem viable to use cell lines of astrocytes or microglia, that are stimulated with serum *in vitro* to assess the affects occurring to these cells too. Notably, the most robust way to model the BBB *in vitro* would be to use a 3D co-culture model.

Secondly, these results are integral in confirming that peripherally-induced inflammation arising as a result of metabolic disorders is detrimental to the brain microvasculature. It is this metaflammation that triggers BBB malfunction. No doubt,

the other cells of the NVU also contribute to the sustained and long-term damage seen at the BBB and in the brain, however it is the metaflammation and immuno-metabolic disturbance that initiates this sequence of events.

It has long been established that T2DM can cause microvessel damage in the peripheral system resulting in secondary complications such as retinopathy, neuropathy and nephropathy. The results from the previous chapters in context with the results from serum stimulation, reveal that neuroinflammation/neurovascular disorders are also a secondary complication of T2DM.

6.3.1 Altered metabolism of brain endothelial cells in MetS/T2DM

Accumulating evidence has indicated that T2DM changes the metabolic signatures in the liver, pancreas, adipose tissue and immune cells, with reports of altered glucose, amino acid, fatty acid, glycerophospholipid and sphingomyelin metabolism (759–763). The altered metabolic state contributes to the progression of T2DM. Given the fundamental role played by the brain endothelial cells as a physical, transport and metabolic barrier; and the disruption incurred to these cells, we hypothesised that changes in metabolism will also contribute to the progressive loss of the BBB and its functionality. This chapters of the thesis begins to explore and describe the differences in different metabolic pathways or metabolic factors seen with HFHS-feeding.

6.3.1.1 The role of glucose at the BBB and in the brain

The brain is very metabolically active and utilises glucose as its primarily fuel to generate energy (127,128). On the whole, fatty acids are not considered to contribute to normal brain energy metabolism however this view had been challenged with reports that up to 20% of energy in the brain can be derived from fatty acid oxidation (764–766). In endothelial cells, there are still mixed reports on whether glycolysis or oxidative phosphorylation is the preferred energy-yielding pathway. Peripheral endothelial cells have low mitochondrial content (767) and therefore it is thought these endothelial cells rely heavily on glycolysis for ATP generation (768–770). In contrast, the cells of the NVU, including the endothelial cells, are densely packed with mitochondria to meet the brain's energetic demand (771). In fact, reports suggest that

glycolysis is the main energy production mechanism in the developing brain with a switch to oxidative phosphorylation in the mature brain (772). Nevertheless, it is well documented that glycolysis is enhanced in cerebral endothelial cells when they acquire tip cell phenotype for angiogenesis (769) or during hypoxic events (773). This has led some to believe that mitochondrial activity is preferentially used in resting cells whereas glycolysis is intensified in activated cells (774). Interestingly, in bEnd3 cells stimulated with serum from HFHS-fed mice, both the use of glycolysis and oxidative phosphorylation is significantly enhanced.

When reviewing glycolysis, HFHS-fed mice serum-stimulated cells have an increased rate of basal glycolysis correlating with increased glucose uptake. The cells are further able to maximise the use of the glycolytic pathway when oxidative phosphorylation was shut down by addition of oligomycin. Results from this chapter and previous chapters clearly demonstrate an increased activation of brain endothelial cells in a diabetic phenotype; therefore the increased glycolytic reserve amount in HFHS-fed mice serum-stimulated cells indicates that brain endothelial cells are able to respond to the energetic demand induced by inflammation and hyperglycaemia. Although the ATP generated by glycolysis has not been calculated, the measurement of all ATP produced by the cells shows an increase in ATP generation by all sources in HFHS-fed mice serum-stimulated cells compared to chow-fed mice serum-stimulated cells.

For normal brain function and energy metabolism, the brain relies on a continuous supply of glucose across the BBB. Usually substrate excess results in the downregulation of its corresponding receptor in order to balance supply and demand. Here, we see no apparent differences in the expression of GLUT-1 between chow-fed and HFHS-fed mice serum-stimulated cells. However other studies using diabetic mice models have reported decreased GLUT-1 and GLUT-3 expression at the BBB (775,776). On the other hand, in AD patients no change is seen in GLUT-1 expression but GLUT-3 expression is decreased (129–131). GLUT-1 is present on both the apical and basolateral membranes of brain endothelial cells (132), GLUT-1 and GLUT-3 are present on astrocytes and GLUT-3 and GLUT-4 are present on neurons. It is therefore possible to hypothesise, that glucose transport across the brain endothelial cells is not impacted by reduction in transporter expression. Instead, astrocytes and neurons have reduced glucose uptake and this contributes to the cognitive impairment seen in neurodegenerative disorders such as AD (129–131). In support of this, human studies

report no change in the concentration of glucose in the brain of diabetic patients vs healthy controls (777–779). This implies that glucose transport across the brain endothelial cells remains intact, but it is the differential uptake and utilisation by the other NVU cells that contributes to brain dysfunction.

To better understand the glucose uptake and utilisation in brain endothelial cells vs. the transport of glucose into the brain for use by other cells, alternative strategies need to be employed such as *in vivo* monitoring or 3D co-culture models. The use of 3D co-culture models will allow for the communication of different cell types and thus impact transporter or receptor expression in a dynamic environment, which is missing in the current bEnd3 model.

6.3.1.2 Insulin in the brain

Within the peripheral system, insulin is a major regulator of blood glucose levels through stimulating uptake of glucose by liver, muscle and adipose tissue (133). In contrast, glucose transport in the brain is largely insulin-independent with GLUT-1 and GLUT-3 not requiring insulin to regulate glucose uptake (136). However the brain is not an insulin-insensitive tissue, with insulin receptors distributed throughout the brain; GLUT-4 present on neurons does require insulin-mediated glucose uptake (136) for neuronal growth, plasticity or neurotransmitters release (137). Therefore, insulin is highly involved in memory and cognition. Evaluation of insulin receptor expression in bEnd3 cells treated with mouse serum, revealed a trend towards insulin receptor downregulation in HFHS-fed mice serum-stimulated cells. Other studies using obese animals, have reported decreased insulin transport across the BBB resulting in reduced CNS insulin levels (780–783).

Additionally, deficiency in insulin and insulin receptors have been reported in patients with AD (396,784,785). A phase III clinical trial in which insulin was administered nasally, improved cognitive function in AD patients (393). Subsequent studies have shown that insulin administration improves AD pathology through restoring metabolic function of neurons. Impaired neuronal insulin signalling is seen in mice with apolipoprotein E (APOE) ε4 allele - the strongest genetic risk factor for AD (786). APOE4 traps the insulin receptor in endosomes preventing its trafficking, thereby causing a reduction in mitochondrial respiration and glycolysis in the neurons (786).

Interestingly, a high fat diet was seen to accelerate the results seen in the APOE4 mice with impaired insulin signalling (786). Epidemiological studies report diabetic patients to have an increased risk of developing AD (787). High fat-feeding in an AD transgenic mouse model results in T2DM-like peripheral insulin resistance concomitant with decreased insulin receptor signalling in the brain, increased Aβ burden and cognitive defects (390,391). In fact, T2DM and transgenic AD mice present with similar vascular dysfunction resulting in cognitive decline that can be attributed to increase Aβ accumulation in both conditions (394,395). The similarities in the T2DM and AD mice linked with insulin sensitivity has therefore lead to the concept that AD is in fact a continuum of DM, termed T3DM (133,396).

Interestingly, insulin therapy was also reported to restore Pgp levels in diabetic rats (145). Pgp has been shown to be involved in the clearance of Aβ (788–791). In serum stimulation of bEnd3 cells with HFHS-fed mice serum, the insulin receptor and Pgp expression showed a downwards trend compared to chow-fed mice serum-stimulated cells. Together, these results implicate how insulin receptor deficiency or insensitivity at the level of brain endothelial cells in diabetes, could subsequently lead to reduced insulin in the brain and therefore induce AD pathology.

6.3.1.3 Mitochondrial respiration in the brain endothelial cells

Upon review of mitochondrial respiration, HFHS-fed mice serum-stimulated cells also increased oxidative phosphorylation compared to chow serum-stimulated cells; this is likely due to the hyperglycaemia and hyperlipidaemia in the HFHS-fed mice (Figure 5.2). In the HFHS-fed mice serum-stimulated cells there is an increase in the basal respiration and ATP production compared to chow-fed mice serum-stimulated cells; the increase in maximal respiration confirms that the cells have the ability to rapidly oxide substrates such as sugars, fats and amino acids, which are augmented in HFHS-feeding. Importantly, the HFHS-fed mice serum-stimulated cells also have a large increase in their spare respiratory capacity suggesting that the bEnd3 cells have the flexibility and fitness to respond to the need of an increased energetic demand. Despite this however, there is increased proton leak, indicative of mitochondrial damage.

Mitochondrial damage has been implicated in diabetes, with reports of altered morphology (reduced size (792) and cristae (793)) and defects in biogenesis and

mitophagy (794) resulting in mitochondrial fragmentation, impaired function and increased ROS production (795). In addition, metabolomic studies in rodents have found that high fat-feeding overloads mitochondria resulting in incomplete β-oxidation and impaired activity (796). Studies conducted in our lab using MS serum on hCMEC/D3 cells showed decreased glycolysis and oxidative phosphorylation, accompanied by mitochondrial hyperpolarisation that could be correlated to an increase in mitochondrial superoxide and NO production (269). Similar experiments are required to be conducted in the HFHS-fed model, to measure how metabolic overload can affect the mitochondrial mass, membrane potential and subsequent function in brain endothelial cells.

6.3.2 Oxidative stress at the BBB

ROS (superoxide anion O_2^-, hydrogen peroxide H_2O_2 and hydroxyl radio HO) are present in all living cells, being produced either endogenously or exogenously. Endogenously, ROS is generated from mitochondria during oxidative phosphorylation and by oxygen metabolising enzymatic reactions (797). Provided redox signalling mechanisms, which control the balance between generation and elimination of ROS remain in intact, the homeostatic levels of ROS are maintained; however an imbalance between pro-oxidants and anti-oxidants and impairment of anti-oxidant defence mechanisms can lead to oxidative stress (798–800). Oxidative stress is damaging to lipids, proteins and nucleic acids of cells and has been implicated in cancers, diabetes, atherosclerosis, aging and neurodegenerative disease (801,802).

In the HFHS-fed mice, both production of cellular ROS and mitochondrial ROS was measured in bEnd3 cells. Results found serum stimulation from mice fed a HFHS-diet induced a greater production of cellular and mitochondrial ROS in comparison to their chow-fed counterparts. This is not surprising, as research has shown diabetes to increase production of free radicals due to chronic hyperglycaemia and hyperlipidaemia (349,350). Metabolic by-products of glycolysis and fatty acids are shunted into the citric acid cycle and ETC for subsequent oxidation (803,804), driving up ROS generation. Additionally, hyperglycaemia hinders the transport of other nutrients e.g. ascorbic acid which act as anti-oxidants and scavenges free radicals. (805–807). Mice fed a HFHS diet have increased circulating glucose and lipid levels,

and serum stimulation of bEnd3 cells increased the rates of glycolysis and mitochondrial respiration compared to chow serum-stimulated cells, accounting for higher ROS measurements.

The changes in nutrient levels, transport ability and pro-inflammatory mediators will also impact the metabolism of other cells such as the astrocytes, microglia and neurons resulting in impaired metabolism and excess ROS generation (808). Importantly, the cells of the NVU are not just producers of ROS but also the target of oxidative stress. For example, NO is produced by the brain to maintain blood flow (809) and for neurotransmission (810); however excessive production of NO by iNOS, nNOS and eNOS can result in the build-up of RNS, such as peroxynitrate, which contributes to oxidative stress (811). The production of RNS has not been measured in the HFHS-fed mice, however Figure 4.16 showed an enhanced expression of iNOS by endothelial cells of the brain microvessels and in microglia of HFHS-fed mice compared to chow-fed mice.

Progressive oxidative damage can lead to cell death and significant loss of cellular function (812,813). Free radicals induce lipid peroxidation through attacking phospholipid components of cellular membranes (814); the neuronal membrane is largely made up of polyunsaturated fatty acids and is therefore highly susceptible to lipid peroxidation, the 4-hyroxynonenal produced in this manner is cytotoxic to neurons (815,816). High levels of 4-hyroxynonenal have been reported in a number of neurodegenerative diseases (817). Oxidative stress in proposed as early event in the progressive neurodegeneration seen in cases of AD (818,819). Additionally, the selective loss of dopamine neurons in PD is due to the high levels of ROS due to enhanced dopamine metabolism (820). The production of ROS by the brain endothelial cells could be a key contributor to the neuroinflammatory state we show and downstream neurodegeneration reported in other diabetic studies (674).

Additionally, a hyperglycaemic environment leads to the non-enzymatic glycosylation of proteins to form AGEs (821). Excess glucose is shunted into other pathways such as polyol pathway where it is converted to sorbitol; a reaction that further depletes NADPH and increases ROS. In turn sorbitol, is converted to fructose leading to production of 3-deoxyglucsone, a reactive aldehyde that contributes to AGE formation

(822). Increased concentrations of AGEs have been found in serum and tissues of diabetic patients and are proposed to play a role in insulin resistance, β-cell failure and diabetic complications through inducing RAGE signalling; thereby increasing ROS formation and downstream inflammatory signalling pathways (823). Whilst the levels of AGEs themselves have not been measured in this current mouse model, Figure 5.8B found an increased expression of RAGE at the brain microvessels of HFHS-fed mice compared to chow-fed mice; abnormal over-expression of RAGE is triggered through inflammation and accumulation of AGEs (821,824). Increased binding of AGE to its receptor can trigger microglia response and chemokine release, and triggers neuronal loss, as seen in AD (825).

Together the measurement of ROS and indirect measurement of RNS and AGEs through expression of iNOS and RAGE show that there are a number of characteristic features within the diabetic mouse model that increase the opportunity for oxidative stress at the BBB and cells of the NVU, to cause neurotoxicity and cell death (378).

One of the major mechanisms for oxidative stress-induced damage at the BBB is through MMP activation (826,827). Previously the role of MMPs in contributing to BBB breakdown have been discussed in Chapter 4 & 5. It was noted in Figure 4.6 that the expression and activity of MMP-2 and MMP-9 was increased at the brain microvessels of HFHS-fed mice in comparison to chow-fed mice. There are two proposed mechanisms by which ROS may regulate MMP activity, either directly or indirectly (826,827). Direct regulation occurs through oxidation or S-nitrosylation of the MMPs to unmask the pro-peptide for activation (828,829). Indirectly, ROS-induced inflammatory cytokines such as IL-1, TNF-α, IL-6 etc. (827) can activate a number of signalling pathways such as MEK1-Erk, MAPK-p38, PI3K-Akt that result in the increased binding of transcription factors AP-1 and NF-κB to the redox-sensitive cis-regulatory elements in the MMP promoter region thereby increasing transcription of MMPs (830). In this manner, we can hypothesise that the activity of MMPs in our model can be related to ROS and inflammatory mediators acting via several signalling pathways that have detrimental effects on BBB breakdown. Future studies will need to focus on the signalling mechanisms involved in the HFHS-fed mice by which this occurs, as these could be potential therapeutic targets.

6.3.3 Role of Annexin A1 in metabolism

As seen in Chapter 5, the treatment of HFHS-fed with hrANXA1 attenuates T2DM development by lowering fasting glucose levels, serum cholesterol and serum triglycerides. Metabolically, the ECAR and OCR profile of cells stimulated with HFHS-fed + hrANXA1 treated mice serum show improvement, with a reduction in glycolysis and mitochondrial respiration, resulting in reduced ROS production. HFHS-fed + hrANXA1 treated mice have reduced iNOS activity (Figure 5.16) and reduced RAGE expression at the brain microvessels, therefore reducing RNS and AGEs (Figure 5.8), contributing to the lowering of oxidative stress. This decline in oxidative reduces the inflammatory mediators and thus lowers MMP activation, contributing to the restoration of BBB integrity seen with hrANXA1 treatment. Other studies have also reported ANXA1 treatment to reduce oxidative stress. For example ANXA1 protected against benzo[a]pyrene (Bap)-induced bronchial epithelium injury through regulating the activity of anti-oxidant defence mechanisms such as glutathione peroxidases and superoxide dismutase, reducing the expression of apoptotic protein Bcl-2 and restoring the PTEN/FAK/PI3K/Akt signalling pathway (831). This is in line with another study, in which the ANXA1 cleavage product Ac2-26 reduced oxidative stress via an FPR1/NOX1-dependent signalling pathway involving PI3K and NF-κB, to orchestrate epithelial repair (832). These results were subsequently confirmed by another study in which ANXA1 overexpression in PC12 cells decreased levels of ROS, IL-6, iNOS and NF-κB (833). Undeniably, HFHS-fed + hrANXA1 treated mice have reduced ROS production, reduced IL-6 levels (Figure 5.8) and reduced iNOS activity (Figure 5.16).

Interestingly, review of oxidative phosphorylation shows that although HFHS-fed + hrANXA1 treated mice serum-stimulated cells retain a high basal respiration rate, the maximal respiration and spare capacity is significantly decreased compared to HFHS-fed mice serum-stimulated cells and is similar to the profile seen in chow-fed mice serum-stimulated cells. This reduction coincides with restored serum glucose and lipids levels (Figure 5.2) and the diminished requirement of energy as a result of reduced metaflammation. On the other hand, the total ATP produced from the cell, irrespective of metabolic pathways shows that HFHS-fed + hrANXA1 treated mice serum-stimulated cells have the highest ATP production compared to chow and HFHS

serum-stimulated cells. These results therefore highlight that although mitochondrial respiration and glycolysis is reduced in HFHS-fed + hrANXA1 treated mice serum-stimulated cells, alternative pathways are being utilised to produce energy. The results clearly demonstrate the endothelial cells are less activated with hrANXA1 treatment, with down-regulation of adhesion molecules and MMPs, therefore the increased energy production serves to question the need for ATP? It can be hypothesised that the extra ATP is required for ANXA1 binding to the actin cytoskeleton for maintenance of TJs. This is supported by a number of studies in which ATP depletion causes disruption to actin cytoskeleton (834–836) binding with TJ proteins ZO-1, ZO-2 and cingulin, thereby causing a reduction in TEER (837).

Importantly, in this study, only the glycolytic and oxidative phosphorylation pathways have been investigated. In order to fully understand the interplay and dynamic shifts between metabolic pathways under stress and inflammation, it would be important to assess the use of other nutrients e.g. glutamine and lactate alongside reviewing the other metabolic pathways of β-oxidation and the citric cycle.

Remarkably, the proton leak in HFHS-fed + hrANXA1 treated mice serum-stimulated cells remains high which indicates that there is still a degree of mitochondrial dysfunction despite the significantly reduced ROS levels. This raises the question of whether ANXA1 has the ability to improve anti-oxidant defence mechanisms or whether ANXA1 itself acts an anti-oxidant to scavenge free radicals.

The effect of ANXA1 on GLUT-1 and insulin receptor expression also warrants further investigation, as the transporter and receptor expression is decreased in HFHS-fed + hrANXA1 treated serum-stimulated cells compared to chow serum-stimulated cells. The lack of glucose transport may affect the function of other cells in the NVU; indeed ANXA1 has been shown to reduce T-cell glycolysis, activation and proliferation (293). In the peripheral system, hrANXA1 in HFHS mice re-sensitized insulin receptor substrate mediated signalling to restore insulin sensitivity (512). This needs to be investigated at the level of the BBB, particularly as ANXA1 treatment in AD mice improves cognitive behaviour, through reducing local inflammation and reducing loss of neurons (Reis et al., manuscript submitted).

The re-establishment of the BBB structure through astrocyte end-feet association to the blood vessel and further metabolic improvements in the brain endothelial cells with hrANXA1 treatment will likely be a key component in the improved neuroinflammatory and neurological state. Astrocytes provide support to neuronal activity (167) through provision of metabolites, neurotransmitter precursors and ion buffering via gap junctions or direct contacts (168,169). Improved, structural, functional, and metabolic activity of the BBB with hrANXA1 treatment will have far reaching impacts within the brain.

6.3.4 Other metabolic factors involved in BBB metabolism

So far, the work investigating metabolism at the brain endothelial cells was conducted in the bEnd3 cell line stimulated with serum extracted from mice. Using the R&D Cytokine Array Panel A Kit, various other metabolic factors were detected in primary brain microvessels isolated from the different mice groups. The differential expression and presence of these factors confirm that the disruption at the BBB is also metabolic in nature and warrants further investigation. Moreover, the investigation of these factors has also been performed in HFHS – Chow reversion diet mice. Although the previous investigations are required to be carried out in this subset of mice, the ability of HFHS – Chow reversion diet mice to restore these metabolic factors implicates that metabolic disruption is occurring as a result of the MetS/T2DM traits and its associated metaflammation.

6.3.4.1 Lipids at the BBB

The role of lipids in brain endothelial cell metabolism was beyond the scope of this study. Nevertheless, the HFHS-fed mice had hyperlipidaemia as seen by raised levels of serum cholesterol and triglyceride compared to chow-fed and HFHS-fed + hrANXA1 treated mice (Figure 5.2). HFHS – Chow reversion diet mice, also had reduced levels of cholesterol and triglycerides compared to HFHS-fed mice, but the levels did not return to chow-fed mice levels.

At the brain microvessels, the expression the expression of LDL-R and protein PCKS9, which are involved in lipid metabolism were detected. The LDL-R is responsible for increasing cholesterol uptake and maintaining lipid homeostasis (838). At the brain microvessels, there was decreased expression of LDL-R in the HFHS-fed mice compared to chow-fed mice. PCSK9 is a protein that binds to LDL-R to prevent LDL-R recycling; blockage of this protein can lower LDL concentrations from the circulation (839). Interestingly the levels of PCSK9 were increased in the brain microvessels of the HFHS-fed mice. The combination of increased PCSK9 and decreased LDL-R in HFHS-fed mice suggest that lipid transport is being affected; and requires pursuit in future studies. Within the brain, fatty acids are taken up by astrocytes for synthesis and transport of cholesterol to neurons for synaptic signalling (840). The decreased uptake of lipids at the BBB could therefore impact the neurotransmission and subsequently memory/cognition. Studies in $LDLR^{-/-}$ mice fed a western diet found a decrease in cognitive processes in these mice versus control mice (841). Crucially, pharmacological and dietary intervention both restored levels of LDL-R and PCSK9 suggesting that lipid metabolism is involved in maintaining the BBB integrity. It would be crucial to investigate whether hrANXA1 and dietary intervention have the ability to restore cognition and memory processes in mice.

6.3.4.2 Adipokines at the BBB

Adipokines are adipose-derived factors which have been implicated to be involved in brain homeostasis and function. A number of these function through affecting food intake and energy expenditure. Four different adipokines were detected in the brain microvessels of chow-fed, HFHS-fed, HFHS-fed + hrANXA1 treated and HFHS – Chow reversion diet mice; these include adiponectin, chemerin, leptin and resistin. Further studies are warranted to understand the exact role of these adipokines within the BBB of the HFHS-fed mice, however the following passages aim to highlight the potential of these hormones to affect the CNS and lead to diabetes-induced neuro-inflammation/degeneration.

Adiponectin is the most abundant adipokine and is involved in mediating a wide range of effects including regulation of insulin sensitivity through controlling glucose and lipid metabolism, improving endothelial function through anti-atherogenic effects, decreasing vascular inflammation, and regulating body weight (842–846). At the BBB, adiponectin supresses IL-6 and TNF-α release from endothelial cells; although it does not cross the BBB itself (847). In the HFHS-fed mice, there is decreased expression of adiponectin in brain microvessels compared to chow-fed mice; decreased adiponectin may contribute to damage induced at the BBB through a rise in pro-inflammatory mediators. There was some restoration of adiponectin levels in HFHS-fed + hrANXA1 mice and significantly increased levels of adiponectin in HFHS – Chow reversion diet mice. This is concomitant with reduced inflammation at the BBB, which is more apparent in the HFHS – Chow reversion diet mice compared to HFHS + hrANXA1 mice (Figure 5.8). Notably, adiponectin also affects astrocytes and neurons. Within neurons, adiponectin has neuroprotective effects through activating the AMPK pathway and regulating NO release (848,849). In contrast, in astrocytes, adiponectin induces a pro-inflammatory response to increase IL-6 levels (850). As adiponectin it is not transported across the BBB, it must enter the brain via the BCSF. The widespread and beneficial vs deleterious effects of adiponectin implicate that changes in levels will affect normal cell and tissue functions.

Resistin levels are positively correlated to adiposity. Like adiponectin, it also regulates the synthesis and secretion of pro-inflammatory TNF-α and IL-6. It mediates its affect through binding to TLR4 and causing activation of pro-inflammatory signalling pathways (851,852). Within the CNS it can affect the hypothalamic insulin response (853). The increased expression of resistin in the HFHS-fed mice compared to chow-fed mice implicates that it may also contribute to the inflammatory state at the BBB. Resistin expression is decreased in HFHS-fed + hrANXA1 treated and HFHS – Chow reversion diet mice, in which inflammation at the BBB is reduced. Moreover, resistin up-regulated PCSK9 which down-modulates LDL-R (854–857). In the HFHS-fed mice, there is increased resistin, increased PCSK9 and decreased LDL-R. Treatment with hrANXA1 and changes in diet restore resistin levels and subsequently PCSK9 and LDL-R. Thus, resistin may be a potential candidate for improving lipid metabolism at the BBB, with implications on neuronal signalling and synaptic plasticity.

Chemerin is associated with regulating glucose metabolism through feeding behaviour (858). High levels of chemerin are a biomarker for obesity and MetS (859–862). Moreover chemerin has shown to be upregulated in AD patients and mouse models, functioning as a receptor for Aβ (863). In the mouse brain microvessels, chemerin levels are increased in HFHS-fed mice compared to chow-fed, HFHS-fed + hrANXA1 treated and HFHS – Chow reversion diet mice. Similarly, low leptin levels have been associated with an increased risk for cardiovascular disease (864) as well as increased risk of AD development (865). In fact, leptin deficiency is thought to impact insulin-controlled pathways. Chronic administration of leptin to AD-transgenic mice reduces the Aβ burden and tau-phosphorylation contributing to improved neurological outcomes (866,867). There appeared to be no differences in the expression of leptin at the BBB of chow-fed and HFHS-fed mice, however levels were increased in HFHS-fed + hrANXA1 treated and HFHS – Chow reversion diet mice. Perhaps hrANXA1 exerts indirect effects on insulin signalling at the CNS via leptin. The potential role of both chemerin and leptin in T3DM development requires further investigation, as these could serve to be candidates to improve AD pathology.

6.3.5 Conclusion

In summary the *in vitro* data on paracellular permeability, junctional proteins and adhesion molecule expression from cells stimulated with mice serum were similar to the *in vivo* and *ex vivo* data of the same parameters. This data confirms that serum-stimulation models are appropriate for the investigation into disease pathology. This is welcome news for the 3Rs of research, as well as for translation studies using human samples *in vitro* to model disease phenotypes.

To our knowledge, our group is the first to investigate the role played by brain endothelial cell metabolism in affecting CNS pathology. To date, the large focus of metabolism-based studies in the CNS have focused on astrocytes and neurons, with the role of brain endothelial cells largely neglected. However, changes to the structural and functional integrity of the BBB implies that metabolic disruption is occurring within these cells. In fact, here we see that HFHS-feeding impairs the glycolytic and oxidative phosphorylation pathways. In the immediate, the increased activity of these pathways provides greater ATP to meet the energetic demand placed upon the cells due to the enhanced inflammatory and immune status. On the other hand, the up-regulation of metabolic pathways contributes to increased oxidative stress. The accumulation of ROS, RNS and AGEs are known to be fatal to neurons leading to neuronal apoptosis. The role of oxidative stress in neurodegenerative disorders of AD and PD have been well-recognised. Given the similarities in T2DM and AD brain pathology, major studies are required into understanding the impact of metaflammation on neuronal activity and subsequently cognition in the HFHS-fed model. Moreover, ROS production can be linked to increased activity of MMPs through direct and indirect regulation via up-regulation of inflammatory mediators and pathways. The results from the previous chapters together with the results from this chapter serve to demonstrate how peripheral inflammation can trigger a neuro-inflammatory response which is self-perpetuating, resulting in a vicious ongoing cycle of damage to the BBB and consequently the brain tissue.

One of the roles of the BBB is to serve as a transport barrier, and therefore alterations to the transport of nutrients and hormones across the BBB will have consequences for the health and functionality of the other cells of the NVU. The results from this chapter have only briefly alluded to the possible effects that changes in insulin, lipid and adipokine transport across the BBB could have for brain activity. Unquestionably, in

depth studies are required to investigate the exact role played by these factors in contributing to T2DM-induced brain neuroinflammation. Notably, insulin signalling is paramount in maintaining the health of neurons, with impaired signalling resulting in Aβ accumulation and cognitive defects. The adipokines resistin and chemerin are also linked to the control of insulin signalling pathways. Our results have shown that peripheral inflammation is the trigger to neuroinflammation through inducing a leaky BBB phenotype impairing its immunological integrity. It can be hypothesised from this chapter that disruption to metabolic transport occurring as a result of the impaired BBB triggers the onset on neurodegeneration that is controlled by nutrient and hormonal factors.

The ability of the intervention arms to restore the metabolism of these cells to the state seen in the chow-fed mice serum stimulated cells is vital, as it serves to demonstrate that these interventions are not merely patching up the cells on the surface but truly working to provide a mechanism to combat the damage that is incurred and to restore the vascular health of these cells. This opens up a huge potential for these interventions in treating neuro-inflammatory/neurodegenerative disorders.

Chapter 7 – Metabolic disorders & the brain: Impact and Implications

The goal of this thesis was to understand whether and how chronic peripheral inflammation arising from metabolic disorders such as MetS or T2DM can impact the brain to initiate a neuroinflammatory response that could lead to neurodegenerative disorders. The BBB serves as the main interface between the peripheral and central systems, protecting the brain microenvironment from damage from peripheral blood-borne materials such as toxins, immune cells and inflammatory mediators (88). Due to the critical role played by the BBB in linking the peripheral and central systems, the focus of this study was to examine changes occurring to the structure, function, and immunological integrity of the BBB under metaflammation.

7.1 The effect of metabolic disorders on the brain: from peripheral inflammation to neuroinflammation

Overall, the results from this project demonstrate that damage to the brain microvasculature is a secondary complication to T2DM, similar to retinopathy, nephropathy and neuropathy. HFHS-feeding caused obesity, hyperglycaemia, hyperlipidaemia, and hyperinsulinemia prompting a low-grade chronic inflammatory state, also known as metaflammation. This metaflammation resulted in the complete breakdown of the BBB vessel structure triggering neuroinflammation. Figure 7.1 provides an overview of the metaflammation-induced damaged at the BBB.

The significant loss of the BBB structure in HFHS-fed mice compared to the chow-fed mice implicates how chronic inflammation is a requirement in initiating the damage to the BBB. In fact, several neurodegenerative disease such as AD, PD, MS, ALS and HD report the presence of pro-inflammatory cytokines and activated immune cells within the peripheral blood (392,571–573). The presence of these circulating factors and immune cells cause brain endothelial dysfunction, leading to increased production of interleukins, cytokines, chemokines and adhesion molecules (320,328,329).

Importantly, immune cell migration is the rate-limiting step in disease onset (156,251). However, as discussed previously, optimal migration of leukocytes across an endothelium barrier requires chemokine signals that initiate from within the CNS (629–631). Astrocytes, microglia and neurons do produce chemotactic factors to

induce leukocyte infiltration (253), highlighting that these cells sense perturbations in the brain or blood milieu early on. In fact, activation of astrocytes and microglia further contributes to the negative inflammatory status through subsequent release of acute-phase proteins, complement components, prostaglandins, cytokines, MMPs and ROS/RNS that promote neuronal cell death (575,576). In addition, the data from this project initiates the conversation on how altered metabolism and transport of nutrients and hormones in the brain endothelial cells of HFHS-fed mice can contribute to oxidative stress build-up and impaired neuronal signalling, which can be huge triggers in neurodegeneration (349,350,821).

Interestingly, the HFHS-fed model not only shows an increase in pro-inflammatory mediators but also anti-inflammatory mediators, indicative of attempts to resolve and combat the damage. Inflammation is an evolutionary-conserved protective response mechanism which involves the coordinated communication of cells through intrinsic molecular signalling cascades. The simultaneous rise of pro- and anti-inflammatory mediators triggers aberrant activation of multiple signalling cascades (340,349–351). This over-active response likely causes confusion in cells and tissues, eventually resulting in loss of control and thereby contributing negatively to the pathological outcome.

These concepts provide a clear pathway between peripheral inflammation and neuroinflammatory response that leads to neurodegeneration (577). In metabolic disorders, where peripheral inflammation is chronic and sustained, the inflammatory microenvironment is likely to propagate a vicious cycle of self-propelling inflammation from the endothelial cells, astrocytes, microglia and neurons that ultimately leads to a self-destructing and deteriorating environment within the brain (578).

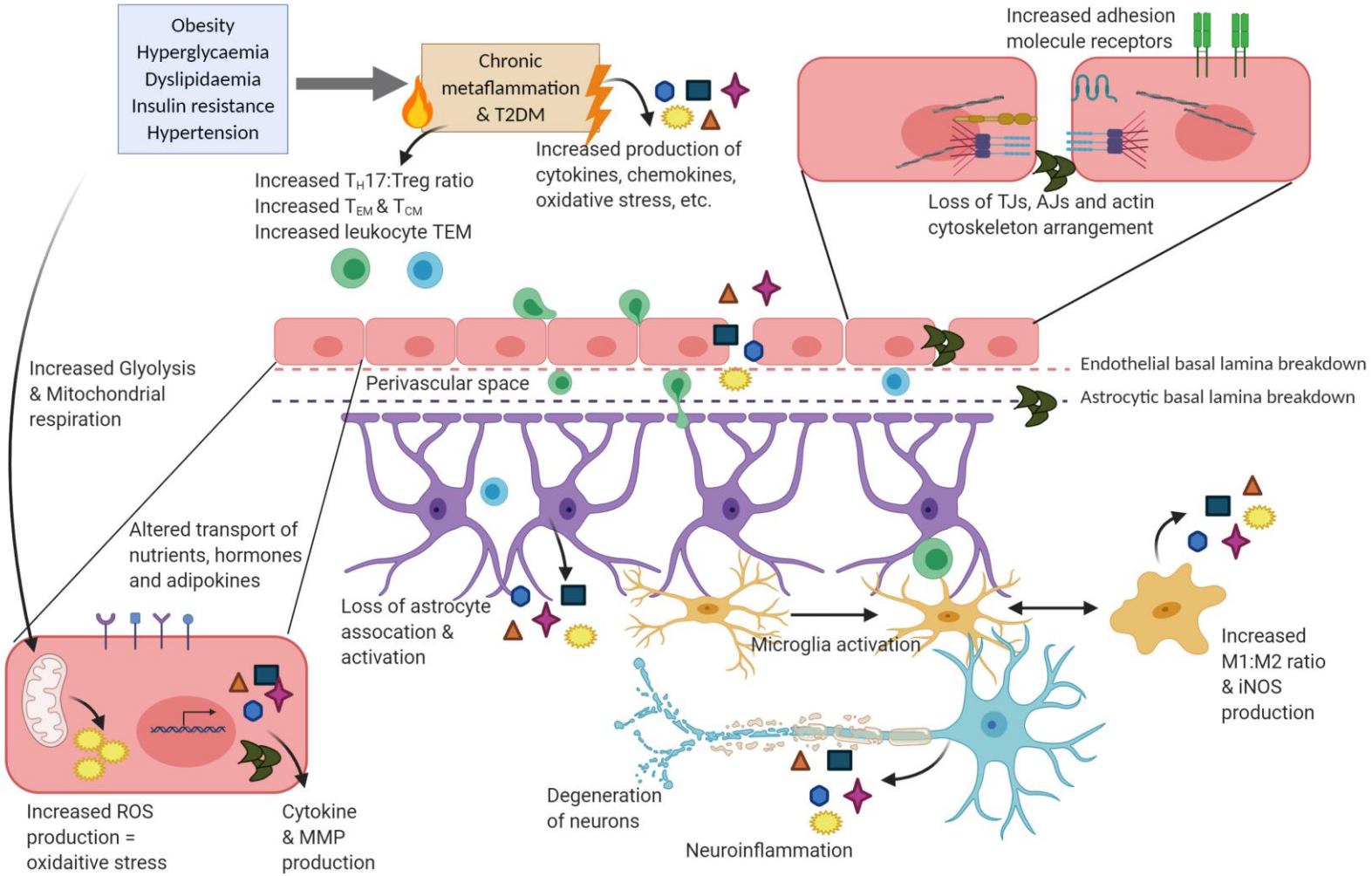
Obesity
Hyperglycaemia
Dyslipidaemia
Insulin resistance
Hypertension
Chronic metaflammation & T2DM
Increased production of cytokines, chemokines, oxidative stress, etc.
Increased T_H17:Treg ratio
Increased T_{EM} & T_{CM}
Increased leukocyte TEM
Increased adhesion molecule receptors
Loss of TJs, AJs and actin cytoskeleton arrangement
Endothelial basal lamina breakdown
Perivascular space
Astrocytic basal lamina breakdown
Increased Glyolysis & Mitochondrial respiration
Altered transport of nutrients, hormones and adipokines
Loss of astrocyte assocation & activation
Microglia activation
Increased M1:M2 ratio & iNOS production
Increased ROS production = oxidaitive stress
Cytokine & MMP production
Degeneration of neurons
Neuroinflammation

Figure 7.1 | Overview of the effect of a HFHS-diet on the disruption of the NVU

The traits of metabolic disorders – obesity, hyperglycaemia, dyslipidaemia, insulin resistance and hypertension, create a low-grade chronic inflammatory state termed metaflammation which results over time in the development of T2DM. Chronic metaflammation is responsible for producing a number of cytokines, chemokines and oxidative stress as well as activating the immune system. The damage by inflammation and the immune system leads to a leaky BBB phenotype that can be correlated to the loss TJs and AJs, the actin cytoskeleton, and the loss of basal lamina α4 on endothelial cells and α2 astrocytic end-feet. This breakdown is mediated by the imbalance of MMPs/TIMPs and results in complete loss of the BBB structure with the disassociation of the astrocytes to the blood vessel. The accumulation of inflammatory mediators and oxidative stress, through increased metabolism of glycolysis and mitochondrial respiration, contributes to the production of these MMPs. The pro-inflammatory microenvironment activates the innate and adaptive arms of the immune system, resulting in the expansion of neutrophils, macrophages, dendritic cells, and T-cells. Within $CD4^+$ T-cells, a diabetic microenvironment encourages the differentiation of T-cells into T_{eff} cells particularly of the T_H17 subset, with reduced Treg presence. Additionally, there are greater T_{EM} and T_{CM} cells. This allows for increased TEM of leukocytes into the brain parenchyma. Here, the peripherally-activated immune cells trigger the activation of microglia cells, skewed towards an M1 phenotype, responsible for producing iNOS which is neurotoxic. The astrocytes, microglia and neurons also sense changes in the brain microenvironment and are likely to respond to the increased presence of inflammatory mediator passage by further up-regulating the release of cytokines, chemokines, MMPs and ROS production that triggers pro-inflammatory signalling pathways. The disruption to the brain endothelial cells alters the transport of nutrients such as glucose and lipids and adipokines such as insulin, adiponectin and chemerin, which likely impact the functional activity of the brain cells. These events together creating a self-destructing environment within the brain triggering neuroinflammation and subsequent neuronal destruction.

7.1.2 Potential mechanism of action for BBB breakdown

In the HFHS-fed mice, the breakdown of the BBB can be correlated to the surge in MMP levels, which are responsible for degrading TJs and the basal laminas (187,547). MMP activity is regulated transcriptionally by cytokines, growth factors, ROS and hormones (187,547,548). Notably, no single factor has been identified to be exclusively responsible for MMP overexpression, although TNF-α and IL-1 are often implicated (868). The activity of MMPs is regulated by transcription, pro-peptide activation and inhibition by TIMPs. The overall inflammatory profile in the HFHS-fed mice creates the perfect mix of factors that aid in the overexpression of MMPs; and as discussed in Chapter 4, the sustained chronic inflammation results in the loss of TIMP-mediated control of MMP expression. Indeed, in the HFHS-fed + hrANXA1 treated mice and HFHS – Chow reversion diet mice, where the inflammatory profile is improved, the MMP expression is reduced and the TIMP-1 levels increase. Although, as discussed in Chapter 5, the balance of MMPs/TIMPs is not fully restored in the HFHS – Chow reversion diet mice in comparison to HFHS-fed + hrANXA1 treated mice; correlating with the different improvements seen in TJ and basal lamina re-establishment between these two groups.

Several studies have been undertaken to uncover the signalling pathways involved in MMP transcription, as the full regulation of MMPs is still largely unknown. Mapping of the MMP-9 promoter regions reveals specific transcription factor binding sites for AP-1 and NF-κB. In contrast, MMP-2 transcription is regulated through NF-κB and caspase-8 (187).

The binding of pro-inflammatory cytokines such as TNF-α or IL-1, growth factors such as VEGF, PAMPs and ROS species to receptors mediates a number of MAPK signalling pathways including ERK 1/2, JNK and p38 which are all upstream to AP-1 (869–872). We therefore propose that the inflammatory environment induced by metaflammation activates these signalling pathways in the brain endothelial cells of HFHS-fed mice, to result in the transcription of MMPs to cause BBB breakdown. Additionally, pro-inflammatory mediators and ROS activate the PI3K/Akt/NF-κB pathway which further promotes MMP transcription (869,873,874) along with further production of IL-1β, IL-6, TNF-α and iNOS (875), creating a vicious circle of inflammation and breakdown in the brain, as previously suggested. In the HFHS-fed mice, the presence of these inflammatory markers, iNOS and MMPs is significantly

enhanced. Moreover, the activation of these pathways has been previously proposed in diabetic models (134,876–879) and in CNS inflammation (872,875,880).

In the HFHS – Chow reversion diet mice, the switch to a chow-diet removes the original source of hyperglycaemia and hyperlipidaemia, thereby resulting in reduced serum glucose and lipid levels and significantly improved inflammatory mediator profile. Importantly, future studies need to confirm that dietary changes also lower ROS and iNOS production by brain endothelial cells. Nonetheless, it can be hypothesised that the reduction of these mediators reduces the activation of the MAPKs and PI3K-Akt signalling pathway, thus limiting MMP transcription. The HFHS – Chow reversion diet mice have reduced MMP-2, MMP-3, and MMP-9 levels/activity.

Cytokines, growth factors, PAMPs and ROS largely bind to G-protein coupled receptors which mediate their downstream effect to MAPKs through the Rho family of GTPases, including Ras, Rac, RhoA and Cdc42 (881–883). Studies in human hepatocellular carcinoma cells and human bladder cancer cells have shown the inhibition of RhoA using anti-tumorigenic compounds Sinulariolide (869) and Flaccidoxide-13-Acetate (874). These compounds reduce transcription of MMP-2 and MMP-9 through supressing the MAPKs and PI3K/Akt pathways. Previous work in our lab, has clearly demonstrated that ANXA1 mediates its affects through the inhibition of RhoA, with $ANXA^{-/-}$ mice having constitutively activated RhoA that contributes to the heightened BBB permeability (297). We can therefore hypothesise, that ANXA1 treatment in HFHS-fed mice reduces the MAPK activity and thus MMP transcription, not only through reduced inflammatory mediators but also direct effects via RhoA. Overall, this contributes to the improved integrity of the BBB vasculature in the HFHS-fed + hrANXA1 treated mice. Moreover, we have previously also demonstrated that inhibition of RhoA in HFHS-fed + hrANXA1 treatment mice is responsible for the attenuation of T2DM and peripheral microvascular complication of nephropathy, through restoring the IRS-1/Akt/GSK-3 signalling pathway (512).

To confirm these hypotheses, signalling pathway studies are currently being undertaken in our lab. Figure 7.2 shows a proposed mechanism of MMP-mediated BBB breakdown in T2DM.

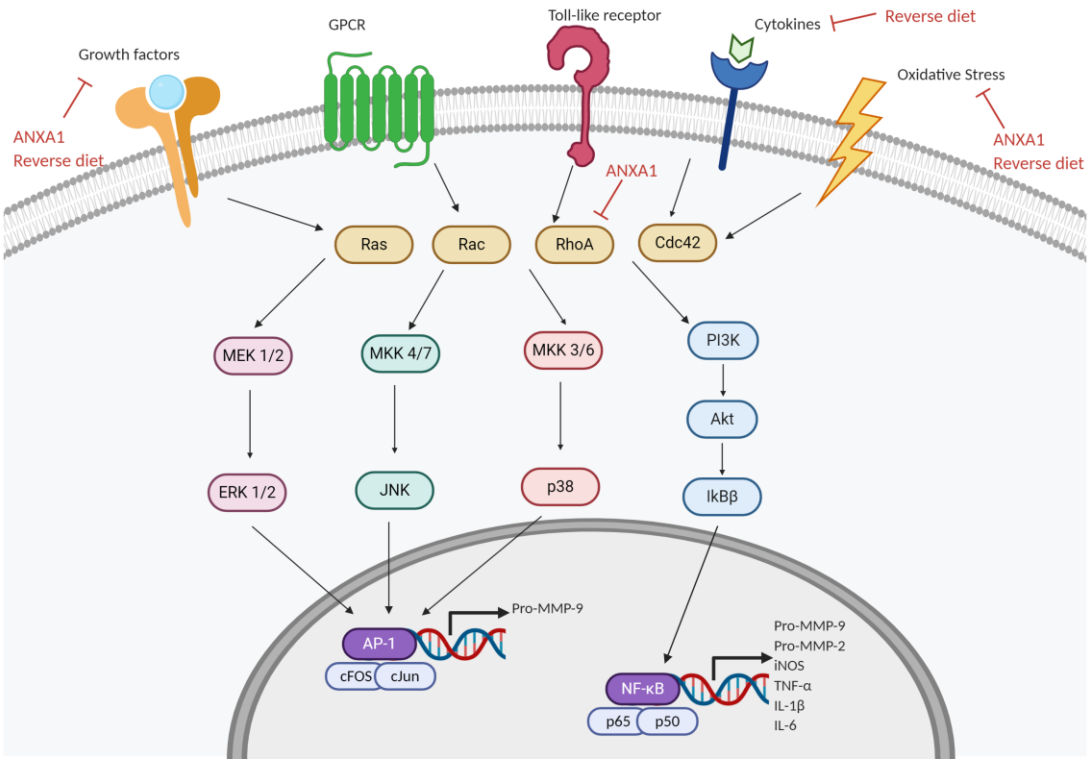

Figure 7.2 | Proposed mechanism of MMP-mediated BBB breakdown in T2DM

MMP activity is regulated transcriptionally by cytokines, growth factors, oxidative, hormones and other cytotoxic molecules. The binding of pro-inflammatory cytokines such as TNF-α or IL-1, growth factors such as VEGF, PAMPs and ROS species to receptors mediates a number of MAPKs signalling pathways including ERK 1/2, JNK and p38 which are all upstream to AP-1. Additionally, pro-inflammatory mediators and ROS activate the PI3K/Akt/NF-κB pathway which further promotes MMP transcription, along with further production of IL-1β, IL-6, TNF-α and iNOS. We propose that the activation of these pathways in the brain endothelial cells of HFHS-fed mice, is responsible of the production of MMPs which degrade the BBB. These inflammatory mediates largely bind to GPCRs which mediate their downstream effects through the Rho family of GTPases including Ras, Rac, RhoA and Cdc42. Dietary reversion and hrANXA1 treatment both have anti-inflammatory effects reducing the presence of these inflammatory triggers and thus we propose the reduced activation of these pathways attenuates MMP production. Additionally, ANXA1has direct effects on inhibiting RhoA and this also mediates the reduction in MMP and pro-inflammatory mediator transcription.

7.2 Metaflammation-induced neuroinflammation: a cocktail for T3DM

The data from this thesis provides an insight into the pathophysiology of how diabetes can trigger inflammatory events within the brain. Whilst this project has not shown the effects on neurons, it is clear that the altered brain microenvironment and CNS inflammation will impact neuronal function adversely. One particular study has shown degenerating neurons in the cortex and hippocampal regions in rodents fed a high-fat and high-fructose diet for 24 weeks (674). Moreover, these mice had impaired spatial learning and memory, as tested using the Morris Water Maze test, that could be linked to the neuronal losses (674). Other studies have also reported impaired cognition in rodents (451,452) and patients (392,450) with T2DM. It is therefore not surprising that epidemiological studies have long reported metabolic disorders to be a risk factor for cognitive decline (5,6) and the development of dementias (7,8). In fact, individuals with T2DM have twice the risk of developing dementia, particularly AD, compared to those without T2DM (9,787).

Further consolidation between T2DM and AD link was shown by a series of studies conducted by Carvalho and colleagues. These studies found that T2DM mice (induced by 20% sucrose feeding for 7 months) and 3x transgenic AD mice presented with similar vascular dysfunction. Both groups of mice showed comparable Evans blue dye leakage into the hippocampus and cortex, accumulation of Aβ and phosphorylated Tau and impaired mitochondrial enzyme activity. Furthermore, both groups of mice also showed similar behavioural and cognitive abnormalities as seen through increased fear and anxiety and impaired learning and memory (394,395). The similarities in the two conditions to cause equivalent CNS dysfunction supports the theory that T2DM causes the development of dementia, namely AD. In line with similar cerebrovascular abnormalities seen in T2DM and AD mice, it has also been reported that AD mice fed a high fat diet have T2DM-like peripheral insulin resistance (390). This results in decreased insulin signalling in the brain that contributes to Aβ burden and cognitive defects (390,391,786). The similarities in the T2DM and AD mice linked with insulin sensitivity has therefore lead to the concept that AD is in fact a continuum of DM, termed T3DM (133,396).

In the HFHS-fed mice, the data demonstrates how disruption to the BBB integrity can impact the transport for nutrients and hormones to other cells of the NVU with particular consequences for neurons. In the HFHS-fed mice there was a downwards

trends towards decreased insulin receptor expression at the brain endothelial cells, as well reduced expression of hormones adiponectin, resistin and chemerin. These adipokines all perform a role in insulin signalling and impairment of their transport will have detrimental effects on neurons, which rely on insulin-mediated uptake of glucose (136) for neuronal growth, plasticity or neurotransmitters release (137). In addition, the increased metabolism (glycolysis and oxidative phosphorylation) of the brain endothelial cells, as a result of high circulating glucose and lipids, can result in the build-up of oxidative stress that contributes to insulin resistance (823).

The central role of insulin in AD has been further confirmed by a phase III clinical trial, in which nasally administered insulin improved cognitive function in AD patients (393). Subsequent studies have shown that insulin administration improves AD pathology through restoring metabolic function of neurons (786), further emphasizing the role played by metabolic dysfunction of the BBB in T2DM to contribute to CNS pathology.

Combined, these studies make a clear case for metaflammation-induced neuroinflammation to be termed T3DM. However, the ability of T2DM to cause AD is a serious cause for concern for the health care and economic system. By 2030, it is projected that 439 million people will have T2DM (310). Diabetes is the third leading cause of death. T2DM patients are 2.5 times more likely to develop CVDs (311,312), which remains the leading cause of death globally, claiming more than 17 million lives/year (313). Equally, the number of people projected to have dementia by 2050 is 150 million (388), of which AD constitutes 60-70% of cases (389). Dementia is the fifth leading cause of death worldwide (309). Both T2DM and dementias are progressive long-term conditions (13). Given that people are living longer and obesity is on the rise (14) we are facing an epidemic crisis, whereby the numbers of individuals who suffer from T2DM, CVDs and AD (or T3DM) is likely to outstrip those who do not suffer from these chronic diseases.

In Chapter 4, it was briefly shown using young (6-week old) mice vs aged (20-week old) mice that a significant degree of damage to the BBB occurs over time, with aged mice having increased paracellular permeability and reduced TEER. The mice fed a HFHS diet were also 20-weeks old, and the ability of T2DM to accelerate the deterioration of the BBB compared to 20-week old chow-fed mice, serves to highlight

how metabolic disorders speed-up the natural aging process to induce neuroinflammatory and neurodegenerative disorders.

Importantly, T2DM is no longer associated with an aged population. Due to the increase incidence in obesity through consumptions of food high in fat and sugar combined with a sedentary lifestyle, individuals are starting to develop T2DM at a younger age (884), with reports of cases of T2DM in children as young as 10 years old (885). Additionally, reports suggest that parental obesity (886) or early-life obesity (887) corresponds to developmental delays in early childhood. Furthermore, childhood and adolescent obesity is related to reduced executive function and attention and lower mathematics and reading achievements (888). These reports implicate how obesity could lead to a significant percentage of the population suffering from cognitive impairments, which is a real cause for concern.

7.2.1. SARS-CoV-2 and Diabetes

Severe acute respiratory syndrome coronavirus 2 (SARS-CoV-2) is the causative agent of coronavirus disease 2019 (COVID-19), which has created the most recent pandemic, as declared on 11th March 2020. Since 31st December 2019 to 7th July 2020, SARS-CoV-2 has infected over 11 million individuals and claimed the lives of over 500,000 persons (889).

Since early in the pandemic, diabetes was classed as a major risk factor for hospitalisation and mortality from SARS-CoV-2 (890). This is perhaps not surprising, as individuals with diabetes demonstrate a higher susceptibility to several infectious diseases including influenza, pneumonia, and tuberculosis. In fact, data from the H_1N_1 influenza pandemic in 2009 has shown that the disease was more severe and lasted for a longer duration in obese patients. Similarly, small retrospective cohort studies from COVID-19 Chinese patients have begun to report that infection rates and deaths are higher in individuals suffering from DM (891,892). DM is a risk factor for infectious diseases due to the low-grade chronic inflammatory state, arising from impaired glycaemic control, which impairs immune response (cytokine production and immune cell activation) to infections (725,728). Moreover, DM patients with abdominal obesity present with mechanical respiratory problems with reduced lung function and

reduced oxygen saturation of the blood (893), pre-disposing to respiratory viruses such as SARS-CoV-2.

Nonetheless, COVID-19 is far from a typical respiratory disorder, with reports emerging of the virus causing neurological defects (894). In the UK, review of 125 seriously ill coronavirus patients have found that nearly half suffered a stroke whilst others have shown brain inflammation, psychosis or dementia-like symptoms (895). A brain autopsy from a patient who developed encephalopathy after presenting with SARS-CoV-2 showed swelling, hyperplasia of glial cells and neuronal necrosis. This was associated with elevated expression of cytokine CXCL9 that corresponded with an infiltration of monocytes, macrophages, and T-cells, as seen by immuno-histochemical analysis (895).

This thesis project demonstrates the link between the peripheral and central system in T2DM, with peripheral inflammation as a responsible factor for the initiation of neuroinflammatory response through BBB breakdown and subsequent T-cell infiltration. Given that we have demonstrated the link of T2DM and the brain through inflammation; this coupled with reports of COVID-19 to produce negative outcomes for both diabetes and the brain as a result of impaired immune responses, suggests there could be a potential link. It has been shown that SARS-CoV-2 can damage endothelial cells, activating inflammatory and thrombotic pathways to cause coagulation resulting in macrovascular damage. So far, SARS-CoV-2 has been linked with inflammation and apoptosis of endothelial cells in the lung, heart, bowel, and kidney, however the effect on the cerebral microvessels has yet to be investigated. Only retrospective cohort studies will be able to determine whether those who suffer from neurological defects, as a side-effect of the virus, are also those individuals who present with underlying metaflammation. We have also discussed the impact of age, and although it appears that mortality rates from coronavirus are higher in the older population (896), investigations will need to be made to determine whether younger individuals who lost their lives suffered from other co-morbidities such as obesity, MetS or T2DM.

7.3 Implications for health care guidance: prevention and management

The progressive development of obesity to T2DM, and T2DM to dementias, in all age groups, poses fundamental calls for the prevention and management of these diseases. In the past two decades, a large proportion of focus has been on the prevention and management of obesity, T2DM and CVDs (897–899), with evidence-based recommendations using a multi-factorial approach of lifestyle, medical and behavioural therapies to produce improvements in disease outcome. Overall comprehensive strategies can reduce the development of micro- and macro-vascular complications in T2DM patients by 50% in approximately 8 years (716).

In the HFHS – Chow reversion diet mice, used in our study, BBB integrity is significantly improved. The key mechanism of this improvement can be related to the ability of dietary changes to reduce inflammation resulting in weight loss and improved peripheral glucose, insulin, and cholesterol levels. Managing these risk factors are the backbone to halting T2DM progression (681,682,684), thereby consolidating the notion that brain microvasculature disruption is a secondary complication of T2DM and should be managed clinically in the same manner.

Currently, WHO prevention guidelines for cognitive decline and dementia do acknowledge that the risk factors for dementia are shared with those of other non-communicable diseases and similar prevention strategies on diet, alcohol and tobacco use and physical activity recommendations should be applied (900). Interestingly, however, the current guidance for the management of individuals who have developed dementias do not offer extensive nutritional therapy approaches other than for VaD. VaD is treated differently as it occurs after stroke which is classed as a CVD and macrovascular complication of T2DM, suggesting that other dementias such AD are treated differently because it is believed that they do not have the same vascular dysfunction. However, as discussed in Section 7.2, AD and T2DM share the same vascular pathologies, suggesting that the management of this dementia or T3DM at least, should also be treated as a complication of T2DM.

The data from the HFHS-fed mice after 10 weeks of feeding clearly demonstrates that the brain microvasculature has been disrupted leading to neuroinflammation that is likely to result in neurodegenerative processes. In the first study of its kind, our data from the HFHS – Chow reversion diet mice prove that dietary change can revert and

restore the damage to the BBB and reduce neuroinflammation. The reduction in inflammatory mediators and MMPs, reduced T_H17 migration, restoration of microglia pro-inflammatory M1 and anti-inflammatory M2 phenotypic balance implicates that signalling responses are being rewired in these mice. This will help to limit neuronal damage and thus improve cognition and memory. Figure 7.3 provides an overview of dietary intervention-based improvement on the BBB and the brain.

Notably, optimal glycaemic control was not achieved in the HFHS – Chow reversion diet mice after 5 weeks on a chow diet which may account for the lack of restoration of TJs and basal laminas at the BBB, along with high activation of immune cells. Previous studies that report improved insulin sensitivity with dietary interventions such as food or calorie restriction (717–719), ketogenic diets (720), herbal formulas (721), reduced glycoxidation products (722) or addition of extra virgin olive oil (723) are employed over a period of 8-24 weeks. Placing the HFHS – Chow reversion diet mice on a longer reversion period is likely to induce significantly greater improvements in BBB integrity. Additionally, further studies are required to understand the effect of BBB metabolism and transport. Nevertheless, the improvement in the adipokine and lipid receptor expression at the BBB serves to demonstrate how diet can repair the functionality of the BBB. The adipokines are key players in insulin signalling, and the restored transport will therefore have huge implications for neuronal function, and reduction of AD-like pathology.

Currently, there is no cure for dementia and no treatment that slows or stops its progression. Medications are largely prescribed to alleviate symptoms such as depression, sleep disturbances, hallucinations, parkinsonism, or agitation and to help improve brain function through boosting levels of chemical messengers involved in memory or learning (901). Our study provides crucial evidence on how dietary change could attenuate T3DM development. Without doubt, more detailed studies are required to understand the impact on neurons, cognition, and behaviour, however this study provides a strong foundation to continue this research with a huge potential for impacting future guidance and management of dementias.

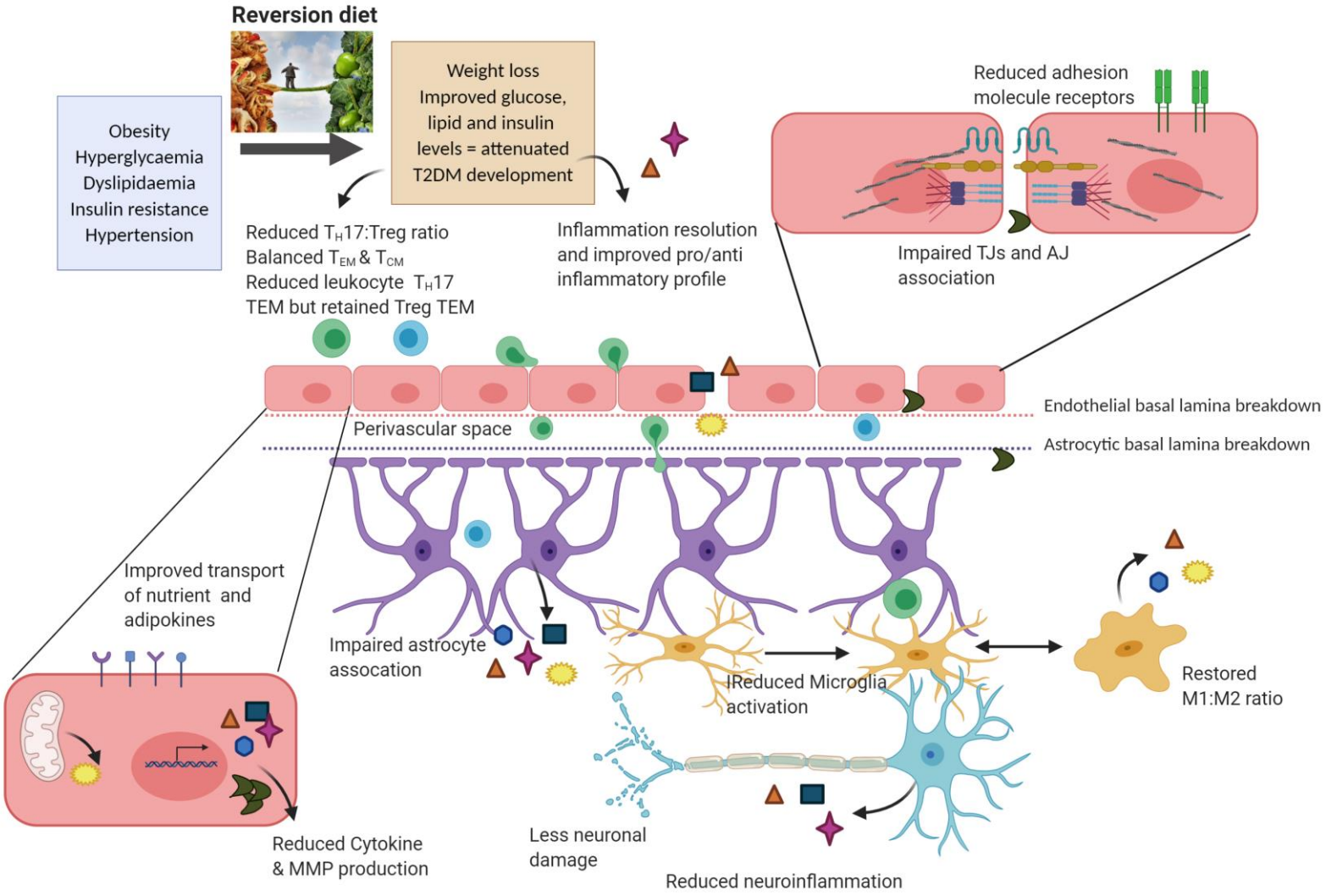
Reversion diet
Obesity
Hyperglycaemia
Dyslipidaemia
Insulin resistance
Hypertension
Weight loss
Improved glucose, lipid and insulin levels = attenuated T2DM development
Reduced T_H17:Treg ratio
Balanced T_{EM} & T_{CM}
Reduced leukocyte T_H17
TEM but retained Treg TEM
Inflammation resolution and improved pro/anti inflammatory profile
Reduced adhesion molecule receptors
Impaired TJs and AJ association
Endothelial basal lamina breakdown
Perivascular space
Astrocytic basal lamina breakdown
Improved transport of nutrient and adipokines
Impaired astrocyte assocation
Reduced Microglia activation
Restored M1:M2 ratio
Reduced Cytokine & MMP production
Less neuronal damage
Reduced neuroinflammation

Figure 7.3 | Overview of the effect of dietary reversion (from a HFHS diet to a chow-diet) on the BBB and the NVU

Dietary intervention of HFHS – Chow reversion diet causes significant weight loss to reduce obesity and improve the glucose, insulin and lipid levels thereby significantly reducing the inflammatory profile and production of MMPs. After 5 weeks of diet intervention, brain endothelial cells show tight junction restoration, and reduced activation via reduced adhesion molecule presence accounting for reduced permeability and improved TEER. However, improvement to the basal lamina is not apparent over 5 weeks of feeding and this prevents the reassociation of the astrocytic end-feet with blood vessel. At the immune cell levels is a reduction in the T_H17/Treg ratio and restored T_{EM} and T_{CM} balance. Whilst there is a reduction in adhesion/migration of T_H17 cells, the Treg cells still transmigrate implicating that T-cells have not lost their ability to migrate however there are changes being made immunologicaly to restore the disease status. Within the brain parenchyma there is considerably reduced microglia activation suggesting that less damaging cells or molecules are passing through. Microglia also show a restoration of balance between M1/M2 phenotype. The reduction in inflammation coupled with improved transport of nutrients and adipokines is likely to prevent activation and production of inflammatory mediators by astrocytes, microglia and neurons which will help to alleviate neuroinflammation and thus prevent neuronal damage.

7.4 Targeting brain damage with ANXA1: the most beneficial brain therapeutic to date?

Aside from dietary intervention, the large focus of this project has been to investigate the use of hrANXA1 as a pharmacological intervention. The role of ANXA1 has been investigated in a number of different conditions including MS, atherosclerosis, inflammatory bowel diseases, rheumatoid arthritis and cancers (294).

Previous studies undertaken in our lab, showed the potential of hrANXA1 as a therapeutic agent in modulating T1DM and T2DM. Prophylactic treatment with hrANXA1 in STZ-induced T1DM mice prevented development of microvascular complications (nephropathy and cardiomyopathy) (678). Furthermore, the therapeutic treatment of hrANXA1 in these STZ-induced T1DM mice which had developed microvascular complications, prevented further decline in cardiac and renal function (678). In a T2DM model of HFHS-feeding, treatment with hrANXA1 prevented further deterioration of T2DM through restoring insulin sensitivity and attenuated the development of renal nephropathy and lipid accumulation within the liver. These studies suggested the potential for hrANXA1 to also prevent T2DM-induced brain microvascular complications such as T3DM.

In fact, in this project we demonstrate that hrANXA1 treatment does reduce, restore, and revert the damage incurred to the BBB under metaflammation. This is not surprising, as the role of ANXA1 in maintaining the BBB integrity has been well-documented, due to its ability to restore junctional proteins through localisation with the actin cytoskeleton (297). Here, we further demonstrate that the role of ANXA1 can be extended to its ability to restore the essential components of the BM, the basal laminas, through rebalancing the MMPs/TIMPs ratio which help to reseal the leaky BBB phenotype.

Immunologically, hrANXA1 treatment in the HFHS-fed mice helped reduce the migratory capacity of T-cells across the BBB through various mechanisms such as reduction of α4β1 integrin-mediated leukocyte binding (482) , L-selectin shedding (280), reduced T-cell activation and balancing of T_H17/Treg levels and thus reducing microglia activation. ANXA1 also mediates neuroprotection through a prominent increase in the percentage of M2 cells that allow for decreased iNOS production. These effects have been previously shown to reduce phagocytosis of non-apoptotic

neurons (279), thereby limiting neurodegeneration. Metabolically, ANXA1 reduced glycolysis and mitochondrial respiration of brain endothelial cells to reduce oxidative stress thereby lowering the inflammatory environment within the brain. In addition, ANXA1 restored the expression of adipokines which would have huge potential for restoring insulin sensitivity, although this requires further investigation.

In summary, ANXA1 confers neuroprotection against metaflammation-induced BBB damage and could be beneficial to limit the progression of neurodegenerative disorders such as T3DM. An overview of ANXA1's effects on the BBB is shown in Figure 7.4.

The use of ANXA1 as a treatment for AD specifically has also been investigated. It has been shown that ANXA1 and the FPR2 receptor are reduced in brain capillaries of AD mice resulting in disruption of the BBB that can be attributed to Aβ-induced RhoA activation (902). Treatment with ANXA1 restores this BBB integrity through inhibiting RhoA. Moreover, ANXA1 is shown to be involved in the degradation and clearance of Aβ through increasing the expression and activity of Aβ-degrading enzyme neprilysin and by increasing microglial Aβ phagocytosis. In addition, ANXA1 reduces Aβ-induced microglial cytokine production (304). Further work has also shown that these effects can be correlated to reduced loss of neurons and improved cognitive behaviour (Reis et al., manuscript submitted). Given the similarities in the T2DM and AD brain pathology with Aβ accumulation, it is likely that ANXA1 will be able to induce the same beneficial effects described above in the brain of T2DM mice to attenuate the development T3DM.

The management of T2DM and CVDs recommends a multi-factorial approach to disease management through lifestyle, medical and behavioural therapies. In a similar way, management of T2DM-related dementias i.e. T3DM would also require a comprehensive management style. The ability of both ANXA1 and dietary changes to induce significant improvement on the BBB integrity implicates that combined, the two interventions could produce even better outcomes.

In addition, the treatment of ANXA1 is provided via i.p.. The ability of ANXA1 to induce such strong anti-inflammatory effects within the CNS without having to consider special drug delivery mechanisms at the BBB further implicates the potential

use of this endogenous molecule as a regulator and therapeutic in neurovascular and neurodegenerative disorders. To date, no other molecule, to our knowledge, has been able to induce similar widespread beneficial effects in the peripheral system, at the BBB and within the brain. ANXA1's potential to limit leukocyte extravasation is mediated through the same mechanism as the current treatment for MS – Natalizumab, a humanised monoclonal antibody against α4β1 integrin (299). Given that ANXA1 is an endogenous molecule, its potential to induce side-effects would be considerably lower, making it further suitable as a therapeutic candidate. Of course, ADME and toxicology studies would be required in primates before considering trials in man. However, the vast array of positive research into ANXA1 implicates its vast therapeutic potential and should be considered by pharmaceutical companies.

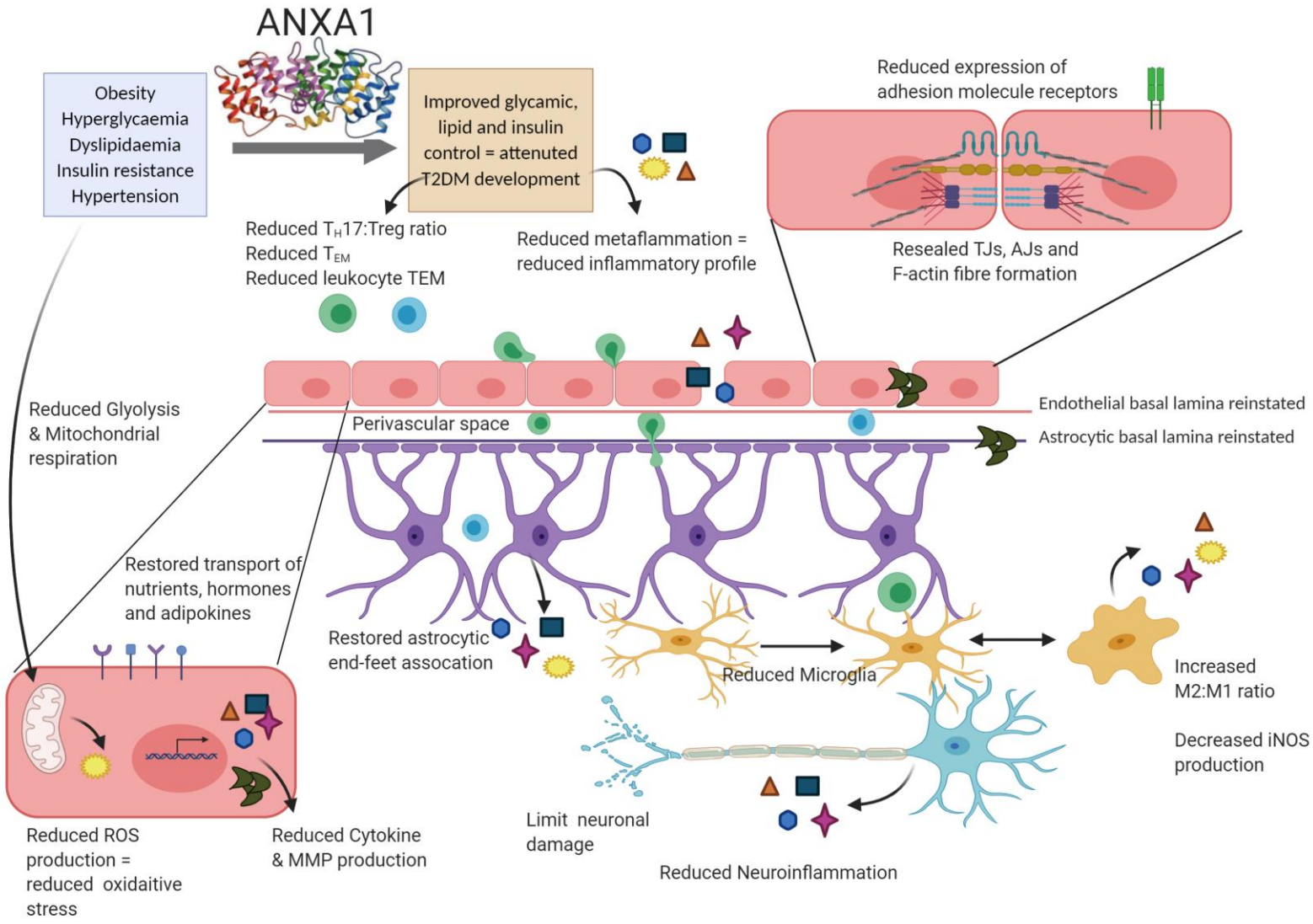
ANXA1
Obesity
Hyperglycaemia
Dyslipidaemia
Insulin resistance
Hypertension
Improved glycamic, lipid and insulin control = attenuted T2DM development
Reduced T_H17:Treg ratio
Reduced T_{EM}
Reduced leukocyte TEM
Reduced metaflammation = reduced inflammatory profile
Reduced expression of adhesion molecule receptors
Resealed TJs, AJs and F-actin fibre formation
Reduced Glyolysis & Mitochondrial respiration
Perivascular space
Endothelial basal lamina reinstated
Astrocytic basal lamina reinstated
Restored transport of nutrients, hormones and adipokines
Restored astrocytic end-feet assocation
Reduced Microglia
Increased M2:M1 ratio
Decreased iNOS production
Reduced ROS production = reduced oxidaitive stress
Reduced Cytokine & MMP production
Limit neuronal damage
Reduced Neuroinflammation

Figure 7.4 | Overview of the effect of hrANXA1 treatment in HFHS-feeding on the BBB and the NVU

Treatment with hrANXA1 attenuates the development of T2DM, by restoring insulin sensitivity and improvement of glucose and lipid levels. At the level of the BBB, treatment with hrANXA1 in the HFHS model has profound effects on restoring the BBB integrity through restoration of TJs (actin-mediated) and BM laminins to allow a resealing of the BBB vasculature through reassociation of astrocytic end-feet to the vessel. This contributes to reduced permeability and TEM. Improved glycaemia and insulin levels reduces glycolysis and mitochondrial respiration, resulting in reduced oxidative stress which contributes to reduced MMP and cytokine production. At the immunological level, hrANXA1 treatment limits T-cell activation and reduces the T_H17/Treg ratio, which can be accounted for by alterations in the interleukins and cytokines. Reduced T-cell activation accompanied by prevention of leukocyte adhesion via L-selectin shedding, amongst possible other mechanisms such as endothelial cell ANXA1 shedding, significantly reduces the migration of peripherally-activated immune cells into the brain parenchyma. Within the brain, hrANXA1 reduces the number of microglia cells and induces a shift from the pro-inflammatory M1 to resolving M2 phenotype, this can have a huge impact on preventing damage to neurons through reduced iNOS production and controlled apoptosis. Additionally, the reinstatement of transport mechanisms for nutrients and adipokines is likely to improve NVU cell functionality to reduce neuroinflammation.

7.5 Limitations and Future Work

The major limitation of the project is the use of all male mice to conduct the studies. Almost 80% of animal-based studies employ the use of male mice to carry out investigations, this is due to the fluctuation of hormones in female mice that can render results uninterpretable (903). However, pre-clinical studies should employ the use of both male and female mice, as this often leads to problems at the clinical stage with differing drug responses. Between 1997-2000, it was estimated that 8-10 drugs were withdrawn by the FDA due to the greater health risks posed for women than for men (904).

Importantly, certain diseases come with their own gender bias. For example, males are more prone to the development of obesity, T2DM and CVDs (905). In contrast, females are more likely to develop dementias (906). It is hypothesised that oestrogen is protective in middle age and when menopause takes place, the risk of CVD and thus dementia development becomes more common in women. Additionally, the results from the Framingham health study suggest that because more men die in middle age due to heart disease, those who survive past 65 may have healthier hearts that provide some protection (907). However, this relies on the concept that dementias begin in old age. As discussed previously, with the rise in obesity, the age at which chronic conditions such as T2DM, CVDs and dementias occur is changing. Only long-term observational studies will be able to determine whether the cases of these conditions at a young age are more prevalent in males or females. Nevertheless, future work on this project should consider the use of male and female mice to determine whether metaflammation-induced neuroinflammation occurs equivalently in both sexes.

Interestingly, previous work from our lab has reported oestrogen-mediated differences at the BBB. Using hCMEC/D3 cells, results showed oestrogen-treatment was protective against inflammation-induced (TNF-α and IFN-γ) barrier defects (908). Oestrogen-treated cells had reduced paracellular permeability, higher TEER, intact TJ integrity and fewer transmigration of leukocytes compared to non-treated cells. Interestingly, these protective effects were mediated through oestrogen-controlled production of ANXA1. However, importantly in this study, it was shown that although young adult female mice (2 months old) had significantly reduced Evans blue leakage compared to male counterparts after LPS-stimulation, reproductively senescent female mice (15 months old) exhibited significantly enhanced Evan's blue dye leakage

compared to 15 month old males (908). We showed in this project that T2DM accelerates the BBB damage in male mice, and therefore a comparison in female mice would be beneficial.

Aside from the potential sex-bias of this study, there is also the limitation of the HFHS – Chow reversion diet mice age difference compared to chow-fed, HFHS-fed and HFHS-fed + hrANXA1 mice. The HFHS – Chow reversion mice are 25-weeks old at cull, compared to 20-weeks old in other 3 groups. The results of this project demonstrate in Figure 4.2, that age itself is a factor in inducing BBB leakage. Therefore, it is possible that the intervention of dietary change could have greater effects on improving BBB integrity and neurovascular health than shown in our results here. Unfortunately, due to limitations of time and money constraints, this preliminary study was unable to compare the effects of dietary intervention against mice of the same age. However, any future studies assessing dietary intervention should be conducted against mice of the same age at cull to remove age as a cofounding factor and to allow for a better comparison of results. Overall, this will help to consolidate the true benefits of dietary changes on improving our neurovascular health.

Another limitation of this study was the use of a 2D *in vitro* model, in which the bEnd3 cells were used. The discussions from this project constantly highlight the complex and dynamic nature of the brain microenvironment due to the interaction of the different cells with each other and the 2D model here does not address the effect on astrocytes or microglia cells. Therefore, to truly mimic the BBB data *in vitro* the use of a 3D culture system needs to be employed. The most ideal 3D culture system would incorporate all the cells of the NVU including brain endothelial cells, astrocytes, pericytes, microglia and neurons (43). In reality, this is not so simple to re-create due to difficulties in set-up, maintenance and cost. Aside from co-culturing, dynamic models are also of benefit such as a cone-plate apparatus in order to place cells under shear stress. Shear stress which is generated by the flow of blood in physiological conditions also affects TJs, transporter expression and leukocyte adhesion (909,910). The best model to incorporate co-culture and shear stress conditions is a microfluidics model, which offers a more robust representation of the BBB (911–915). To date, a true model of the BBB which offers all these conditions has yet to be designed. Moreover, whilst some models are good for examining TJs, they are not sufficient for

measuring permeability and therefore choosing a single model that can be used to investigate a variety of effects often hinders the use of costly *in vitro* models (910). Therefore, the large majority of *in vitro* studies continue to be conducted in 2D models. Perhaps, one way to improve our 2D model in this project would be to use primary brain endothelial cell cultures in place of bEnd3 cells for stimulation with mouse serum.

Finally, a key method to consolidate the findings in this project would be to use human samples of serum and PBMCs to determine whether diabetic patients have raised inflammatory factors that mediate BBB damage *in vitro* that can induce leukocyte migration. Using 3D models, it would be beneficial to see examine the effects of microglia activation and cytokine production, and potentially on neuronal damage/apoptosis. To conduct such studies, samples would be required from healthy individuals, patients with MetS who are not on medication and patients with T2DM who are taking medications.

7.6 Closing remarks

In conclusion, the data from this thesis demonstrates a clear mechanistic link and pathway between metaflammation to neuroinflammation. The BBB is the interface between the peripheral and central systems, therefore structural, functional, metabolic, and immunological integrity of the BBB is of paramount importance for maintaining brain health.

The results collectively showcase how neurovascular complications of the brain microvasculature must also be termed under the umbrella of T2DM-related secondary complications. For many years, the brain has been considered a 'separate' entity from the rest of the body. However, research is accumulating which continually breaks this paradigm – from the discovery of the glymphatic system, the role of the gut-brain axis and the link of the peripheral to central immune systems, all indicating the need for a holistic approach to disease management.

As the way we live changes, so do the diseases we encounter. Therefore, our management and treatment of these conditions must also change with time. This requires constant review of disease management guidelines, public health measures and treatment strategies. The work here combines several different fields of science including inflammation, metabolism, immunology and pharmacology; giving us a new perspective on the way we view T2DM and neurological disorders. The ability of hrANXA1 and a dietary intervention to reduce and restore the metaflammation-induced BBB damage provides hope for the way we can slow down T3DM disease progression. The growing population of individuals with chronic conditions such as obesity, T2DM and dementias requires the need for innovative therapeutic approaches for healthcare. I hope the work here helps to serve to this need, with the hope that this work will be taken further for exploration into the benefit it can serve to provide for effective therapies and a better quality of life.

Importantly the discoveries here are only one piece of a larger puzzle, with many more avenues to explore being opened. The intricacies and details of our body and how it works continues to fascinate scientists around the world. Afterall, this is the beauty of science – there is always more to learn.

References

1. Eckel RH, Grundy SM, Zimmet PZ. The metabolic syndrome. In: Lancet. 2005. p. 1415–28.
2. Keller KB, Lemberg L. Obesity and the metabolic syndrome. Am J Crit Care [Internet]. 2003;12(2):167–70.
3. OMS/WHO. Cardiovascular diseases (CVD), fact sheet n°317 [Internet]. 2013.
4. Engelhardt B, Ransohoff RM. Capture, crawl, cross: The T cell code to breach the blood-brain barriers. Vol. 33, Trends in Immunology. 2012. p. 579–89.
5. Luchsinger JA, Reitz C, Patel B, Tang MX, Manly JJ, Mayeux R. Relation of diabetes to mild cognitive impairment. Arch Neurol [Internet]. 2007;64(4):570–5.
6. Arvanitakis Z, Wilson RS, Bienias JL, Evans DA, Bennett DA. Diabetes Mellitus and Risk of Alzheimer Disease and Decline in Cognitive Function. Arch Neurol [Internet]. 2004;61(5):661–6.
7. Ott A, Stolk RP, Van Harskamp F, Pols HAP, Hofman A, Breteler MMB. Diabetes mellitus and the risk of dementia: The Rotterdam Study. Neurology. 1999;53(9):1937–42.
8. Leibson CL, Rocca WA, Hanson VA, Cha R, Kokmen E, O'Brien PC, et al. Risk of dementia among persons with diabetes mellitus: A population- based cohort study. Am J Epidemiol [Internet]. 1997;145(4):301–8.
9. American Diabetes Association. Diagnosis and classification of diabetes mellitus. Diabetes Care. 2009;32(SUPPL. 1):43–8.
10. Ferreira LSS, Fernandes CS, Vieira MNN, De Felice FG. Insulin Resistance in Alzheimer's Disease [Internet]. Vol. 12, Frontiers in Neuroscience . 2018. p. 830.
11. Nguyen TT, Ta QTH, Nguyen TTD, Le TT, Vo VG. Role of Insulin Resistance in the Alzheimer's Disease Progression. Neurochem Res [Internet]. 2020;45(7):1481–91.
12. Nguyen TT, Ta QTH, Nguyen TKO, Nguyen TTD, Van Giau V. Type 3 Diabetes and Its Role Implications in Alzheimer's Disease. Int J Mol Sci [Internet]. 2020 Apr 30;21(9):3165.
13. Hill . J, Hicks . D, James . J, Vanterpool G, Gillespie C, Fox C, et al. Diabetes and Dementia Guidance on Practical Management [Internet]. 2013.
14. Vaamonde JG, Álvarez-Món MA. Obesity and overweight [Internet]. Vol. 13, Medicine (Spain). 2020. p. 767–76.
15. Kandel ER, Schwartz JH, Jessell TM, Siegelbaum SA, Hudspeth AJ. Principles of Neural Science, Fifth Edition [Internet]. Vol. 3, Neurology. 2014. 1760 p.
16. Abbott NJ, Patabendige AAK, Dolman DEM, Yusof SR, Begley DJ. Structure and function of the blood–brain barrier. Neurobiol Dis. 2009;37:13–25.

17. Openstax college. Anatomy and Physiology [Internet]. Anatomy and physiology. 2013. 207–242 p.
18. Langlet F, Mullier A, Bouret SG, Prevot V, Dehouck B. Tanycyte-like cells form a blood-cerebrospinal fluid barrier in the circumventricular organs of the mouse brain. J Comp Neurol. 2013;521(15):3389–405.
19. Mullier A, Bouret SG, Prevot V, Dehouck B. Differential distribution of tight junction proteins suggests a role for tanycytes in blood-hypothalamus barrier regulation in the adult mouse brain. J Comp Neurol. 2010;518(7):943–62.
20. Persidsky Y, Ramirez SH, Haorah J, Kanmogne GD. Blood-brain barrier: Structural components and function under physiologic and pathologic conditions. In: Journal of Neuroimmune Pharmacology. 2006. p. 223–36.
21. Abbott NJ, Rönnbäck L, Hansson E. Astrocyte–endothelial interactions at the blood–brain barrier. Nat Rev Neurosci [Internet]. 2006;7(1):41–53.
22. Weiss N, Miller F, Cazaubon S, Couraud PO. The blood-brain barrier in brain homeostasis and neurological diseases. Vol. 1788, Biochimica et Biophysica Acta - Biomembranes. 2009. p. 842–57.
23. Johanson CE, Stopa EG, McMillan PN. The blood-cerebrospinal fluid barrier: structure and functional significance. Vol. 686, Methods in molecular biology (Clifton, N.J.). 2011. p. 101–31.
24. Redzic ZB, Segal MB. The structure of the choroid plexus and the physiology of the choroid plexus epithelium. Vol. 56, Advanced Drug Delivery Reviews. 2004. p. 1695–716.
25. Wolburg H, Paulus W. Choroid plexus: Biology and pathology. Vol. 119, Acta Neuropathologica. 2010. p. 75–88.
26. Solár P, Zamani A, Kubíčková L, Dubový P, Joukal M. Choroid plexus and the blood-cerebrospinal fluid barrier in disease. Vol. 17, Fluids and Barriers of the CNS. 2020.
27. Brown PD, Davies SL, Speake T, Millar ID. Molecular mechanisms of cerebrospinal fluid production. Neuroscience. 2004;129(4):955–68.
28. Damkier HH, Brown PD, Praetorius J. Cerebrospinal fluid secretion by the choroid plexus. Vol. 93, Physiological Reviews. 2013. p. 1847–92.
29. Laterra J, Keep R, Betz LA, Goldstein GW. Blood—Cerebrospinal Fluid Barrier. In: Siegel GJ, Agranoff BW, Albers RW, et al., editors. Basic Neurochemistry: Molecular, Cellular and Medical Aspects. 6th edition. Siegel G, Agranoff B, Albers, RW, et al. E, editors. Philadelphia: Lippincott-Raven; 1999.

30. Falcão AM, Marques F, Novais A, Sousa N, Palha JA, Sousa JC. The path from the choroid plexus to the subventricular zone: Go with the flow! Vol. 6, Frontiers in Cellular Neuroscience. 2012.
31. Cserr HF. Physiology of the choroid plexus. Vol. 51, Physiological reviews. 1971. p. 273–311.
32. Sakka L, Coll G, Chazal J. Anatomy and physiology of cerebrospinal fluid. Vol. 128, European Annals of Otorhinolaryngology, Head and Neck Diseases. 2011. p. 309–16.
33. Brinker T, Stopa E, Morrison J, Klinge P. A new look at cerebrospinal fluid circulation. Vol. 11, Fluids and Barriers of the CNS. 2014.
34. Welch K, Friedman V. The cerebrospinal fluid valves. Brain. 1960;83(3):454–69.
35. Sørensen PS, Thomsen C, Gjerris F, Henriksen O. Brain water accumulation in pseudotumour cerebri demonstrated by MR-imaging of brain water self-diffusion. Acta Neurochir Suppl (Wien). 1990;51:363–5.
36. Cserr HF, Patlak CS. Secretion and Bulk Flow of Interstitial Fluid. In 1992. p. 245–61.
37. Abbott NJ. Evidence for bulk flow of brain interstitial fluid: Significance for physiology and pathology. Neurochem Int. 2004;45(4):545–52.
38. Shetty AK, Zanirati G. The interstitial system of the brain in health and disease. Vol. 11, Aging and Disease. 2020. p. 200–11.
39. Lei Y, Han H, Yuan F, Javeed A, Zhao Y. The brain interstitial system: Anatomy, modeling, in vivo measurement, and applications. Vol. 157, Progress in Neurobiology. 2017. p. 230–46.
40. Nicholson C, Kamali-Zare P, Tao L. Brain extracellular space as a diffusion barrier. Comput Vis Sci. 2011;14(7):309–25.
41. Milhorat TH. The third circulation revisited. J Neurosurg. 1975;42(6):628–45.
42. Rua R, McGavern DB. Advances in Meningeal Immunity. Vol. 24, Trends in Molecular Medicine. 2018. p. 542–59.
43. Weller RO, Sharp MM, Christodoulides M, Carare RO, Møllgård K. The meninges as barriers and facilitators for the movement of fluid, cells and pathogens related to the rodent and human CNS. Vol. 135, Acta Neuropathologica. 2018. p. 363–85.
44. Protasoni M, Sangiorgi S, Cividini A, Culuvaris GT, Tomei G, Dell'Orbo C, et al. The collagenic architecture of human dura mater: Laboratory investigation. J Neurosurg. 2011;114(6):1723–30.
45. Absinta M, Ha SK, Nair G, Sati P, Luciano NJ, Palisoc M, et al. Human and nonhuman primate meninges harbor lymphatic vessels that can be visualized noninvasively by MRI. Elife. 2017;6.

46. Hartman AL. Normal Anatomy of the Cerebrospinal Fluid Compartment. In: Cerebrospinal Fluid in Clinical Practice. 2009. p. 5–10.
47. Stock AD, Gelb S, Pasternak O, Ben-Zvi A, Putterman C. The blood brain barrier and neuropsychiatric lupus: new perspectives in light of advances in understanding the neuroimmune interface. Vol. 16, Autoimmunity Reviews. 2017. p. 612–9.
48. Miyata S. New aspects in fenestrated capillary and tissue dynamics in the sensory circumventricular organs of adult brains. Vol. 9, Frontiers in Neuroscience. 2015.
49. Langlet F, Levin BE, Luquet S, Mazzone M, Messina A, Dunn-Meynell AA, et al. Tanycytic VEGF-A boosts blood-hypothalamus barrier plasticity and access of metabolic signals to the arcuate nucleus in response to fasting. Cell Metab. 2013;17(4):607–17.
50. Noback CR. Circumventrikulare Organe des Zwischenhirns. (Circumventricular Organs of the Diencephalon). By M. Hofer. In: Primatologia (Handbook of Primatology), Edited by H. Hofer, A. H. Schultz, and D. Starck. Vol. 2, part 2, no. 13, pp. 104; 45 figures, S. Karger . Am J Phys Anthropol. 1966;24(2):285–6.
51. Gross PM, Weindl A. Peering through the windows of the brain. Vol. 7, Journal of Cerebral Blood Flow and Metabolism. 1987. p. 663–72.
52. Smith GM, Shine HD. Immunofluorescent labeling of tight junctions in the rat brain and spinal cord. Int J Dev Neurosci. 1992;10(5):387–92.
53. Petrov T, Howarth AG, Krukoff TL, Stevenson BR. Distribution of the tight junction-associated protein ZO-1 in circumventricular organs of the CNS. Mol Brain Res. 1994;21(3–4):235–46.
54. Nag S, Begley DJ. Blood-brain barrier, exchange of metabolites and gases. 1st ed. Kalimo H, editor. Pathology and Genetics. Cerebrovascular Diseases. Wiley-Blackwell; 2005. 22–29 p.
55. Purves D, Augustine G, Fitzpatrick D, Katz L, LaMantia A-S, McNamara J, et al. Neuroscience. 2nd edition: Autonomic Regulation of Cardiovascular Function. Sunderland (MA): Sinauer Associates; 2001. 2001. p. 109–12.
56. Cipolla M. Chapter 2 Anatomy and Ultrastructure The Microcirculation and the Neurovascular Unit. Boek. 2009;(Figure 4):1–11.
57. Hutchings M, Weller RO. Anatomical relationships of the pia mater to cerebral blood vessels in man. J Neurosurg. 1986;65(3):316–25.
58. Zhang ET, Inman CB, Weller RO. Interrelationships of the pia mater and the perivascular (Virchow-Robin) spaces in the human cerebrum. J Anat [Internet]. 1990;170:111–23.
59. Weller RO. Microscopic morphology and histology of the human meninges. Morphologie. 2005;89(284):22–34.

60. Morris AWJ, Sharp MMG, Albargothy NJ, Fernandes R, Hawkes CA, Verma A, et al. Vascular basement membranes as pathways for the passage of fluid into and out of the brain. Acta Neuropathol. 2016;131(5):725–36.
61. Charidimou A, Hong YT, Jäger HR, Fox Z, Aigbirhio FI, Fryer TD, et al. White Matter Perivascular Spaces on Magnetic Resonance Imaging: Marker of Cerebrovascular Amyloid Burden? Stroke. 2015;46(6):1707–9.
62. Pollock H, Hutchings M, Weller RO, Zhang ET. Perivascular spaces in the basal ganglia of the human brain: Their relationship to lacunes. J Anat. 1997;191(3):337–46.
63. Criswell TP, Sharp MMG, Dobson H, Finucane C, Weller RO, Verma A, et al. The structure of the perivascular compartment in the old canine brain: A case study. Clin Sci. 2017;131(22):2737–44.
64. Carare RO, Bernardes-Silva M, Newman TA, Page AM, Nicoll JAR, Perry VH, et al. Solutes, but not cells, drain from the brain parenchyma along basement membranes of capillaries and arteries: Significance for cerebral amyloid angiopathy and neuroimmunology. Neuropathol Appl Neurobiol. 2008;34(2):131–44.
65. Anatomy and Ultrastructure. Curator Museum J. 2010;25(3):234–55.
66. Rennels ML, Nelson E. Capillary innervation in the mammalian central nervous system: An electron microscopic demonstration. Am J Anat. 1975;144(2):233–41.
67. Kulik T, Kusano Y, Aronhime S, Sandler AL, Winn HR. Regulation of cerebral vasculature in normal and ischemic brain. Neuropharmacology. 2008;55(3):281–8.
68. Kiliç T, Akakin A. Anatomy of cerebral veins and sinuses. Vol. 23, Frontiers of neurology and neuroscience. 2008. p. 4–15.
69. Yamazaki Y, Kanekiyo T. Blood-brain barrier dysfunction and the pathogenesis of alzheimer's disease. Vol. 18, International Journal of Molecular Sciences. 2017.
70. Jessen NA, Munk ASF, Lundgaard I, Nedergaard M. The Glymphatic System: A Beginner's Guide. Neurochem Res. 2015;40(12):2583–99.
71. Engelhardt B, Carare RO, Bechmann I, Flügel A, Laman JD, Weller RO. Vascular, glial, and lymphatic immune gateways of the central nervous system. Vol. 132, Acta Neuropathologica. 2016. p. 317–38.
72. ERBSLOH F, BERNSMEIER A, HILLESHEIM H. [The glucose consumption of the brain & its dependence on the liver]. Arch Psychiatr Nervenkr Z Gesamte Neurol Psychiatr [Internet]. 1958;196(6):611–26.
73. Camandola S, Mattson MP. Brain metabolism in health, aging, and neurodegeneration. EMBO J. 2017;36(11):1474–92.

74. Fantini S, Sassaroli A, Tgavalekos KT, Kornbluth J. Cerebral blood flow and autoregulation: current measurement techniques and prospects for noninvasive optical methods. Neurophotonics. 2016;3(3):031411.
75. Zlokovic B V. Neurovascular pathways to neurodegeneration in Alzheimer's disease and other disorders. Nat Rev Neurosci. 2011;12(12):723–8.
76. Iadecola C. Neurovascular regulation in the normal brain and in Alzheimer's disease. Nat Rev Neurosci. 2004;5(5):347–60.
77. Kisler K, Nelson AR, Montagne A, Zlokovic B V. Cerebral blood flow regulation and neurovascular dysfunction in Alzheimer disease. Vol. 18, Nature Reviews Neuroscience. 2017. p. 419–34.
78. Attwell D, Buchan AM, Charpak S, Lauritzen M, MacVicar BA, Newman EA. Glial and neuronal control of brain blood flow. Vol. 468, Nature. 2010. p. 232–43.
79. Kleinfeld D, Mitra PP, Helmchen F, Denk W. Fluctuations and stimulus-induced changes in blood flow observed in individual capillaries in layers 2 through 4 of rat neocortex. Proc Natl Acad Sci U S A. 1998;95(26):15741–6.
80. Hudetz AG. Blood flow in the cerebral capillary network: A review emphasizing observations with intravital microscopy. Vol. 4, Microcirculation. 1997. p. 233–52.
81. Zonta M, Angulo MC, Gobbo S, Rosengarten B, Hossmann KA, Pozzan T, et al. Neuron-to-astrocyte signaling is central to the dynamic control of brain microcirculation. Nat Neurosci. 2003;6(1):43–50.
82. Kur J, Newman EA. Purinergic control of vascular tone in the retina. J Physiol. 2014;592(3):491–504.
83. Horiuchi T, Dietrich HH, Tsugane S, Dacey RG. Analysis of purine- and pyrimidine-induced vascular responses in the isolated rat cerebral arteriole. Am J Physiol - Hear Circ Physiol. 2001;280(2 49-2).
84. Lovatt D, Xu Q, Liu W, Takano T, Smith NA, Schnermann J, et al. Neuronal adenosine release, and not astrocytic ATP release, mediates feedback inhibition of excitatory activity. Proc Natl Acad Sci U S A. 2012;109(16):6265–70.
85. Mulligan SJ, MacVicar BA. Calcium transients in astrocyte endfeet cause cerebrovascular constrictions. Nature. 2004;431(7005):195–9.
86. Takano T, Tian GF, Peng W, Lou N, Libionka W, Han X, et al. Astrocyte-mediated control of cerebral blood flow. Nat Neurosci. 2006;9(2):260–7.
87. Iadecola C. The Pathobiology of Vascular Dementia. Vol. 80, Neuron. 2013. p. 844–66.
88. Risau W, Wolburg H. Development of the blood-brain barrier. Vol. 13, Trends in Neurosciences. 1990. p. 174–8.

89. Pardridge WM. Blood-brain barrier biology and methodology. J Neurovirol. 1999;5(6):556–69.
90. Ballabh P, Braun A, Nedergaard M. The blood-brain barrier: An overview: Structure, regulation, and clinical implications. Vol. 16, Neurobiology of Disease. 2004. p. 1–13.
91. Crone C, Olesen SP. Electrical resistance of brain microvascular endothelium. Brain Res. 1982;241(1):49–55.
92. Crone C, Christensen O. Electrical resistance of a capillary endothelium. J Gen Physiol [Internet]. 1981;77(4):349–71.
93. Hartsock A, Nelson WJ. Adherens and tight junctions: Structure, function and connections to the actin cytoskeleton. Vol. 1778, Biochimica et Biophysica Acta - Biomembranes. 2008. p. 660–9.
94. Schulze C, Firth JA. Immunohistochemical localization of adherens junction components in blood-brain barrier microvessels of the rat. J Cell Sci. 1993;104(3):773–82.
95. Vorbrodt AW, Dobrogowska DH. Molecular anatomy of intercellular junctions in brain endothelial and epithelial barriers: Electron microscopist's view. Vol. 42, Brain Research Reviews. 2003. p. 221–42.
96. Dejana E, Tournier-Lasserve E, Weinstein BM. The Control of Vascular Integrity by Endothelial Cell Junctions: Molecular Basis and Pathological Implications. Vol. 16, Developmental Cell. 2009. p. 209–21.
97. Tietz S, Engelhardt B. Brain barriers: Crosstalk between complex tight junctions and adherens junctions. Vol. 209, Journal of Cell Biology. 2015. p. 493–506.
98. Furuse M, Sasaki H, Tsukita S. Manner of interaction of heterogeneous claudin species within and between tight junction strands. J Cell Biol. 1999;147(4):891–903.
99. Hirase T, Staddon JM, Saitou M, Ando-Akatsuka Y, Itoh M, Furuse M, et al. Occludin as a possible determinant of tight junction permeability in endothelial cells. J Cell Sci. 1997;110 (Pt 1:1603–13.
100. Gonzalezmariscal L. Tight junction proteins. Prog Biophys Mol Biol. 2003;81(1):1–44.
101. Citi, S. & Cordenonsi M. Tight junction proteins. Biochim Biophys, Acta. 1998;1448(1):1–11.
102. Wolburg H, Lippoldt A. Tight junctions of the blood-brain barrier: Development, composition and regulation. Vol. 38, Vascular Pharmacology. 2002. p. 323–37.
103. Petty MA, Lo EH. Junctional complexes of the blood-brain barrier: Permeability changes in neuroinflammation. Vol. 68, Progress in Neurobiology. 2002. p. 311–23.

104. Steinberg MS, McNutt PM. Cadherins and their connections: Adhesion junctions have broader functions. Vol. 11, Current Opinion in Cell Biology. 1999. p. 554–60.
105. Nagafuchi A. Molecular architecture of adherens junctions. Curr Opin Cell Biol [Internet]. 2001;13(5):600–3.
106. Taddei A, Giampietro C, Conti A, Orsenigo F, Breviario F, Pirazzoli V, et al. Endothelial adherens junctions control tight junctions by VE-cadherin-mediated upregulation of claudin-5. Nat Cell Biol [Internet]. 2008;10(8):923–34.
107. Huber F, Boire A, López MP, Koenderink GH. Cytoskeletal crosstalk: When three different personalities team up. Vol. 32, Current Opinion in Cell Biology. 2015. p. 39–47.
108. Wong a J, Pollard TD, Herman IM. Actin filament stress fibers in vascular endothelial cells in vivo. Science (80-) [Internet]. 1983;219(February):867–9.
109. Small J V, Rottner K, Kaverina I. Functional design in the actin cytoskeleton. Curr Opin Cell Biol. 1999;11(1):54–60.
110. Prasain N, Stevens T. The actin cytoskeleton in endothelial cell phenotypes. Microvasc Res. 2009;77(1):53–63.
111. Lai CH, Kuo KH, Leo JM. Critical role of actin in modulating BBB permeability. Vol. 50, Brain Research Reviews. 2005. p. 7–13.
112. Shasby DM, Ries DR, Shasby SS, Winter MC. Histamine stimulates phosphorylation of adherens junction proteins and alters their link to vimentin. Am J Physiol Lung Cell Mol Physiol [Internet]. 2002;282(6):L1330–8.
113. Stamatovic S, Keep R, Andjelkovic A. Brain Endothelial Cell-Cell Junctions: How to “Open” the Blood Brain Barrier. Curr Neuropharmacol [Internet]. 2008;6(3):179–92.
114. Cardoso FL, Brites D, Brito MA. Looking at the blood-brain barrier: Molecular anatomy and possible investigation approaches. Vol. 64, Brain Research Reviews. 2010. p. 328–63.
115. Worzfeld T, Schwaninger M. Apicobasal polarity of brain endothelial cells. J Cereb Blood Flow Metab [Internet]. 2016;36(2):340–62.
116. Bendayan R, Ronaldson PT, Gingras D, Bendayan M. In situ localization of P-glycoprotein (ABCB1) in human and rat brain. J Histochem Cytochem [Internet]. 2006;54(10):1159–67.
117. Tewes BJ, Galla HJ. Lipid polarity in brain capillary endothelial cells. Endothelium [Internet]. 2001;8(3):207–20.
118. Hudson N, Powner MB, Sarker MH, Burgoyne T, Campbell M, Ockrim ZK, et al. Differential apicobasal VEGF signaling at vascular blood-neural barriers. Dev Cell. 2014;30(5):541–52.

119. Boado RJ, Li JY, Pardridge WM. Developmental Regulation of the Rabbit Blood-Brain Barrier LAT1 Large Neutral Amino Acid Transporter mRNA and Protein. Pediatr Res. 2004;55(4):557–60.
120. Boado RJ, Li JY, Nagaya M, Zhang C, Pardridge WM. Selective expression of the large neutral amino acid transporter at the blood-brain barrier. Proc Natl Acad Sci U S A [Internet]. 1999;96(21):12079–84.
121. Dallas S, Miller DS, Bendayan R. Multidrug resistance-associated proteins: expression and function in the central nervous system. Pharmacol Rev. 2006;58(2):140–61.
122. Dauchy S, Dutheil F, Weaver RJ, Chassoux F, Daumas-Duport C, Couraud PO, et al. ABC transporters, cytochromes P450 and their main transcription factors: Expression at the human blood-brain barrier. J Neurochem. 2008;107(6):1518–28.
123. Begley DJ. ABC transporters and the blood-brain barrier. Curr Pharm Des [Internet]. 2004;10(12):1295–312.
124. Demeule M, Régina A, Jodoin J, Laplante A, Dagenais C, Berthelet F, et al. Drug transport to the brain: Key roles for the efflux pump P-glycoprotein in the blood-brain barrier. Vol. 38, Vascular Pharmacology. 2002. p. 339–48.
125. Liu Y, Hu M. P-glycoprotein and bioavailability-implication of polymorphism. Clin Chem Lab Med [Internet]. 2000;38(9):877–81.
126. Engelhardt B, Wolburg H. Mini review: Transendothelial migration of leukocytes: Through the front door or around the side of the house? Vol. 34, European Journal of Immunology. 2004. p. 2955–63.
127. Kety SS. The circulation and energy metabolism of the brain. Vol. 9, Clinical neurosurgery. 1963. 56–66 p.
128. Sokoloff L, Fitzgerald G, Kaufman E. Cerebral nutrition and energy metabolism. In: Nutrition and the brain determinants of the availability of nutrients to the brain. Wurtman R, Wurtman J, editors. New York: Raven; 1977. 83–139 p.
129. Maher F, Vannucci SJ, Simpson IA. Glucose transporter proteins in brain. FASEB J. 1994;8(13):1003–11.
130. Harr SD, Simonian N, Hyman BT. Functional alterations in alzheimers disease Decreased glucose transporter 3 immunoreactivity in the perforant pathway terminal zone. J Neuropathol Exp Neurol. 1995;54(1):38–41.
131. Landau SM, Harvey D, Madison CM, Reiman EM, Foster NL, Aisen PS, et al. Comparing predictors of conversion and decline in mild cognitive impairment. Neurology. 2010;75(3):230–8.

132. Kumagai AK, Dwyer KJ, Pardridge WM. Differential glycosylation of the GLUT1 glucose transporter in brain capillaries and choroid plexus. BBA - Biomembr. 1994;1193(1):24–30.
133. Banks WA, Owen JB, Erickson MA. Insulin in the brain: There and back again. Vol. 136, Pharmacology and Therapeutics. 2012. p. 82–93.
134. Huang X, Liu G, Guo J, Su ZQ. The PI3K/AKT pathway in obesity and type 2 diabetes. Vol. 14, International Journal of Biological Sciences. 2018. p. 1483–96.
135. James DE, Brown R, Navarro J, Pilch PF. Insulin-regulatable tissues express a unique insulin-sensitive glucose transport protein. Nature. 1988;333(6169):183–5.
136. McEwen BS, Reagan LP. Glucose transporter expression in the central nervous system: Relationship to synaptic function. Eur J Pharmacol. 2004;490(1–3):13–24.
137. Arnold SE, Arvanitakis Z, Macauley-Rambach SL, Koenig AM, Wang HY, Ahima RS, et al. Brain insulin resistance in type 2 diabetes and Alzheimer disease: Concepts and conundrums. Vol. 14, Nature Reviews Neurology. 2018. p. 168–81.
138. Havrankova J, Roth J, Brownstein M. Insulin receptors are widely distributed in the central nervous system of the rat. Nature. 1978;272(5656):827–9.
139. Wozniak M, Rydzewski B, Baker SP, Raizada MK. The cellular and physiological actions of insulin in the central nervous system. Vol. 22, Neurochemistry International. 1993. p. 1–10.
140. Unger J, McNeill TH, Moxley RT, White M, Moss A, Livingston JN. Distribution of insulin receptor-like immunoreactivity in the rat forebrain. Neuroscience. 1989;31(1):143–57.
141. Banks WA. Role of the blood-brain barrier in the evolution of feeding and cognition. Ann N Y Acad Sci. 2012;1264(1):13–9.
142. Woods SC, Porte D. The role of insulin as a satiety factor in the central nervous system. Vol. 10, Advances in metabolic disorders. 1983. p. 457–68.
143. Debons AF, Krimsky I, From A. A direct action of insulin on the hypothalamic satiety center. Am J Physiol. 1970;219(4):938–43.
144. Schwartz MW, Figlewicz DP, Baskin DG, Woods SC, Porte D. Insulin in the brain: A hormonal regulator of energy balance. Endocr Rev. 1992;13(3):387–414.
145. Liu H, Liu X, Jia L, Liu Y, Yang H, Wang G, et al. Insulin therapy restores impaired function and expression of P-glycoprotein in blood-brain barrier of experimental diabetes. Biochem Pharmacol. 2008;75(8):1649–58.
146. Shawahna R, Uchida Y, Declèves X, Ohtsuki S, Yousif S, Dauchy S, et al. Transcriptomic and quantitative proteomic analysis of transporters and drug metabolizing enzymes in freshly isolated human brain microvessels. Mol Pharm. 2011;8(4):1332–41.

147. Strazielle N, Ghersi-Egea JF. Factors affecting delivery of antiviral drugs to the brain. Rev Med Virol [Internet]. 2005;15(2):105–33.
148. Hotamisligil GS, Shargill NS, Spiegelman BM. Adipose expression of tumor necrosis factor-α: Direct role in obesity-linked insulin resistance. Science (80-). 1993;259(5091):87–91.
149. Benarroch EE. Blood-Brain barrier: Recent developments and clinical correlations. Neurology. 2012;78(16):1268–76.
150. Abrahamson DR. Recent studies on the structure and pathology of basement membranes. Vol. 149, The Journal of Pathology. 1986. p. 257–78.
151. Sorokin LM, Pausch F, Frieser M, Kröger S, Ohage E, Deutzmann R. Developmental regulation of the laminin chain suggests a role in epithelial and endothelial cell maturation. Dev Biol. 1997;189(2):285–300.
152. Yousif LF, Di Russo J, Sorokin L. Laminin isoforms in endothelial and perivascular basement membranes. Vol. 7, Cell Adhesion and Migration. 2013. p. 101–10.
153. Kapellos GE, Alexiou TS. Modeling Momentum and Mass Transport in Cellular Biological Media: From the Molecular to the Tissue Scale. In: Transport in Biological Media. 2013. p. 1–40.
154. Endo T. Dystroglycans. In: Comprehensive Glycoscience: From Chemistry to Systems Biology. 2007. p. 285–96.
155. Owens T, Bechmann I, Engelhardt B. Perivascular spaces and the two steps to neuroinflammation. Vol. 67, Journal of Neuropathology and Experimental Neurology. 2008. p. 1113–21.
156. Sixt M, Engelhardt B, Pausch F, Hallmann R, Wendler O, Sorokin LM. Endothelial cell laminin isoforms, laminins 8 and 10, play decisive roles in T cell recruitment across the blood-brain barrier in experimental autoimmune encephalomyelitis. J Cell Biol. 2001;153(5):933–45.
157. Kutuzov N, Flyvbjerg H, Lauritzen M. Contributions of the glycocalyx, endothelium, and extravascular compartment to the blood–brain Barrier. Proc Natl Acad Sci U S A. 2018;115(40):E9429–38.
158. Reitsma S, Slaaf DW, Vink H, Van Zandvoort MAMJ, Oude Egbrink MGA. The endothelial glycocalyx: Composition, functions, and visualization. Vol. 454, Pflugers Archiv European Journal of Physiology. 2007. p. 345–59.
159. Alphonsus CS, Rodseth RN. The endothelial glycocalyx: A review of the vascular barrier. Vol. 69, Anaesthesia. 2014. p. 777–84.
160. Yong VW. Metalloproteinases: Mediators of pathology and regeneration in the CNS. Vol. 6, Nature Reviews Neuroscience. 2005. p. 931–44.

161. Peppiatt CM, Howarth C, Mobbs P, Attwell D. Bidirectional control of CNS capillary diameter by pericytes. Nature. 2006;443(7112):700–4.
162. Armulik A, Genové G, Mäe M, Nisancioglu MH, Wallgard E, Niaudet C, et al. Pericytes regulate the blood-brain barrier. Nature. 2010;468(7323):557–61.
163. Sá-Pereira I, Brites D, Brito MA. Neurovascular unit: A focus on pericytes. Vol. 45, Molecular Neurobiology. 2012. p. 327–47.
164. Wolburg H. The Endothelial Frontier. In: Blood-Brain Barriers: From Ontogeny to Artificial Interfaces. 2007. p. 75–107.
165. Kacem K, Lacombe P, Seylaz J, Bonvento G. Structural organization of the perivascular astrocyte endfeet and their relationship with the endothelial glucose transporter: A confocal microscopy study. Glia. 1998;23(1):1–10.
166. Gordon GRJ, Mulligan SJ, MacVicar BA. Astrocyte control of the cerebrovasculature. Vol. 55, Glia. 2007. p. 1214–21.
167. Santello M, Calì C, Bezzi P. Gliotransmission and the tripartite synapse. Adv Exp Med Biol. 2012;970:307–31.
168. Farhy-Tselnicker I, Allen NJ. Astrocytes, neurons, synapses: A tripartite view on cortical circuit development. Vol. 13, Neural Development. 2018.
169. Figley CR, Stroman PW. The role(s) of astrocytes and astrocyte activity in neurometabolism, neurovascular coupling, and the production of functional neuroimaging signals. Vol. 33, European Journal of Neuroscience. 2011. p. 577–88.
170. Banerjee S, Bhat MA. Neuron-glial interactions in blood-brain barrier formation. Annu Rev Neurosci. 2007;30:235–58.
171. Ousman SS, Kubes P. Immune surveillance in the central nervous system. Vol. 15, Nature Neuroscience. 2012. p. 1096–101.
172. Helmut K, Hanisch UK, Noda M, Verkhratsky A. Physiology of microglia. Physiol Rev. 2011;91(2):461–553.
173. Ginhoux F, Lim S, Hoeffel G, Low D, Huber T. Origin and differentiation of microglia. Frontiers in Cellular Neuroscience. 2013.
174. Haruwaka K, Ikegami A, Tachibana Y, Ohno N, Konishi H, Hashimoto A, et al. Dual microglia effects on blood brain barrier permeability induced by systemic inflammation. Nat Commun. 2019;10(1).
175. Hanisch UK, Kettenmann H. Microglia: Active sensor and versatile effector cells in the normal and pathologic brain. Vol. 10, Nature Neuroscience. 2007. p. 1387–94.
176. Cross CE. Bloom and Fawcett: A Textbook of Histology. JAMA J Am Med Assoc. 1995;274(4):352.

177. Baumann N, Pham-Dinh D. Biology of oligodendrocyte and myelin in the mammalian central nervous system. Vol. 81, Physiological Reviews. 2001. p. 871–927.
178. Burdo JR, Martin J, Menzies SL, Dolan KG, Romano MA, Fletcher RJ, et al. Cellular distribution of iron in the brain of the Belgrade rat. Neuroscience. 1999;93(3):1189–96.
179. Uranova N, Orlovskaya D, Vikhreva O, Zimina I, Kolomeets N, Vostrikov V, et al. Electron microscopy of oligodendroglia in severe mental illness. Brain Res Bull. 2001;55(5):597–610.
180. Yokoo M, Sato E. Cumulus-oocyte complex interactions during oocyte maturation. Int Rev Cytol. 2004;235:251–91.
181. Descamps L, Coisne C, Dehouck B, Cecchelli R, Torpier G. Protective effect of glial cells against lipopolysaccharide-mediated blood-brain barrier injury. Glia. 2003;42(1):46–58.
182. Arai K, Lo EH. An oligovascular niche: Cerebral endothelial cells promote the survival and proliferation of oligodendrocyte precursor cells. J Neurosci. 2009;29(14):4351–5.
183. Hayakawa K, Seo JH, Pham LDD, Miyamoto N, Som AT, Guo S, et al. Cerebral endothelial derived vascular endothelial growth factor promotes the migration but not the proliferation of oligodendrocyte precursor cells in vitro. Neurosci Lett. 2012;513(1):42–6.
184. Seo JH, Maki T, Maeda M, Miyamoto N, Liang AC, Hayakawa K, et al. Oligodendrocyte precursor cells support blood-brain barrier integrity via TGF-β signaling. PLoS One. 2014;9(7).
185. Garwood J, Garcion E, Dobbertin A, Heck N, Calco V, Ffrench-Constant C, et al. The extracellular matrix glycoprotein Tenascin-C is expressed by oligodendrocyte precursor cells and required for the regulation of maturation rate, survival and responsiveness to platelet-derived growth factor. Eur J Neurosci. 2004;20(10):2524–40.
186. Larsen PH, Yong VW. The expression of matrix metalloproteinase-12 by oligodendrocytes regulates their maturation and morphological differentiation. J Neurosci. 2004;24(35):7597–603.
187. Rempe RG, Hartz AMS, Bauer B. Matrix metalloproteinases in the brain and blood-brain barrier: Versatile breakers and makers. Vol. 36, Journal of Cerebral Blood Flow and Metabolism. 2016. p. 1481–507.
188. Koehler RC, Gebremedhin D, Harder DR. Role of astrocytes in cerebrovascular regulation. Vol. 100, Journal of Applied Physiology. 2006. p. 307–17.

189. Muoio V, Persson PB, Sendeski MM. The neurovascular unit - concept review. Vol. 210, Acta Physiologica. 2014. p. 790–8.
190. Liao S, Padera TP. Lymphatic function and immune regulation in health and disease. Lymphat Res Biol. 2013;11(3):136–43.
191. Petrova T V., Koh GY. Biological functions of lymphatic vessels. Science (80-). 2020;369(6500).
192. Skandalakis JE, Skandalakis LJ, Skandalakis PN. Anatomy of the Lymphatics. Vol. 16, Surgical Oncology Clinics of North America. 2007. p. 1–16.
193. Alitalo K, Tammela T, Petrova T V. Lymphangiogenesis in development and human disease. Vol. 438, Nature. 2005. p. 946–53.
194. Olszewski WL. The lymphatic system in body homeostasis: physiological conditions. Vol. 1, Lymphatic research and biology. 2003.
195. Wang Z, Ying Z, Bosy-Westphal A, Zhang J, Heller M, Later W, et al. Evaluation of specific metabolic rates of major organs and tissues: Comparison between nonobese and obese women. Obesity. 2012;20(1):95–100.
196. Iliff JJ, Nedergaard M. Is there a cerebral lymphatic system? In: Stroke. 2013.
197. Iliff JJ, Wang M, Liao Y, Plogg BA, Peng W, Gundersen GA, et al. A paravascular pathway facilitates CSF flow through the brain parenchyma and the clearance of interstitial solutes, including amyloid β. Sci Transl Med. 2012;4(147).
198. Benveniste H, Liu X, Koundal S, Sanggaard S, Lee H, Wardlaw J. The Glymphatic System and Waste Clearance with Brain Aging: A Review. Gerontology. 2019;65(2):106–19.
199. Johnston M, Zakharov A, Papaiconomou C, Salmasi G, Armstrong D. Evidence of connections between cerebrospinal fluid and nasal lymphatic vessels in humans, non-human primates and other mammalian species. Cerebrospinal Fluid Res. 2004;1.
200. Murtha LA, Yang Q, Parsons MW, Levi CR, Beard DJ, Spratt NJ, et al. Cerebrospinal fluid is drained primarily via the spinal canal and olfactory route in young and aged spontaneously hypertensive rats. Fluids Barriers CNS. 2014;11(1).
201. Iliff JJ, Chen MJ, Plog BA, Zeppenfeld DM, Soltero M, Yang L, et al. Impairment of glymphatic pathway function promotes tau pathology after traumatic brain injury. J Neurosci. 2014;34(49):16180–93.
202. Sun BL, Wang L hua, Yang T, Sun J yi, Mao L lei, Yang M feng, et al. Lymphatic drainage system of the brain: A novel target for intervention of neurological diseases. Vols. 163–164, Progress in Neurobiology. 2018. p. 118–43.
203. Weller RO, Djuanda E, Yow HY, Carare RO. Lymphatic drainage of the brain and the pathophysiology of neurological disease. Vol. 117, Acta Neuropathologica. 2009. p. 1–14.

204. Albargothy NJ, Johnston DA, MacGregor-Sharp M, Weller RO, Verma A, Hawkes CA, et al. Convective influx/glymphatic system: tracers injected into the CSF enter and leave the brain along separate periarterial basement membrane pathways. Acta Neuropathol. 2018;136(1):139–52.
205. Hawkes CA, Härtig W, Kacza J, Schliebs R, Weller RO, Nicoll JA, et al. Perivascular drainage of solutes is impaired in the ageing mouse brain and in the presence of cerebral amyloid angiopathy. Acta Neuropathol. 2011;121(4):431–43.
206. Schley D, Carare-Nnadi R, Please CP, Perry VH, Weller RO. Mechanisms to explain the reverse perivascular transport of solutes out of the brain. J Theor Biol. 2006;238(4):962–74.
207. Arbel-Ornath M, Hudry E, Eikermann-Haerter K, Hou S, Gregory JL, Zhao L, et al. Interstitial fluid drainage is impaired in ischemic stroke and Alzheimer's disease mouse models. Acta Neuropathol. 2013;126(3):353–64.
208. Diem AK, Sharp MMG, Gatherer M, Bressloff NW, Carare RO, Richardson G. Arterial pulsations cannot drive intramural periarterial drainage: Significance for Aβ drainage. Front Neurosci. 2017;11(AUG).
209. Weller RO, Boche D, Nicoll JAR. Microvasculature changes and cerebral amyloid angiopathy in Alzheimer's disease and their potential impact on therapy. Vol. 118, Acta Neuropathologica. 2009. p. 87–102.
210. Hawkes CA, Jayakody N, Johnston DA, Bechmann I, Carare RO. Failure of perivascular drainage of β-amyloid in cerebral amyloid angiopathy. In: Brain Pathology. 2014. p. 396–403.
211. Dohgu S, Yamauchi A, Takata F, Naito M, Tsuruo T, Higuchi S, et al. Transforming growth factor-beta1 upregulates the tight junction and P-glycoprotein of brain microvascular endothelial cells. Cell Mol Neurobiol. 2004;24(3):491–7.
212. Patnaik R, Mohanty S, Sharma HS. Blockade of histamine H2 receptors attenuate blood-brain barrier permeability, cerebral blood flow disturbances, edema formation and cell reactions following hyperthermic brain injury in the rat. Acta Neurochir Suppl. 2000;76:535–9.
213. Reuss B, Dono R, Unsicker K. Functions of fibroblast growth factor (FGF)-2 and FGF-5 in astroglial differentiation and blood-brain barrier permeability: evidence from mouse mutants. J Neurosci. 2003;23(16):6404–12.
214. Zhang ZG, Zhang L, Jiang Q, Zhang R, Davies K, Powers C, et al. VEGF enhances angiogenesis and promotes blood-brain barrier leakage in the ischemic brain. J Clin Invest. 2000;106(7):829–38.

215. Gerwien H, Hermann S, Zhang X, Korpos E, Song J, Kopka K, et al. Imaging matrix metalloproteinase activity in multiple sclerosis as a specific marker of leukocyte penetration of the blood-brain barrier. Sci Transl Med. 2016;8(364):364ra152-364ra152.
216. Abbott NJ. Inflammatory mediators and modulation of blood-brain barrier permeability. Cell Mol Neurobiol. 2000;20(2):131–47.
217. Argaw AT, Zhang Y, Snyder BJ, Zhao M, Kopp N, Lee SC, et al. IL-1beta Regulates Blood-Brain Barrier Permeability via Reactivation of the Hypoxia-Angiogenesis Program. J Immunol. 2006;177(8):5574–84.
218. Dimitrijevic OB, Stamatovic SM, Keep RF, Andjelkovic A V. Effects of the chemokine CCL2 on blood-brain barrier permeability during ischemia-reperfusion injury. J Cereb blood flow Metab. 2006;26(6):797–810.
219. Lum H, Roebuck KA. Oxidant stress and endothelial cell dysfunction. Am J Physiol Cell Physiol. 2001;280(4):C719-41.
220. Garcia JG, Schaphorst KL. Regulation of endothelial cell gap formation and paracellular permeability. J InvestigMed. 1995;43(1081-5589 (Print)):117–26.
221. Stamatovic S, Keep R, Andjelkovic A. Brain Endothelial Cell-Cell Junctions: How to “Open” the Blood Brain Barrier. Curr Neuropharmacol. 2008;6(3):179–92.
222. Potter MD, Barbero S, Cheresh DA. Tyrosine phosphorylation of VE-cadherin prevents binding of p120- and β-catenin and maintains the cellular mesenchymal state. J Biol Chem. 2005;280(36):31906–12.
223. Morgan L, Shah B, Rivers LE, Barden L, Groom AJ, Chung R, et al. Inflammation and dephosphorylation of the tight junction protein occludin in an experimental model of multiple sclerosis. Neuroscience. 2007;147(3):664–73.
224. Clarke H, Soler AP, Mullin JM. Protein kinase C activation leads to dephosphorylation of occludin and tight junction permeability increase in LLC-PK1 epithelial cell sheets. J Cell Sci. 2000;113(18):3187–96.
225. Lohmann C, Krischke M, Wegener J, Galla HJ. Tyrosine phosphatase inhibition induces loss of blood-brain barrier integrity by matrix metalloproteinase-dependent and -independent pathways. Brain Res. 2004;995(2):184–96.
226. Hotulainen P, Lappalainen P. Stress fibers are generated by two distinct actin assembly mechanisms in motile cells. J Cell Biol. 2006;173(3):383–94.
227. Stamatovic SM, Keep RF, Kunkel SL, Andjelkovic A V. Potential role of MCP-1 in endothelial cell tight junction “opening”: signaling via Rho and Rho kinase. J Cell Sci. 2003;116(Pt 22):4615–28.

228. Zlokovic B V. The Blood-Brain Barrier in Health and Chronic Neurodegenerative Disorders. Vol. 57, Neuron. 2008. p. 178–201.
229. Medzhitov R. Inflammation 2010: New Adventures of an Old Flame. Vol. 140, Cell. 2010. p. 771–6.
230. Scarborough J, Majno G. The Healing Hand: Man and Wound in the Ancient World. Am Hist Rev. 1977;82(1):66.
231. Huang AL, Vita JA. Effects of systemic inflammation on endothelium-dependent vasodilation. Vol. 16, Trends in Cardiovascular Medicine. 2006. p. 15–20.
232. Serhan CN, Savill J. Resolution of inflammation: The beginning programs the end. Vol. 6, Nature Immunology. 2005. p. 1191–7.
233. Cray C, Zaias J, Altman NH. Acute phase response in animals: A review. Vol. 59, Comparative Medicine. 2009. p. 517–26.
234. Chakraborty A, Ghosh S, Mukhopadhyay P, Dinara SM, Bag A, Mahata MK, et al. Trapping effect analysis of AlGaN/InGaN/GaN Heterostructure by conductance frequency measurement [Internet]. Vol. XXXIII, MRS Proceedings. 2014. 81–87 p.
235. Zhou T, Hu Z, Yang S, Sun L, Yu Z, Wang G. Role of Adaptive and Innate Immunity in Type 2 Diabetes Mellitus. Vol. 2018, Journal of Diabetes Research. 2018.
236. Raphael I, Nalawade S, Eagar TN, Forsthuber TG. T cell subsets and their signature cytokines in autoimmune and inflammatory diseases. Vol. 74, Cytokine. 2015. p. 5–17.
237. Zhu J, Yamane H, Paul WE. Differentiation of effector CD4+ T cell populations. Annu Rev Immunol. 2010;28:445–89.
238. Sakaguchi S, Yamaguchi T, Nomura T, Ono M. Regulatory T Cells and Immune Tolerance. Vol. 133, Cell. 2008. p. 775–87.
239. Murphy JB. Conditions Determining the Transplantability of Tissues in the Brain. J Exp Med [Internet]. 1923;38(2):183–97.
240. Medawar PB. Immunity to homologous grafted skin; the fate of skin homografts transplanted to the brain, to subcutaneous tissue, and to the anterior chamber of the eye. Br J Exp Pathol. 1948;29(1):58–69.
241. Louveau A, Harris TH, Kipnis J. Revisiting the concept of CNS immune privilege. Trends Immunol. 2015;36(10):569–77.
242. Carson MJ, Doose JM, Melchior B, Schmid CD, Ploix CC. CNS immune privilege: Hiding in plain sight. Vol. 213, Immunological Reviews. 2006. p. 48–65.
243. Nourshargh S, Alon R. Leukocyte Migration into Inflamed Tissues. Vol. 41, Immunity. 2014. p. 694–707.

244. Muller W a. Mechanisms of leukocyte transendothelial migration. Annu Rev Pathol [Internet]. 2011;6:323–44.
245. Woodfin A, Voisin MB, Imhof BA, Dejana E, Engelhardt B, Nourshargh S. Endothelial cell activation leads to neutrophil transmigration as supported by the sequential roles of ICAM-2, JAM-A, and PECAM-1. Blood. 2009;113(24):6246–57.
246. Nourshargh S, Hordijk PL, Sixt M. Breaching multiple barriers: Leukocyte motility through venular walls and the interstitium. Nat Rev Mol Cell Biol [Internet]. 2010;11(5):366–78.
247. Ransohoff RM, Kivisäkk P, Kidd G. Three or more routes for leukocyte migration into the central nervous system. Vol. 3, Nature Reviews Immunology. 2003. p. 569–81.
248. Lai CH, Kuo KH. The critical component to establish in vitro BBB model: Pericyte. Vol. 50, Brain Research Reviews. 2005. p. 258–65.
249. Becher B, Prat A, Antel JP. Brain-immune connection: Immuno-regulatory properties of CNS-resident cells. Vol. 29, GLIA. 2000. p. 293–304.
250. Wu C, Ivars F, Anderson P, Hallmann R, Vestweber D, Nilsson P, et al. Endothelial basement membrane laminin alpha5 selectively inhibits T lymphocyte extravasation into the brain. Nat Med. 2009;15(5):519–27.
251. Agrawal S, Anderson P, Durbeej M, Van Rooijen N, Ivars F, Opdenakker G, et al. Dystroglycan is selectively cleaved at the parenchymal basement membrane at sites of leukocyte extravasation in experimental autoimmune encephalomyelitis. J Cell Biol. 2006;173(2):1007–19.
252. Pagenstecher A, Lassmann S, Carson MJ, Kincaid CL, Stalder AK, Campbell IL. Astrocyte-Targeted Expression of IL-12 Induces Active Cellular Immune Responses in the Central Nervous System and Modulates Experimental Allergic Encephalomyelitis. J Immunol [Internet]. 2000;164(9):4481–92.
253. Boztug K, Carson MJ, Pham-Mitchell N, Asensio VC, DeMartino J, Campbell IL. Leukocyte Infiltration, But Not Neurodegeneration, in the CNS of Transgenic Mice with Astrocyte Production of the CXC Chemokine Ligand 10. J Immunol [Internet]. 2002;169(3):1505–15.
254. Krakowski ML, Owens T. Naive T lymphocytes traffic to inflamed central nervous system, but require antigen recognition for activation. Eur J Immunol. 2000;30(4):1002–9.
255. de Vos AF, van Meurs M, Brok HP, Boven LA, Hintzen RQ, van der Valk P, et al. Transfer of Central Nervous System Autoantigens and Presentation in Secondary Lymphoid Organs. J Immunol. 2002;169(10):5415–23.

256. Cserr HF, Harling-Berg CJ, Knopf PM. Drainage of Brain Extracellular Fluid into Blood and Deep Cervical Lymph and its Immunological Significance. Vol. 2, Brain Pathology. 1992. p. 269–76.
257. Barker CF, Billingham RE. Immunologically privileged sites and tissues. In: Corneal Graft Failure. 2008. p. 79–104.
258. Stoll G, Jander S, Schroeter M. Detrimental and beneficial effects of injury-induced inflammation and cytokine expression in the nervous system. Vol. 513, Advances in Experimental Medicine and Biology. 2002. p. 87–113.
259. Dirnagl U, Iadecola C, Moskowitz MA. Pathobiology of ischaemic stroke: An integrated view. Trends Neurosci. 1999;22(9):391–7.
260. Aronowski J, Strong R, Grotta JC. Reperfusion injury: Demonstration of brain damage produced by reperfusion after transient focal ischemia in rats. J Cereb Blood Flow Metab. 1997;17(10):1048–56.
261. Planas AM, Gorina R, Chamorro Á. Signalling pathways mediating inflammatory responses in brain ischaemia. In: Biochemical Society Transactions. 2006. p. 1267–70.
262. Rosenberg GA, Estrada EY, Dencoff JE. Matrix metalloproteinases and TIMPs are associated with blood-brain barrier opening after reperfusion in rat brain. Stroke. 1998;29(10):2189–95.
263. Asahi M, Wang X, Mori T, Sumii T, Jung JC, Moskowitz MA, et al. Effects of matrix metalloproteinase-9 gene knock-out on the proteolysis of blood-brain barrier and white matter components after cerebral ischemia. J Neurosci. 2001;21(19):7724–32.
264. Brew K, Nagase H. The tissue inhibitors of metalloproteinases (TIMPs): An ancient family with structural and functional diversity. Vol. 1803, Biochimica et Biophysica Acta - Molecular Cell Research. 2010. p. 55–71.
265. Nagase H, Murphy G. Tailoring TIMPs for selective metalloproteinase inhibition. In: The Cancer Degradome: Proteases and Cancer Biology. 2008. p. 787–810.
266. Minagar A, Jy W, Jimenez JJ, Alexander JS. Multiple sclerosis as a vascular disease. Neurol Res [Internet]. 2006;28(3):230–5.
267. Boz C, Ozmenoglu M, Velioglu S, Kilinc K, Orem A, Alioglu Z, et al. Matrix metalloproteinase-9 (MMP-9) and tissue inhibitor of matrix metalloproteinase (TIMP-1) in patients with relapsing-remitting multiple sclerosis treated with interferon beta. Clin Neurol Neurosurg. 2006;108(2):124–8.

268. Minagar A, Ostanin D, Long AC, Jennings M, Kelley RE, Sasaki M, et al. Serum from patients with multiple sclerosis downregulates occludin and VE-cadherin expression in cultured endothelial cells [Internet]. Vol. 9, Multiple Sclerosis. 2003. p. 235–8.
269. Sheikh MH, Henson SM, Loiola RA, Mercurio S, Colamatteo A, Maniscalco GT, et al. Immuno-metabolic impact of the multiple sclerosis patients' sera on endothelial cells of the blood-brain barrier. J Neuroinflammation. 2020;17(1).
270. Lewandowski KC, Banach E, Bieńkiewicz M, Lewiński A. Matrix metalloproteinases in type 2 diabetes and non-diabetic controls: Effects of short-term and chronic hyperglycaemia. Arch Med Sci. 2011;7(2):294–303.
271. Alessandri AL, Sousa LP, Lucas CD, Rossi AG, Pinho V, Teixeira MM. Resolution of inflammation: Mechanisms and opportunity for drug development. Vol. 139, Pharmacology and Therapeutics. 2013. p. 189–212.
272. Blackwell GJ, Carnuccio R, Di Rosa M, Flower RJ, Parente L, Persico P. Macrocortin: a polypeptide causing the anti-phospholipase effect of glucocorticoids. Nature [Internet]. 1980;287(5778):147–9.
273. Bena S, Brancaleone V, Wang JM, Perretti M, Flower RJ. Annexin A1 interaction with the FPR2/ALX receptor: Identification of distinct domains and downstream associated signaling. J Biol Chem. 2012;287(29):24690–7.
274. Solito E, Nuti S, Parente L. Dexamethasone-induced translocation of lipocortin (annexin) 1 to the cell membrane of U-937 cells. In: British Journal of Pharmacology. 1994. p. 347–8.
275. Flower RJ, Blackwell GJ. Anti-inflammatory steroids induce biosynthesis of a phospholipase A2 inhibitor which prevents prostaglandin generation. Nature. 1979;278:456–9.
276. Hannon R, Croxtall JD, Getting SJ, Roviezzo F, Yona S, Paul-Clark MJ, et al. Aberrant inflammation and resistance to glucocorticoids in annexin 1-/- mouse. FASEB J. 2003;17(2):253–5.
277. Parente L, Solito E. Annexin 1: More than an anti-phospholipase protein. Vol. 53, Inflammation Research. 2004. p. 125–32.
278. Solito E, De Coupade C, Canaider S, Goulding NJ, Perretti M. Transfection of annexin 1 in monocytic cells produces a high degree of spontaneous and stimulated apoptosis associated with caspase-3 activation. Br J Pharmacol. 2001;133:217–28.
279. McArthur S, Cristante E, Paterno M, Christian H, Roncaroli F, Gillies GE, et al. Annexin A1: A Central Player in the Anti-Inflammatory and Neuroprotective Role of Microglia. J Immunol [Internet]. 2010;185(10):6317–28.

280. De Coupade C, Solito E, Levine JD. Dexamethasone enhances interaction of endogenous Annexin 1 with L-selectin and triggers shedding of L-selectin in the monocytic cell line U-937. Br J Pharmacol. 2003;140(1):133–45.
281. Oliani SM, Paul-Clark MJ, Christian HC, Flower RJ, Perretti M. Neutrophil interaction with inflamed postcapillary venule endothelium alters annexin 1 expression. Am J Pathol. 2001;158(2):603–15.
282. Walther A, Riehemann K, Gerke V. A novel ligand of the formyl peptide receptor: annexin I regulates neutrophil extravasation by interacting with the FPR. Mol Cell. 2000;5(5):831–40.
283. Solito E, De Coupade C, Canaider S, Goulding NJ, Perretti M. Transfection of annexin 1 in monocytic cells produces a high degree of spontaneous and stimulated apoptosis associated with caspase-3 activation. Br J Pharmacol. 2001;133(2):217–28.
284. Wang HG, Pathan N, Ethell IM, Krajewski S, Yamaguchi Y, Shibasaki F, et al. Ca2+-Induced Apoptosis Through Calcineurin Dephosphorylation of BAD. Science (80-) [Internet]. 1999;284(5412):339–43.
285. Solito E, Kamal A, Russo-Marie F, Buckingham JC, Marullo S, Perretti M. A novel calcium-dependent proapoptotic effect of annexin 1 on human neutrophils. FASEB J. 2003;17(11):1544–6.
286. Arur S, Uche UE, Rezaul K, Fong M, Scranton V, Cowan AE, et al. Annexin I is an endogenous ligand that mediates apoptotic cell engulfment. Vol. 4, Developmental Cell. 2003. p. 587–98.
287. Goulding NJ, Godolphin JL, Sharland PR, Maddison PJ, Sampson M, Peers SH, et al. Anti-inflammatory lipocortin 1 production by peripheral blood leucocytes in response to hydrocortisone. Lancet. 1990;335(8703):1416–8.
288. D'Acquisto F, Merghani A, Lecona E, Rosignoli G, Raza K, Buckley CD, et al. Annexin-1 modulates T-cell activation and differentiation. Blood. 2007;109(3):1095–102.
289. Paschalidis N, Iqbal AJ, Maione F, Wood EG, Perretti M, Flower RJ, et al. Modulation of experimental autoimmune encephalomyelitis by endogenous Annexin A1. J Neuroinflammation. 2009;6.
290. Yang YH, Song W, Deane JA, Kao W, Ooi JD, Ngo D, et al. Deficiency of Annexin A1 in CD4 + T Cells Exacerbates T Cell–Dependent Inflammation . J Immunol. 2013;190(3):997–1007.
291. Yazid S, Gardner PJ, Carvalho L, Chu CJ, Flower RJ, Solito E, et al. Annexin-A1 restricts Th17 cells and attenuates the severity of autoimmune disease. J Autoimmun. 2015;58:1–11.

292. Kamal AM, Smith SF, De Silva Wijayasinghe M, Solito E, Corrigan CJ. An annexin 1 (ANXA1)-derived peptide inhibits prototype antigen-driven human T cell Th1 and Th2 responses in vitro. Clin Exp Allergy. 2001;31(7):1116–25.
293. Colamatteo A, Maggioli E, Azevedo Loiola R, Hamid Sheikh M, Calì G, Bruzzese D, et al. Reduced Annexin A1 Expression Associates with Disease Severity and Inflammation in Multiple Sclerosis Patients. J Immunol. 2019;203(7):1753–65.
294. Sheikh MH, Solito E. Annexin A1: Uncovering the many talents of an old protein. Vol. 19, International Journal of Molecular Sciences. 2018.
295. Fava RA, McKanna J, Cohen S. Lipocortin I (p35) is abundant in a restricted number of differentiated cell types in adult organs. J Cell Physiol. 1989;141(2):284–93.
296. McArthur S, Loiola RA, Maggioli E, Errede M, Solito E, Virgintino D. The restorative role of annexin A1 at the blood–brain barrier. Fluids Barriers CNS. 2016;13(1):17.
297. Cristante E, McArthur S, Mauro C, Maggioli E, Romero IA, Wylezinska-Arridge M, et al. Identification of an essential endogenous regulator of blood-brain barrier integrity, and its pathological and therapeutic implications. Proc Natl Acad Sci U S A [Internet]. 2013;110(3):832–41.
298. Alvarez JI, Cayrol R, Prat A. Disruption of central nervous system barriers in multiple sclerosis. Vol. 1812, Biochimica et Biophysica Acta - Molecular Basis of Disease. 2011. p. 252–64.
299. Langer-Gould A, Atlas SW, Green AJ, Bollen AW, Pelletier D. Progressive multifocal leukoencephalopathy in a patient treated with natalizumab. N Engl J Med. 2005;353(4):375–81.
300. Gavins FNE, Dalli J, Flower RJ, Granger DN, Perretti M. Activation of the annexin 1 counter-regulatory circuit affords protection in the mouse brain microcirculation. FASEB J [Internet]. 2007;21(8):1751–8.
301. Relton JK, Strijbos PJ, O'Shaughnessy CT, Carey F, Forder RA, Tilders FJ, et al. Lipocortin-1 is an endogenous inhibitor of ischemic damage in the rat brain. J Exp Med. 1991;174(2):305–10.
302. Fetler L, Amigorena S. Brain under surveillance: The microglia patrol. Vol. 309, Science. 2005. p. 392–3.
303. Ransohoff RM, Perry VH. Microglial physiology: Unique stimuli, specialized responses. Annu Rev Immunol [Internet]. 2009;27(1):119–45.
304. Ries M, Loiola R, Shah UN, Gentleman SM, Solito E, Sastre M. The anti-inflammatory Annexin A1 induces the clearance and degradation of the amyloid-β peptide. J Neuroinflammation. 2016;13(1).

305. Luo ZZ, Gao Y, Sun N, Zhao Y, Wang J, Tian B, et al. Enhancing the interaction between annexin-1 and formyl peptide receptors regulates microglial activation to protect neurons from ischemia-like injury. J Neuroimmunol. 2014;276(1–2):24–36.
306. Chatterjee S, Khunti K, Davies MJ. Type 2 diabetes. Vol. 389, The Lancet. 2017. p. 2239–51.
307. Rother KI. Diabetes treatment - Bridging the divide. N Engl J Med. 2007;356(15):1499–501.
308. Hu FB, Manson JE, Stampfer MJ, Colditz G, Liu S, Solomon CG, et al. Diet, lifestyle, and the risk of type 2 diabetes mellitus in women. N Engl J Med. 2001;345(11):790–7.
309. Forouzanfar MH, Afshin A, Alexander LT, Biryukov S, Brauer M, Cercy K, et al. Global, regional, and national comparative risk assessment of 79 behavioural, environmental and occupational, and metabolic risks or clusters of risks, 1990–2015: a systematic analysis for the Global Burden of Disease Study 2015. Lancet. 2016;388(10053):1659–724.
310. Chamnan P, Simmons RK, Forouhi NG, Luben RN, Khaw KT, Wareham NJ, et al. Incidence of type 2 diabetes using proposed HbA1c diagnostic criteria in the european prospective investigation of cancer-norfolk cohort: Implications for preventive strategies. Diabetes Care. 2011;34(4):950–6.
311. Pendlebury M. Facts and Truth-making. Topoi. 2010;29(2):137–45.
312. Siddiqi K. Non-communicable diseases. Public Heal An action Guid to Improv Heal. 2010;
313. Hannah Ritchie, Max Roser. Causes of Death - Our World in Data [Internet]. Our World in Data. 2020.
314. Nathan AJ, Scobell A. How China sees America. Foreign Aff. 2012;91(5).
315. NCD Risk Factor Collaboration. Worldwide trends in diabetes since 1980: a pooled analysis of 751 population-based studies with 4.4 million participants. Lancet (London, England). 2016;387(10027):1513–30.
316. Chawla A, Chawla R, Jaggi S. Microvasular and macrovascular complications in diabetes mellitus: Distinct or continuum? Vol. 20, Indian Journal of Endocrinology and Metabolism. 2016. p. 546–53.
317. Cade WT. Diabetes-related microvascular and macrovascular diseases in the physical therapy setting. Phys Ther. 2008;88(11):1322–35.
318. Fowler MJ. Microvascular and macrovascular complications of diabetes. Clin Diabetes. 2011;29(3):116–22.
319. Facts F, Diabetes ON. National Diabetes Fact Sheet , 2011. Centers Dis Control Prev US Dep Heal Hum Serv. 2011;CS217080A(Division of Diabetes Translation):1–12.

320. Tabit CE, Chung WB, Hamburg NM, Vita JA. Endothelial dysfunction in diabetes mellitus: Molecular mechanisms and clinical implications. Vol. 11, Reviews in Endocrine and Metabolic Disorders. 2010. p. 61–74.
321. Heiss C, Rodriguez-Mateos A, Kelm M. Central Role of eNOS in the Maintenance of Endothelial Homeostasis. Antioxidants Redox Signal. 2015;22(14):1230–42.
322. Widlansky ME, Gokce N, Keaney JF, Vita JA. The clinical implications of endothelial dysfunction. J Am Coll Cardiol. 2003;42(7):1149–60.
323. Sessa WC. eNos at a glance. Vol. 117, Journal of Cell Science. 2004. p. 2427–9.
324. Dimmeler S, Fleming I, Fisslthaler B, Hermann C, Busse R, Zeiher AM. Activation of nitric oxide synthase in endothelial cells by Akt- dependent phosphorylation. Nature. 1999;399(6736):601–5.
325. Zeng G, Nystrom FH, Ravichandran L V., Cong LN, Kirby M, Mostowski H, et al. Roles for insulin receptor, PI3-kinase, and Akt in insulin-signaling pathways related to production of nitric oxide in human vascular endothelial cells. Circulation. 2000;101(13):1539–45.
326. Muniyappa R, Montagnani M, Koh KK, Quon MJ. Cardiovascular actions of insulin. Vol. 28, Endocrine Reviews. 2007. p. 463–91.
327. Kim JA, Montagnani M, Kwang KK, Quon MJ. Reciprocal relationships between insulin resistance and endothelial dysfunction: Molecular and pathophysiological mechanisms. Circulation. 2006;113(15):1888–904.
328. Nacci C, Tarquinio M, Montagnani M. Molecular and clinical aspects of endothelial dysfunction in diabetes. Intern Emerg Med. 2009;4(2):107–16.
329. Wheatcroft SB, Williams IL, Shah AM, Kearney MT. Pathophysiological implications of insulin resistance on vascular endothelial function. Vol. 20, Diabetic Medicine. 2003. p. 255–68.
330. Meigs JB, Larson MG, Fox CS, Keaney JF, Vasan RS, Benjamin EJ. Association of oxidative stress, insulin resistance, and diabetes risk phenotypes: The Framingham Offspring Study. Diabetes Care. 2007;30(10):2529–35.
331. Keaney JF, Larson MG, Vasan RS, Wilson PWF, Lipinska I, Corey D, et al. Obesity and systemic oxidative stress: Clinical correlates of oxidative stress in the Framingham study. Arterioscler Thromb Vasc Biol. 2003;23(3):434–9.
332. Ting HH, Timimi FK, Boles KS, Creager SJ, Ganz P, Creager MA. Vitamin C improves endothelium-dependent vasodilation in patients with non-insulin-dependent diabetes mellitus. J Clin Invest. 1996;97(1):22–8.
333. Quintero M, Colombo SL, Godfrey A, Moncada S. Mitochondria as signaling organelles in the vascular endothelium. Proc Natl Acad Sci U S A. 2006;103(14):5379–84.

334. Yu T, Robotham JL, Yoon Y. Increased production of reactive oxygen species in hyperglycemic conditions requires dynamic change of mitochondrial morphology. Proc Natl Acad Sci U S A. 2006;103(8):2653–8.
335. Parish R, Petersen KF. Mitochondrial dysfunction and type 2 diabetes. Curr Diab Rep. 2005;5(3):177–83.
336. El Midaoui A, De Champlain J. Prevention of hypertension, insulin resistance, and oxidative stress by α-lipoic acid. Hypertension. 2002;39(2 I):303–7.
337. Hotamisligil GS, Arner P, Caro JF, Atkinson RL, Spiegelman BM. Increased adipose tissue expression of tumor necrosis factor-α in human obesity and insulin resistance. J Clin Invest [Internet]. 1995;95(5):2409–15.
338. Kern PA, Saghizadeh M, Ong JM, Bosch RJ, Deem R, Simsolo RB. The expression of tumor necrosis factor in human adipose tissue: Regulation by obesity, weight loss, and relationship to lipoprotein lipase. J Clin Invest. 1995;95(5):2111–9.
339. Wellen KE, Hotamisligil GS. Inflammation, stress, and diabetes. Vol. 115, Journal of Clinical Investigation. 2005. p. 1111–9.
340. Monteiro R, Azevedo I. Chronic inflammation in obesity and the metabolic syndrome. Mediators Inflamm. 2010;2010.
341. Dandona P, Weinstock R, Thusu K, Abdel-Rahman E, Aljada A, Wadden T. Tumor necrosis factor-α in sera of obese patients: Fall with weight loss. J Clin Endocrinol Metab. 1998;83(8):2907–10.
342. Vozarova B, Weyer C, Hanson K, Tataranni PA, Bogardus C, Pratley RE. Circulating interleukin-6 in relation to adiposity, insulin action, and insulin secretion. Obes Res. 2001;9(7):414–7.
343. Festa A, D'Agostino R, Howard G, Mykkänen L, Tracy RP, Haffner SM. Chronic subclinical inflammation as part of the insulin resistance syndrome: The insulin resistance atherosclerosis study (IRAS). Circulation. 2000;102(1):42–7.
344. Caputo T, Gilardi F, Desvergne B. From chronic overnutrition to metaflammation and insulin resistance: adipose tissue and liver contributions. Vol. 591, FEBS Letters. 2017. p. 3061–88.
345. de Zeeuw P, Wong BW, Carmeliet P. Metabolic adaptations in diabetic endothelial cells. Circ J. 2015;79(5):934–41.
346. Eelen G, De Zeeuw P, Simons M, Carmeliet P. Endothelial cell metabolism in normal and diseased vasculature. Vol. 116, Circulation Research. 2015. p. 1231–44.
347. Qatanani M, Lazar MA. Mechanisms of obesity-associated insulin resistance: Many choices on the menu. Vol. 21, Genes and Development. 2007. p. 1443–55.

348. Cusi K, Maezono K, Osman A, Pendergrass M, Patti ME, Pratipanawatr T, et al. Insulin resistance differentially affects the PI 3-kinase- and MAP kinase-mediated signaling in human muscle. J Clin Invest. 2000;105(3):311–20.
349. Yamagishi SI, Maeda S, Matsui T, Ueda S, Fukami K, Okuda S. Role of advanced glycation end products (AGEs) and oxidative stress in vascular complications in diabetes. Biochim Biophys Acta - Gen Subj. 2012;1820(5):663–71.
350. Dias IHK, Griffiths HR. Oxidative stress in diabetes - circulating advanced glycation end products, lipid oxidation and vascular disease. Ann Clin Biochem. 2014;51(2):125–7.
351. Rudich A, Kanety H, Bashan N. Adipose stress-sensing kinases: linking obesity to malfunction. Vol. 18, Trends in Endocrinology and Metabolism. 2007. p. 291–9.
352. Yuan M, Konstantopoulos N, Lee J, Hansen L, Li ZW, Karin M, et al. Reversal of obesity- and diet-induced insulin resistance with salicylates or targeted disruption of Ikkβ. Science (80-). 2001;293(5535):1673–7.
353. Hundal RS, Petersen KF, Mayerson AB, Randhawa PS, Inzucchi S, Shoelson SE, et al. Mechanism by which high-dose aspirin improves glucose metabolism in type 2 diabetes. J Clin Invest. 2002;109(10):1321–6.
354. Fernández-Real JM, Pickup JC. Innate immunity, insulin resistance and type 2 diabetes. Trends Endocrinol Metab. 2008;19(1):10–6.
355. Xu M, Liu PP, Li H. Innate immune signaling and its role in metabolic and cardiovascular diseases. Physiol Rev. 2019;99(1):893–948.
356. Hotamisligil GS. Inflammation and metabolic disorders. Vol. 444, Nature. 2006. p. 860–7.
357. Hotamisligil GS. Inflammation, metaflammation and immunometabolic disorders. Vol. 542, Nature. 2017. p. 177–85.
358. Dalmas E. Role of innate immune cells in metabolism: from physiology to type 2 diabetes. Vol. 41, Seminars in Immunopathology. 2019. p. 531–45.
359. Mosser DM, Edwards JP. Exploring the full spectrum of macrophage activation. Vol. 8, Nature Reviews Immunology. 2008. p. 958–69.
360. Fujisaka S, Usui I, Bukhari A, Ikutani M, Oya T, Kanatani Y, et al. Regulatory mechanisms for adipose tissue M1 and M2 macrophages in diet-induced obese mice. Diabetes. 2009;58(11):2574–82.
361. Lumeng CN, Delproposto JB, Westcott DJ, Saltiel AR. Phenotypic switching of adipose tissue macrophages with obesity is generated by spatiotemporal differences in macrophage subtypes. Diabetes. 2008;57(12):3239–46.

362. Weisberg SP, McCann D, Desai M, Rosenbaum M, Leibel RL, Ferrante AW. Obesity is associated with macrophage accumulation in adipose tissue. J Clin Invest. 2003;112(12):1796–808.
363. Xia C, Rao X, Zhong J. Role of T Lymphocytes in Type 2 Diabetes and Diabetes-Associated Inflammation. Vol. 2017, Journal of Diabetes Research. 2017.
364. Nekoua MP, Fachinan R, Atchamou AK, Nouatin O, Amoussou-Guenou D, Amoussou-Guenou MK, et al. Modulation of immune cells and Th1/Th2 cytokines in insulin-treated type 2 diabetes mellitus. Afr Health Sci. 2016;16(3):712–24.
365. Francisco CO, Catai AM, Moura-Tonello SCG, Arruda LCM, Lopes SLB, Benze BG, et al. Cytokine profile and lymphocyte subsets in type 2 diabetes. Brazilian J Med Biol Res. 2016;49(4).
366. Harford KA, Reynolds CM, McGillicuddy FC, Roche HM. Fats, inflammation and insulin resistance: Insights to the role of macrophage and T-cell accumulation in adipose tissue. Proc Nutr Soc. 2011;70(4):408–17.
367. Zhang C, Xiao C, Wang P, Xu W, Zhang A, Li Q, et al. The alteration of Th1/Th2/Th17/Treg paradigm in patients with type 2 diabetes mellitus: Relationship with diabetic nephropathy. Hum Immunol. 2014;75(4):289–96.
368. Zeng C, Shi X, Zhang B, Liu H, Zhang L, Ding W, et al. The imbalance of Th17/Th1/Tregs in patients with type 2 diabetes: Relationship with metabolic factors and complications. J Mol Med. 2012;90(2):175–86.
369. Golubovskaya V, Wu L. Different subsets of T cells, memory, effector functions, and CAR-T immunotherapy. Vol. 8, Cancers. 2016.
370. Mauro C, Smith J, Cucchi D, Coe D, Fu H, Bonacina F, et al. Obesity-Induced Metabolic Stress Leads to Biased Effector Memory CD4+ T Cell Differentiation via PI3K p110δ-Akt-Mediated Signals. Cell Metab. 2017;25(3):593–609.
371. Rattik S, Engelbertsen D, Wigren M, Ljungcrantz I, Östling G, Persson M, et al. Elevated circulating effector memory T cells but similar levels of regulatory T cells in patients with type 2 diabetes mellitus and cardiovascular disease. Diabetes Vasc Dis Res. 2019;16(3):270–80.
372. Nishimura S, Manabe I, Nagasaki M, Eto K, Yamashita H, Ohsugi M, et al. CD8+ effector T cells contribute to macrophage recruitment and adipose tissue inflammation in obesity. Nat Med. 2009;15(8):914–20.
373. Srenathan U, Steel K, Taams LS. IL-17+ CD8+ T cells: Differentiation, phenotype and role in inflammatory disease. Immunol Lett. 2016;178:20–6.
374. Rausch ME, Weisberg S, Vardhana P, Tortoriello D V. Obesity in C57BL/6J mice is characterized by adipose tissue hypoxia and cytotoxic T-cell infiltration. Int J Obes. 2008;32(3):451–63.

375. DeFuria J, Belkina AC, Jagannathan-Bogdan M, Snyder-Cappione J, Carr JD, Nersesova YR, et al. B cells promote inflammation in obesity and type 2 diabetes through regulation of T-cell function and an inflammatory cytokine profile. Proc Natl Acad Sci U S A. 2013;110(13):5133–8.
376. Winer DA, Winer S, Shen L, Wadia PP, Yantha J, Paltser G, et al. B cells promote insulin resistance through modulation of T cells and production of pathogenic IgG antibodies. Nat Med. 2011;17(5):610–7.
377. Blackshaw S, Eliasson MJL, Sawa A, Watkins CC, Krug D, Gupta A, et al. Species, strain and developmental variations in hippocampal neuronal and endothelial nitric oxide synthase clarify discrepancies in nitric oxide-dependent synaptic plasticity. Neuroscience. 2003;119(4):979–90.
378. Wang F, Cao Y, Ma L, Pei H, Rausch WD, Li H. Dysfunction of Cerebrovascular Endothelial Cells: Prelude to Vascular Dementia. Front Aging Neurosci. 2018;10.
379. Kahn SE, Cooper ME, Del Prato S. Pathophysiology and treatment of type 2 diabetes: Perspectives on the past, present, and future. Vol. 383, The Lancet. 2014. p. 1068–83.
380. Tenenbaum A, Fisman EZ, Motro M. Metabolic syndrome and type 2 diabetes mellitus: Focus on peroxisome proliferator activated receptors (PPAR). Cardiovasc Diabetol. 2003;2.
381. Samuel VT, Liu ZX, Qu X, Elder BD, Bilz S, Befroy D, et al. Mechanism of hepatic insulin resistance in non-alcoholic fatty liver disease. J Biol Chem. 2004;279(31):32345–53.
382. Kim YB, Shulman GI, Kahn BB. Fatty acid infusion selectively impairs insulin action on Akt1 and protein kinase C Nζ but not on glycogen synthase kinase-3. J Biol Chem. 2002;277(36):32915–22.
383. Ruotolo G, Howard B V. Dyslipidemia of the metabolic syndrome. Curr Cardiol Rep. 2002;4(6):494–500.
384. Kolovou GD, Anagnostopoulou KK, Cokkinos D V. Pathophysiology of dyslipidaemia in the metabolic syndrome. Vol. 81, Postgraduate Medical Journal. 2005. p. 358–66.
385. Yanai H, Tomono Y, Ito K, Furutani N, Yoshida H, Tada N. The underlying mechanisms for development of hypertension in the metabolic syndrome. Vol. 7, Nutrition Journal. 2008.
386. Nation DA, Sweeney MD, Montagne A, Sagare AP, D'Orazio LM, Pachicano M, et al. Blood–brain barrier breakdown is an early biomarker of human cognitive dysfunction. Vol. 25, Nature Medicine. 2019. p. 270–6.

387. Montagne A, Barnes SR, Sweeney MD, Halliday MR, Sagare AP, Zhao Z, et al. Blood-Brain barrier breakdown in the aging human hippocampus. Neuron. 2015;85(2):296–302.
388. World Health Organization. Dementia. Fact sheet N°362. May 2017. World Health Organization. 2017.
389. WHO. WHO | 10 facts on dementia. Who. 2019.
390. Ho L, Qin W, Pompl PN, Xiang Z, Wang J, Zhao Z, et al. Diet-induced insulin resistance promotes amyloidosis in a transgenic mouse model of Alzheimer's disease. FASEB J. 2004;18(7):902–4.
391. Qiu WQ, Walsh DM, Ye Z, Vekrellis K, Zhang J, Podlisny MB, et al. Insulin-degrading enzyme regulates extracellular levels of amyloid β- protein by degradation. J Biol Chem. 1998;273(49):32730–8.
392. Pugazhenthi S, Qin L, Reddy PH. Common neurodegenerative pathways in obesity, diabetes, and Alzheimer's disease. Biochim Biophys Acta - Mol Basis Dis. 2017;1863(5):1037–45.
393. Freiherr J, Hallschmid M, Frey WH, Brünner YF, Chapman CD, Hölscher C, et al. Intranasal insulin as a treatment for alzheimer's disease: A review of basic research and clinical evidence. Vol. 27, CNS Drugs. 2013. p. 505–14.
394. Carvalho C, Cardoso S, Correia SC, Santos RX, Santos MS, Baldeiras I, et al. Metabolic alterations induced by sucrose intake and Alzheimer's disease promote similar brain mitochondrial abnormalities. Diabetes. 2012;61(5):1234–42.
395. Carvalho C, Machado N, Mota PC, Correia SC, Cardoso S, Santos RX, et al. Type 2 diabetic and alzheimer's disease mice present similar behavioral, cognitive, and vascular anomalies. J Alzheimer's Dis. 2013;35(3):623–35.
396. Steen E, Terry BM, Rivera EJ, Cannon JL, Neely TR, Tavares R, et al. Impaired insulin and insulin-like growth factor expression and signaling mechanisms in Alzheimer's disease - Is this type 3 diabetes? J Alzheimer's Dis. 2005;7(1):63–80.
397. Filous AR, Silver J. "Targeting astrocytes in CNS injury and disease: A translational research approach." Vol. 144, Progress in Neurobiology. 2016. p. 173–87.
398. Rodríguez JJ, Olabarria M, Chvatal A, Verkhratsky A. Astroglia in dementia and Alzheimer's disease. Vol. 16, Cell Death and Differentiation. 2009. p. 378–85.
399. Bushong EA, Martone ME, Jones YZ, Ellisman MH. Protoplasmic astrocytes in CA1 stratum radiatum occupy separate anatomical domains. J Neurosci. 2002;22(1):183–92.
400. Oberheim NA, Wang X, Goldman S, Nedergaard M. Astrocytic complexity distinguishes the human brain. Trends Neurosci. 2006;29(10):547–53.

401. Pekny M, Nilsson M. Astrocyte activation and reactive gliosis. Vol. 50, Glia. 2005. p. 427–34.
402. Price BR, Norris CM, Sompol P, Wilcock DM. An emerging role of astrocytes in vascular contributions to cognitive impairment and dementia. Vol. 144, Journal of Neurochemistry. 2018. p. 644–50.
403. Engelhardt S, Patkar S, Ogunshola OO. Cell-specific blood-brain barrier regulation in health and disease: A focus on hypoxia. Vol. 171, British Journal of Pharmacology. 2014. p. 1210–30.
404. Lu DY, Yu WH, Yeh WL, Tang CH, Leung YM, Wong KL, et al. Hypoxia-induced matrix metalloproteinase-13 expression in astrocytes enhances permeability of brain endothelial cells. J Cell Physiol. 2009;220(1):163–73.
405. Argaw AT, Asp L, Zhang J, Navrazhina K, Pham T, Mariani JN, et al. Astrocyte-derived VEGF-A drives blood-brain barrier disruption in CNS inflammatory disease. J Clin Invest. 2012;122(7):2454–68.
406. Mani N, Khaibullina A, Krum JM, Rosenstein JM. Astrocyte growth effects of vascular endothelial growth factor (VEGF) application to perinatal neocortical explants: Receptor mediation and signal transduction pathways. Exp Neurol. 2005;192(2):394–406.
407. Schachtrup C, Ryu JK, Helmrick MJ, Vagena E, Galanakis DK, Degen JL, et al. Fibrinogen triggers astrocyte scar formation by promoting the availability of active TGF-β after vascular damage. J Neurosci. 2010;30(17):5843–54.
408. Chen A, Akinyemi RO, Hase Y, Firbank MJ, Ndung'u MN, Foster V, et al. Frontal White matter hyperintensities, clasmatodendrosis and gliovascular abnormalities in ageing and post-stroke dementia. Brain. 2016;139(1):242–58.
409. Bridges LR, Andoh J, Lawrence AJ, Khoong CHL, Poon WW, Esiri MM, et al. Blood-brain barrier dysfunction and cerebral small vessel disease (arteriolosclerosis) in brains of older people. J Neuropathol Exp Neurol. 2014;73(11):1026–33.
410. Gadea A, Schinelli S, Gallo V. Endothelin-1 regulates astrocyte proliferation and reactive gliosis via a JNK/c-Jun signaling pathway. J Neurosci. 2008;28(10):2394–408.
411. Kersaitis C, Halliday GM, Kril JJ. Regional and cellular pathology in frontotemporal dementia: Relationship to stage of disease in cases with and without Pick bodies. Acta Neuropathol. 2004;108(6):515–23.
412. Norden DM, Godbout JP. Review: Microglia of the aged brain: Primed to be activated and resistant to regulation. Vol. 39, Neuropathology and Applied Neurobiology. 2013. p. 19–34.

413. Huber JD, Campos CR, Mark KS, Davis TP. Alterations in blood-brain barrier ICAM-1 expression and brain microglial activation after λ-carrageenan-induced inflammatory pain. Am J Physiol - Hear Circ Physiol. 2006;290(2).
414. Shibata M, Ohtani R, Ihara M, Tomimoto H. White matter lesions and glial activation in a novel mouse model of chronic cerebral hypoperfusion. In: Stroke. 2004. p. 2598–603.
415. Ryu JK, McLarnon JG. A leaky blood-brain barrier, fibrinogen infiltration and microglial reactivity in inflamed Alzheimer's disease brain. J Cell Mol Med. 2009;13(9 A):2911–25.
416. Truettner JS, Alonso OF, Dietrich WD. Influence of therapeutic hypothermia on matrix metalloproteinase activity after traumatic brain injury in rats. J Cereb Blood Flow Metab. 2005;25(11):1505–16.
417. Filley CM, Fields RD. White matter and cognition: Making the connection. Vol. 116, Journal of Neurophysiology. 2016. p. 2093–104.
418. Rosenberg GA, Wallin A, Wardlaw JM, Markus HS, Montaner J, Wolfson L, et al. Consensus statement for diagnosis of subcortical small vessel disease. Vol. 36, Journal of Cerebral Blood Flow and Metabolism. 2016. p. 6–25.
419. Wilkins A, Majed H, Layfield R, Compston A, Chandran S. Oligodendrocytes promote neuronal survival and axonal length by distinct intracellular mechanisms: A novel role for oligodendrocyte-derived glial cell line-derived neurotrophic factor. J Neurosci. 2003;23(12):4967–74.
420. Wolf G, Lotan A, Lifschytz T, Ben-Ari H, Merzel TK, Tatarskyy P, et al. Differentially severe cognitive effects of compromised cerebral blood flow in aged mice: Association with myelin degradation and microglia activation. Front Aging Neurosci. 2017;9(JUN).
421. Barker R, Wellington D, Esiri MM, Love S. Assessing white matter ischemic damage in dementia patients by measurement of myelin proteins. J Cereb Blood Flow Metab. 2013;33(7):1050–7.
422. Simpson JE, Fernando MS, Clark L, Ince PG, Matthews F, Forster G, et al. White matter lesions in an unselected cohort of the elderly: Astrocytic, microglial and oligodendrocyte precursor cell responses. Neuropathol Appl Neurobiol. 2007;33(4):410–9.
423. Blakemore WF. Pattern of remyelination in the CNS. Nature. 1974;249(5457):577–8.
424. Wood PM, Bunge RP. The origin of remyelinating cells in the adult central nervous system: The role of the mature oligodendrocyte. Glia. 1991;4(2):225–32.

425. Back SA, Gan X, Li Y, Rosenberg PA, Volpe JJ. Maturation-dependent vulnerability of oligodendrocytes to oxidative stress-induced death caused by glutathione depletion. J Neurosci. 1998;18(16):6241–53.
426. French HM, Reid M, Mamontov P, Simmons RA, Grinspan JB. Oxidative stress disrupts oligodendrocyte maturation. J Neurosci Res. 2009;87(14):3076–87.
427. Back SA, Tuohy TMF, Chen H, Wallingford N, Craig A, Struve J, et al. Hyaluronan accumulates in demyelinated lesions and inhibits oligodendrocyte progenitor maturation. Nat Med. 2005;11(9):966–72.
428. Miron VE, Boyd A, Zhao JW, Yuen TJ, Ruckh JM, Shadrach JL, et al. M2 microglia and macrophages drive oligodendrocyte differentiation during CNS remyelination. Nat Neurosci. 2013;16(9):1211–8.
429. Wang B, Han S. Inhibition of Inducible Nitric Oxide Synthase Attenuates Deficits in Synaptic Plasticity and Brain Functions Following Traumatic Brain Injury. Cerebellum. 2018;17(4):477–84.
430. Chaitanya G V., Schwaninger M, Alexander JS, Babu PP. Granzyme-b is involved in mediating post-ischemic neuronal death during focal cerebral ischemia in rat model. Neuroscience. 2010;165(4):1203–16.
431. Cheon SY, Cho KJ, Kim SY, Kam EH, Lee JE, Koo BN. Blockade of apoptosis signal-regulating kinase 1 attenuates matrix metalloproteinase 9 activity in brain endothelial cells and the subsequent apoptosis in neurons after ischemic injury. Front Cell Neurosci. 2016;10(SEP2016).
432. Ye L, Huang Y, Zhao L, Li Y, Sun L, Zhou Y, et al. IL-1β and TNF-α induce neurotoxicity through glutamate production: A potential role for neuronal glutaminase. J Neurochem. 2013;125(6):897–908.
433. Neniskyte U, Vilalta A, Brown GC. Tumour necrosis factor alpha-induced neuronal loss is mediated by microglial phagocytosis. FEBS Lett. 2014;588(17):2952–6.
434. Patel S, Rauf A. Adaptogenic herb ginseng (Panax) as medical food: Status quo and future prospects. Vol. 85, Biomedicine and Pharmacotherapy. 2017. p. 120–7.
435. Moraes JC, Coope A, Morari J, Cintra DE, Roman EA, Pauli JR, et al. High-fat diet induces apoptosis of hypothalamic neurons. PLoS One. 2009;4(4).
436. Price TO, Farr SA, Niehoff ML, Ercal N, Morley JE, Shah GN. Protective Effect of Topiramate on Hyperglycemia-Induced Cerebral Oxidative Stress, Pericyte Loss and Learning Behavior in Diabetic Mice. Int Libr diabetes Metab [Internet]. 2015;1(1):6–12.

437. Banks WA, Gray AM, Erickson MA, Salameh TS, Damodarasamy M, Sheibani N, et al. Lipopolysaccharide-induced blood-brain barrier disruption: Roles of cyclooxygenase, oxidative stress, neuroinflammation, and elements of the neurovascular unit. J Neuroinflammation [Internet]. 2015;12(1):223.
438. Harris AK, Hutchinson JR, Sachidanandam K, Johnson MH, Dorrance AM, Stepp DW, et al. Type 2 diabetes causes remodeling of cerebrovasculature via differential regulation of matrix metalloproteinases and collagen synthesis: Role of endothelin-1. Diabetes. 2005;54(9):2638–44.
439. Kanoski SE, Zhang Y, Zheng W, Davidson TL. The effects of a high-energy diet on hippocampal function and blood-brain barrier integrity in the rat. J Alzheimer's Dis. 2010;21(1):207–19.
440. Stranahan AM, Hao S, Dey A, Yu X, Baban B. Blood-brain barrier breakdown promotes macrophage infiltration and cognitive impairment in leptin receptor-deficient mice. J Cereb Blood Flow Metab [Internet]. 2016;36(12):2108–21.
441. Pannacciulli N, Del Parigi A, Chen K, Le DSNT, Reiman EM, Tataranni PA. Brain abnormalities in human obesity: A voxel-based morphometric study. Neuroimage. 2006;31(4):1419–25.
442. van Bloemendaal L, Ijzerman RG, ten Kulve JS, Barkhof F, Diamant M, Veltman DJ, et al. Alterations in white matter volume and integrity in obesity and type 2 diabetes. Metab Brain Dis. 2016;31(3):621–9.
443. Raji CA, Ho AJ, Parikshak NN, Becker JT, Lopez OL, Kuller LH, et al. Brain structure and obesity. Hum Brain Mapp. 2010;31(3):353–64.
444. Madden DJ, Bennett IJ, Burzynska A, Potter GG, Chen N kuei, Song AW. Diffusion tensor imaging of cerebral white matter integrity in cognitive aging. Biochim Biophys Acta - Mol Basis Dis [Internet]. 2012;1822(3):386–400.
445. Moran C, Phan TG, Chen J, Blizzard L, Beare R, Venn A, et al. Brain atrophy in type 2 diabetes: Regional distribution and influence on cognition. Diabetes Care. 2013;36(12):4036–42.
446. Hoogenboom WS, Marder TJ, Flores VL, Huisman S, Eaton HP, Schneiderman JS, et al. Cerebral white matter integrity and resting-state functional connectivity in middle-aged patients with type 2 diabetes. Diabetes. 2014;63(2):728–38.
447. Bierhaus A, Humpert PM, Morcos M, Wendt T, Chavakis T, Arnold B, et al. Understanding RAGE, the receptor for advanced glycation end products. Vol. 83, Journal of Molecular Medicine. 2005. p. 876–86.
448. Li XH, Lv BL, Xie JZ, Liu J, Zhou XW, Wang JZ. AGEs induce Alzheimer-like tau pathology and memory deficit via RAGE-mediated GSK-3 activation. Neurobiol Aging. 2012;33(7):1400–10.

449. Hsu TM, Kanoski SE. Blood-brain barrier disruption: Mechanistic links between western diet consumption and dementia. Vol. 6, Frontiers in Aging Neuroscience. 2014.
450. Rhea EM, Salameh TS, Logsdon AF, Hanson AJ, Erickson MA, Banks WA. Blood-Brain Barriers in Obesity. AAPS J [Internet]. 2017;19(4):921–30.
451. Murray AJ, Knight NS, Cochlin LE, McAleese S, Deacon RMJ, Rawlins JNP, et al. Deterioration of physical performance and cognitive function in rats with short-term high-fat feeding. FASEB J [Internet]. 2009;23(12):4353–60.
452. Kanoski SE, Davidson TL. Different Patterns of Memory Impairments Accompany Short- and Longer-Term Maintenance on a High-Energy Diet. J Exp Psychol Anim Behav Process [Internet]. 2010;36(2):313–9.
453. Morris MC. Nutritional determinants of cognitive aging and dementia. In: Proceedings of the Nutrition Society. 2012. p. 1–13.
454. Morris MC. Nutrition and risk of dementia: Overview and methodological issues. Ann N Y Acad Sci. 2016;1367(1):31–7.
455. Knowler WC, Barrett-Connor E, Fowler SE, Hamman RF, Lachin JM, Walker EA, et al. Reduction in the incidence of type 2 diabetes with lifestyle intervention or metformin. N Engl J Med. 2002;346(6):393–403.
456. Tuomilehto J, Lindström J, Eriksson JG, Valle TT, Hamäläinen H, Ianne-Parikka P, et al. Prevention of type 2 diabetes mellitus by changes in lifestyle among subjects with impaired glucose tolerance. N Engl J Med. 2001;344(18):1343–50.
457. Van Den Brink AC, Brouwer-Brolsma EM, Berendsen AAM, Van De Rest O. The Mediterranean, Dietary Approaches to Stop Hypertension (DASH), and Mediterranean-DASH Intervention for Neurodegenerative Delay (MIND) Diets Are Associated with Less Cognitive Decline and a Lower Risk of Alzheimer's Disease-A Review. Vol. 10, Advances in Nutrition. 2019. p. 1040–65.
458. Morris MC, Sacks F, Barnes L, Aggarwal N, Arfanakis K. MIND Diet Intervention and Cognitive Decline (MIND) [Internet]. 2017.
459. Thibault L. Animal Models of Dietary-Induced Obesity. In: Animal Models for the Study of Human Disease. 2013. p. 277–303.
460. Al-Goblan AS, Al-Alfi MA, Khan MZ. Mechanism linking diabetes mellitus and obesity. Diabetes, Metab Syndr Obes Targets Ther. 2014;7:587–91.
461. Fang JY, Lin CH, Huang TH, Chuang SY. In vivo rodent models of type 2 diabetes and their usefulness for evaluating flavonoid bioactivity. Vol. 11, Nutrients. 2019.
462. Zhang D, Christianson J, Liu ZX, Tian L, Choi CS, Neschen S, et al. Resistance to high-fat diet-induced obesity and insulin resistance in mice with very long-chain acyl-CoA dehydrogenase deficiency. Cell Metab [Internet]. 2010;11(5):402–11.

463. Sclafani A. Animal models of obesity: classification and characterization. Int J Obes. 1984;8(5):491–508.
464. Surwit RS, Kuhn CM, Cochrane C, McCubbin JA, Feinglos MN. Diet-induced type II diabetes in C57BL/6J mice. Diabetes. 1988;37(9):1163–7.
465. Collins S, Martin TL, Surwit RS, Robidoux J. Genetic vulnerability to diet-induced obesity in the C57BL/6J mouse: Physiological and molecular characteristics. Vol. 81, Physiology and Behavior. 2004. p. 243–8.
466. Bégin-Heick N. Of mice and women: the beta 3-adrenergic receptor leptin and obesity. Biochem Cell Biol [Internet]. 1996;74(5):615–22.
467. Wang C, Liao JK. A Mouse Model of Diet-Induced Obesity and Insulin Resistance. Methods Mol Biol [Internet]. 2012;821(5):1–11.
468. Heydemann A. An Overview of Murine High Fat Diet as a Model for Type 2 Diabetes Mellitus. Vol. 2016, Journal of Diabetes Research. 2016.
469. Buettner R, Schölmerich J, Bollheimer LC. High-fat diets: Modeling the metabolic disorders of human obesity in rodents. Vol. 15, Obesity. 2007. p. 798–808.
470. Heydemann A. An Overview of Murine High Fat Diet as a Model for Type 2 Diabetes Mellitus. Vol. 2016, Journal of Diabetes Research. 2016.
471. Grundy SM, Cleeman JI, Daniels SR, Donato KA, Eckel RH, Franklin BA, et al. Diagnosis and management of the metabolic syndrome: An American Heart Association/National Heart, Lung, and Blood Institute scientific statement. Circulation. 2005;112(17):2735–52.
472. Parekh PI, Petro AE, Tiller JM, Feinglos MN, Surwit RS. Reversal of diet-induced obesity and diabetes in C57BL/6J mice. Metabolism. 1998;47(9):1089–96.
473. Al Zoubi SY. Diabetes and the cardiac dysfunction caused by experimental sepsis [Internet]. Queen Mary, University of London; 2018.
474. Purvis GSD. The role of Annexin-A1 in the pathophysiology of diabetes. [Internet]. Queen Mary, University of London; 2017.
475. Hull W. Treating the Changing Face of Western Medicine: Pharmacological Interventions on the Jak/STAT Pathway in Diabetic Complications and its Relationship to Ageing [Internet]. Queen Mary, University of London; 2017.
476. Patel HB, Kornerup KN, Sampaio AL, D'Acquisto F, Seed MP, Girol AP, et al. The impact of endogenous annexin A1 on glucocorticoid control of inflammatory arthritis. Ann Rheum Dis [Internet]. 2012;71(11):1872–80.
477. Pederzoli-Ribeil M, Maione F, Cooper D, Al-Kashi A, Dalli J, Perretti M, et al. Design and characterization of a cleavage-resistant Annexin A1 mutant to control inflammation in the microvasculature. Blood. 2010;116(20):4288–96.

478. Kusters DHM, Chatrou ML, Willems BAG, De Saint-Hubert M, Bauwens M, Van Der Vorst E, et al. Pharmacological treatment with annexin A1 reduces atherosclerotic plaque burden in LDLR-/- mice on Western Type Diet. PLoS One. 2015;10(6).
479. Perretti M, Getting SJ, Solito E, Murphy PM, Gao JL. Involvement of the receptor for formylated peptides in the in vivo anti-migratory actions of annexin 1 and its mimetics. Am J Pathol. 2001;158(6):1969–73.
480. Gavins FNE, Yona S, Kamal AM, Flower RJ, Perretti M. Leukocyte antiadhesive actions of annexin 1: ALXR- and FPR-related anti-inflammatory mechanisms. Blood. 2003;101(10):4140–7.
481. Ernst S, Lange C, Wilbers A, Goebeler V, Gerke V, Rescher U. An Annexin 1 N-Terminal Peptide Activates Leukocytes by Triggering Different Members of the Formyl Peptide Receptor Family. J Immunol [Internet]. 2004;172(12):7669–76.
482. Solito E, Romero IA, Marullo S, Russo-Marie F, Weksler BB. Annexin 1 Binds to U937 Monocytic Cells and Inhibits Their Adhesion to Microvascular Endothelium: Involvement of the 4 1 Integrin. J Immunol [Internet]. 2000;165(3):1573–81.
483. Rodrigues-Lisoni FC, Mehemet DK, Peitl P, John CD, Tajara E, Buckingham JC, et al. In vitro and in vivo studies on CCR10 regulation by Annexin A1. FEBS Lett. 2006;580(5):1431–8.
484. Hayhoe RPG, Kamal AM, Solito E, Flower RJ, Cooper D, Perretti M. Annexin 1 and its bioactive peptide inhibit neutrophil-endothelium interactions under flow: Indication of distinct receptor involvement. Blood. 2006;107(5):2123–30.
485. Rodrigues-Lisoni FC, Oliani S, Buckingham J, Solito E, Tajara EH. Annexin A1: From gene organization to physiology. Vol. 2, Annexins. 2005.
486. Dunn TB. Normal and pathologic anatomy of the reticular tissue in laboratory mice, with a classification and discussion of neoplasms. J Natl Cancer Inst. 1954;14(6):1281–433.
487. Bowe JE, Franklin ZJ, Hauge-Evans AC, King AJ, Persaud SJ, Jones PM. Assessing glucose homeostasis in rodent models. J Endocrinol. 2014;222(3):13–25.
488. Muniyappa R, Lee S, Chen H, Quon MJ. Current approaches for assessing insulin sensitivity and resistance in vivo: Advantages, limitations, and appropriate usage. Vol. 294, American Journal of Physiology - Endocrinology and Metabolism. 2008.
489. Heikkinen S, Argmann CA, Champy MF, Auwerx J. Evaluation of glucose homeostasis. Vol. Chapter 29, Current protocols in molecular biology / edited by Frederick M. Ausubel ... [et al.]. 2007.
490. Andrikopoulos S, Blair AR, Deluca N, Fam BC, Proietto J. Evaluating the glucose tolerance test in mice. Am J Physiol - Endocrinol Metab. 2008;295(6).

491. Ayala JE, Bracy DP, McGuinness OP, Wasserman DH. Considerations in the design of hyperinsulinemic-euglycemic clamps in the conscious mouse. Diabetes. 2006;55(2):390–7.
492. Yen LF, Wei VC, Kuo EY, Lai TW. Distinct Patterns of Cerebral Extravasation by Evans Blue and Sodium Fluorescein in Rats. PLoS One. 2013;8(7).
493. Saria A, Lundberg JM. Evans blue fluorescence: quantitative and morphological evaluation of vascular permeability in animal tissues. J Neurosci Methods. 1983;8(1):41–9.
494. Yao L, Xue X, Yu P, Ni Y, Chen F. Evans Blue Dye: A Revisit of Its Applications in Biomedicine. Contrast Media Mol Imaging. 2018;2018.
495. Manaenko A, Chen H, Kammer J, Zhang JH, Tang J. Comparison Evans Blue injection routes: Intravenous versus intraperitoneal, for measurement of blood-brain barrier in a mice hemorrhage model. J Neurosci Methods. 2011;195(2):206–10.
496. Greenwood J, Luthert PJ, Pratt OE, Lantos PL. Hyperosmolar opening of the blood-brain barrier in the energy-depleted rat brain. Part 1. Permeability studies. J Cereb Blood Flow Metab [Internet]. 1988;8(1):9–15.
497. Radu M, Chernoff J. An in vivo assay to test blood vessel permeability. J Vis Exp. 2013;(73):e50062.
498. Morrey JD, Olsen AL, Siddharthan V, Motter NE, Wang H, Taro BS, et al. Increased blood-brain barrier permeability is not a primary determinant for lethality of West Nile virus infection in rodents. J Gen Virol [Internet]. 2008;89(2):467–73.
499. Montesano R, Pepper MS, Möhle-Steinlein U, Risau W, Wagner EF, Orci L. Increased proteolytic activity is responsible for the aberrant morphogenetic behavior of endothelial cells expressing the middle T oncogene. Cell. 1990;62(3):435–45.
500. Dehouck M -P, Jolliet-Riant P, Brée F, Fruchart J -C, Cecchelli R, Tillement J -P. Drug Transfer Across the Blood-Brain Barrier: Correlation Between In Vitro and In Vivo Models. J Neurochem [Internet]. 1992;58(5):1790–7.
501. Cristante E. Impact of peripheral inflammation in the brain : new roles for the anti-inflammatory molecule Annexin A1 [Internet]. Imperial College London; 2013.
502. Seahorse Bioscience Inc. User Manual: XF Glycolysis Stress Test kit. Kit User Guide. 2012.
503. Guide U. Agilent Seahorse XF Cell Mito Stress Test Kit. Agil Technol. 2017;103016–400.
504. King AJF. The use of animal models in diabetes research. Vol. 166, British Journal of Pharmacology. 2012. p. 877–94.
505. Speakman J, Hambly C, Mitchell S, Król E. Animal models of obesity. Vol. 8, Obesity Reviews. 2007. p. 55–61.

506. Chatzigeorgiou A, Halapas A, Kalafatakis K, Kamper EF. The use of animal models in the study of diabetes mellitus. Vol. 23, In Vivo. 2009. p. 245–58.
507. McCarthy MI. Genomics, type 2 diabetes, and obesity. Vol. 363, New England Journal of Medicine. 2010. p. 2339–50.
508. Leiter EH. Selecting the "right" mouse model for metabolic syndrome and type 2 diabetes research. Methods Mol Biol. 2009;560:1–17.
509. Hariri N, Gougeon R, Thibault L. A highly saturated fat-rich diet is more obesogenic than diets with lower saturated fat content. Nutr Res. 2010;30(9):632–43.
510. Kubant R, Poon AN, Sánchez-Hernández D, Domenichiello AF, Huot PSP, Pannia E, et al. A comparison of effects of lard and hydrogenated vegetable shortening on the development of high-fat diet-induced obesity in rats. Nutr Diabetes. 2015;5.
511. Collins S, Martin TL, Surwit RS, Robidoux J. Genetic vulnerability to diet-induced obesity in the C57BL/6J mouse: Physiological and molecular characteristics. Vol. 81, Physiology and Behavior. 2004. p. 243–8.
512. Purvis GSD, Collino M, Loiola RA, Baragetti A, Chiazza F, Brovelli M, et al. Identification of Annexina1 as an endogenous regulator of RhoA, and its role in the pathophysiology and experimental therapy of type-2 diabetes. Front Immunol. 2019;10(MAR).
513. Stamatovic SM, Keep RF, Andjelkovic A V. Brain endothelial cell-cell junctions: how to "open" the blood brain barrier. Curr Neuropharmacol [Internet]. 2008;6(3):179–92.
514. van Hinsbergh VW, van Nieuw Amerongen GP. Intracellular signalling involved in modulating human endothelial barrier function [Internet]. Vol. 200, J Anat. 2002. p. 549-60.
515. Soma T, Chiba H, Kato-Mori Y, Wada T, Yamashita T, Kojima T, et al. Thr 207 of claudin-5 is involved in size-selective loosening of the endothelial barrier by cyclic AMP. Exp Cell Res. 2004;300(1):202–12.
516. Kago T, Takagi N, Date I, Takenaga Y, Takagi K, Takeo S. Cerebral ischemia enhances tyrosine phosphorylation of occludin in brain capillaries. Biochem Biophys Res Commun. 2006;339(4):1197–203.
517. Bazzoni G. Endothelial Cell-to-Cell Junctions: Molecular Organization and Role in Vascular Homeostasis. Physiol Rev [Internet]. 2004;84(3):869–901.
518. Libby P. Inflammation in atherosclerosis. Nature [Internet]. 2002;420(6917):868–74.
519. Szmitko PE, Wang C-H, Weisel RD, de Almeida JR, Anderson TJ, Verma S. New markers of inflammation and endothelial cell activation: Part I. Circulation [Internet]. 2003;108(16):1917–23.

520. de Vries MA, Alipour A, Klop B, van de Geijn G-JM, Janssen HW, Njo TL, et al. Glucose-dependent leukocyte activation in patients with type 2 diabetes mellitus, familial combined hyperlipidemia and healthy controls. Metabolism [Internet]. 2015;64(2):213–7.
521. van Oostrom AJ, van Wijk JP, Sijmonsma TP, Rabelink TJ, Castro Cabezas M. Increased expression of activation markers on monocytes and neutrophils in type 2 diabetes. Neth J Med [Internet]. 2004;62(9):320–5.
522. Morigi M, Angioletti S, Imberti B, Donadelli R, Micheletti G, Figliuzzi M, et al. Leukocyte-endothelial interaction is augmented by high glucose concentrations and hyperglycemia in a NF-kB-dependent fashion. J Clin Invest. 1998;101(9):1905–15.
523. Yang H, Youm Y-H, Vandanmagsar B, Ravussin A, Gimble JM, Greenway F, et al. Obesity Increases the Production of Proinflammatory Mediators from Adipose Tissue T Cells and Compromises TCR Repertoire Diversity: Implications for Systemic Inflammation and Insulin Resistance. J Immunol [Internet]. 2010;185(3):1836–45.
524. Kintscher U, Hartge M, Hess K, Foryst-Ludwig A, Clemenz M, Wabitsch M, et al. T-lymphocyte infiltration in visceral adipose tissue: A primary event in adipose tissue inflammation and the development of obesity-mediated insulin resistance. Arterioscler Thromb Vasc Biol. 2008;28(7):1304–10.
525. Winer S, Chan Y, Paltser G, Truong D, Tsui H, Bahrami J, et al. Normalization of obesity-associated insulin resistance through immunotherapy. Nat Med [Internet]. 2009;15(8):921–9.
526. Feuerer M, Herrero L, Cipolletta D, Naaz A, Wong J, Nayer A, et al. Lean, but not obese, fat is enriched for a unique population of regulatory T cells that affect metabolic parameters. Nat Med [Internet]. 2009;15(8):930–9.
527. Marques CP, Cheeran MCJ, Palmquist JM, Hu S, Lokensgard JR. Microglia are the major cellular source of inducible nitric oxide synthase during experimental herpes encephalitis. J Neurovirol. 2008;14(3):229–38.
528. Mosser RE, Maulis MF, Moullé VS, Dunn JC, Carboneau BA, Arasi K, et al. High-fat diet-induced β-cell proliferation occurs prior to insulin resistance in C57Bl/6J male mice. Am J Physiol - Endocrinol Metab. 2015;308(7):E573–82.
529. Fraulob JC, Ogg-Diamantino R, Fernandes-Santos C, Aguila MB, Mandarim-de-Lacerda CA. A mouse model of metabolic syndrome: Insulin resistance, fatty liver and Non-Alcoholic Fatty Pancreas Disease (NAFPD) in C57BL/6 mice fed a high fat diet. J Clin Biochem Nutr. 2010;
530. Williams LM, Campbell FM, Drew JE, Koch C, Hoggard N, Rees WD, et al. The development of diet-induced obesity and glucose intolerance in C57Bl/6 mice on a high-fat diet consists of distinct phases. PLoS One. 2014;9(8).

531. Al Zoubi S, Chen J, Murphy C, Martin L, Chiazza F, Collotta D, et al. Linagliptin Attenuates the Cardiac Dysfunction Associated With Experimental Sepsis in Mice With Pre-existing Type 2 Diabetes by Inhibiting NF-κB. Front Immunol. 2018;9:2996.
532. Vaidya HB, Gangadaran S, Cheema SK. An obesogenic diet enriched with blue mussels protects against weight gain and lowers cholesterol levels in C57BL/6 mice. Nutr Res. 2017;46:31–7.
533. Hannocks MJ, Pizzo ME, Huppert J, Deshpande T, Abbott NJ, Thorne RG, et al. Molecular characterization of perivascular drainage pathways in the murine brain. J Cereb Blood Flow Metab. 2018;38(4):669–86.
534. Kazama T, Yaoita E, Ito M, Sato Y. Charge-selective permeability of dermo-epidermal junction: Tracer studies with cationic and anionic ferritins. J Invest Dermatol. 1988;91(6):560–5.
535. Rennke HG, Cotran RS, Venkatachalam MA. Role of molecular charge in glomerular permeability: Tracer studies with cationized ferritins. J Cell Biol. 1975;67(3):638–46.
536. Rennke HG, Venkatachalam MA. Glomerular permeability: in vivo tracer studies with polyanionic and polycationic ferritins. Kidney Int. 1977;11(1):44–53.
537. Brightman MW. The brain's interstitial clefts and their glial walls. J Neurocytol. 2002;31(8–9):595–603.
538. Hajiluian G, Nameni G, Shahabi P, Mesgari-Abbasi M, Sadigh-Eteghad S, Farhangi MA. Vitamin D administration, cognitive function, BBB permeability and neuroinflammatory factors in high-fat diet-induced obese rats. Int J Obes. 2017;41(4):639–44.
539. Davidson TL, Monnot A, Neal AU, Martin AA, Horton JJ, Zheng W. The effects of a high-energy diet on hippocampal-dependent discrimination performance and blood-brain barrier integrity differ for diet-induced obese and diet-resistant rats. Physiol Behav. 2012;107(1):26–33.
540. Freeman LR, Granholm ACE. Vascular changes in rat hippocampus following a high saturated fat and cholesterol diet. J Cereb Blood Flow Metab [Internet]. 2012;32(4):643–53.
541. Hernandez-Guillamon M, Mawhirt S, Blais S, Montaner J, Neubert TA, Rostagno A, et al. Sequential amyloid-β degradation by the matrix metalloproteases MMP-2 and MMP-9. J Biol Chem. 2015;290(24):15078–91.
542. Gardner J, Ghorpade A. Tissue Inhibitor of Metalloproteinase (TIMP)-1: The TIMPed Balance of Matrix Metalloproteinases in the Central Nervous System. Vol. 74, Journal of Neuroscience Research. 2003. p. 801–6.

543. Derosa G, D'Angelo A, Tinelli C, Devangelio E, Consoli A, Miccoli R, et al. Evaluation of metalloproteinase 2 and 9 levels and their inhibitors in diabetic and healthy subjects. Diabetes Metab. 2007;33(2):129–34.
544. Seung WL, Kyoung ES, Dong SS, Sung MA, Eun SH, Dae JK, et al. Alterations in peripheral blood levels of TIMP-1, MMP-2, and MMP-9 in patients with type-2 diabetes. Diabetes Res Clin Pract. 2005;69(2):175–9.
545. Chung AWY, Yang HHC, Sigrist MK, Brin G, Chum E, Gourlay WA, et al. Matrix metalloproteinase-2 and-9 exacerbate arterial stiffening and angiogenesis in diabetes and chronic kidney disease. Cardiovasc Res. 2009;84(3):494–504.
546. Loukovaara S, Robciuc A, Holopainen JM, Lehti K, Pessi T, Liinamaa J, et al. Ang-2 upregulation correlates with increased levels of MMP-9, VEGF, EPO and TGFβ1 in diabetic eyes undergoing vitrectomy. Acta Ophthalmol. 2013;91(6):531–9.
547. Rosenberg GA. Matrix metalloproteinases in neuroinflammation. Glia. 2002;39(3):279–91.
548. Rosenberg GA. Matrix metalloproteinases and their multiple roles in neurodegenerative diseases. Vol. 8, The Lancet Neurology. 2009. p. 205–16.
549. Bugno M, Witek B, Bereta J, Bereta M, Edwards DR, Kordula T. Reprogramming of TIMP-1 and TIMP-3 expression profiles in brain microvascular endothelial cells and astrocytes in response to proinflammatory cytokines. FEBS Lett. 1999;448(1):9–14.
550. Suryadevara R, Holter S, Borgmann K, Persidsky R, Labenz-Zink C, Persidsky Y, et al. Regulation of tissue inhibitor of metalloproteinase-1 by astrocytes: Links to HIV-1 dementia. Glia. 2003;44(1):47–56.
551. Pagenstecher A, Stalder AK, Kincaid CL, Shapiro SD, Campbell IL. Differential expression of matrix metalloproteinase and tissue inhibitor of matrix metalloproteinase genes in the mouse central nervous system in normal and inflammatory states. Am J Pathol. 1998;152(3):729–41.
552. Szymocha R, Akaoka H, Brisson C, Beurton-Marduel P, Chalon A, Bernard A, et al. Astrocytic alterations induced by HTLV type 1-infected T lymphocytes: A role for Tax-1 and tumor necrosis factor α. AIDS Res Hum Retroviruses. 2000;16(16):1723–9.
553. Khuth S-T, Akaoka H, Pagenstecher A, Verlaeten O, Belin M-F, Giraudon P, et al. Morbillivirus Infection of the Mouse Central Nervous System Induces Region-Specific Upregulation of MMPs and TIMPs Correlated to Inflammatory Cytokine Expression. J Virol. 2001;75(17):8268–82.

554. Ghorpade A, Persidskaia R, Suryadevara R, Che M, Liu XJ, Persidsky Y, et al. Mononuclear Phagocyte Differentiation, Activation, and Viral Infection Regulate Matrix Metalloproteinase Expression: Implications for Human Immunodeficiency Virus Type 1-Associated Dementia. J Virol. 2001;75(14):6572–83.
555. Clark AW, Krekoski CA, Bou SS, Chapman KR, Edwards DR. Increased gelatinase A (MMP-2) and gelatinase B (MMP-9) activities in human brain after focal ischemia. Neurosci Lett. 1997;238(1–2):53–6.
556. Solé S, Petegnief V, Gorina R, Chamorro Á, Planas AM. Activation of Matrix Metalloproteinase-3 and Agrin Cleavage in Cerebral Ischemia/Reperfusion. J Neuropathol Exp Neurol. 2004;63(4):338–49.
557. Lo EH, Wang X, Louise Cuzner M. Extracellular proteolysis in brain injury and inflammation: Role for plasminogen activators and matrix metalloproteinases. Vol. 69, Journal of Neuroscience Research. 2002. p. 1–9.
558. Rosell A, Ortega-Aznar A, Alvarez-Sabín J, Fernández-Cadenas I, Ribó M, Molina CA, et al. Increased brain expression of matrix metalloproteinase-9 after ischemic and hemorrhagic human stroke. Stroke. 2006;37(6):1399–406.
559. Rosenberg GA, Navratil M, Barone F, Feuerstein G. Proteolytic cascade enzymes increase in focal cerebral ischemia in rat. J Cereb Blood Flow Metab. 1996;16(3):360–6.
560. Heo JH, Lucero J, Abumiya T, Koziol JA, Copeland BR, Del Zoppo GJ. Matrix metalloproteinases increase very early during experimental focal cerebral ischemia. J Cereb Blood Flow Metab. 1999;19(6):624–33.
561. Cheung HH, Lynn Kelly N, Liston P, Korneluk RG. Involvement of caspase-2 and caspase-9 in endoplasmic reticulum stress-induced apoptosis: A role for the IAPs. Exp Cell Res. 2006;312(12):2347–57.
562. Sumii T, Lo EH. Involvement of matrix metalloproteinase in thrombolysis-associated hemorrhagic transformation after embolic focal ischemia in rats. Stroke. 2002;33(3):831–6.
563. Amour A, Slocombe PM, Webster A, Butler M, Knight CG, Smith BJ, et al. TNF-α converting enzyme (TACE) is inhibited by TIMP-3. FEBS Lett. 1998;435(1):39–44.
564. Smookler DS, Mohammed FF, Kassiri Z, Duncan GS, Mak TW, Khokha R. Cutting Edge: Tissue Inhibitor of Metalloproteinase 3 Regulates TNF-Dependent Systemic Inflammation. J Immunol. 2006;176(2):721–5.
565. Hoe HS, Cooper MJ, Burns MP, Lewis PA, Van Der Brug M, Chakraborty G, et al. The metalloprotease inhibitor TIMP-3 regulates amyloid precursor protein and apolipoprotein E receptor proteolysis. J Neurosci. 2007;27(40):10895–905.

566. Dunckley T, Beach TG, Ramsey KE, Grover A, Mastroeni D, Walker DG, et al. Gene expression correlates of neurofibrillary tangles in Alzheimer's disease. Neurobiol Aging. 2006;27(10):1359–71.
567. Dewing JM, Carare RO, Lotery AJ, Ratnayaka JA. The Diverse Roles of TIMP-3: Insights into Degenerative Diseases of the Senescent Retina and Brain. Cells. 2019;9(1).
568. Prattichizzo F, De Nigris V, Spiga R, Mancuso E, La Sala L, Antonicelli R, et al. Inflammageing and metaflammation: The yin and yang of type 2 diabetes. Vol. 41, Ageing Research Reviews. 2018. p. 1–17.
569. Mahajan SD, Parikh NU, Woodruff TM, Jarvis JN, Lopez M, Hennon T, et al. C5a alters blood-brain barrier integrity in a human in vitro model of systemic lupus erythematosus. Immunology. 2015;146(1):130–43.
570. Xiong F, Leonov S, Howard AC, Xiong S, Zhang B, Mei L, et al. Receptor for Advanced Glycation End products (RAGE) prevents endothelial cell membrane resealing and regulates F-actin remodeling in a β-catenin-dependent manner. J Biol Chem. 2011;286(40):35061–70.
571. Nuzzo D, Picone P, Caruana L, Vasto S, Barera A, Caruso C, et al. Inflammatory mediators as biomarkers in brain disorders. Inflammation. 2014;37(3):639–48.
572. Swardfager W, Lanctt K, Rothenburg L, Wong A, Cappell J, Herrmann N. A meta-analysis of cytokines in Alzheimer's disease. Biol Psychiatry. 2010;68(10):930–41.
573. Zhang R, Miller RG, Madison C, Jin X, Honrada R, Harris W, et al. Systemic immune system alterations in early stages of Alzheimer's disease. J Neuroimmunol. 2013;256(1–2):38–42.
574. Krstic D, Madhusudan A, Doehner J, Vogel P, Notter T, Imhof C, et al. Systemic immune challenges trigger and drive Alzheimer-like neuropathology in mice. J Neuroinflammation. 2012;9.
575. Wyss-Coray T. Inflammation in Alzheimer disease: Driving force, bystander or beneficial response? Vol. 12, Nature Medicine. 2006. p. 1005–15.
576. Wyss-Coray T, Rogers J. Inflammation in Alzheimer disease-A brief review of the basic science and clinical literature. Cold Spring Harb Perspect Med. 2012;2(1).
577. Thomson CA, McColl A, Cavanagh J, Graham GJ. Peripheral inflammation is associated with remote global gene expression changes in the brain. J Neuroinflammation. 2014;11.
578. Spielman LJ, Little JP, Klegeris A. Inflammation and insulin/IGF-1 resistance as the possible link between obesity and neurodegeneration. Vol. 273, Journal of Neuroimmunology. 2014. p. 8–21.

579. Town T, Tan J, Flavell RA, Mullan M. T-cells in Alzheimer's disease. Vol. 7, NeuroMolecular Medicine. 2005. p. 255–64.
580. Vom Berg J, Prokop S, Miller KR, Obst J, Kälin RE, Lopategui-Cabezas I, et al. Inhibition of IL-12/IL-23 signaling reduces Alzheimer's diseasea-like pathology and cognitive decline. Nat Med. 2012;18(12):1812–9.
581. Becher B, Durell BG, Noelle RJ. IL-23 produced by CNS-resident cells controls T cell encephalitogenicity during the effector phase of experimental autoimmune encephalomyelitis. J Clin Invest. 2003;112(8):1186–91.
582. Juge-Aubry CE, Somm E, Chicheportiche R, Burger D, Pernin A, Cuénod-Pittet B, et al. Regulatory effects of interleukin (IL)-1, interferon-β, and IL-4 on the production of IL-1 receptor antagonist by human adipose tissue. In: Journal of Clinical Endocrinology and Metabolism. 2004. p. 2652–8.
583. Juge-Aubry CE, Somm E, Giusti V, Pernin A, Chicheportiche R, Verdumo C, et al. Adipose tissue is a major source of interleukin-1 receptor antagonist: Upregulation in obesity and inflammation. Diabetes. 2003;52(5):1104–10.
584. Surendar J, Mohan V, Rao MM, Babu S, Aravindhan V. Increased levels of both Th1 and Th2 cytokines in subjects with metabolic syndrome (CURES-103). Diabetes Technol Ther. 2011;13(4):477–82.
585. Dandona P, Ghanim H, Monte S V., Caruana JA, Green K, Abuaysheh S, et al. Increase in the mediators of asthma in obesity and obesity with type 2 diabetes: Reduction with weight loss. Obesity. 2014;22(2):356–62.
586. Rakotoarivelo V, Lacraz G, Mayhue M, Brown C, Rottembourg D, Fradette J, et al. Inflammatory Cytokine Profiles in Visceral and Subcutaneous Adipose Tissues of Obese Patients Undergoing Bariatric Surgery Reveal Lack of Correlation With Obesity or Diabetes. EBioMedicine. 2018;30:237–47.
587. Lee BC, Lee J. Cellular and molecular players in adipose tissue inflammation in the development of obesity-induced insulin resistance. Vol. 1842, Biochimica et Biophysica Acta - Molecular Basis of Disease. 2014. p. 446–62.
588. Sankowski R, Mader S, Valdés-Ferrer SI. Systemic inflammation and the brain: Novel roles of genetic, molecular, and environmental cues as drivers of neurodegeneration. Front Cell Neurosci. 2015;9(FEB).
589. Orihuela CJ, Fillon S, Smith-Sielicki SH, El Kasmi KC, Gao G, Soulis K, et al. Cell wall-mediated neuronal damage in early sepsis. Infect Immun. 2006;74(7):3783–9.
590. Allan SM. The role of pro- and antiinflammatory cytokines in neurodegeneration. Ann N Y Acad Sci. 2000;917:84–93.

591. Barry JC, Shakibakho S, Durrer C, Simtchouk S, Jawanda KK, Cheung ST, et al. Hyporesponsiveness to the anti-inflammatory action of interleukin-10 in type 2 diabetes. Sci Rep. 2016;6.
592. Mayo L, Cunha AP Da, Madi A, Beynon V, Yang Z, Alvarez JI, et al. IL-10-dependent Tr1 cells attenuate astrocyte activation and ameliorate chronic central nervous system inflammation. Brain. 2016;139(7):1939–57.
593. Joniec-Maciejak I, Ciesielska A, Wawer A, Sznejder-Pachołek A, Schwenkgrub J, Cudna A, et al. The influence of AAV2-mediated gene transfer of human IL-10 on neurodegeneration and immune response in a murine model of Parkinson's disease. Pharmacol Reports. 2014;66(4):660–9.
594. Chakrabarty P, Li A, Ceballos-Diaz C, Eddy JA, Funk CC, Moore B, et al. IL-10 Alters Immunoproteostasis in APP Mice, Increasing Plaque Burden and Worsening Cognitive Behavior. Neuron. 2015;85(3):519–33.
595. Kiyota T, Okuyama S, Swan RJ, Jacobsen MT, Gendelman HE, Ikezu T. CNS expression of anti-inflammatory cytokine interleukin-4 attenuates Alzheimer's disease-like pathogenesis in APP+PS1 bigenic mice. FASEB J. 2010;24(8):3093–102.
596. Kiyota T, Ingraham KL, Swan RJ, Jacobsen MT, Andrews SJ, Ikezu T. AAV serotype 2/1-mediated gene delivery of anti-inflammatory interleukin-10 enhances neurogenesis and cognitive function in APPPS1 mice. Gene Ther. 2012;19(7):724–33.
597. Han J, Sun L, Fan X, Wang Z, Cheng Y, Zhu J, et al. Role of regulatory b cells in neuroimmunologic disorders. Vol. 94, Journal of Neuroscience Research. 2016. p. 693–701.
598. Cua DJ, Hutchins B, LaFace DM, Stohlman SA, Coffman RL. Central Nervous System Expression of IL-10 Inhibits Autoimmune Encephalomyelitis. J Immunol. 2001;166(1):602–8.
599. Lobo-Silva D, Carriche GM, Castro AG, Roque S, Saraiva M. Balancing the immune response in the brain: IL-10 and its regulation. Vol. 13, Journal of Neuroinflammation. 2016.
600. Kahn SE, Hull RL, Utzschneider KM. Mechanisms linking obesity to insulin resistance and type 2 diabetes. Vol. 444, Nature. 2006. p. 840–6.
601. Sakaguchi S, Ono M, Setoguchi R, Yagi H, Hori S, Fehervari Z, et al. Foxp3+CD25+CD4+ natural regulatory T cells in dominant self-tolerance and autoimmune disease. Vol. 212, Immunological Reviews. 2006. p. 8–27.

602. Murphy TJ, Choileain NN, Zang Y, Mannick JA, Lederer JA. CD4 + CD25 + Regulatory T Cells Control Innate Immune Reactivity after Injury . J Immunol. 2005;174(5):2957–63.
603. Garidou L, Pomié C, Klopp P, Waget A, Charpentier J, Aloulou M, et al. The Gut Microbiota Regulates Intestinal CD4 T Cells Expressing RORγt and Controls Metabolic Disease. Cell Metab. 2015;22(1):100–12.
604. Abdel-Moneim A, Bakery HH, Allam G. The potential pathogenic role of IL-17/Th17 cells in both type 1 and type 2 diabetes mellitus. Vol. 101, Biomedicine and Pharmacotherapy. 2018. p. 287–92.
605. Sumarac-Dumanovic M, Stevanovic D, Ljubic A, Jorga J, Simic M, Stamenkovic-Pejkovic D, et al. Increased activity of interleukin-23/interleukin-17 proinflammatory axis in obese women. Int J Obes. 2009;33(1):151–6.
606. Winer S, Paltser G, Chan Y, Tsui H, Engleman E, Winer D, et al. Obesity predisposes to Th17 bias. Eur J Immunol. 2009;39(9):2629–35.
607. Zúñiga LA, Shen W-J, Joyce-Shaikh B, Pyatnova EA, Richards AG, Thom C, et al. IL-17 Regulates Adipogenesis, Glucose Homeostasis, and Obesity. J Immunol [Internet]. 2010;185(11):6947–59.
608. Hamilton MK, Boudry G, Lemay DG, Raybould HE. Changes in intestinal barrier function and gut microbiota in high-fat diet-fed rats are dynamic and region dependent. Am J Physiol - Gastrointest Liver Physiol. 2015;308(10):G840–51.
609. Welling MM, Nabuurs RJA, Van Der Weerd L. Potential role of antimicrobial peptides in the early onset of Alzheimer's disease. Alzheimer's Dement. 2015;11(1):51–7.
610. Durelli L, Conti L, Clerico M, Boselli D, Contessa G, Ripellino P, et al. T-helper 17 cells expand in multiple sclerosis and are inhibited by interferon-β. Ann Neurol. 2009;65(5):499–509.
611. Brucklacher-Waldert V, Stuerner K, Kolster M, Wolthausen J, Tolosa E. Phenotypical and functional characterization of T helper 17 cells in multiple sclerosis. Brain. 2009;132(12):3329–41.
612. Lock C, Hermans G, Pedotti R, Brendolan A, Schadt E, Garren H, et al. Gene-microarray analysis of multiple sclerosis lesions yields new targets validated in autoimmune encephalomyelitis. Nat Med. 2002;8(5):500–8.
613. Komiyama Y, Nakae S, Matsuki T, Nambu A, Ishigame H, Kakuta S, et al. IL-17 Plays an Important Role in the Development of Experimental Autoimmune Encephalomyelitis. J Immunol. 2006;177(1):566–73.

614. Saresella M, Calabrese E, Marventano I, Piancone F, Gatti A, Alberoni M, et al. Increased activity of Th-17 and Th-9 lymphocytes and a skewing of the post-thymic differentiation pathway are seen in Alzheimer's disease. Brain Behav Immun. 2011;25(3):539–47.
615. Oberstein TJ, Taha L, Spitzer P, Hellstern J, Herrmann M, Kornhuber J, et al. Imbalance of circulating Th17 and regulatory T cells in Alzheimer's disease: A case control study. Front Immunol. 2018;9(JUN).
616. Zhang J, Ke KF, Liu Z, Qiu YH, Peng YP. Th17 Cell-Mediated Neuroinflammation Is Involved in Neurodegeneration of Aβ1-42-Induced Alzheimer's Disease Model Rats. PLoS One. 2013;8(10).
617. Reynolds AD, Stone DK, Hutter JAL, Benner EJ, Mosley RL, Gendelman HE. Regulatory T Cells Attenuate Th17 Cell-Mediated Nigrostriatal Dopaminergic Neurodegeneration in a Model of Parkinson's Disease. J Immunol. 2010;184(5):2261–71.
618. Dansokho C, Ait Ahmed D, Aid S, Toly-Ndour C, Chaigneau T, Calle V, et al. Regulatory T cells delay disease progression in Alzheimer-like pathology. Brain. 2016;139(4):1237–51.
619. Rosenkranz D, Weyer S, Tolosa E, Gaenslen A, Berg D, Leyhe T, et al. Higher frequency of regulatory T cells in the elderly and increased suppressive activity in neurodegeneration. J Neuroimmunol. 2007;188(1–2):117–27.
620. Daglas M, Draxler DF, Ho H, McCutcheon F, Galle A, Au AE, et al. Activated CD8+ T Cells Cause Long-Term Neurological Impairment after Traumatic Brain Injury in Mice. Cell Rep. 2019;29(5):1178-1191.e6.
621. Cao YL, Zhang FQ, Hao FQ. Th1/Th2 cytokine expression in diabetic retinopathy. Genet Mol Res. 2016;15(3).
622. Lynch LA, O'Connell JM, Kwasnik AK, Cawood TJ, O'Farrelly C, O'Shea DB. Are natural killer cells protecting the metabolically healthy obese patient? Obesity. 2009;17(3):601–5.
623. Huh JY, Kim JI, Park YJ, Hwang IJ, Lee YS, Sohn JH, et al. A Novel Function of Adipocytes in Lipid Antigen Presentation to iNKT Cells. Mol Cell Biol. 2013;33(2):328–39.
624. Schipper HS, Rakhshandehroo M, Van De Graaf SFJ, Venken K, Koppen A, Stienstra R, et al. Natural killer T cells in adipose tissue prevent insulin resistance. J Clin Invest. 2012;122(9):3343–54.
625. Lynch L, Nowak M, Varghese B, Clark J, Hogan AE, Toxavidis V, et al. Adipose Tissue Invariant NKT Cells Protect against Diet-Induced Obesity and Metabolic Disorder through Regulatory Cytokine Production. Immunity. 2012;37(3):574–87.

626. Hams E, Locksley RM, McKenzie ANJ, Fallon PG. Cutting Edge: IL-25 Elicits Innate Lymphoid Type 2 and Type II NKT Cells That Regulate Obesity in Mice. J Immunol. 2013;191(11):5349–53.
627. Kohlgruber A, Lynch L. Adipose Tissue Inflammation in the Pathogenesis of Type 2 Diabetes. Vol. 15, Current Diabetes Reports. 2015.
628. Ji Y, Sun S, Xu A, Bhargava P, Yang L, Lam KSL, et al. Activation of natural killer T cells promotes M2 macrophage polarization in adipose tissue and improves systemic glucose tolerance via interleukin-4 (IL-4)/STAT6 protein signaling axis in obesity. J Biol Chem. 2012;287(17):13561–71.
629. Asensio VC, Kincaid C, Campbell IL. Chemokines and the inflammatory response to viral infection in the central nervous system with a focus on lymphocytic choriomeningitis virus. J Neurovirol. 1999;5(1):65–75.
630. Lane TE, Asensio VC, Yu N, Paoletti AD, Campbell IL, Buchmeier MJ. Dynamic regulation of alpha- and beta-chemokine expression in the central nervous system during mouse hepatitis virus-induced demyelinating disease. J Immunol [Internet]. 1998;160(2):970–8.
631. Asensio VC, Campbell IL. Chemokine gene expression in the brains of mice with lymphocytic choriomeningitis. J Virol. 1997;71(10):7832–40.
632. Bachmann MF, Kopf M, Marsland BJ. Opinion: Chemokines: More than just road signs. Vol. 6, Nature Reviews Immunology. 2006. p. 159–64.
633. Williams JL, Holman DW, Klein RS. Chemokines in the balance: Maintenance of homeostasis and protection at CNS barriers. Vol. 8, Frontiers in Cellular Neuroscience. 2014.
634. McCandless EE, Wang Q, Woerner BM, Harper JM, Klein RS. CXCL12 Limits Inflammation by Localizing Mononuclear Infiltrates to the Perivascular Space during Experimental Autoimmune Encephalomyelitis. J Immunol. 2006;177(11):8053–64.
635. Bradley LM, Watson SR. Lymphocyte migration into tissue: The paradigm derived from CD4 subsets. Curr Opin Immunol. 1996;8(3):312–20.
636. Butcher EC, Picker LJ. Lymphocyte homing and homeostasis. Science (80-). 1996;272(5258):60–6.
637. Kivisäkk P, Mahad DJ, Callahan MK, Trebst C, Tucky B, Wei T, et al. Human cerebrospinal fluid central memory CD4+ T cells: Evidence for trafficking through choroid plexus and meninges via P-selectin. Proc Natl Acad Sci U S A. 2003;100(14):8389–94.

638. Kivisäkk P, Trebst C, Liu Z, Tucky BH, Sørensen TL, Rudick RA, et al. T-cells in the cerebrospinal fluid express a similar repertoire of inflammatory chemokine receptors in the absence or presence of CNS inflammation: Implications for CNS trafficking. Clin Exp Immunol. 2002;129(3):510–8.
639. Shirakawa K, Yan X, Shinmura K, Endo J, Kataoka M, Katsumata Y, et al. Obesity accelerates T cell senescence in murine visceral adipose tissue. J Clin Invest. 2016;126(12):4626–39.
640. Hickey WF, Hsu BL, Kimura H. T-lymphocyte entry into the central nervous system. J Neurosci Res. 1991;28(2):254–60.
641. Hatterer E, Davoust N, Didier-Bazes M, Vuaillat C, Malcus C, Belin MF, et al. How to drain without lymphatics? Dendritic cells migrate from the cerebrospinal fluid to the B-cell follicles of cervical lymph nodes. Blood. 2006;107(2):806–12.
642. Takeshita Y, Ransohoff RM. Inflammatory cell trafficking across the blood-brain barrier: Chemokine regulation and in vitro models. Immunol Rev. 2012;248(1):228–39.
643. Engelhardt B, Vestweber D, Hallmann R, Schulz M. E- and P-selectin are not involved in the recruitment of inflammatory cells across the blood-brain barrier in experimental autoimmune encephalomyelitis. Blood. 1997;90(11):4459–72.
644. Tran EH, Hoekstra K, van Rooijen N, Dijkstra CD, Owens T. Immune invasion of the central nervous system parenchyma and experimental allergic encephalomyelitis, but not leukocyte extravasation from blood, are prevented in macrophage-depleted mice. J Immunol [Internet]. 1998;161(7):3767–75.
645. Cross AH, O'Mara T, Raine CS. Chronologic localization of myelin-reactive cells in the lesions of relapsing eae: Implications for the study of multiple sclerosis. Neurology. 1993;43(5):1028–33.
646. Tian M, Jacobson C, Gee SH, Campbell KP, Carbonetto S, Jucker M. Dystroglycan in the cerebellum is a laminin α2-chain binding protein at the glial-vascular interface and is expressed in Purkinje cells. Eur J Neurosci. 1996;8(12):2739–47.
647. Song J, Wu C, Korpos E, Zhang X, Agrawal SM, Wang Y, et al. Focal MMP-2 and MMP-9 Activity at the Blood-Brain Barrier Promotes Chemokine-Induced Leukocyte Migration. Cell Rep. 2015;10(7):1040–54.
648. Körner H, Riminton DS, Strickland DH, Lemckert FA, Pollard JD, Sedgwick JD. Critical points of tumor necrosis factor action in central nervous system autoimmune inflammation defined by gene targeting. J Exp Med. 1997;186(9):1585–90.

649. Ho HH, Antoniv TT, Ji J-D, Ivashkiv LB. Lipopolysaccharide-Induced Expression of Matrix Metalloproteinases in Human Monocytes Is Suppressed by IFN-γ via Superinduction of ATF-3 and Suppression of AP-1. J Immunol. 2008;181(7):5089–97.
650. Di Girolamo N, Indoh I, Jackson N, Wakefield D, McNeil HP, Yan W, et al. Human Mast Cell-Derived Gelatinase B (Matrix Metalloproteinase-9) Is Regulated by Inflammatory Cytokines: Role in Cell Migration. J Immunol. 2006;177(4):2638–50.
651. Weaver CT, Hatton RD, Mangan PR, Harrington LE. IL-17 family cytokines and the expanding diversity of effector T cell lineages. Annu Rev Immunol. 2007;25:821–52.
652. Cepok S, Jacobsen M, Schock S, Omer B, Jaekel S, Böddeker I, et al. Patterns of cerebrospinal fluid pathology correlate with disease progression in multiple sclerosis. Brain. 2001;124(11):2169–76.
653. Kooij G, Kopplin K, Blasig R, Stuiver M, Koning N, Goverse G, et al. Disturbed function of the blood-cerebrospinal fluid barrier aggravates neuro-inflammation. Acta Neuropathol. 2014;128(2):267–77.
654. Ransohoff RM. Immunology: In the beginning. Vol. 462, Nature. 2009. p. 41–2.
655. Ott BR, Jones RN, Daiello LA, de la Monte SM, Stopa EG, Johanson CE, et al. Blood-cerebrospinal fluid barrier gradients in mild cognitive impairment and Alzheimer's disease: Relationship to inflammatory cytokines and chemokines. Front Aging Neurosci. 2018;10(AUG).
656. Altmann C, Schmidt MHH. The role of microglia in diabetic retinopathy: Inflammation, microvasculature defects and neurodegeneration. Vol. 19, International Journal of Molecular Sciences. 2018.
657. Graeber MB, Li W, Rodriguez ML. Role of microglia in CNS inflammation. Vol. 585, FEBS Letters. 2011. p. 3798–805.
658. Streit WJ, Mrak RE, Griffin WST. Microglia and neuroinflammation: A pathological perspective. J Neuroinflammation. 2004;1.
659. Cherry JD, Olschowka JA, O'Banion MK. Neuroinflammation and M2 microglia: The good, the bad, and the inflamed. Vol. 11, Journal of Neuroinflammation. 2014.
660. Martin E, Boucher C, Fontaine B, Delarasse C. Distinct inflammatory phenotypes of microglia and monocyte-derived macrophages in Alzheimer's disease models: effects of aging and amyloid pathology. Aging Cell. 2017;16(1):27–38.
661. Kamphuis W, Kooijman L, Schetters S, Orre M, Hol EM. Transcriptional profiling of CD11c-positive microglia accumulating around amyloid plaques in a mouse model for Alzheimer's disease. Biochim Biophys Acta - Mol Basis Dis. 2016;1862(10):1847–60.

662. Olmos-Alonso A, Schetters STT, Sri S, Askew K, Mancuso R, Vargas-Caballero M, et al. Pharmacological targeting of CSF1R inhibits microglial proliferation and prevents the progression of Alzheimer's-like pathology. Brain. 2016;139(3):891–907.
663. Kamphuis W, Orre M, Kooijman L, Dahmen M, Hol EM. Differential cell proliferation in the cortex of the APPswePS1dE9 Alzheimer's disease mouse model. Glia. 2012;60(4):615–29.
664. Boehme SA, Lio FM, Maciejewski-Lenoir D, Bacon KB, Conlon PJ. The Chemokine Fractalkine Inhibits Fas-Mediated Cell Death of Brain Microglia. J Immunol. 2000;165(1):397–403.
665. Maciejewski-Lenoir D, Chen S, Feng L, Maki R, Bacon KB. Characterization of fractalkine in rat brain cells: migratory and activation signals for CX3CR-1-expressing microglia. J Immunol [Internet]. 1999;163(3):1628–35.
666. Mendiola AS, Garza R, Cardona SM, Mythen SA, Lira SA, Akassoglou K, et al. Fractalkine signaling attenuates perivascular clustering of microglia and fibrinogen leakage during systemic inflammation in mouse models of diabetic retinopathy. Front Cell Neurosci. 2017;10.
667. Rogers JT, Morganti JM, Bachstetter AD, Hudson CE, Peters MM, Grimmig BA, et al. CX3CR1 deficiency leads to impairment of hippocampal cognitive function and synaptic plasticity. J Neurosci. 2011;31(45):16241–50.
668. Bachstetter AD, Morganti JM, Jernberg J, Schlunk A, Mitchell SH, Brewster KW, et al. Fractalkine and CX 3CR1 regulate hippocampal neurogenesis in adult and aged rats. Neurobiol Aging. 2011;32(11):2030–44.
669. Lee S, Varvel NH, Konerth ME, Xu G, Cardona AE, Ransohoff RM, et al. CX3CR1 deficiency alters microglial activation and reduces beta-amyloid deposition in two Alzheimer's disease mouse models. Am J Pathol. 2010;177(5):2549–62.
670. Fuhrmann M, Bittner T, Jung CKE, Burgold S, Page RM, Mitteregger G, et al. Microglial Cx3cr1 knockout prevents neuron loss in a mouse model of Alzheimer's disease. Nat Neurosci. 2010;13(4):411–3.
671. Bhaskar K, Konerth M, Kokiko-Cochran ON, Cardona A, Ransohoff RM, Lamb BT. Regulation of tau pathology by the microglial fractalkine receptor. Neuron. 2010;68(1):19–31.
672. Cho SH, Sun B, Zhou Y, Kauppinen TM, Halabisky B, Wes P, et al. CX3CR1 protein signaling modulates microglial activation and protects against plaque-independent cognitive deficits in a mouse model of Alzheimer disease. J Biol Chem. 2011;286(37):32713–22.
673. Wolf Y, Yona S, Kim KW, Jung S. Microglia, seen from the CX3CR1 angle. Front Cell Neurosci. 2013;(MAR).

674. Takechi R, Lam V, Brook E, Giles C, Fimognari N, Mooranian A, et al. Blood-brain barrier dysfunction precedes cognitive decline and neurodegeneration in diabetic insulin resistant mouse model: An implication for causal link. Front Aging Neurosci. 2017;9(DEC).
675. Yashin AI, Arbeev KG, Kulminski A, Akushevich I, Akushevich L, Ukraintseva S V. Health decline, aging and mortality: How are they related? Biogerontology. 2007;8(3):291–302.
676. Castelo-Branco C, Soveral I. The immune system and aging: A review. Vol. 30, Gynecological Endocrinology. 2014. p. 16–22.
677. Franceschi C, Bonafè M, Valensin S, Olivieri F, De Luca M, Ottaviani E, et al. Inflamm-aging. An evolutionary perspective on immunosenescence. Ann N Y Acad Sci. 2000;908:244–54.
678. Purvis GSD, Chiazza F, Chen J, Azevedo-Loiola R, Martin L, Kusters DHM, et al. Annexin A1 attenuates microvascular complications through restoration of Akt signalling in a murine model of type 1 diabetes. Diabetologia. 2018;61(2):482–95.
679. Solito E, McArthur S, Christian H, Gavins F, Buckingham JC, Gillies GE. Annexin A1 in the brain - undiscovered roles? Vol. 29, Trends in Pharmacological Sciences. 2008. p. 135–42.
680. Brown SA. Studies of educational interventions and outcomes in diabetic adults: A meta-analysis revisited. Patient Educ Couns. 1990;16(3):189–215.
681. NICE guidelines. Type 2 diabetes in adults Type 2 diabetes: management of type 2 diabetes in adults provisional. Natl Inst Heal Care Excell [Internet]. 2015;NG28(December 2015):1–86.
682. WHO. Global Gudelines for type 2 diabetes. Glob Guidel Type 2 Diabetes [Internet]. 2012;2–4.
683. Standards of medical care in diabetes-2014. Vol. 37, Diabetes Care. 2014.
684. Deanfield J, Sattar N, Simpson I, Wood D, Bradbury K, Fox K, et al. Joint British Societies' consensus recommendations for the prevention of cardiovascular disease (JBS3). Vol. 100, Heart. 2014.
685. McGrattan AM, McGuinness B, McKinley MC, Kee F, Passmore P, Woodside J V., et al. Diet and Inflammation in Cognitive Ageing and Alzheimer's Disease. Vol. 8, Current Nutrition Reports. 2019. p. 53–65.
686. Petersson SD, Philippou E. Mediterranean diet, cognitive function, and dementia: A systematic review of the evidence. Adv Nutr. 2016;7(5):889–904.
687. Lourida I, Soni M, Thompson-Coon J, Purandare N, Lang IA, Ukoumunne OC, et al. Mediterranean diet, cognitive function, and dementia: A systematic review. Epidemiology. 2013;24(4):479–89.

688. Chiazza F, Couturier-Maillard A, Benetti E, Mastrocola R, Nigro D, Cutrin JC, et al. Targeting the NLRP3 inflammasome to reduce diet-induced metabolic abnormalities in mice. Mol Med. 2015;21:1025–37.
689. Gual P, Le Marchand-Brustel Y, Tanti JF. Positive and negative regulation of insulin signaling through IRS-1 phosphorylation. In: Biochimie. 2005. p. 99–109.
690. Myers MG, Sun XJ, White MF. The IRS-1 signaling system. Vol. 19, Trends in Biochemical Sciences. 1994. p. 289–93.
691. Fredman G, Kamaly N, Spolitu S, Milton J, Ghorpade D, Chiasson R, et al. Targeted nanoparticles containing the proresolving peptide Ac2-26 protect against advanced atherosclerosis in hypercholesterolemic mice. Sci Transl Med. 2015;7(275).
692. Kang H, Ko J, Jang SW. The role of annexin A1 in expression of matrix metalloproteinase-9 and invasion of breast cancer cells. Biochem Biophys Res Commun. 2012;423(1):188–94.
693. Liu QH, Shi ML, Bai J, Zheng JN. Identification of ANXA1 as a lymphatic metastasis and poor prognostic factor in pancreatic ductal adenocarcinoma. Asian Pacific J Cancer Prev. 2015;16(7):2719–24.
694. Tu Y, Johnstone CN, Stewart AG. Annexin A1 influences in breast cancer: Controversies on contributions to tumour, host and immunoediting processes. Vol. 119, Pharmacological Research. 2017. p. 278–88.
695. Guo C, Liu S, Sun M-Z. Potential role of Anxa1 in cancer. Futur Oncol. 2013;9(11):1773–93.
696. Thrailkill KM, Clay Bunn R, Fowlkes JL. Matrix metalloproteinases: their potential role in the pathogenesis of diabetic nephropathy. Vol. 35, Endocrine. 2009. p. 1–10.
697. Busti C, Falcinelli E, Momi S, Gresele P. Matrix metalloproteinases and peripheral arterial disease. Vol. 5, Internal and Emergency Medicine. 2010. p. 13–25.
698. Oliani SM, Perretti M. Cell localization of the anti-inflammatory protein annexin 1 during experimental inflammatory response. Ital J Anat Embryol. 2001;106(2 Suppl 1):69–77.
699. Pitzalis C, Pipitone N, Bajocchi G, Hall M, Goulding N, Lee A, et al. Corticosteroids Inhibit Lymphocyte Binding to Endothelium and Intercellular Adhesion: An Additional Mechanism for Their Anti-Inflammatory and Immunosuppressive Effect. J Immunol. 1997;158(10):5007–16.
700. Goulding NJ, Ogbourn S, Pipitone N, Biagini P, Gerli R, Pitzalis C. The inhibitory effect of dexamethasone on lymphocyte adhesion molecule expression and intercellular aggregation is not mediated by lipocortin 1. Clin Exp Immunol. 1999;118(3):376–83.

701. Moffatt OD, Devitt A, Bell ED, Simmons DL, Gregory CD. Macrophage recognition of ICAM-3 on apoptotic leukocytes. J Immunol [Internet]. 1999;162(11):6800–10.
702. Sugimoto MA, Vago JP, Teixeira MM, Sousa LP. Annexin A1 and the Resolution of Inflammation: Modulation of Neutrophil Recruitment, Apoptosis, and Clearance. Vol. 2016, Journal of Immunology Research. 2016.
703. Salmond RJ, Emery J, Okkenhaug K, Zamoyska R. MAPK, Phosphatidylinositol 3-Kinase, and Mammalian Target of Rapamycin Pathways Converge at the Level of Ribosomal Protein S6 Phosphorylation to Control Metabolic Signaling in CD8 T Cells. J Immunol [Internet]. 2009;183(11):7388–97.
704. McArthur S, Gobbetti T, Juban G, Desgeorges T, Theret M, Gondin J, et al. Annexin A1 drives macrophage skewing towards a resolving phenotype to accelerate the regeneration of muscle injury through AMPK activation. bioRxiv. 2018;375709.
705. Li Y, Cai L, Wang H, Wu P, Gu W, Chen Y, et al. Pleiotropic regulation of macrophage polarization and tumorigenesis by formyl peptide receptor-2. Oncogene. 2011;30(36):3887–99.
706. Moraes LA, Kar S, Foo SL, Gu T, Toh YQ, Ampomah PB, et al. Annexin-A1 enhances breast cancer growth and migration by promoting alternative macrophage polarization in the tumour microenvironment. Sci Rep. 2017;7(1).
707. YAZAWA H, YU Z-X, TAKEDA K, LE Y, GONG W, FERRANS VJ, et al. β Amyloid peptide (Aβ 42) is internalized via the G-protein-coupled receptor FPRL1 and forms fibrillar aggregates in macrophages 1 . FASEB J. 2001;15(13):2454–62.
708. Patel DM, Ahmad SF, Weiss DG, Gerke V, Kuznetsov SA. Annexin A1 is a new functional linker between actin filaments and phagosomes during phagocytosis. J Cell Sci. 2011;124(4):578–88.
709. Williams AE, van Dam AM, Man-A-Hing WKH, Berkenbosch F, Eikelenboom P, Fraser H. Cytokines, prostaglandins and lipocortin-1 are present in the brains of scrapie-infected mice. Brain Res. 1994;654(2):200–6.
710. Williams A, Van Dam AM, Ritchie D, Eikelenboom P, Fraser H. Immunocytochemical appearance of cytokines, prostaglandin E2and lipocortin-1 in the CNS during the incubation period of murine scrapie correlates with progressive PrP accumulations. Brain Res. 1997;754(1–2):171–80.
711. Young KA, Hirst WD, Solito E, Wilkin GP. De novo expression of lipocortin-1 in reactive microglia and astrocytes in kainic acid lesioned rat cerebellum. Glia. 1999;26(4):333–43.

712. Elhayany A, Lustman A, Abel R, Attal-Singer J, Vinker S. A low carbohydrate Mediterranean diet improves cardiovascular risk factors and diabetes control among overweight patients with type 2 diabetes mellitus: A 1-year prospective randomized intervention study. Diabetes, Obes Metab. 2010;12(3):204–9.
713. Shai I, Schwarzfuchs D, Henkin Y, Shahar DR, Witkow S, Greenberg I, et al. Weight loss with a low-carbohydrate, Mediterranean, or low-fat diet. N Engl J Med. 2008;359(3):229–41.
714. de Lorgeril M, Renaud S, Salen P, Monjaud I, Mamelle N, Martin JL, et al. Mediterranean alpha-linolenic acid-rich diet in secondary prevention of coronary heart disease. Lancet. 1994;343(8911):1454–9.
715. De Lorgeril M, Salen P, Martin JL, Monjaud I, Delaye J, Mamelle N. Mediterranean diet, traditional risk factors, and the rate of cardiovascular complications after myocardial infarction: Final report of the Lyon Diet Heart Study. Circulation. 1999;99(6):779–85.
716. Gæde P, Vedel P, Larsen N, Jensen GVH, Parving HH, Pedersen O. Multifactorial intervention and cardiovascular disease in patients with type 2 diabetes. N Engl J Med. 2003;348(5):383–93.
717. Wei S, Zhao J, Bai M, Li C, Zhang L, Chen Y. Comparison of glycemic improvement between intermittent calorie restriction and continuous calorie restriction in diabetic mice. Nutr Metab. 2019;16(1).
718. Wei S, Han R, Zhao J, Wang S, Huang M, Wang Y, et al. Intermittent administration of a fasting-mimicking diet intervenes in diabetes progression, restores β cells and reconstructs gut microbiota in mice. Nutr Metab. 2018;15(1).
719. da Rosa CVD, de Campos JM, de Sá Nakanishi AB, Comar JF, Martins IP, de Freitas Mathias PC, et al. Food restriction promotes damage reduction in rat models of type 2 diabetes mellitus. PLoS One. 2018;13(6).
720. Zhang Q, Xu L, Xia J, Wang D, Qian M, Ding S. Treatment of Diabetic Mice with a Combination of Ketogenic Diet and Aerobic Exercise via Modulations of PPARs Gene Programs. PPAR Res. 2018;2018:1–13.
721. Winters WD, Huo YS, Yao DL. Inhibition of the progression of type 2 diabetes in the C57BL/6J mouse model by an anti-diabetes herbal formula. Phyther Res. 2003;17(6):591–8.
722. Hofmann SM, Dong HJ, Li Z, Cai W, Altomonte J, Thung SN, et al. Improved insulin sensitivity is associated with restricted intake of dietary glycoxidation products in the db/db mouse. Diabetes. 2002;51(7):2082–9.

723. Jurado-Ruiz E, Álvarez-Amor L, Varela LM, Berná G, Parra-Camacho MS, Oliveras-Lopez MJ, et al. Extra virgin olive oil diet intervention improves insulin resistance and islet performance in diet-induced diabetes in mice. Sci Rep. 2019;9(1).
724. Arroba AI, Alcalde-Estevez E, García-Ramírez M, Cazzoni D, de la Villa P, Sánchez-Fernández EM, et al. Modulation of microglia polarization dynamics during diabetic retinopathy in db/db mice. Biochim Biophys Acta - Mol Basis Dis. 2016;1862(9):1663–74.
725. Moutschen MP, Scheen AJ, Lefebvre PJ. Impaired immune responses in diabetes mellitus: Analysis of the factors and mechanisms involved. Relevance to the increased susceptibility of diabetic patients to specific infections. Vol. 18, Diabete et Metabolisme. 1992. p. 187–201.
726. Giovannucci E, Harlan DM, Archer MC, Bergenstal RM, Gapstur SM, Habel LA, et al. Diabetes and cancer: A consensus report. In: Diabetes Care. 2010. p. 1674–85.
727. Habib SL, Rojna M. Diabetes and Risk of Cancer. ISRN Oncol. 2013;2013:1–16.
728. Joshi N, Caputo GM, Weitekamp MR, Karchmer AW. Infections in patients with diabetes mellitus. Vol. 341, New England Journal of Medicine. 1999. p. 1906–12.
729. Larsen CM, Faulenbach M, Vaag A, Vølund A, Ehses JA, Seifert B, et al. Interleukin-1-receptor antagonist in type 2 diabetes mellitus. N Engl J Med. 2007;356(15):1517–26.
730. Gómez-Pinilla F. Brain foods: The effects of nutrients on brain function. Vol. 9, Nature Reviews Neuroscience. 2008. p. 568–78.
731. Wu A, Ying Z, Gomez-Pinilla F. Dietary curcumin counteracts the outcome of traumatic brain injury on oxidative stress, synaptic plasticity, and cognition. Exp Neurol. 2006;197(2):309–17.
732. Wu A, Ying Z, Gomez-Pinilla F. Oxidative stress modulates Sir2α in rat hippocampus and cerebral cortex. Eur J Neurosci. 2006;23(10):2573–80.
733. Greenwood CE, Winocur G. High-fat diets, insulin resistance and declining cognitive function. In: Neurobiology of Aging. 2005. p. 42–5.
734. Lee JY, Ye J, Gao Z, Youn HS, Lee WH, Zhao L, et al. Reciprocal modulation of toll-like receptor-4 signaling pathways involving MyD88 and phosphatidylinositol 3-kinase/AKT by saturated and polyunsaturated fatty acids. J Biol Chem. 2003;278(39):37041–51.
735. Huang S, Rutkowsky JM, Snodgrass RG, Ono-Moore KD, Schneider DA, Newman JW, et al. Saturated fatty acids activate TLR-mediated proinflammatory signaling pathways. J Lipid Res. 2012;53(9):2002–13.

736. Liang H, Hussey SE, Sanchez-Avila A, Tantiwong P, Musi N. Effect of Lipopolysaccharide on Inflammation and Insulin Action in Human Muscle. PLoS One. 2013;8(5).
737. Manco M, Putignani L, Bottazzo GF. Gut microbiota, lipopolysaccharides, and innate immunity in the pathogenesis of obesity and cardiovascular risk. Vol. 31, Endocrine Reviews. 2010. p. 817–44.
738. Guo S, Al-Sadi R, Said HM, Ma TY. Lipopolysaccharide causes an increase in intestinal tight junction permeability in vitro and in vivo by inducing enterocyte membrane expression and localization of TLR-4 and CD14. Am J Pathol. 2013;182(2):375–87.
739. Davis JE, Gabler NK, Walker-Daniels J, Spurlock ME. Tlr-4 deficiency selectively protects against obesity induced by diets high in saturated fat. Obesity. 2008;16(6):1248–55.
740. Kleinridders A, Schenten D, Könner AC, Belgardt BF, Mauer J, Okamura T, et al. MyD88 Signaling in the CNS Is Required for Development of Fatty Acid-Induced Leptin Resistance and Diet-Induced Obesity. Cell Metab. 2009;10(4):249–59.
741. Rogero MM, Calder PC. Obesity, inflammation, toll-like receptor 4 and fatty acids. Vol. 10, Nutrients. 2018.
742. Ahola AJ, Lassenius MI, Forsblom C, Harjutsalo V, Lehto M, Groop PH. Dietary patterns reflecting healthy food choices are associated with lower serum LPS activity. Sci Rep. 2017;7(1).
743. Perez-Pardo P, Dodiya HB, Engen PA, Forsyth CB, Huschens AM, Shaikh M, et al. Role of TLR4 in the gut-brain axis in Parkinson's disease: A translational study from men to mice. Gut. 2018;
744. Scheen AJ, Esser N, Paquot N. Antidiabetic agents: Potential anti-inflammatory activity beyond glucose control. Vol. 41, Diabetes and Metabolism. 2015. p. 183–94.
745. Harris JJ, Jolivet R, Attwell D. Synaptic Energy Use and Supply. Vol. 75, Neuron. 2012. p. 762–77.
746. Hyder F, Rothman DL, Bennett MR. Cortical energy demands of signaling and nonsignaling components in brain are conserved across mammalian species and activity levels. Vol. 110, Proceedings of the National Academy of Sciences of the United States of America. 2013. p. 3549–54.
747. Rangaraju V, Calloway N, Ryan TA. Activity-driven local ATP synthesis is required for synaptic function. Cell. 2014;156(4):825–35.
748. Pathak D, Shields LY, Mendelsohn BA, Haddad D, Lin W, Gerencser AA, et al. The role of mitochondrially derived ATP in synaptic vesicle recycling. J Biol Chem. 2015;290(37):22325–36.

749. Engelhardt B, Sorokin L. The blood-brain and the blood-cerebrospinal fluid barriers: Function and dysfunction. Vol. 31, Seminars in Immunopathology. 2009. p. 497–511.
750. Pontzer H, Brown MH, Raichlen DA, Dunsworth H, Hare B, Walker K, et al. Metabolic acceleration and the evolution of human brain size and life history. Nature. 2016;533:390–2.
751. Watts ME, Pocock R, Claudianos C. Brain energy and oxygen metabolism: Emerging role in normal function and disease. Vol. 11, Frontiers in Molecular Neuroscience. 2018.
752. Schinkel AH. P-Glycoprotein, a gatekeeper in the blood-brain barrier. Vol. 36, Advanced Drug Delivery Reviews. 1999. p. 179–94.
753. Seino K, Azuma M, Bashuda H, Fukao K, Yagita H, Okumura K. CD86 (B70/B7-2) on endothelial cells co-stimulates allogeneic CD4+T cells. Int Immunol. 1995;7(8):1331–7.
754. Omari KIM, Dorovini-Zis K. Expression and function of the costimulatory molecules B7-1 (CD80) and B7-2 (CD86) in an in vitro model of the human blood-brain barrier. J Neuroimmunol. 2001;113(1):129–41.
755. Khan Academy. Oxidative phosphorylation and the electron transport chain. KhanacademyOrg [Internet]. 2015;1.
756. Berg J, Tymoczko J, Stryer L. Biochemistry, 5th edition. Biochemistry. 2002.
757. van den Brom CE, Bulte CSE, Loer SA, Bouwman RA, Boer C. Diabetes, perioperative ischaemia and volatile anaesthetics: Consequences of derangements in myocardial substrate metabolism. Vol. 12, Cardiovascular Diabetology. 2013.
758. Furukawa S, Fujita T, Shimabukuro M, Iwaki M, Yamada Y, Nakajima Y, et al. Increased oxidative stress in obesity and its impact on metabolic syndrome. J Clin Invest [Internet]. 1752;114(12).
759. Van Der Pouw Kraan TCTM, Chen WJ, Bunck MCM, Van Raalte DH, Van Der Zijl NJ, Van Genugten RE, et al. Metabolic changes in type 2 diabetes are reflected in peripheral blood cells, revealing aberrant cytotoxicity, a viral signature, and hypoxia inducible factor activity. BMC Med Genomics. 2015;8(1).
760. Jiang G, Zhang BB. Glucagon and regulation of glucose metabolism. Vol. 284, American Journal of Physiology - Endocrinology and Metabolism. 2003.
761. Edgerton DS, Moore MC, Winnick JJ, Scott M, Farmer B, Naver H, et al. Changes in glucose and fat metabolism in response to the administration of a hepato-preferential insulin analog. Diabetes. 2014;63(11):3946–54.

762. Xu F, Tavintharan S, Sum CF, Woon K, Lim SC, Ong CN. Metabolic signature shift in type 2 diabetes mellitus revealed by mass spectrometry-based metabolomics. J Clin Endocrinol Metab. 2013;98(6).
763. Haythorne E, Rohm M, van de Bunt M, Brereton MF, Tarasov AI, Blacker TS, et al. Diabetes causes marked inhibition of mitochondrial metabolism in pancreatic β-cells. Nat Commun. 2019;10(1).
764. Kuge Y, Yajima K, Kawashima H, Yamazaki H, Hashimoto N, Miyake Y. Brain uptake and metabolism of [1-11C]octanoate in rats: Pharmacokinetic basis for its application as a radiopharmaceutical for studying brain fatty acid metabolism. Ann Nucl Med. 1995;9(3):137–42.
765. Edmond J, Robbins RA, Bergstrom JD, Cole RA, de Vellis J. Capacity for substrate utilization in oxidative metabolism by neurons, astrocytes, and oligodendrocytes from developing brain in primary culture. J Neurosci Res. 1987;18(4):551–61.
766. Ebert D, Haller RG, Walton ME. Energy contribution of octanoate to intact rat brain metabolism measured by 13C nuclear magnetic resonance spectroscopy. J Neurosci. 2003;23(13):5928–35.
767. Groschner LN, Waldeck-Weiermair M, Malli R, Graier WF. Endothelial mitochondria-less respiration, more integration. Pflugers Arch Eur J Physiol. 2012;464(1):63–76.
768. Dagher Z, Ruderman N, Tornheim K, Ido Y. Acute regulation of fatty acid oxidation and AMP-activated protein kinase in human umbilical vein endothelial cells. Circ Res. 2001;88(12):1276–82.
769. De Bock K, Georgiadou M, Schoors S, Kuchnio A, Wong BW, Cantelmo AR, et al. Role of PFKFB3-driven glycolysis in vessel sprouting. Cell. 2013;154(3):651–63.
770. Mertens S, Noll T, Spahr R, Krutzfeldt A, Piper HM. Energetic response of coronary endothelial cells to hypoxia. Am J Physiol - Hear Circ Physiol. 1990;258(3 27-3).
771. Grammas P, Martinez J, Miller B. Cerebral microvascular endothelium and the pathogenesis of neurodegenerative diseases. Vol. 13, Expert reviews in molecular medicine. 2011.
772. Bauernfeind AL, Babbitt CC. The appropriation of glucose through primate neurodevelopment. J Hum Evol. 2014;77:132–40.
773. Fraisl P, Mazzone M, Schmidt T, Carmeliet P. Regulation of Angiogenesis by Oxygen and Metabolism. Vol. 16, Developmental Cell. 2009. p. 167–79.
774. Cheng SC, Joosten LAB, Netea MG. The interplay between central metabolism and innate immune responses. Vol. 25, Cytokine and Growth Factor Reviews. 2014. p. 707–13.

775. Hou WK, Xian YX, Zhang L, Lai H, Hou XG, Xu YX, et al. Influence of blood glucose on the expression of glucose transporter proteins 1 and 3 in the brain of diabetic rats. Chin Med J (Engl). 2007;120(19):1704–9.
776. Pardridge WM, Triguero D, Farrell CR. Downregulation of blood-brain barrier glucose transporter in experimental diabetes. Diabetes. 1990;39(9):1040–4.
777. Seaquist ER, Tkac I, Damberg G, Thomas W, Gruetter R. Brain glucose concentrations in poorly controlled diabetes mellitus as measured by high-field magnetic resonance spectroscopy. Metabolism. 2005;54(8):1008–13.
778. Gruetter R, Novotny EJ, Boulware SD, Rothman DL, Shulman RG. 1H NMR studies of glucose transport in the human brain. J Cereb Blood Flow Metab. 1996;16(3):427–38.
779. Hasselbalch SG, Knudsen GM, Capaldo B, Postiglione A, Paulson OB. Blood-brain barrier transport and brain metabolism of glucose during acute hyperglycemia in humans. J Clin Endocrinol Metab. 2001;86(5):1986–90.
780. Stein LJ, Dorsa DM, Baskin DG, Figlewicz DP, Porte D, Woods SC. Reduced effect of experimental peripheral hyperinsulinemia to elevate cerebrospinal fluid insulin concentrations of obese zucker rats. Endocrinology. 1987;121(5):1611–5.
781. Gerozissis K, Orosco M, Rouch C, Nicolaidis S. Basal and hyperinsulinemia-induced immunoreactive hypothalamic insulin changes in lean and genetically obese Zucker rats revealed by microdialysis. Brain Res. 1993;611(2):258–63.
782. Kaiyala KJ, Prigeon RL, Kahn SE, Woods SC, Schwartz MW. Obesity induced by a high-fat diet is associated with reduced brain insulin transport in dogs. Diabetes. 2000;49(9):1525–33.
783. Baskin DG, Stein LJ, Ikeda H, Woods SC, Figlewicz DP, Porte D, et al. Genetically obese zucker rats have abnormally low brain insulin content. Life Sci. 1985;36(7):627–33.
784. Craft S, Cholerton B, Baker LD. Insulin and Alzheimer's disease: Untangling the web. Vol. 33, Journal of Alzheimer's Disease. 2013.
785. Hoyer S. Glucose metabolism and insulin receptor signal transduction in Alzheimer disease. Eur J Pharmacol. 2004;490(1–3):115–25.
786. Zhao N, Liu CC, Van Ingelgom AJ, Martens YA, Linares C, Knight JA, et al. Apolipoprotein E4 Impairs Neuronal Insulin Signaling by Trapping Insulin Receptor in the Endosomes. Neuron. 2017;96(1):115-129.e5.
787. Schrijvers EMC, Witteman JCM, Sijbrands EJG, Hofman A, Koudstaal PJ, Breteler MMB. Insulin metabolism and the risk of Alzheimer disease: The Rotterdam Study. Neurology. 2010;75(22):1982–7.

788. Cirrito JR, Deane R, Fagan AM, Spinner ML, Parsadanian M, Finn MB, et al. P-glycoprotein deficiency at the blood-brain barrier increases amyloid-β deposition in an Alzheimer disease mouse model. J Clin Invest. 2005;115(11):3285–90.
789. Kuhnke D, Jedlitschky G, Grube M, Krohn M, Jucker M, Mosyagin I, et al. MDR1-P-glycoprotein (ABCB1) mediates transport of Alzheimer's amyloid-β peptides - Implications for the mechanisms of Aβ clearance at the blood-brain barrier. Brain Pathol. 2007;17(4):347–53.
790. Lam FC, Liu R, Lu P, Shapiro AB, Renoir JM, Sharom FJ, et al. β-Amyloid efflux mediated by p-glycoprotein. J Neurochem. 2001;76(4):1121–8.
791. Hartz AMS, Miller DS, Bauer B. Restoring blood-brain barrier P-glycoprotein reduces brain amyloid-β in a mouse model of Alzheimer's disease. Mol Pharmacol. 2010;77(5):715–23.
792. Boudina S, Sena S, Theobald H, Sheng X, Wright JJ, Xia XH, et al. Mitochondrial energetics in the heart in obesity-related diabetes: Direct evidence for increased uncoupled respiration and activation of uncoupling proteins. Diabetes. 2007;56(10):2457–66.
793. Bugger H, Boudina S, Hu XX, Tuinei J, Zaha VG, Theobald HA, et al. Type 1 diabetic akita mouse hearts are insulin sensitive but manifest structurally abnormal mitochondria that remain coupled despite increased uncoupling protein 3. Diabetes. 2008;57(11):2924–32.
794. Bach D, Pich S, Soriano FX, Vega N, Baumgartner B, Oriola J, et al. Mitofusin-2 determines mitochondrial network architecture and mitochondrial metabolism: A novel regulatory mechanism altered in obesity. J Biol Chem. 2003;278(19):17190–7.
795. Tang X, Luo YX, Chen HZ, Liu DP. Mitochondria, endothelial cell function, and vascular diseases. Vol. 5 MAY, Frontiers in Physiology. 2014.
796. Muoio DM, Newgard CB. Mechanisms of disease: Molecular and metabolic mechanisms of insulin resistance and β-cell failure in type 2 diabetes. Nat Rev Mol Cell Biol. 2008;9(3):193–205.
797. Sarsour EH, Kumar MG, Chaudhuri L, Kalen AL, Goswami PC. Redox control of the cell cycle in health and disease. Vol. 11, Antioxidants and Redox Signaling. 2009. p. 2985–3011.
798. Valko M, Leibfritz D, Moncol J, Cronin MTD, Mazur M, Telser J. Free radicals and antioxidants in normal physiological functions and human disease. Vol. 39, International Journal of Biochemistry and Cell Biology. 2007. p. 44–84.
799. Trachootham D, Lu W, Ogasawara MA, Valle NR Del, Huang P. Redox regulation of cell survival. Vol. 10, Antioxidants and Redox Signaling. 2008. p. 1343–74.

800. Mariani E, Polidori MC, Cherubini A, Mecocci P. Oxidative stress in brain aging, neurodegenerative and vascular diseases: An overview. J Chromatogr B Anal Technol Biomed Life Sci. 2005;827(1):65–75.
801. Halliwell B. Oxygen and nitrogen are pro-carcinogens. Damage to DNA by reactive oxygen, chlorine and nitrogen species: Measurement, mechanism and the effects of nutrition. Mutat Res - Genet Toxicol Environ Mutagen. 1999;443(1–2):37–52.
802. Evans JL, Goldfine ID, Maddux BA, Grodsky GM. Oxidative stress and stress-activated signaling pathways: A unifying hypothesis of type 2 diabetes. Endocr Rev. 2002;23(5):599–622.
803. Bouché C, Serdy S, Kahn CR, Goldfine AB. The cellular fate of glucose and its relevance in type 2 diabetes. Vol. 25, Endocrine Reviews. 2004. p. 807–30.
804. Lopaschuk GD. Fatty Acid Oxidation and Its Relation with Insulin Resistance and Associated Disorders. In: Annals of Nutrition and Metabolism. 2016. p. 15–20.
805. Agus DB, Gambhir SS, Pardridge WM, Spielholz C, Baselga J, Vera JC, et al. Vitamin C crosses the blood-brain barrier in the oxidized form through the glucose transporters. J Clin Invest. 1997;100(11):2842–8.
806. Huang J, Agus DB, Winfree CJ, Kiss S, Mack WJ, McTaggart RA, et al. Dehydroascorbic acid, a blood-brain barrier transportable form of vitamin C, mediates potent cerebroprotection in experimental stroke. Proc Natl Acad Sci U S A. 2001;98(20):11720–4.
807. Minamizono A, Tomi M, Hosoya KI. Inhibition of dehydroascorbic acid transport across the rat blood-retinal and -brain barriers in experimental diabetes. Biol Pharm Bull. 2006;29(10):2148–50.
808. Popa-Wagner A, Mitran S, Sivanesan S, Chang E, Buga AM. ROS and brain diseases: The good, the bad, and the ugly. Oxidative Medicine and Cellular Longevity. 2013.
809. Toda N, Ayajiki K, Okamura T. Cerebral blood flow regulation by nitric oxide: Recent advances. Vol. 61, Pharmacological Reviews. 2009. p. 62–97.
810. Dawson TM, Snyder SH. Gases as biological messengers: Nitric oxide and carbon monoxide in the brain. Vol. 14, Journal of Neuroscience. 1994. p. 5147–59.
811. Förstermann U. Nitric oxide and oxidative stress in vascular disease. Vol. 459, Pflugers Archiv European Journal of Physiology. 2010. p. 923–39.
812. Halliwell B. Antioxidant defence mechanisms: From the beginning to the end (of the beginning). In: Free Radical Research. 1999. p. 261–72.
813. Bresgen N, Karlhuber G, Krizbai I, Bauer H, Bauer HC, Eckl PM. Oxidative stress in cultured cerebral endothelial cells induces chromosomal aberrations, micronuclei, and apoptosis. J Neurosci Res. 2003;72(3):327–33.

814. Halliwell B. Role of free radicals in the neurodegenerative diseases: Therapeutic implications for antioxidant treatment. Vol. 18, Drugs and Aging. 2001. p. 685–716.
815. Markesbery WR, Lovell MA. Four-hydroxynonenal, a product of lipid peroxidation, is increased in the brain in Alzheimer's disease. Neurobiol Aging. 1998;19(1):33–6.
816. Butterfield DA, Bader Lange ML, Sultana R. Involvements of the lipid peroxidation product, HNE, in the pathogenesis and progression of Alzheimer's disease. Vol. 1801, Biochimica et Biophysica Acta - Molecular and Cell Biology of Lipids. 2010. p. 924–9.
817. Zarkovic K. 4-Hydroxynonenal and neurodegenerative diseases. In: Molecular Aspects of Medicine. 2003. p. 293–303.
818. Good PF, Werner P, Hsu A, Olanow CW, Perl DP. Evidence for neuronal oxidative damage in Alzheimer's disease. Am J Pathol. 1996;149(1):21–8.
819. Schapira AHV. Mitochondrial dysfunction in neurodegenerative diseases. Vol. 33, Neurochemical Research. 2008. p. 2502–9.
820. Dauer W, Przedborski S. Parkinson's disease: Mechanisms and models. Vol. 39, Neuron. 2003. p. 889–909.
821. Schmidt AM, Yan S Du, Yan SF, Stern DM. The multiligand receptor RAGE as a progression factor amplifying immune and inflammatory responses. Vol. 108, Journal of Clinical Investigation. 2001. p. 949–55.
822. Wautier JL, Schmidt AM. Protein glycation: A firm link to endothelial cell dysfunction. Vol. 95, Circulation Research. 2004. p. 233–8.
823. Nowotny K, Jung T, Höhn A, Weber D, Grune T. Advanced glycation end products and oxidative stress in type 2 diabetes mellitus. Vol. 5, Biomolecules. 2015. p. 194–222.
824. Chuah YK, Basir R, Talib H, Tie TH, Nordin N. Receptor for advanced glycation end products and its involvement in inflammatory diseases. Vol. 2013, International Journal of Inflammation. 2013.
825. Younessi P, Yoonessi A. Advanced glycation end-products and their receptor-mediated roles: Inflammation and oxidative stress. Vol. 36, Iranian Journal of Medical Sciences. 2011. p. 154–66.
826. Freeman LR, Keller JN. Oxidative stress and cerebral endothelial cells: Regulation of the blood-brain-barrier and antioxidant based interventions. Vol. 1822, Biochimica et Biophysica Acta - Molecular Basis of Disease. 2012. p. 822–9.
827. Lehner C, Gehwolf R, Tempfer H, Krizbai I, Hennig B, Bauer HC, et al. Oxidative stress and blood-brain barrier dysfunction under particular consideration of matrix metalloproteinases. Vol. 15, Antioxidants and Redox Signaling. 2011. p. 1305–23.

828. Gu Z, Kaul M, Yan B, Kridel SJ, Cui J, Strongin A, et al. S-nitrosylation of matrix metalloproteinases: Signaling pathway to neuronal cell death. Science (80-). 2002;297(5584):1186–90.
829. Meli DN, Christen S, Leib SL. Matrix metalloproteinase-9 in pneumococcal meningitis: Activation via an oxidative pathway. J Infect Dis. 2003;187(9):1411–5.
830. Huang CY, Fujimura M, Noshita N, Chang YY, Chan PH. SOD1 down-regulates NF-κB and c-Myc expression in mice after transient focal cerebral ischemia. J Cereb Blood Flow Metab. 2001;21(2):163–73.
831. Cui Y, Yang S. Overexpression of Annexin A1 protects against benzo[a]pyrene-induced bronchial epithelium injury. Mol Med Rep. 2018;18(1):349–57.
832. Leoni G, Alam A, Alexander Neumann P, Lambeth JD, Cheng G, McCoy J, et al. Annexin A1, formyl peptide receptor, and NOX1 orchestrate epithelial repair. J Clin Invest. 2013;123(1):443–54.
833. Kiani-Esfahani A, Sheykhshabani SK, Peymani M, Hashemi MS, Ghaedi K, Nasr-Esfahani MH. Overexpression of annexin A1 suppresses pro-inflammatory factors in PC12 cells induced by 1-methyl-4-phenylpyridinium. Cell J. 2016;18(2):197–204.
834. Epstein FH, Fish EM, Molitoris BA. Alterations in epithelial polarity and the pathogenesis of disease states. Vol. 330, New England Journal of Medicine. 1994. p. 1580–8.
835. Bacallao R, Garfinkel A, Monke S, Zampighi G, Mandel LJ. ATP depletion: A novel method to study junctional properties in epithelial tissues: I - Rearrangement of the actin cytoskeleton. J Cell Sci. 1994;107(12):3301–13.
836. Nurko S, Sogabe K, Davis JA, Roeser NF, Defrain M, Chien A, et al. Contribution of actin cytoskeletal alterations to ATP depletion and calcium-induced proximal tubule cell injury. Am J Physiol. 1996;270(1 PART 2).
837. Tsukamoto T, Nigam SK. Tight junction proteins form large complexes and associate with the cytoskeleton in an ATP depletion model for reversible junction assembly. J Biol Chem. 1997;272(26):16133–9.
838. Go GW, Mani A. Low-density lipoprotein receptor (LDLR) family orchestrates cholesterol homeostasis. Vol. 85, Yale Journal of Biology and Medicine. 2012. p. 19–28.
839. Poirier S, Mayer G, Benjannet S, Bergeron E, Marcinkiewicz J, Nassoury N, et al. The proprotein convertase PCSK9 induces the degradation of low density lipoprotein receptor (LDLR) and its closest family members VLDLR and ApoER2. J Biol Chem. 2008;283(4):2363–72.
840. Barber CN, Raben DM. Lipid metabolism crosstalk in the brain: Glia and neurons. Vol. 13, Frontiers in Cellular Neuroscience. 2019.

841. Rutkowsky JM, Lee LL, Puchowicz M, Golub MS, Befroy DE, Wilson DW, et al. Reduced cognitive function, increased bloodbrain-barrier transport and inflammatory responses, and altered brain metabolites in LDLr-/-And C57BL/6 mice fed a western diet. PLoS One. 2018;13(2).
842. Whitehead JP, Richards AA, Hickman IJ, Macdonald GA, Prins JB. Adiponectin - A key adipokine in the metabolic syndrome. Vol. 8, Diabetes, Obesity and Metabolism. 2006. p. 264–80.
843. Okamoto Y, Kihara S, Ouchi N, Nishida M, Arita Y, Kumada M, et al. Adiponectin reduces atherosclerosis in apolipoprotein E-deficient mice. Circulation. 2002;106(22):2767–70.
844. Deepa SS, Dong LQ. Appl1: Role in adiponectin signaling and beyond. Vol. 296, American Journal of Physiology - Endocrinology and Metabolism. 2009.
845. Berg AH, Combs TP, Scherer PE. ACRP30/adiponectin: An adipokine regulating glucose and lipid metabolism. Vol. 13, Trends in Endocrinology and Metabolism. 2002. p. 84–9.
846. Thundyil J, Pavlovski D, Sobey CG, Arumugam T V. Adiponectin receptor signalling in the brain. Vol. 165, British Journal of Pharmacology. 2012. p. 313–27.
847. Spranger J, Verma S, Göhring I, Bobbert T, Seifert J, Sindler AL, et al. Adiponectin does not cross the blood-brain barrier but modifies cytokine expression of brain endothelial cells. Diabetes. 2006;55(1):141–7.
848. Qiu G, Wan R, Hu J, Mattson MP, Spangler E, Liu S, et al. Adiponectin protects rat hippocampal neurons against excitotoxicity. Age (Omaha). 2011;33(2):155–65.
849. Nishimura M, Izumiya Y, Higuchi A, Shibata R, Qiu J, Kudo C, et al. Adiponectin prevents cerebral ischemic injury through endothelial nitric oxide synthase-dependent mechanisms. Circulation. 2008;117(2):216–23.
850. Wan Z, Mah D, Simtchouk S, Klegeris A, Little JP. Globular adiponectin induces a pro-inflammatory response in human astrocytic cells. Biochem Biophys Res Commun. 2014;446(1):37–42.
851. Bokarewa M, Nagaev I, Dahlberg L, Smith U, Tarkowski A. Resistin, an Adipokine with Potent Proinflammatory Properties. J Immunol. 2005;174(9):5789–95.
852. Silswal N, Singh AK, Aruna B, Mukhopadhyay S, Ghosh S, Ehtesham NZ. Human resistin stimulates the pro-inflammatory cytokines TNF-α and IL-12 in macrophages by NF-κB-dependent pathway. Biochem Biophys Res Commun. 2005;334(4):1092–101.

853. Kosari S, Rathner JA, Badoer E. Central Resistin Enhances Renal Sympathetic Nerve Activity via Phosphatidylinositol 3-Kinase but Reduces the Activity to Brown Adipose Tissue via Extracellular Signal-Regulated Kinase 1/2. J Neuroendocrinol. 2012;24(11):1432–9.
854. Melone M, Wilsie L, Palyha O, Strack A, Rashid S. Discovery of a new role of human resistin in hepatocyte low-density lipoprotein receptor suppression mediated in part by proprotein convertase subtilisin/kexin type 9. J Am Coll Cardiol. 2012;59(19):1697–705.
855. Horton JD, Cohen JC, Hobbs HH. PCSK9: A convertase that coordinates LDL catabolism. Vol. 50, Journal of Lipid Research. 2009.
856. Hampton EN, Knuth MW, Li J, Harris JL, Lesley SA, Spraggon G. The self-inhibited structure of full-length PCSK9 at 1.9 Å reveals structural homology with resistin within the C-terminal domain. Proc Natl Acad Sci U S A. 2007;104(37):14604–9.
857. Park HK, Kwak MK, Kim HJ, Ahima RS. Linking resistin, inflammation, and cardiometabolic diseases. Vol. 32, Korean Journal of Internal Medicine. 2017. p. 239–47.
858. Helfer G, Wu QF. Chemerin: A multifaceted adipokine involved in metabolic disorders. Vol. 238, Journal of Endocrinology. 2018. p. R79–94.
859. Bozaoglu K, Bolton K, McMillan J, Zimmet P, Jowett J, Collier G, et al. Chemerin is a novel adipokine associated with obesity and metabolic syndrome. Endocrinology. 2007;148(10):4687–94.
860. Bozaoglu K, Segal D, Shields KA, Cummings N, Curran JE, Comuzzie AG, et al. Chemerin is associated with metabolic syndrome phenotypes in a Mexican-American population. J Clin Endocrinol Metab. 2009;94(8):3085–8.
861. Sell H, Laurencikiene J, Taube A, Eckardt K, Cramer A, Horrighs A, et al. Chemerin is a novel adipocyte-derived factor inducing insulin resistance in primary human skeletal muscle cells. Diabetes. 2009;58(12):2731–40.
862. Chakaroun R, Raschpichler M, Klöting N, Oberbach A, Flehmig G, Kern M, et al. Effects of weight loss and exercise on chemerin serum concentrations and adipose tissue expression in human obesity. Metabolism. 2012;61(5):706–14.
863. Peng L, Yu Y, Liu J, Li S, He H, Cheng N, et al. The chemerin receptor CMKLR1 is a functional receptor for amyloid-β peptide. J Alzheimer's Dis. 2014;43(1):227–42.
864. Ku IA, Farzaneh-Far R, Vittinghoff E, Zhang MH, Na B, Whooley MA. Association of low leptin with cardiovascular events and mortality in patients with stable coronary artery disease: The Heart and Soul Study. Atherosclerosis. 2011;217(2):503–8.

865. Lieb W, Beiser AS, Vasan RS, Tan ZS, Au R, Harris TB, et al. Association of plasma leptin levels with incident Alzheimer disease and MRI measures of brain aging. JAMA - J Am Med Assoc. 2009;302(23):2565–72.
866. Fewlass DC, Noboa K, Pi-Sunyer FX, Johnston JM, Yan SD, Tezapsidis N. Obesity-related leptin regulates Alzheimer's Aβ. FASEB J. 2004;18(15):1870–8.
867. Greco SJ, Sarkar S, Johnston JM, Tezapsidis N. Leptin regulates tau phosphorylation and amyloid through AMPK in neuronal cells. Biochem Biophys Res Commun. 2009;380(1):98–104.
868. Löffek S, Schilling O, Franzke CW. Series "matrix metalloproteinases in lung health and disease" edited by J. Müller-Quernheim and O. Eickelberg number 1 in this series: Biological role of matrix metalloproteinases: A critical balance. Eur Respir J. 2011;38(1):191–208.
869. Wu YJ, Neoh CA, Tsao CY, Su JH, Li HH. Sinulariolide suppresses human hepatocellular carcinoma cell migration and invasion by inhibiting matrix metalloproteinase-2/-9 through MAPKs and PI3K/Akt signaling pathways. Int J Mol Sci. 2015;16(7):16469–82.
870. Dutra FF, Bozza MT. Heme on innate immunity and inflammation. Vol. 5 MAY, Frontiers in Pharmacology. 2014.
871. Cho A, Graves J, Reidy MA. Mitogen-activated protein kinases mediate matrix metalloproteinase-9 expression in vascular smooth muscle cells. Arterioscler Thromb Vasc Biol. 2000;20(12):2527–32.
872. Wang T, Liao Y, Sun Q, Tang H, Wang G, Zhao F, et al. Upregulation of matrix metalloproteinase-9 in primary cultured rat astrocytes induced by 2-chloroethanol via MAPK signal pathways. Front Cell Neurosci. 2017;11.
873. Cheng CY, Hsieh HL, Hsiao L Der, Yang CM. PI3-K/Akt/JNK/NF-κB is essential for MMP-9 expression and outgrowth in human limbal epithelial cells on intact amniotic membrane. Stem Cell Res. 2012;9(1):9–23.
874. Neoh CA, Wu WT, Dai GF, Su JH, Liu CI, Su TR, et al. Flaccidoxide-13-acetate extracted from the soft coral cladiella kashmani reduces human bladder cancer cell migration and invasion through reducing activation of the FAK/PI3K/AKT/mTOR signaling pathway. Molecules. 2018;23(1).
875. Bachstetter AD, Van Eldik LJ. The p38 map kinase family as regulators of proinflammatory cytokine production in degenerative diseases of the CNS. Vol. 1, Aging and Disease. 2010. p. 199–211.
876. Zhao Y, Tang Z, Zhu X, Wang X, Wang C, Zhang W, et al. TAB3 involves in hepatic insulin resistance through activation of MAPK pathway. Gen Comp Endocrinol. 2015;224:228–34.

877. Pan Y, Wang Y, Zhao Y, Peng K, Li W, Wang Y, et al. Inhibition of JNK phosphorylation by a novel curcumin analog prevents high glucose-induced inflammation and apoptosis in cardiomyocytes and the development of diabetic cardiomyopathy. Diabetes. 2014;63(10):3497–511.
878. Gao Y, Kang L, Li C, Wang X, Sun C, Li Q, et al. Resveratrol Ameliorates Diabetes-Induced Cardiac Dysfunction Through AT1R-ERK/p38 MAPK Signaling Pathway. Cardiovasc Toxicol. 2016;16(2):130–7.
879. Gogg S, Smith U, Jansson PA. Increased MAPK activation and impaired insulin signaling in subcutaneous microvascular endothelial cells in type 2 diabetes: The role of endothelin-1. Diabetes. 2009;58(10):2238–45.
880. Bathina S, Das UN. Dysregulation of PI3K-Akt-mTOR pathway in brain of streptozotocin-induced type 2 diabetes mellitus in Wistar rats. Lipids Health Dis. 2018;17(1).
881. Heasman SJ, Ridley AJ. Mammalian Rho GTPases: New insights into their functions from in vivo studies. Vol. 9, Nature Reviews Molecular Cell Biology. 2008. p. 690–701.
882. Bustelo XR, Sauzeau V, Berenjeno IM. GTP-binding proteins of the Rho/Rac family: Regulation, effectors and functions in vivo. Vol. 29, BioEssays. 2007. p. 356–70.
883. Boureux A, Vignal E, Faure S, Fort P. Evolution of the Rho family of Ras-like GTPases in eukaryotes. Mol Biol Evol. 2007;24(1):203–16.
884. Centers for Disease Control and Prevention. National Diabetes Statistics Report: Estimates of Diabetes and its Burden in the United States. US Dep Heal Hum Serv. 2014;
885. Pettitt DJ, Talton J, Dabelea D, Divers J, Imperatore G, Lawrence JM, et al. Prevalence of diabetes in U.S. Youth in 2009: The SEARCH for diabetes in youth study. Diabetes Care. 2014;37(2):402–8.
886. Duffany KO, McVeigh KH, Kershaw TS, Lipkind HS, Ickovics JR. Maternal Obesity: Risks for Developmental Delays in Early Childhood. Matern Child Health J. 2016;20(2):219–30.
887. Li N, Yolton K, Lanphear BP, Chen A, Kalkwarf HJ, Braun JM. Impact of Early-Life Weight Status on Cognitive Abilities in Children. Obesity. 2018;26(6):1088–95.
888. Wang C, Chan JSY, Ren L, Yan JH. Obesity Reduces Cognitive and Motor Functions across the Lifespan. Vol. 2016, Neural Plasticity. 2016.
889. ECDC. COVID-19 situation update worldwide, as of 13 May 2020. European Centre for Disease Prevention and Control. 2020. p. 1–9.
890. Guo W, Li M, Dong Y, Zhou H, Zhang Z, Tian C, et al. Diabetes is a risk factor for the progression and prognosis of COVID-19. Diabetes Metab Res Rev. 2020;

891. Cristelo C, Azevedo C, Marques JM, Nunes R, Sarmento B. SARS-CoV-2 and diabetes: New challenges for the disease. Vol. 164, Diabetes Research and Clinical Practice. 2020.
892. Sten Madsbad. COVID-19 Infection in People with Diabetes. Touch endriconology [Internet]. 2020;1–28.
893. Dixon AE, Peters U. The effect of obesity on lung function. Vol. 12, Expert Review of Respiratory Medicine. 2018. p. 755–67.
894. Varatharaj A, Thomas N, Ellul M, Davies NW, Pollak T, Tenorio EL, et al. UK-Wide Surveillance of Neurological and Neuropsychiatric Complications of COVID-19: The First 153 Patients. SSRN Electron J. 2020;
895. Ellul M, Benjamin L, Singh B, Lant S, Michael B, Kneen R, et al. Neurological Associations of COVID-19. SSRN Electron J. 2020;
896. Verity R, Okell LC, Dorigatti I, Winskill P, Whittaker C, Imai N, et al. Estimates of the severity of coronavirus disease 2019: a model-based analysis. Lancet Infect Dis. 2020;20(6):669–77.
897. Jain A, Davis AM. Primary Prevention of Cardiovascular Disease. Vol. 322, JAMA - Journal of the American Medical Association. 2019. p. 1817–8.
898. Ley SH, Hamdy O, Mohan V, Hu FB. Prevention and management of type 2 diabetes: Dietary components and nutritional strategies. Vol. 383, The Lancet. 2014. p. 1999–2007.
899. Dyson PA, Kelly T, Deakin T, Duncan A, Frost G, Harrison Z, et al. Diabetes UK evidence-based nutrition guidelines for the prevention and management of diabetes. Diabet Med. 2011;28(11):1282–8.
900. Dua T, Seeher KM, Sivananthan S, Chowdhary N, Pot AM, Saxena S. Risk reduction of cognitive decline and dementia. Vol. 13, Alzheimer's & Dementia. 2017. 1450–1451 p.
901. National Institute for Health and Care Excellence. National Institute for Health and Care Excellence (NICE). Grants Regist 2019. 2019;540–540.
902. Park JC, Baik SH, Han SH, Cho HJ, Choi H, Kim HJ, et al. Annexin A1 restores Aβ1-42-induced blood–brain barrier disruption through the inhibition of RhoA-ROCK signaling pathway. Aging Cell. 2017;16(1):149–61.
903. Hughes RN. Sex does matter: Comments on the prevalence of male-only investigations of drug effects on rodent behaviour. Vol. 18, Behavioural Pharmacology. 2007. p. 583–9.
904. U.S. Government Accountability Office. Drug safety: Most drugs withdrawn in recent years had greater health risks for women. Gao-01-286R [Internet]. 2001;343(25):1–8.

905. Maas AHEM, Appelman YEA. Gender differences in coronary heart disease. Vol. 18, Netherlands Heart Journal. 2010. p. 598–603.
906. Podcasy JL, Epperson CN. Considering sex and gender in Alzheimer disease and other dementias. Dialogues Clin Neurosci. 2016;18(4):437–46.
907. Satizabal CL, Beiser AS, Chouraki V, Chêne G, Dufouil C, Seshadri S. Incidence of dementia over three decades in the Framingham heart study. N Engl J Med. 2016;374(6):523–32.
908. Maggioli E, McArthur S, Mauro C, Kieswich J, Kusters DHM, Reutelingsperger CPM, et al. Estrogen protects the blood–brain barrier from inflammation-induced disruption and increased lymphocyte trafficking. Brain Behav Immun. 2016;51:212–22.
909. He Y, Yao Y, Tsirka S., Cao Y. Cell-Culture Models of the Blood–Brain Barrier. Stroke. 2014;45(8):2514–26.
910. Stone NL, England TJ, O'Sullivan SE. A novel transwell blood brain barrier model using primary human cells. Front Cell Neurosci. 2019;13.
911. Takeshita Y, Obermeier B, Cotleur A, Sano Y, Kanda T, Ransohoff RM. An in vitro blood-brain barrier model combining shear stress and endothelial cell/astrocyte co-culture. J Neurosci Methods. 2014;232:165–72.
912. Cucullo L, McAllister MS, Kight K, Krizanac-Bengez L, Marroni M, Mayberg MR, et al. A new dynamic in vitro model for the multidimensional study of astrocyte-endothelial cell interactions at the blood-brain barrier. Brain Res. 2002;951(2):243–54.
913. Griep LM, Wolbers F, De Wagenaar B, Ter Braak PM, Weksler BB, Romero IA, et al. BBB on CHIP: Microfluidic platform to mechanically and biochemically modulate blood-brain barrier function. Biomed Microdevices. 2013;15(1):145–50.
914. Adriani G, Ma D, Pavesi A, Goh ELK, Kamm RD. Modeling the Blood-Brain Barrier in a 3D triple co-culture microfluidic system. In: Proceedings of the Annual International Conference of the IEEE Engineering in Medicine and Biology Society, EMBS. 2015. p. 338–41.
915. Wang JD, Khafagy ES, Khanafer K, Takayama S, Elsayed MEH. Organization of Endothelial Cells, Pericytes, and Astrocytes into a 3D Microfluidic in Vitro Model of the Blood-Brain Barrier. Mol Pharm. 2016;13(3):895–906.